
THESES SIS/LIBRARY
R.G. MENZIES LIBRARY BUILDING NO:2
THE AUSTRALIAN NATIONAL UNIVERSITY
CANBERRA ACT 0200 AUSTRALIA

TELEPHONE: +61 2 6125 4631
FACSIMILE: +61 2 6125 4063
EMAIL: library.theses@anu.edu.au

USE OF THESES

This copy is supplied for purposes
of private study and research only.
Passages from the thesis may not be
copied or closely paraphrased without the
written consent of the author.

Errata

- p. 23, ref(22): read "Lawrance" instead of "Lawarance"
- p. 41, 1.3: read "trans-bis(trimethylenediamine)dichloroplatinum(IV) dichloride" instead of "Bis(trimethylenediamine)trans-dichloroplatinum(IV) dichloride"
- p. 42, 1.-6,: read "Anal. Calc. for "[C₁₄H₃₆Cl₄N₆Pt]": C, 26.89; H, 5.80; N, 13.44. Found: C, 17.41; H, 3.95; N, 7.88" instead of "Anal. Calc. for "[C₁₄H₃₆Cl₄N₆Pt]": C, 26.89; H, 5.80; N, 13.44; Cl, 22.68. Found: C, 17.41; H, 3.95; N, 7.88"
- p. 43, 1.20: read "Bis(1,1,1-tris(aminomethyl)ethane)platinum(IV) tetrachloride monohydrate" instead of "Bis(1,1,1-tris(aminomethyl)ethane)platinum(IV) tetrachloridemonohydrate"
- p. 48, 1.1: read "[[(6,14-diethyl-1,5,9,13,20,24-hexamethyl-18,22-diamonio-3,7,11,15-tetraazapentacyclo[10.4.4.4⁴⁻⁹.0⁷⁻²³.0¹⁵⁻¹⁹]tetracosane)platinum(II) tetrachloride" instead of "[[(6,14-diethyl-1,5,9,13,20,23-hexamethyl-3,7,11,15,18,22-hexaazapentacyclo[10.4.4.4⁴⁻⁹.0⁷⁻²³.0¹⁵⁻¹⁹]tetracosane)platinum(II) tetrachloride"
- p. 51, 1.20 read "[[(1,5,9,13-tetramethyl-18,22-diamonio-3,7,11,15-tetraazapentacyclo[10.4.4.4⁴⁻⁹.0⁷⁻²³.0¹⁵⁻¹⁹]tetracosane)platinum(II) tetrachloride" instead of "[[(1,4,9,12-tetramethyl-3,7,11,15,18,23-hexaazapentacyclo[10.4.4.4⁴⁻⁹.0⁷⁻²².0¹⁵⁻¹⁹]tetracosane)platinum(II) tetrachloride"
- p. 56, 1.1, -1; p 57, 1.1; 131, 1.8: read "[Pt(Me₅-N₆-tricosanetriimine)](ZnCl₄)_{1.5}.Cl.2H₂O" and not "[Pt(Me₅-N₆-tricosanetriimine)](ZnCl₄)_{1.5}.Cl" (see also note on page 32)
- p. 75, 1.1: Insert "NMR" between "¹³C" and "spectrum"
- p. 153, 1.6: delete the sentence "The peak currents were higher using the EPG electrodes than those using the gold disc electrodes".
- p. 173, ref 9: read "Cotton, F.A.; Wilkinson, G." instead of "Cotton, F.A.; G. Wilkinson"
- p. 188, 1.-5: insert "in" before "MeCN"
- p. 204, 1.4, 1.6, 1.9: read "CVs" instead of "CV's"
- p. 235, 1.3: read "(1,1,1-tris(5-amino-2-azapentyl)ethane)chromium(III)" instead of "1,1,1-tris(5-amino-2-azapentyl)ethane) chromium(III)"
- p. 236, 1-7, -9: read "HCl" instead of "HCL"
- p. 238, 1.16: read "K₂SO₄" instead of "K₂SO₅"
- Appendix A, p.i, -1: read "18,22-diamonio-3,7,11,15-tetraazapentacyclo[10.4.4.4⁴⁻⁹.0⁷⁻²³.0¹⁵⁻¹⁹]tetracosane" instead of "3,7,11,15,18,22-hexaazapentacyclo[10.4.4.4⁴⁻⁹.0⁷⁻²³.0¹⁵⁻¹⁹]tetracosane"
- Appendix B(I): read "[Pt(Me₅-N₆-tricosanetriimine)](ZnCl₄)_{1.5}.Cl.2H₂O" and not "[Pt(Me₅-N₆-tricosanetriimine)](ZnCl₄)_{1.5}.Cl" (see also note on page 32)

**Synthesis and Properties of Expanded Cage
Complexes of Pt(IV), Pt(II), Co(III) and Cr(III)**

A Thesis Submitted for the Degree of Doctor of Philosophy

at

The Australian National University

by

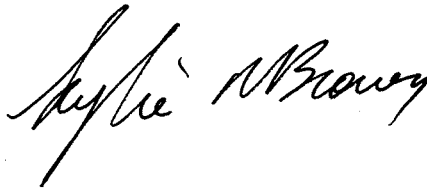
Kylie Nancy Brown

Research School of Chemistry, Canberra, ACT

October 1994

Declaration

The work presented in this thesis is the original work of the author, except where due reference is made in the text.



Kylie Nancy Brown

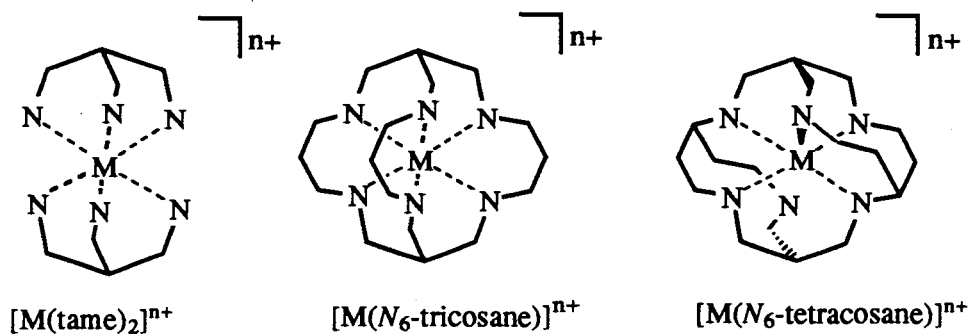


Acknowledgments

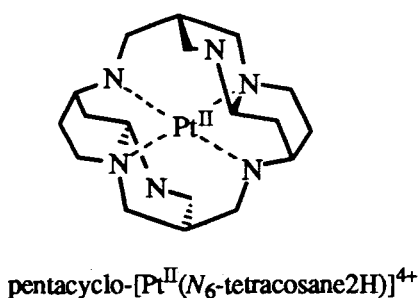
I specially thank my supervisor Professor Alan Sargeson for the opportunity to work with him and his group. I thank Drs Peter Osvath, Patricia Angus, Paul Bernhardt, Chris Crane and Stephen Ralph for their tolerance and efforts in helping me to write this thesis. Thanks to the members of the Sargeson Group for many provocative discussions, not all of them related to chemistry. Others to thank include Professor Alan Bond at LaTrobe University for many discussions and advice regarding the electrochemistry. Thanks also to Dr. Chunnian Shi at the Californian Institute of Technology for assistance with the electrochemistry of the some of the platinum complexes, and to Dr. G. Heath and his group for his assistance with the mercury electrode. Thanks also to Jullian Kelly, Drs Hans Riesen, Elmars Krausz and Lucian Dubicki for their expertise with the electronic spectroscopy and for increasing my knowledge in this area. Thanks also to the staff at the University NMR centre, for their much needed assistance. I am grateful to the crystallographers Drs. Trevor Hambley, at the University of Sydney, David Hockless and Tony Willis at the Research School of Chemistry. I also thank Ben Andrews and my family for their encouragement and support during these last few years. Next, but not least, thanks to the rest of those who tempered the chemistry and made my stay in Canberra more exciting. Finally, I am grateful to Persy and Kelpy for their secretarial skills in the typing of this thesis.

Abstract

This thesis addresses the template synthesis of cage complexes of the N_6 -tricosane and N_6 -tetracosane framework (below) using the template $[M(\text{tame})_2]^{n+}$ in acetonitrile, where $M = \text{Pt(IV)}$, Co(III) and Cr(III) .



Three different types of cages were produced from the $[\text{Pt}(\text{tame})_2]^{4+}$ template reactions. Two cages were synthesised directly from the reaction of the template with (a) propanal and formaldehyde and (b) propanal only, to yield the N_6 -tricosanetriimine and N_6 -tetracosanediimine type cages, respectively. The mechanisms for the synthesis of these cages is addressed. Attempts to selectively reduce the imines in the N_6 -tetracosanediimine type cages only resulted in reduction of Pt(IV) ion, accompanied by a ligand rearrangement to form pentacyclic Pt(II) complexes of the type shown below. The electrochemistry of these complexes were complicated. The cyclic voltammograms of the Pt(IV) complexes exhibited irreversible responses for the $\text{Pt(IV)}/\text{Pt(II)}$ couple, which reflected the conversion of the six coordinate Pt(IV) to square planar Pt(II) by a two electron reduction which was accompanied by extensive ligand rearrangement.



The reaction of $[\text{Co}(\text{tame})_2]^{3+}$ with propanal in the presence of base in acetonitrile produced $[\text{Co}(\text{Et}_2\text{-Me}_6\text{-}N_6\text{-tetracosanediimine})]^{3+}$. Subsequent reduction of the imines produced $[\text{Co}(\text{Et}_2\text{-Me}_6\text{-}N_6\text{-tetracosane})]^{3+}$. The crystal structures of both the diimine and saturated complexes show unusual tetragonal compression of the $\text{Co}N_6^{3+}$ chromophore and this was manifested in their NMR and absorption spectra and in the electron transfer properties. The self exchange rate constant of the $[\text{Co}(\text{Et}_2\text{-Me}_6\text{-}N_6\text{-tetracosane})]^{3+/2+}$ couple was deduced from the cross reaction of the Co(II) member

with $[\text{Co}(\text{azacpten})]^{3+}$ and was found to be $k_{\text{ex}} = 200 \text{ M}^{-1}\text{s}^{-1}$. This is one of the largest yet reported for saturated $\text{CoN}_6^{3+/2+}$ couples.

The reaction of $[\text{Cr}(\text{tame})_2]^{3+}$ with propanal and formaldehyde in basic acetonitrile produced $[\text{Cr}(\text{Me}_5\text{-N}_6\text{-tricosanetriimine})]^{3+}$. Reduction of the imines afforded the saturated cage, $[\text{Cr}(\text{Me}_5\text{-N}_6\text{-tricosane})]^{3+}$. This complex exhibits reversible Cr(III)/Cr(II) electrochemistry and is photostable over long periods of irradiation. The ${}^2\text{E}_g$ state lifetime at 298 K of $[\text{Cr}(\text{Me}_5\text{-N}_6\text{-tricosane})]^{3+}$ in acid solution was found to be the longest yet reported for Cr(III) hexaamine complexes ($\tau = 230 \mu\text{s}$ at pH ~ 2.2). It was also examined for its potential as a photosensitiser, using the quenching reagents iodide, azide, EDTA, DCTA, oxalate and $[\text{Fe}(\text{CN})_6]^{4-}$.

The N_6 -tetracosane synthesis generated a whole new class of cage complexes. These cages are anticipated to encapsulate large metal ions and further the study of macrocyclic chemistry.

Table of Contents

Declaration

Acknowledgements

Abstract

Contents

Abbreviations

CHAPTER 1 Introduction

1.1	General.....	2
1.2	Template Synthesis.....	2
1.3	Sepulchrates and Sarcophagine Cage Complexes.....	4
	(a) Nomenclature	4
	(b) General Properties of Cage Complexes.....	5
1.4	Applications of Cage Complexes	9
1.5	Details of the Syntheses of Cage Complexes.....	10
	(a) Overview of Sep and Sar Cage Syntheses.....	10
	(b) Synthesis of Cage Complexes with Expanded Cavities	14
1.6	Encapsulation of Metal Ions Using Non-Template Methods	18
1.7	Other Synthetic Approaches to Cages with Large Cavities	19
1.8	Aims.....	21
1.9	References.....	22

CHAPTER 2 Experimental

2.1	Starting Materials	29
2.2	Solvents.....	29
2.3	Ligands	30

2.4	Chromatography	31
2.5	Hazards and Special Precautions	31
2.6	NMR Spectroscopy	31
2.7	Structure Determinations.....	32
2.8	Electrochemistry	33
2.9	Visible Spectroscopy.....	35
2.10	References.....	36

CHAPTER 3 The Synthesis of Expanded Pt(IV) and Pt(II) Cages

3.1.	Introduction.....	38
3.1.1	Sar Cage Complexes of Pt(IV)	38
3.1.2	Proposed Syntheses of Pt(IV) <i>N</i> ₆ -tricosane Cage Complexes.....	38
3.1.3	Substitution Reactions about Pt(IV) with the Free Cage Ligands	40
3.2.	Synthesis.....	41
3.2.1	Synthesis of the Templates.....	41
3.2.2	Reactions of [Pt(tame) ₂] ⁴⁺ with Propanal.....	44
3.2.3	Reaction of [Pt(tame) ₂] ⁴⁺ with Acetaldehyde.....	49
3.2.4	Reaction of [Pt(tame) ₂] ⁴⁺ with Acetylacetone	52
3.3.	Results	54
3.3.1	Pt(IV) Substitution Reactions.....	54
3.3.2	Reactions of [Pt(tame) ₂] ⁴⁺ with Propanal.....	55
	(a) Synthesis of [Pt(^α Me ₅ - <i>N</i> ₆ -tricosanetriimine)] ⁴⁺	55
	(b) Attempted Reduction of [Pt(^α Me ₅ - <i>N</i> ₆ -tricosanetriimine)] ⁴⁺	62
	(c) Synthesis of [Pt(Et ₂ -Me ₆ - <i>N</i> ₆ -tetracosanediimine)] ⁴⁺	66
	(b) Reduction of [Pt(Et ₂ -Me ₆ - <i>N</i> ₆ -tetracosanediimine)] ⁴⁺	77

(b) Reduction of $[\text{Pt}(\text{Et}_2\text{-Me}_6\text{-N}_6\text{-tricosanetriimine})]^{4+}$	77
3.3.3 Reactions of $[\text{Pt}(\text{tame})_2]^{4+}$ with Acetaldehyde.....	84
(a) Synthesis of $[\text{Pt}(\beta\text{Me}_5\text{-N}_6\text{-tricosanetriimine})]^{4+}$	84
(b) Synthesis of $[\text{Pt}(\text{Me}_4\text{-N}_6\text{-tetracosanediimine})]^{4+}$	89
(c) Reduction of $[\text{Pt}(\text{Me}_4\text{-N}_6\text{-tetracosanediimine})]^{4+}$	93
3.3.4 Reactions of $[\text{Pt}(\text{tame})_2]^{4+}$ with Acetylacetone	95
(a) Synthesis of $[\text{Pt}(\text{tame}_2\text{-2,4-pentanediiiminate})]^{3+}$	95
(b) Reduction of $[\text{Pt}(\text{tame}_2\text{-2,4-pentanediiiminate})]^{3+}$	98
(c) Reaction of $[\text{Pt}(\text{tame})_2]^{4+}$ with 3,3-dimethyl-2,4-pentanedione	100
3.4. Discussion	101
3.4.1 General	101
3.4.2 Substitution Reactions of Pt(IV).....	101
3.4.3 Reactions of $[\text{Pt}(\text{tame})_2]^{4+}$ with Propanal.....	106
(a) Synthesis of $[\text{Pt}(\alpha\text{Me}_5\text{-N}_6\text{-tricosanetriimine})]^{4+}$	106
(b) Attempted Reduction of $[\text{Pt}(\alpha\text{Me}_5\text{-N}_6\text{-tricosanetriimine})]^{4+}$	114
(c) Synthesis of $[\text{Pt}(\text{Et}_2\text{-Me}_6\text{-N}_6\text{-tetracosanediimine})]^{4+}$	115
(d) Reduction of $[\text{Pt}(\text{Et}_2\text{-Me}_6\text{-N}_6\text{-tetracosanediimine})]^{4+}$	126
3.4.4 Reaction of $[\text{Pt}(\text{tame})_2]^{4+}$ with Acetaldehyde.....	129
(a) Synthesis of $[\text{Pt}([\beta\text{Me}_5\text{-N}_6\text{-tricosanetriimine})]^{4+}$	129
(b) Synthesis of $[\text{Pt}(\text{Me}_4\text{-N}_6\text{-tetracosanediimine})]^{4+}$	129
(c) Hydrogenation of the $[\text{Pt}(\text{Me}_4\text{-N}_6\text{-tetracosanediimine})]^{4+}$	133
3.4.5 Reaction of $[\text{Pt}(\text{tame})_2]^{4+}$ with Acetylacetone	134
3.4.6 Conclusion	136
3.4.7 References.....	137

CHAPTER 4	Electrochemical Behaviour of the Expanded Pt(IV) Cages	
4.1.	Introduction.....	142
4.1.1.	General.....	142
4.1.2.	Overview of Pt(III) Complexes.....	142
4.1.3.	Electrochemical Behaviour of Pt(IV) Sar Cage Complexes	143
4.2.	Experimental.....	146
4.2.1	Electrochemistry.....	146
4.3.	Results	147
4.3.1	General	147
4.3.2	[Pt ^{IV} (tame) ₂] ⁴⁺	147
4.3.2	[Pt ^{IV} (α Me ₅ -N ₆ -tricosanetriimine)] ⁴⁺	148
4.3.3	[Pt ^{IV} (Me ₄ -N ₆ -tetracosanediimine)] ⁴⁺	151
4.3.4	[Pt ^{IV} (Et ₂ -Me ₆ -N ₆ -tetracosanediimine)] ⁴⁺	153
4.3.5	Pentacyclo-[Pt ^{II} (Et ₂ -Me ₆ -N ₆ -tetracosane2H)] ⁴⁺	163
4.4.	Discussion	166
4.4.1	General	166
4.4.2	[Pt ^{IV} (tame) ₂] ⁴⁺	166
4.4.3	[Pt ^{IV} (α Me ₅ -N ₆ -tricosanetriimine)] ⁴⁺	167
4.4.4	[Pt ^{IV} (Et ₂ -Me ₆ -N ₆ -tetracosanediimine)] ⁴⁺	168
4.4.5	References.....	173
CHAPTER 5	Synthesis and Properties of Expanded Cobalt(III) Cages	
5.1.	Introduction.....	178
5.1.1	General	178
5.1.2	Overview of [Co(Me ₅ -N ₆ -tricosane)] ³⁺	178

(a) Spectral Properties.....	179
(b) Redox Properties	179
(c) Electron Transfer Rates	179
5.1.3 Effect of Ligand Rigidity	180
(a) [M(sar)] ⁿ⁺ Cage Complexes	180
(b) [M(N ₆ -tricosane)] ⁿ⁺ Complexes	181
5.1.4 Synthetic Strategies for Expanded Cavity Cages	182
5.1.5 New Scope for Cage Chemistry.....	183
5.2. Experimental.....	184
5.2.1 Synthesis	184
5.2.2 Procedures	189
5.3. Results	190
5.3.1 Reaction of Propanal with [Co(tame) ₂] ³⁺	190
5.3.2. Reduction of [Co(Et ₂ -Me ₆ -N ₆ -tetracosanediimine)] ³⁺	196
5.3.3 Reaction of [Co(tame) ₂] ³⁺ with Acetaldehyde.....	201
5.3.4 Electronic Spectra	201
5.3.5 Electrochemistry of the Co(III) N ₆ -tetracosane Complexes.....	204
5.3.6 Self Exchange Rate Constants.....	205
5.4. Discussion	206
5.4.1 Synthesis.....	206
5.4.2 Properties of the Co(III) N ₆ -tetracosane Complexes.....	210
(a) Electronic Spectroscopy	210
(b) Electrochemistry.....	212
(c) Correlation between Spectroscopic and Electrochemical Properties.....	214

(d) Self Exchange Rate Constant	215
5.4.3 References.....	218
CHAPTER 6 Synthesis and Properties of Expanded Chromium(III) Cages	
6.1. Introduction.....	223
6.1.1 General	223
6.1.2 General Spectroscopy for Cr(III) Hexaamine Complexes.....	223
6.1.3 Synthesis of Cr(III) Cage Complexes	229
6.1.4 Suitability of the Cr(III)/Cr(II) Couple in the Photocatalytic Cycle	232
6.2. Experimental.....	234
6.2.1 Synthesis.....	234
6.2.2 Procedures	239
6.3. Results	243
6.3.1 Synthesis.....	243
(a) Synthesis of the Templates.....	243
(b) Synthesis of the [Cr(Me ₅ -N ₆ -tricosane)] ³⁺ -Type Complexes	243
(c) Attempted Synthesis of [Cr(Me ₂ -N ₆ -tricosane)Cl ₃].....	244
6.3.2 Electrochemistry of Cr(III) Hexaamine Complexes.....	245
6.3.3 Electronic Spectra	251
6.3.3 Conformational Analysis.....	263
6.3.5 Quenching Experiments	264
6.4. Discussion	268
6.4.1 Template Synthesis of Chromium(III) Hexamine Complexes	268
6.4.2 Electrochemistry.....	272

6.4.3 Absorption and Emission Spectra	272
(a) Spin Allowed Transitions.....	272
(b) Spectroelectrochemistry	273
(c) Spin Forbidden Transitions	274
6.4.4 Comparison of the Lifetimes of the 2E_g State.....	275
6.4.5 A Potential Photosensitiser — the $[\text{Cr}(\text{Me}_5\text{-}N_6\text{-tricosane})]^{3+}$ Ion?	281
6.4.5 References.....	283

Appendices

Appendix A	i
Appendix B	iii
Appendix C	xviii
Appendix D	xxiii
Appendix E	xxiv
Appendix F	xxxiii
Appendix G.....	xlii
Appendix H.....	xlvii

Abbreviations

acac	acetylacetone
APT	attached proton test
AR	analytical reagent
bpy	bipyridine
chxn	cyclohexandiamine
COSY	correlation spectroscopy
CV	cyclic voltammogram
DCTA	1,2-cyclohexanediaminetetraacetic acid
DEPT	distortionless polarisation transfer
DQF	double quantum filtered
D ₂ O	deuterium oxide
diammac	6,13-dimethyl-1,4,8,11-tetraazacyclotetradecane-6,13-diamine
dien	diethylenetriamine
DMF	dimethylformamide
dmg	dimethylglyoxime
DMSO	dimethylsulfoxide
EDTA	ethylenediaminetetraacetic acid
en	ethylenediamine
<i>fac</i>	facial
fn	fourier number
FT	fourier transform
HMBC	heteronuclear multiple-pulse bond correlation
HMQC	heteronuclear multiple-pulse quantum correlation
NHE	normal hydrogen electrode
IR	infrared
L	litre, dm ³

MeCN	acetonitrile
<i>mer</i>	meridional
<i>N</i> ₆ -tetracosanediimine	3,7,11,15,18,22-hexaazatricyclo[10.4.4.4 ⁹⁻¹⁴]tetracosane-18,22-diene
<i>N</i> ₆ -tetracosane	3,7,11,15,18,22-hexaazatricyclo[10.4.4.4 ⁹⁻⁴]tetracosane
NMR	nuclear magnetic resonance
NOE	nuclear Overhauser effect
<i>N</i> ₆ -tricosane	3,7,11,15,18,22-hexaazabicyclo[7.7.7]tricosane
<i>N</i> ₆ -tricosanetriimine	3,7,11,15,18,22-hexaazabicyclo[7.7.7]tricosane-3,14,18-triene
ni	number of increments
np	number of points
nt	number of transients
pn	1,2-propanediamine
PVA	polyvinylalcohol
py	pyridine
sar	sarcophagine; 3,6,10,13,16,19-hexaazabicyclo[6.6.6]icosane
SCE	standard calomel electrode
sen	1,1,1-tris(4-amino-2-azabutyl)ethane
sep	sepulchrane; 1,3,6,8,10,13,16,19-octaazabicyclo[6.6.6]icosane
stn	1,1,1-tris(5-amino-2-azapentyl)ethane
tacn	1,4,7-triazacyclononane
tame	1,1,1-tris(aminomethyl)ethane
tn	trimethylenediamine; 1,3-propanediamine
trien	triethylenetetraamine
UV	ultra violet
vis	visible

Chapter 1

Introduction

1.1. General

The thermodynamic, kinetic, redox and spectral properties of metal ion macropolycycles have been shown to differ dramatically from those of their mono-, di-, tri- and polydentate acyclic analogues. These properties depend on a combination of effects, including the ability of the ligand to adopt the preferred geometry of the metal ion (and vice versa), the match between the size of the metal ion and the cavity of the ligand and the type of ligating atoms. These effects may be systematically examined by subtly altering the ligand framework either by adding substituents, by expanding the cavity, or changing the donor atoms. Aspects of the behaviour are relevant to understanding some biological systems, namely, the stability of the metal ion coordinated in some biological ligands and the rapidity of some electron transfer reactions in proteins.

This work explores the template synthesis of organic ligands about metal ions to form polyazamacrocyclic complexes. As the ligand essentially forms a cage about the metal ion, these complexes are hereafter referred to as "cage complexes".

1.2. Template Synthesis

Regular organic syntheses of macrocyclic ligands are often tedious, requiring a number of steps to produce the desired product and frequently yields are low.¹⁻⁴ Entropy effects involved in ring closure of long chains are large and negative. The ends of long chains are not likely to be in proximity so that the probability of their interaction, which is required for cyclisation, is low. These problems may be overcome by using a template complex which includes fragments of the final molecule. The complex is used to direct and control a sequence of small ring cyclisations, often in a one-pot synthesis. The template metal complex organises and also activates the precursors,^{2,5,6} while also stabilising reactive intermediates. In some cases, the product macrocycle is stabilised by the metal ion, while in others, it may be possible to remove this metal ion to yield the free ligand. This strategy can provide an efficient and useful route to the synthesis of macrocyclic ligands which may then be coordinated to other metal ions.

Many examples of template synthesis have used Schiff base condensations around metal amine complexes,^{2,4} involving coordinated imine intermediates. The coordination of an imine to a metal ion enhances its susceptibility towards nucleophilic attack and also decreases its propensity towards hydrolysis. The order of reactivity of imines is depicted in Fig. 1.1. Protonated imines readily undergo hydrolysis, free imines are less reactive, whereas coordination to a metal ion confers intermediate reactivity to the imine.

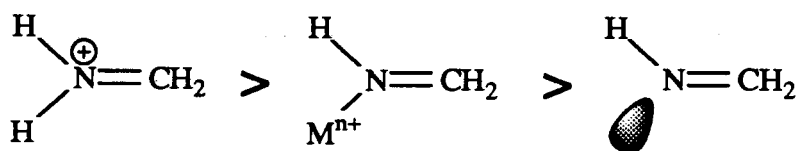
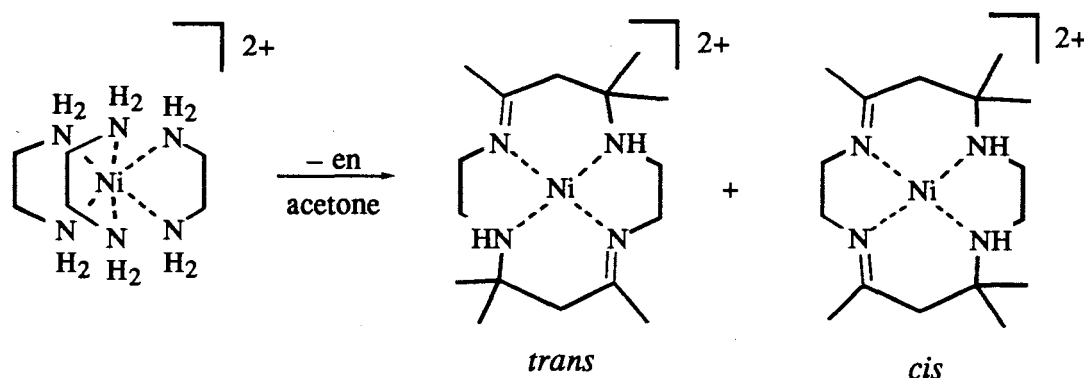


Figure 1.1: Order of reactivity of imines.

One of the earliest template syntheses involved the condensation of acetone with $[\text{Ni}(\text{en})_3]^{2+}$ (en = ethylenediamine), to form stable $[\text{Ni}(\text{Me}_6\text{-[14]aneN}_4\text{diene})]^{2+}$ complexes (Scheme 1.1).⁷ In this reaction, the $[\text{Ni}(\text{en})_3]^{2+}$ ion loses an ethylenediamine group and condenses with acetone to form a coordinated imine, which then undergoes nucleophilic attack by an acetonyl carbanion. Condensation of the carbonyl with an adjacent amine takes place and leads to ring closure. The amines on the opposite face of the complex react in the same way. Other metal ions have been observed to react similarly,⁷ e.g., Cu(II), Co(II), Co(III), Pd(II), Pt(II), Fe(II), Mg(II) and Mo(V).⁸



Scheme 1.1: Reaction of $[\text{Ni}(\text{en})_3]^{2+}$ with acetone.

There are numerous other examples of this kind or of similar processes, generally for complexes with an $[\text{MN}_4]$ core.^{2,4,9} The Schiff base route has also been used for synthesising three dimensional unsaturated macropolycycles, some of which are depicted in Fig. 1.2.^{10,11}

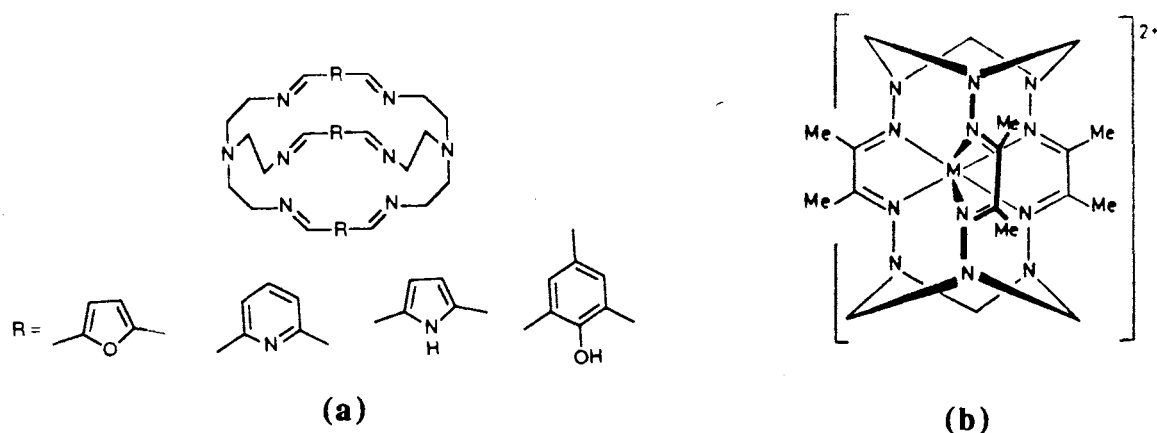
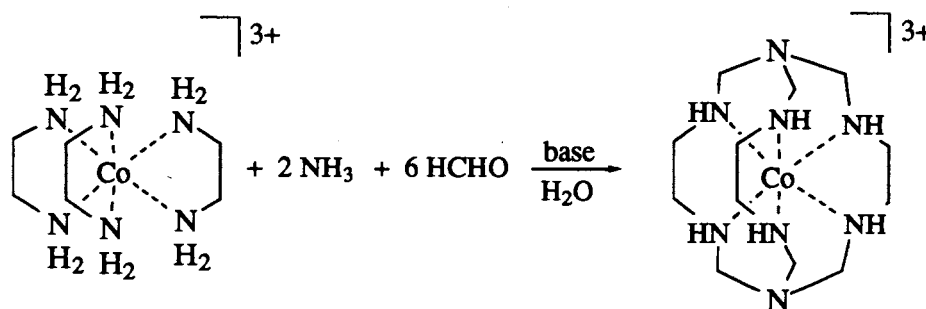


Figure 1.2: Macrobicyclic complexes formed using Schiff base methods. (a) $\text{M} = \text{Na}^+$,¹⁰ (b) $\text{M} = \text{Fe}(\text{II}), \text{Ni}(\text{II})$.¹¹

1.3. Sepulchrates and Sarcophagine Cage Complexes

The first metal directed synthesis of a saturated cage was achieved using the imine strategy, by reacting $[\text{Co}(\text{en})_3]^{3+}$ with NH_3 and CH_2O in the presence of base, producing $[\text{Co}(\text{sep})]^{3+}$ (sep = sepulchrates = 1,3,6,8,10,13,16,19-octaazabicyclo[6.6.6]icosane) in 80% yield (Scheme 1.2).¹²⁻¹⁴ A proposed reaction mechanism and other synthetic details are addressed later.



Scheme 1.2: Template synthesis of $[\text{Co}(\text{sep})]^{3+}$.

This methodology was later extended to form cages with different apical substituents by using different nucleophiles.¹⁵⁻¹⁸ Other modifications have produced cages with both sulfur and nitrogen donor atoms.¹⁹⁻²¹ Extrusion of the cobalt ion from the sar cages has been achieved and various other metals introduced.²² Organic routes have been used to synthesise cage complexes with six sulfur donor atoms.^{23,24}

(a) Nomenclature

Trivial names are used in the bulk of this thesis for brevity and ease of communication. The IUPAC names and structures described in this work are compiled in Appendix A. The term "small cage" refers primarily to the sar complexes, which comprise both five- and six-membered chelate ring systems. The term "large cage" refers primarily to the N_6 -tricosane complexes, comprising only six-membered chelate rings. Cages of the latter type often have longer than typical M-N bonds. The basic framework of cage complexes commonly referred to in this thesis are depicted in Fig. 1.3.

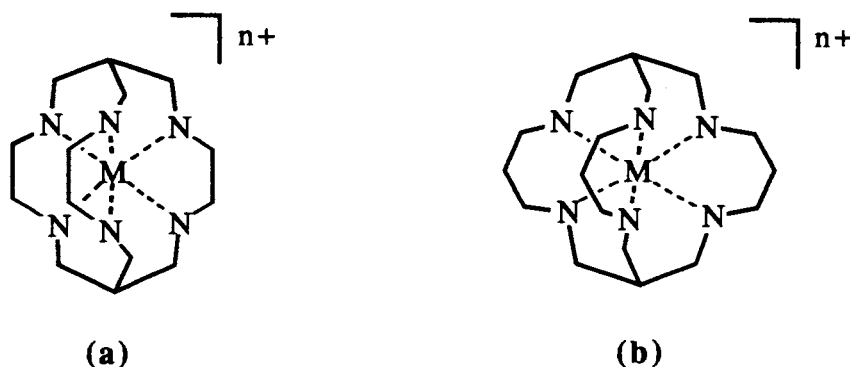


Figure 1.3: Metal ion complexes of (a) sarcophagine and (b) N_6 -tricosane (amine protons have been omitted for clarity).

(b) General Properties of Cage Complexes

I. Stability

One of the most important features of encapsulated metal ions is their kinetic and thermodynamic stability. As the increased stability of macromonocycles has been thought of as an extension of the chelate effect, the enhanced stability of macropolycycles has also been regarded as an extension of this macrocyclic effect.²⁵ Substitution reactions of the cage complexes are minimised due to the nature of the hexadentate bicyclic ligand. When bond rupture takes place, movement of the dissociated ligating atom away from the metal ion is restricted and recoordination is fast. Normally labile metal ions may therefore be rendered kinetically inert, as it is inconceivable that all six metal-donor bonds will simultaneously break. For example, the stability and inertness of $[\text{Co}(\text{sep})]^{2+}$ has been demonstrated by its negligible exchange with a $^{60}\text{Co}(\text{aq})^{2+}$ tracer over 24 hours.¹²

The thermodynamic stability of the cage complexes is high and establishing the dissociation equilibrium is difficult as the process is generally very slow. Only for $[\text{Hg}(\text{sar})]^{2+}$ and $[\text{Hg}(\text{NH}_3)_2\text{sar}]^{2+}$ has this property been measured ($K_{\text{stab}} \sim 10^{28}$ for both complexes).²⁶ In comparison, $K_{\text{stab}} \sim 10^{23}$ for $[\text{Hg}(\text{cyclam})]^{2+}$ is significantly lower.²⁶ The implication in this data is that the Co(II), Ni(II), Cu(II), Zn(II), Cd(II), Fe(II) and Mn(II) complexes are all as stable, or more so than the Hg(II) analogues.

II. Electron Transfer Rates

The self exchange rate constants of encapsulated Co(III)/Co(II) hexaamine couples are 5-7 orders of magnitude greater than their nonencapsulated analogues.²⁷ For example, the self exchange rate constants of the [Co(sep)]^{3+/2+}, [Co(en)]^{3+/2+} and [Co(NH₃)₆]^{3+/2+} couples are 5.1,¹³ 5×10^{-5} ,²⁸ and $\sim 10^{-7} \text{M}^{-1} \text{s}^{-1}$,²⁹ respectively. Briefly, one hypothesis is that the increased rate of electron transfer for the cages arises from non optimal Co-N bond lengths in both the Co(III) and Co(II) states.^{30,31} This introduces strain in both members of the redox couple, such that an entactic state³² is attained. The strain aids elongation and compression of the Co(III)-N and Co(II)-N bonds respectively, so that the energy required to form the activated complex from which electron transfer takes place is less than that in the less strained acyclic systems.^{30,31}

III. Electrochemical Behaviour of Cage Complexes

Most encapsulated metal ions exhibit reversible electrochemistry, even those with normally labile metal ions as they are held within the cage on the cyclic voltammetric (CV) timescale.^{33,34} For example, the CoN₆^{3+/2+} couple of sar complexes is reversible, whereas nonencapsulated CoN₆^{3+/2+} couples are generally irreversible on the CV timescale, as the ligand dissociation rate in the latter case for Co(II) is competitive with the reoxidation rate. The electrochemical behaviour of the sar complexes may be modulated by altering the ligating atoms,^{19,21,23,24} metal ions,³⁰ substituents^{33,35} and potential cavity size.³⁶⁻⁴¹ Reduction potentials ranging from +1 to -1 V at increments of 0.1 V, have been achieved through such modifications.³⁰ These effects are exemplified in the CoN₆^{3+/2+} couple, and Table 1.1 includes reduction potentials for a range of CoN₆^{3+/2+} cage complexes where the ligand framework has been systematically modified.

(i) Effect of the Donor Atom

The polarisability of the donor atoms will influence the relative stabilities of each member of the redox couple. This is exemplified in the substitution of the nitrogen donor atoms by sulfur donor atoms in the cages. Sulfur donor atoms are able to stabilise the lower oxidation states of metal ions and therefore the reduction potentials of the cages with sulfur donor atoms are more positive than those with nitrogen donor atoms.^{19,21,23,24} The S₆ donor cages stabilise lower oxidation states more than the N₆ cages on the CV timescale, for example, the Co(II)/Co(I) couple is quasireversible for the S₆- cage complexes,^{23,24} but it is irreversible for the N₃S₃ systems.

(ii) Effect of the Metal Ions

The reduction potentials of the complexes are related to small differences in the thermochemical properties of the metal ion.⁴² These are essentially, the ionisation potential, hydration enthalpy and heats of formation. For example, the effect of decreasing ionisation potential going down a group is demonstrated by a negative shift of the reduction potential. In the example of the $[\text{Co}(\text{sep})]^{3+/2+}$ couple,³³ its reduction potential (in acetone) is 1.53 V more positive compared to the $[\text{Rh}(\text{sep})]^{3+/2+}$ couple under the same conditions.⁴³ The ionisation potentials for the ions $\text{Co(II)} \rightarrow \text{Co(III)}$ and $\text{Rh(II)} \rightarrow \text{Rh(III)}$ are 33.49 and 31.0 eV, respectively.⁴⁴

(iii) Substituent Effects

The ability of the ligand to remove electron density from the metal ion facilitates its reduction.³³ Electron withdrawing substituents such as $-\text{NO}_2$ and $-\text{Cl}$ shift the reduction potentials of Co(III)/Co(II) couple to more positive values, while the opposite occurs for electron donating substituents, such as alkyl groups. The range spanned by the $\text{Co}^{3+}/\text{Co}^{2+}$ couples for N_6 cages by varying the substituents is ~ 0.6 V.³⁰ Correlations have been observed between the inductive effects of substituents with reduction potentials and NMR spectra.³⁵

Table 1.1: The effect of substituents, donor atom and ligand size on some Co(III)/Co(II) reduction potentials.

Complex	$E_{1/2}^{\S}$	Complex	$E_{1/2}^{\S}$
$[\text{Co}(\text{NH}_3)_6]^{3+/2+}$	-0.019^{33}	$[\text{Co}(\text{en})_3]^{3+/2+}$	-0.18^{27}
$[\text{Co}(\text{sep})]^{3+/2+}$	-0.30^{27}	$[\text{Co}(\text{sar})]^{3+/2+}$	-0.40^{27}
$[\text{Co}(\text{Me}_2\text{-N}_6\text{-sar})]^{3+/2+}$	-0.48^{41}	$[\text{Co}((\text{NH}_3)_2\text{sar})]^{5+/4+}$	$+0.04^{27}$
$[\text{Co}(\text{OH})_2\text{sar}]^{3+/2+}$	-0.20^{33}	$[\text{Co}(\text{NO}_2)_2\text{sar}]^{3+/2+}$	$+0.06^{33}$
$[\text{Co}(\text{Me-oxo-sar})]^{3+/2+}$	-0.58^{33}	$[\text{Co}(\text{Cl}_2\text{sar})]^{3+/2+}$	-0.13^{33}
$[\text{Co}(\text{Me-N}_3\text{S}_3\text{-sar})]^{3+/2+}$	-0.07^{24}	$[\text{Co}(\text{Me}_2\text{-S}_6\text{-sar})]^{3+/2+}$	$+0.27^{24}$
$[\text{Co}(\text{Me}_5\text{-N}_6\text{-tricosane})]^{3+/2+}$	$+0.08^{40}$	$[\text{Co}(\text{Me}_2\text{-S}_6\text{-tricosane})]^{3+/2+}$	$+0.40^{23}$

\S V vs NHE.

(iv) Ligand Cavity Size

The ease with which a ligand accommodates each member of the redox couple is related to its preferred cavity size.⁴⁵ Metal ions within ligands with smaller cavities are harder to reduce than those in larger cavities.³³ In some cases, the generation of a large cation within the cavity results in ligand rupture (e.g., Pt(III)^{34,46}), or dissociation of the metal ion (e.g., Cu(I)⁴⁷). Ligands with extra atoms in their framework have inherently larger cavities, and hence may readily accommodate larger ions. This is evident in the reduction potential of the $[\text{Co}(\text{Me}_5\text{-N}_6\text{-tricosane})]^{3+/2+}$ couple,⁴⁰ which is 0.56 V more positive than that of $[\text{Co}(\text{Me}_2\text{-N}_6\text{-sar})]^{3+/2+}$.⁴¹ Ligand rigidity may also limit changes in cavity size during reduction.² For example, the reduction potential of the $[\text{Co}(\text{ClCH}_2)_2, \text{Cl-absar}]^{3+/2+}$ couple (-0.36 V vs SCE), where one of the caps is constricted (Fig. 1.3(a)) is 0.10 V more negative than the $[\text{Co}(\text{Cl}, \text{Me-sar})]^{3+/2+}$ couple (Fig. 1.4(b)).³³

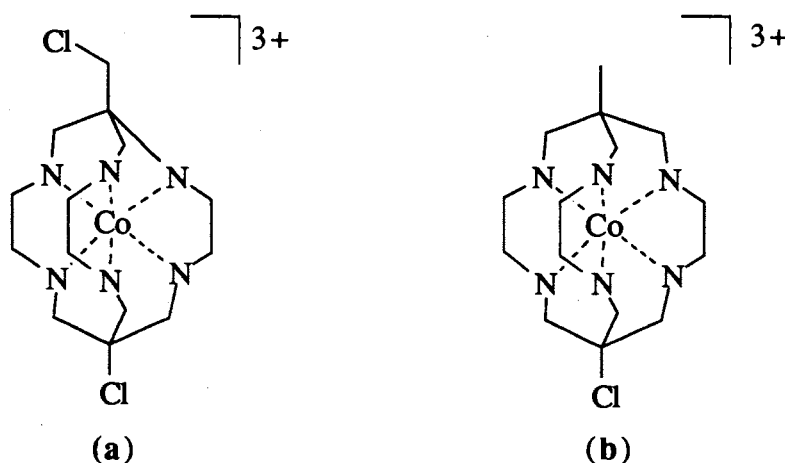


Figure 1.4: (a) $[\text{Co}(\text{ClCH}_2)_2, \text{Cl-absar}]^{3+}$ and (b) $[\text{Co}(\text{Cl}, \text{Me-sar})]^{3+}$ (amine protons have been omitted for clarity).

IV. Spectroscopy of Cage Complexes

The spectral features of a complex are governed mainly by the M-L bond length and also the stereochemistry around the metal ion, which is a compromise between the geometries preferred by the ligand and the metal. The effect of encapsulation on the spectral behaviour of some metal ions has been quite striking for the Cr(III) sar complexes.^{48,49} The distortion away from octahedral symmetry for $[\text{Cr}(\text{NH}_2)_2\text{sar}]^{3+}$ is manifested in the absorption spectra, where the absorption coefficients of the bands arising from the ${}^4\text{A}_{2g}(\text{O}_h) \rightarrow {}^4\text{T}_{2g}$ and ${}^4\text{A}_{2g}(\text{O}_h) \rightarrow {}^4\text{T}_{1g}$ transitions are $\epsilon_{456,447}=203, 208$ and $\epsilon_{346}=109 \text{ M}^{-1}\text{cm}^{-1}$, respectively (the first spin allowed transition, $({}^4\text{A}_{2g}(\text{O}_h) \rightarrow {}^4\text{T}_{2g})$ is split). In contrast, the absorption coefficients of the same bands for $[\text{Cr}(\text{en})_3]^{3+}$ are considerably less ($\epsilon_{456}=72$ and $\epsilon_{353}=63 \text{ M}^{-1}\text{cm}^{-1}$). Another unexpected spectroscopic phenomenon of the sar complexes is that the lifetime of their

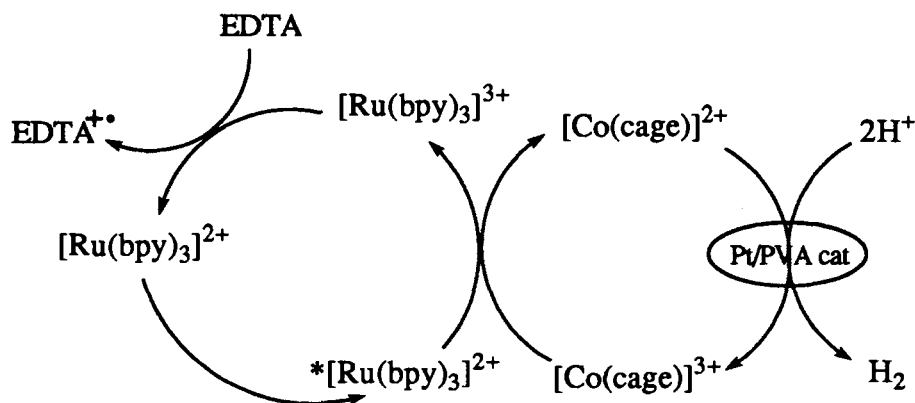
2E_g states is negligible at 298 K (<10 ns). This is not due to increased rates of photodissociation.^{48,49} In contrast, the nonencapsulated $[\text{Cr}(\text{en})_3]^{3+}$ analogue has a longer 2E_g lifetime (1.5 μs) under the same conditions.

Increasing the M-L bond lengths by expanding the preferred cavity size of the cage ligand may also produce dramatic differences in the spectral properties of the metal ion. The $[\text{Rh}(\text{X}, \text{Y}-\text{N}_6\text{-tricosane})]^{3+}$ ($\text{X}=\text{NO}_2$, NH_3^+ , $\text{Y}=\text{NO}_2$, NH_3^+ , Me) complexes, for example, not only have a decreased ligand field strength, but their emission lifetimes at 77 K are much longer (ranging from 160-205 μs) than their sar analogues, whose emission lifetimes are less than 10 ns under the same conditions.⁵⁰

1.4. Applications of Cage Complexes

Clearly the benefits arising from the stability, fast electron transfer rates of metal ions, redox and spectral properties of the cage complexes may be harnessed. Potential applications for cage type ligands include chelation therapy for those suffering from Wilson's disease.⁵¹ The sar ligands bind rapidly and almost irreversibly to Cu(II) from various copper pools in mouse liver cells to form $[\text{Cu}(\text{R}_2\text{sar})]^{2+}$ ($\text{R}=\text{H}$, NH_2).⁵¹ The cage ligands have several advantages compared to some chelation agents currently in use, e.g., penicillamine. Once coordinated within the cage, the copper ion does not undergo exchange with other physiological ligands.

The increased electron transfer rates and the reversibility and accessibility of the Co(III)/Co(II) couple, as well as the stability of both redox members may be utilised. This is exemplified by the $[\text{Co}(\text{sar})]^{3+/2+}$, $[\text{Co}(\text{sep})]^{3+/2+}$ ⁵²⁻⁵⁵ and analogous N_3S_3 sar couples,²¹ acting as electron transfer agents in the photoreduction of water (Scheme 1.3). In the presence of $[\text{Ru}(\text{bpy})_3]^{2+}$ as sensitiser and Pt/PVA as catalyst, the Co(III) cage complex acts as an electron transfer agent. In earlier studies, methylviologen was used as the electron transfer agent, which is toxic and less stable in its reduced form than the cage. The excited state $[\text{Ru}(\text{bpy})_3]^{2+}$ is a powerful reductant and reduces the Co(III) cage complexes to Co(II). The Co(II) complex, in the presence of the Pt/PVA catalyst, then reduces water to dihydrogen. A sacrificial electron donor (e.g., EDTA) returns the $[\text{Ru}(\text{bpy})_3]^{3+}$ to its original Ru(II) state, so completing the cycle.



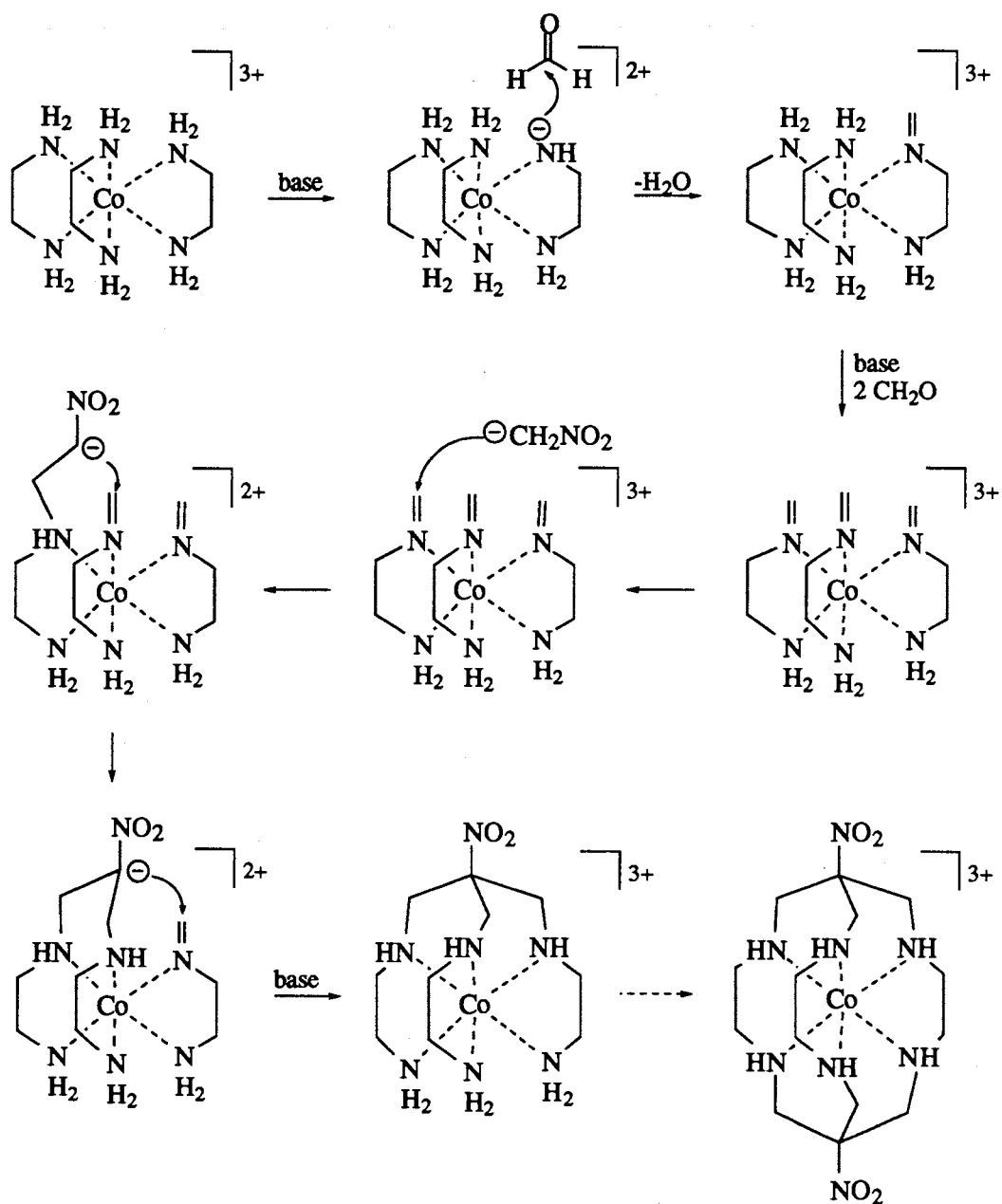
Scheme 1.3: The use of Co(III) cage complexes as electron transfer agents for the photoreduction of water.

Dihydrogen production has also been observed in electrochemical studies of Pt(IV) sar complexes.⁴⁶ At low temperature, in acetone, a Pt(III) sar ion generates hydrogen gas at the surface of the electrode, and regenerates the deprotonated Pt(IV) complex. There are implications in this experiment for the use of such molecules as electrocatalysts in the reduction of water to dihydrogen at low overpotentials. However, at ambient temperatures and also in aqueous media, the Pt(IV) based responses were irreversible, as the intermediate Pt(III) ion rapidly disproportionated to form Pt(II) and Pt(IV) complexes with ruptured cage ligands. No hydrogen formation was observed under these conditions.

1.5. Details of the Syntheses of Cage Complexes

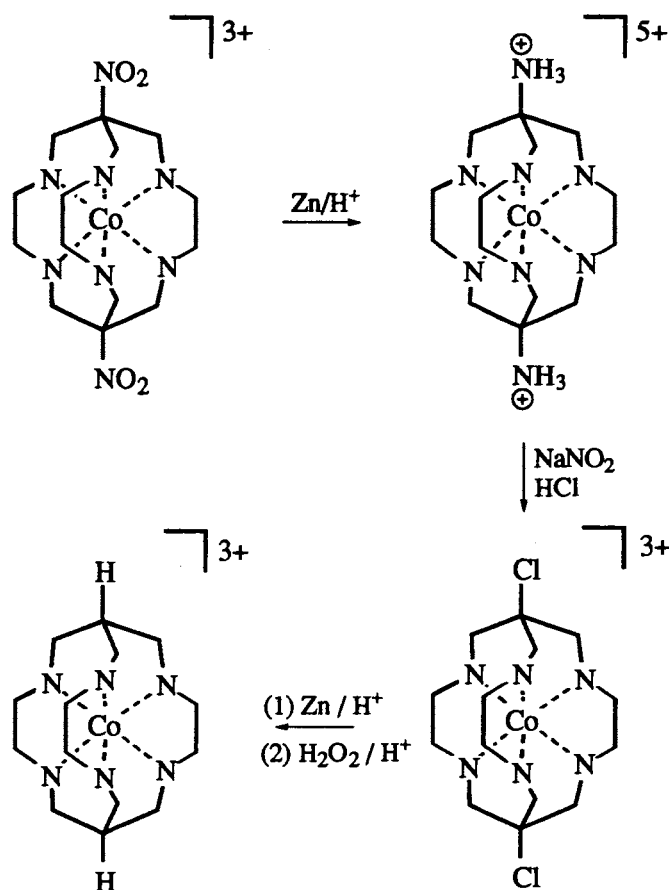
(a) Overview of Sep and Sar Cage Syntheses

The general strategy for the synthesis of this class of cage complexes has been based on the intermolecular condensation of aldehydes with coordinated primary amines to give coordinated imines, catalysed by a mild base. The metal directs the orientation of the imine organic fragments and also stabilises the intermediate imines towards hydrolysis, so that the desired reactions become more competitive. The coordinated imine intermediates then react with a nucleophile such as nitromethane carbanion,¹⁸ ammonia,¹² or an enolate anion⁵⁶ leading to encapsulation of the metal ion. Scheme 1.4 describes a mechanism for the template synthesis of $[\text{Co}((\text{NO}_2)_2\text{sar})]^{3+}$ from the reaction of $[\text{Co}(\text{en})_3]^{3+}$ with nitromethane and formaldehyde in water.¹³ Other metal ions, such as Pt(IV),⁴⁶ Ir(III),⁴³ Rh(III)⁴³ and Ni(II),⁵⁷ have been encapsulated using this route.



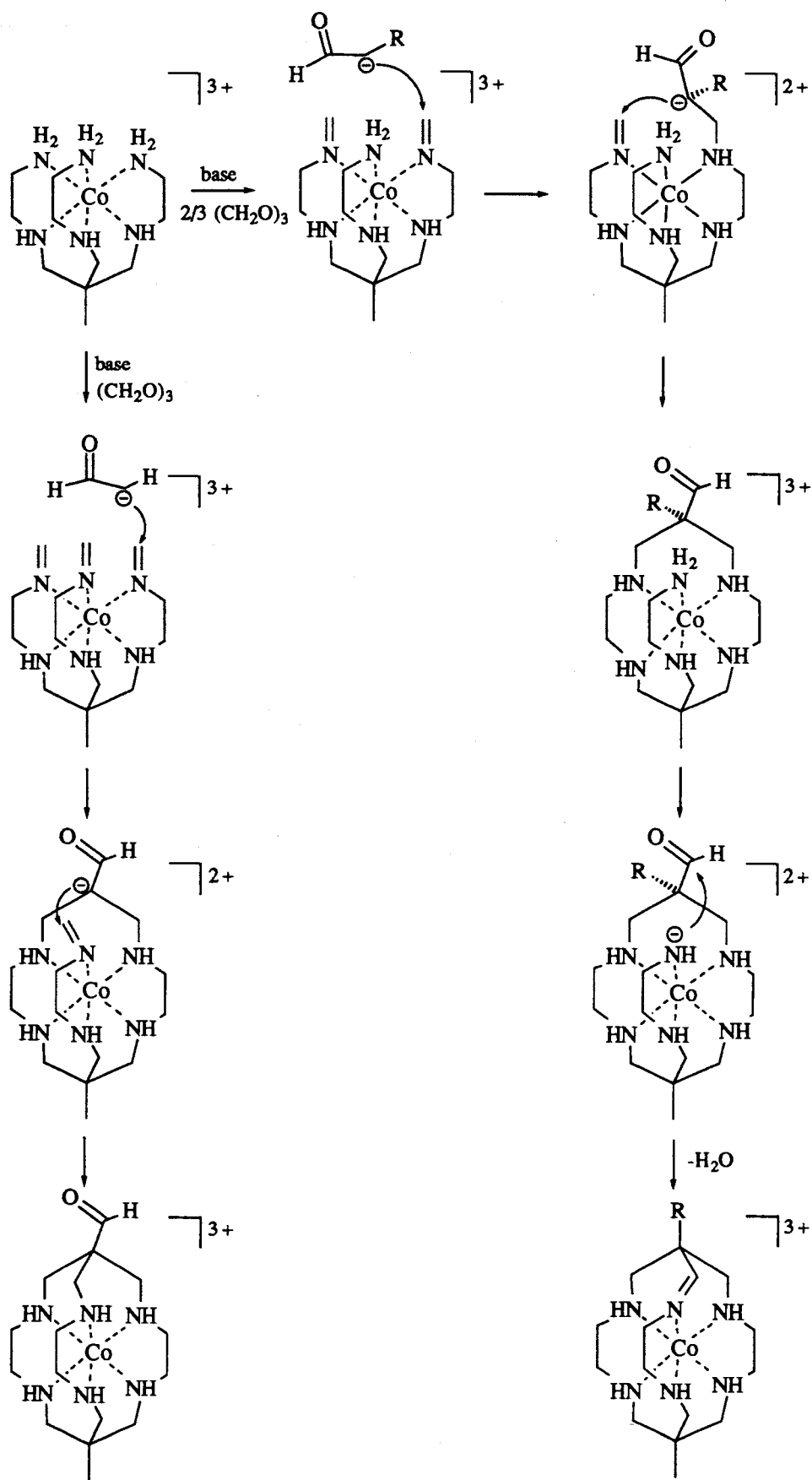
Scheme 1.4: A mechanism for the synthesis of $[\text{Co}((\text{NO}_2)_2\text{sar})]^{3+}$.

The apical nitro groups have been subsequently reduced with zinc in the presence of acid, to produce amine substituents (Scheme 1.5).¹⁸ Diazotisation of the amine capped $[\text{Co}(\text{NH}_2)_2\text{sar}]^{3+}$ cage produces $[\text{Co}(\text{Cl}_2\text{sar})]^{3+}$, from which $[\text{Co}(\text{sar})]^{3+}$ is obtained.^{18,22}



Scheme 1.5: Reduction of apical substituents $-\text{NO}_2$, $-\text{NH}_3^+$, $-\text{Cl}$ and to $-\text{H}$ (amine protons have been omitted for clarity).

Other Co(III) templates have been capped in this way and the apical substituents modified. For example, capping $lel_3\text{-}[\text{Co}(\text{chxn})_3]^{3+}$ ($\text{chxn} = (R, R, \text{ or } S, S)\text{-trans-1,2-cyclohexanediamine}$) forms $lel_3\text{-}[\text{Co}((\text{NH}_2)_2\text{char})]^{3+}$,⁵⁸ and similarly, $[\text{Co}(\text{pn})_3]^{3+}$ ($\text{pn} = 1,2\text{-propanediamine}$) forms $lel_3\text{-}[\text{Co}((\text{NH}_2)_2\text{-Me}_3\text{sar})]^{3+}$.^{59,60} Its ob_3 analogue, however, has not been capped, but by extruding the cobalt ion from the lel_3 complex and reinserting the Co(III) ion into the free cage ligand, the ob_3 complex has been obtained.^{59,60} Improved yields may be obtained when starting with the template $[\text{Co}(\text{sen})]^{3+}$ ($\text{sen} = 1,1,1\text{-tris(4-amino-2-azabutyl)ethane}$) to form, for example, $[\text{Co}(\text{NO}_2, \text{Mesar})]^{3+}$, where only one face needs to be capped.¹³ The use of nonaqueous solvents, primarily MeCN, has increased the choice of nucleophiles, particularly aromatic and aliphatic aldehydes⁵⁶ for example, acetaldehyde,⁵⁶ propanal,⁵⁶ AsH_3 ,¹⁵ PH_3 ,⁶¹ diethyl malonate¹⁷ and substituted pyridines.¹⁶ This has increased the range of substituents on the cap. Scheme 1.6 shows a mechanism for capping of $[\text{Co}(\text{sen})]^{3+}$ with an aldehyde carbanion in acetonitrile.⁵⁶

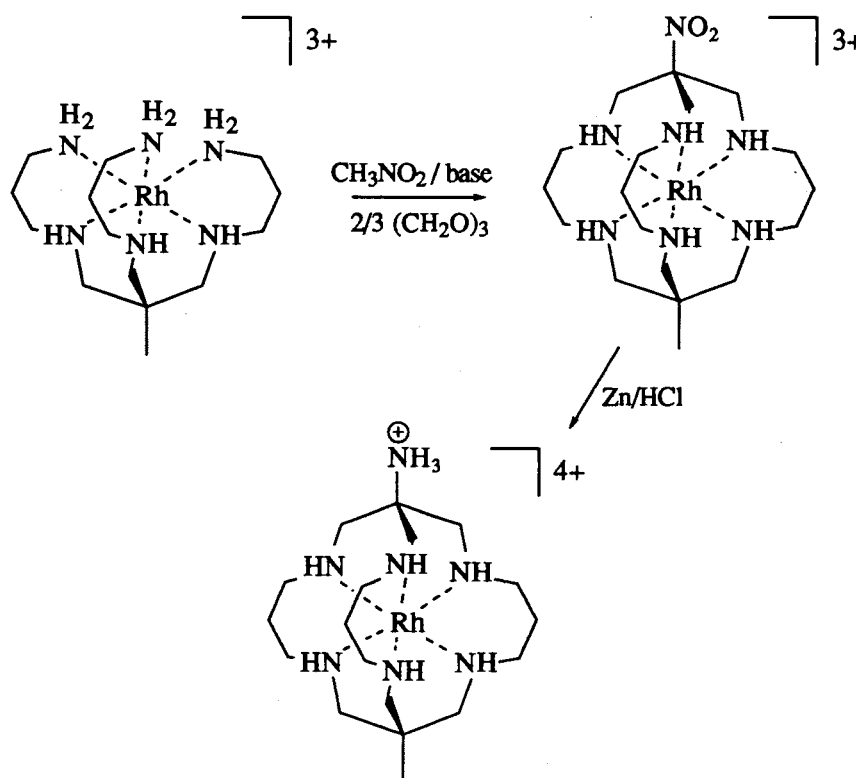


Scheme 1.6: Condensation of mixed aldehydes with $[M(\text{sen})]^{3+}$.

*(b) Synthesis of Cage Complexes with Expanded Cavities***I. Capping Reactions**

Using the route described above for capping inert metal ion templates, it was anticipated that the analogous six-membered chelate ring precursor complexes $[M(\text{tn})_3]^{n+}$ ($\text{tn} = 1,3\text{-propanediamine}$) and $[M(\text{stn})]^{n+}$ ($\text{stn} = 1,1,1\text{-tris}(5\text{-amino-}2\text{-azapentyl)ethane}$) could be capped. This procedure would form cage ligands which have potentially larger cavities, namely, the N_6 -tricosane complexes (N_6 -tricosane = 3,7,11,15,18,22-hexaazabicyclo[7.7.7]tricosane, Fig. 1.3(b)).

The $[\text{Rh}(\text{tn})_3]^{3+}$ and $[\text{Rh}(\text{stn})]^{3+}$ templates have been capped in this manner by treating them with nitromethane and formaldehyde in the presence of base, to form $[\text{Rh}(\text{NO}_2)_2\text{-}N_6\text{-tricosane}]^{3+}$ and $[\text{Rh}(\text{Me},\text{NO}_2\text{-}N_6\text{-tricosane})]^{3+}$ (Scheme 1.8).⁵⁰ The Rh(III)-N bond lengths in these complexes are $\sim 0.05 \text{ \AA}$ longer than those in the sar analogues. Reduction of the nitro substituents yielded the amine analogues.⁵⁰



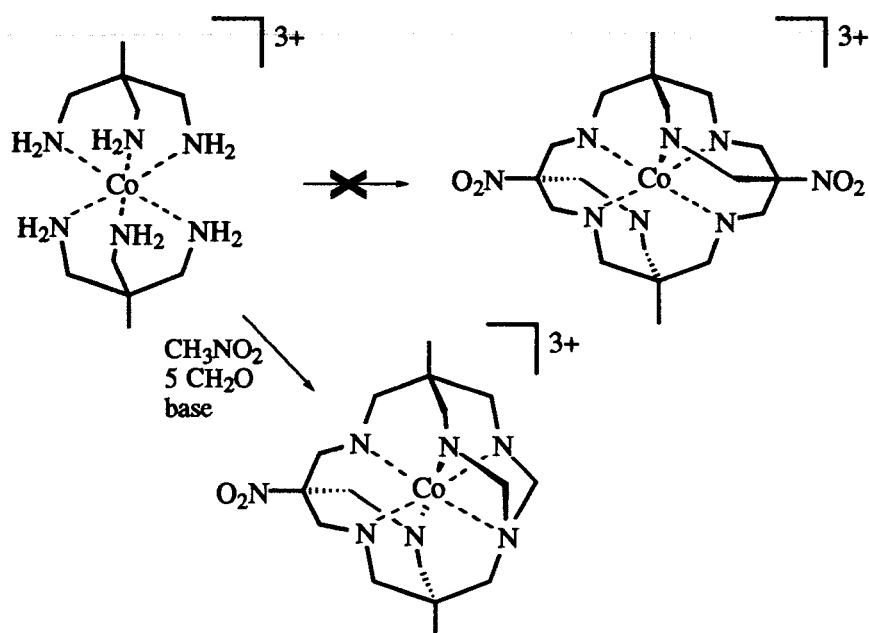
Scheme 1.8: Capping $[\text{Rh}(\text{stn})]^{3+}$ to form $[\text{Rh}(\text{X},\text{Me-}N_6\text{-tricosane})]^{3+}$ (where $\text{X}=\text{NO}_2$ and NH_3^+).

However, attempts to cap the $[\text{Co}(\text{tn})_3]^{3+}$ and $[\text{Co}(\text{stn})]^{3+}$ templates in the same way have not been successful.⁶² A possible reason is that the reaction conditions may allow the reduction of Co(III) intermediates to their labile Co(II) forms to occur. This may be achieved by the oxidation of formaldehyde to formic acid, as this is favourable under basic conditions.⁶³ Since $[\text{Co}(\text{tn})_3]^{3+}$ is more easily reduced than $[\text{Co}(\text{en})_3]^{3+}$, the driving force for reduction to Co(II) with formaldehyde would be greater and this may explain the difficulty in capping six-membered ring CoN_6^{3+} templates. In contrast, the reduction potentials for the analogous Rh(III) templates are more negative and formation of labile reduced species would be less competitive with cyclisation.

I. Strapping Reactions

To overcome some of the problems associated with unstable intermediates and possible conformational difficulties in the synthesis of expanded Co(III) cage complexes, the tridentate ligand, tame (tame = 1,1,1-tris(aminomethyl)ethane), was used.^{39,64} The $[\text{M}(\text{tame})_2]^{3+}$ bears the preformed cap components, and the amines on opposite tame ligands may be linked to form an encapsulated entity. In the early experiments, $[\text{Co}(\text{tame})_2]^{3+}$ was treated with formaldehyde and nitromethane in water, in an attempt to synthesise a tetracapped N_6 -docosane complex (Scheme 1.9).

The target N_6 -docosane complex was not isolated. Instead, a large number of complicated complexes containing methylene bridges were isolated, one of which is represented in Scheme 1.9.³⁹ Under these reaction conditions, the formation of methylene bridged species competes with the processes leading to strap formation and so reducing the yield of target cage complex. Clearly, this route was not successful in producing the desired symmetrical molecule. Other routes to limit the condensation of formaldehyde with the template and also control the reactivity of the coordinated imines were investigated. The first requirement has been achieved by using paraformaldehyde instead of aqueous formaldehyde. This polymer slowly hydrolyses to form monomeric formaldehyde so limiting its multiple condensation with the template. Secondly, the propensity for methylene bridge formation appears to be decreased for $[\text{Co}(\text{tame})_2]^{3+}$ when the condensation reactions are performed in acetonitrile.⁶⁵

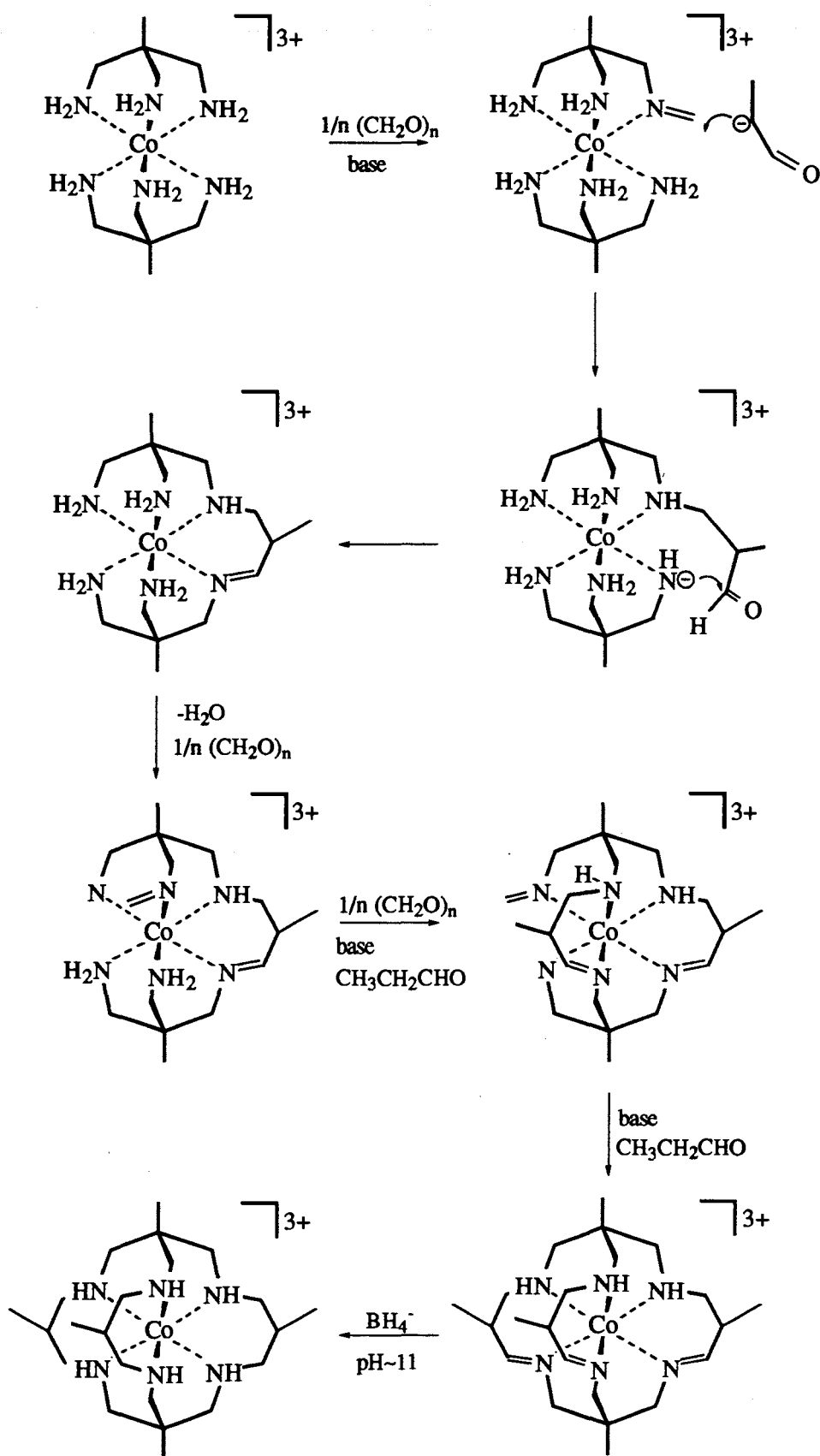


Scheme 1.9: Aqueous strapping reaction of $[\text{Co}(\text{tame})_2]^{3+}$ to form complex with three caps.

(i) Synthesis of $[\text{Co}(\text{Me}_5\text{-}N_6\text{-tricosane})]^{3+}$

$[\text{Co}(\text{tame})_2]^{3+}$ was treated with paraformaldehyde and propanal in the presence of base to produce the C_3 -symmetrical complex $[\text{Co}(\text{Me}_5\text{-}N_6\text{-tricosanetriimine})]^{3+}$.⁴⁰ Quantitative reduction of the triimine with sodium borohydride in basic aqueous media subsequently produced the saturated $[\text{Co}(\text{Me}_5\text{-}N_6\text{-tricosane})]^{3+}$, in ~20% yield. A mechanism for the strapping reaction in acetonitrile has been proposed (Scheme 1.10).⁴⁰ The series of reactions leading to the cage is complicated and the order proposed in this scheme may not be precisely as indicated. Despite the relatively low yield, the initial one pot synthesis gives rise to a large molecule of considerable complexity and it is doubtful that a regular organic synthesis, step by step, would achieve a better result.

Other Co(III) and Co(II) N_6 -tricosane complexes have been synthesised, by substituting isobutanal for propanal to produce the $[\text{Co}(\text{Me}_8\text{-}N_6\text{-tricosanetriimine})]^{3+}$.⁴¹ Treatment of this complex with NaBH_4 in basic conditions reduced not only the imines, but also Co(III) to Co(II). To date, the oxidation of $[\text{Co}(\text{Me}_8\text{-}N_6\text{-tricosane})]^{2+}$ to the Co(III) complex has not been achieved.



Scheme 1.10: A possible mechanism for strapping $[\text{Co}(\text{tame})_2]^{3+}$ in acetonitrile to form $[\text{Co}(\text{Me}_5\text{-N}_6\text{-tricosane})]^{3+}$.

1.6. Encapsulation of Metal Ions Using Non-Template Methods

Non-template methods have been used to encapsulate the more labile metal ions which are less suited to the imine strategy. The cage ligand is first synthesised around a Co(III) template from which the cobalt ion is subsequently extruded, by firstly reducing the Co(III) to the more labile Co(II). With the aid of a strongly complexing ligand (e.g. CN^-), in the absence of oxygen, the Co(II) ion is sequestered from the nitrogen donor atoms to form finally the very stable $[\text{Co}(\text{CN})_6]^{3-}$ ion,²² allowing the free cage ligand to be isolated. An alternative strategy uses zinc in strong acid (concentrated HCl or HBr) to reduce the Co(III) complex to Co(II).^{66,67} In excess acid, the protons compete with the Co(II) ion in binding to amine donor atoms leading to displacement of the metal ion, yielding the uncomplexed ligand and CoX_4^{4-} , where $\text{X} = \text{Cl}^-$ or Br^- . The anions also assist extrusion of the metal by binding to the metal and the effect they have on the rates of extrusion is in the following order: $\text{Br}^- > \text{Cl}^- \gg \text{ClO}_4^-$.³⁰

Free sar and $\text{Me}_5\text{-N}_6$ -tricosane ligands have been isolated in this way and used to coordinate a number of metal ions in various oxidation states. To date, the metal ions which have been stabilised in the sar cage ligands in this way are Li(I),⁶⁸ Mg(II),⁶⁹ V(IV),⁷⁰ Cr(III),^{48,49} Mn(III),⁷¹ Mn(II),⁷¹ Fe(III),⁷² Fe(II),⁷² Co(III),³⁶ Co(II),¹³ Ni(II),^{73,74} Ni(III),^{73,74} Cu(II),⁴⁷ Zn(II),²⁶ Cd(II),²⁶ Hg(II),²⁶ Ga(III),⁶⁶ In(III),⁶⁶ Ru(II).⁷⁵ Similarly, the following ions have been introduced into the $\text{Me}_5\text{-N}_6$ -tricosane ligands:⁷⁶ Cr(III), Co(III), Co(II), Ni(II), Cu(II), Zn(II), Cd(II), Hg(II) and Pb(II).

Whether a metal ion can be complexed by these cages appears to depend on the metal - ligand dissociation rate, the size and preferred oxidation state of the metal ion in an N_6 ligand field and the stereochemistry preferred by both the metal ion and the ligand.

Very labile metal ions are difficult to maintain in the cages. For example, $[\text{Li}((\text{NH}_2)_2\text{-N}_6\text{-sar})](\text{CF}_3\text{SO}_3)$ has been isolated from dry acetonitrile and structurally characterised.⁶⁸ Li(I) generally prefers oxygen donors to nitrogen and in water, rapid dissociation takes place to yield the free ligand. Other group I metal ions have not yet been encapsulated in these cages.

Very large metal ions, such as Pb(II), have been excluded from sar cages, but $[\text{Pb}(\text{Me}_5\text{-N}_6\text{-tricosane})]^{2+}$ has been synthesised.⁷⁶

The ability of the ligand to adopt the stereochemistry preferred by the metal ion (and vice versa) influences the stability of the complex. In extreme cases, such as for the Pt(II)⁴⁶ and Pd(II)⁷⁷ ions, the metal ion prefers square planar geometries, while for Cu(II)³⁰ in acid media, only four nitrogen donors are coordinated. In most cases, the observed stereochemistry of the complex is a compromise between steric effects from

the ligand and electronic effects which arise from the metal ion.^{69,78} The ligand distortion may be quantified using the trigonal twist angle,⁶⁹ ϕ_t , which is defined in Fig. 1.5. For octahedral geometries the twist angle is 60° , whereas the free sar ligand has a preferred twist angle of $\sim 24^\circ$ ⁶⁹ and distortion occurs in order to accommodate the metal ion. The ability of the metal ion to dominate the resulting stereochemistry has been related to its ligand field splitting.⁶⁹ Metal ions with d^0 , d^1 , d^2 , high spin d^5 , high spin d^6 and d^{10} configurations have their stereochemistry dominated by the ligand.⁶⁹ The twist angles range from $\sim 18^\circ$ for $[\text{V}((\text{NH}_3)_2\text{sar})]^{4+}$ and $\sim 28.6^\circ$ for high spin $[\text{Fe}((\text{NH}_3)_2\text{sar})]^{4+}$. For all other transition metal ion complexes of the sar, electronic factors pertaining to the metal ions are dominant and the overall symmetry around the metal centre is closer to octahedral. The stereochemical preferences for the N_6 -tricosane complexes are currently being examined.⁷⁹

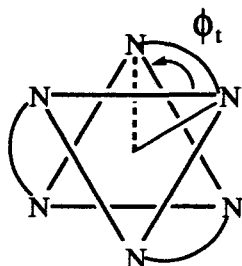
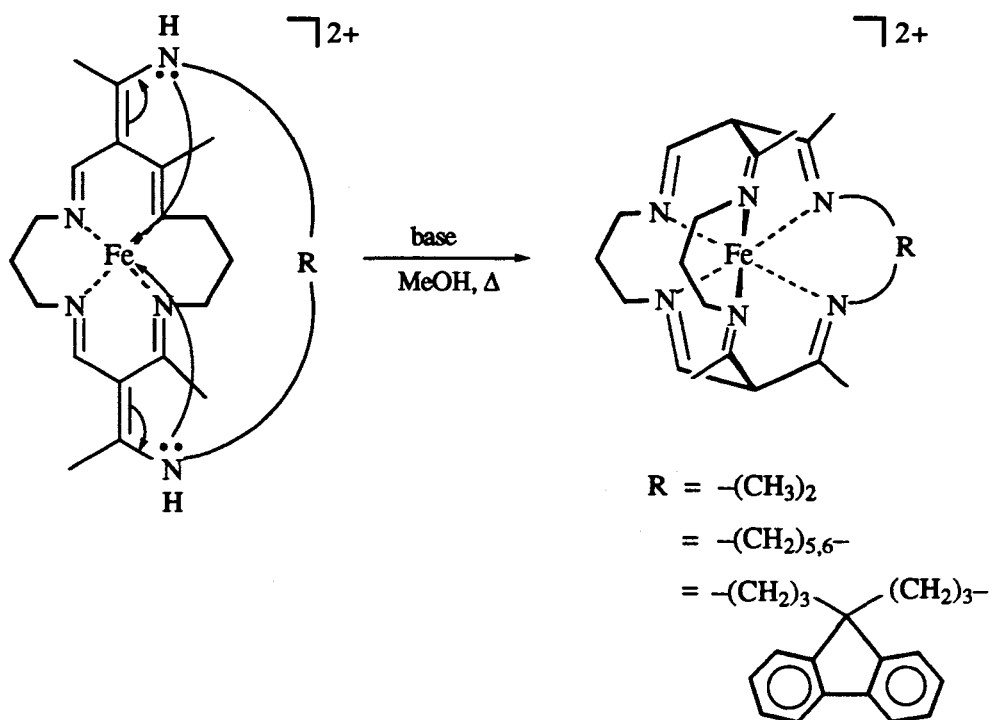


Figure 1.5: Defining the twist angle, ϕ_t .

1.7. Other Synthetic Approaches to Cages with Large Cavities

Another method for synthesising larger cage complexes involves the rearrangement of a tetraimine 16-membered macrocyclic complex of high spin Fe(II) (Scheme 1.11).⁸⁰⁻⁸⁵ The ligand bears two non-coordinating amines, which are connected by alkyl spacers. Internal electronic rearrangement of the ligand occurs such that these exo-nitrogen atoms coordinate to the high spin Fe(II), to form a stable hexaimine low spin Fe(II) complex. The formation of the hexadentate complex is driven largely by the formation of low spin Fe(II) hexaimine species, which is a very stable configuration for this ion. The internal rearrangement described in Scheme 1.11 is not observed using other metal ions. A symmetrical cage complex has not yet been synthesised using this method; in particular, rearranged complexes with the spacer $(-\text{CH}_2)_3$ have not been reported. The spacer length between the exo-nitrogen atoms appears to influence whether or not rearrangement occurs.



Scheme 1.11: Rearrangement of a 16-membered macrocycle to form a hexaimine macrobicyclic.

Macrobicyclic ligands with expanded cavities have been synthesised using organic methods, and metal ions have been introduced. For example, the coordination of Pu(IV) in a siderophore analogue to form a stable complex has been achieved.⁸⁶ Metal ions which coordinate with oxygen donors, such as Fe(III) and Ga(III) and alkali metal ions, have been encapsulated in ligands with straps derived from catechol or cyclic ethers, one of which is represented in Fig. 1.6(a)^{87,88} Other macrocycles of the cyclophane type⁸⁹ (Fig. 1.6(b)) have been reported to bind anions inside the cavity.

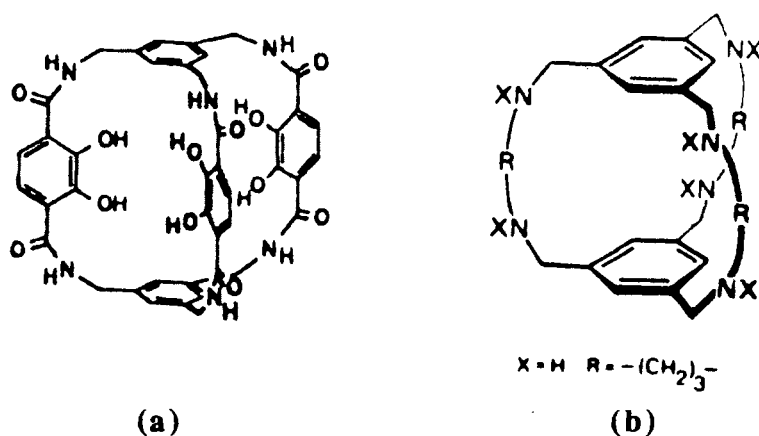


Figure 1.6: Cages derived from (a) catechol^{87,88} and (b) cyclophane⁸⁹ (diagrams reproduced from these references).

1.8. Aims

Clearly, the cage ligands are able to alter the behaviour of metal ions compared to their simpler nonencapsulated analogues. This thesis focuses on the synthesis of a series of hexaaza cage complexes of Pt(IV), Co(III) and Cr(III) with expanded cavities and compares their properties with those of the analogous sar complexes. Some reasons for synthesising such complexes are given below.

(a) Pt(IV) Cage Complexes

The electrochemical behaviour of the Pt(IV) sar cage complexes at 298 K and in aqueous media has been attributed to the mismatch of the ligand cavity and the larger Pt(III) ion.⁴⁶ Reduction of the Pt(IV) ion to Pt(III) without rupturing the ligand may be possible in ligands which are able to tolerate larger ions.

(b) Co(III) Cage Complexes

To gain insight to the redox properties and electron transfer of the $\text{CoN}_6^{3+/2+}$ couple, new macropolycyclic complexes with increased rigidity and longer than usual Co-N bond lengths need to be synthesised and their properties investigated. Such complexes may further enlarge the scope of cage chemistry, as larger metal ions may be encapsulated after the cobalt ion has been removed from the ligand.

(c) Cr(III) Cage Complexes

It is not clear why the excited state lifetime in the N_6 -tricosane complexes of Rh(III) is considerably longer than for the sar complexes. It was anticipated that the larger cages could be used to explore the excited state behaviour of other metal ions such as Cr(III), particularly for delineating the factors governing the lifetimes of a series of Cr(III) hexaamine cage complexes and their photoreactivity. It was anticipated that the template strategy would be better suited for the direct synthesis of Cr(III) cage complexes as Cr-N bond lengths are generally longer than for Co(III)-N and six-membered chelate rings are more stable for CrN_6^{3+} systems than for CoN_6^{3+} .

1.9. References

- (1) House, D. A. *Comprehensive Coordination Chemistry*; Pergamon Press: Oxford, 1987; Vol. 2, and references therein.
- (2) Lindoy, L. F. *The Chemistry of Macrocyclic Ligand Complexes*; Cambridge University Press: Cambridge, 1989, and references therein.
- (3) Melson, G. A. *Coordination Chemistry of Macrocyclic Compounds*; Plenum Press: New York, 1979.
- (4) Dietrich, B.; Viout, P.; Lehn, J.-M. *Macrocyclic Chemistry*; VCH Verlagsgesellschaft Inc.: New York, 1993, and references therein.
- (5) Sargeson, A. M. *Proc. Roy. Aust. Chem. Inst.* **1976**, 229.
- (6) de Sousa Healy, M.; Rest, A. J. *Adv. Inorg. Chem. & Radiochem* **1978**, 21, 1, and references therein.
- (7) Curtis, N. F. *Coord. Chem. Rev.* **1968**, 3, 3, and references therein.
- (8) Ashurova, N. K.; Yakubov, K. G.; Tsivadze, A. Y. *Russ. J. Coord. Chem.* **1994**, 20, 411.
- (9) Lawrance, G. A.; Lye, P. G. *Comments Inorg. Chem.* **1994**, 15, 339, and references therein.
- (10) McKee, V.; Dorrity, M. R. J.; Malone, J. F.; Marrs, D.; Nelson, J. *J. Chem. Soc., Chem. Commun.* **1992**, 383.
- (11) Goedken, V. L.; Peng, S.-M. *J. Chem. Soc., Chem. Commun.* **1973**, 62.
- (12) Creaser, I. I.; Harrowfield, J. M.; Herlt, A. J.; Sargeson, A. M.; Springborg, J.; Geue, R. J.; Snow, M. R. *J. Am. Chem. Soc.* **1977**, 99, 3181.
- (13) Creaser, I. I.; Geue, R. J.; Harrowfield, J. M.; Herlt, A. J.; Sargeson, A. M.; Snow, M. R.; Springborg, J. *J. Am. Chem. Soc.* **1982**, 104, 6016.
- (14) Harrowfield, J. M.; Herlt, A. J.; Sargeson, A. M. *Inorg. Synth.* **1980**, 20, 85.
- (15) Höhn, A.; Geue, R. J.; Sargeson, A. M.; Willis, A. C. *J. Chem. Soc., Chem. Commun.* **1989**, 1648.
- (16) Geue, R. J.; Korybut-Daskiewicz, B.; Sargeson, A. M. *J. Chem. Soc., Chem. Commun.* **1993**, 1454.

- (17) Geue, R. J.; Petri, W. R.; Sargeson, A. M.; Snow, M. R. *Aust. J. Chem.* **1992**, *45*, 1681.
- (18) Geue, R. J.; Hambley, T. W.; Harrowfield, J. M.; Sargeson, A. M.; Snow, M. R. *J. Am. Chem. Soc.* **1984**, *106*, 5478.
- (19) Gahan, L. R.; Hambley, T. W.; Sargeson, A. M.; Snow, M. R. *Inorg. Chem.* **1982**, *21*, 2699.
- (20) Bruce, J.; Gahan, L.; Hambley, T. W.; Stranger, R. *J. Chem. Soc., Chem. Commun.* **1993**, 702.
- (21) Lay, P. A.; Lydon, J. D.; Mau, A. W. H.; Osvath, P.; Sargeson, A. M.; Sasse, W. H. F. *Aust. J. Chem.* **1993**, *46*, 641.
- (22) Bottomley, G. A.; Clark, I. J.; Creaser, I. I.; Engelhardt, L. M.; Geue, R. J.; Hagen, K. S.; Harrowfield, J. M.; Lawrance, G. A.; Lay, P. A.; Sargeson, A. M.; See, A. J.; Skelton, B. W.; White, A. H.; Wilner, F. R. *Aust. J. Chem.* **1994**, *47*, 143.
- (23) Osvath, P.; Sargeson, A. M. *J. Chem. Soc., Chem. Commun.*, **1993**, 40.
- (24) Osvath, P.; Sargeson, A. M.; Skelton, B. W.; White, A. H. *J. Chem. Soc., Chem. Commun.* **1991**, 1036.
- (25) Lamb, J. D.; Izatt, R. M.; Christensen, J. J.; Eatough, D. J. *Coordination Chemistry of Macrocyclic Compounds*; Plenum Press: New York, 1979, Chapter 3, and references therein.
- (26) Sargeson, A. M. *Pure. Appl. Chem.* **1986**, *587*, 1552, and references therein.
- (27) Creaser, I. I.; Sargeson, A. M.; Zanella, A. W. *Inorg. Chem.* **1983**, *22*, 4022, and references therein.
- (28) Dwyer, F. P.; Sargeson, A. M. *J. Phys. Chem.* **1961**, *65*, 1892.
- (29) Hammershøi, A.; Geselowitz, D. A.; Taube, H. *Inorg. Chem.* **1983**, *23*, 979; Value extrapolated from 40°C and 2.5 M KCl to 25° C and 0.2 M KCl.
- (30) Sargeson, A. M. *Pure. Appl. Chem.* **1984**, *56*, 1603, and references therein.
- (31) Pizer, R.; Geue, R. J.; Sargeson, A. M. In *183rd ACS National Meeting*; Las Vegas, 1982.
- (32) Vallee, B. L.; Williams, R. J. P. *Proc. Natl. Acad. Sci.* **1968**, *50*, 498.

- (33) Bond, A. M.; Lawrance, G. A.; Lay, P. A.; Sargeson, A. M. *Inorg. Chem.* **1983**, *22*, 2010.
- (34) Lay, P. A. Ph.D. Thesis, Australian National University, 1981.
- (35) Lawrance, G. A.; Lay, P. A.; Sargeson, A. M. *Inorg. Chem.* **1990**, *29*, 2808.
- (36) Geue, R. J.; Hendry, A. J.; Sargeson, A. M. *J. Chem. Soc., Chem. Commun.* **1989**, 1646.
- (37) Hammershøi, A.; Lawrance, G. A.; Sargeson, A. M. *Aust. J. Chem.* **1986**, *39*, 2183.
- (38) Hammershøi, A.; Sargeson, A. M. *Inorg. Chem.* **1983**, *22*, 3554.
- (39) Gainsford, G. J.; Geue, R. J.; Sargeson, A. M. *J. Chem. Soc., Chem. Commun.* **1982**, 233.
- (40) Geue, R. J.; Höhn, A.; Ralph, S. F.; Sargeson, A. M.; Willis, A. C. *J. Chem. Soc., Chem. Commun.* **1994**, 1513.
- (41) Höhn, A.; Sargeson, A. M., Unpublished results **1989**.
- (42) Buckingham, D. A.; Sargeson, A. M. In *Chelating Agents and Metal Chelates*; F. P. Dwyer and P. D. Mellor, Eds.; Academic Press: New York, 1964.
- (43) Harrowfield, J. M.; Herlt, A. J.; Lay, P. A.; Sargeson, A. M.; Bond, A. M.; Mulac, W. A.; Sullivan, J. C. *J. Am. Chem. Soc.* **1983**, *105*, 5503.
- (44) Cotton, F. A.; Wilkinson, G. *Advanced Inorganic Chemistry*; 2nd ed.; John Wiley: New York, 1966.
- (45) Hung, Y.; Martin, L. Y.; Jackels, S. C.; Tait, M.; Busch, D. H. *J. Am. Chem. Soc.* **1977**, *99*, 4029.
- (46) Boucher, H. A.; Lawrance, G. A.; Lay, P. A.; Sargeson, A. M.; Bond, A. M.; Sangster, D. F.; Sullivan, J. C. *J. Am. Chem. Soc.* **1983**, *105*, 4652.
- (47) Creaser, I. I.; Harrowfield, J. M.; Lawrance, G. A.; Mulac, W.; Sangster, D.; Sargeson, A. M.; Schmidt, K.; Sullivan, J. C. *J. Coord. Chem.* **1991**, *23*, 389.
- (48) Comba, P.; Creaser, I. I.; Gahan, L. R.; Harrowfield, J. M.; Lawrance, G. A.; Martin, L. L.; Mau, A. W. H.; Sargeson, A. M.; Sasse, W. H. F.; Snow, M. R. *Inorg. Chem.* **1986**, *25*, 384.

- (49) Comba, P.; Mau, A. W. H.; Sargeson, A. M. *J. Phys. Chem.* **1985**, *89*, 394.
- (50) Geue, R. J.; McDonnell, M. B.; Mau, A. W. H.; Sargeson, A. M.; Willis, A. C. *J. Chem. Soc., Chem. Commun.* **1994**, 667.
- (51) McArdle, H. J.; Gross, S. M.; Creaser, I. I.; Sargeson, A. M.; Danks, D. M. *Am. J. Physiol.* **1989**, *256*, G667.
- (52) Lay, P. A.; Mau, A. W. H.; Sasse, W. H. F.; Creaser, I. I.; Gahan, L. R.; Sargeson, A. M. *Inorg. Chem.* **1983**, *22*, 2347.
- (53) Creaser, I. I.; Gahan, L. R.; Geue, R. J.; Launikonis, A.; Lay, P. A.; Lydon, J. D.; McCarthy, M. G.; Mau, A. W. H.; Sargeson, A. M.; Sasse, W. H. F. *Inorg. Chem.* **1985**, *24*, 2671.
- (54) Creaser, I. I.; Hammershøi, A.; Launikonis, A.; Mau, A. W. H.; Sargeson, A. M.; Sasse, W. H. F. *Photochem. Photobiol.* **1989**, *49*, 19.
- (55) Mok, C. Y.; Zanella, A. W.; Creutz, C.; Sutin, N. *Inorg. Chem.* **1984**, *23*, 2891.
- (56) Höhn, A.; Geue, R. J.; Sargeson, A. M. *J. Chem. Soc., Chem. Commun.* **1990**, 1473.
- (57) Suh, M. P.; Shin, W.; Kim, D.; Kim, S. *Inorg. Chem.* **1984**, *23*, 618.
- (58) Geue, R. J.; McCarthy, M. G.; Sargeson, A. M. *J. Am. Chem. Soc.* **1984**, *106*, 8282.
- (59) Hendry, A. J. Ph.D. Thesis, Australian National University, 1986.
- (60) Hendry, A. J.; Naidoo, K. J.; Thornton, D. A. *J. Chem. Soc., Chem. Commun.* **1989**, 998.
- (61) Höhn, A.; Geue, R. J.; Sargeson, A. M.; Willis, A. C. *J. Chem. Soc., Chem. Commun.* **1989**, 1644.
- (62) McDonnell, M. B., Unpublished observations.
- (63) March, J. *Advanced Inorganic Chemistry*; 4th ed.; John Wiley and Sons: New York, 1992, pp 1233-1235.
- (64) Geue, R. J.; McCarthy, M. G.; Sargeson, A. M.; Skelton, B. W.; White, A. H. *Inorg. Chem.* **1985**, *24*, 1607.

- (65) Qin, C. J., Personal communication 1994.
- (66) Creaser, I. I., Unpublished results.
- (67) Anderson, P. A.; Creaser, I. I.; Dean, C.; Harrowfield, J. M.; Horn, E.; Martin, L. L.; Sargeson, A. M.; Snow, M. R.; Tiekink, E. R. T. *Aust. J. Chem.* **1993**, *46*, 449, and references therein.
- (68) Hagen, K.; Sargeson, A. M., Unpublished results.
- (69) Comba, P.; Sargeson, A. M.; Engelhardt, L. M.; Harrowfield, J. M.; White, A. H.; Horn, E.; Snow, M. R. *Inorg. Chem.* **1985**, *24*, 2325, and references therein.
- (70) Comba, P.; Engelhardt, L. M.; Harrowfield, J. M.; Lawrance, G. A.; Martin, L. L.; Sargeson, A. M.; White, A. H. *J. Chem. Soc., Chem. Commun.* **1985**, 174.
- (71) Creaser, I. I.; Engelhardt, L. M.; Harrowfield, J. M.; Sargeson, A. M.; Skelton, B. W.; White, A. H. *Aust. J. Chem.* **1993**, *46*, 465.
- (72) Martin, L. L. Ph.D. Thesis, Australian National University, 1986, and references therein.
- (73) Engelhardt, L. M.; Harrowfield, J. M.; Sargeson, A. M.; White, A. H. *Aust. J. Chem.* **1993**, *46*, 127.
- (74) Clark, I. J.; Creaser, I. I.; Engelhardt, L. M.; Harrowfield, J. M.; Krausz, E. R.; Moran, G. M.; Sargeson, A. M.; White, A. H. *Aust. J. Chem.* **1993**, *46*, 111.
- (75) Bernhard, P.; Sargeson, A. M. *J. Chem. Soc., Chem. Commun.* **1985**, 1516.
- (76) Ralph, S. F., Personal Communication 1990-1993.
- (77) Spiccia, L., Unpublished Results.
- (78) Comba, P.; Sargeson, A. M. *Phosphorus and Sulfur* **1986**, *28*, 137.
- (79) Bernhardt, P. V., Personal communication 1994.
- (80) Herron, N.; Chavan, M. Y.; Busch, D. H. *J. Chem. Soc., Dalton Trans.* **1984**, 1491.
- (81) Riley, D. P.; Stone, J. A.; Busch, D. H. *J. Am. Chem. Soc.* **1976**, *98*, 1752.
- (82) Riley, D. P.; Stone, J. A.; Busch, D. H. *J. Am. Chem. Soc.* **1977**, *99*, 767.

- (83) Mertes, K. B.; Corfield, P. W. R.; Busch, D. H. *Inorg. Chem.* **1977**, *16*, 3226.
- (84) Herron, N.; Grzybowski, J. J.; Matsumoto, N.; Zimmer, L. L.; Christoph, G. G.; Busch, D. H. *J. Am. Chem. Soc.* **1982**, *104*, 1999.
- (85) Busch, D. *Pure. Appl. Chem.* **1980**, *52*, 2477.
- (86) Xu, J.; Stack, T. D. P.; Raymond, K. N. *Inorg. Chem.* **1992**, *31*, 4903.
- (87) Kiggen, W.; Vögtle, F.; Franken, S.; Puff, H. *Tetrahedron* **1986**, *42*, 1859.
- (88) Katalinić, J. P.; Ebmeyer, F.; Seel, C.; Vögtle, F. *Chem. Ber.* **1989**, *122*, 2391.
- (89) Heyer, D.; Lehn, J. M. *Tet. Lett.* **1986**, *27*, 5869.

Chapter 2

Experimental

2.1. Starting Materials

All chemicals (AR grade) were used as received unless otherwise specified. $K_2[PtCl_6]$ was synthesised from Pt powder (recovered from residues) according to published methods¹ or from $H_2[PtCl_6]$ (Johnson Matthey) by recrystallisation from an aqueous solution of KCl.

For synthesising tetrachlorozincate salts, a stock solution was made by dissolving $ZnCl_2$ (4 g) in concentrated HCl (40 mL) and which was then diluted with water (80 mL), to form a 4 M HCl solution. This solution was added dropwise to an acidified solution containing the chloride salt of the complex. Unless otherwise specified, the trifluoromethanesulphonate (triflate) salts were prepared by suspending or dissolving the chloride salt of the complex in neat, dry trifluoromethanesulphonic acid (triflic) acid, in a three necked r.b. flask connected to a stream of nitrogen and an air condenser. The reaction solution was purged with nitrogen for 6-12 hours to remove HCl and gentle heating over a steam bath was sometimes required. Ether was then slowly added to the flask to precipitate the triflate salt which was filtered off. The residue was washed thoroughly with ether and the complex recrystallised either from water, water/ethanol, acetonitrile or acetonitrile/ether. The complexes were dried *in vacuo* over silica gel. Perchlorate salts were formed by addition of a concentrated solution of the chloride salt to a hot solution of 6 M $NaClO_4$ and the solution stirred for approximately five minutes. The resulting precipitate was filtered off and then recrystallised from water/ethanol or from acetonitrile. The complexes were dried *in vacuo* over silica gel.

2.2. Solvents

Distilled water was used for all chromatography and recrystallisations. Solvents (AR grade) were used as received unless they were purified further by literature methods.² All rotary evaporations were conducted at 15 mm Hg and at not more than $\sim 40^\circ C$, unless otherwise stated.

Standard inert atmosphere techniques³ were used where stated in the text, using either house nitrogen (boil-off from liquid nitrogen) or argon (CIG, high purity). Where required, solvents were thoroughly purged with inert gas immediately prior to use.

2.3. Ligands

(a) *1,1,1-tris(aminomethyl)ethane trihydrochloride (tame.3HCl)* .

Tame.3HCl was prepared as described previously.⁴ 1,1,1-tris(benzenesulfonato methyl)ethane was heated with excess liquid ammonia at ~115 °C and ~ 60 atmospheres for 2-3 days. The resulting amine was then purified and crystallised as the chloride salt and further purified by sorption on Dowex 50W-X2 cation exchange resin. The resin was washed with water, 1 M HCl and the ligand was eluted with 3 M HCl and the eluent evaporated to near dryness. The product was recrystallised from water. **NMR** (δ , D₂O): ¹H: 1.31 (CH₃), 3.23 (CH₂), ¹³C: 17.77 (CH₃), 36.11 (quaternary carbon), 43.55 (CH₂)

(b) *1,1,1-tris(aminomethyl)ethane (tame)*

Tame.3HCl (25.5 g) was suspended in 1 L hot ethanol and added slowly to a warm solution of NaOH (13.5 g) in ethanol (200 mL). The mixture was refluxed under a stream of nitrogen for 3 hours. The ethanol was evaporated and the tame ligand was extracted from the white residue using hot chloroform. The suspension was filtered and the solvent evaporated to yield a pale yellow oil. **NMR** (δ , D₂O): ¹H: 0.80 (CH₃), 2.45 (CH₂). ¹³C: 18.64 (CH₃), 39.81 (quaternary carbon), 45.64 (CH₂).

(c) *1,1,1-tris(5-amino-2-azapentyl)ethane hexahydrochloride dihydrate (stn.6HCl.2H₂O)*

Stn.6HCl was prepared as described previously.⁴ 1,1,1-tris(benzenesulfonato-methyl)ethane was refluxed with a large excess of trimethylenediamine for 48 hours. The excess trimethylenediamine was evaporated from the reaction mixture and the resulting yellow oil was diluted to 10 L and acidified to pH ~ 3. This was sorbed on a column of Dowex 50W-X2 cation resin (200-400 mesh), washed with water and 1 M HCl and the protonated ligand was eluted with 4 M HCl. The eluate was evaporated to dryness and the resulting solid was recrystallised with water and ethanol. **NMR** (δ , D₂O): ¹H: 1.40 (CH₃), 2.20 (CH₂, strap), 3.10 (CH₂, strap), 3.28 (CH₂, strap), 3.42 (CH₂, cap). ¹³C: 18.4 (CH₃), 24.4 (CH₂ strap), 36.9 (CH₂ cap), 37.4 (quaternary carbon), 47.5 (CH₂ strap), 52.47 (CH₂ strap).

(d) *1,1,1-tris(5-amino-2-azapentyl)ethane (stn)*

Stn.6HCl.2H₂O (20 g) was dissolved in water (750 mL) and added to a column (150 cm x 10 cm) of Dowex (100-200 mesh AG1-X8) anion exchange resin (OH⁻ form). The column was washed with water (10 L) to elute the free ligand which then was evaporated to yield a pale yellow oil. **NMR** (δ , D₂O): ¹H: 0.91 (CH₃, cap), 1.60

(CH₂, strap), 2.45 (CH₂ cap), 2.61 (CH₂, strap) ¹³C: 20.9 (CH₃), 32.2 (CH₂ strap), 38.2 (CH₂ strap), 39.6 (quaternary carbon), 48.5 (CH₂ strap), 55.8 (CH₂ strap).

2.4. Chromatography

Dowex 50W-X2 cation exchange resin (Bio-Rad, 200-400 mesh) was used for separation of species based on their charge in an aqueous solution. The H⁺ form was used unless otherwise specified. Where required, the Na⁺ form was made by treating the H⁺ form with 5 M NaOH (3 volumes) and the resin was then washed with ~5 volumes of water. To separate complexes of similar charge, SP-Sephadex C-25 (Pharmacia Fine Chemicals) was used. Anion exchange resins used include Dowex AG3-X4A (200-400 mesh) and AG1-X8 (100-200 mesh), in the chloride forms, which were converted to the OH⁻ form by washing the resins with a solution of 1 M NaOH (20 volumes) and then rinsing with water until the eluant became neutral. The OH⁻ form of the resin was then converted to different anion forms using 2 M solutions of the corresponding acids (4 volumes) followed by thorough rinsing with water until the eluant became neutral.

Specific desalting procedures are described in the text. Essentially, eluants obtained from chromatography with SP-Sephadex resin (which contained either 0.05-0.5 M K₂SO₄, 0.05-0.2 M Na₃citrate, 0.05-0.1 M NaCl) were sorbed onto Dowex cation exchange resin (H⁺ form) which was then thoroughly washed with water. The resin was then washed with 1 M HCl and the desired cationic complex was eluted with the appropriate concentration of HCl. Generally, 6 M HCl was used for the Pt(IV) hexamine complexes and 3-4 M HCl for the Co(III) and Cr(III) complexes.

2.5. Hazards and Special Precautions

In the synthetic procedures, care was taken to avoid contact with the fumes when quenching the condensation reactions with hydrochloric acid, as carcinogenic haloethers may have formed.⁵ Condensation reactions involving the Pt(IV) and Cr(III) templates were performed and quenched in the dark to limit any possible photoinduced decomposition. Details of subsequent treatment are stated in the text. Perchlorate salts were handled carefully as they are potentially explosive.

2.6. NMR Spectroscopy

All ¹H and ¹³C NMR spectra were acquired using either Varian Gemini 300 MHz, or Varian VXR 300 MHz or Varian VXRS 500 MHz spectrometers using standard Varian software. D₂O, DCl, D₃-MeCN, D₆-acetone, CDCl₃, D₇-DMF and D₆-DMSO (all Merck) were used without further purification. All spectra were referenced internally against 1,4-dioxane (3.744 ppm vs TMS for the ¹H NMR spectra and 67.3

ppm vs TMS for ^{13}C NMR spectra).⁶ Chemical shifts (δ) are in ppm and are reported as positive at frequencies higher than TMS. Uncertainties in the chemical shift are typically 0.05 ppm for ^1H and 0.5 ppm for ^{13}C . In some of the less concentrated samples in D_2O , the H-OD signal was selectively presaturated for 5 seconds. Typically, 16-32 transients were required for the one-dimensional ^1H NMR spectra and ~40,000 transients for most of the one-dimensional ^{13}C NMR spectra. The geminal coupling constants were determined from the one-dimensional ^1H NMR spectra. The small ^3J and long range homonuclear coupling constants ($^{4,5}\text{J}_{\text{H-H}}$) were often too small to be determined from the one-dimensional ^1H NMR spectra, especially for complicated splitting patterns. In these instances, they were estimated from the F_2 dimension in the DQF COSY spectra. However, coupling constants measured in this way tend to be overestimated,⁷ so some of these coupling constants quoted in this work may only be approximate. The $^{2,3}\text{J}_{\text{Pt-H,C}}$ coupling constants were determined from the one-dimensional ^1H and ^{13}C NMR spectra.

The two-dimensional experiments were obtained using either the Varian VXR 300 MHz (phase sensitive-DQF COSY (hereafter referred to as DQF COSY), NOESY) or Varian VXR 500 MHz (DQF COSY, TOCSY, HMQC, HMBC) spectrometers, in conjunction with standard Varian software. The pretransient delay times (d_1) and recycling times for the experiments were typically 0.5–2 s and 1–6 s, respectively. Relevant parameters (number of increments (ni), and transients acquired (nt), the number of points used (np), sweep width (sw), Fourier number (fn), etc) are stated in the figure caption for each spectrum. Sinebell weighting functions were used in both dimensions prior to Fourier transformation for DQF COSY, HMQC and HMBC spectra and 30° or 60° shifted sine weighting functions used for the NOESY spectra. No ^{13}C decoupling was used when acquiring the HMQC spectra, therefore the resonances in the F_2 dimension (^1H) are split into doublets. In this case, the middle of the signal was taken as the peak frequency when assigning its corresponding one dimensional ^{13}C NMR spectrum.

2.7. Structure Determinations

The X-ray structures for $[\text{Pt}(\alpha\text{Me}_5\text{-}N_6\text{-tricosanetriimine})](\text{ZnCl})_{1.5}\text{Cl}$, $[\text{Co}(\text{Et}_2\text{-Me}_6\text{-}N_6\text{-tetracosanediimine})]\text{Cl}_3 \cdot 5\text{H}_2\text{O}$ and $[\text{Co}(\text{Et}_2\text{-Me}_6\text{-}N_6\text{-tetracosane})]\text{Cl}_3 \cdot 4\text{H}_2\text{O}$ were determined by Dr T.W. Hambley at the University of Sydney, using a Enraf-Nonius CAD-4F four circle diffractometer employing graphite monochromated $\text{MoK}\alpha$ radiation. The conditions under which the experimental data were acquired are described in Appendices B(I) and E (for $[\text{Pt}(\alpha\text{Me}_5\text{-}N_6\text{-tricosanetriimine})](\text{ZnCl})_{1.5}\text{Cl}$ and the cobalt complexes, respectively).

The X-ray structure for $[\text{Pt}(\text{Et}_2\text{-Me}_6\text{-N}_6\text{-tetracosanediimine-H})](\text{PF}_6)_3 \cdot 5\text{H}_2\text{O}$ was determined by Dr. A.C. Willis at the Australian National University, using a Rigaku AFC-6R diffractometer with graphite monochromated $\text{Cu-K}\alpha$ radiation and a Rigaku RU-200B rotating anode X-ray generator. The conditions under which the experimental data were acquired are described in Appendix B(II).

The X-ray structures for pentacyclo- $[\text{Pt}(\text{Et}_2\text{-Me}_6\text{-N}_6\text{-tetracosane2H})]\text{Cl}_4 \cdot 9\text{H}_2\text{O}$ and the $[\text{Pt}(\beta\text{Me}_5\text{-N}_6\text{-tricosanetriimine})](\text{ZnCl}_4)(\text{ZnCl}_3)_2 \cdot 0.5\text{H}_2\text{O} \cdot 4\text{HCl}$ were determined by Dr. D.C.R. Hockless at the Australian National University, using a Rigaku AFC-6R diffractometer with graphite monochromated $\text{Cu-K}\alpha$ radiation and Rigaku RU-200B rotating anode generator. The conditions under which the experimental data were acquired are described in Appendices B(III) and B(IV).

2.8. Electrochemistry

(a) Electrolytes

The electrolytes used in the aqueous electrochemistry were of AR grade and were used without further purification. The electrolyte concentration in the aqueous electrochemistry was typically 0.1 M or 1 M.

Electrolytes used for nonaqueous electrochemistry were tetra(1-butyl)ammonium tetrafluoroborate (TBATFB, BDH, AR grade), tetramethylammonium triflate (TMAT) and tetra(1-butyl)ammonium perchlorate (TBAClO₄). The TBATFB was recrystallised three to four times from ethyl acetate and ether⁸ and dried using a vacuum pump. The TBATFB was stored under argon in the dark, to minimise contamination by water and photodecomposition. The TMAT was prepared by Dr. L.L. Martin and used without further purification, and the TBAClO₄ was prepared by Dr. S. Gheller, and was used without further purification. The concentration of electrolyte used was about 0.1 M.

The concentration of the electroactive species was generally 1-5 mM. All samples were purged for ~ 15 minutes with a continuous flow of argon or house nitrogen prior to data acquisition. Measurements were acquired under a blanket of nitrogen or argon at $\sim 293 \pm 1$ K unless otherwise specified. As different reference electrodes were used, in order to allow comparison between experiments, the potentials cited in the text are referenced to the normal hydrogen electrode (NHE) unless otherwise specified.

(b) Cyclic Voltammetry

The cyclic voltammograms (CV's) using a mercury drop working electrode were recorded using a Princeton Applied Research Model-174 Polarographic Analyser (PAR-170, DC polarographic mode) or Model-173 Universal Programmer (PAR-173) in conjunction with a Model-175 Potentiostat/Galvanostat (PAR-175). Both systems were interfaced with a Hewlett-Packard 7046A (X,Y) plotter. The mercury electrode (Metrohm 663 VA stand, interfaced with an RSC Model-411 interface unit) was generally used as a hanging mercury drop (HMDE). The three-electrode configuration included an auxiliary electrode, which was a carbon rod (~0.4 cm diameter, ~8 cm in length), and the reference electrode, which was either a Ag/AgCl/KCl_(sat) (199 mV vs NHE)⁹ or a standard calomel electrode (SCE, 241 mV vs NHE).⁹

Some of the aqueous and all of the non aqueous electrochemical measurements using disc electrodes were recorded using a BAS-100 Electrochemical Analyser. Using BAS File Transfer Software, the data was transferred to a personal computer, which was then converted to Macintosh-readable form. The CV's were displayed using a suitable graphics program. The three-electrode configuration included an auxiliary electrode (a platinum wire (0.5 mm diameter, ~4 cm in length)) and a working electrode, which was either a BAS glassy carbon (3 mm diameter), a platinum (1.5 mm diameter) or a gold (1.5 mm) disc electrode. These were polished using a suspension of BAS polishing alumina on a polishing cloth. The electrode was then rinsed thoroughly with distilled water and carefully wiped dry with lens tissue. In aqueous media, the reference electrode was the standard calomel electrode, (241 mV vs NHE). For the aqueous electrochemistry, the reference electrode was separated from the cell using a salt bridge containing an aqueous solution of ~1.5 M NaCl. In acetone, the reference electrode was an Ag/AgCl/LiCl_(sat. acetone) electrode and in acetonitrile, an Ag/AgCl/TBATFB(0.1 M, MeCN) electrode.

The electrochemistry using the edge plane pyrolytic graphite (EPG) carbon electrodes were performed by Dr Chunnian Shi at the Californian Institute of Technology, Pasadena, CA, using a Pine EPG rotating disc electrode or and a Union Carbide stationary disc EPG electrode on a Pine Institute Co. Bi potentiostat (model AFRDE-4). Some of the CV's using the HMDE (using a Metrohm E410 stand) and gold disc electrode in aqueous solution were also recorded in this laboratory. The results were recorded using a Kipp-Zonen Recorder (BD91).

(c) Controlled Potential Electrolysis.

The controlled potential electrolyses were performed using a BAS-100 Electrochemical Analyser. The solution containing only the electrolyte was electrolysed for up to 1.5 hours until the background current became negligible. The electro-active species was then added. Generally, a mercury pool was used as the working electrode, with a platinum auxiliary electrode and the SCE reference electrode. The auxiliary and reference electrodes were separated from the bulk solution using salt bridges containing an aqueous solution of ~1.5 M NaCl. The mercury pool was stirred with a magnetic flea. All electrolyses were performed under a blanket of nitrogen.

2.9. Visible Spectroscopy

The electronic absorption spectra were measured in water using a Hewlett Packard 8450 A UV/visible spectrophotometer with 1 cm or 0.1 cm quartz cells. The data was converted to Macintosh-readable form and the spectra displayed using a suitable graphics program.

2.10. References

- (1) Giedt, D. C.; Nyman, C. J. *Inorganic Syntheses* **1966**, *8*, 239.
- (2) Perrin, D. D.; Armarego, W. L. F. *Purification of Laboratory Chemicals*; Pergamon Press: Exeter, 1988.
- (3) Shriver, D. F.; Drezdson, M. A. *The Manipulation of Air Sensitive Compounds*; 2nd ed.; Wiley: New York, 1986.
- (4) Geue, R. J.; Searle, G. H. *Aust. J. Chem.* **1983**, *36*, 927.
- (5) Nelson, N. *Ecotoxicol. Environ. Saf.* **1977**, *1*, 289.
- (6) Pretsch, E.; Clerc, T.; Seibl, J.; Simon, W. *Tables of Spectral Data for Structural Determinations of Organic Compounds.*; 2nd ed.; Springer-Verlag: Berlin, 1989.
- (7) Derome, A. E. *Modern NMR Techniques for Chemistry Research*; Pergamon: Oxford, 1987.
- (8) Moulton, R.; Widman, T.; Peter, K.; Volhardt, C.; Bard, A. J. *Inorg. Chem.* **1986**, *25*, 1846.
- (9) Lide, D. R. *CRC Handbook of Chemistry and Physics*; 73rd ed.; CRC Publishing Co.: Boca Raton, 1992-1993, and references therein.

Chapter 3

The Synthesis of Pt(IV) and Pt(II) Expanded Cage Complexes

3.1. Introduction

3.1.1. Sar Cage Complexes of Pt(IV)

The sar cage complexes of Pt(IV) have been synthesised previously, (namely, $[\text{Pt}(\text{sep})]^{4+}$, $[\text{Pt}(\text{NO}_2)_2\text{sar}]^{4+}$, and $[\text{Pt}(\text{NHOH})_2\text{sar}]^{4+}$ (Fig. 3.1)). These cage complexes were made using $[\text{Pt}(\text{en})_3]^{4+}$ as a template,¹ in analogy to the aqueous template capping methods devised for $[\text{Co}(\text{en})_3]^{3+}$ encapsulation.² The mechanism for this type of template synthesis was addressed in Chapter 1.

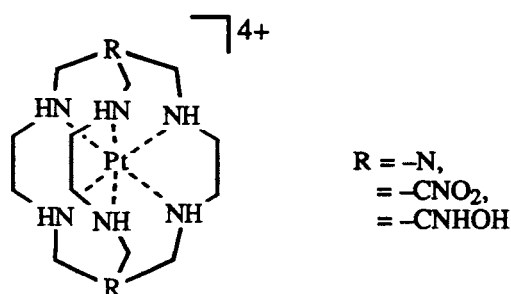


Figure 3.1: $[\text{Pt}((\text{R})_2\text{sar})]^{4+}$.

3.1.2. Proposed Syntheses of Pt(IV) N_6 -tricosane Cage Complexes

It was anticipated that $[\text{Pt}(\text{Me}_2\text{-}N_6\text{-tricosane})]^{4+}$ could be synthesised using a modified capping route described in Chapter 1 for $[\text{Rh}(\text{NO}_2)\text{Me-}N_6\text{-tricosane}]^{3+}$. The average Pt-N bond length for saturated PtN_6^{4+} complexes is $\sim 2.07 \text{ \AA}$, which is comparable to that of Rh-N in saturated RhN_6^{3+} systems (2.09 \AA).³ Therefore, the synthesis of Pt(IV) N_6 -tricosane complexes should be feasible using either $[\text{Pt}(\text{tn})_3]^{4+}$ or $[\text{Pt}(\text{stn})]^{4+}$ as templates. However, the syntheses of the necessary precursors for the Pt(IV) capping reactions, namely, $[\text{Pt}(\text{tn})_3]^{4+}$ and $[\text{Pt}(\text{stn})]^{4+}$, have not been reported, and this aspect needs to be explored.

An alternative route to the synthesis of Pt(IV) N_6 -tricosane cage complexes is by the strapping methods with mixed aldehydes around the template $[\text{Pt}(\text{tame})_2]^{4+}$ to form $[\text{Pt}(\text{Me}_n\text{-}N_6\text{-tricosanetriimine})]^{4+}$ ($n = 2, 5, 8$, for ethanal, propanal and 2-butanal, respectively). This strategy was also described in Chapter 1 for Co(III) analogues. The synthesis for the $[\text{Pt}(\text{tame})_2]^{4+}$ template has also not been reported.

A third potential route to Pt(IV) macrobicycles is to condense metal ion hexaamine complexes with diketones. Condensation of β -diketones with metal amine complexes to form bidentate complexes and $[\text{x}]_n\text{aneN}_4$ macrocycles ($x = 12-14$) have been reported.⁴⁻⁶ Pertinent examples for this study involve the condensation of Pt(IV) hexaamines with acetylacetonone (acac). In the presence of a mild base, $[\text{Pt}(\text{NH}_3)_6]^{4+}$ condenses with acetylacetonone to form mono- *cis*- and *trans*- *bis*- 2,4-pentanediiiminate

complexes⁷⁻⁹ (Figs 3.2(a)-(c), respectively). In these Pt(IV) complexes, the methylene-protons of the pentanediimine strap deprotonates, to give rise to a delocalised six-membered chelate ring. The complex containing three acetylacetonate units was not detected. The deprotonation and delocalisation appear to reduce the acidity of the other coordinating amines and thereby influence further condensations with acetylacetonate. Condensation of acetylacetonate with $[\text{Pt}(\text{en})_3]^{4+}$ has also been reported,⁹ however, the major isolated product contained only one acetylacetonate unit.

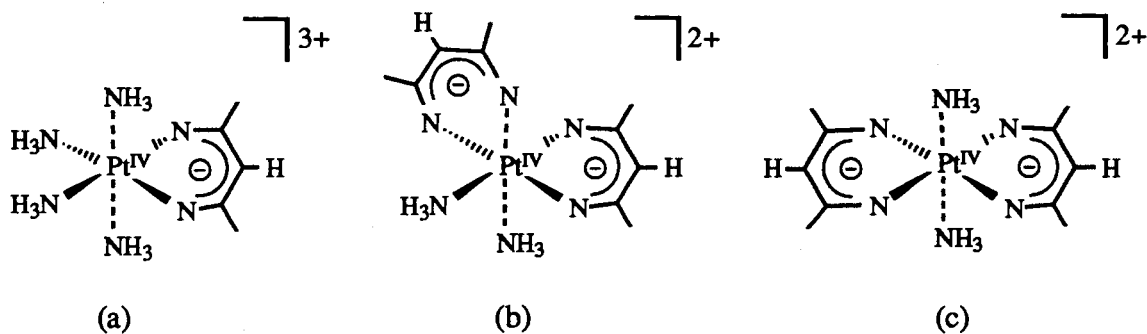
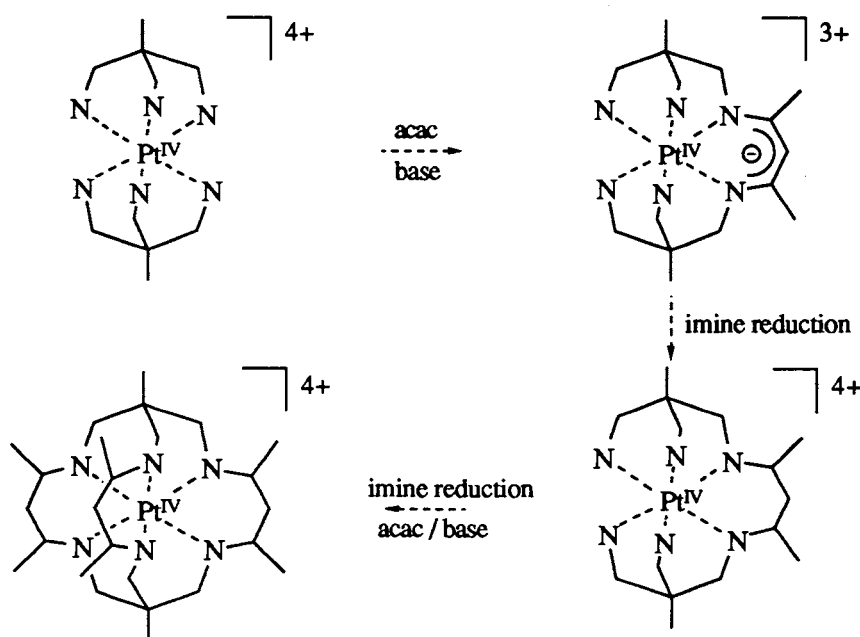


Figure 3.2: (a) mono- (b)*cis*- and (c)*trans*- bis- 2,4-pentanediiimate complexes obtained from condensation of $[\text{Pt}(\text{NH}_3)_6]^{4+}$ with acetylacetonate.

The complex obtained from condensation of three acetylacetonate units with the template $[\text{Pt}(\text{tame})_2]^{4+}$ could provide an alternative route to encapsulation. If the imines could be reduced selectively then the acidity of the amine sites may be restored. Sequential addition of further acetylacetonate units followed by selective reduction of the resulting imines would yield $[\text{Pt}(\text{Me}_8\text{-N}_6\text{-tricosane})]^{4+}$.



Scheme 3.1: A possible synthesis for $[\text{Pt}(\text{Me}_8\text{-N}_6\text{-tricosane})]^{4+}$ (amine protons have been omitted for clarity).

The substituted diketone, 3,3-dimethyl-2,4-pentanedione, is also a likely prospect for condensation reactions, as once it has condensed with the template, deprotonation at the strap methylene and delocalisation is not possible. Therefore, the amine acidity may be maintained such that further condensations with the diketone may be possible, without the necessity of selectively reducing the imines.

3.1.3. Substitution Reactions about Pt(IV) with the Free Cage Ligands

The syntheses of Pt(IV) hexaamine cages will not be confined to template methods. It has been observed that the reaction of $[\text{PtCl}_6]^{2-}$ or $[\text{PtCl}_4]^{2-}$ with free $(\text{NH}_2)_2\text{sar}$ resulted in the metal ions coordinating to four of the donor amines, with the uncoordinated nitrogen donor atoms lying on the same side of the PtN_4 plane.¹⁰ Introduction of the Pt(IV) ion into free $\text{Me}_5\text{-}N_6\text{-tricosane}$ may be possible by such a route, provided the remaining two nitrogen donor atoms can be induced to coordinate.

In this chapter, the syntheses of the templates required for synthesising the $[\text{Pt}(N_6\text{-tricosane})]^{4+}$ type complexes are addressed. The template synthesis of these cages, as well as other Pt(IV) hexaamine cage complexes are presented, and their properties and possible mechanisms for their syntheses are explored.

3.2. Synthesis

3.2.1. Synthesis of the Pt(IV) Templates

(a) *Bis(trimethylenediamine)trans-dichloroplatinum(IV) dichloride*

The many attempts to synthesise $[\text{Pt}(\text{tn})_3]^{4+}$ were not successful. The following preparation is a typical example of the procedure which was modified from the synthesis of $[\text{Pt}(\text{en})_3]^{4+}$ in ethanol.¹¹ Other solvents systems also were tried, namely methanol, water, 50% ethanol/water, DMF and DMSO. All of these reactions produced mixtures of $[\text{Pt}(\text{tn})_2]\text{Cl}_2$, *trans*- $[\text{Pt}(\text{tn})_2\text{Cl}_2]\text{Cl}_2$, traces of $[\text{Pt}(\text{tn})\text{Cl}_2]$ and red polymeric products. Similar results have been obtained by others.^{10,12}

$\text{H}_2\text{PtCl}_6 \cdot 6 \text{H}_2\text{O}$ (1g) was dissolved in ethanol (10 mL) and the resulting solution was cooled in an ice bath. Trimethylenediamine (98%, 5 equivalents, 1 mL) was added dropwise to the solution. The reaction mixture was heated for 3 hours at 60° C, then it was diluted to 500 mL and acidified with HCl to pH~4. The solution was sorbed onto a column of Dowex 50W-X2 cation exchange resin, which was washed with water (1 L), 1 M HCl (1 L), 2 M HCl (500 mL), 4 M HCl (500 mL), 6 M HCl (500 mL) and 50% HCl/ethanol. The 2 M and 4 M eluates were evaporated to near dryness to yield colourless powders. These powders were recrystallised from water/HCl and dried *in vacuo*. The ^1H NMR spectrum of the powder from the 2 M eluate showed that it contained a mixture of $[\text{Pt}(\text{tn})_2]\text{Cl}_2$ and *trans*- $[\text{Pt}(\text{tn})_2\text{Cl}_2]\text{Cl}_2$. The two complexes were separated by fractional crystallisation. The ^1H NMR spectrum of the 4 M eluate showed that it contained mostly *trans*- $[\text{Pt}(\text{tn})_2\text{Cl}_2]^{2+}$. The 6 M and 50% HCl/ethanol eluates were taken to dryness. The ^1H NMR spectrum of the 6 M eluate did not show any appreciable signal while the ^1H NMR spectrum of the 50% HCl/ethanol eluate was broad and featureless. Combined yield from 2 M and 4 M eluates: ~65 % .

Anal. Calc. for $[\text{C}_6\text{H}_{20}\text{Cl}_2\text{N}_4\text{Pt}]$: C, 17.40; H, 4.87; N, 13.52; Cl, 17.12. Found: C, 17.65; H, 4.88; N, 13.31; Cl, 17.34. Anal. Calc. for $[(\text{C}_6\text{H}_{20}\text{Cl}_4\text{N}_4\text{Pt}) \cdot 5\text{H}_2\text{O}]$: C, 12.53; H, 5.26; N, 9.74; Cl, 24.65. Found: C, 12.58; H, 4.42; N, 9.21; Cl, 24.73.

NMR (δ (ppm), D_2O) $[\text{Pt}(\text{tn})_2]^{2+}$: ^1H : 2.10 (m), 3.13 (d of d). ^{13}C : 25.65, 37.47

NMR (δ , D_2O) *trans*- $[\text{Pt}(\text{tn})_2\text{Cl}_2]^{2+}$: ^1H : 1.82 (m), 2.82 (d of d). ^{13}C : 28.01, 43.26

The procedure for the attempted synthesis of the $[\text{Pt}(\text{tn})_3]^{4+}$ ion was modified from the synthesis of $[\text{Pt}(\text{pn})(\text{en})_2]\text{Cl}_4$.¹³

Trimethylenediaminedihydrochloride (0.45 g) was added to a stirred boiling solution of 5 M sodium acetate (11 mL). K_2PtCl_4 (1g) was added to this solution. A peach precipitate ($[\text{Pt}(\text{tn})\text{Cl}_2]$) was formed after five minutes and was filtered and washed with a minimum volume of iced water. The $[\text{Pt}(\text{tn})\text{Cl}_2]$ was suspended in water (10 mL) and purged with chlorine gas for 10 minutes to form a dark orange precipitate $[\text{Pt}(\text{tn})\text{Cl}_4]$. This was filtered and washed with ethanol. Yield: 55%.

Anal. Calc. for $[\text{C}_3\text{H}_{10}\text{Cl}_4\text{N}_2\text{Pt}]$: C, 8.77; H, 2.45; N, 6.82; Cl, 34.50. Found: C, 8.84; H, 2.54; N, 6.41; Cl, 34.45

Trimethylenediamine (~2 equivalents, 0.04 mL), was added to a suspension of $[\text{Pt}(\text{tn})\text{Cl}_4]$ (0.1 g) in DMF (1.5 mL) and K_2PtCl_4 (~5 mg). The mixture was stirred for 3 hours, during which the orange suspension became paler. A solution of acetone and concentrated HCl was added to the reaction mixture which was then heated gently for 10 minutes and then cooled. The resulting colourless precipitate was filtered and washed with ethanol. The ^1H NMR spectrum of the powder indicated that *trans*- $[\text{Pt}(\text{tn})_2\text{Cl}_2]\text{Cl}_2$ was formed and therefore no microanalysis was sought.

(b) Reaction of H_2PtCl_6 with 1,1,1-tris(5-amino-2-azapentyl)ethane (stn)

Free stn (1 equivalent, 0.6 g) was slowly added to a stirred suspension of $\text{H}_2\text{PtCl}_6 \cdot 6\text{H}_2\text{O}$ (1.07 g) and triethylamine (2 equivalents, 0.6 mL) in ethanol (50 mL). K_2PtCl_4 (~5 mg) was added to catalyse the reaction and the reaction vessel was wrapped in foil. The solution was heated at 60° for 2 hours. The precipitate was filtered and washed with ethanol to yield a colourless powder. The powder was recrystallised from water/HCl. The ^1H NMR spectrum of the powder was complicated, indicating that many products had been formed. Similar results were obtained by others.^{12,14} The red solution was sorbed onto SP-Sephadex cation exchange resin, but no separation of products was observed using 0.1 M NaCl, 0.05 M K_2SO_4 and 0.05 M $\text{Na}_3\text{citrate}$ as eluants. A broad, featureless band moved through the column, leaving behind a red/brown band at the top of the resin column, which could not be desorbed, even after treatment with 5 M NaCl. Anal. Calc. for $[\text{C}_{14}\text{H}_{36}\text{Cl}_4\text{N}_6\text{Pt}]$: C, 26.89; H, 5.80; N, 13.44; Cl, 22.68. Found: C, 17.41; H, 3.95; N, 7.88.

The colourless powder was converted to the triflate salt by addition of neat triflic acid, in the manner described in Chapter 2. The suspension was purged with nitrogen for 12 hours. Ether was added to the resulting pale brown suspension and the reaction was filtered, to yield a cream rubbery solid, which was insoluble in water, methanol, ethanol, isopropanol, DMF and DMSO. This product was not identified.

The substitution procedure described above was repeated using $\text{H}_2\text{PtCl}_6 \cdot 6\text{H}_2\text{O}$ (1.44 g), stn (1.9 g), triethylamine (1 equivalent, 4 mL) and DMF (15 mL), and the reaction was heated at 40° C for 6 hours. A cream powder was isolated from a red mother liquor and the former was recrystallised from water. Its ^1H NMR spectrum contained many peaks, and no microanalysis was therefore sought.

(c) Reaction of (Me₅-N₆-tricosane) with H₂PtCl₆ in DMF

Triethylamine (2.5 equivalents, 0.05 mL) was added to a suspension of $\text{H}_2\text{PtCl}_6 \cdot 6\text{H}_2\text{O}$ (0.065 g) in DMF (2 mL). Free (Me₅-N₆-tricosane) (0.05 g) and K_2PtCl_4 (~5 mg) were then added to the stirred suspension which was then heated at 40° overnight. The resulting colourless precipitate was filtered from a red-brown mother liquor. The ^1H NMR of the precipitate indicated that it was free ligand, whilst that of the mother liquor was complicated.

The above procedure was repeated in 50% ethanol/water. Triethylamine (2.5 equivalents, 0.02 mL) was added to a suspension of $\text{H}_2\text{PtCl}_6 \cdot 6\text{H}_2\text{O}$ (0.04 g) in water (1 mL). Free Me₅-N₆-tricosane (0.03 g) was suspended in ethanol (2 mL) and added to the water solution, followed by addition of K_2PtCl_4 (~5 mg). The suspension which was then heated at 40° for 20 hours. The resulting cream precipitate was filtered from a red mother liquor. The ^1H NMR spectrum of the precipitate again indicated that it was free ligand and that of the mother liquor was complicated.

*(d) Bis(1,1,1-tris(aminomethyl)ethane)platinum(IV) tetrachloridemonohydrate.
([Pt(tame)₂]Cl₄·H₂O)*

The tame ligand (2 equivalents, 1.0 g) was added dropwise to a stirring suspension of K_2PtCl_6 (2 g) in DMF (15 mL). K_2PtCl_4 (~5 mg) was added to catalyse the reaction and the vessel was wrapped in foil to minimise possible photoreduction. A clear orange solution formed after the tame was added and within ~5 minutes, a colourless precipitate became evident. The reaction was heated at 40° C for 30 hours to drive it to completion. The suspension was diluted to 500 mL with water, the pH adjusted to 4-5 with HCl and then the mixture was sorbed onto a column (15 cm x 3 cm) of Dowex 50W-X2 cation exchange resin. The column was washed with water (500 mL) and 2 M HCl (500 mL) and the complex eluted with 6 M HCl. Evaporation of the eluate to near dryness yielded a colourless powder which was filtered, washed with ethanol and then isopropyl alcohol. The powder was dried *in vacuo* over molecular sieves. Yield: 75 %. Anal. Calc. for $[\text{C}_{10}\text{H}_{30}\text{Cl}_4\text{N}_6\text{Pt}]\cdot\text{H}_2\text{O}$: C, 20.38; H, 5.47; N, 14.26; Cl, 24.06; Pt, 33.11. Found: C, 20.35; H, 5.71; N, 14.13; Cl, 24.67; Pt, 32.95. $\text{pK}_{\text{a}1}$: 7.0 ± 0.1 , $\text{pK}_{\text{a}2}$: 11 ± 0.1

NMR (δ (ppm), D₂O) [Pt(tame)₂]Cl₄: ¹H: 1.10 (s, 1H, CH₃) 2.87 (s, 1H, CH₂).
¹³C: 21.80 (s, CH₃), 45.15 (t, quaternary), 47.20 (t, CH₂)

²J_{Pt-H} (Hz): ²J_{Pt-H}=44.2. ^xJ_{Pt-C} (Hz): ²J_{Pt-C}=8.4; ³J_{Pt-C}=44.2

[Pt(tame)₂]Cl₄ was converted to the triflate salt by treating the chloride salt (2.5 g) with excess distilled neat triflic acid (~5 mL) in a 3 necked round bottom flask which was fitted with an air condenser and a nitrogen bleed. Nitrogen was bubbled vigorously for 12 hours. Ether was added to the creamy slurry and the precipitate was filtered and washed with ether. The complex was recrystallised from water.

3.2.2. Reactions of [Pt(tame)₂]⁴⁺ with Propanal

(a) (1,5,9,13,20-pentamethyl-3,7,11,15,18,22-hexaazabicyclo[7.7.7]tricosanetriimine)platinum(IV) tetrachloride ([Pt(^{α} Me₅-N₆-tricosanetriimine)]Cl₄) (the α superscript indicates that the methyl substituents on the six membered ring chelate straps are on the carbon atoms alpha to the imine (i.e., atoms 5,11,20))

[Pt(tame)₂]Cl₄.H₂O (2 g) was suspended in acetonitrile (20 mL). Anhydrous NaClO₄ (4 g) was suspended in acetonitrile (15 mL) and added to the [Pt(tame)₂]Cl₄ solution and the suspension was cooled in an ice bath. Triethylamine (3 equivalents, 1.5 mL) was added dropwise (an orange colour developed, indicating that deprotonation had taken place), followed by aqueous formaldehyde (37 %, 5 equivalents, 1.4 mL) to the stirred suspension. Propanal (15 equivalents, 3.8 mL) was then added and the reaction was stirred for 3 hours in the dark before being quenched with concentrated HCl (~2 mL), resulting in a colourless suspension in a brown mother liquor. This reaction mixture was diluted to 1 L, giving rise to an orange solution which was loaded onto a (5 x 10 cm) column of Dowex 50 W-X2 cation exchange resin. The resin washed with water (1 L), 1 M HCl (1 L) and the complex was eluted with 6 M HCl (~1 L). The 6 M eluate was evaporated to near dryness to yield a colourless suspension, which was filtered and the resulting colourless powder was washed with a small amount of ethanol. This residue was recrystallised from water and concentrated HCl, to yield fragile colourless crystals which crumbled as they dried. Yield ~50%.

Anal. Calc. for [C₂₂H₄₂Cl₄N₆Pt].5H₂O.0.5HCl: C, 31.61; H, 6.33; N, 10.05; Cl, 19.09. Found: C, 31.84; H, 6.53; N, 9.80; Cl, 19.04. The chloride salt was converted to the tetrachlorozincate salt by dissolving [Pt(^{α} Me₅-N₆-tricosanetriimine)]Cl₄ (100 mg) in a minimum volume of water (2 mL) and adding 5 drops of a solution containing ZnCl₂ in 4 M HCl (~5 g/100 mL). Crystals suitable for an X-ray crystallographic analysis were obtained after ~ 36 hours. These were filtered by gravity on filter paper and allowed to dry in air.

NMR (δ (ppm), D₂O) [Pt(α Me₅-N₆-tricosanetriimine)]Cl₄ **¹H**: 1.12 (s, 1H, cap CH₃, H₁₀), 1.22 (s, 1H, cap(imine) CH₃, H₁), 1.40 (s, 9H, strap CH₃, H₆), 2.16 (d of t, 1H, cap CH₂, H_{7a}), 2.21 (d of t, 1H, strap CH₂, H_{8a}), 2.86 (d, 1H, cap CH₂, H_{7b}), 3.16 (d, 1H, cap CH₂, H_{8b}), 3.84 (d of t, 1H, cap CH₂, H_{3a}), 4.39 (d, 1H, cap CH₂, H_{3b}), 8.86 (t, 1H, imine, H₄).

¹³C: 16.0 (s, strap CH₃, C₆), 21.6 (s, cap CH₃, C₁₀), 22.2 (s, cap CH₃, C₁), 35.0 (broad t, strap CH/CD, C₅), 40.1 (t, quaternary, C₂), 42.2, (t, quaternary, C₉), 55.7 (s, strap CH₂, C₇), 56.3 (s, cap CH₂, C₈), 65.9 (t, cap CH₂, C₃), 189.5 (s, C_{imine}, C₄).

²J_{H-H} (Hz): ²J_{3a-3b}=14.1; ²J_{7a-7b}=16.2; ²J_{8a-8b}=14.4. **³J_{Pt-H}** (Hz): ³J_{Pt-3a}=42; ³J_{Pt-4}=69.2; ³J_{Pt-7a}=57.5; ³J_{Pt-8a}=54.4. **⁴J_{H-H}** (Hz): ⁴J_{3a-4}=2.8; ⁴J_{3b-4}=4.9; ⁴J_{4-7a}=4.4. **²J_{Pt-C}** (Hz): ²J_{Pt-C3}=19.6. **³J_{Pt-C}** (Hz): ³J_{Pt-C2} = 37.9; ³J_{Pt-C5}=25.1; ³J_{Pt-C9}=54.8.

I. Hydrogenation of [Pt(α Me₅-N₆-tricosanetriimine)]⁴⁺

[Pt(α Me₅-N₆-tricosanetriimine)]Cl₄ (50 mg) was dissolved in D₂O (0.5 mL) in an NMR tube and the Pd/C catalyst (10%, ~5 mg) was introduced. The suspension was purged with argon for 20 minutes. The NMR tube was sealed and then centrifuged for 5 minutes before the ¹H and ¹³C NMR spectra were acquired. The sample was purged with hydrogen for 30 minutes and then again purged for 5 minutes with argon, and after centrifugation, the ¹H and ¹³C NMR spectra were acquired. The sample was again purged with hydrogen for a further 1.5 hours, then with argon and centrifuged, before the ¹H and ¹³C NMR spectra were acquired. Hydrogen was then bubbled through the sample for 16 hours and the ¹H NMR spectrum was again acquired.

NMR (δ (ppm), D₂O) **¹H**: The spectrum was very complicated and the only notable signals after 2 hours included: methyl region: 0.91 (2H), 0.98, (1H), 1.44 (2H), 4.98 (2H), 8.39 (1H).

¹³C: Additional peaks after 2 hours: 14.0, 14.6, 14.7, 17.8, 23.1, 38.5, 39., 44.7, 51.7, 51.9, 56.4, 57.2, 68.4, 68.7, 94.6 (putative carbinolamine), 182.3 (imine).

(b) [(19,23-diethyl-1,5,9,13,20,24-hexamethyl-3,7,11,15,18,22-hexaazatricyclo[10.4.4.4⁴⁻⁹]tetracos-3,11-diene)platinum(IV) tetrachloride. ([Pt(Et₂-Me₆-N₆-tetracosanediimine)Cl₄.H₂O))

[Pt(tame)₂]Cl₄ (2 g) was suspended in a solution of anhydrous NaClO₄ (3 g) in acetonitrile (40 mL) and stirred. Propanal (15 equivalents, 3.9 mL), followed by triethylamine (2 equivalents, 1 mL) was added. After 4 hours, the reaction was quenched with concentrated HCl (~3 mL). The orange-brown reaction solution was diluted to 1 L with water and sorbed onto a (5 x 10 cm) column of Dowex 50 W-X2 cation exchange resin, which was washed with water (1 L), 1 M HCl (1 L) and the complex was eluted with 6 M HCl (~1 L). The eluate was evaporated to near dryness to yield a colourless suspension which was filtered and the resulting colourless powder was recrystallised from water. This colourless powder was sufficiently pure for most purposes. However, further purification was achieved by redissolving the complex (~200 mg) and loading onto a (25 x 3 cm) column of SP-Sephadex cation exchange resin. The resin was washed with water (500 mL). Three yellow bands separated using 0.05 M Na₃citrate. After separation of the three bands became obvious, the complexes were eluted by flash chromatography with compressed air in order to minimise the time that the complexes were exposed to the citrate solution. The first band was narrow and came off rapidly, and after desalting on a column of Dowex cation exchange resin, its ¹H NMR spectrum was broad and featureless and the complexes were not identified. The second band was desalted on a (3 x 7.5 cm) column of Dowex 50W-X2 cation exchange resin and the 6 M HCl eluate was evaporated to near dryness to yield a colourless suspension and a colourless powder was isolated upon filtering. The ¹H and ¹³C NMR spectra of the colourless powder were complicated, but appeared to arise from one complex, consistent with that of a partially strapped complex, [Pt(12,19-diethyl-1,5,9,13,20-pentamethyl-3,7,11,15,18,22-hexaazabicyclo[10.4.4]docosa-3,14-diene)]Cl₄ (hereafter abbreviated as [Pt(Et₂-Me₅-N₆-docosanediimine)]Cl₄). The third band contained only [Pt(Et₂-Me₆-N₆-tetracosanediimine)Cl₄. Neutral aqueous solutions of this complex were orange but colourless crystals were obtained from solutions of ~4 M HCl. The colourless crystals were fragile and crumbled upon drying. A sample of the complex (50 mg) was dissolved in water, the solution was acidified to pH ~ 3 and KPF₆ (0.5 g) was then added to the solution. The resulting yellow precipitate was filtered and recrystallised from warm water to form crystals suitable for X-ray analysis. Yield [Pt(Et₂-Me₅-N₆-docosanediimine)Cl₄: ~15%. Anal. Calc. for [C₂₅H₅₀Cl₄N₆Pt]10H₂O: C, 31.55; H, 7.41; N, 8.83. Found: C, 31.42; H, 7.02; N, 8.78. Yield [Pt(Et₂-Me₆-N₆-tetracosanediimine)Cl₄.3H₂O: 65 %. Anal. Calc. for [C₂₈H₅₄Cl₄N₆Pt].3H₂O: C, 38.85; H, 6.99; N, 9.71; Cl, 16.38. Found: C, 38.77; H, 7.94; N, 9.61; Cl, 16.62. pK_{a1}: 1.9±0.5, pK_{a2}: 9.6±0.1.

NMR (δ (ppm), ~ 0.1 M DCl, [Pt(Et₂-Me₅-N₆-docosanediiimine)Cl₄): ¹H: 0.88 (t, 3H, ³J_{H-H}=7.4 Hz), 0.99 (t, 3H, ³J_{H-H}=6.9 Hz), 1.05 (s, 3H), 1.08 (d, 3H, ³J_{H-H}=7.1 Hz), 1.12 (s, 3H), 1.48 (overlapping pair of d's, 6H, ³J_{H-H}=7.4 Hz), 1.61-1.97 (3 overlapping pairs of multiplets, 3H), 2.02-2.23 (3 overlapping pairs of multiplets, 3H), 2.39 (d, 1H, ²J_{H-H}=14.0 Hz), 2.58 (d, 1H ²J_{H-H}=8.6Hz), 2.62 (d, 1H, ²J_{H-H}=9.0 Hz), 2.84 (d of d, 2H, ²J_{H-H}=9.0 Hz), 2.95 (d, 1H, ²J_{H-H}=13.2 Hz), next three resonances give a combined integral 4H: 3.24 (d of d, ²J_{H-H}=13.8 Hz, ³J_{H-H}=3.2 Hz), 3.30 (broad s), 3.39 (d, ²J_{H-H}=13.6 Hz). next two resonances give a combined integral 3H: 3.68 (d, ²J_{H-H}=14.5 Hz), 3.75 (d, ²J_{H-H}=14.8 Hz). 4.02-4.16 (multiplet, 1H), 4.24 (d, 1H, ²J_{H-H}=13.4Hz), 4.40 (d, 1H, ²J_{H-H}=14.6 Hz), 8.38 (t, 1H, ³J_{Pt-H}=71.4 Hz), 8.77(t, 1H, ³J_{Pt-H}=64.0 Hz).

¹³C: 12.4 (s), 13.4 (s), 15.3 (two overlapping singlets), 20.7 (s), 21.6 (s), 22.2 (s), 24.0 (s), 24.4 (s), 24.5 (s), 39.7 (s), 41.4 (s), 41.7(t, ³J_{Pt-C}=60 Hz), 41.9 (s), 44.0 (t, ³J_{Pt-C}=68.5 Hz), 46.0 (s), 50.7 (s), 51.4 (s), 54.1 (s), 64.0 (broad s), 64.7 (s), 65.6 (s), 67.6 (s), 189.5 (s, imine), 196.7 (s, imine).

NMR (δ (ppm), ~ 0.1 M DCl) [Pt(Et₂-Me₆-N₆-tetracosanediiimine)Cl₄: ¹H: 1.00 (overlapping d of d, 3H, H₈), 1.20 (s, 3H, H₁), 1.25 (d, 3H, H₁₀), 1.59 (d, 3H, H₁₃), 1.73-1.87 (m, 1H, H_{7a}), 1.92-2.07 (m, 1H, H_{7b}), 2.26-2.41 (m, 1H, H₉), 2.69, (overlapping s and d, 2H, H_{5a} and H₁₁), 2.90 (broad d with unresolved ¹⁹⁵Pt satellites, 1H, H_{3a}), 3.08 (d, 1H, H_{5b}), 3.46 (d, 1H, H_{3b}), 3.64 (overlapping s and d, 1H, H₆ and H_{4a}), 4.07-4.18 (m, 1H, H₁₂), 4.71 (d, 1H, H_{4b}), 8.49 (t, 1H, H₁₄).

¹³C (D₂O): 14.1 (s, CH₃), 15.8 (s, CH₃), 21.2 (s, CH₃), 22.3 (s, CH₃), 24.7 (broad m, CH₂), 35.3 (broad, CH), 41.6 (broad, 2 x CH), 42.2 (s, quaternary), 50.2 (s, CH₂), 64.0 (s, CH₂), 64.2 (s, CH) 197 (only observed using indirect detection methods, Cimine).

²J_{H-H} (Hz): ²J_{3a-3b}=13.0; ²J_{4a-4b}=13.1; ²J_{5a-5b}=12.8; ²J_{7a-7b}=14.9 Hz. ³J_{H-H}: ³J₆₋₉=11.8; ³J_{7a,b-8}=7.0; ³J₉₋₁₀=6.9; ³J₁₂₋₁₃=7.4 Hz. ⁴J_{H-H}: ⁴J_{4b-14}=3.1 Hz.

It was possible to generate [Pt(Et₂-Me₆-N₆-tetracosanediiimine)Cl₄ from [Pt(Et₂-Me₅-N₆-docosanediiimine)Cl₄, by suspending the latter complex in a solution of acetonitrile containing ~ 2 -4 g anhydrous NaClO₄, followed by addition of propanal (~ 15 equivalents) and triethylamine (~ 3 equivalents). After 4 hours, the reaction was quenched with HCl and diluted with water, and the reaction mixture was worked up as described previously.

(b) [(6,14-diethyl-1,5,9,13,20,23-hexamethyl-3,7,11,15,18,22-hexaazapentacyclo[10.4.4.4⁴⁻⁹.0⁷⁻²³.0¹⁵⁻¹⁹]tetracosane)platinum(II) tetrachloride.
(pentacyclo-[Pt^{II}(Et₂-Me₆-N₆-tetracosaneH₂)Cl₄)

[Pt(Et₂-Me₆-N₆-tetracosanediimine)Cl₄.H₂O (100 mg) was dissolved in water (10 mL) in a two-necked flask, the Pd/C catalyst (10%, ~ 10 mg) was introduced. The solution was cooled to ~275 K, purged with nitrogen and then purged with hydrogen for about 5 hours. As the hydrogenation proceeded, the solution rapidly turned from orange to green over 5 minutes and then became colourless. The colourless solution was then filtered in air to remove the catalyst, the residue was washed with water and the filtrate was taken to dryness on a rotary evaporator to yield a colourless powder.

Crystals of the chloride salt were grown by slow evaporation from a solution of D₂O.

Yield pentacyclo-[Pt^{II}(Et₂-Me₆-N₆-tetracosaneH₂)Cl₄: ~ 95 %.

Anal. Calc. for [C₂₈H₅₆Cl₄N₆Pt]5H₂O.0.5HCl: C, 36.48; H, 7.27; N, 9.11; Cl, 17.30. Found: C, 36.22; H, 6.69; N, 9.50; Cl, 17.63.

NMR (δ (ppm), D₂O) pentacyclo-[Pt^{II}(Et₂-Me₆-N₆-tetracosaneH₂)Cl₄: ¹H: 1.11 (s, 3H, cap CH₃, H₁), 1.13 (overlapping d of d, 3H, ethyl CH₃, H₈) 1.23 (d, 3H, cross strap CH₃, H₁₃), 1.38 (d, 3H, strap CH₃, H₁₀), 1.79-1.88 (m, 1H, ethyl CH₂, H_{7a}), 1.93-2.01 (m, 1H, ethyl CH₂, H_{7b}), 2.10 (overlapping q of d of d, 1H, cross strap CH, H₁₂), 2.23 (q of d of d, 1H, strap CH, H₉), 2.80 (d, 1H, cap CH₂, H_{4a}), 2.88 (d, 1H, cap CH₂, H_{3a}), 2.91 (broad s, 1H, junction CH, H₁₁), 3.16 (d, 1H, cap CH₂, H_{4b}), 3.19 (d, 1H, cap CH₂, H_{5a}), 3.57 (d, 2H, cap CH₂, H_{3b}, partially overlaps with H_{5b}), 3.61 (d, 2H, cap CH₂, H_{5b}, partially overlaps with H_{3b}), 3.63 (d, 1H, cross strap CH, H₁₄), 4.54-4.58 (multiplet, 1H, strap CH, H₆).

¹³C: 12.9 (s, ethyl CH₃, C₈), 15.3 (s, cross strap CH₃, C₁₃), 18.9 (s, strap CH₃, C₁₀), 23.0 (s, ethyl CH₂, C₇), 25.5 (s, cap CH₃, C₁), 31.4 (s, CH, C₉), 32.5 (s, quaternary, C₂), 44.8 (s, CH, C₁₂), 52.8 (s, CH₂, C₄), 57.4 (s, CH₂, C₃), 57.6 (s, CH₂, C₅), 62.5 (s, CH, C₁₁), 72.1 (s, CH, C₆), 75.6 (s, CH, C₁₄).

²J_{H-H} (Hz): ²J_{3a-3b}=12.1; ²J_{4a-4b}=13.5; ²J_{5a-5b}=14.3; ²J_{7a-7b}= 15.1. ³J_{H-H} (Hz): ³J₆₋₉=7.5; ³J_{7a,b-8}=15.1; ³J₉₋₁₀=11.5 Hz; , ³J₁₂₋₁₃=12; ³J₁₂₋₁₄=15.

I. Electrochemical generation of pentacyclo-[Pt^{II}(Et₂-Me₆-N₆-tetracosaneH₂)Cl₄]

Controlled potential electrolysis of [Pt(Et₂-Me₆-N₆-tetracosanediimine)Cl₄.H₂O (100 mg) in 1 M H₂SO₄ (20 mL) at -800 mV vs SCE using a mercury pool working electrode was undertaken. The electrolysis indicated that only 1.5 electrons per Pt had been passed. After 3.5 hours, the solution was diluted to 100 mL and sorbed onto (3 x 10 cm) column of Dowex 50W-X2 cation exchange resin. This was washed with water (500 mL), 1 M HCl, (500 mL) and the complex eluted with 5 M HCl. The 5 M eluate was evaporated to dryness to yield a colourless powder, whose ¹H and ¹³C NMR spectra indicated that only one product had been formed. The ¹H NMR spectrum was similar and ¹³C NMR spectrum was identical to the product obtained from the hydrogenation of [Pt(Et₂-Me₆-N₆-tetracosanediimine)]⁴⁺.

NMR (δ (ppm), D₂O) pentacyclo-[Pt^{II}(Et₂-Me₆-N₆-tetracosaneH₂)Cl₄: ¹H: 1.11 (overlapping s and t, 6H, cap CH₃ and strap ethyl CH₃, H₁ and H₈, respectively), 1.21 (d, 3H, cross strap CH₃, H₁₃), 1.35 (d, 3H, strap CH₃, H₁₀), 1.71-1.88 (m, 1H, H_{7a}), 1.88-2.09 (m, 1H, H_{7b}), 2.11-2.27 (2 overlapping multiplets, 2H, H₁₂ and H₉), 2.83, (2 overlapping d's, 2H, H_{4a} and H_{3a}) 2.90 (broad s, 1H, H₁₁), 3.18 (d, 1H, H_{4b}), 3.21 (d, 1H, H_{5a}), 3.60 (2 overlapping d's, 2H, H_{5b} and H_{3b}), 3.68 (d, 1H, H₁₄), 4.64 (multiplet, 1H, H₆).

¹³C: same as for hydrogenated product.

²J_{H-H} (Hz): ²J_{3a-3b}=12.5; ²J_{4a-4b}=13.5; ²J_{5a-5b}=14.1; ²J_{7a-7b}= 15.1. ³J_{H-H} (Hz): ³J₆₋₉=8; ³J_{7a,b-8}=16.1; ³J₉₋₁₀=12; , ³J₁₂₋₁₃=11; ³J₁₂₋₁₄=14.

3.2.3. Reaction of [Pt(tame)₂]⁴⁺ with Acetaldehyde

(a) [(1,6,9,12,21-pentamethyl-3,7,11,15,18,22-hexaazabicyclo[7.7.7]tricosane-3,18,15-triimine)]platinum(IV) tetrachlorozincate. [Pt(^{β} Me₅N₆-tricosanetriimine)](ZnCl₄)₂. (The ^{β} superscript indicates that the methyl substituents on the six membered ring chelate straps are on the carbon atoms beta to the imine, (i.e., on atoms 6,12,21))

and

(b) [(1,4,9,12-tetramethyl-3,7,11,15,18,23-hexaazatricyclo[10.4.4.4⁴⁻⁹]tetracosane-18,23-diene)platinum(IV) tetrachloride. ([Pt(Me₄-N₆-tetracosanediimine)Cl₄.H₂O)]

[Pt(tame)₂]Cl₄.H₂O (1 g) was suspended in a solution of acetonitrile (15 mL) containing anhydrous NaClO₄ (2 g) and the suspension cooled to ~275 K. Triethylamine (2 equivalents, 0.5 mL) was added, followed by acetaldehyde (20 equivalents, 2 mL). After 30 minutes, the reaction was quenched with concentrated HCl (~2 mL). The solution was diluted to 1 L with water and then sorbed on a (3 x 10 cm) column of Dowex 50W-X2 cation exchange resin which was then washed with water

(500 mL) followed by 1 M HCl (1 L). The complexes were eluted with 6 M HCl (~1 L). The 6 M HCl eluate was evaporated to near dryness to yield a yellow oil. Concentrated HCl was added to the oil, followed by a few drops of ethanol, to form a cream suspension, which was filtered and the residue was washed with a small volume of cold ethanol. The ^1H NMR spectrum of the mother liquor was complicated. The ^1H NMR spectrum of the cream powder indicated that two complexes, $[\text{Pt}(\beta\text{Me}_5\text{-N}_6\text{-tricosanetriimine})]^{4+}$ and $[\text{Pt}(\text{Me}_4\text{-N}_6\text{-tetracosanediimine})]^{4+}$ were present in approximately equal amounts. Attempts to separate the two products using a (40 x 5 cm) column of SP-Sephadex cation exchange resin and a various eluants (0.05 M K_2SO_4 , 0.1 M NaCl and 0.05 M $\text{Na}_3\text{citrate}$) were not successful. Only one broad yellow band each was obtained using either the eluants K_2SO_4 or NaCl, and after desalting using on Dowex 50W-X2 cation exchange resin, the ^1H NMR spectra indicated that the band still had both complexes present. Two broad yellow bands were separated when eluting with 0.05 M $\text{Na}_3\text{-citrate}$ and after desalting each band on Dowex 50W-X2 cation exchange resin, the ^1H NMR spectra showed that the first band was complicated, presumably due to base catalysed decomposition during separation. The second band still contained both complexes.

The two complexes were separated by fractional crystallisation by dissolving the cream powder in ~6 M HCl and then adding 1-2 mL of a solution of ZnCl_2 in 4 M HCl (~5g/100 mL). After one week, crystals of $[\text{Pt}(\beta\text{Me}_5\text{N}_6\text{-tricosanetriimine})](\text{ZnCl}_4)_2 \cdot 3\text{H}_2\text{O} \cdot 1.5\text{HCl}$ were isolated and after a further two days, crystals of $[\text{Pt}(\text{Me}_4\text{-N}_6\text{-tetracosanediimine})(\text{ZnCl}_4)_2]$ were obtained from the acidified mother liquor. These were twinned and therefore not suitable for an X-ray analysis. Attempts to regrow these crystals from HCl and DCl still gave rise to twinning. Combined yield of both complexes: ~45%. Anal. Calc. for $\beta[\text{C}_{22}\text{H}_{42}\text{Cl}_8\text{N}_6\text{PtZn}_2]3\text{H}_2\text{O} \cdot 1.5\text{HCl}$: C, 23.83; H, 4.50; N, 7.58; Cl, 30.37. Found: C, 23.25; H, 4.61; N, 7.36; Cl, 30.72. Anal. Calc. for $[\text{C}_{22}\text{H}_{42}\text{Cl}_4\text{N}_6\text{Pt}]3\text{H}_2\text{O}$: C, 33.81; H, 6.19; N, 10.75; Cl, 18.14. Found: C, 33.62; H, 6.99; N, 10.49; Cl, 18.14.

NMR (δ (ppm), D_2O) $[\text{Pt}(\beta\text{Me}_5\text{-N}_6\text{-tricosanetriimine})]^{4+}$: ^1H : 1.31 (s, 1H, cap CH_3 , H_{10}), 1.35 (s, 1H, cap CH_3 , H_1), 1.63 (d, 3H, strap CH_3 , H_7); 2.80 (d of t, 1H, cap CH_2 , H_{8a}), 3.45 (d, 1H, cap CH_2 , H_{8b}), 3.57 (d of t, 1H, cap CH, H_6), 3.85 (d of t, 1H, cap CH_2 , H_{3a}), 4.3 (broad d of low intensity probably due to solvent exchange, tentatively strap CH_2 , H_{5b}), 4.53 (d, 1H, cap CH_2 , H_{3b}), 8.86 (t, 1H, imine, H_4).

^{13}C : 17.1 (s, CH_3 , C_7), 20.1 (s, CH_3 , C_{10}), 21.9 (s, CH_3 , C_1), 35.6 (broad multiplet, CH/CD, C_5), 40.0 (t, quaternary, C_2), 41.6 (t, quaternary, C_9), 47.6 (s, CH_2 , C_8), 56.1 (s, CH_2 , C_6), 65.0 (s, CH_2 , C_3), 186.6 (t, C_{imine} , C_4).

$^2J_{\text{H-H}}$ (Hz): $^3J_{3a-3b}=13.5$; $^3J_{5a-5b}\sim 12$ (poorly resolved) ; $^2J_{8a-8b}=13.6$. $^3J_{\text{H-H}}$ (Hz): $^3J_{6-7}=6.9$. $^3J_{\text{Pt-H}}$ (Hz): $^3J_{\text{Pt-}3a}\sim 48$; $^3J_{\text{Pt-}4}=73.8$; $^3J_{\text{Pt-}6}=18.2$; $^3J_{\text{Pt-}8a}=41.3$. $^xJ_{\text{Pt-C}}$ (Hz): $^3J_{\text{Pt-C}7}=36$; $^3J_{\text{Pt-C}2}=30$; $^3J_{\text{Pt-C}9}=56$; $^2J_{\text{Pt-C}4}=14$.

NMR (δ (ppm), D₂O) [Pt(Me₄-N₆-tetracosanediimine)]⁴⁺: ^1H : 1.29 (s, 3H, cap CH₃, H₁), 1.41 (d, 3H, strap CH₃, H₇), 2.12 (d of t, 1H, strap CH₂, H_{8a}), 2.53 (d of t, 1H, strap CH₂, H_{8b}; partially overlaps H_{3a}), 2.61 (d of t, 1H, cap CH₂, H_{3a}; partially overlaps H_{8b}), 2.94 (d of t, 1H, cap CH₂, H_{5a}), 3.14 (d, 1H, cap CH₂, H_{3b}), 3.33 (d of t, 1H, junction CH, H₉), 3.54 (d, 1H, cap CH₂, H_{5b}), 3.80 (overlapping d of t, 1H, cap CH₂, H_{4a}), 4.06 (broad m, 1.3H, strap CH, H₆, partially overlapped with the acidic proton, H_{10b}), 4.95 (d, 1H, strap CH₂, H_{4b}), 8.76 (t, 1H, imine, H₁₁), cross strap methylene protons, H_{10a} and H_{10b}, are not observed due to solvent exchange.

^{13}C : 18.0 (s, cap CH₃, C₁), 21.8 (s, strap CH₃, C₇), 30.8 (s, strap CH, C₆), 37.1 (broadened due to solvent exchange, cross strap CH₂, C₁₀), 40.9 (t, quaternary, C₂), 48.8 (s, strap CH₂, C₈), 49.3 (s, cap CH₂, C₃), 52.9 (s, cap CH₂, C₅), 55.4 (s, cap CH₂, C₄) 63.4 (s, CH, C₉), 186.6 (s, C_{imine}, C₁₁).

$^2J_{\text{H-H}}$ (Hz): $^2J_{3a-3b}=14.0$; $^2J_{4a-4b}=15$; $^2J_{5a-5b}=13.1$; $^2J_{8a-8b}=16.9$ Hz. $^3J_{\text{H-H}}$ (Hz): $^3J_{7-6}=6.3$; $^3J_{6-8a}=10.6$; $^3J_{6-8b}=4.4$; $^3J_{9-8a}=4.6$; $^3J_{9-8b}=12.0$ Hz. $^4J_{\text{H-H}}$ (Hz): $^4J_{\text{H}4a-\text{H}11}\sim 3.1$; $^4J_{4b-11}=5.1$ Hz. $^xJ_{\text{Pt-H}}$ (Hz): $^3J_{\text{Pt-}3a}$ =present, but unresolvable; $^3J_{\text{Pt-}4a}=47$; $^3J_{\text{Pt-}5a}=41.0$; $^3J_{\text{Pt-}11}=74.6$ Hz. $^xJ_{\text{Pt-C}}$ (Hz): $^3J_{\text{Pt-}8}=14$; $^3J_{\text{Pt-}2}=48.3$ Hz.

(c) [(1,4,9,12-tetramethyl-3,7,11,15,18,23-hexaazapentacyclo [10.4.4.4⁴-9.0⁷-22.0¹⁵-19]tetracosane)platinum(II) tetrachloride. (pentacyclo-[Pt^{II}(Me₄-N₆-tetracosaneH₂)Cl₄)

[Pt(Me₄-N₆-tetracosanediimine)(ZnCl₄)₂ (100 mg) was dissolved in water (10 mL) in a 2 necked flask, the Pd/C catalyst (10%, ~ 10 mg) was introduced. The solution was cooled to ~275 K and purged with nitrogen and then with hydrogen. The original orange solution rapidly turned green within 5 minutes and then became colourless, as the hydrogenation proceeded. To ensure complete reduction of the Pt complex, the hydrogen was bubbled for a further 5 hours. The colourless solution was then filtered in air, the residue washed with water and the filtrate was taken to dryness on a rotary evaporator to yield a colourless powder. Yield pentacyclo-[Pt^{II}(Me₄-N₆-tetracosane2H)Cl₄: ~ 95 %.

NMR (δ (ppm), D₂O) pentacyclo-[Pt^{II}(Me₄-N₆-tetracosane2H)Cl₄: ^1H : 1.09 (s, 3H, cap CH₃, H₁), 1.32 (d, 3H, strap CH₃, H₇), 1.63-1.68 (d of d of d of d, 1H, strap CH₂, H_{8a}), 1.83 (d of d of d of d, 1H, cross strap CH₂, H_{10a}), 2.57-2.63 (multiplet, 1H, cross strap CH₂, H_{10b}), 2.65-2.70 (d of d of d of d of t, 1H, strap CH₂, H_{8b}),

2.81 (d, 1H, cap CH₂, H_{5a}), 2.87 (d, 1H, cap CH₂, H_{4a}), 2.97 (d, 1H, cap CH₂, H_{3a}), 3.20 (d, 1H, cap CH₂, H₅; partial overlap with H₉), 3.23 (broad s, 1H, junction CH, H₉), 3.32 (d, 1H, cap CH₂, H_{4b}), 3.49 (d, 1H, cap CH₂, H_{3b}), 4.15 (d of d, 1H, cross strap CH, H₁₁), 4.65 (d of d of q, 1H, strap CH, H₆).

¹³C: 17.5 (s, strap CH₃, C₇), 26.1 (s, cap CH₃, C₁), 29.3 (s, strap CH₂, C₈), 32.6 (s, quaternary, C₂), 35.4 (s, cross strap CH₂, C₁₀), 50.1 (s, junction CH, C₉), 53.5 (s, cap CH₂, C₃), 56.0 (s, cap CH₂, C₅), 58.4 (s, cap CH₂, C₄), 59.2 (s, CH, C₆), 68.1 (s, cross strap CH, C₁₁).

²J_{H-H} (Hz): ²J_{3a-3b}=13.2; ²J_{4a-4b}=15.5; ²J_{5a-5b}=13.2; ²J_{8a-8b}=12.4; ²J_{10a-10b}=7.5.

³J_{H-H} (Hz): ³J_{5a-6}=16.5; ³J₆₋₇=6.6; ³J_{6-8a}=16.6; ³J_{6-8b}=3.3; ³J_{8a-9}=2.7; ³J_{8b-9}=7.0;

³J_{9-10b}=6.6; ³J_{10a-11}=15; ³J_{10b-11}=1.29. ³J_{Pt-H} (Hz): ³J_{Pt-10b}=1.3. ⁴J_{H-H} (Hz):

⁴J_{3a-5b}=1.8; ⁴J_{4b-5b}=4.1.

3.2.4. Reaction of [Pt(tame)₂]⁴⁺ with Acetylacetonone

(a) [2,10-tetrakis(aminomethyl)-5,7-dimethyl-4,8-diazaundeca-5,7-dienato] platinum(IV) trichloride. [Pt(tame)₂-(2,4-pentanediiminate)]Cl₃

The weakly basic anion exchange resin (Biorad, (AG3 - X4, 200 - 400 mesh, 2.8 milliequivalents per dry gram), 6 equivalents, 3.75 g) was converted to the hydroxide form by washing the resin with 0.5 M NaOH solution (20 volumes) and then with water (10 volumes). The resin was suspended in water (~10 mL) and a solution of [Pt(tame)₂]Cl₄.H₂O (1.0 g) in water (10 mL) was added, followed by acetylacetonone (12 equivalents, 2.12 mL). The suspension changed from colourless to orange after 10 minutes. The reaction was stirred for 12 hours and then filtered. The residue was washed with water and the filtrate was evaporated to near dryness to yield an orange solid. Yield: 70 %. Anal. Calc. for [C₁₅H₂₉Cl₃N₆Pt]5.5H₂O.0.25HCl : C, 25.63; H, 5.77; N, 11.95; Cl, 16.39. Found: C, 25.69; H, 5.89; N, 11.96; Cl, 16.75.

NMR (δ (ppm), D₂O): ¹H: 1.09 (s, 3H, CH₃, H₁), 2.25 (s, 3H, CH₃, H₆), 2.38, (d of d plus ¹⁹⁵Pt satellites, 1H, CH₂, ²J_{H-H}=14.0 Hz, ³J_{Pt-H}=42.3 Hz), 2.60 (d, 1H, CH₂, ²J_{H-H}=12.5 Hz), 2.67 (d plus ¹⁹⁵Pt satellites, CH₂, ²J_{H-H}=13.4 Hz, ³J_{Pt-H}~22 Hz), 3.01 (d, 1H, CH₂, ²J_{H-H}=13.0 Hz), 3.40 (d plus ¹⁹⁵Pt satellites, 1H, CH₂, ²J_{H-H}=14.5 Hz, ³J_{Pt-H}=47 Hz), 3.79 (d, 1H, CH₂, ²J_{H-H}=13 Hz).

¹³C: 22.3 (s, CH₃, C₇), 25.3 (t, CH₃, C₁, ⁴J_{Pt-C1}=21 Hz), 45.7 (t, quaternary, C₂, ³J_{Pt-C2}=68 Hz), 46.8 (s, CH₂, C₅), 46.9 (s, CH₂, C₄), 56.3 (s, CH₂, C₃), 98.9 (broad resonance, CD, C₈), 162.5 (s, C_{imine}, C₆).

(b) *Hydrogenation of [2,10-tetra(aminomethyl)-5,7-dimethyl-4,8-diazaundeca-5,7-dienato]platinum(IV)] trichloride.*

[Pt(tame₂-(2,4-pentanediiminate)]Cl₃ (92 mg) was dissolved in water (50 mL) in a two-necked flask and the Pd/C catalyst (10%, ~10 mg) was introduced. The solution was purged with nitrogen for 20 minutes and then purged with hydrogen for 12 hours. The solution rapidly acquired a green colour and ~5 minutes the solution became colourless. The reaction solution was filtered in air and the residue washed with water. The filtrate was evaporated to dryness to yield a colourless powder. Yield: ~ 90 %.

NMR: (δ (ppm), D₂O) ¹H: 1.07 (s, 3H, cap CH₃), 1.15 (s, 3H, cap CH₃), 2.45 (s, 6H, strap CH₃), 2.81-3.25 (multiplet, 6H, CH₂, includes overlapping d of d's at 3.15), 3.74-4.08 (multiplet, 3H, CH₂).

¹³C: 17.6 (s, cap CH₃), 18.9 (s, cap CH₃), 23.9 (s, strap CH₃ x 2), 38.8 (s, quaternary C), 45.1 (s, CH₂) 46.3 (s, CH₂), 49.1 (s, CH₂) 49.7 (s, CH₂) 54.2 (broad t, CH/CD), 59.7 (s, CH₂) 60.3 (s, CH₂ x 2), 180.5 (s, C_{imine}).

3.3. Results

3.3.1. Pt(IV) Substitution Reactions

(a) Attempted Synthesis of $[Pt(tn)_3]^{4+}$

The attempted syntheses of the elusive tris(trimethylenediamine)platinum(IV) ion, $[Pt(tn)_3]^{4+}$, were based on modifications of the reported synthesis of $[Pt(en)_3]^{4+}$ ¹¹ and $[Pt(en)_x(pn)_{3-x}]^{4+}$ ($x=3,2,1,0$).¹³ They involved ligand substitution at $[PtCl_6]^{2-}$ in the presence of a catalytic amount of $[PtCl_4]^{2-}$, or substitution at $[PtCl_4]^{2-}$, followed by oxidation of Pt(II) to Pt(IV).

(1) Addition of excess trimethylenediamine to a solution containing $[PtCl_6]^{2-}$ in the presence of a catalytic amount of $[PtCl_4]^{2-}$ produced $[Pt(tn)Cl_2]$, *trans*- $[Pt(tn)_2Cl_2]^{2+}$ and red polymeric species. The effect of various solvents (water, ethanol, DMSO and DMF) on the outcome of the reaction was explored but in no case was the target product obtained.

(2) Substitution at $[PtCl_4]^{2-}$ by trimethylenediamine formed $[Pt(tn)Cl_2]$, which was oxidised readily with chlorine gas to form $[Pt(tn)Cl_4]$. The addition of excess trimethylenediamine to this complex in both ethanol and DMF, in the presence of a catalytic amount of $[PtCl_4]^{2-}$, gave *trans*- $[Pt(tn)_2Cl_2]^{2+}$.

The products of both methods were purified using ion exchange chromatography and fractional crystallisation. The $[Pt(tn)_3]^{4+}$ ion was not detected after workup of the 2, 4, 6 M HCl eluants and also in the 50% ethanol/HCl eluant. The products of the reactions, $[Pt(tn)_2]^{2+}$ and *trans*- $[Pt(tn)_2Cl_2]^{2+}$, were characterised by elemental analysis and ¹H and ¹³C NMR spectroscopy.

(b) Attempted Synthesis of $[Pt(stn)]^{4+}$

Reaction of $H_2[PtCl_6]$ with free stn in ethanol at 60 °C produced a red solution and evaporation to near dryness allowed a cream powder to be isolated from the red mother liquor. The ¹H NMR spectrum was poorly resolved, indicating that many products had formed. Separation of the products was not successful using SP-Sephadex cation exchange resin or by fractional crystallisation. When the powder was redissolved in water, a blood red solution was obtained. The same reaction carried out in DMF also produced a red solution. Treating the powder with neat triflic acid produced a cream pliant solid which was too insoluble to be investigated further.

(c) Attempted Direct Synthesis of [Pt(Me₅-N₆-tricosane)]⁴⁺

No substitution was evident from the reaction of K₂[PtCl₆] and free Me₅-N₆-tricosane with a catalytic amount of K₂[PtCl₄] in DMF. The free ligand was recovered after two days of reaction. Heating Me₅-N₆-tricosane in 50% water/ethanol with K₂[PtCl₆] produced a red solution, whose ¹H NMR spectrum was complicated, indicating that many products were present. Similarly, reaction of K₂[PtCl₄] and the ligand in water, DMF or ethanol as solvents¹⁵ gave rise to products whose ¹H and ¹³C NMR spectra contained many signals. Partial coordination may have occurred, to form PtN₄ or PtN₂Cl₂ species, which have been observed in attempted substitutions of Pt(II) with sar type cage ligands.¹⁰

(d) Synthesis of [Pt(tame)₂]⁴⁺

Good yields (~75%) of [Pt(tame)₂]⁴⁺ were obtained when free tame was added to a solution of K₂[PtCl₆] dissolved in warm DMF, in the presence of a catalytic amount of K₂[PtCl₄], and heated at 40° for 30 hours. When the reaction was performed using ethanol as the solvent and heated for 3 hours at 70°,¹¹ a lower yield (~60%) of the desired product was obtained, along with increased amounts of red products, possibly Pt(II) and Pt(O) species. [Pt(tame)₂]Cl₄ was characterised by elemental analysis and ¹H and ¹³C NMR spectroscopy.

3.3.2. Reactions of [Pt(tame)₂]⁴⁺ with Propanal

(a) Synthesis of [Pt(^αMe₅-N₆-tricosanetriimine)]⁴⁺

I. Properties of [Pt(^αMe₅-N₆-tricosanetriimine)]⁴⁺

The reaction of [Pt(tame)₂]Cl₄ with aqueous formaldehyde and propanal in MeCN, in the presence of triethylamine and NaClO₄ gave [Pt(^αMe₅-N₆-tricosanetriimine)]Cl₄ in reasonable yield (~50%). After removal of the organic components, the chloride salt of the complex was isolated as a colourless powder from a red-brown mother liquor. The ¹H NMR spectrum of the mother liquor indicated that many other complexes had also been formed in low yield. Separation of these complexes was not successful using SP-Sephadex cation exchange resin (0.2 M K₂SO₄ as the eluant). A slightly higher yield of [Pt(^αMe₅-N₆-tricosanetriimine)]Cl₄ was obtained when [Pt(tame)₂](CF₃SO₃)₄ was used instead of the chloride salt. The [Pt(^αMe₅-N₆-tricosanetriimine)]⁴⁺ ion is quite acidic and readily deprotonates in water, giving rise to an orange solution. The chloride and tetrachlorozincate salts of the complex are soluble in water. The BF₄⁻ and PF₆⁻ salts are sparingly soluble in MeCN and acetone, but deprotonation in these solvents still occurs, as evident from the pale orange colour of the suspensions. The [Pt(^αMe₅-N₆-tricosanetriimine)]⁴⁺ ion is stable indefinitely in aqueous solutions, pH ≤ 6.

II. Crystal Structure of $[\text{Pt}(\alpha\text{Me}_5\text{-}N_6\text{-tricosanetriimine})](\text{ZnCl}_4)_{1.5}\text{Cl}$

An X-ray crystallographic analysis of the tetrachlorozincate salt was obtained. The anions were very disordered. Crystals of the chloride salt were also obtained, but they crumbled in air. The ORTEP diagram of the cation and the atom numbering scheme are shown in Fig. 3.3. The interatomic distances and angles are listed in Tables 3.1 and 3.2, respectively. Other relevant crystallographic data are in Appendix B(I).

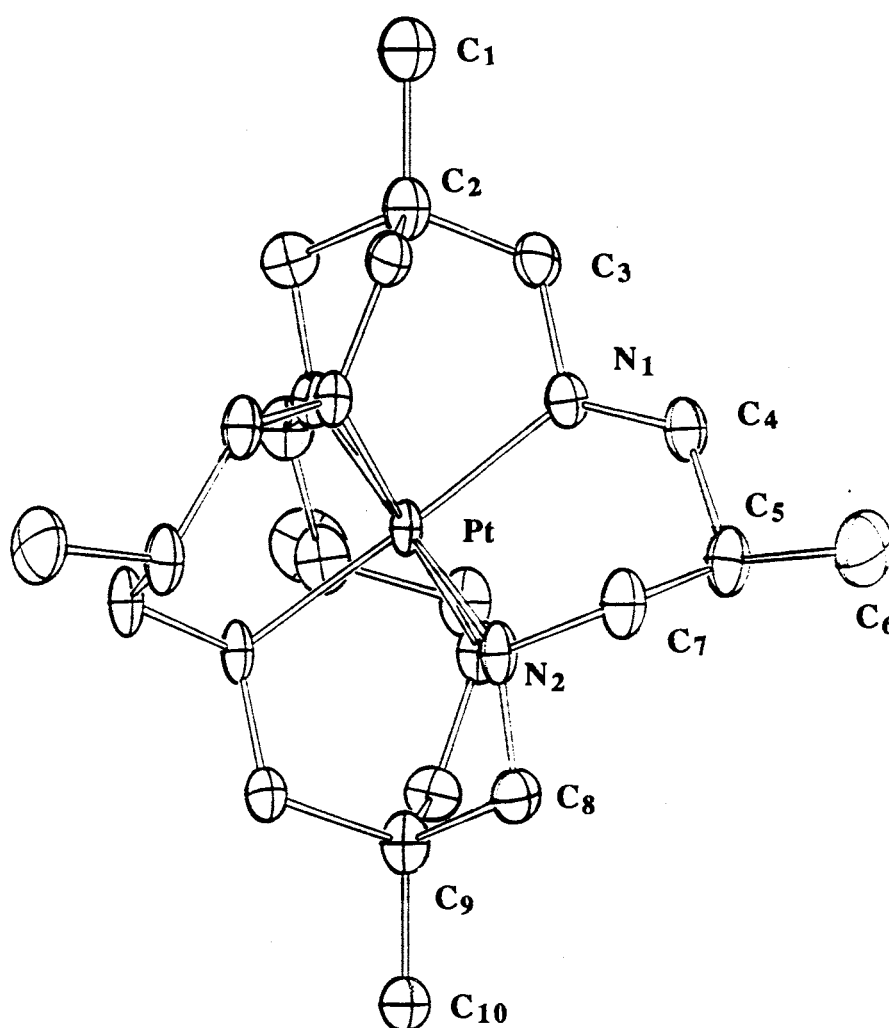


Figure 3.3: ORTEP diagram of the cation in $[\text{Pt}(\alpha\text{Me}_5\text{-}N_6\text{-tricosanetriimine})](\text{ZnCl}_4)_{1.5}\text{Cl}$.

Table 3.1: Relevant bond lengths of the cation in $[\text{Pt}(\alpha\text{Me}_5\text{-N}_6\text{-tricosanetriimine})](\text{ZnCl}_4)_{1.5}\text{Cl}$ (space group = $R\bar{3}c$).

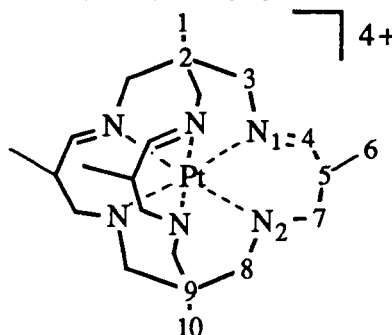
Bond Distance	(Å)
Pt-N(1)	2.051(6)
Pt-N(2)	2.083(5)

Bond Distance	(Å)	Bond Distance	(Å)
N(1)-C(3)	1.464(9)	N(2)-C(8)	1.479(9)
N(1)-C(4)	1.280(8)	N(2)-C(7)	1.459(9)
C(2)-C(1)	1.548(23)	C(10)-C(9)	1.583(20)
C(3)-C(2)	1.521(10)	C(9)-C(8)	1.548(9)
C(5)-C(4)	1.508(10)	C(7)-C(5)	1.542(11)
C(5)-C(6)	1.521(10)	Zn(2)-Cl(1)	2.245(4)
Zn(2)-Cl(2)	2.373(7)	Zn(2)-Cl(3)	2.220(7)

Table 3.2: Relevant bond angles of the cation in $[\text{Pt}(\alpha\text{Me}_5\text{-N}_6\text{-tricosanetriimine})](\text{ZnCl}_4)_{1.5}\text{Cl}$.

Bond Angles	Degrees	Bond Angles	Degrees
N(1)-Pt-N(1)'	86.7(2)	N(2)-Pt-N(2)'	88.9(2)
N(2)-Pt-N(1)	92.4(2)	N(2)-Pt-N(1)'	92.4(2)
Pt-N(1)-C(3)	115.0(5)	Pt-N(2)-C(8)	114.3(4)
Pt-N(1)-C(4)	126.1(5)	Pt-N(2)-C(7)	116.4(5)
N(1)-C(3)-C(2)	111.4(8)	N(2)-C(8)-C(9)	112.8(8)
C(4)-N(1)-C(3)	118.7(7)	C(8)-N(2)-C(7)	109.0(6)
N(1)-C(4)-C(5)	124.9	N(2)-C(7)-C(5)	114.6(6)
C(3)-C(2)-C(1)	111.9(2)	C(10)-C(9)-C(8)	107.9(6)
C(3)-C(2)-C(3)'	110.0(7)	C(8)-C(9)-C(8)'	111.0(6)
C(6)-C(5)-C(4)	111.1(7)	C(7)-C(5)-C(6)	110.9(7)
C(7)-C(5)-C(4)	109.8(6)		

§ Primes indicate atoms generated by the symmetry operation (1-x,1-y,1-z)



The $[\text{Pt}(\alpha\text{Me}_5\text{-N}_6\text{-tricosanetriimine})]^{4+}$ cation lies on a site of C_3 symmetry. The geometry about the Pt(IV) ion is slightly distorted from octahedral. The two tame residues are connected by three six-membered chelate rings at the amines (referred to as "straps"). Each of these chelate rings bears an imine, and all three imines are connected to the same tame residue on one face of the octahedron, to form the *facial*-triimine complex. The imines force the six membered chelate rings to adopt a flattened skew-boat conformation. There are seven chiral centres in the complex, three chiral centres arising from the secondary nitrogens, three from the methine carbon atoms in the strap and one from the Pt(IV) ion. From the crystal structure, the configuration about the Pt(IV) centre is Λ , all three secondary nitrogens ($3 \times \text{N}_2$) are in the *S* configuration, and the methine carbon atoms ($3 \times \text{C}_5$) of the straps are all in the *R* configuration. The numbering system presented in the crystal structure is used to describe the NMR spectra. Discounting degenerate isomers, there are 48 possible isomers, but only one is evident from this crystal structure.

III. NMR spectroscopy of $[\text{Pt}(\alpha\text{Me}_5\text{-N}_6\text{-tricosanetriimine})]^{4+}$

The chloride salt of this complex was also characterised by ^1H and ^{13}C NMR spectroscopy. The ^1H NMR spectrum of the complex in D_2O is depicted in Fig. 3.4. The DQF COSY spectrum (Fig. 3.5) was necessary for assignment of the ^1H signals and for estimating the smaller coupling constants. The ^{13}C NMR spectrum in 99% D_2O is depicted in Fig. 3.6(a). The APT (Figs 3.6(b) and 3.6(c)) and HMBC (Appendix C) spectra were helpful in assigning the ^{13}C NMR spectrum.

The nitrogen protons rapidly exchange with solvent and are not observed in D_2O . Eleven proton environments were anticipated in the ^1H NMR spectrum, but only ten were observed, as the methine proton (H_5) on the carbon atom alpha to the imine had also exchanged with D_2O . All methylene protons are magnetically inequivalent and give rise to pairs of doublets. ^{195}Pt satellites (natural abundance of $^{195}\text{Pt} = 33.8\%$, $s=1/2$) are observed in the signals at 2.16, 2.21, 3.84 and 8.86 ppm, arising from coupling with only one in each pair of methylene protons (H_{3a} , H_{7a} , H_{8a}) and the imine (H_4) ($^3J_{\text{Pt-H}_{3a}} = 42$; $^3J_{\text{Pt-H}_{7a}} = 57.5$; $^3J_{\text{Pt-H}_{8a}} = 54.4$; $^3J_{\text{Pt-H}_4} = 69.2$ Hz). The strength of the vicinal homonuclear coupling and the ^{195}Pt coupling is essentially dependent on the dihedral angle (in the latter case, Pt-N-C-H). Coupling is minimal when the dihedral angle is 90° and strongest when the angle is either 0 or 180° .¹⁶ The DQF COSY spectrum implies that long range coupling occurs between the imine proton (H_4) and the cap (H_{3a} , H_{3b}) and the strap methylene protons (H_{7a}) where $^4J_{\text{H}_{3a}\text{-H}_4} = 2.8$; $^4J_{\text{H}_{3b}\text{-H}_4} = 4.9$ and $^4J_{\text{H}_4\text{-H}_{7a}} = 4.4$ Hz. These protons are part of a "W" conformation. This conformation, in conjunction with the π -system imparted by the imine, makes an efficient pathway for coupling.¹⁶

The protons H_6 and $H_{7a,b}$ exhibit relatively simple splitting patterns in the 1H NMR spectrum and this indicates that H_5 exchanges with solvent. The signal for the strap methyl protons (H_6 , 1.4 ppm) is expected to be a doublet, but instead it is observed as a singlet. Furthermore, there are no cross or diagonal peaks observed for H_6 with H_5 in the DQF COSY spectrum. In addition, the adjacent strap methylene protons (H_{7a} and H_{7b} , centred at 2.16, 2.86 ppm) are observed as pairs of doublets ($^2J_{7a-7b} = 16.2$ Hz) and apart from the ^{195}Pt coupling with H_{7a} ($^3J_{Pt-H_{7a}} = 57.5$ Hz), there is with no additional splitting by H_5 . The coupling of the methine carbon atom (C_5) with deuterium is also evident from APT spectra (Fig. 3.6(b) and (c)). In 99% D_2O (Fig. 3.6(b)), the ^{13}C signal for this methine atom is broad (35.0 ppm) and has the same phase as the methylene and quaternary carbon atoms. When the methine carbon atom is protonated, as observed in the APT spectrum of the complex in 90% H_2O / 10% D_2O (Fig. 3.6(c)), its resonance is considerably sharper and has the same phase as the methyl and the imine carbon atoms.

Coupling of carbon atoms with the ^{195}Pt nucleus was observed for both of the quaternary carbon atoms of the caps (C_2 and C_9), the strap methine carbon atom (C_5) and, to a small degree with the imine (C_4). The largest ^{195}Pt -C coupling was with the quaternary carbon atom in the same residue connected to the saturated side of the complex, $^3J_{Pt-C_9} = 54.8$ Hz.

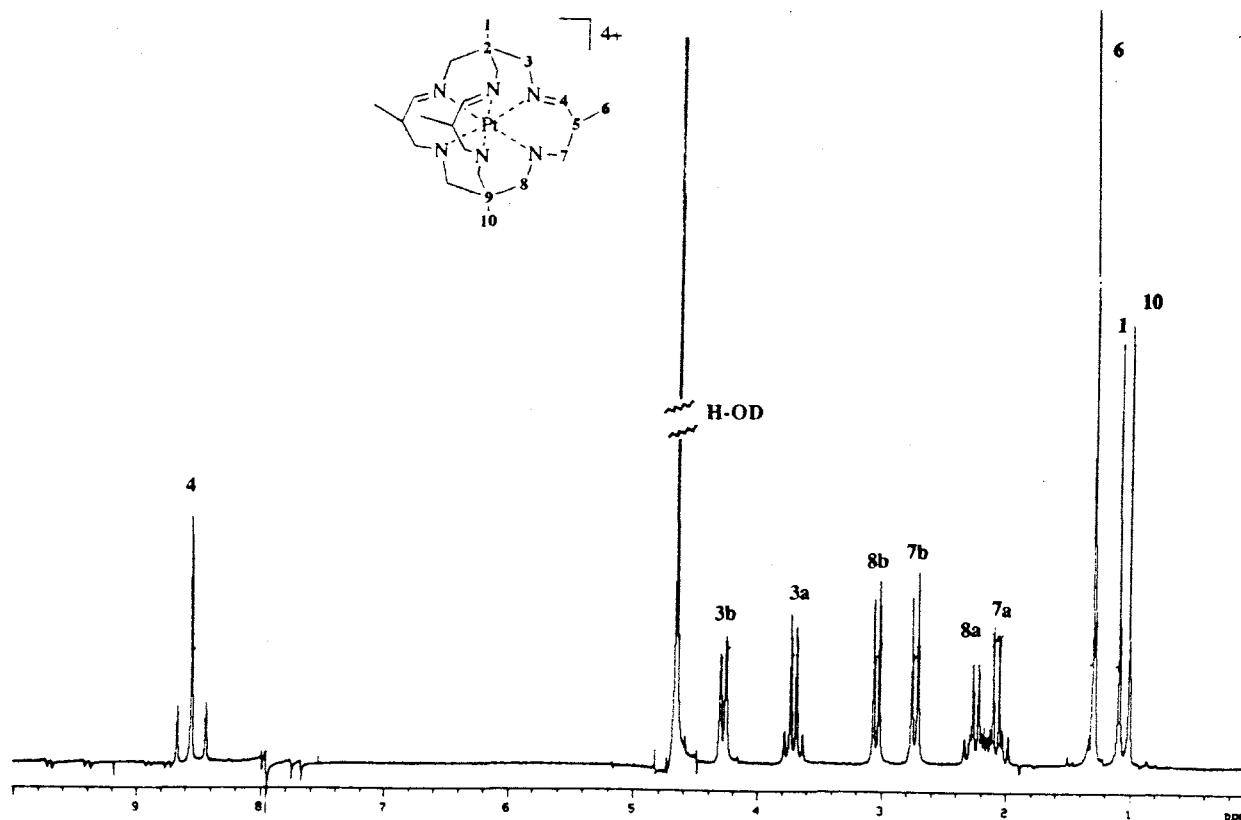


Figure 3.4: 500 MHz 1H NMR spectrum of $[Pt(\alpha Me_5-N_6\text{-tricosanetriimine})]Cl_4$, in D_2O , 293 K.

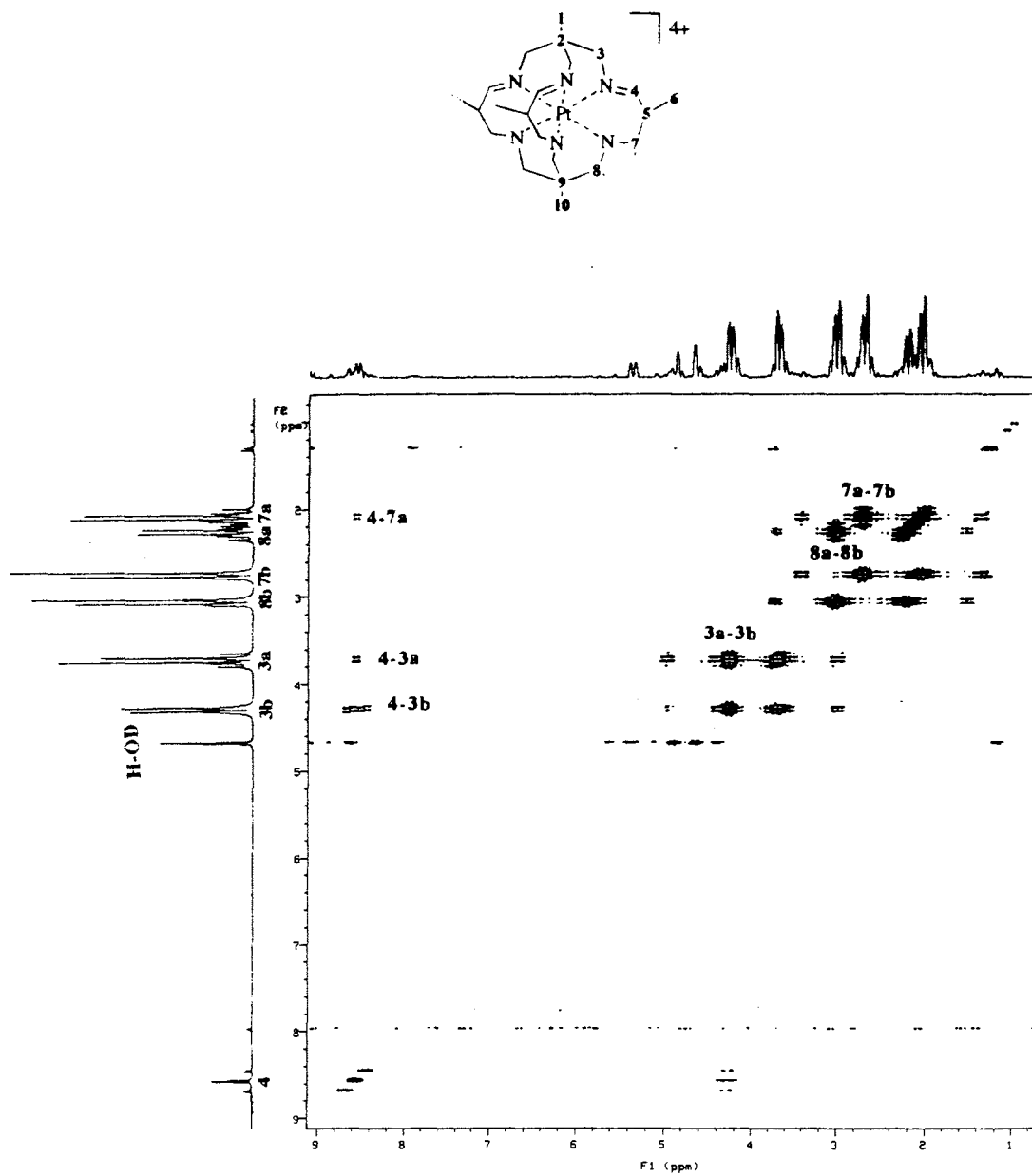


Figure 3.5: 500 MHz DQF COSY spectrum of $[\text{Pt}(\alpha\text{Me}_5\text{-N}_6\text{-tricosanetriimine})]\text{Cl}_4$ in D_2O . $n_p = 2048$, $sw = 2522.7$ Hz, $d_1 = 0.5$ s, $nt = 32$, $ni = 128$, $fn = 4096$, $fn_1 = 4096$.

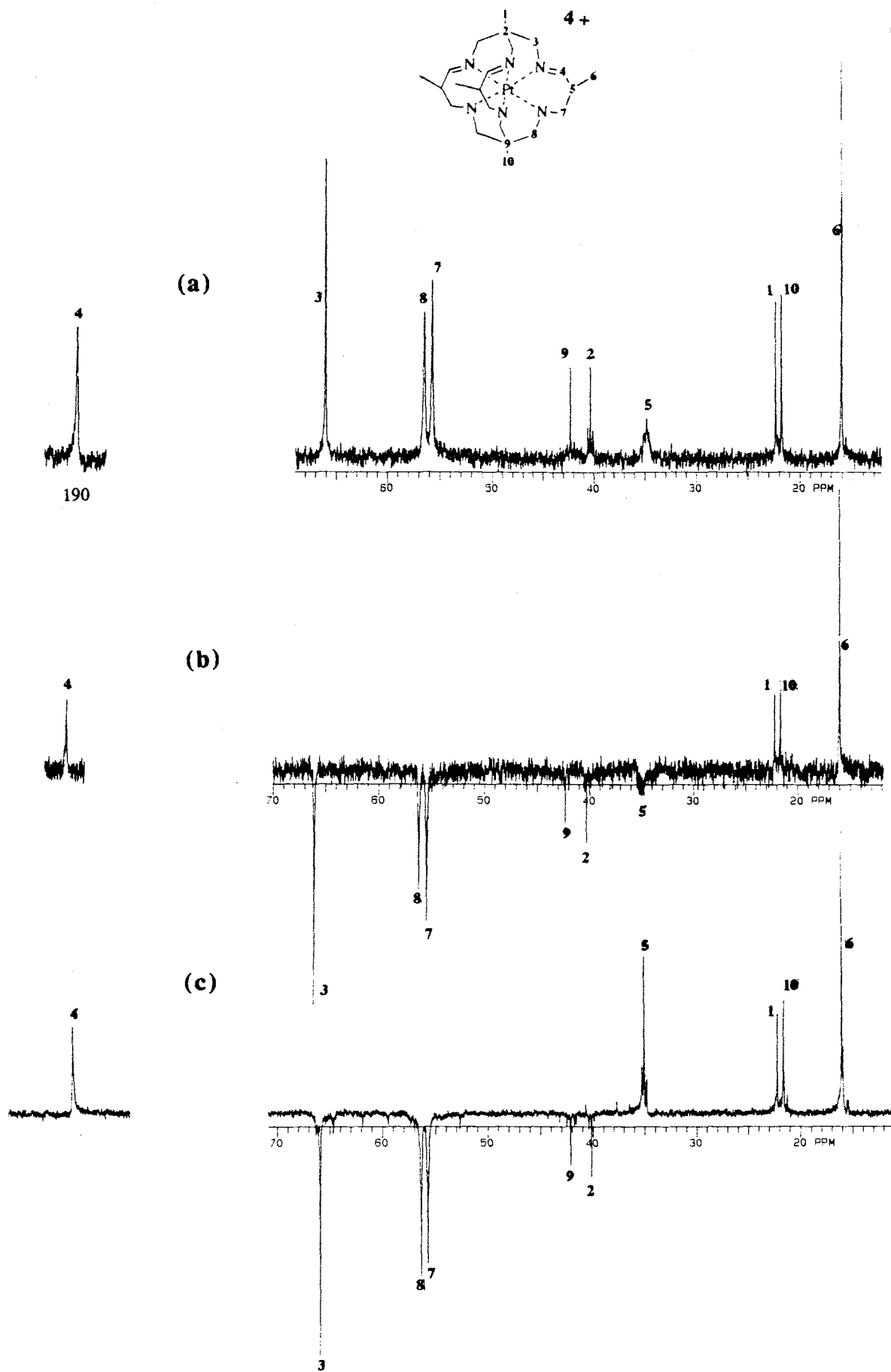


Figure 3.6: 300 MHz ^{13}C NMR Spectra of $[\text{Pt}(\alpha\text{Me}_5\text{-N}_6\text{-tricosanetriimine})]\text{Cl}_4$ (a) 99 % D_2O ; APT spectra in (b) 99 % D_2O and (c) 90% $\text{H}_2\text{O}/10\%$ D_2O .

(b) Attempted Reduction of the imines in $[Pt(\alpha Me_5-N_6-tricosanetriimine)]^{4+}$

Selective reduction of the imines in $[Pt(\alpha Me_5-N_6-tricosanetriimine)]Cl_4$ proved to be difficult using a number of different reductants that had been successful for selectively reducing imines in similar cage complexes of Co(III)¹⁷ (Chapter 5) and Cr(III) (Chapter 6). These included NaBH₄ (pH~11, aqueous media, Na₂CO₃), NaBH₃CN (pH~4, acetic acid) Na₂S₂O₄ (pH~4, acetic acid). The complicated ¹H and ¹³C NMR spectra of the products indicated that more than one species had formed during each of these reactions. These were thought to be mostly Pt(II) species, as inferred from the change in colour from orange to colourless during the reactions. The reaction of the complex using BH₄⁻ resulted in reduction of the Pt(IV) to a black solid, presumably platinum metal, which had precipitated out during the reaction and also during quenching on Dowex cation exchange resin (Na⁺ form).

Hydrogenation of the complex using H₂ over a 10% Pd/C catalyst at 275 K and atmospheric pressure in water (initially an orange solution) gave rise to a transient green (which has not yet been characterised) and then a colourless solution. It was originally thought that the reduction was incomplete after three hours, as signals in the imine region were still apparent. It was anticipated therefore, that hydrogenation at a higher pressure would completely reduce the imines. However, hydrogenation of the complex at ~8 kPa over a 10% Pd/C catalyst in water for two days at room temperature produced many different products, as inferred from the complicated ¹H NMR spectra. To investigate the processes occurring during the hydrogenation, the ¹H and ¹³C NMR spectra were acquired after 30 minutes and 2 hours of reaction.

The ¹H NMR spectra of the reaction at 0, 0.5, 2 and 16 hours are depicted in Figs 3.7(a)-(d) and the ¹³C NMR spectra acquired after 30 minutes and two hours are depicted in Figs 3.8(a)-(b). The ¹H NMR spectrum after 30 minutes (Fig. 3.7(b)), shows three new signals at 0.91, 0.98 and 1.44 ppm, in the methyl region. The signals at 0.91 and 1.44 ppm are twice the intensity of that at 0.98; the total area is consistent with 5 new methyl environments. There are also new signals at 4.98 and 8.39 ppm, which are attributed to carbinolamine and imine protons, respectively. The putative imine signal does not exhibit ¹⁹⁵Pt coupling, as did the original signal, and this implies that this imine group is not coordinated to the metal centre. After two hours of hydrogenation, signals from the original complex are no longer present. After longer periods of hydrogenation, there is an increase in the number of resonances in the NMR spectra due to decomposition products. Bubbling hydrogen through the solution in the presence of the Pd/C catalyst overnight resulted in a very complicated ¹H NMR spectrum (Fig. 3.7(d)) which did not resemble the spectra of the starting material and the first intermediate which was recorded after two hours of hydrogenation. The ¹³C NMR

spectrum after 30 minutes of hydrogenation exhibited 16 new resonances (Fig. 3.8(a)), notably, five new signals in the methyl region at 14.0, 14.6, 14.7, 17.8, 23.1 ppm and two resonances at 94.7 and at 182.3 ppm. The peak at 94.7 ppm is attributed to a carbinolamine resonance as such signals are observed in this region with cage ligands involving Co(III). The peak at 182.3 ppm is attributed to a coordinated imine carbon atom.

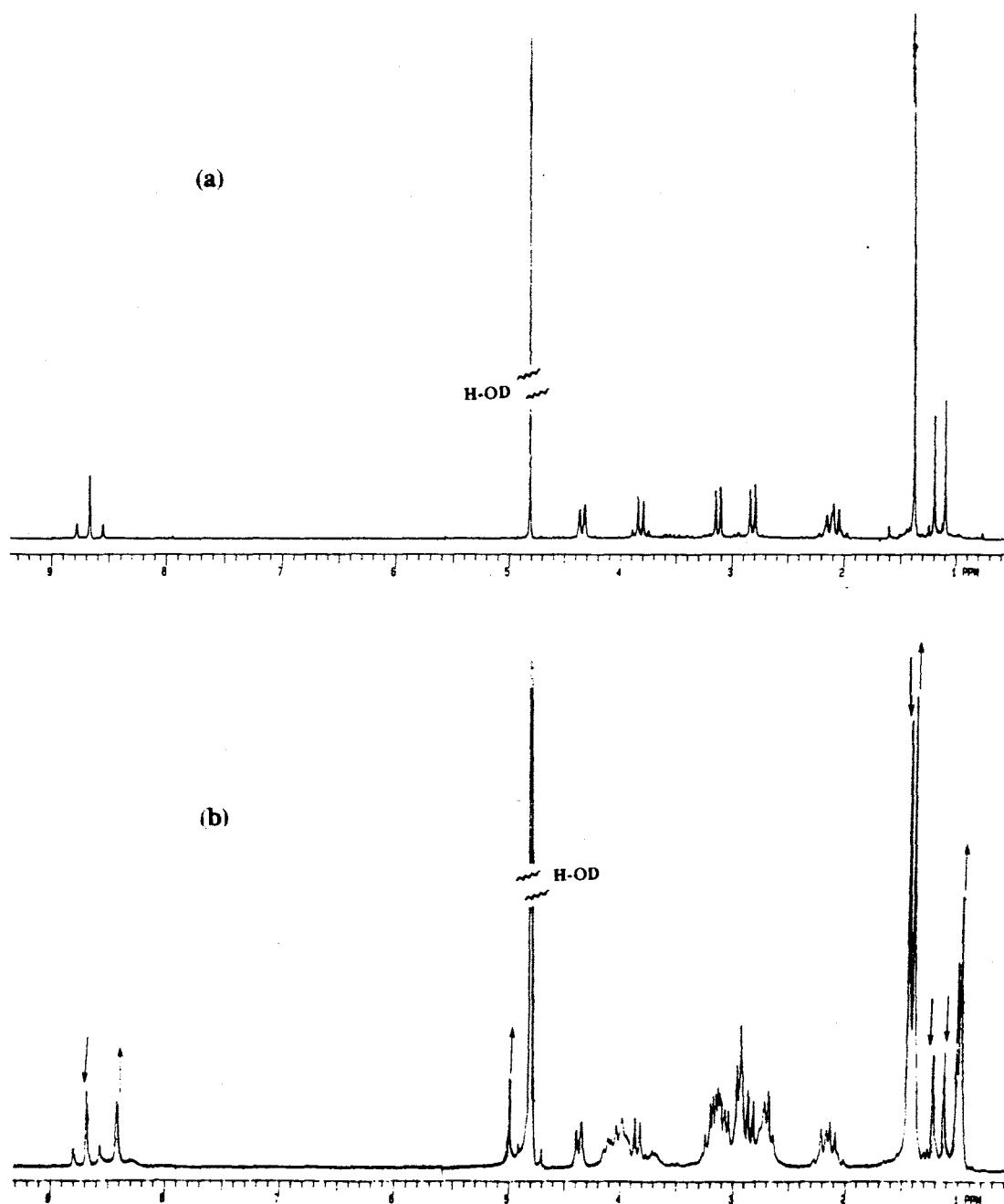


Figure 3.7: 300 MHz ^1H NMR spectra of $[\text{Pt}(\alpha\text{Me}_5\text{-}N_6\text{-tricosanetriimine})]\text{Cl}_4$ taken at (a) 0 h, (b) 0.5 h, (c), 2 h and (d) 16 h of hydrogenation in D_2O .

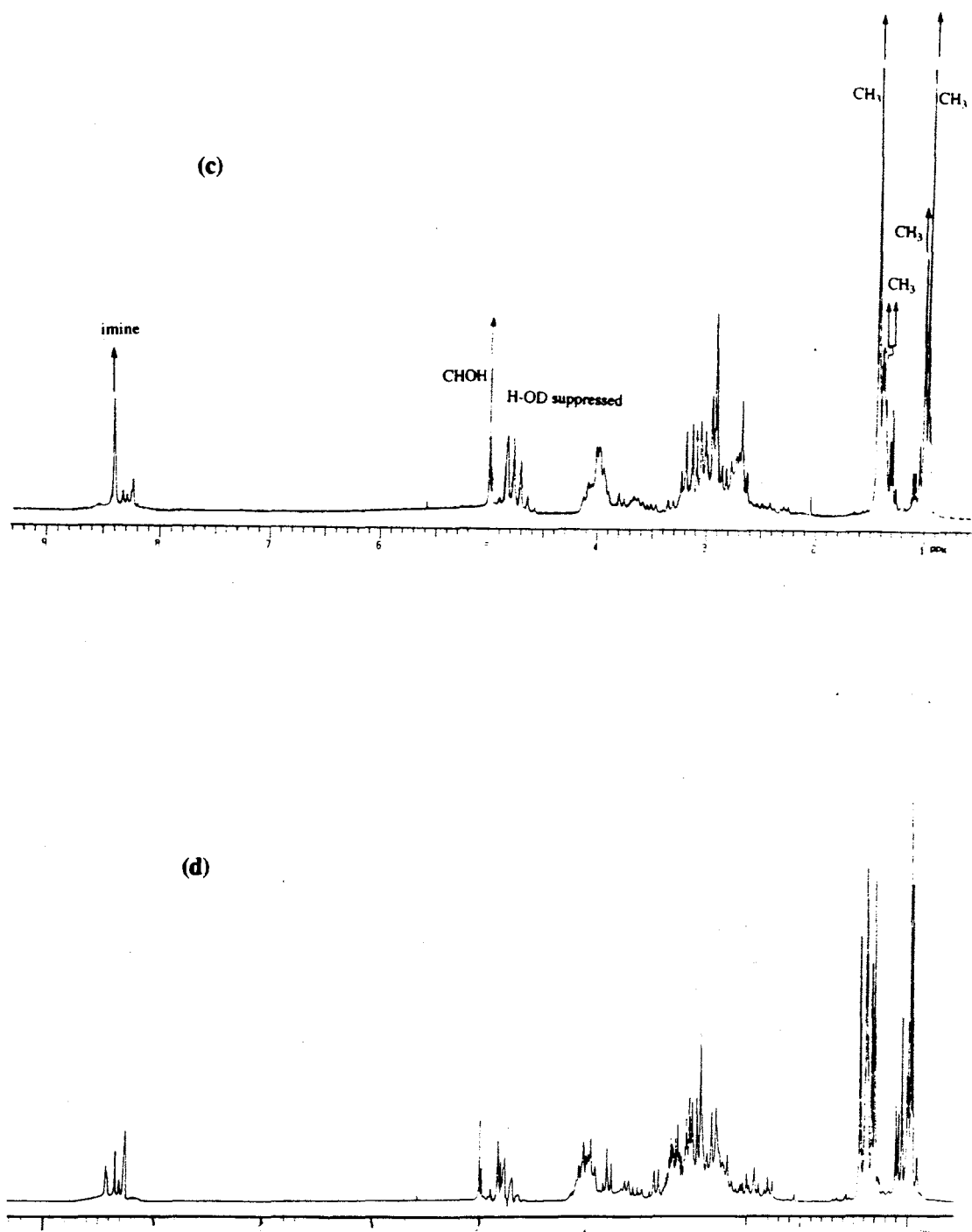


Figure 3.7: 300 MHz ^1H NMR spectra of $[\text{Pt}(\alpha\text{Me}_5\text{-N}_6\text{-tricosanetriimine})]\text{Cl}_4$ taken at (a) 0 h, (b) 0.5 h, (c), 2 h and (d) 16 h of hydrogenation in D_2O .

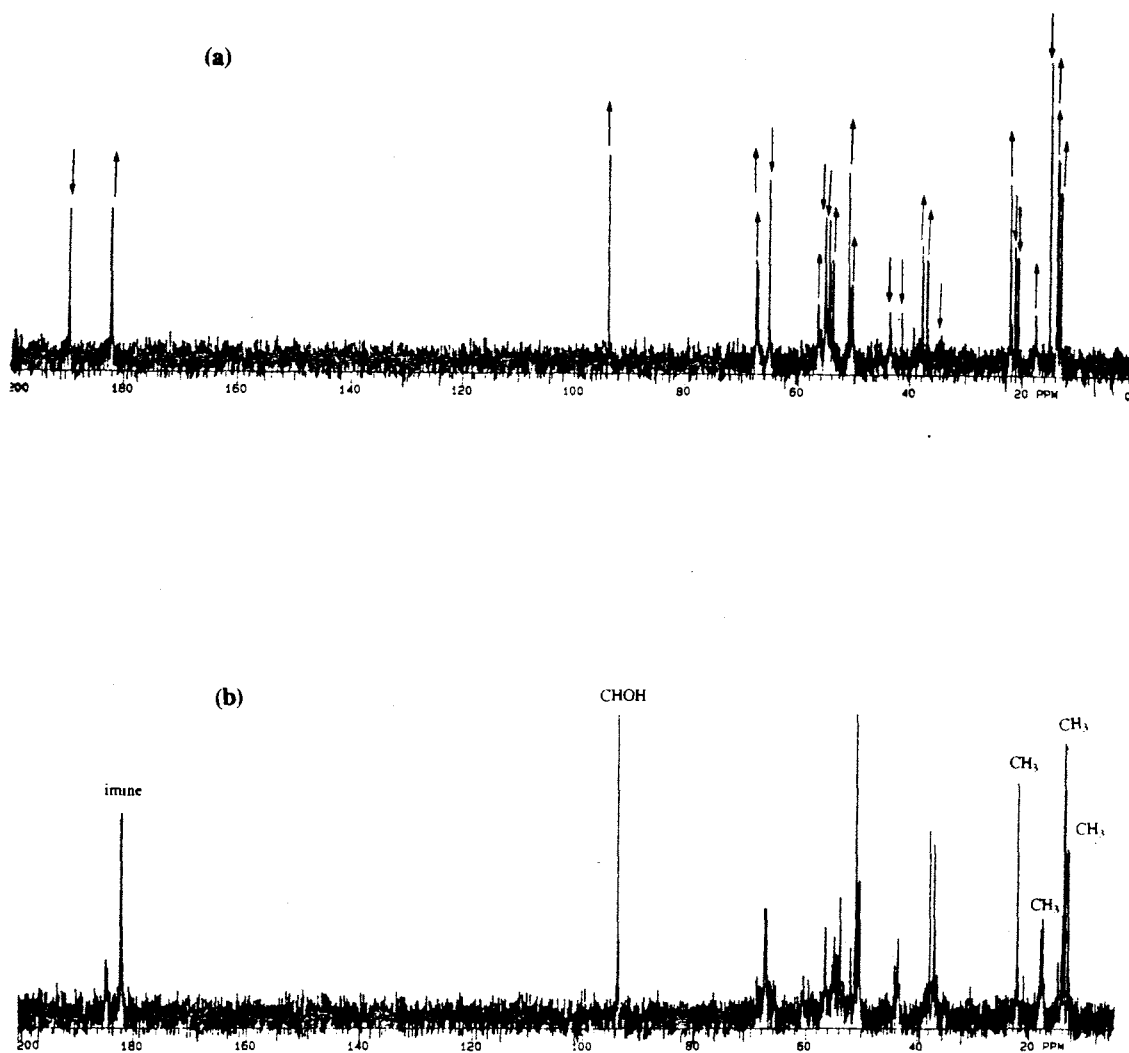


Figure 3.8: 300 MHz ^{13}C NMR spectra of $[\text{Pt}(\alpha\text{Me}_5\text{-N}_6\text{-tricosanetriimine})]\text{Cl}_4$ taken at (a) 0.5 h, (b), 2 h.

A possible structure for the first complex arising from the hydrogenation is depicted in Fig. 3.9. The proposed complex has 22 different carbon environments, but there is a pseudo mirror plane which may simplify the number of carbon signals to 16, the number observed. Rearrangement takes place after prolonged hydrogenation, to form many different products, including carbinolamine complexes and partially strapped complexes.

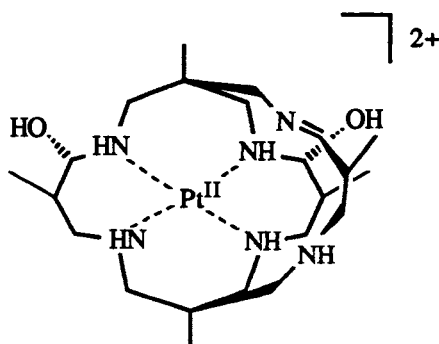


Figure 3.9: Proposed structure of the product arising after two hours of hydrogenation of $[\text{Pt}(\alpha\text{Me}_5\text{-N}_6\text{-tricosanetriimine})]^{4+}$.

(c) Synthesis of $[\text{Pt}(\text{Et}_2\text{-Me}_6\text{-N}_6\text{-tetracosanediimine})]^{4+}$

Reaction of $[\text{Pt}(\text{tame})_2](\text{CF}_3\text{SO}_3)_4$ under the conditions developed previously for the synthesis for $[\text{Co}(\text{Me}_5\text{-N}_6\text{-tricosane})]^{3+}$ (using $[\text{Co}(\text{tame})_2]^{3+}$, triethylamine, paraformaldehyde and propanal in a 1:2:5:15 ratio in MeCN),¹⁷ unexpectedly gave $[\text{Pt}(\text{Et}_2\text{-Me}_6\text{-N}_6\text{-tetracosanediimine})]\text{Cl}_4$ in reasonable yield (65%). Not surprisingly, this complex was also formed in good yield by reaction of the template $[\text{Pt}(\text{tame})_2]^{4+}$ with only propanal in the presence of a catalytic amount of triethylamine. The use of $[\text{Pt}(\text{tame})_2]\text{Cl}_4$ with NaClO_4 in MeCN gave a similar yield to that obtained when the triflate salt was used.

I. General Properties of $[\text{Pt}(\text{Et}_2\text{-Me}_6\text{-N}_6\text{-tetracosanediimine})]^{4+}$

The chloride salt of the complex has limited solubility in water, ethanol, MeCN, DMF, DMSO and acetone. The ClO_4^- , CF_3SO_3^- , BF_4^- and PF_6^- salts are even less soluble in water than the Cl^- salt, although the ClO_4^- , BF_4^- and PF_6^- salts are more soluble in MeCN and acetone. The relatively high yield of the complex allowed it to be easily separated from the by-products after initial purification on Dowex cation exchange resin (unlike condensation reactions using $[\text{Co}(\text{tame})_2]^{3+}$ and $[\text{Cr}(\text{tame})_2]^{3+}$ as the templates, where extensive chromatography using SP-Sephadex cation exchange resin was required).

The complex is quite acidic, $\text{pK}_{\text{a}(1)} = 1.8$ and $\text{pK}_{\text{a}(2)} = 9.6$ and this acidity manifests itself in a number of ways. The chloride salt is colourless, but when dissolved

in water, the complex is deprotonated, giving rise to a deep orange solution. The complex is most stable in acidic solutions, but decomposes in solutions where the $\text{pH} \geq 3$. Acidification with HCl , H_2SO_4 , $\text{CF}_3\text{SO}_3\text{H}$ and HClO_4 , in order to decrease the rate of decomposition, resulted in immediate precipitation of the much less soluble protonated complex from the orange mother liquor. In non aqueous solvents, MeCN , acetone, DMF and DMSO , deprotonation was evident from the pale orange colour of the resulting suspension. The acidity, poor solubility and the relatively slow decomposition influenced the methods used for its characterisation. The NMR and electrochemical data were acquired using low concentrations, usually of the more soluble deprotonated complex.

II. Crystal Structure of $[\text{Pt}(\text{Et}_2\text{-Me}_6\text{-N}_6\text{-tetracosanediimine-H})](\text{PF}_6)_3 \cdot 5\text{H}_2\text{O}$

An X-ray crystallographic analysis was carried out on a single crystal of the orange mono-deprotonated complex, isolated as the PF_6^- salt. Crystals of the chloride salt of the fully protonated complex were also grown, but were not suitable for X-ray crystallographic analysis. The ORTEP diagram is depicted in Fig. 3.10. The numbering scheme presented here is also used in the description of the NMR spectra. The bond lengths and angles are compiled in Tables 3.3 and 3.4. Other relevant crystallographic data are in Appendix B(II).

The X-ray structure shows that the cation has C_i symmetry. A total of six propanal units condensed with the $[\text{Pt}(\text{tame})_2]^{4+}$ template. The structure shows that two pairs of propanal molecules had condensed to form two six membered chelate rings ("straps") linking the two tame residues, in such a way that the two remaining primary amine groups were *trans* to each other. Each strap is also linked to one of these *trans* amines by a propanal residue (these links are referred to as "cross" straps) bearing imines that are *trans* to each other, to afford a new type of cage. The two *trans* straps linking the two tame caps are in the skewboat conformation and the two six membered chelate rings arising from the cross straps are in a flattened skewboat conformation. Fourteen chiral centres were generated in the reaction, ten associated with the carbon framework and four associated with the secondary nitrogens. In one half of the complex, the carbon atoms C_2 , C_6 , C_9 , C_{11} and C_{12} have *S,S,S* and *R* configurations respectively, and the secondary nitrogens N_1 and N_3 both have the *S* configuration. The chiral centres one side of the molecule have configurations enantiomeric to those on the other side of the inversion centre.

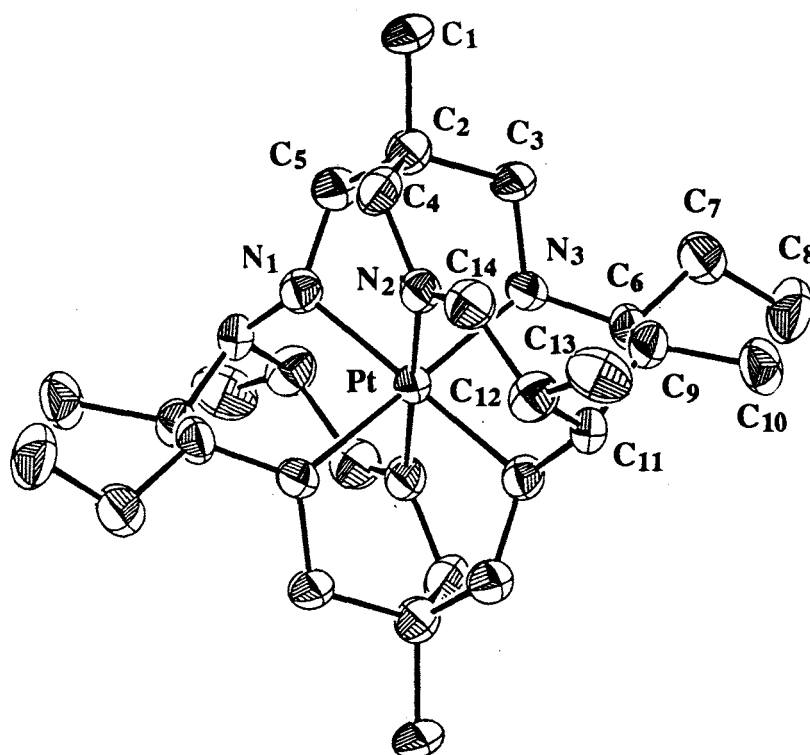


Figure 3.10: ORTEP diagram of the cation in [Pt(Et₂-Me₆-N₆-tetracosane-diimine-H)](PF₆)₃·5H₂O.

Table 3.3: Relevant bond lengths for the cation in [Pt(Et₂-Me₆-N₆-tetracosane-diimine-H)](PF₆)₃·5H₂O.[§]

Bond	Distance (Å)
Pt-N(1)	2.087(7)
Pt-N(2)	2.035(6)
Pt-N(3)	2.109(7)

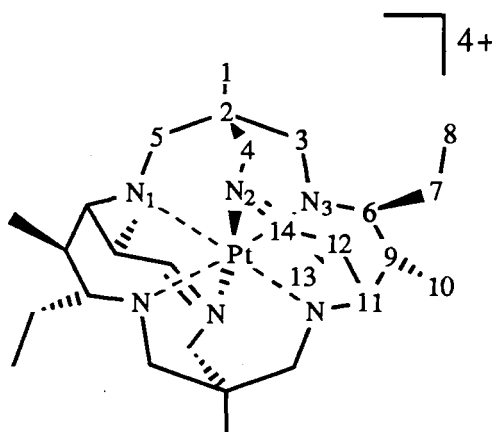
Bond	Distance (Å)	Bond	Distance (Å)
N(1)-C(5)	1.48(1)	N(1)-C(11)'	1.43(1)
N(2)-C(4)	1.46(1)	N(2)-C(14)	1.28(1)
N(3)-C(3)	1.50(1)	N(3)-C(6)	1.49(1)
C(1)-C(2)	1.56(1)	C(2)-C(5)	1.55(1)
C(2)-C(4)	1.54(1)	C(2)-C(3)	1.52(1)
C(6)-C(7)	1.53(1)	C(6)-C(9)	1.54(1)
C(7)-C(8)	1.51(1)	C(9)-C(10)	1.57(1)
C(9)-C(11)	1.54(1)	C(11)-C(12)	1.58(1)
C(12)-C(13)	1.47(1)	C(12)-C(14)	1.55(1)

[§] Primes indicate atoms generated by the symmetry operation ($1/2-x, 1/2-y, 1-z$)

Table 3.4: Relevant bond angles for the cation in [Pt(Et₂-Me₆-N₆-tetracosanediimine-H)](PF₆)₃·5H₂O.[§]

Bond Angles	Degrees	Bond Angles	Degrees
N(1)-Pt-N(2)	86.3(3)	N(1)-Pt-N(3)	93.7(3)
N(1)-Pt-N(1)'	180.0(-)	N(1)-Pt-N(2)'	93.7(3)
N(1)-Pt-N(3)'	86.3(3)	N(2)-Pt-N(3)	82.5(3)
N(2)-Pt-N(2)'	180.0(-)	N(2)-Pt-N(3)'	97.5(3)
N(3)-Pt-N(3)'	180.0(-)	Pt-N(1)-C(5)	114.5(5)
Pt-N(1)-C(11)'	114.4(5)	C(5)-N(1)-C(11)'	114.8(7)
Pt-N(2)-C(4)	115.3(5)	Pt-N(2)-C(14)	126.5(6)
C(4)-N(2)-C(14)	117.2(7)	Pt-N(3)-C(3)	113.2(5)
Pt-N(3)-C(6)	115.6(5)	C(3)-N(3)-C(6)	113.7(6)
C(1)-C(2)-C(5)	107.7(7)	C(1)-C(2)-C(4)	109.6(7)
C(1)-C(2)-C(3)	106.1(7)	C(5)-C(2)-C(4)	110.8(7)
C(5)-C(2)-C(3)	111.1(7)	C(4)-C(2)-C(3)	111.3(7)
N(1)-C(5)-C(2)	108.2(7)	N(2)-C(4)-C(2)	109.7(7)
N(3)-C(3)-C(2)	115.4(7)	N(3)-C(6)-C(7)	109.0(7)
N(3)-C(6)-C(9)	111.3(6)	C(7)-C(6)-C(9)	115.5(7)
C(6)-C(7)-C(8)	114.7(8)	C(6)-C(9)-C(10)	111.6(7)
C(6)-C(9)-C(11)	115.0(7)	C(10)-C(9)-C(11)	107.1(7)
C(9)-C(11)-C(12)	112.2(7)	C(9)-C(11)-N(1)'	111.7(7)
C(12)-C(11)-N(1)'	112.7(7)	C(11)-C(12)-C(13)	114.4(8)
C(11)-C(12)-C(14)	109.5(7)	C(13)-C(12)-C(14)	110.0(8)
N(2)-C(14)-C(12)	125.5(8)		

§ Primes indicate atoms generated by the symmetry operation ($1/2-x, 1/2-y, 1-z$)



III. NMR Spectroscopy of $[\text{Pt}(\text{Et}_2\text{-Me}_6\text{-N}_6\text{-tetracosanediimine})]^{4+}$

The NMR spectra were complicated by proton exchange with the solvent, ^{195}Pt coupling with the ^1H and ^{13}C nuclei and signals due to a decomposition product. The data from experiments using more sophisticated pulse sequences and therefore longer experimental times (2-3 days), were complicated by resonances from the decomposition product. The NMR spectra were of $[\text{Pt}(\text{Et}_2\text{-Me}_6\text{-N}_6\text{-tetracosanediimine})]\text{Cl}_4$ in D_2O which had 1-3 drops of DCl added in an attempt to retard decomposition and proton exchange. The resulting acidities of the solutions were estimated from pH indicator paper (the solutions with one drop and 3 drops of DCl were pH ~ 4 and ~ 1). Attempts to increase further the acidity of the solution using the deuterated acids DCl , D_2SO_4 and $\text{CF}_3\text{SO}_3\text{D}$, resulted in precipitation of the less soluble colourless protonated complex from the orange mother liquor. The acquisition of ^1H NMR spectra of the protonated complex in other solvents, D_6 -acetone, D_3 - MeCN-d_3 , D_7 -DMF was not achieved, as deprotonation was still evident from the orange colour of the resulting solution and the resulting signals were broader and less resolved than those obtained from the chloride salt in D_2O . The NMR data were not entirely consistent with those of the analogous Co(III) complex. It was only after the crystal structure was solved that the NMR spectra could be interpreted.

The ^1H NMR spectra in D_2O at pH ~ 4 and ~ 1 are shown in Figs. 3.11(a) and 3.11(b), respectively. In Fig. 3.11(a), most of the signals are broad and not resolved. The proton resonances for H_{11} and H_{12} are not discernible due to their exchange with solvent. The assignment of the ^1H NMR spectrum acquired at pH ~ 4 was aided by a poorly resolved DQF COSY spectrum that was acquired under the same conditions (Appendix C). In this DQF COSY spectrum, the cross peaks from the decomposition product coincided with those of the complex and were relatively intense, indicating that some coupling constants in the decomposition product were larger than those of the original material. In contrast, the DQF COSY for $[\text{Pt}(\text{Et}_2\text{-Me}_6\text{-N}_6\text{-tetracosanediimine})]^{4+}$ acquired at pH ~ 1 was relatively less complicated, as decomposition and solvent exchange were partly suppressed under these conditions (Fig. 3.12). The ^1H NMR and DQF COSY spectra of $[\text{Pt}(\text{Et}_2\text{-Me}_6\text{-N}_6\text{-tetracosanediimine})]^{4+}$ at pH ~ 1 are reminiscent of that for $[\text{Co}(\text{Et}_2\text{-Me}_6\text{-N}_6\text{-tetracosanediimine})]^{3+}$ (Chapter 5). Hence assignments of the ^1H NMR spectrum at pH ~ 1 were aided by those made for from the analogous Co(III) complex and in part for the analogous Pt(IV) complex derived from acetaldehyde (discussed later). The Co(III) complex was more stable so long experimental timescales were possible. In addition, improved resolution of the ^1H NMR spectrum was obtained using the 500 MHz NMR spectrometer. This was not possible with $[\text{Pt}(\text{Et}_2\text{-Me}_6\text{-N}_6\text{-tetracosanediimine})]^{4+}$ as the resolution decreased markedly with

the higher magnetic field due to chemical shift anisotropy. This type of behaviour is not unexpected for Pt(IV) hexaamine complexes.¹⁸⁻²⁰ A 300 MHz instrument was suitable for observing splitting patterns and to ascertain some 2J and 3J coupling constants. The signals for the methylene protons $H_{3a,3b}$ and $H_{5a,5b}$ are indistinguishable and their assignments may be interchanged. The methylene cap proton, H_{4b} , strongly couples with the imine proton in the cross strap, H_{14} ($^4J_{H_{4b}-H_{14}} \sim 3.1$ Hz), as evident from the intense cross peak in the DQF COSY spectrum. This behaviour has also been observed with analogous Pt(IV) (discussed later) and Co(III) complexes (Chapter 5).

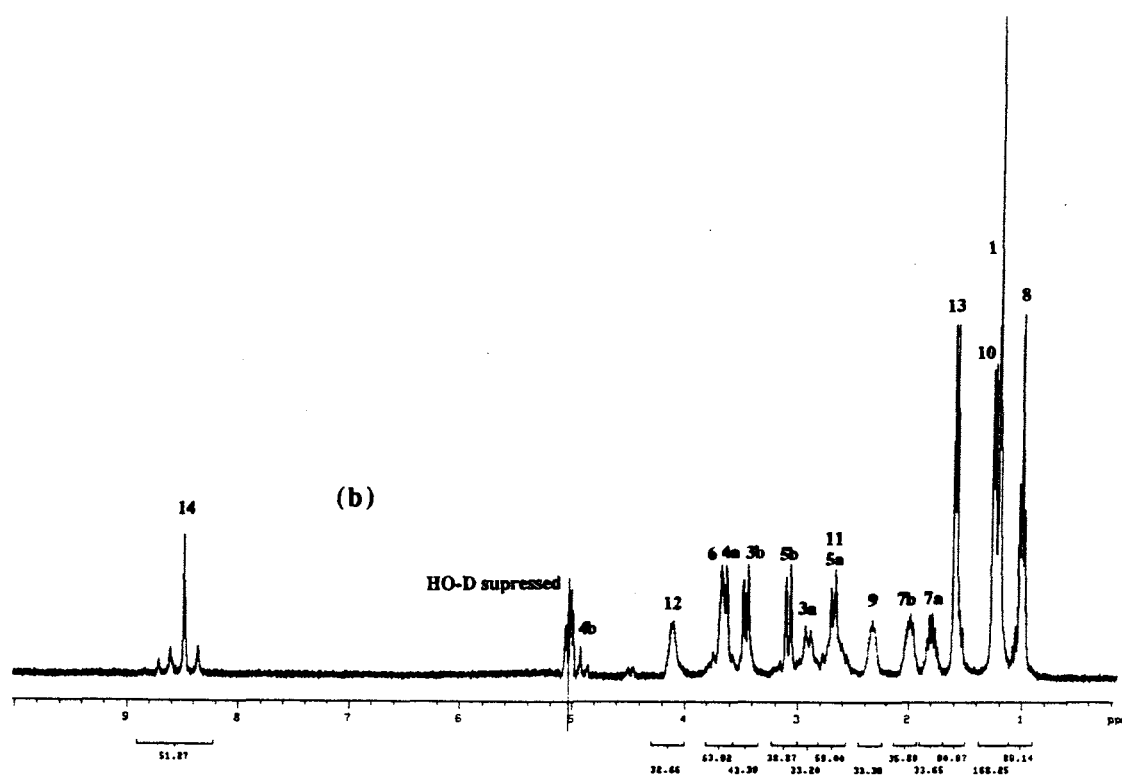
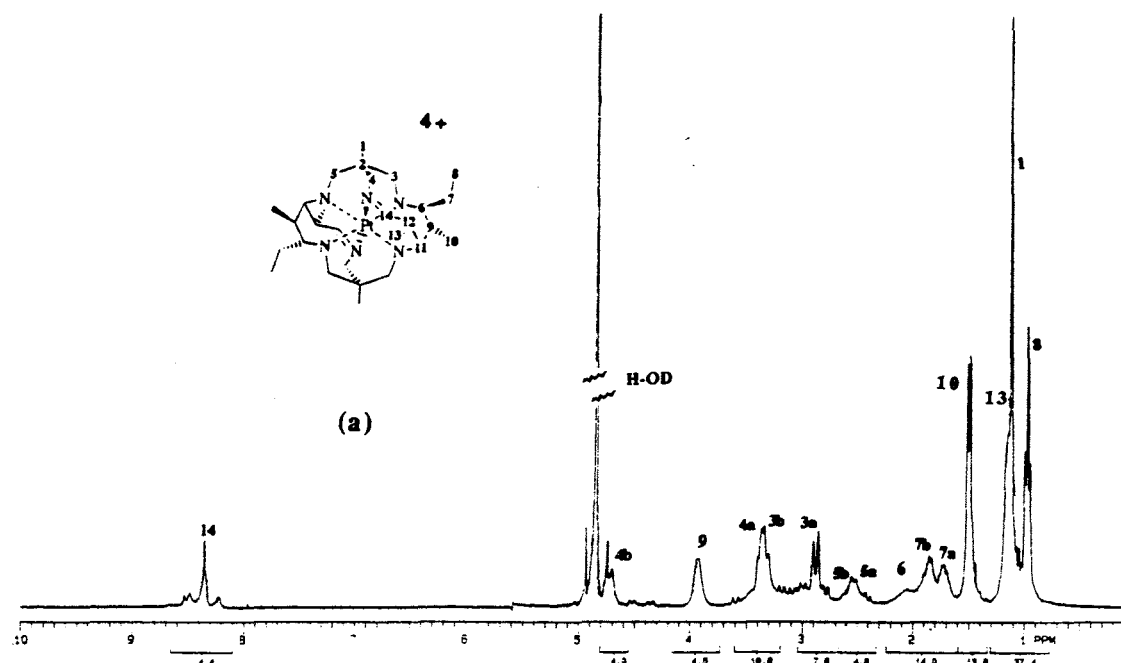


Figure 3.11: 300 MHz ^1H NMR spectrum of $[\text{Pt}(\text{Et}_2\text{-Me}_6\text{-N}_6\text{-tetracosanediimine})]\text{Cl}_4$ in D_2O at (a) pH \sim 4 and (b) pH \sim 1.

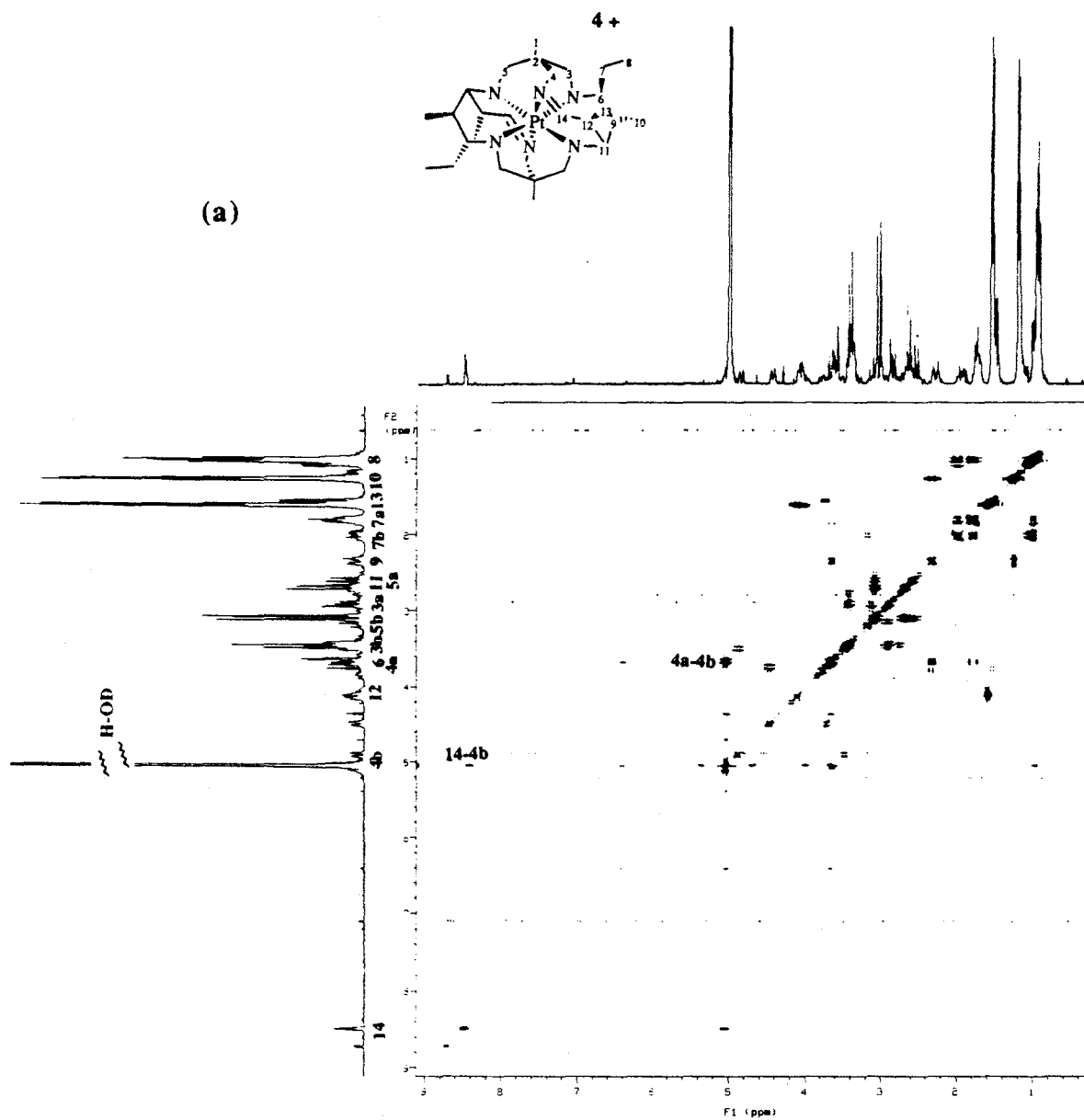
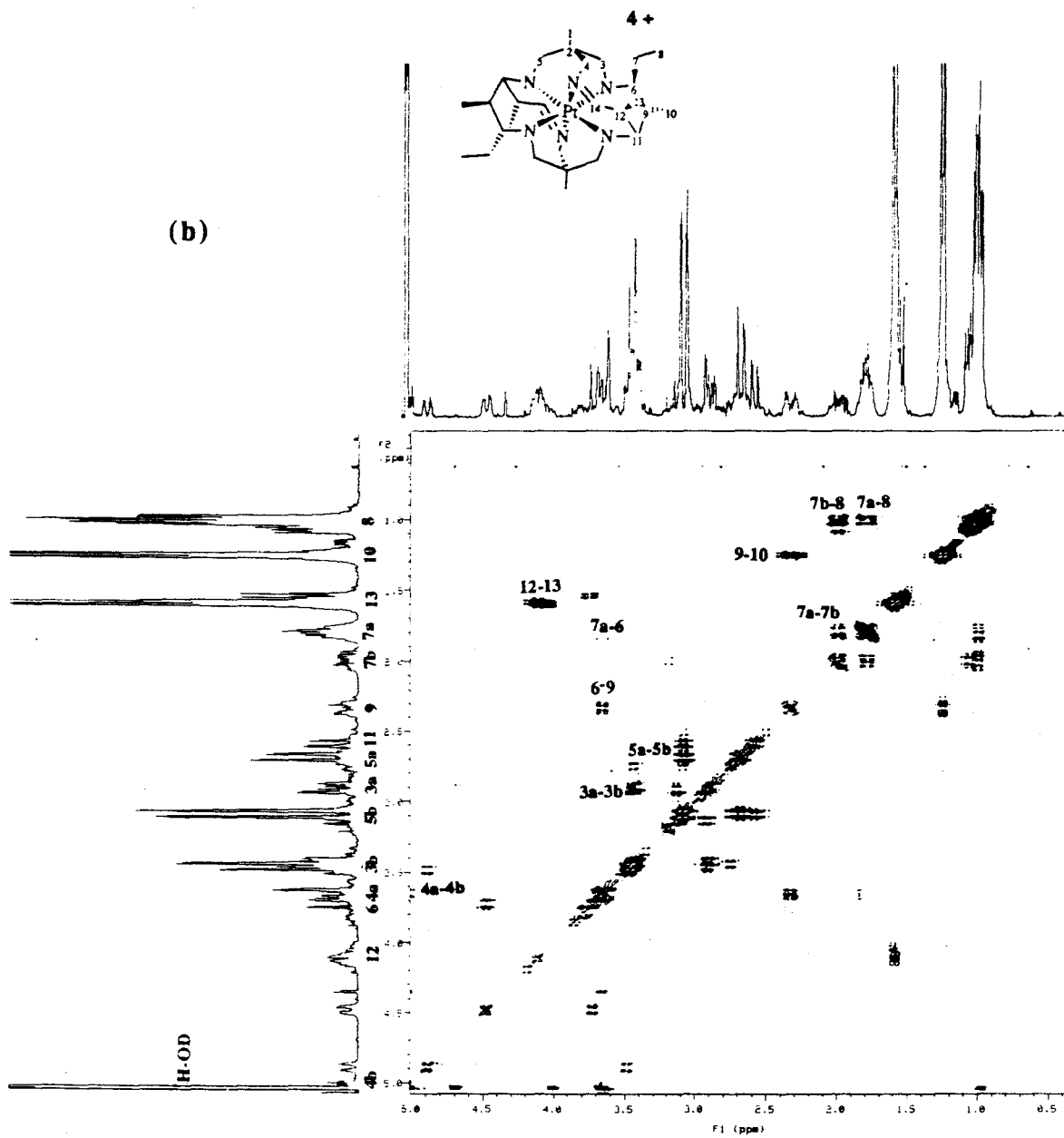


Figure 3.12: 300 MHz DQF COSY spectrum of $[\text{Pt}(\text{Et}_2\text{-Me}_6\text{-N}_6\text{-tetracosane-diimine})]\text{Cl}_4$ at pH ~1. $n_p = 2048$, $sw = 2646.9$ Hz, $d_1 = 1.2$ s, $nt = 168$, $ni = 220$, $fn = 4096$, $fn_1 = 4096$. (a) Full spectrum and (b) expanded spectrum 0–5.0 ppm (next page).



The one dimensional ^{13}C spectrum (Fig. 3.13) does not provide sufficient data to deduce the structure. In the light of the crystal structure analysis, fourteen ^{13}C resonances are expected in the ^{13}C NMR spectrum, but only 11 are discernible. Some signals are broad and overlap with other signals. In addition, the imine carbon signal was not observed in the range 0–250 ppm and a relaxation time of 5 s. The analogous signals in related Pt(IV) and Co(III) complexes occur at ~ 180 –200 ppm. The imine ^{13}C resonance was detected by indirect two dimensional NMR spectroscopic methods, namely, HMQC spectroscopy (Fig. 3.14). A cross peak at 197 ppm was obtained for the imine proton and the imine carbon atoms. The resolution of the methyl, methylene and methine groups was not important for this experiment, so the use of the 500 MHz spectrometer was justified. The relaxation time of the imine was much longer than anticipated. Complete assignment of the ^{13}C NMR spectrum so far has not been possible. The multiplicities indicated in Fig. 3.13 are derived from APT and DEPT spectra acquired at pH \sim 4 in 99 % D_2O .

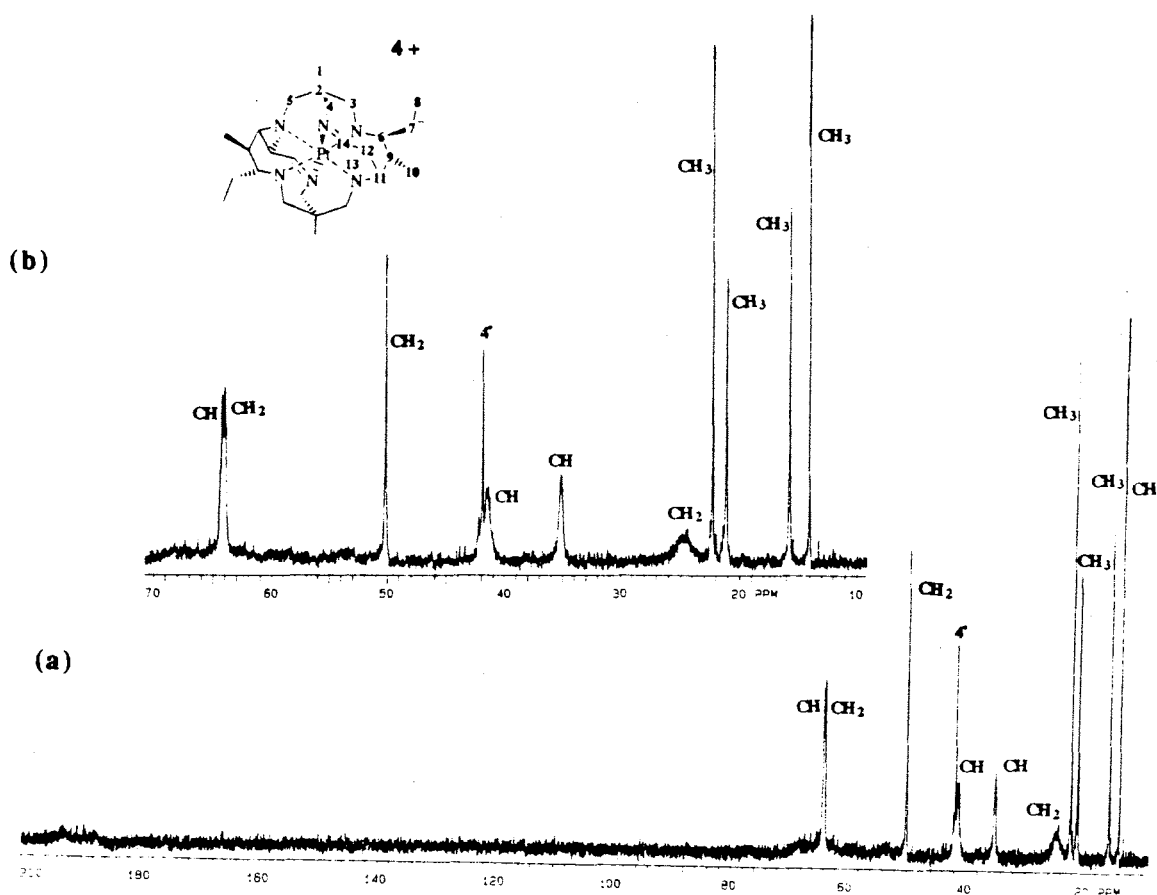


Figure 3.13: 300 MHz ^{13}C NMR spectrum of $[\text{Pt}(\text{Et}_2\text{-Me}_6\text{-N}_6\text{-tetracosanediimine})]^{4+}$ in 99% D_2O (a) 0-200 ppm, (b) expanded section.

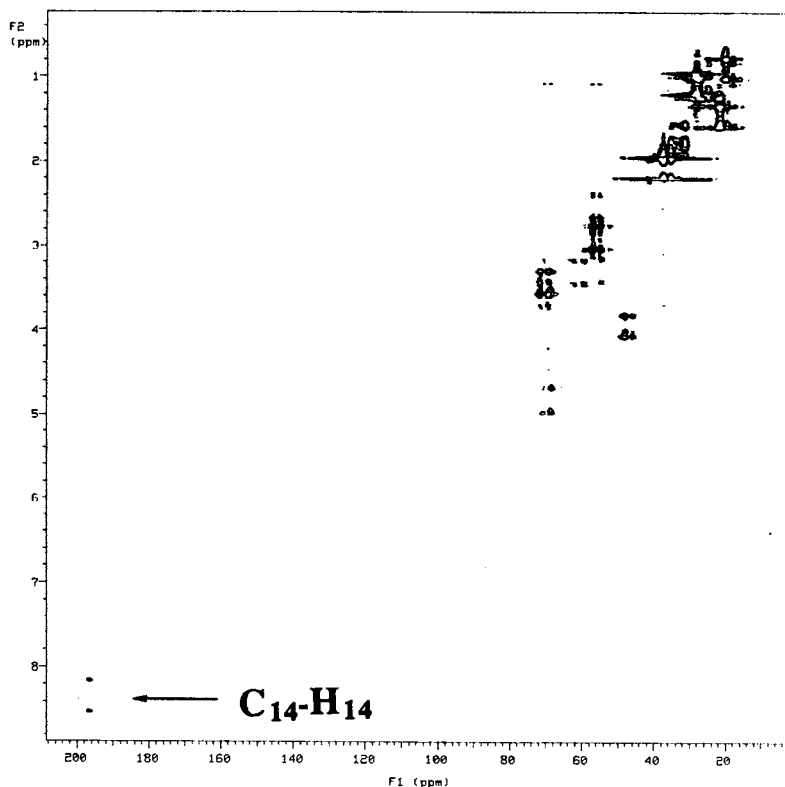


Figure 3.14: 500 MHz HMQC spectrum of $[\text{Pt}(\text{Et}_2\text{-Me}_6\text{-N}_6\text{-tetracosanediimine})]^{4+}$ in D_2O . $\text{np} = 2048$, $\text{sw} = 5000.0$ Hz, $\text{d1} = 0.8$ s, $\text{nt} = 256$, $\text{J} = 180$ Hz, $\text{ni} = 128$, $\text{fn} = 2048$, $\text{fn1} = 2048$, $\text{mbond} = \text{n}$, $\text{null} = 0.35$, $\text{taumb} = 0$.

IV. Decomposition of $[\text{Pt}(\text{Et}_2\text{-Me}_6\text{-N}_6\text{-tetracosanediimine})]^{4+}$

Aqueous solutions of $[\text{Pt}(\text{Et}_2\text{-Me}_6\text{-N}_6\text{-tetracosanediimine})]^{4+}$ (pH 3-4) left to stand at ~ 293 K after two days give rise to a product that had complicated ^1H and ^{13}C NMR spectra (Figs 3.15(a) and (b) respectively). The ^1H NMR spectrum is characterised by the presence of seven signals in the methyl region and two imine signals at 8.37 and 8.78 ppm, coupled with ^{195}Pt ($^3J_{\text{Pt-H}(8.37)} = 72.3$, $^3J_{\text{Pt-H}(8.78)} = 63.5$ Hz). In the ^{13}C NMR spectrum, there are 25 different signals, including 2 imine signals at 189.5 and 196.7 ppm. The 25 peaks in the ^{13}C NMR spectrum indicate that the complex is asymmetric and the microanalysis of this complex gave a C:N ratio of 25:6. The loss of a propanal residue is consistent with the 25 carbon atoms indicated by the ^{13}C NMR spectrum and its microanalysis. Treatment of this complex with an excess of propanal and an equivalent of base in MeCN regenerated $[\text{Pt}(\text{Et}_2\text{-Me}_6\text{-N}_6\text{-tetracosanediimine})]^{4+}$. It is therefore proposed that this decomposition product is also an intermediate in the formation of the cage complex.

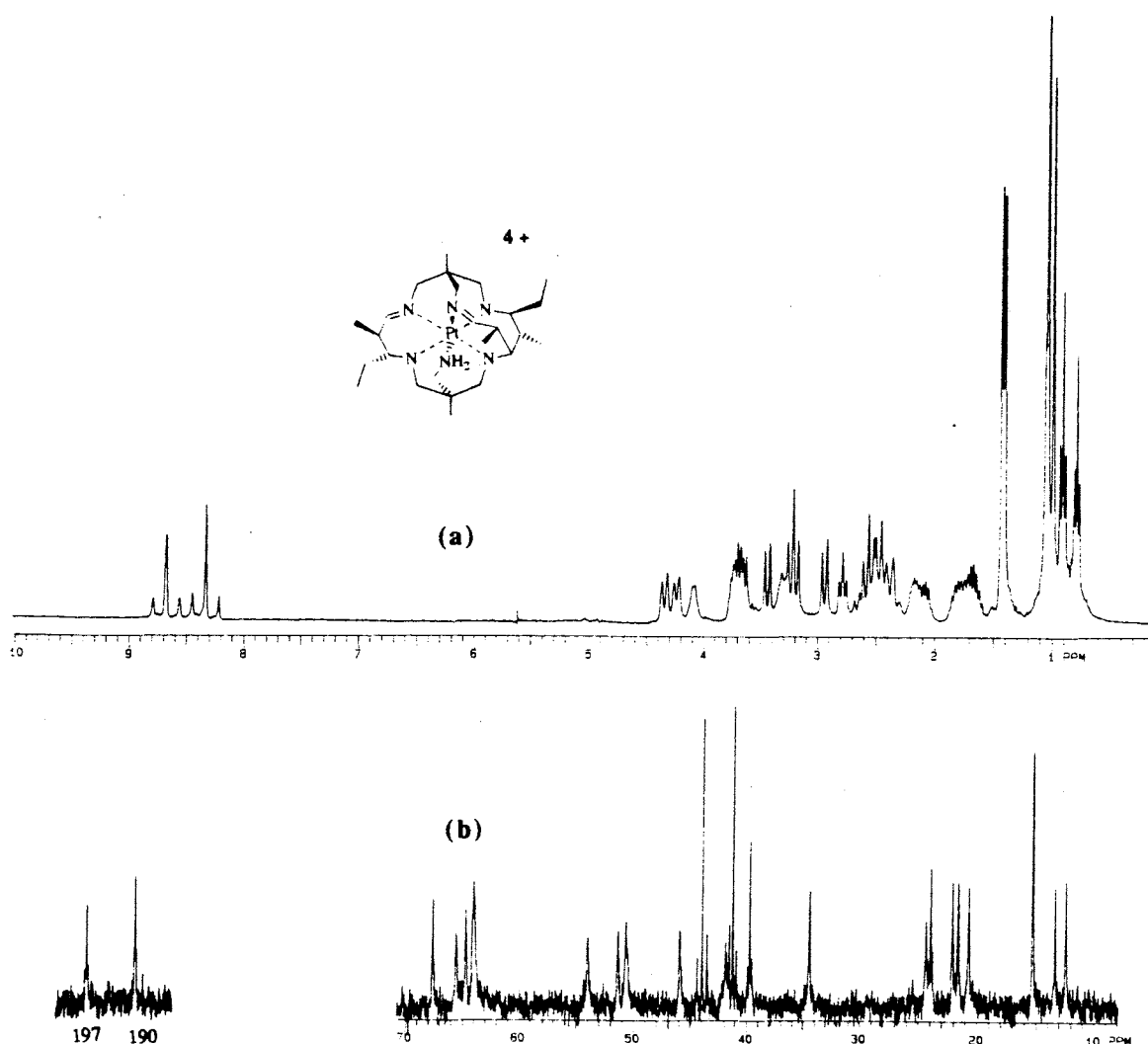


Figure 3.15: 300 MHz (a) ^1H and (b) ^{13}C NMR spectrum of the decomposition product of $[\text{Pt}(\text{Et}_2\text{-Me}_6\text{-N}_6\text{-tetracosanediimine})]^{4+}$, in D_2O .

(b) Reduction of the $[\text{Pt}(\text{Et}_2\text{-Me}_6\text{-N}_6\text{-tetracosanediimine})]^{4+}$

Selective reduction of the imine groups in $[\text{Pt}(\text{Et}_2\text{-Me}_6\text{-N}_6\text{-tetracosanediimine})]^{4+}$ proved difficult. Treatment with NaBH_4 at high pH (as for the Co(III) cages) formed a number of different products and the NMR spectra of the reaction solution after chromatography on Dowex cation exchange resin (Na^+ form) implied that they have low symmetry. As the reduction proceeded, the colour changed from orange to colourless, indicating that the Pt(IV) was reduced to various Pt(II) species, accompanied by extensive ligand rearrangement. When the complex was exposed to BH_4^- for more than 15 minutes, a black solid precipitated, presumably platinum metal. Milder and more imine-selective reductants ($\text{S}_2\text{O}_4^{2-}$ and NaBH_3CN at

pH 3-4) also gave a variety of complexes with ruptured ligands, as evident from the complicated NMR spectra of the products. A possible pathway involves initial reduction of Pt(IV) to Pt(III) followed by disproportionation to form Pt(II) and Pt(IV) complexes, while the ligand ruptures, by analogy with the $[\text{Pt}(\text{NHOH})_2\text{sar}]^{4+}$ electrochemistry.¹

Hydrogenation of $[\text{Pt}(\text{Et}_2\text{-Me}_6\text{-N}_6\text{-tetracosanediimine})]^{4+}$ over a 10% Pd/C catalyst in water (pH 3-4) at ~275 K at one atmosphere pressure gave rise to a transient green and then to a colourless solution, which after filtration of the catalyst and solvent evaporation, afforded a colourless powder whose NMR spectra were consistent with one product containing no imines. The nature of the green intermediate has not yet been elucidated. The process is exothermic and decomposition occurs rapidly if the reaction temperature is higher than ~278 K.

Bulk electrolysis of the $[\text{Pt}(\text{Et}_2\text{-Me}_6\text{-N}_6\text{-tetracosanediimine})]^{4+}$ in 1 M H_2SO_4 using a mercury pool electrode at -800 mV vs SCE, after ion exchange chromatography gave a single complex whose ^{13}C NMR spectrum was identical to the above hydrogenated complex obtained at 275 K. After 3.5 hours, the rate of accumulation of current was very slow, even though only 1.5 electrons per Pt complex had been consumed, instead of the anticipated two. This was attributed to passivation of the mercury surface by the product and this aspect is discussed in more detail in Chapter 4. The NMR spectral evidence indicates that this product is the same complex as that obtained from the hydrogenation of $[\text{Pt}(\text{Et}_2\text{-Me}_6\text{-N}_6\text{-tetracosanediimine})]^{4+}$.

I. Properties of pentacyclo- $[\text{Pt}^{\text{II}}(\text{Et}_2\text{-Me}_6\text{-N}_6\text{-tetracosaneH}_2)]^{4+}$

The chloride salt of the complex was isolated as a colourless powder from a colourless mother liquor. It was more stable, less acidic and the chloride salt was marginally more soluble in water than its parent diimine complex.

II. Crystal Structure of pentacyclo- $[\text{Pt}^{\text{II}}(\text{Et}_2\text{-Me}_6\text{-N}_6\text{-tetracosaneH}_2)]\text{Cl}_4 \cdot 9\text{H}_2\text{O}$

The X-ray crystallographic analysis of crystals of the product obtained from the hydrogenation reaction showed that it was a complicated [16]ane N_4 square planar Pt(II) complex, in which the N_6 -tetracosanediimine ligand had undergone a complicated rearrangement to form a macropentacycle. No ligand rupture was evident. The interatomic distances and angles of the cation are listed in Table 3.5. Other crystallographic data is compiled in Appendix B(III). The ORTEP diagram of the cation is depicted in Fig. 3.16.

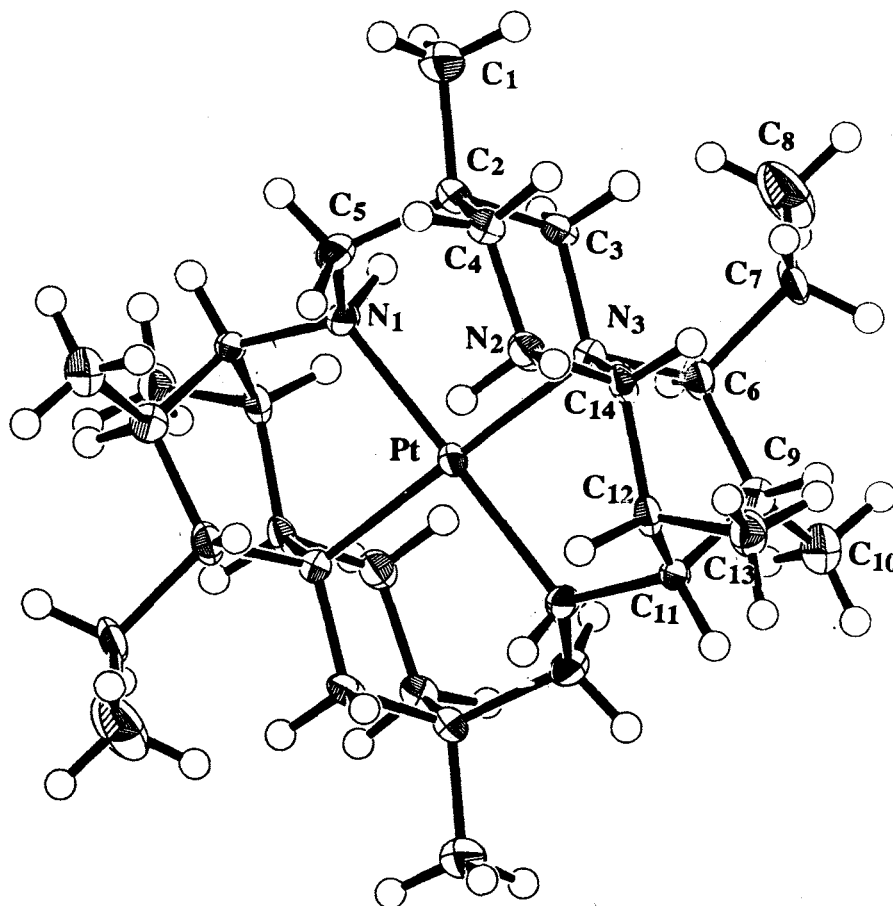


Figure 3.16: ORTEP diagram of the cation of the pentacyclo-[Pt^{II}(Et₂-Me₆-N₆-tetracosaneH₂)]Cl₄.9H₂O.

Table 3.5: Relevant bond lengths for the cation in pentacyclo-[Pt^{II}(Et₂-Me₆-N₆-tetracosaneH₂)]Cl₄.9H₂O (space group is R $\bar{3}$ (#148)).

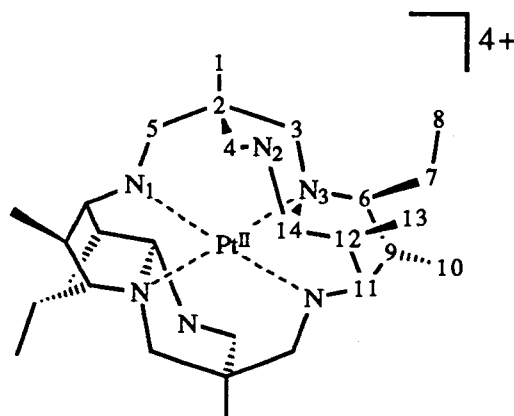
Bond Distance	(Å)
Pt-N(1)	2.061(7)
Pt-N(3)	2.092(7)
Pt-N(2) [§]	3.354(7)

§, non bonding Pt-N.

Bond Distance	(Å)	Bond Distance	(Å)
N(1)-C(5)	1.46(1)	C(2)-C(3)	1.53(1)
N(2)-C(4)	1.50(1)	C(6)-C(7)	1.55(1)
N(3)-C(3)	1.480(10)	C(7)-C(8)	1.54(1)
N(1)-C(11)	1.48(1)	C(6)-C(9)	1.56(1)
N(2)-C(14)	1.48(1)	C(9)-C(10)	1.51(1)
N(3)-C(6)	1.57(1)	C(9)-C(11)	1.51(1)
N(3)-C(14)	1.487(10)	C(11)-C(12)	1.57(1)
C(1)-C(2)	1.54(1)	C(12)-C(13)	1.52(1)
C(2)-C(5)	1.56(1)	C(12)-C(14)	1.55(1)
C(2)-C(4)	1.51(1)		

Table 3.6: Relevant bond angles for the cation in pentacyclo-[Pt^{II}(Et₂-Me₆-N₆-tetracosaneH₂)]Cl₄.9H₂O.

Bond Angles	Degrees	Bond Angles	Degrees
N(1)-Pt-N(3)	88.5(3)	C(4)-C(2)-C(3)	106.8(7)
N(3)-C(3)-C(2)	114.0(7)	Pt-N(1)-C(5)	111.0(5)
N(3)-C(6)-C(7)	114.3(7)	Pt-N(1)-C(11)	113.6(5)
N(3)-C(6)-C(9)	110.5(6)	Pt-N(3)-C(3)	111.7(5)
C(7)-C(6)-C(9)	109.5(7)	Pt-N(3)-C(6)	107.5(5)
C(6)-C(7)-C(8)	114.3(8)	Pt-N(3)-C(14)	110.8(5)
C(6)-C(9)-C(10)	112.3(7)	C(5)-N(1)-C(11)	116.6(7)
C(6)-C(9)-C(11)	111.9(7)	C(4)-N(2)-C(14)	115.6(7)
C(10)-C(9)-C(11)	118.7(8)	N(1)-C(11)-C(12)	108.7(7)
N(1)-C(11)-C(9)	114.9(8)	C(3)-N(3)-C(6)	108.8(6)
N(1)-C(5)-C(2)	113.4(7)	C(3)-N(3)-C(14)	109.3(6)
C(9)-C(11)-C(12)	109.5(7)	C(6)-N(3)-C(14)	108.7(6)
C(11)-C(12)-C(13)	111.9(7)	C(1)-C(2)-C(5)	109.3(7)
C(11)-C(12)-C(14)	110.0(7)	C(1)-C(2)-C(4)	107.9(7)
C(13)-C(12)-C(14)	110.4(7)	C(1)-C(2)-C(3)	107.0(7)
N(2)-C(14)-N(3)	109.9(6)	C(4)-C(2)-C(3)	106.8(7)
N(2)-C(4)-C(2)	111.4(7)	C(5)-C(2)-C(4)	110.8(7)
N(2)-C(14)-C(12)	108.0(6)	C(5)-C(2)-C(3)	114.7(7)
N(3)-C(14)-C(12)	112.9(7)		



The complex cation lies on a centre of inversion. There are 16 stereogenic centres in the complex, twelve associated with the carbon sites on the ligand and four associated with the coordinating nitrogen sites. The configurations about C₂, C₆, C₉, C₁₁, C₁₂ and C₁₄ are S,S,S,S,R and R, respectively. The configurations about the coordinating nitrogen atoms N₁ and N₃ are R and S, respectively. All configurations about the chiral centres are the same as those for the parent Pt(IV) diimine, except for N₁. The configurations of the chiral centres on one side of the Pt(II) centre are catoptric

to those on the other side. The nitrogen donor atoms originating from the imines in the cross straps are no longer coordinated to the Pt(II) ion and lie on opposite sides of the PtN_4^{2+} plane at a distance 3.354 Å from the Pt(II) ion. These nitrogen atoms are protonated so the overall charge of the cation is 4+. Each cross strap is fused with one of the chelate rings in the same cap. The conformation of the unfused chelate ring in the same cap is skew boat and the ring fused with the strap is in the chair conformation. The six-membered chelate rings in the straps and cross straps are in chair conformations. The rings are unable to undergo conformational changes and this results in a rather rigid complex.

III. NMR Spectroscopy of pentacyclo-[Pt^{II}(Et₂-Me₆-N₆-tetracosaneH₂)]⁴⁺

Unlike the parent diimine structure, no proton exchange with the solvent was evident from the NMR spectra. The ¹H NMR spectra of the products obtained from the electrochemical reduction and the hydrogenation are both complicated by overlapping peaks and unusual splitting patterns (Figs 3.17(a) and 3.17(b)). The spectra are very similar, although they are not identical. The ¹H NMR spectrum appears to be slightly sensitive to acid, however, the solution containing the hydrogenated complex (Fig. 3.17(b)) is less acidic than that of the electrolysed complex (Fig. 3.17(a)). The connectivities of the spin systems in both samples are identical, as ascertained from their DQF COSY spectra. The DQF COSY spectrum of the hydrogenated product is depicted in Fig. 3.18, and that of the electrochemically reduced complex is in Appendix C. Assignment of the ¹H NMR spectra was aided by the improved resolution at 500 MHz compared to that obtained at 300 MHz. The assignments for the pairs of cap methylene protons H_{3a,b} and H_{5a,b} may be interchanged. The anticipated fourteen peaks were all observed in the ¹³C NMR spectra for both complexes and the peak positions are identical. The ¹³C NMR spectrum of the hydrogenated product is depicted in Fig. 3.19, which was assigned from the HMQC spectrum (Appendix C).

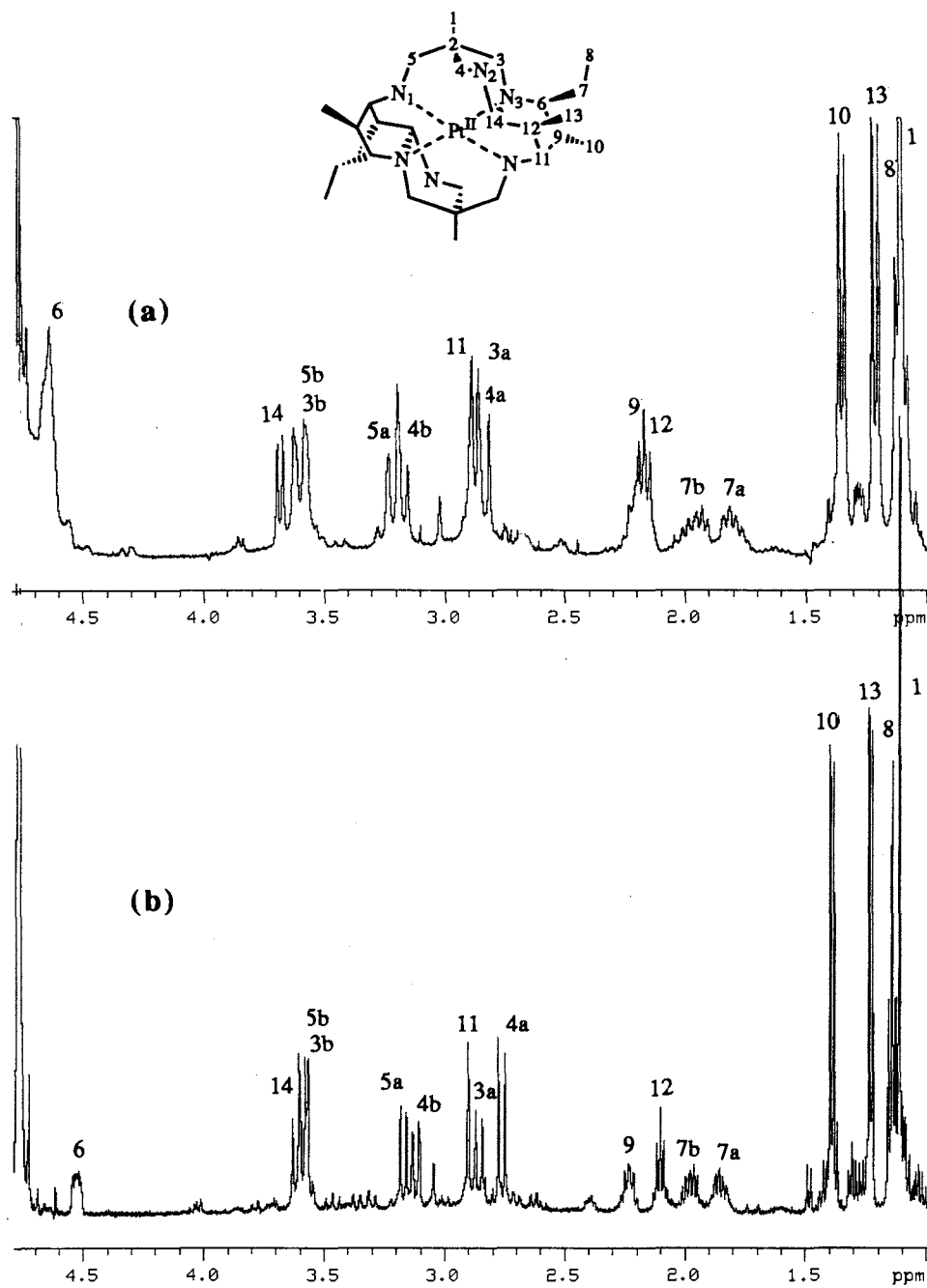


Figure 3.17: ¹H NMR spectra of pentacyclo-[Pt^{II}(Et₂-Me₆-N₆-tetracosaneH₂)]⁴⁺ formed from (a) electrochemical reduction (300 MHz) and (b) hydrogenation (500 MHz) of [Pt(Et₂-Me₆-N₆-tetracosanediimine)]⁴⁺ (D₂O).

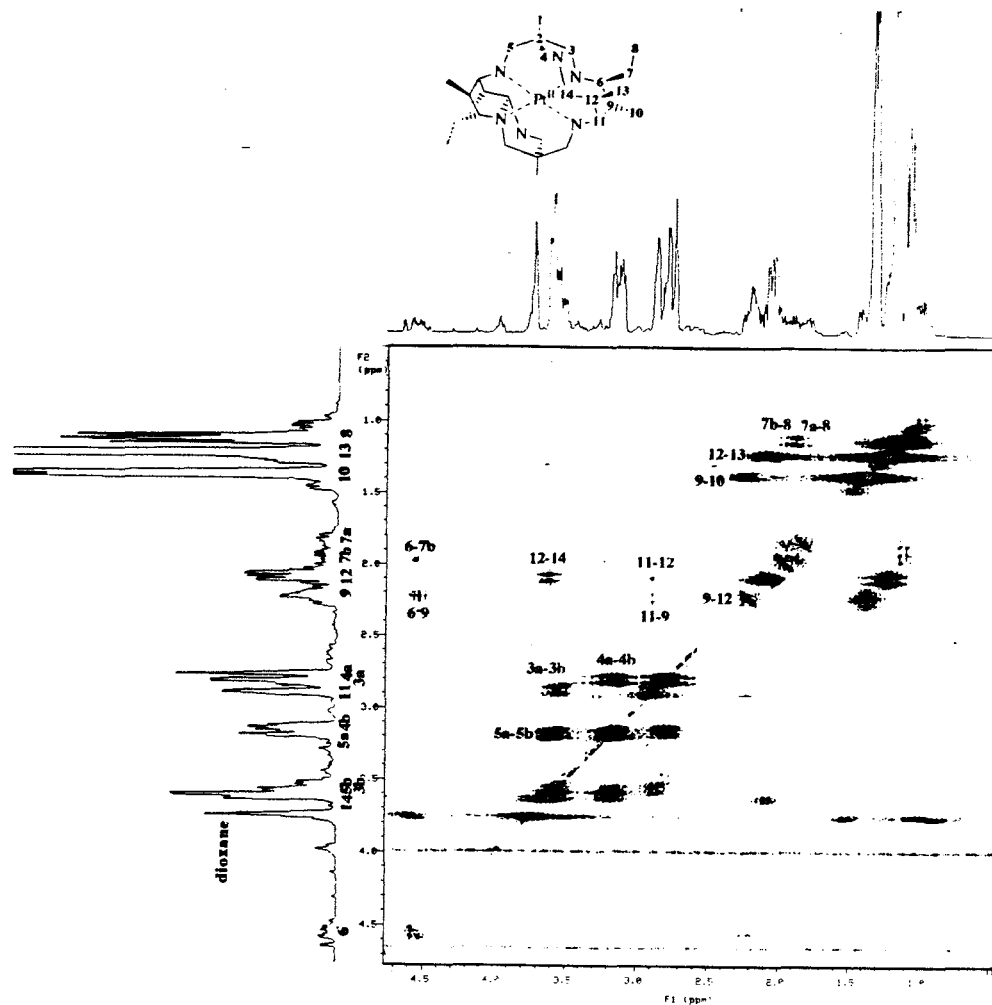


Figure 3.18: 300 MHz DQF COSY spectrum of the hydrogenated product; pentacyclo-[Pt^{II}(Et₂-Me₆-N₆-tetracosaneH₂)]⁴⁺ in D₂O, np = 2048, sw = 1753.5 Hz, d1 = 1.5 s, nt = 144, ni = 300, fn = 4096, fn1 = 4096.

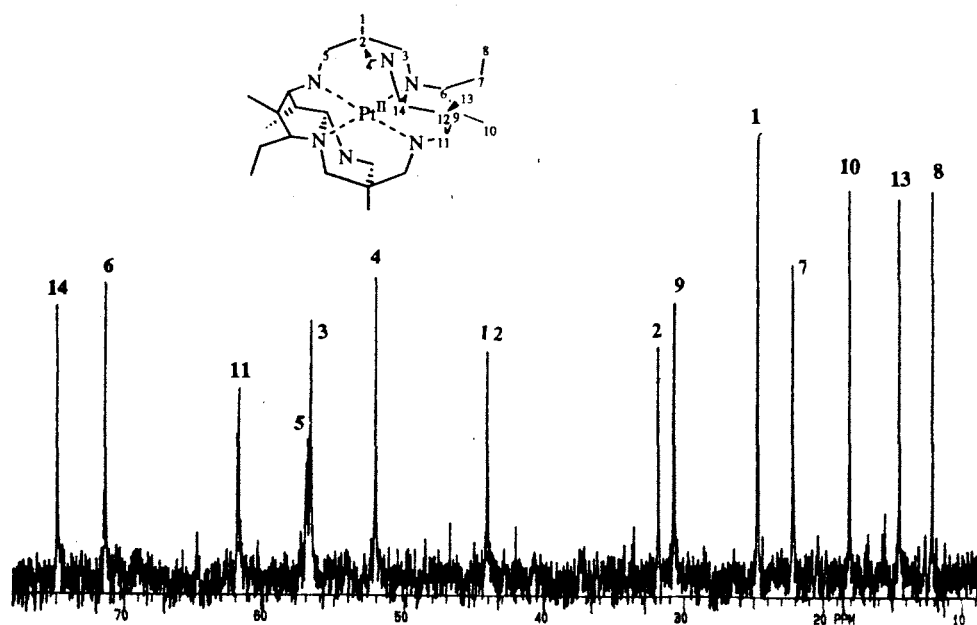


Figure 3.19: 300 MHz ¹³C NMR spectrum of the hydrogenated product, pentacyclo-[Pt^{II}(Et₂-Me₆-N₆-tetracosaneH₂)]⁴⁺ in D₂O.

3.3.3. Reactions of $[\text{Pt}(\text{tame})_2]^{4+}$ with Acetaldehyde

Two major products were isolated from the reaction of $[\text{Pt}(\text{tame})_2]\text{Cl}_4$ with CH_3CHO in a solution of acetonitrile and NaClO_4 in the presence of base, in ~1:1 ratio. These were the $[\text{Pt}(\beta\text{Me}_5\text{-}N_6\text{-tricosanetriimine})]^{4+}$ (Fig. 3.20(a)) and the $[\text{Pt}(\text{Me}_4\text{-}N_6\text{-tetracosanediimine})]^{4+}$ (Fig. 3.20(b)). Reaction at either 275 or 298 K did not alter the relative ratios of these complexes. Similarly, the reaction undertaken in water gave the same ratio, except that the combined yield of the products was less. Lastly, using between one and three equivalents of base in MeCN also gave the same ratio. Separation of the products was difficult using SP-Sephadex cation exchange resin ($\text{Na}_3\text{citrate}$, K_2SO_4 and NaCl as the eluants). Fractional crystallisation using the ZnCl_4^{2-} anion in acidic solutions allowed separation of the products. These complexes were characterised by ^1H and ^{13}C NMR spectroscopy and the structure of the $[\text{Pt}(\beta\text{Me}_5\text{-}N_6\text{-tricosanetriimine})]^{4+}$ cation was confirmed by an X-ray crystallographic analysis.

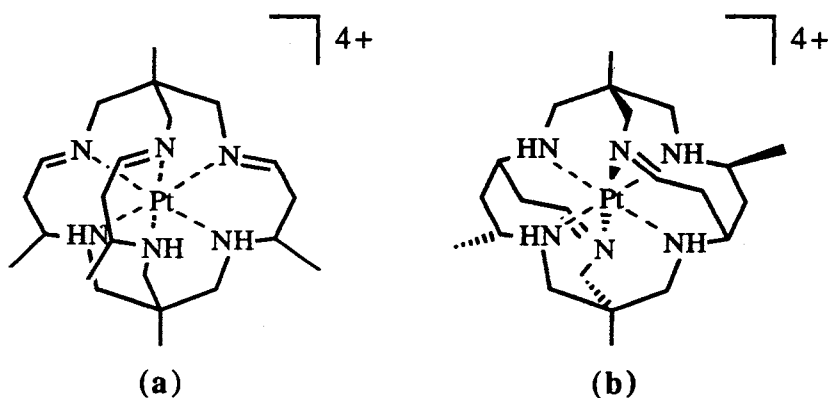


Figure 3.20: Products isolated from reaction of $[\text{Pt}(\text{tame})_2]^{4+}$ with acetaldehyde. (a) $[\text{Pt}(\beta\text{Me}_5\text{-}N_6\text{-tricosanetriimine})]^{4+}$ and (b) $[\text{Pt}(\text{Me}_4\text{-}N_6\text{-tetracosanediimine})]^{4+}$.

(a) Characterisation of $[\text{Pt}(\beta\text{Me}_5\text{-}N_6\text{-tricosanetriimine})]^{4+}$

I. Properties of $[\text{Pt}(\beta\text{Me}_5\text{-}N_6\text{-tricosanetriimine})]^{4+}$

Crystals which initially analysed as $[\text{C}_{22}\text{H}_{42}\text{Cl}_8\text{N}_6\text{PtZn}_2]3\text{H}_2\text{O} \cdot 1.5\text{HCl}$ were isolated as the protonated form from aqueous media. The complex is rather acidic and deprotonation is evident when dissolved in water, as inferred from the orange colour of the solution, as well as from its NMR spectra. This triimine complex is isomeric with the $[\text{Pt}(\alpha\text{Me}_5\text{-}N_6\text{-tricosanetriimine})]^{4+}$ ion obtained from the reaction of $[\text{Pt}(\text{tame})_2]^{4+}$ with aqueous formaldehyde and propanal, where the methyl substituents on the straps are now on the carbon atoms beta to the imine.

II. Crystal Structure of $[\text{Pt}(\beta\text{Me}_5\text{-}N_6\text{-tricosanetriimine})](\text{ZnCl}_4)(\text{ZnCl}_3)_2 \cdot 0.5\text{H}_2\text{O} \cdot 0.4\text{HCl}$

At 298 K, the complex decomposed slightly in the X-ray beam, as indicated by the change in space group from $R\bar{3}(\#148)$ during data acquisition. This was attributed to solvent loss from the lattice. As the anions were disordered, their composition is not certain. The microanalysis of the crystals gave an empirical formula consistent with $[\text{Pt}(\beta\text{Me}_5\text{-}N_6\text{-tricosanetriimine})](\text{ZnCl}_4)_2 \cdot 3\text{H}_2\text{O} \cdot 1.5\text{HCl}$. However, the X-ray crystallographic analysis was performed about six months after the microanalysis had been acquired and it is possible that the composition had changed during this time, and the empirical formula was found to be $[\text{C}_{44}\text{H}_{87}\text{Cl}_{20}\text{N}_{12}\text{OPt}_2\text{Zn}_6]0.5\text{H}_2\text{O} \cdot 0.4\text{HCl}$. Although the connectivity of the cation established in the crystal structure was consistent with the ^1H and ^{13}C NMR spectra, the bond lengths and angles etc, were not precisely determined. The numbering system is also used in the description of the NMR data. The PLUTO structure of the cation is depicted in Fig. 3.21. Table 3.7 lists the relevant bond lengths and angles. Other crystallographic data are listed in Appendix B(IV).

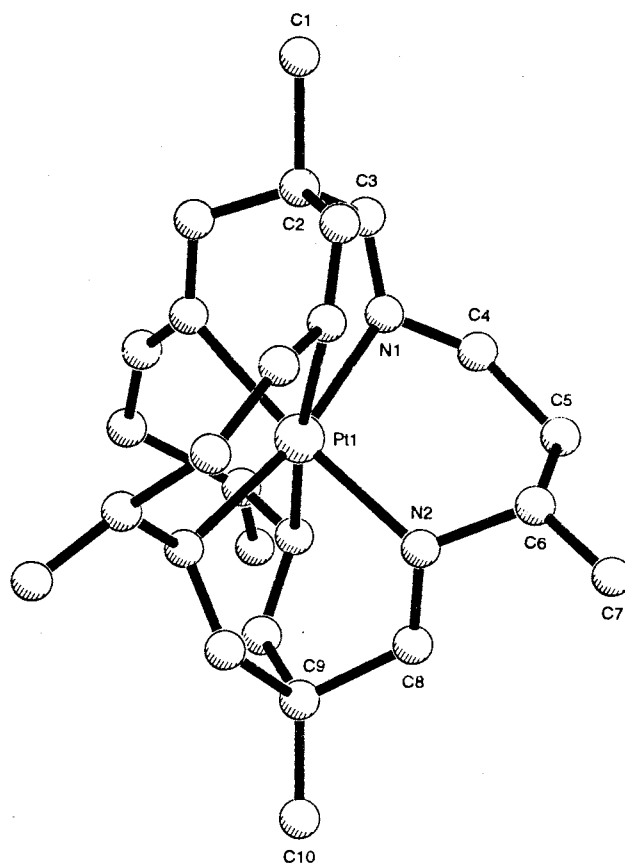


Figure 3.21: PLUTO diagram of the cation in $[\text{Pt}(\beta\text{Me}_5\text{-}N_6\text{-tricosanetriimine})](\text{ZnCl}_4)(\text{ZnCl}_3)_2 \cdot 0.5\text{H}_2\text{O} \cdot 0.4\text{HCl}$.

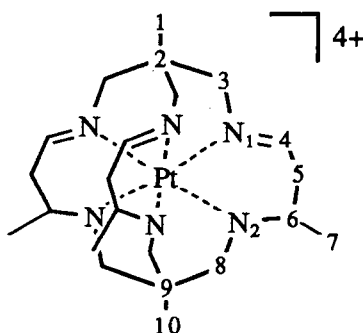
Table 3.7: Relevant bond lengths and angles for the cation in [Pt(β Me₅-N₆-tricosanetriimine)](ZnCl₄)(ZnCl₃)₂·0.5H₂O·4HCl.

Bond Distance	(Å)
Pt-N(1)	2.05(7)
Pt-N(2)	2.11(6)

Bond Distance	(Å)	Bond Distance	(Å)
N(1)-C(3)	1.25(8)	C(4)-C(5)	1.5(1)
N(1)-C(4)	1.2(1)	C(5)-C(6)	1.7(1)
N(2)-C(6)	1.49(9)	C(6)-C(7)	1.4(1)
N(2)-C(8)	1.35(7)	C(8)-C(9)	1.54(9)
C(2)-C(3)	1.34(8)	C(9)-C(10)	1.5(2)

Table 3.8: Relevant angles for the cation in [Pt(β Me₅-N₆-tricosanetriimine)](ZnCl₄)(ZnCl₃)₂·0.5H₂O·4HCl.

Bond Angles	Degrees	Bond Angles	Degrees
N(1)-Pt-N(1)	73	N(2)-Pt-N(2)	85
N(1)-Pt-N(2)	106	N(1)-Pt-N(2)'	96
Pt-N(1)-C(4)	101	Pt-N(2)-C(6)	115
Pt-N(1)-C(3)	130	Pt-N(2)-C(8)	113
N(1)-C(3)-C(2)	110	N(2)-C(8)-C(9)	121
N(1)-C(4)-C(5)	153	N(2)-C(6)-C(5)	109
C(4)-N(1)-C(3)	122	C(8)-N(2)-C(6)	115
C(3)-C(2)-C(3)'	113	C(8)-C(9)-C(8)'	103
C(6)-C(5)-C(4)	112	C(7)-C(6)-C(5)	124
C(3)-C(2)-C(1)	105	C(10)-C(9)-C(8)	115



The crystal structure of the cation in $[\text{Pt}(\beta\text{Me}_5\text{-N}_6\text{-tricosanetriimine})](\text{ZnCl}_4)(\text{ZnCl}_3)_2 \cdot 0.5\text{H}_2\text{O} \cdot 4\text{HCl}$ shows that the two tame caps are linked by three six-membered chelate rings, each containing one imine. All three six-membered chelate rings of the tame residue are in the boat conformation, and the three six-membered chelate rings arising from the straps are in a flattened skewboat conformation. The imines lie on one face of the octahedron to form the *facial*-triimine complex. There are seven chiral centres in the complex, three arising from the saturated nitrogens, three from the methine carbon atoms in the straps and one at the Pt(IV) ion. From the crystal structure, the absolute configuration about the Pt(IV) centre is Δ . The configurations about all three nitrogen atoms are the same (R), and all the methine carbon atoms have the S configuration.

II. NMR Spectroscopy of $[\text{Pt}(\beta\text{Me}_5\text{-N}_6\text{-tricosanetriimine})]^{4+}$

The $[\text{Pt}(\beta\text{Me}_5\text{-N}_6\text{-tricosanetriimine})]^{4+}$ complex was characterised by ^1H and ^{13}C NMR spectroscopic methods, using multiple-pulse experiments - APT and DEPT. The NMR spectra were of the tetrachlorozincate salt in ~ 1 M DCl. The assignment of the resonances in the ^1H NMR spectrum (Fig. 3.22(a)) was made on the basis of one-dimensional decoupling experiments and also in part by analogy with the isomeric $[\text{Pt}(\alpha\text{Me}_5\text{-N}_6\text{-tricosanetriimine})]^{4+}$ complex. Only ten different proton signals were observed, instead of the anticipated eleven, and this is attributed to solvent exchange of the protons on the methylene carbon atom alpha to the imine in the strap (H_{5a} and H_{5b}). Evidence for proton exchange is from the splitting pattern of the methine proton of the strap (H_6), which is only a quartet and not the anticipated quartet of doublet of doublets. While one of these methylene protons (nominally H_{5a}) rapidly undergoes proton exchange, the other proton, H_{5b} (at $\delta \sim 4.4$ ppm), is still discernible in the ^1H NMR spectrum, implying that its rate of proton exchange is slower. It is anticipated that this proton occupies the equatorial position of the six-membered chelate ring, as this lies in the same plane as the imine, while the faster exchanging proton occupies the axial position (nominally, H_{5a}).²¹ Vicinal coupling between the ^{195}Pt nucleus and some of the methylene protons is large and the magnitude depends essentially on the dihedral angles. The ^{13}C NMR spectrum (Fig. 3.22(b)) shows the anticipated 11 resonances. The resonance for the methylene carbon atom on the strap (C_5) is broad due to coupling with deuterium and this behaviour is similar to that for the isomeric $[\text{Pt}(\alpha\text{Me}_5\text{-N}_6\text{-tricosanetriimine})]^{4+}$ complex. The assignments shown in Fig. 3.22(b) were assigned on the basis of the APT and DEPT spectra and in part, by analogy with $[\text{Pt}(\alpha\text{Me}_5\text{-N}_6\text{-tricosanetriimine})]^{4+}$. Vicinal coupling of the carbon atoms with the ^{195}Pt nucleus was dependent on the dihedral angles.

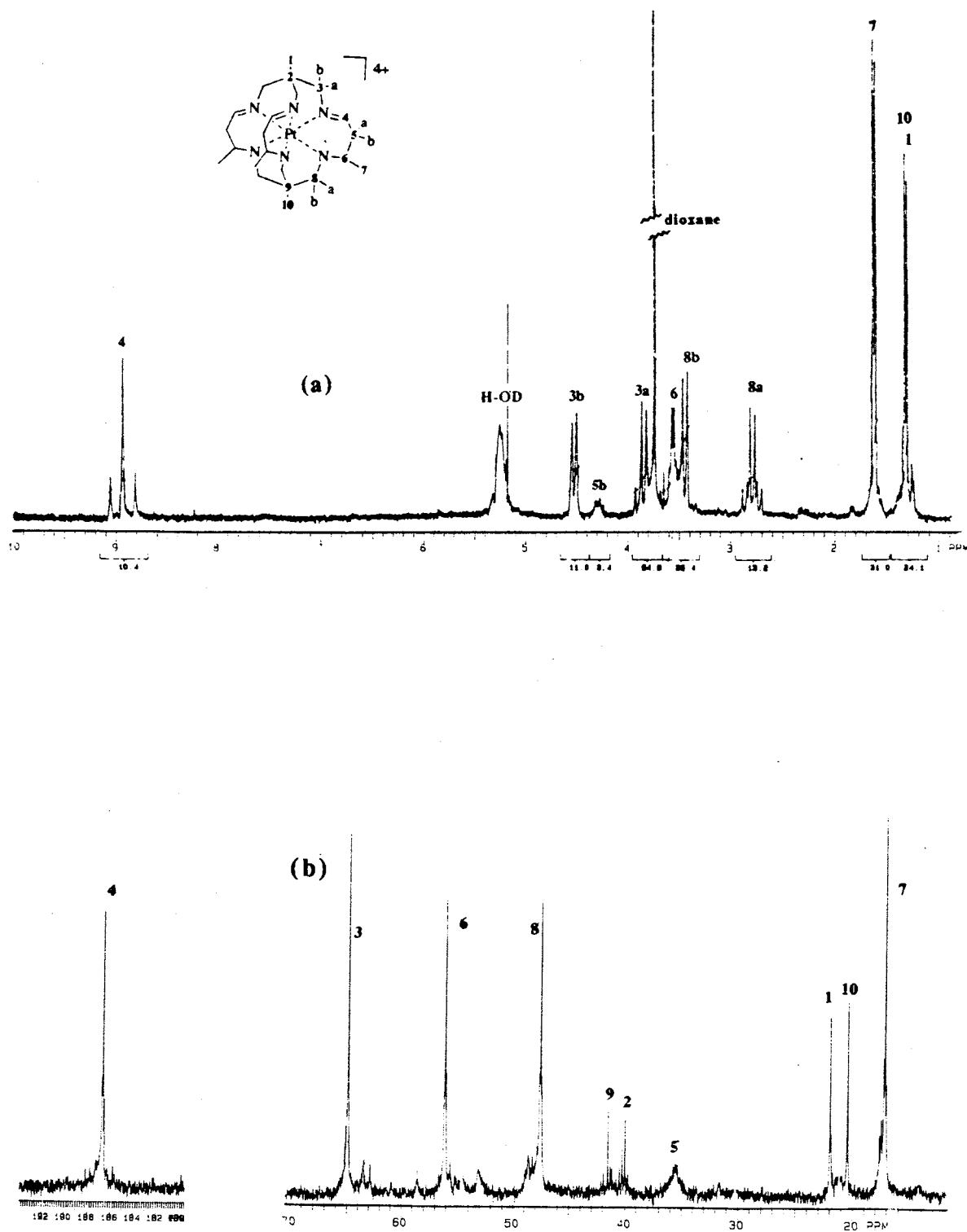


Figure 3.24: 300 MHz (a) ^1H and (b) ^{13}C NMR spectrum $[\text{Pt}(\beta\text{Me}_5\text{-N}_6\text{-tricosane-triimine})](\text{ZnCl}_4)_2$ in $\sim 1 \text{ M DCl}$.

(b) Characterisation of $[Pt(Me_4-N_6-tetracosanediimine)]^{4+}$

II. Properties of the $[Pt(Me_4-N_6-tetracosanediimine)]^{4+}$

$[Pt(Me_4-N_6-tetracosanediimine)]^{4+}$ is quite acidic in water and readily deprotonates, as indicated from the orange colour of the solution. The complex is more soluble and less predisposed to undergo loss of an acetaldehyde residue than the analogous $[Pt(Et_2-Me_6-N_6-tetracosanediimine)]Cl_4$. Poor quality colourless crystals were obtained after addition of a few drops of a solution of $ZnCl_2$ in 4 M HCl to the mother liquor after $[Pt(\beta-Me_5-N_6-tricosanetriimine)](ZnCl_4)_2$ had been first filtered. These were recrystallised from an acidified solution of $[Pt(Me_4-N_6-tetracosanediimine)](ZnCl_4)_2$ in ~2 M DCl. These were found to be twinned and therefore unsuitable for X-ray crystallographic analysis. Further attempts to grow suitable crystals have not yet been successful.

II. NMR Spectroscopy of $[Pt(Me_4-N_6-tetracosanediimine)]^{4+}$

All NMR spectra recorded were of the tetrachlorozincate salt in ~2 M DCl, in an attempt to suppress proton exchange with the solvent and to improve resolution. The 1H and DQF COSY NMR spectra of the $[Pt(Me_4-N_6-tetracosanediimine)]^{4+}$ (Figs 3.23 and 3.24) are reminiscent of those of the analogous $[Pt(Et_2-Me_6-N_6-tetracosanediimine)]^{4+}$ complex at pH~1. However, the NMR spectra for these two complexes are different in a number of ways, firstly, the $[Pt(Me_4-N_6-tetracosanediimine)]^{4+}$ NMR spectra are better resolved, and this aided assignment of the signals. The $[Pt(Me_4-N_6-tetracosanediimine)]^{4+}$ ion did not exhibit any chemical shift anisotropy at the higher magnetic fields. Well-resolved spectra were recorded using both 300 and 500 MHz spectrometers. Lastly, the ^{13}C NMR spectrum (Fig. 3.25) exhibits the eleven anticipated signals, in contrast to $[Pt(Et_2-Me_6-N_6-tetracosanediimine)]^{4+}$.

Assignment of the 1H spectrum was aided by the DQF COSY spectrum and also by comparison with the spectra for $[Co(Et_2-Me_6-N_6-tetracosanediimine)]^{3+}$. Decomposition of $[Pt(Me_4-N_6-tetracosanediimine)]^{4+}$ was slower than $[Pt(Et_2-Me_6-N_6-tetracosanediimine)]^{4+}$, so cross peaks arising from the decomposition product were not very intense. All methylene protons are magnetically inequivalent and are observed as pairs of doublets. The pairs of methylene protons H_{3a}, H_{5a} and H_{3b}, H_{5b} are indistinguishable and the assignments for these pairs may be interchanged. The methylene cap protons (H_{4b} and H_{4a}) couple with the imine proton in the cross strap, H_{11} , as evident from the cross peaks in the DQF COSY spectrum ($^4J_{H_{4a}-H_{11}} \sim 3.1$, $^4J_{H_{4b}-H_{11}} \sim 5.1$ Hz, estimated from the DQF COSY spectrum). This behaviour has also been observed with analogous Pt(IV) and Co(II) complexes. The protons H_{3a} , H_{4a} , H_{5a} , H_9 and H_{11} exhibit coupling with ^{195}Pt . Solvent exchange with the protons alpha

to the imine ($H_{10a,b}$) is evident in the 1H NMR spectrum. At least one of the methylene protons in the cross strap (nominally, H_{10a}) is not observed, while a signal attributed to the geminal proton (H_{10b}) is just discernible at $\delta \sim 4.06$ ppm, which is partially overlapped by that for H_6 . The rate of exchange of H_{10b} may not be as fast as that for H_{10a} . It is anticipated that the former proton occupies the equatorial position of the six-membered chelate ring in the cross strap, while the more rapidly exchanging proton (H_{10a}) occupies the axial position.²¹ The DQF COSY spectrum did not exhibit cross peaks associated for coupling of protons with H_{10a} or H_{10b} .

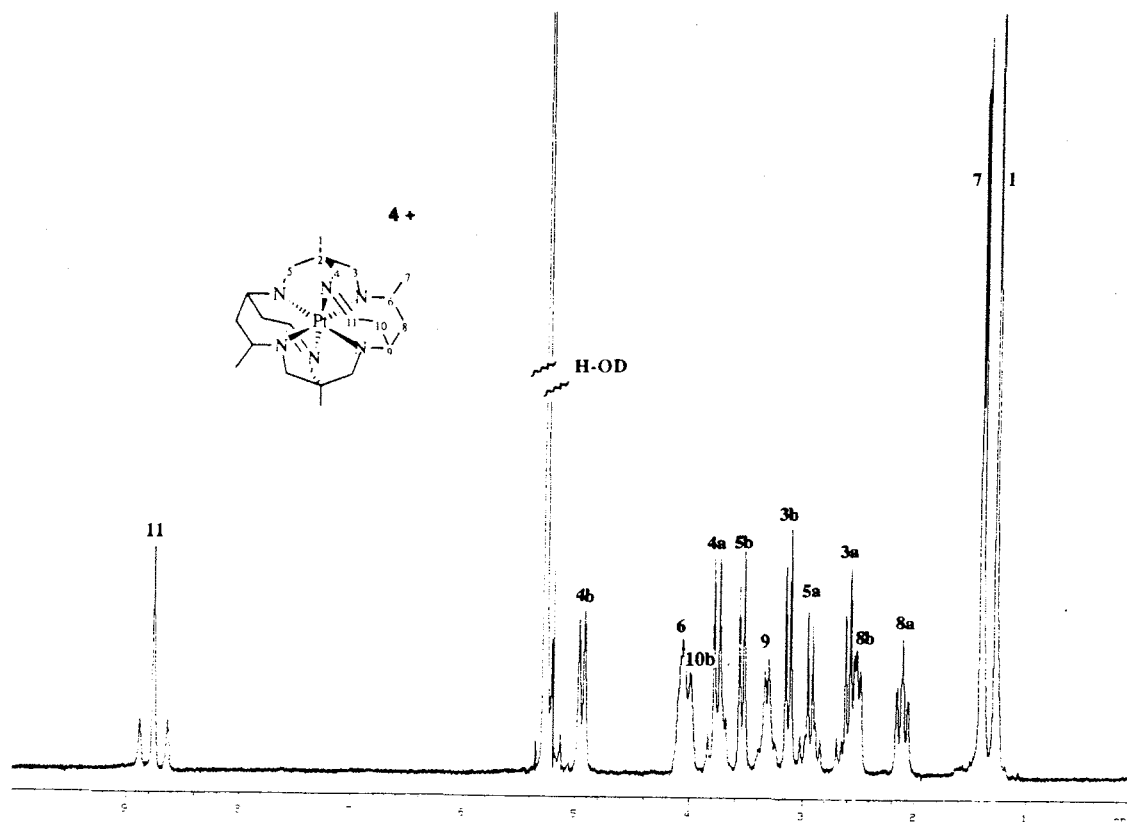


Figure 3.23: 300 MHz 1H NMR spectrum of $[Pt(Me_4-N_6\text{-tetracosanediimine})](ZnCl_4)_2$ in ~ 2 M DCl.

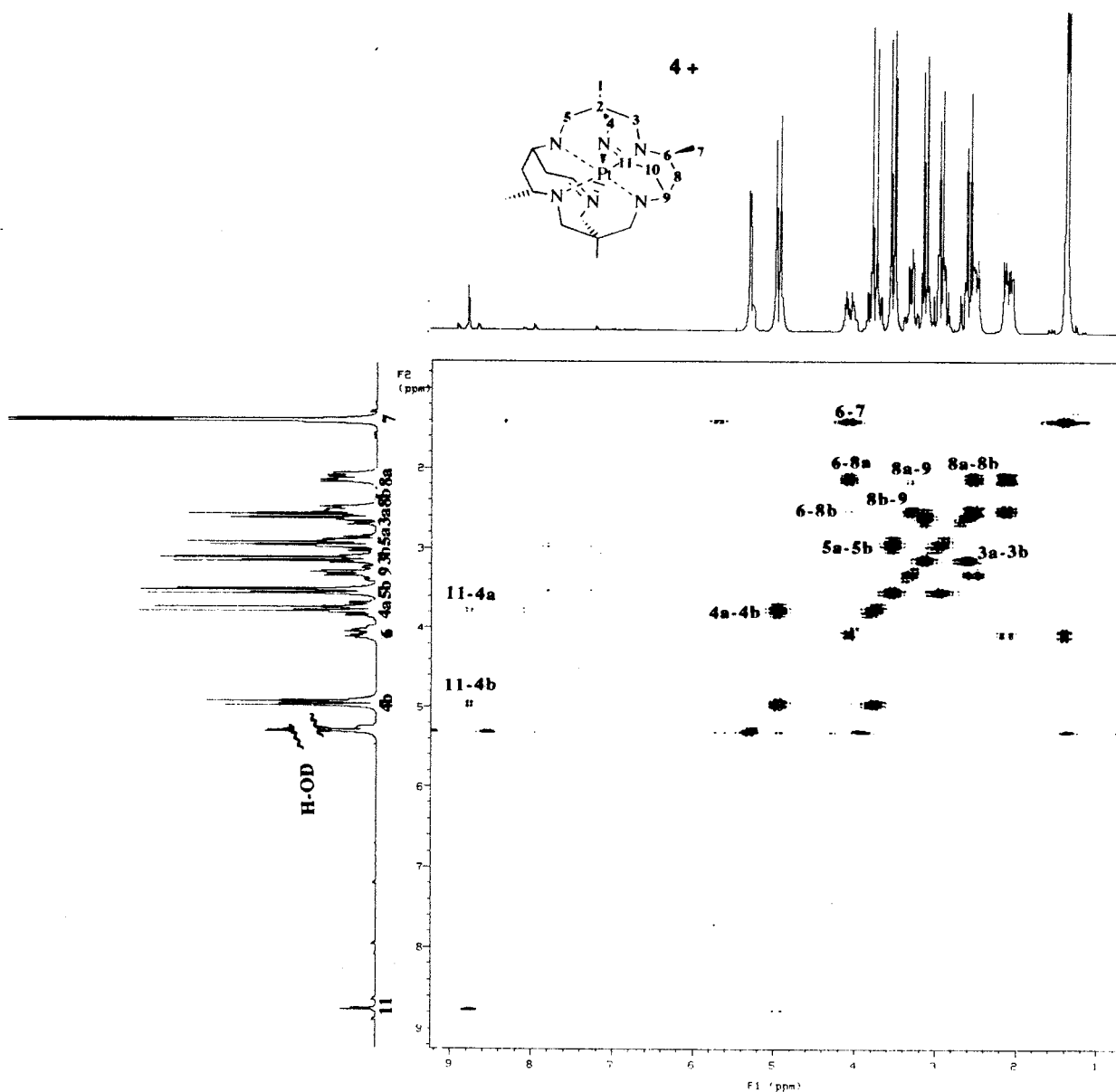


Figure 3.24: 300 MHz DQF COSY spectrum of $[\text{Pt}(\text{Me}_4\text{-}N_6\text{-tetracosanediimine})]^{4+}$ in ~ 2 M DCl. $np = 2048$, $sw = 2568.1$ Hz, $d1 = 1.0$ s, $nt = 160$, $ni = 124$, $fn = 2048$, $fn1 = 2048$.

The ^{13}C NMR spectrum (Fig. 3.25) is consistent with the proposed N_6 -tetracosanediimine structure. Unlike that for $[\text{Pt}(\text{Et}_2\text{-Me}_6\text{-}N_6\text{-tetracosanediimine})]^{4+}$, all the anticipated eleven signals were observed, including that for the imine carbon atom at $\delta \sim 187$ ppm, even using relatively short delay and acquisition times (0.2 and 0.5 s respectively). The ^{13}C NMR spectrum was assigned on the basis of the DEPT spectrum and by analogy with the $[\text{Co}(\text{Et}_2\text{-Me}_6\text{-}N_6\text{-tetracosanediimine})]^{3+}$ spectrum. The carbon atom alpha to the imine (C_{10} , centred at 37.1 ppm) was broadened, due to deuterium coupling. ^{195}Pt coupling was observed for carbon atoms which were three bonds away with the quaternary carbon atom of the cap (C_2) having the largest coupling constant for this complex ($^3J_{\text{Pt-C}_2} = 48$ Hz).

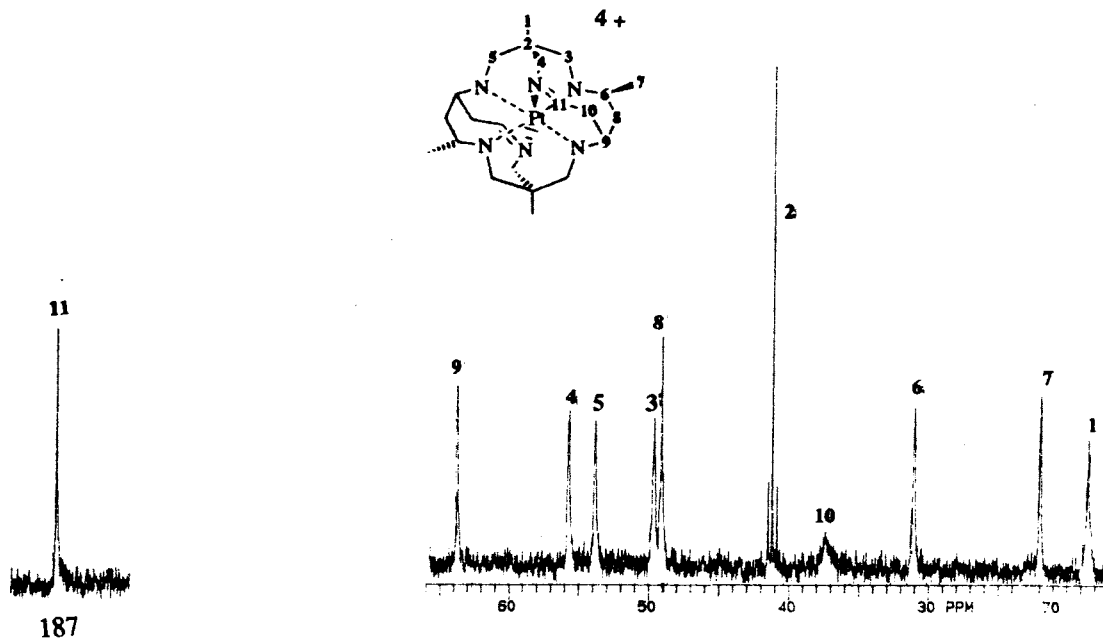


Figure 3.25: 300 MHz ^{13}C NMR spectrum of $[\text{Pt}(\text{Me}_4\text{-}N_6\text{-tetracosanediimine})]^{4+}$ in $\sim 2\text{M DCl}$, $d_1 = 0$ s, $at = 0.5$ s.

III. Decomposition of $[\text{Pt}(\text{Me}_4\text{-}N_6\text{-tetracosanediimine})]^{4+}$

Although $[\text{Pt}(\text{Me}_4\text{-}N_6\text{-tetracosanediimine})]^{4+}$ is more robust than its propanal-derived analogue, imine hydrolysis and subsequent loss of an acetaldehyde residue was still apparent in solutions ($\text{pH} > 3$) more than one week old. The ^1H and ^{13}C NMR spectra are consistent with the proposed complex $[\text{Pt}(\text{Me}_4\text{-}N_6\text{-docosanediimine})]^{4+}$. The multiplicities shown in the ^{13}C NMR spectrum (Fig. 3.26) were assigned on the basis of the DEPT spectrum. No further assignment has been achieved to date.

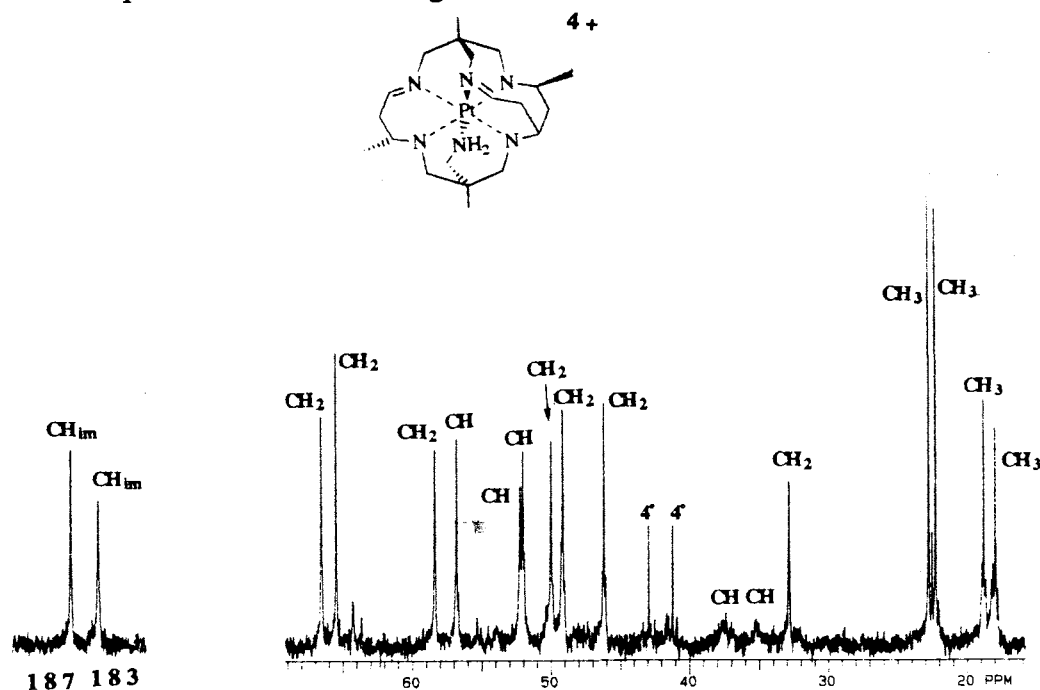


Figure 3.26: 300 MHz ^{13}C NMR spectra of the decomposition product of $[\text{Pt}(\text{Me}_4\text{-}N_6\text{-tetracosanediimine})](\text{ZnCl}_4)_2$ in D_2O .

(c) Reduction of $[Pt(Me_4-N_6-tetracosanediimine)]^{4+}$

Reduction with H_2 over a 10% Pd/C catalyst in aqueous media at 275 K at atmospheric pressure, gave rise to a complex with similar properties to that obtained from the hydrogenation of the analogous $[Pt(Et_2-Me_6-N_6-tetracosanediimine)]^{4+}$ under the same conditions. Prior to reduction, the colour of the solution was orange, arising from deprotonation. As hydrogenation proceeded, the solution became green and then colourless after about 30 minutes. The loss of colour indicates that the complex is no longer deprotonated and the loss of acidity is ascribed to the formation of a Pt(II) centre. The NMR spectra of the hydrogenated product showed that the imine signal was no longer present. Therefore, by analogy with behaviour of the product obtained from the hydrogenation of $[Pt(Et_2-Me_6-N_6-tetracosanediimine)]^{4+}$, it is proposed that the Pt(IV) centre has been reduced to square planar Pt(II) accompanied by a ligand rearrangement that removes the imine. The postulated product, pentacyclo- $[Pt^{II}(Me_4-N_6-tetracosane2H)]^{4+}$, is depicted in Fig. 3.27. No crystals have yet been grown. The chloride salt of the complex is stable at room temperature.

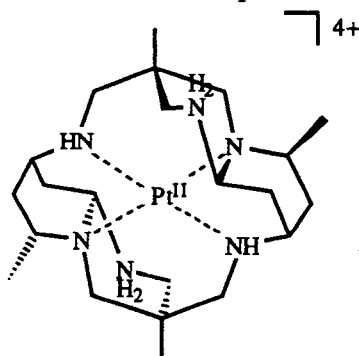


Figure 3.27: Proposed structure of the product arising from the hydrogenation of $[Pt(Me_4-N_6-tetracosanediimine)]^{4+}$.

I. NMR Spectroscopy of pentacyclo- $[Pt^{II}(Me_4-N_6-tetracosane2H)]^{4+}$

The chloride salt of the complex in D_2O was used for acquiring all NMR spectra. The 500 MHz 1H and ^{13}C NMR spectra are depicted in Figs 3.28 and 3.29. All anticipated 19 signals are observed in the 1H NMR spectrum, indicating that no proton exchange occurs. Assignment of the 1H NMR spectrum was aided by the DQF COSY spectrum (Fig. 3.30). The pairs of methylene protons $H_{3a,3b}$ and $H_{5a,5b}$ are indistinguishable and the assignments for these may be interchanged. The methine proton (H_9) at the junction of the strap with the cross strap couples more strongly to H_{8b} than to H_{8a} and also more strongly to H_{10b} than to H_{10a} , presumably the magnitude of the couplings are dependent on the dihedral angles.

The ^{13}C NMR spectrum depicts the 11 anticipated ^{13}C resonances and is consistent with the proposed structure. The assignments shown in Fig. 3.29 were assessed on the basis of the APT, DEPT, coupled ^{13}C and HMBC spectra.

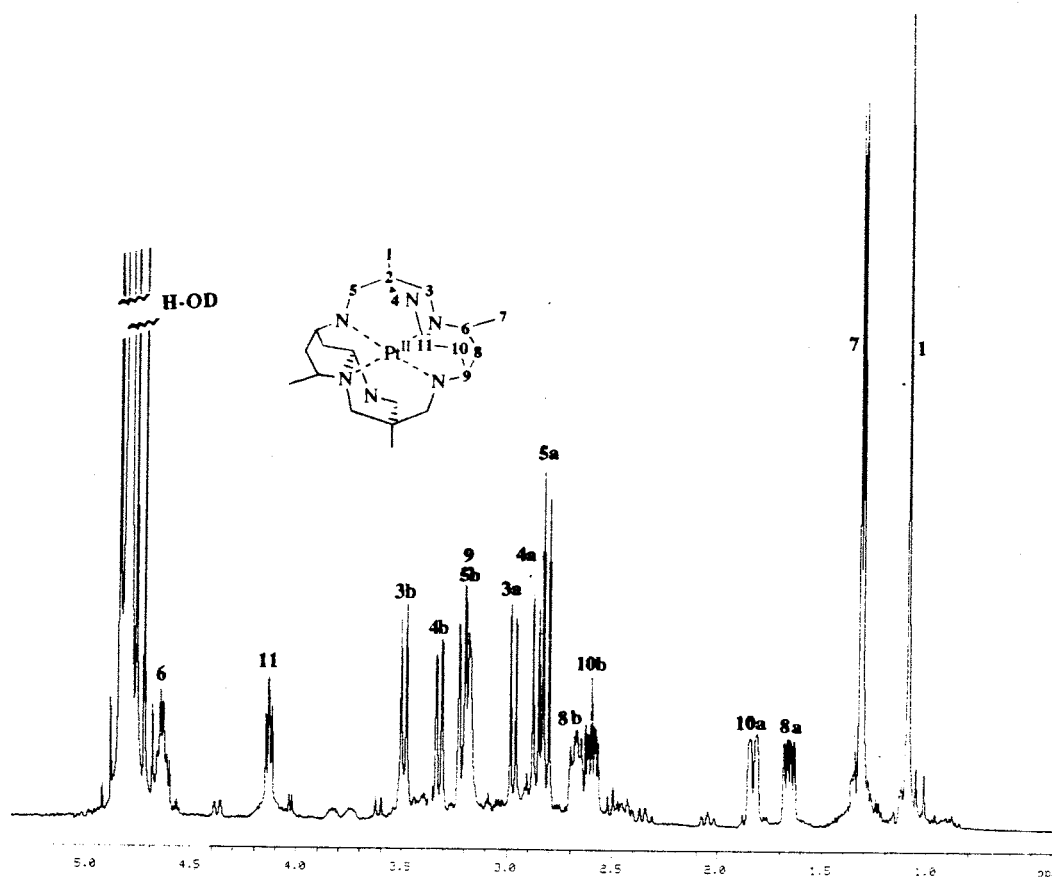


Figure 3.28: 500 MHz ^1H NMR spectrum of pentacyclo-[Pt^{II}(Me₄-N₆-tetracosane2H)]Cl₄ in D₂O.

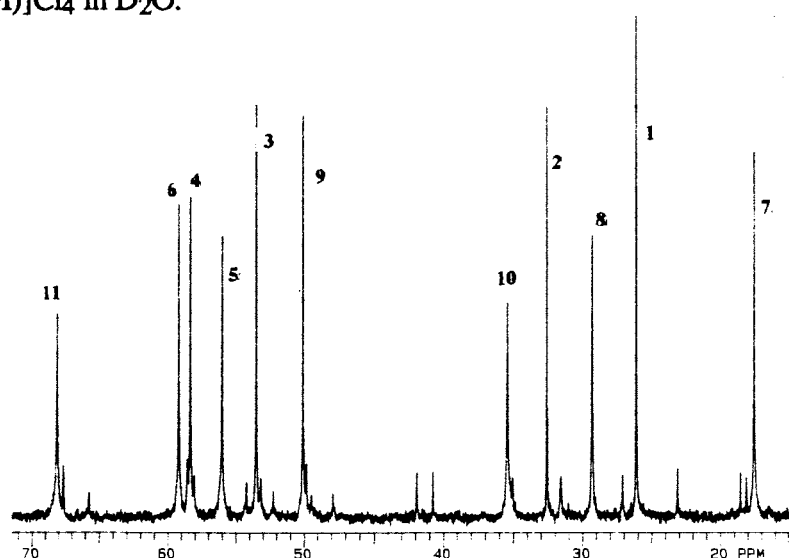


Figure 3.29: 300 MHz ^{13}C NMR spectrum of pentacyclo-[Pt^{II}(Me₄-N₆-tetracosane2H)]Cl₄ in D₂O.

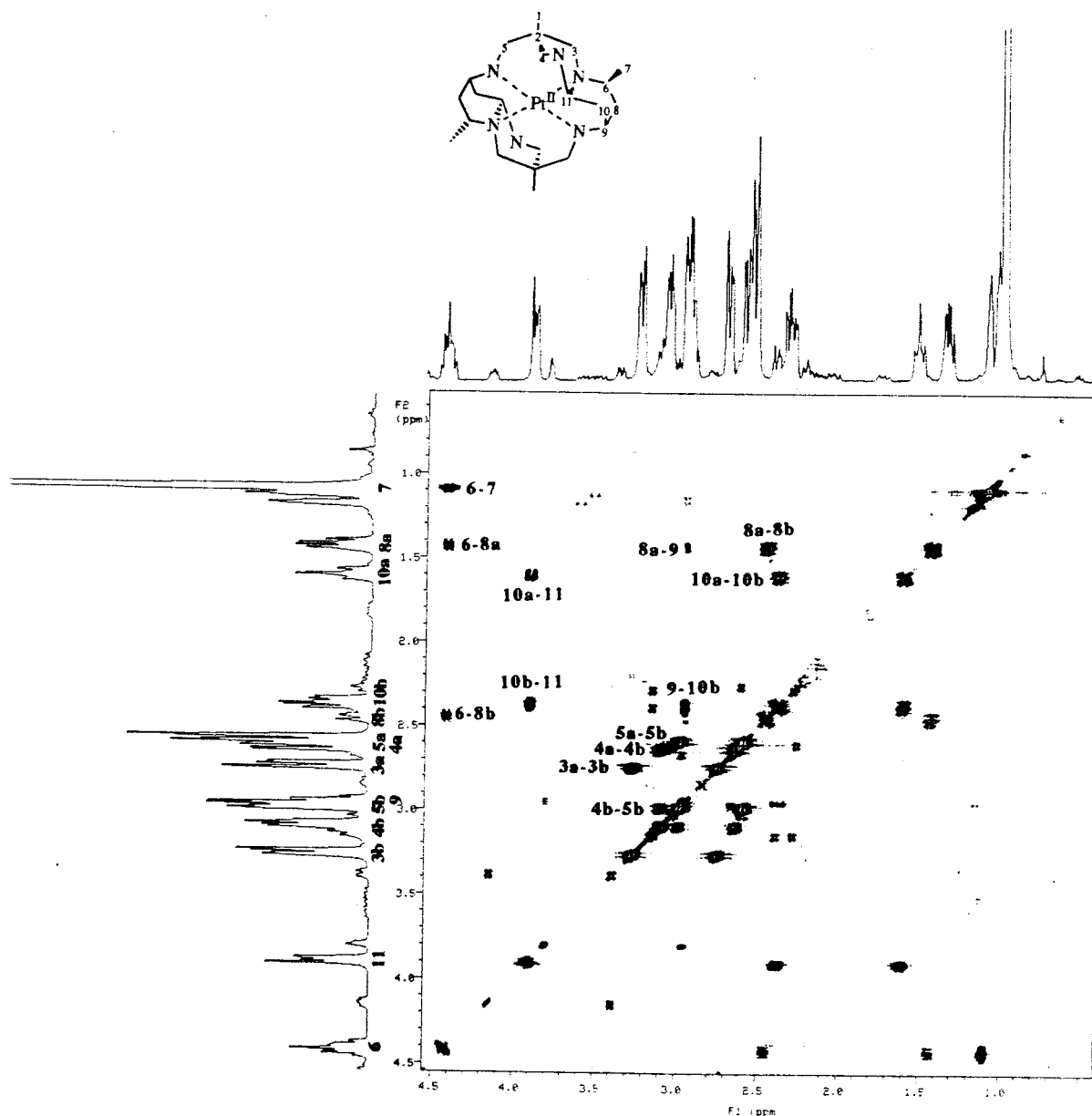


Figure 3.30: 500 MHz DQF COSY spectrum of pentacyclo-[Pt^{II}(Me₄-N₆-tetracosane₂H)]Cl₄ in D₂O. np = 4096, sw = 2537.6 Hz, d1 = 1.5 s, nt = 64, ni = 256, fn = 4096, fn1 = 4096.

3.3.4. Reactions of [Pt(tame)₂]⁴⁺ with Acetylacetonone

(a) Synthesis of [Pt(tame₂-2,4-pentanediiminate)]Cl₃

Reaction of [Pt(tame)₂]⁴⁺ with an excess of acetylacetonone gave rise to a complex with one condensed acetylacetonone unit (Fig. 3.31), where the two tame caps are linked by one delocalised six-membered chelate ring that was derived from an acetylacetonone residue. Complexes with more than one acetylacetonone unit linking the tame caps were not detected, even using an excess of acetylacetonone.

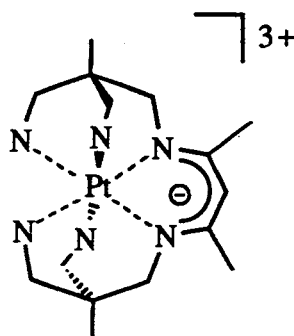


Figure 3.31: Proposed structure of the product from the reaction of $[\text{Pt}(\text{tame})_2]^{4+}$ with acetylacetonate, $[\text{Pt}(\text{tame}_{2-2,4}\text{-pentanediiiminate})]^{3+}$

I. Properties of $[\text{Pt}(\text{tame}_{2-2,4}\text{-pentanediiiminate})]\text{Cl}_3$

The bright orange complex was eluted from Dowex cation exchange resin with 2 M HCl, indicating a lower charge than anticipated for a Pt(IV) hexaamine complex. The microanalysis of the chloride salt is consistent with an empirical formula of $[\text{C}_{15}\text{H}_{23}\text{Cl}_3\text{N}_6\text{Pt}]$ and an overall charge of the cation of +3. The complex is bright orange even in the solid state, unlike the preceding Pt(IV) cages with coordinated imines, which are colourless. This complex is stable indefinitely in solution and is more soluble in water than the preceding Pt(IV) and Pt(II) complexes. Crystals suitable for an X-ray crystallographic analysis have not yet been grown. Treatment of the complex with neat triflic acid in an inert atmosphere gave rise to an ^1H NMR spectrum consistent with $[\text{Pt}(\text{tame})_2]^{4+}$, indicating that the acetylacetonate unit had been cleaved from the complex.

II. NMR Spectroscopy of $[\text{Pt}(\text{tame}_{2-2,4}\text{-pentanediiiminate})]^{3+}$

All NMR spectra of the chloride salt were recorded in D_2O and are consistent with the proposed structure. The ^1H and ^{13}C NMR spectra are depicted in Figs. 3.32(a) and 3.32(b). The multiplicities in the ^{13}C NMR spectrum were assigned on the basis of the APT and DEPT spectra. The methylene carbon atoms in the cap (C_4 and C_5), are indistinguishable and their assignments may also be interchanged. The imine carbon atom (C_6) is observed at 162.5 ppm, as anticipated for diketone and diimine systems.²² The frequency of the resonance attributed to the strap carbon atom (C_8 ; δ -98.8 ppm) is higher than expected for a multiplicity of CH_2 and is also quite broad, due to coupling with deuterium. This implies that the protons undergo proton exchange with the solvent. One of the methylene protons is sufficiently acidic such that it remains deprotonated and this allows the carbon atom to be incorporated in a delocalised six-membered chelate ring system, similar to that observed in the $[\text{Pt}(\text{en})_3\text{-(2,4-pentanediiiminate)}]^{3+}$ and $[\text{Pt}(\text{NH}_3)_4\text{(2,4-pentanediiiminate)}]^{3+}$ complexes.⁷⁻⁹ ^{195}Pt satellites are observed in the signals at 25.3 and 45.7 ppm which are ascribed to the methyl (C_1) and quaternary

carbon atoms in the tame residue (C₂). The ¹⁹⁵Pt coupling with the latter site is the largest value observed for complexes of this type (³J_{Pt-C2}=68 Hz).

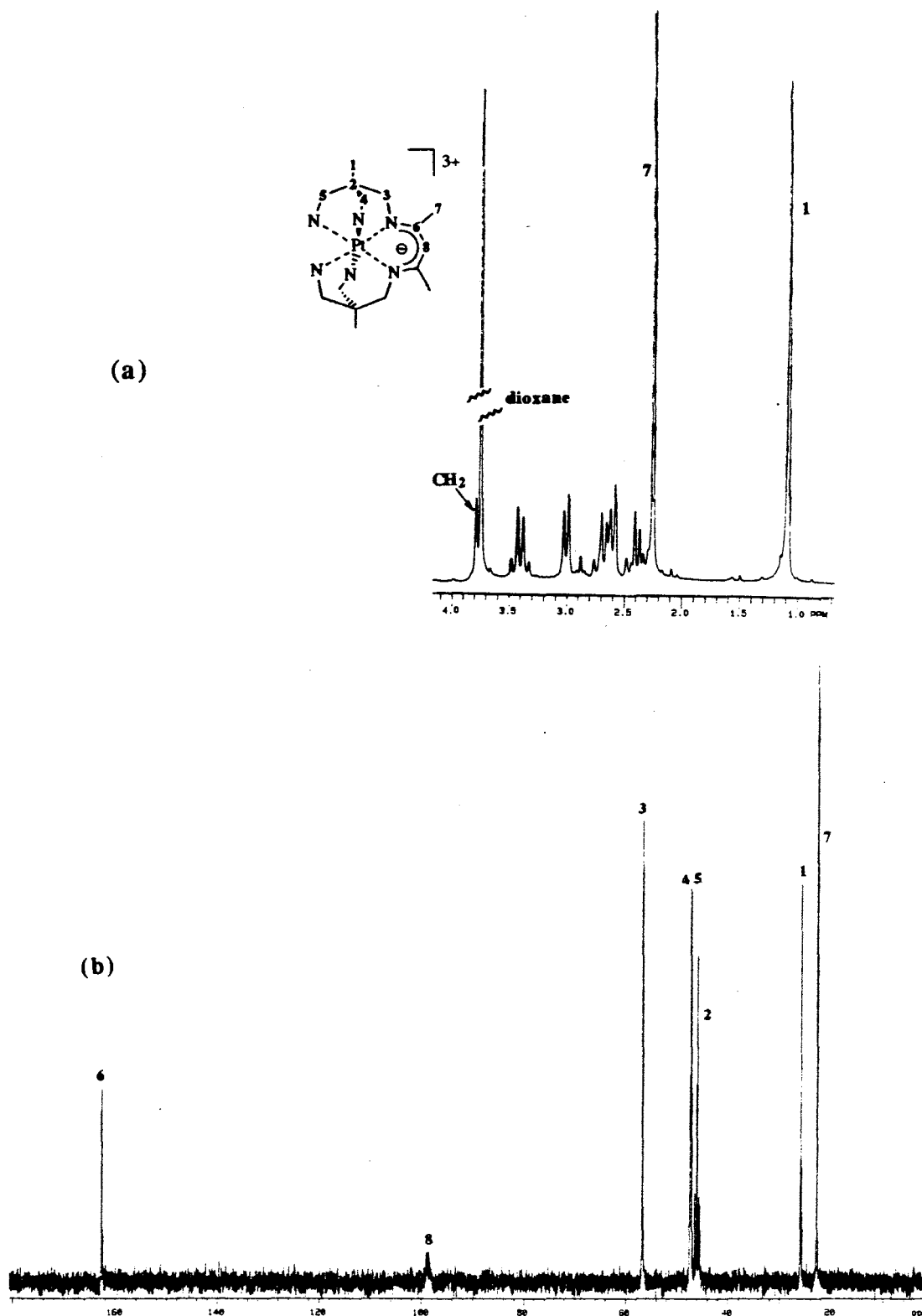


Figure 3.32: 300 MHz (a) ¹H and (b) ¹³C NMR spectrum of [Pt(tame₂-2,4-pentanediiiminate)]Cl₃ in D₂O.

(b) Hydrogenation of $[Pt(\text{tame}_2\text{-}2,4\text{-pentanediiminate})]^{3+}$

The diiminate complex was hydrogenated overnight at room temperature and pressure, in the presence of Pd(10%)/C as the catalyst. After about 5 minutes, the orange solution became green and then colourless, as observed with $[Pt(\alpha\text{Me}_5\text{-}N_6\text{-tricosanetriimine})]^{4+}$ and the N_6 -tetracosanedimine complexes. The complex was isolated from the reaction solution after filtering off the catalyst and evaporation of the solvent. The NMR spectra of the reduced complex indicated that only one product had formed, but that an imine was still present. It is probable that the hydrogenation reduced the octahedral Pt(IV) to square planar Pt(II), and a structure of the product is postulated in Fig. 3.33. The colourless chloride salt of the product was soluble and stable in aqueous solution. Crystals suitable for X-ray crystallographic analysis have not yet been grown.

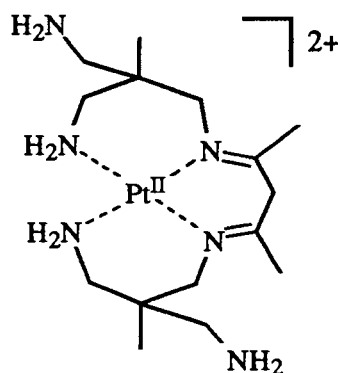


Figure 3.33: Proposed structure of the product arising from the hydrogenation of $[Pt(\text{tame}_2\text{-}2,4\text{-pentanediiminate})]^{3+}$.

I. NMR Spectroscopy of the Hydrogenated Complex

All NMR spectra of the chloride salt were recorded at 300 MHz in D_2O . The 1H NMR spectrum (Fig. 3.34(a)) indicates that there are three different methyl proton environments and a number of overlapping multiplets which are attributed to methylene protons. The multiplicities shown in the ^{13}C NMR spectrum (Fig. 3.34(b)) were assigned on the basis of the APT and DEPT spectra. On first inspection, there appears to be 13 carbon signals, including the broad resonance centred at 54.2 ppm and two nearly overlapping signals at ~ 39 ppm. The signal at 180 ppm is attributed to the imine carbon atoms (C_6 and C_9) and the frequency is higher than that for the precursor diiminate complex (162.5 ppm). The broadness of the signal at 54.2 ppm implies that proton exchange with the solvent occurs. This resonance is therefore attributed to the carbon atom (C_8) in the chelate ring derived from the acetylacetone residue, as this site is likely to be the most acidic, being adjacent to two coordinated imines. The frequency of C_8 is more negative compared to the analogous parent diiminate complex. This shift, along

with the shift of the imine resonance to more a positive frequency compared to the parent Pt(IV) precursor, implies that the six-membered chelate ring in the Pt(II) complex is no longer delocalised.

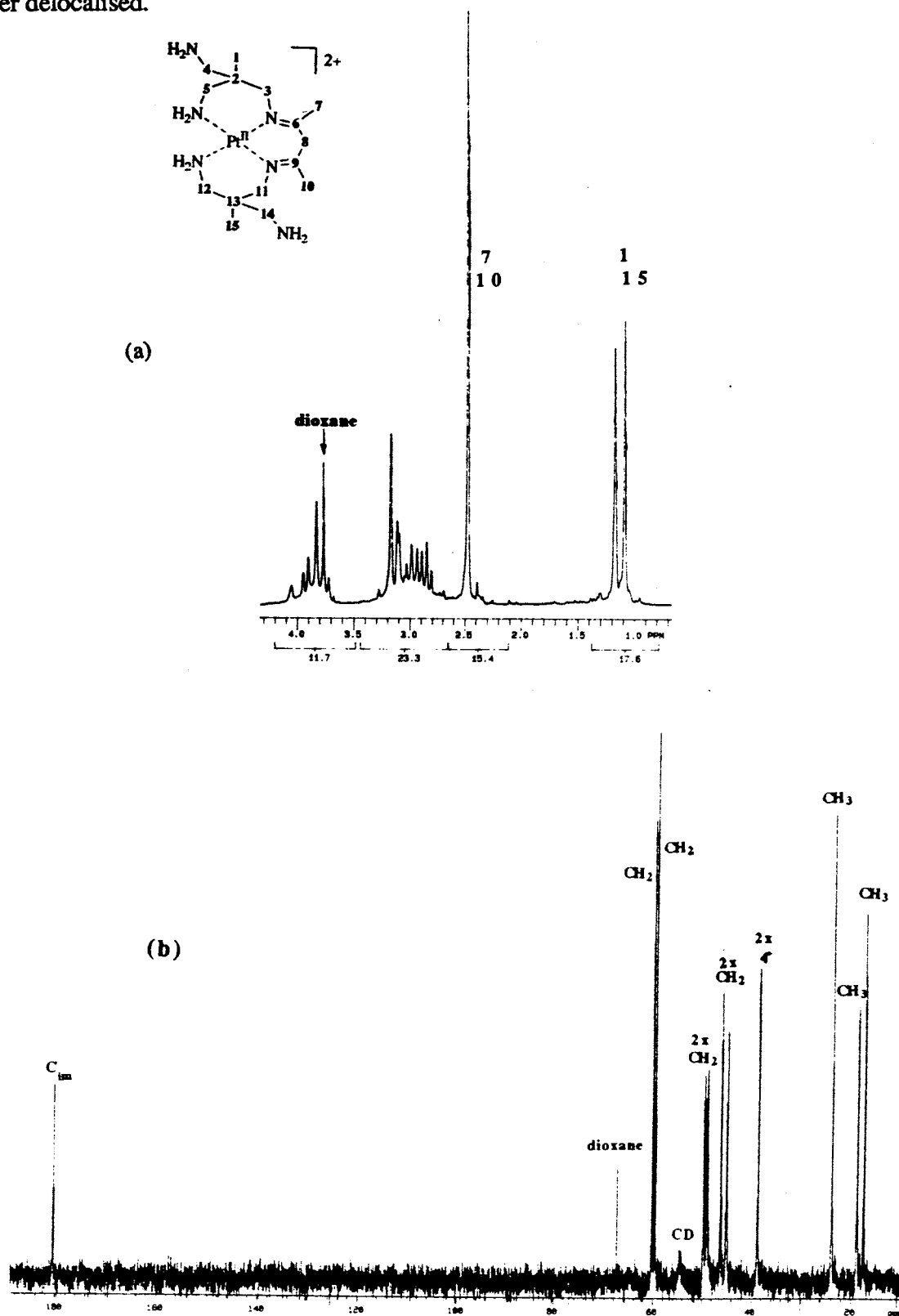


Figure 3.34: 300 MHz NMR spectrum in D₂O of the product arising from the hydrogenation of [Pt(tame₂-2,4-pentandiimine)]³⁺ (a) ¹H and (b) ¹³C.

(c) Reaction of $[\text{Pt}(\text{tame})_2]^{4+}$ with 3,3-dimethyl-2,4-pentanedione

Attempts to condense $[\text{Pt}(\text{tame})_2]^{4+}$ with an excess of the diketone 3,3-dimethyl-2,4-pentanedione in either MeCN or water, in the presence of triethylamine, were not successful. No chelate ring formation was observed, in either nonaqueous or aqueous media. Presumably, the driving force for condensation lies in the formation of the stable 6-membered delocalised chelate ring, which is only possible if the methine carbon of the acetylacetonate residue becomes deprotonated. This behaviour is consistent with that observed during the attempted protonation of the $[\text{Pt}(\text{tame})_2\text{-2,4-pentanedione}]^{3+}$ complex using triflic acid.

3.4. Discussion

3.4.1. General

This first part of this discussion addresses the mechanism of the substitution at $[\text{PtCl}_6]^{2-}$ involving the syntheses of the templates $[\text{Pt}(\text{tn})_3]^{4+}$ (Fig. 3.47(a)), $[\text{Pt}(\text{stn})]^{4+}$ (Fig. 3.47(b)) and $[\text{Pt}(\text{tame})_2]^{4+}$ (Fig. 3.47(c)) and also reactions with the free cage ligand to form $[\text{Pt}(\text{Me}_5\text{-}N_6\text{-tricosane})]^{4+}$ (Fig. 3.47(d)). The only successful substitution reaction was the synthesis of $[\text{Pt}(\text{tame})_2]^{4+}$. Hence the large cages in this chapter are all derived from aldehyde condensations with this template in acetonitrile. Secondly, the condensation reactions leading up to the synthesis of the cages are discussed and alternative routes leading to Pt(IV) cages are proposed.

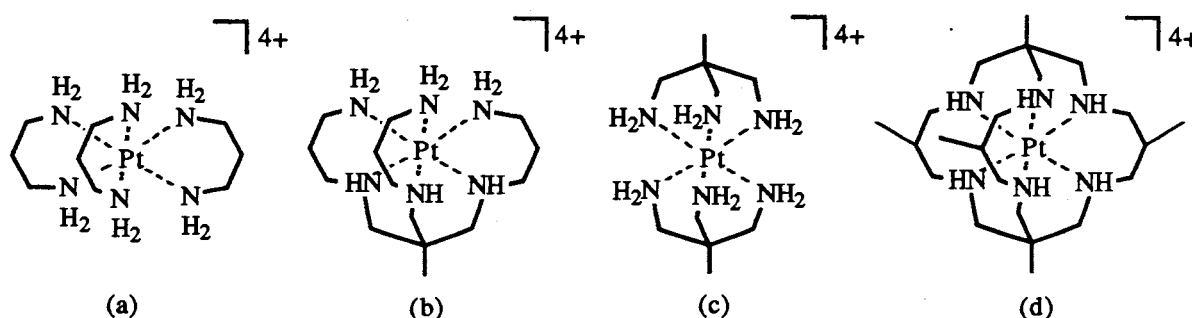
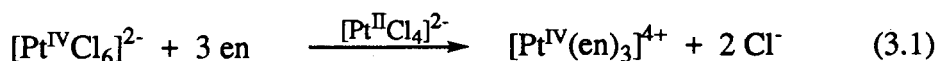


Figure 3.47: (a) $[\text{Pt}(\text{tn})_3]^{4+}$; (b) $[\text{Pt}(\text{stn})]^{4+}$; (c) $[\text{Pt}(\text{tame})_2]^{4+}$; (d) $[\text{Pt}(\alpha\text{Me}_5\text{-}N_6\text{-tricosane})]^{4+}$.

3.4.2. Substitution Reactions of Pt(IV)

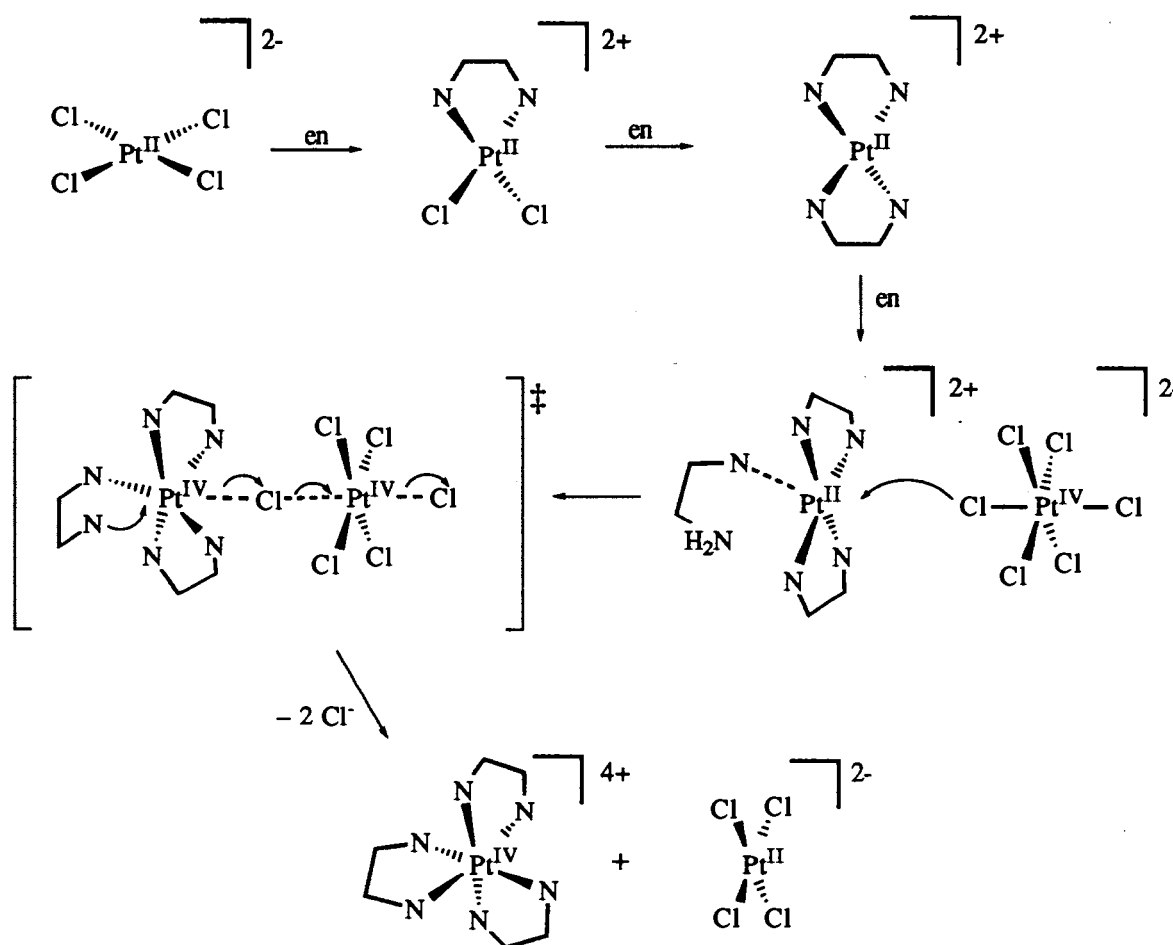
(a) $[\text{Pt}(\text{tn})_3]^{4+}$

Despite numerous attempts, the synthesis of $[\text{Pt}(\text{tn})_3]^{4+}$ by substitution of Cl^- in $[\text{PtCl}_6]^{2-}$ in the presence of a catalytic amount of $[\text{PtCl}_4]^{2-}$ was not successful. It is not clear why such a simple molecule such as $[\text{Pt}(\text{tn})_3]^{4+}$ is difficult to synthesise using methods that have been successful for the synthesis of $[\text{Pt}(\text{NH}_3)_6]^{4+}$, $[\text{Pt}(\text{en})_3]^{4+}$ and $[\text{Pt}(\text{pn})_3]^{4+}$. The reason may lie in the general mechanism of Pt(IV) ligand substitution, as summarised in equation 3.1 (using ethylenediamine as the substituting ligand).



Pt(IV) complexes are very inert and their substitution is dominated by electron transfer and substitution mechanisms utilising Pt(II) complexes as catalysts.²³⁻²⁸ The mechanism involves the transfer of a ligand (e.g. Cl^-) from a Pt(IV) centre to a Pt(II)

centre with concomitant oxidation of the Pt(II) species to Pt(IV). Scheme 3.2 depicts a mechanism proposed for substitution around $[\text{PtCl}_6]^{2-}$ using bidentate ethylenediamine as the incoming ligand to form $[\text{Pt}(\text{en})_3]^{4+}$ in the presence of a catalytic amount of $[\text{PtCl}_4]^{2-}$.



Scheme 3.2: General mechanism for Pt(IV) substitution complexes, catalysed by Pt(II) (amine protons have been omitted for clarity).

Initially, substitution of $[\text{PtCl}_6]^{2-}$ by two ethylenediamine ligands takes place to form $[\text{Pt}(\text{en})_2]^{2+}$, by the standard Pt(II) associative substitution mechanism.²⁸⁻³⁰ A third ethylenediamine ligand coordinates to form a square pyramidal Pt(II) intermediate species. A chloride ligand from a $[\text{PtCl}_6]^{2-}$ centre coordinates at the remaining vacant coordination site of the Pt(II) complex, which forms a bridge between the two metal ions. A two electron transfer ensues, resulting in oxidation of the Pt(II) centre to Pt(IV). This process is accompanied by coordination of the nitrogen donor of the uncoordinated end of the third ethylenediamine ligand to the Pt centre of the $[\text{Pt}^{\text{IV}}(\text{en})_2]$ moiety and

dissociation of the $[\text{Pt}^{\text{II}}\text{Cl}_6]^{4-}$ entity occurs.[†] In order for the unbound end of the third ethylenediamine ligand to coordinate with the metal centre, the two coordinated ethylenediamine chelate rings must rearrange, for example, by folding back. This rearrangement appears to be dependent on the nature of these non-bridging ligands. The steric and electronic effects exerted by the non-bridging ligands appear to influence the rate of substitution.²⁴ It has been previously demonstrated that bulky ligands, as in the substitution of 1,1,2,2-tetramethylethylenediamine (Me_4en), to form *trans*- $[\text{Pt}(\text{Me}_4\text{en})_2\text{Cl}_2]^{2+}$, are slow to substitute, as bridge formation is hindered.²⁴ Similar reasoning may be used to explain the difficulty of substitution of the third trimethylenediamine ligand to form the target complex, $[\text{Pt}(\text{tn})_3]^{4+}$.

The major product formed in these preparations was $[\text{Pt}(\text{tn})_2]^{2+}$, and some *trans*- $[\text{Pt}(\text{tn})_2\text{Cl}_2]^{2+}$ was also isolated. After further treatment of both complexes with excess trimethylenediamine, no additional ligand substitution was observed. This may be related to the stability and relative rates of formation and collapse of the transient bridged complex. Bridge formation may be inhibited in the Pt-tn system as the non-bridging trimethylenediamine chelate rings may be more sterically hindering than the ethylenediamine rings. Alternatively, the bridged transient may not be sufficiently stable and collapses before the pendant nitrogen donor of the third trimethylenediamine ligand has time to coordinate with the Pt centre. Ring closure rates for six-membered chelate ring systems are slower and they are also less stable than five-membered chelate rings,²⁹ so collapse of the bridged transient may be more competitive in the trimethylenediamine reaction. Improving the stability of the putative bridged species may enhance the formation of the third chelate ring. It has been observed that the rates of substitution are dependent on the type of bridging ligand, the order of reactivity is $\text{I} \gg \text{Br} > \text{SCN} > \text{Cl}^- \gg \text{OH}^-$.²⁴ In the trimethylenediamine substitution reactions described here, the bridging atom was Cl^- and this ion would not give rise to the most stable bridged complex. Using the iodide as the bridging atom may increase the lifetime of the bridged species, and thus enhance the probability of formation of the third trimethylenediamine ring. This may be achieved by using $[\text{PtI}_6]^{2-}$ in the presence of $[\text{PtI}_4]^{2-}$.

[†] The reduction potential of the $[\text{PtCl}_6]^{2-}/[\text{PtCl}_4]^{2-}$ is ~ 0.7 V, compared with that of $[\text{Pt}(\text{NH}_3)_6]^{4+}/[\text{Pt}(\text{NH}_3)_4]^{2+}$ at ~ 0.4 V.³¹ Hence the $[\text{PtCl}_6]^{2-}$ entity in the bridged intermediate is that which is reduced.

(b) [Pt(stn)]⁴⁺

The synthesis of [Pt(stn)]⁴⁺, by way of substitution of [PtCl₆]²⁻ by free stn in the presence of a catalytic amount of [PtCl₄]²⁻, was also not successful. Many products were obtained from the reaction, including highly coloured polymeric products. The initial substitution mechanism is probably similar to that described in Scheme 3.2. Namely, ligand substitution occurs around a Pt(II) centre to form a square planar PtN₄²⁺ species. Electron transfer then takes place from the Pt(II) centre by way of a bridging ligand to a Pt(IV) centre with concurrent ligand transfer from the Pt(IV) to the Pt(II) species. However, there are many opportunities for the Pt(II) centre to coordinate with four nitrogen donors of the hexadentate stn ligand and many isomers are possible. In addition, coordination of more than one Pt(II) centre to the ligand is possible, giving rise to dimeric and polymeric species. Finally, in order to form the target complex, the two uncoordinated nitrogen donor atoms must be on the same side of the PtN₄²⁺ plane such that formation of the inner sphere bridged intermediate will not be hindered. Extensive rearrangement must also occur for the remaining nitrogen donor to coordinate during the lifetime of the bridged transient. Folding back of the coordinated trimethylenediamine straps, for example, is likely to be inhibited as the tripod cap restricts movement of these straps unless Pt^{IV}-N bond cleavage takes place. This is unlikely, as Pt^{IV}-N dissociation is very slow. Unless there is some way to enhance the lability of the Pt(IV) ion, the coordination of stn (and likewise sen) is unlikely.

(c) [Pt(Me₅-N₆-tricosane)]⁴⁺

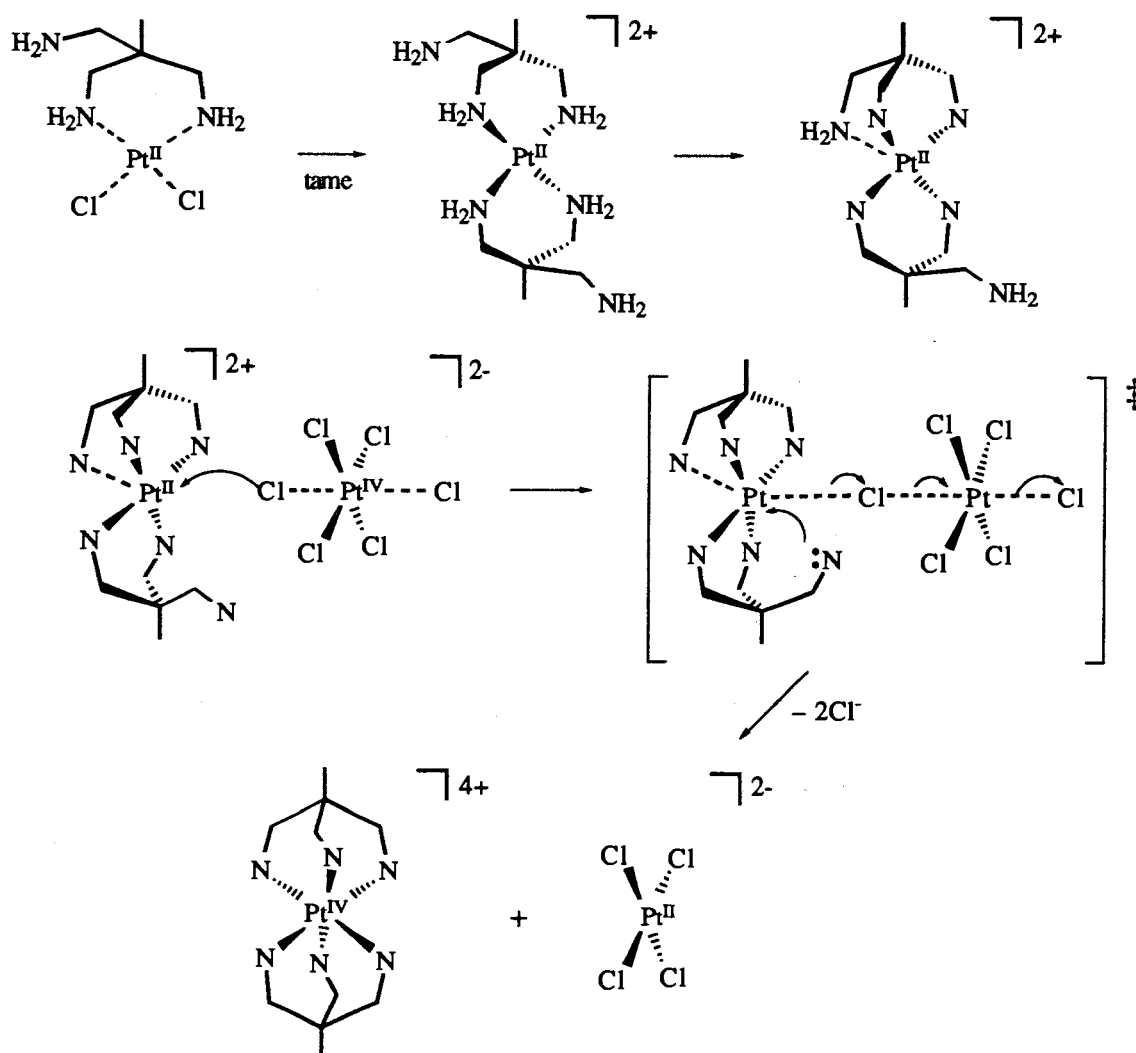
The attempted synthesis of [Pt(Me₅-N₆-tricosane)]⁴⁺ by reacting [PtCl₆]²⁻ with the free ligand, in the presence of a catalytic amount of [PtCl₂]²⁻, in DMF at 40° for two days was not achieved. Attempted substitution of both Pt(IV) and Pt(II) with free Me₅-N₆-tricosane ligand in other solvents (water, ethanol, DMSO and 50% water / ethanol) have also been reported to be unsuccessful¹⁵ and many different complexes were also formed. The number of complexes produced in this reaction appeared to be fewer than in the stn system, judging from the less complicated ¹H NMR spectra. The same residues restrict the amine donors in their spatial orientation so that coordination of the ligand with more than one metal ion is less likely than for the stn system.

Clearly, the mechanism for substitution about Pt(IV) using polydentate ligands with more than four ligating nitrogen donors is not conducive to the formation of Pt(IV) polydentate complexes.

(d) $[Pt(tame)_2]^{4+}$

The reaction of $[PtCl_6]^{2-}$ with free tame in the presence of a catalytic amount of $K_2[PtCl_4]$ produced the bis (tridentate) $[Pt(tame)_2]^{4+}$ complex. It is likely that the ligand substitution takes place around the Pt(II) ion, followed by the formation of a bridged complex with $[PtCl_6]^{2-}$. A plausible mechanism is proposed in Scheme 3.3.

Square planar $[Pt(tame)_2]^{2+}$ forms first, where the noncoordinating amine group on each tame residue lies on opposite sides of the PtN_4^{2+} plane. Similar stereochemistry has been observed in $[Pt(tacn)_2]^{2+}$.³² One of the pendant amines coordinates to form a square pyramidal complex, followed by coordination of a chloride ion from $[PtCl_6]^{2-}$ to form the bridge. The pendant nitrogen donor atom of the second tame ligand coordinates with the Pt centre, accompanied by dissociation of the $[PtCl_4]^{2-}$ entity (and two chloride atoms), giving rise to $[Pt(tame)_2]^{4+}$.

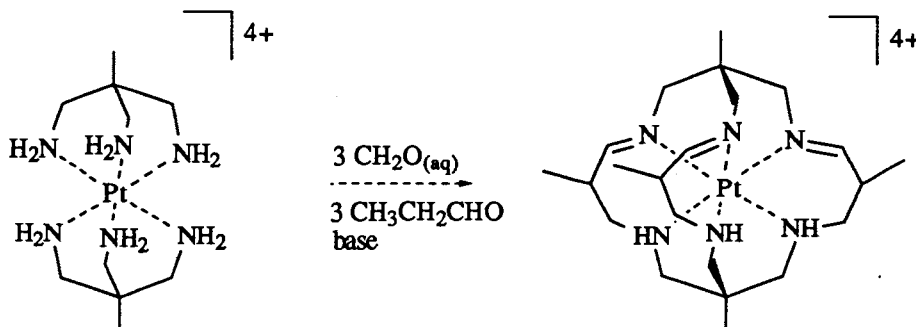


Scheme 3.3: Proposed mechanism for $[Pt(tame)_2]^{4+}$ synthesis (some amine protons have been omitted for clarity).

3.4.3. Reactions of $[\text{Pt}(\text{tame})_2]^{4+}$ with Propanal

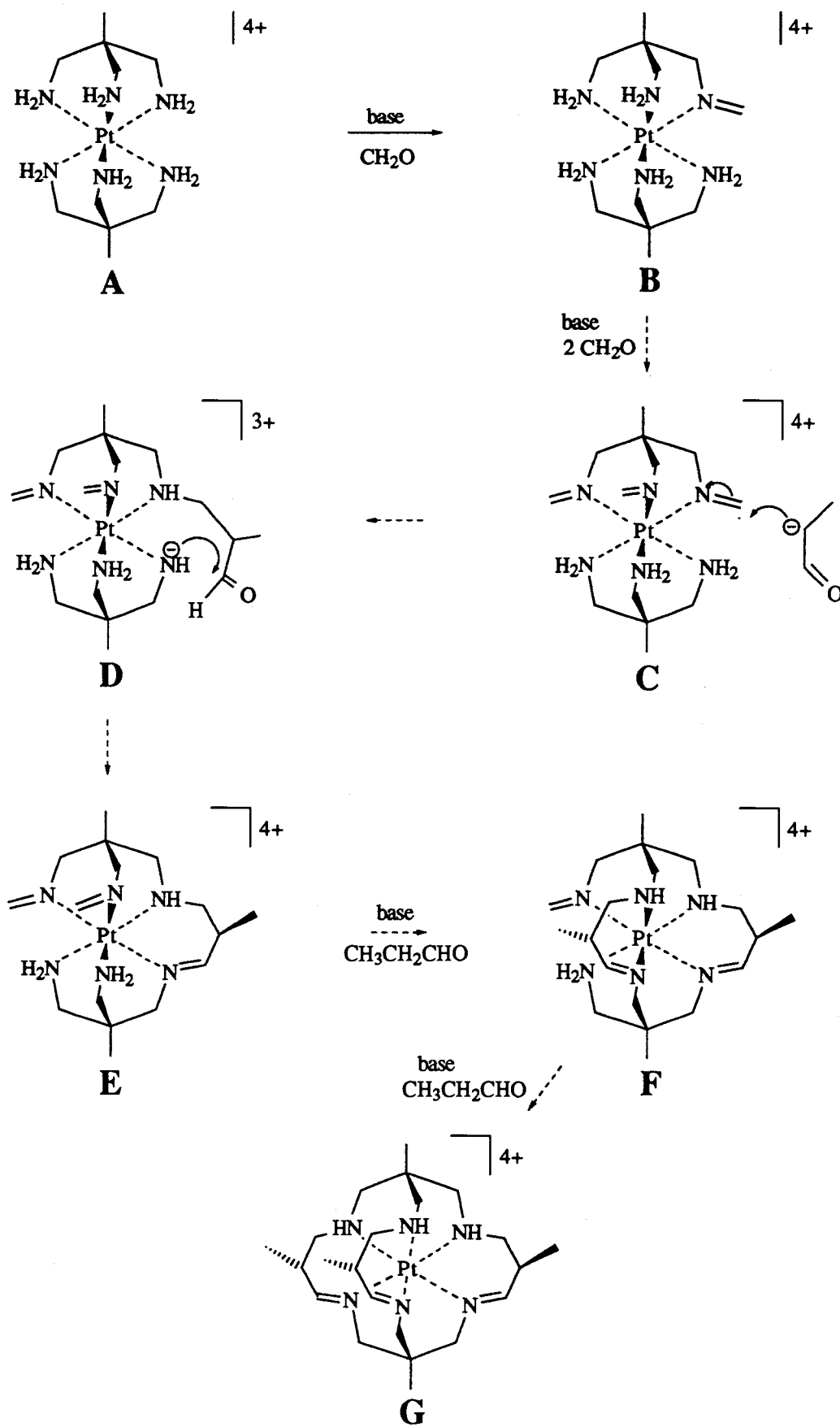
(a) Synthesis of $[\text{Pt}(\alpha\text{Me}_5\text{-N}_6\text{-tricosanetriimine})]^{4+}$

When $[\text{Pt}(\text{tame})_2]^{4+}$ was treated with aqueous formaldehyde and propanal in basic MeCN in a one pot template synthesis, the major product was $[\text{Pt}(\alpha\text{Me}_5\text{-N}_6\text{-tricosanetriimine})]^{4+}$ (Scheme 3.4). All three imines lie on the same face of the octahedron, attached to the same tame ligand. The yield of $[\text{Pt}(\alpha\text{Me}_5\text{-N}_6\text{-tricosanetriimine})]^{4+}$ obtained from this reaction (~50%) was considerably higher than that for the analogous Co(III) reaction (~20%)¹⁷ and this may be attributed to the greater acidity of the N-H groups of the $[\text{Pt}(\text{tame})_2]^{4+}$ template. Condensation reactions of the aldehydes with Pt(IV) hexaamines are therefore faster and take place at a lower pH than those in the Co(III) system. The lower pH used for the Pt(IV) systems also reduces the rate of base catalysed side reactions (e.g., self condensation, polymerisation, etc), hence higher concentrations of reactants are available for condensation with the template. Possible by-products formed in the reaction are discussed later.



Scheme 3.4: Synthesis of $[\text{Pt}(\alpha\text{Me}_5\text{-N}_6\text{-tricosanetriimine})]^{4+}$.

A mechanism is proposed in Scheme 3.5, which attempts to address the regio- and stereoselectivity of the reaction. A combination of inter- and intramolecular condensation reactions is involved and several pathways are possible. It is not certain why the *facial*-triimine isomer predominates, but the observed regioselectivity may result from a subtle combination of intraligand electronic and steric effects which direct the sequence of condensation reactions. However, the former effects are not well understood in terms of how they govern the relative acidities of coordinating amines. Formation of the first imine may affect the relative acidities of the remaining uncondensed amines and the differences appear to be related to whether the amines are *cis* or *trans* to the coordinated imine and also on which template ligand the imine resides.



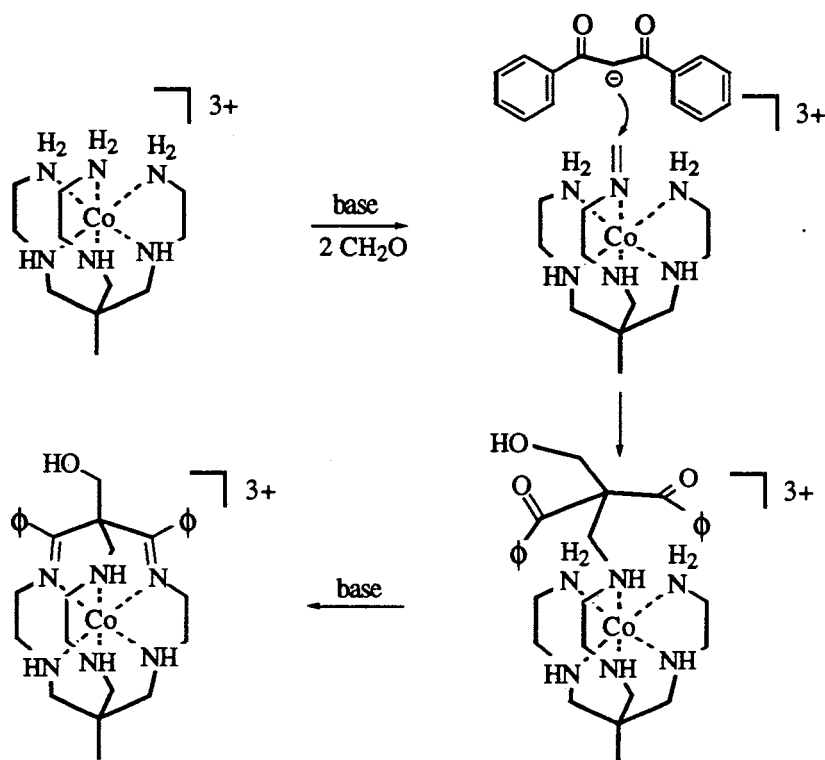
Scheme 3.5: Proposed mechanism for $[\text{Pt}(\alpha\text{Me}_5\text{-N}_6\text{-tricosanetriimine})]^{4+}$.

Work relating the acidities of stereoisomers of $[\text{Pt}(\text{NH}_3)_x(\text{en})(\text{Cl})_{x-1}(\text{py})_y]^{n+}$ ($x=3,2,1,0$, $y=0,1,2$) to electronic effects implies that amines *cis* to the pyridine groups are more acidic than those that are *trans*.^{33,34} Selective deprotonation of the *cis* amine in *mer*- $[\text{Pt}(\text{en})(\text{py})\text{Cl}_3]^+$ has also been claimed.³⁵ If the pyridine ligand in these systems is regarded as an imine analogue, then amine sites *cis* to coordinated imines are likely to be more acidic than those which are *trans*. Extending this conclusion to the condensation reactions reported in this work, the remaining amines *cis* to the first imine should be more acidic. Additional support for this interpretation may be drawn from the lack of evidence for a $[\text{Pt}(\text{Me}_5\text{-}N_6\text{-tricosanetriimine})]^{4+}$ complex where the three imines lie on an octahedral meridian (*mer*-triimine). Some *mer*-triimine may have formed along with numerous other products, since only ~50% of the template was accounted for in the products, but it was not present as a substantial component. Similar observations have been noted in other strapping reactions giving rise to N_6 -tricosanetriimine complexes, such as in the reaction of $[\text{Pt}(\text{tame})_2]^{4+}$ with acetaldehyde (discussed later) and in mixed aldehyde condensation reactions with the $[\text{Co}(\text{tame})_2]^{3+}$ template.¹⁷

In Scheme 3.5, likely intermediates are denoted by capital letters. The $[\text{Pt}(\text{tame})_2]^{4+}$ template, **A**, deprotonates and condenses first with a formaldehyde unit to form a monomethanimine complex, **B**. The $[\text{Pt}(\text{tame})_2]^{4+}$ condenses first with formaldehyde as it is more reactive than propanal. Condensation of propanal with the template will only be competitive when the concentration of formaldehyde is low, in which case other cage complexes are formed (discussed later). To ensure that the concentration of formaldehyde in solution is not limiting, aqueous formaldehyde is used in these reactions. Fortunately, methylene-bridged species did not appear to be a problem in this reaction, unlike the analogous $[\text{Co}(\text{tame})_2]^{4+}$ reactions.^{36,37}

Intermediate **B** condenses with a second formaldehyde unit, presumably with the amine *cis* to the first imine, on the same tame ligand. These two methanimines doubly activate the remaining primary amine on the same tame ligand to react with a third formaldehyde unit, to form a *fac*-tris(methanimine) complex, **C**. Evidence from other condensation reactions (for example, in Scheme 3.6) implies that intermolecular nucleophilic attack of a propanal carbanion with one of the imines is likely, producing intermediate **D**, which bears a pendant carbonyl moiety. Dreiding models indicate that the pendant carbonyl is well poised for intramolecular attack by an adjacent deprotonated amine on the opposite tame ligand, and this condensation yields intermediate **E**. The remaining two methanimines condense sequentially with two propanal carbanions in a manner similar to that of the first imine, to form first the intermediate **F** and then the final complex, **G**.

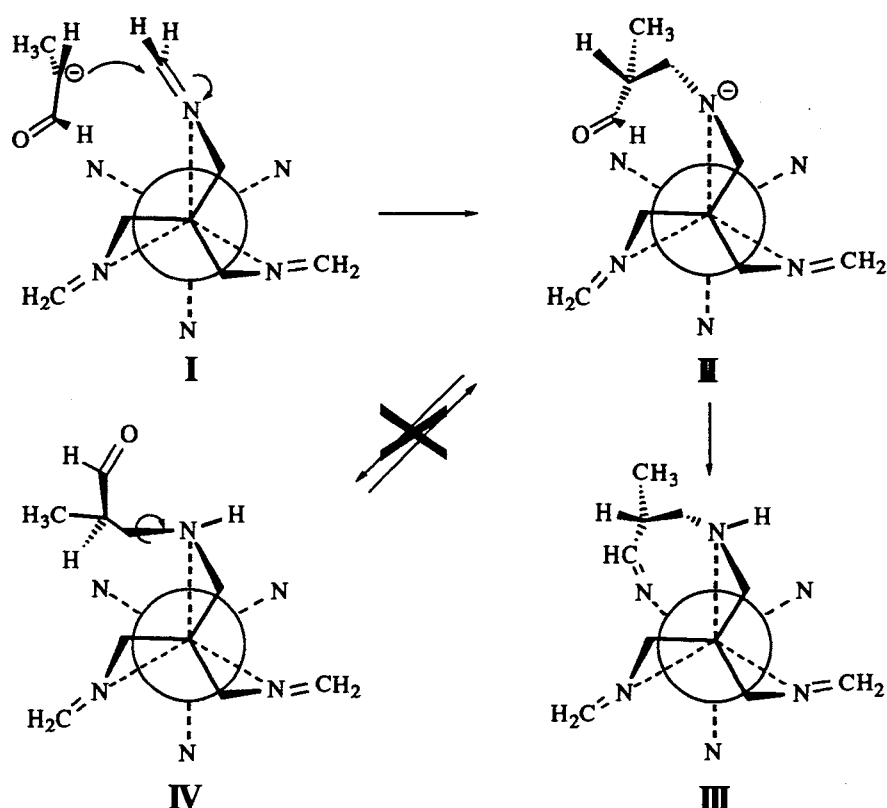
Such intermolecular attack of a carbanion at a coordinated imine followed by rapid intramolecular condensation leading to ring closure has been established in other systems, e.g., the reaction of 1,3-diphenyl-1,3-propanedione, formaldehyde and $[\text{Co}(\text{sen})]^{3+}$ to form the cage complex with two phenyl substituents in the cap, as depicted in Scheme 3.6.³⁸ In this system, the formaldehyde condenses to form a methanimine intermediate which is then attacked by the deprotonated carbanion. In the absence of formaldehyde, the dione does not condense with the template and this is consistent with the sequence of reactions occurring in the order described.³⁸



Scheme 3.6: Reaction of 1,3-diphenyl-1,3-propanedione with $[\text{Co}(\text{sen})]^{3+}$ in the presence of CH_2O .

The process in Scheme 3.5 however, is more intricate, since it must account for the reaction of six organic fragments with the template such that seven stereogenic centres are produced, two associated with each strap (at the secondary nitrogen and the methine carbon), plus the $\text{Pt}(\text{IV})$ ion. After taking into account degenerate stereoisomers, 48 isomers are possible. The crystal structure of $[\text{Pt}(\alpha\text{Me}_5\text{-N}_6\text{-tricosanetriimine})](\text{ZnCl}_4)_2$ has the Λ configuration about $\text{Pt}(\text{IV})$ and the configurations of the three methine carbon atoms in the strap and three secondary nitrogens in the final complex are R and S, respectively. It is not clear whether the observed configurations are established under kinetic or thermodynamic control, however, there is much stereochemical control in the process. Epimerisation may be possible at the nitrogen sites since they undergo proton exchange during the reaction and their configurations may not be fixed until the final stages of the reaction. However, the methine centres are less

acidic than the amine sites, so the configuration developed about these centres may control the overall configuration. Dreiding models show that the condensation of the first propanal with the imine appears to determine the stereochemistry of the product. The orientation of the incoming propanal carbanion to form the first strap leading to formation of the Λ isomer about the Pt(IV) centre is described in Scheme 3.7. The first propanal carbanion approaches either equivalent side of a methanimine, oriented such that steric interactions of its carbonyl and methyl groups with the same methylene protons and the other two methanimines are avoided (I). The methyl group is expected to be oriented away from the template, as shown. Attack of the propanal carbanion at the imine and subsequent protonation of the nitrogen creates two stereogenic centres, one at the carbanion carbon and the other at the nitrogen centre (II). However, the nitrogen proton rapidly exchanges with solvent so its configuration may not be controlled at this point. Condensation of the pendant carbonyl with an amine on the opposite tame ligand leads to the formation of an methanimine at this site (as in III). If the propanal carbanion condenses with the imine with its carbonyl oriented away from the amine on the opposite tame ligand, the intermediate IV results and Dreiding models show that rotation about the axis indicated in structure IV is sterically hindered. Cyclisation is therefore obviated, unless retro-aldol condensation occurs.



Scheme 3.7: Possible approach of the first propanal carbanion to the tris(methanimine) intermediate, C.

Similar steric requirements pertain to the formation of the remaining straps. In forming the second strap, the configuration of its methine can be established when the second propanal carbanion condenses with one of the two remaining methanimines. This propanal can condense with either of the remaining two methanimines in four possible ways, as depicted in Fig. 3.48.

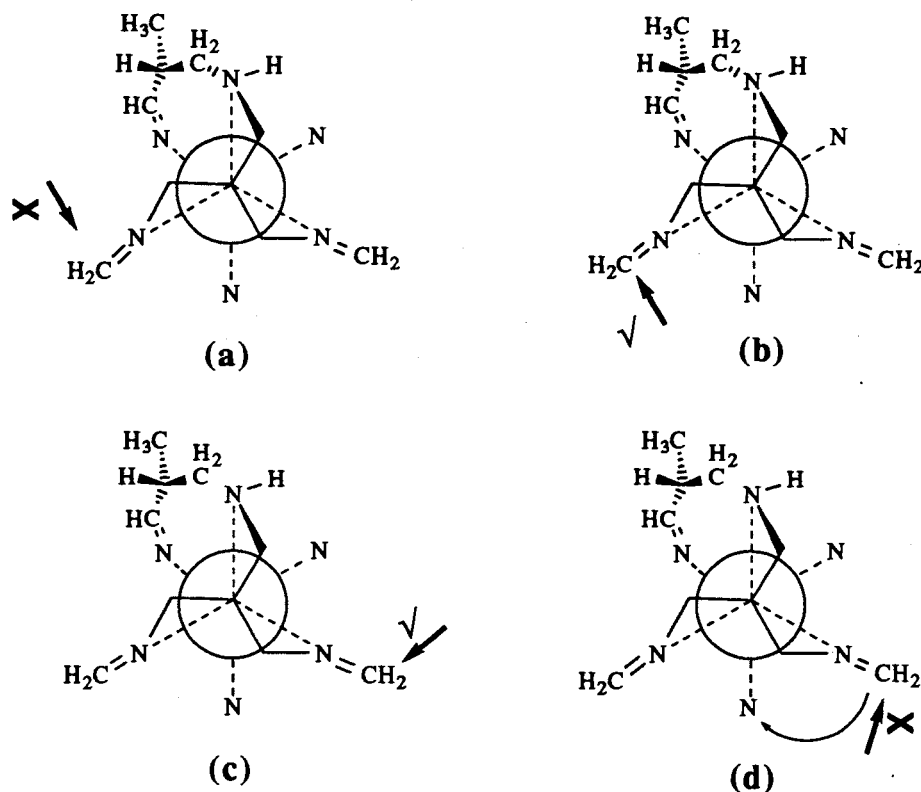


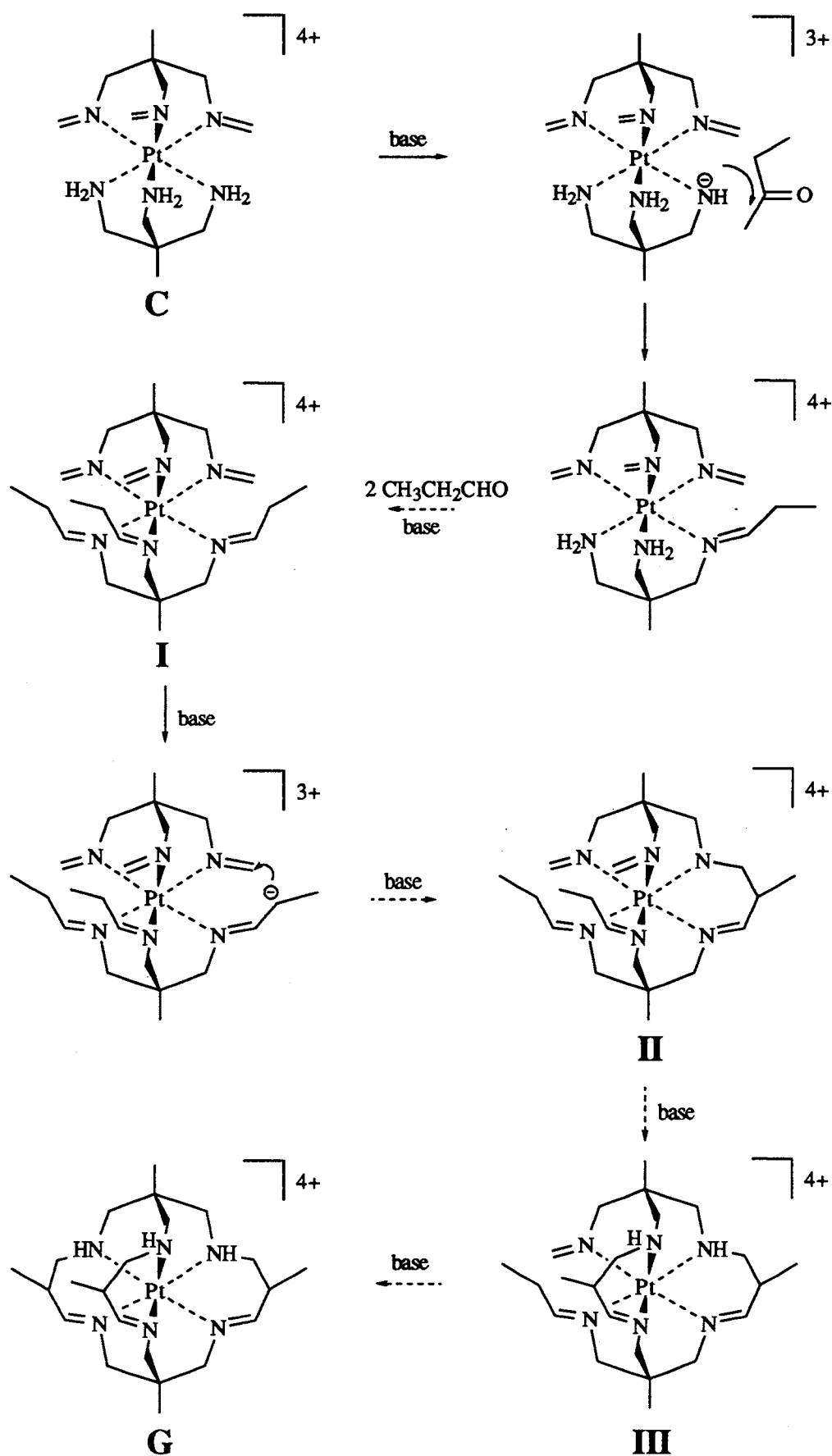
Figure 3.48: Approach of second propanal carbanion to either of the two remaining methanimines of intermediate E. (a): most hindered side for attack; (b) and (c) attack from this side yields same methine configuration as that in the first strap; (d) attack from this side yields the complex with the newly formed chelate rings *trans* to each other.

Attack by the second propanal carbanion at the face of the methanimine indicated in Fig. 3.48(a) is not likely, as Dreiding models show that the first strap hinders the approach of the carbanion to this face of the imine. On the other hand, hindrance is less if the propanal carbanion approaches the other side of the same imine, as depicted in Fig. 3.48(b). Hindrance is also less in Figs 3.48(c) and (d). If attack takes place as in Figs 3.48(b) or (c), then the resulting configuration about the strap methine centre will be the same as that in the first strap. However, if the carbanion approaches and condenses with the methanimine from the side shown as in Fig. 3.48(d), its pendant carbonyl would condense with the amine on the opposite tame cap, as indicated, giving rise to a complex with the straps *trans* to each other. Dreiding models show that the pendant carbonyl of Fig. 3.48(d) is more favourably aligned with the *trans* amine site, than with the *cis* amine site. Therefore, formation of the third strap to form the triimine

complex is obviated. Attack at this site to give the *trans*-strapped complex is not statistically favoured, the ratio of the mixed configuration product (as in Fig. 3.48(d)) to that resulting from Figs 3.48(b) and (c) is 1:2. The reaction of the remaining methanimine is subject to the same considerations as formation of the second strap. The C_3 symmetrical isomer is favoured by these steric and statistical influences.

The most stable conformation of the complex arises when the configurations about the methine centres of the six-membered chelate rings are the same, with the methyl substituents in the equatorial position. If the less favoured configurations are produced in the pendant carbonyl complex (i.e., by condensing in the manner Scheme 3.7, structure IV), then cyclisation may be slower or that retro-aldol condensation of the pendant propanal may occur to reform the methanimine. Formation and isolation of largely one stereoisomer out of a possible 48 is truly remarkable. As outlined above, this can be rationalised in terms of a combination of thermodynamic and kinetically controlled condensation reactions driven by the steric effects of the chelate conformations and their substituents.

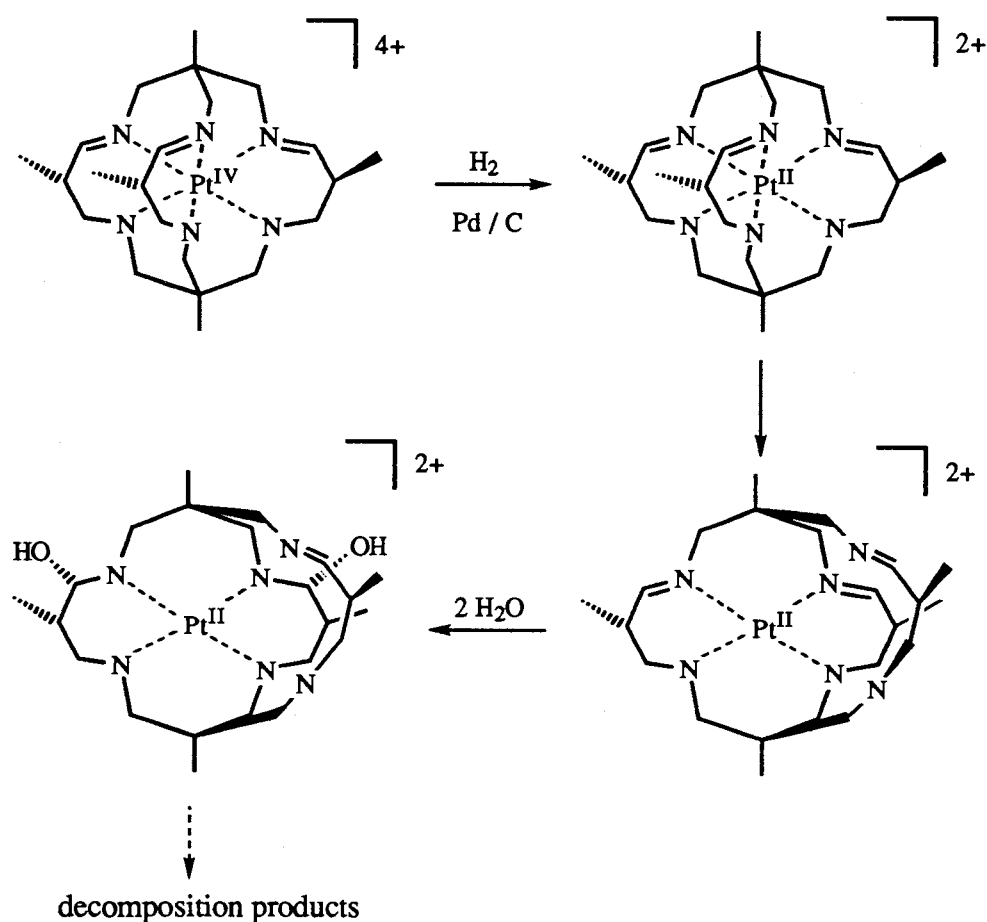
Other possible mechanisms should be briefly considered. One such mechanism is outlined in Scheme 3.8, using the tris(methanimine) species, C, introduced previously in Scheme 3.5. The intermediates in Scheme 3.8 are denoted by Roman numerals. Intermediate C may sequentially condense with three propanal molecules to form the hexaimine species, I. The protons on the carbon atoms alpha to the imines in the propanimines may be deprotonated under the reaction conditions to form internal nucleophiles. In the presence of base, intramolecular attack by a propanimine carbanion on a coordinated methanimine on the opposite same ligand leads to ring closure to form the intermediate II, and similar reactions occur to form species III and finally, G. This route, like the intermolecular route described in Scheme 3.5, accounts for the regio- and stereoselectivity of the reaction. However, while there is some support for the carbanion routes from other studies described in Schemes 3.5 and 3.6,³⁸ there is none for this pathway. It seems unlikely that the condensation of the tris(methanimine) intermediate (C) with three less reactive propanal molecules to form the putative mixed aldehyde hexaimine species (I) is competitive with further condensation of formaldehyde. Moreover, the formation of hexamine I must be competitive with the direct condensation of the propanal carbanion with the methanimines in intermediate C. Lastly, for intramolecular condensation to occur, the propanimines must all be *endo* and this seems unlikely as the propanal molecule must approach the amine with the ethyl group directed towards the imine. Dreiding models show that this is not the least sterically hindered approach.



Scheme 3.8: Possible mechanism for formation of $[Pt(\alpha Me_5-N_6\text{-tricosanetriimine})]^{4+}$ by way of a tris(methanimine)tris(propanimine) intermediate.

(b) Attempted Reduction of $[\text{Pt}(\alpha\text{Me}_5\text{-N}_6\text{-tricosanetriimine})]^{4+}$

It was not possible to reduce selectively the imines in $[\text{Pt}(\alpha\text{Me}_5\text{-N}_6\text{-tricosanetriimine})]^{4+}$ to the fully saturated $[\text{Pt}(\text{Me}_5\text{-N}_6\text{-tricosane})]^{4+}$ complex using borohydride, dithionite or cyanoborohydride reagents. Too many complexes were produced for separation on a small scale. It was initially thought that hydrogenation of the imines was a likely route for the selective reduction of the imines as the NMR spectra of the reaction solution after a few hours were considerably simpler than those obtained from the borohydride, dithionite and cyanoborohydride reactions. Monitoring the hydrogenation of the complex by ^1H and ^{13}C NMR spectroscopy showed that one complex is formed initially, but is unstable and reacts further to form different products. The ^{13}C NMR spectrum of this complex shows that there are 16 different carbon environments in the complex, including one signal for an uncoordinated imine, one carbinolamine signal and five methyl signals. The ^1H NMR spectrum also supports these assignments.

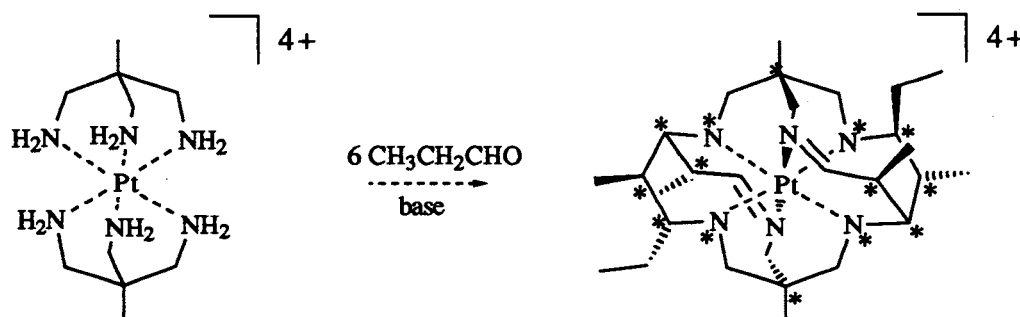


Scheme 3.9: Hydrogenation of $[\text{Pt}(\alpha\text{Me}_5\text{-N}_6\text{-tricosanetriimine})]^{4+}$ (amine protons have been omitted for clarity).

A possible mechanism for reduction and rearrangement is depicted in Scheme 3.9. It is proposed that the Pt(IV) state is reduced first to Pt(II) by way of an observed green transient, possibly a Pt(III) species. As Pt(II) favours a square planar environment, dissociation of two nitrogen atoms of one strap takes place to form a PtN_4^{2+} entity. This accounts for the presence of an uncoordinated imine. The other two coordinated imines become hydrated to form carbinolamines. Dreiding models show that the postulated complex has a pseudo mirror plane through the tame caps, so that similar environments in the complex may have similar peak frequencies, e.g., the strap methyl protons, the coordinating cap and strap methylene protons. The configurations about the coordinated nitrogens and the methine carbon atoms on the strap are expected to be preserved during the hydrogenation, as epimerisation at the nitrogen and methine sites in the less acidic Pt(II) state is probably slow. This would account for the mere 16 peaks observed in the ^{13}C NMR spectrum, instead of the anticipated 22. Further reaction takes place to form a number of different complexes as observed in the NMR spectra after longer hydrogenation times. Such processes may include inversion about the nitrogen donors and hydrolysis of the imine on the noncoordinating strap. Reduction of the imines in $[\text{Pt}(\alpha\text{Me}_5\text{-N}_6\text{-tricosanetriimine})]^{4+}$ while retaining the Pt(IV) oxidation state and the integrity of the cage framework is yet to be achieved.

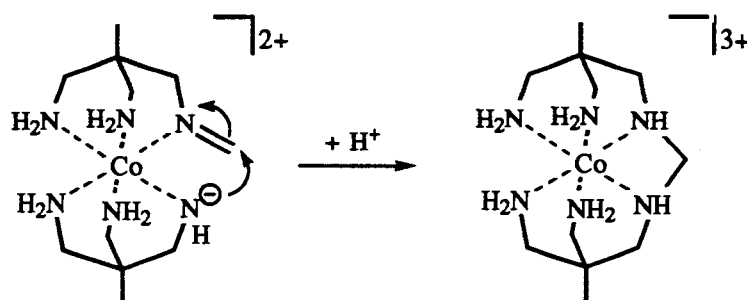
(c) Synthesis of $[\text{Pt}(\text{Et}_2\text{-Me}_6\text{-N}_6\text{-tetracosanediimine})]^{4+}$

When conditions suited for strapping $[\text{Co}(\text{tame})_2]^{3+}$ to form $[\text{Co}(\text{Me}_5\text{-N}_6\text{-tricosanetriimine})]^{3+}$ were used with $[\text{Pt}(\text{tame})_2]^{4+}$, a high yield of a new class of cage complex, $[\text{Pt}(\text{Et}_2\text{-Me}_6\text{-N}_6\text{-tetracosanediimine})]^{4+}$ (Scheme 3.10) was instead formed. There was no evidence that formaldehyde had participated in this reaction. In the absence of paraformaldehyde, the reaction affords the same complex in about the same yield. The crystal structure of this complex shows that the complex has C_i symmetry. The 14 chiroptic sites that were generated in this reaction are denoted by asterisks in Scheme 3.10. Four are associated with the secondary nitrogens and ten are associated with the methine carbon atoms in the straps and cross straps that link the two tame caps. Although the nitrogen protons rapidly exchange with solvent, even in neutral solution, their stereochemistry is controlled by the inflexibility of the ligand and of the chiral carbon centres.



Scheme 3.10: Product arising from reaction of $[Pt(tame)_2]^{4+}$ and propanal (some amine protons have been omitted for clarity).

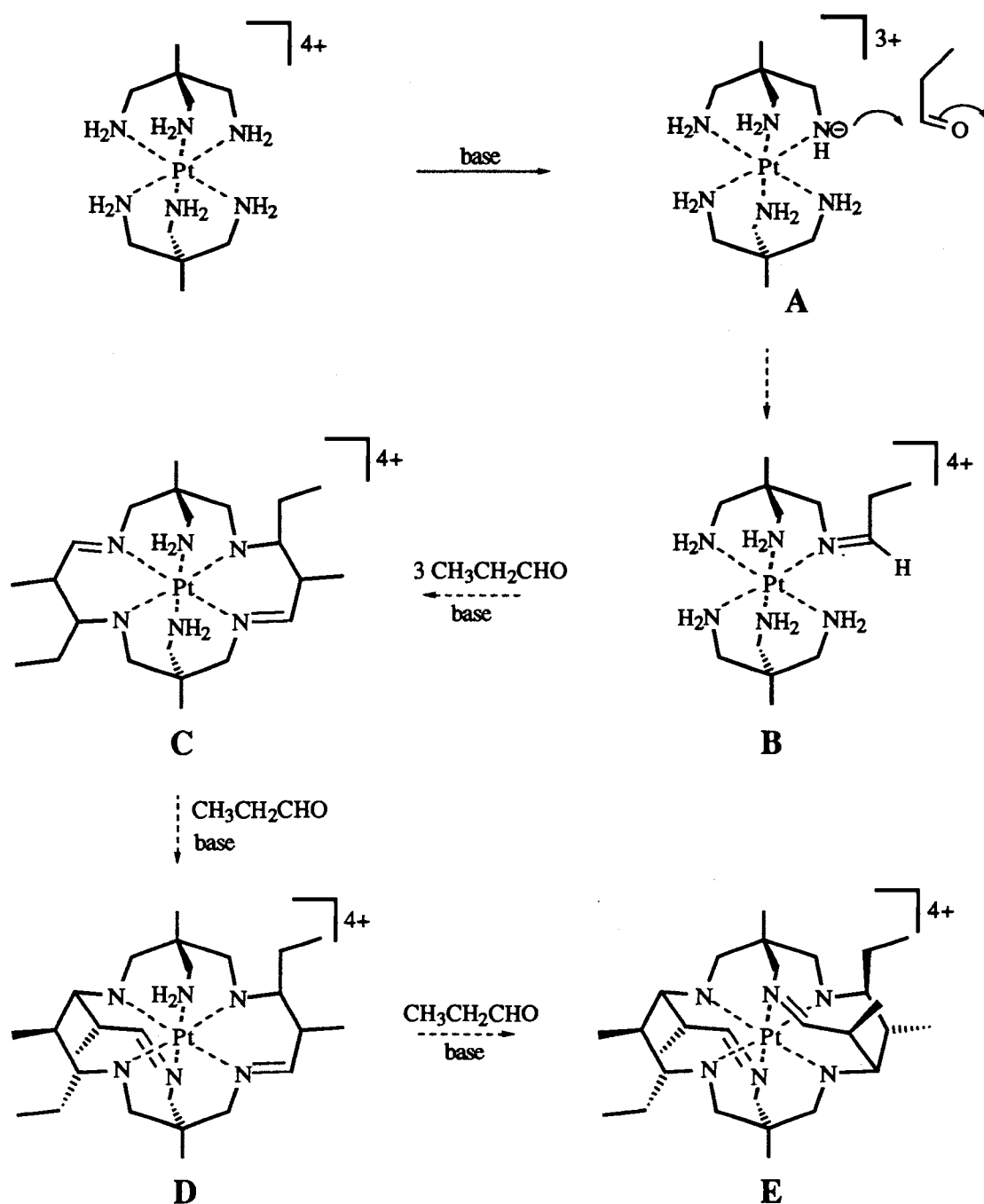
Some explanation is needed for why different products are obtained, depending on whether aqueous formaldehyde or paraformaldehyde is used. The source of formaldehyde used in $[M(tame)_2]^{4+}$ Schiff-base reactions in MeCN governs the product composition. Aqueous formaldehyde is necessary to form $[Pt(\alpha Me_5-N_6\text{-tricosanetriimine})]^{4+}$, whereas paraformaldehyde appears to be necessary for the synthesis of the analogous Co(III) complex. In both systems, the template condenses preferentially with formaldehyde to form coordinated methanimines. In the $[Co(tame)_2]^{3+}$ reactions, intramolecular condensation of the coordinated methanimine with a nearby deprotonated amine is facile (Scheme 3.11). These intramolecular condensation reactions appear to be faster than the rate of intermolecular condensation of the propanal carbanion with the coordinated methanimines. The resulting methylene-bridged species are very stable and such reactions reduce the yield of the desired cage. Furthermore, excess formaldehyde appears to increase the number of methylene-bridges in the template. Hence, slow release of monomeric formaldehyde *in situ* is necessary in order to limit the formation of methylene-bridged species in the $[Co(tame)_2]^{3+}$ reactions. This is achieved by using paraformaldehyde, which is not very soluble in acetonitrile.³⁹ In the presence of traces of water, hydrolysis of paraformaldehyde releases formaldehyde, slowly, therefore limiting its concentration. The water originates from hydrated template complexes, from traces in the solvent and also as a result of the carbonyl condensation reactions. In contrast, $[Pt(tame)_2]^{4+}$ condensation reactions are much faster than those with $[Co(tame)_2]^{3+}$, and formation of methylene-bridged species does not appear to be important. When the concentration of monomeric formaldehyde is low, due to the relatively slow hydrolysis of paraformaldehyde, or not present at all, the deprotonated template $[Pt(tame)_2-H]^{3+}$ condenses with other aldehydes which are present, in this instance, with propanal.



Scheme 3.11: Formation of methylene bridges in $[\text{Co}(\text{tame})_2]^{3+}$.

The mechanism for the formation of the $[\text{Pt}(\text{Et}_2\text{-Me}_6\text{-N}_6\text{-tetracosanediimine})]^{4+}$ has not been fully elucidated. A combination of inter- and intramolecular Schiff base and aldol-type condensation reactions are involved, in a manner similar to those discussed previously for the synthesis of $[\text{Pt}(\alpha\text{Me}_5\text{-N}_6\text{-tricosanetriimine})]^{4+}$ (Scheme 3.5). The exact sequence of events is not clear and it is possible that several pathways occur concurrently. Some intermediates, however, are more likely than others and basic aspects of the pathway are outlined in Scheme 3.12, where these intermediates are denoted by capital letters. The less certain intermediates are discussed later in more detailed schemes and these are labelled with Roman numerals. The overall regio- and stereoselectivity of the reaction must also be accounted for.

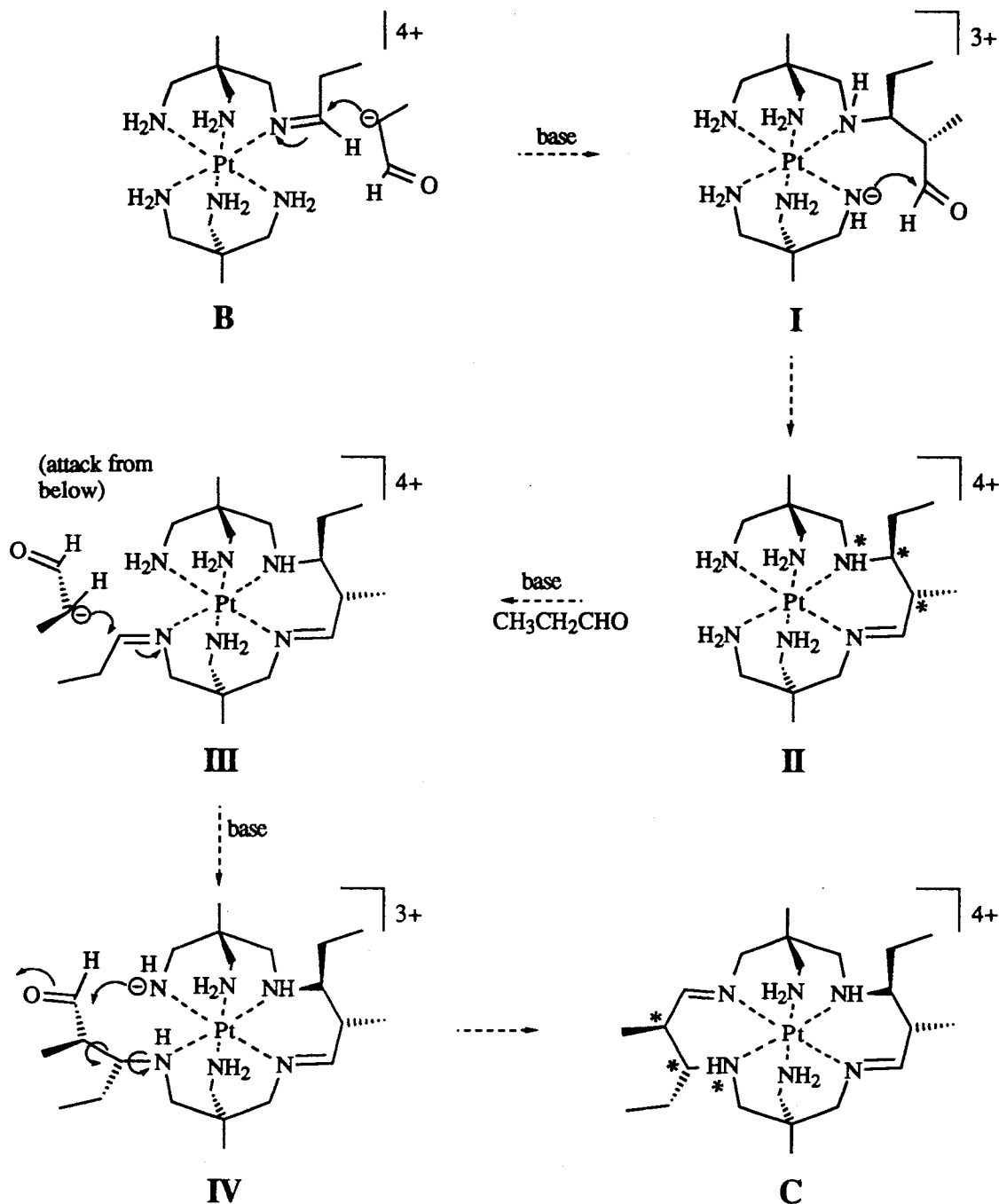
The template deprotonates to form intermediate **A**, which condenses with a propanal molecule, to form the propanimine species, **B**. Intermediate **B** may react with three more propanal units in a number of different ways, to form the *trans*-strapped complex, **C**, which is required for the final stages of the synthesis. It is not clear how complex **C** forms from **B**, and this is addressed later. Intermediate **C** has the imines located *trans* to each other, as are the primary amines, and the latter cannot be readily linked. Hence, once intermediate **C** has formed, formation of the triimine complex (with C_3 symmetry) is not feasible. Sequential condensation of each strap imine with the fifth and sixth propanal units then forms the cross straps, as represented by complexes **D** and the final encapsulated N_6 -tetracosanediimine complex, **E**. Complex **D** is relatively stable and has been characterised independently.



Scheme 3.12: A basic mechanism for synthesis of [Pt(Et₂-Me₆-N₆-tetracosanedimine)]⁴⁺ (some amine protons have been omitted for clarity).

The sequence of events from the monopropylimine complex **B** to the *trans*-strapped diimine, **C**, is less well understood. The order of condensation reactions that produce the observed stereoisomer is probably governed by a combination of electronic and steric effects. A possible route is proposed in Scheme 3.13.

A propanal carbanion attacks the propanimine species, **B**, to form intermediate **I**, which bears a pendant carbonyl. There is no preference for which side of the imine the carbanion attacks **B**. To minimise steric interaction with the ethyl group of the imine, the carbanion is oriented so that its methyl group is pointed away from the complex and its carbonyl group is oriented towards the adjacent amine of the opposite tame ligand. Three chiral centres are generated from this condensation, one from the carbanion carbon and two from the propanimine (as shown). The crystal structure of the product shows these three configurations are the same. Condensation of the pendant carbonyl with an adjacent deprotonated amine on the opposite tame ligand occurs, resulting in formation of the first six-membered chelate strap and the generation of an imine at this site, as shown in intermediate **II**. This chelate ring is in a skewboat conformation. Dreiding models show that when this ring adopts the chair conformation, there is a substantial steric clash of the ethyl substituents with the primary amine on the same tame ligand. The condensation of the third propanal takes place with an amine *cis* to the imine in **II** as this is expected to be more acidic than that *trans*^{33,34} (for reasons discussed previously), so forming the propanimine species, **III**. The other *cis* amine, on the opposite tame ligand is not likely to undergo condensation with this propanal as Dreiding models show that this site it is sterically hindered by the ethyl group on the first strap. The fourth propanal carbanion approaches the propanimine in intermediate **III** from the least sterically hindered face, which is from below the imine, as shown in Scheme 3.13, to form a complex with a pendant carbonyl species, **IV**. Dreiding models show that attack from above this imine is sterically hindered by the first strap. The propanal carbanion approaches the propanimine with its methyl group pointing away from the complex and the carbonyl oriented towards the opposite tame ligand. Three more chiral sites are generated during this condensation, two arising at the nitrogen and carbon of the imine and one at the carbanion carbon. The crystal structure shows that the configurations generated at these sites are catoptric to the corresponding sites on the first strap. Once the pendant carbonyl is formed it condenses with the adjacent amine site on the opposite tame cap, to form the second strap and an imine at this site. The imines in the straps are *trans* to each other, as are the remaining primary amines (complex **C**). The condensation with the supposedly less acidic amine *trans* to the strap imine is not impossible, but it may be slower than if it could condense at the other sites. However, Dreiding models show that rotation about the bonds indicated in **IV** is severely restricted and the carbonyl is very favourably poised for condensation at the *trans* amine site, such that its reaction with the other sites is much less likely. Like the first strap, the second is also in a skewboat conformation, due to steric restrictions imposed by the ethyl substituent. Complex **C** has six chiral centres and its overall symmetry is C_i .

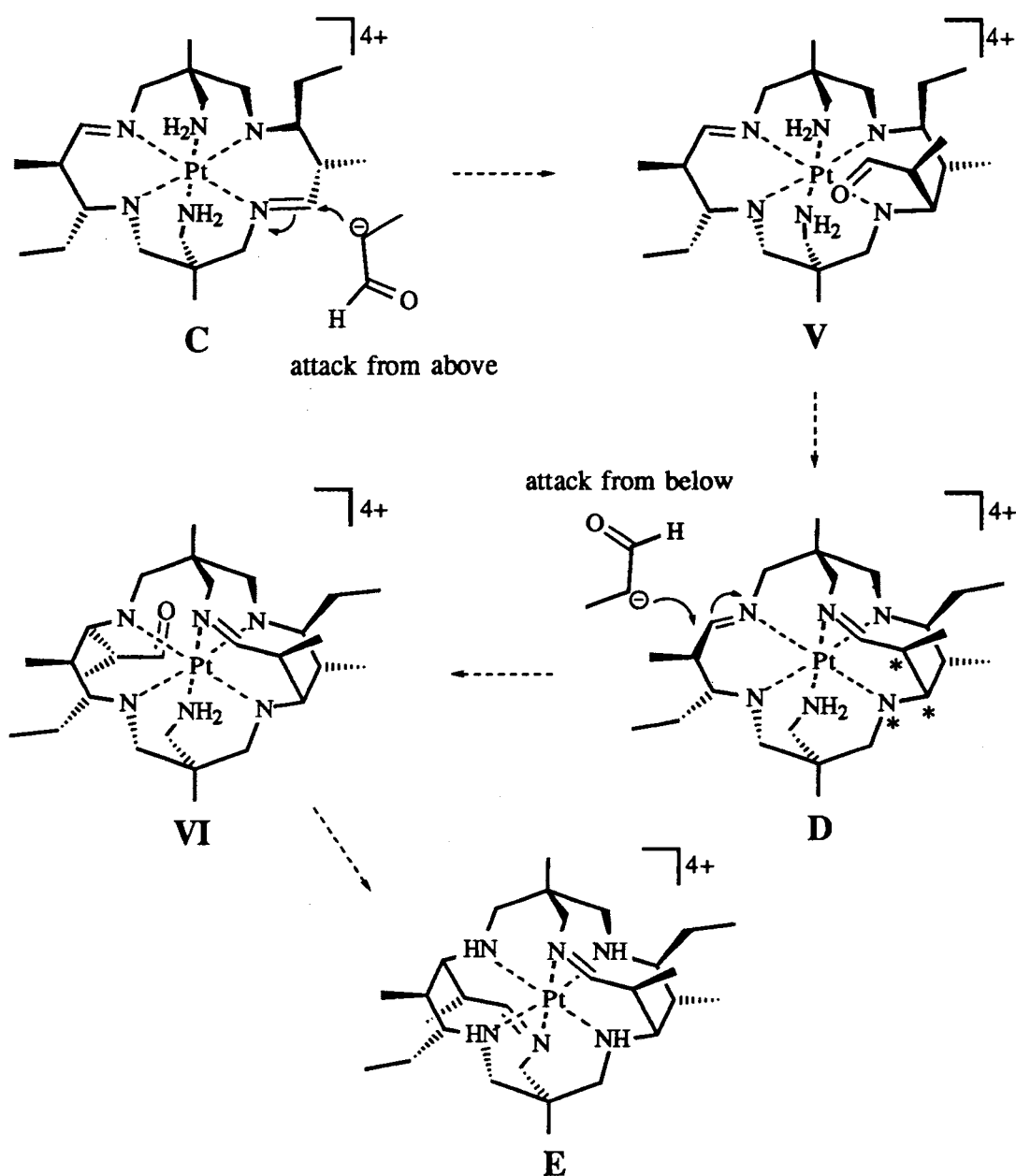


Scheme 3.13: Proposed mechanism for synthesis of complex C. Putative intermediates are labelled I, II, etc.

Scheme 3.14 proposes a series of events which leads to the formation of the cage (E) from complex C. A fifth propanal carbanion attacks one of the strap imines of complex C. Dreiding models indicate that attack only from the top of the imine (as shown) is feasible. Addition at the imine face from below is hindered by the primary amine group on this same residue and therefore less favoured. The carbanion approaches the top face of the imine with its methyl group directed away from the complex to form

intermediate **V**. The resulting pendant carbonyl group is oriented favourably for attack by the primary deprotonated amine on the opposite tame ligand and the condensation results in the formation of the first "cross strap", containing an imine at this site ($[\text{Pt}(\text{Et}_2\text{-Me}_5\text{-N}_6\text{-docosanediiimine})]^{4+}$, **D**). Three chiral centres are generated by addition of this propanal to the imine, one at the methine derived from the carbanion and the other two arising from the nitrogen and carbon in the strap imine. The crystal structure shows that the three centres in this cross strap have the same configuration, but opposite to the others in the strap to which this cross strap is connected. The formation of the second cross strap is subject to the same restrictions; namely that attack by the sixth propanal unit on the other strap imine occurs from below the face of the imine, as shown. The configurations of the chiral sites generated by the condensation are catoptric to those already formed in its connecting strap, as shown in intermediate **VI** and also to those in the first cross strap. Condensation of the pendant carbonyl with the remaining primary amine occurs, giving rise to the product, **E**, with fourteen stereogenic centres, which are related as seven enantiomeric pairs, so the net result is an achiral complex, with C_i symmetry.

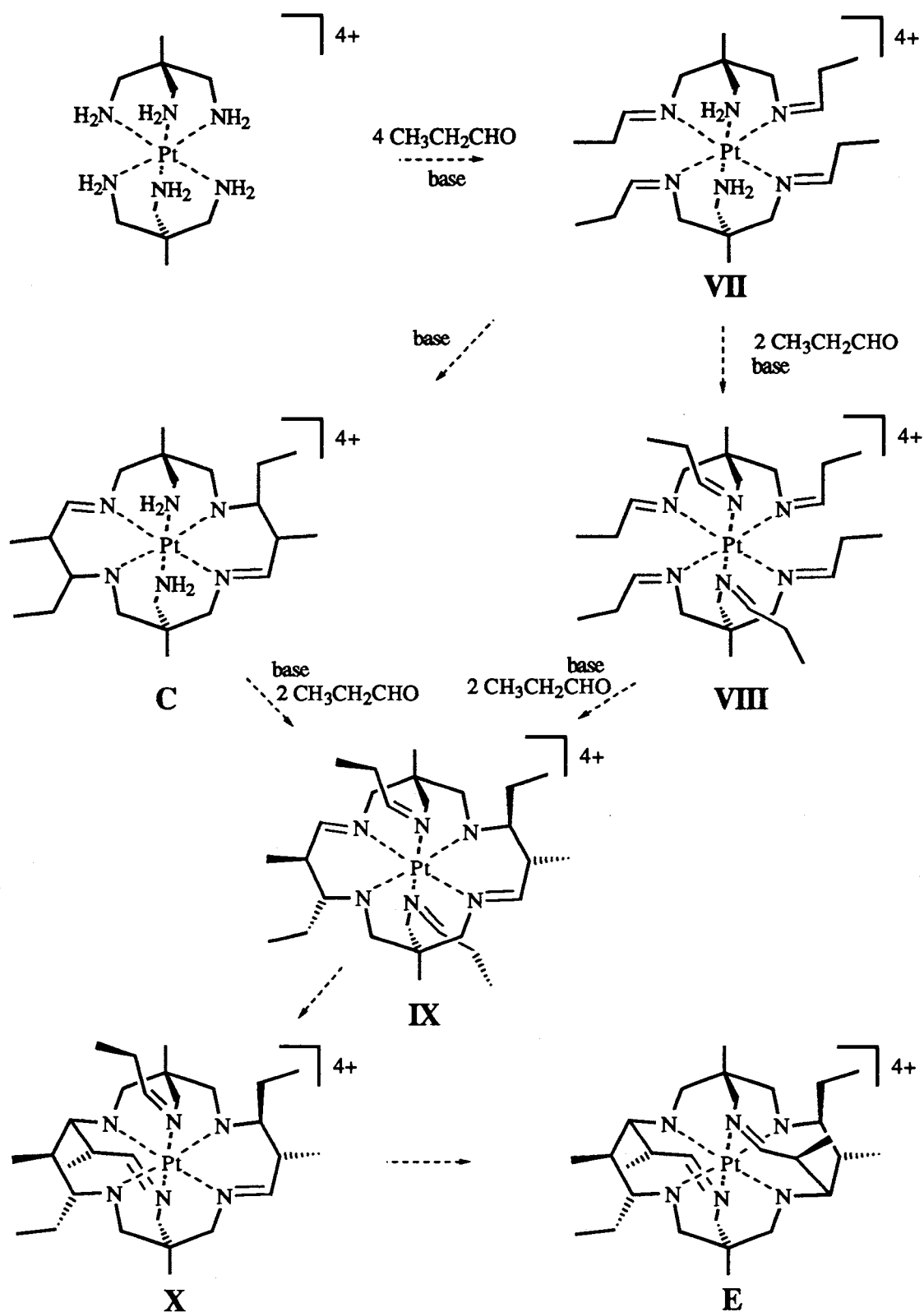
Dreiding models of $[\text{Pt}(\text{Et}_2\text{-Me}_6\text{-N}_6\text{-tetracosanediiimine})]^{4+}$ show that it is rather strained, particularly in the vicinity of the straps bearing the imines. To relieve some of this strain, one of the imines hydrolyses, via retro-Schiff base and retro-aldol reactions, resulting in loss of a propanal residue, to reform **D**, as indicated by the microanalysis of the product and its complicated ^{13}C NMR spectrum. This hydrolysis is enhanced at $\text{pH} > 3$. Regeneration of $[\text{Pt}(\text{Et}_2\text{-Me}_6\text{-N}_6\text{-tetracosanediiimine})]^{4+}$ was accomplished by treating this complex with excess propanal under the original reaction conditions. These observations imply that $[\text{Pt}(\text{Et}_2\text{-Me}_5\text{-N}_6\text{-docosanediiimine})]^{4+}$ (**D**) is an intermediate in the formation of $[\text{Pt}(\text{Et}_2\text{-Me}_6\text{-N}_6\text{-tetracosanediiimine})]^{4+}$.



Scheme 3.14: Condensation of the fifth and sixth propanal units to form the final complex (some amine protons have been omitted for clarity).

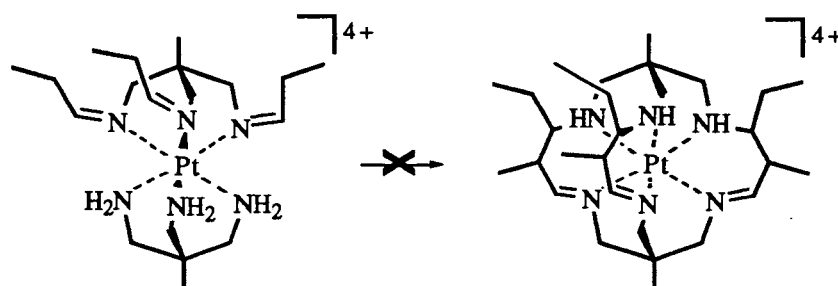
The *trans* strapped diimine intermediate, **C**, and the final complex, **E**, may arise from other routes, for example, by way of intramolecular nucleophilic condensation of coordinated propanimines, similar to the formation of methylene-bridged complexes in reactions using formaldehyde.³⁶ One such pathway (Scheme 3.15) involves the condensation of four propanal units with the template to form the tetraimine intermediate, **VII**, having two propanimines linked to each tame ligand and *trans* primary amines. On each tame ligand, one propanimine must be *endo* and the other *exo*. Specific deprotonation of each of the *endo* propanimines occurs to form internal nucleophiles which intramolecularly condense with the *exo* propanimines on the opposite tame ligand, leading to the formation of the *trans*-strapped complex **C**. The *trans* primary amines of complex **C** could condense with two more propanal units, to form intermediate **IX**, which has *trans* pendant propanimines. Alternatively, the tetraimine species (**VII**) could continue to condense with two propanal molecules, to form a hexaimine species, **VIII**. Deprotonation of carbon sites alpha to the imines of the *endo* propanimines that are also *trans* to each other, followed by intramolecular attack on the *exo* propanimines on the opposite tame residue could also form intermediate **IX**. In principle, after deprotonation at the methine sites alpha to the imines, each of the pendant *trans* propanimines could intramolecularly attack the imines in their adjacent straps, to form the final complex, **E**.

However, the pathways described in Scheme 3.15 are not likely. Firstly, there is a low probability of the propanimines in either intermediates **VII** or **VIII** all having the correct initial conformation required for cyclisation to form **C** or **IX**. Secondly, there is no reason for the formation of intermediate **C** from **VII**, where two remaining primary amines (in **VII**) occupy *trans* sites, and similarly, selective reaction of the *trans* propanimines in **VIII** to form **IX** is not likely. Thirdly, there is no reason for the *endo* propanimines to be preferentially deprotonated such that they are able to attack the *exo* propanimines in an intramolecular manner. Fourthly, Dreiding models show that the pendant *trans* propanimines in **IX** are very poorly aligned with the strap imines for nucleophilic attack to form the cross straps (reactions **IX** to **X** and then to **E**). Finally, the evidence to date favours the intermolecular attack of a carbanion on a coordinated imine rather than the intramolecular attack of two coordinated imines as the path to cyclisation. Overall, Scheme 3.15 cannot be considered as a viable route compared to the carbanion pathway described in Schemes 3.12, 3.13 and 3.14.

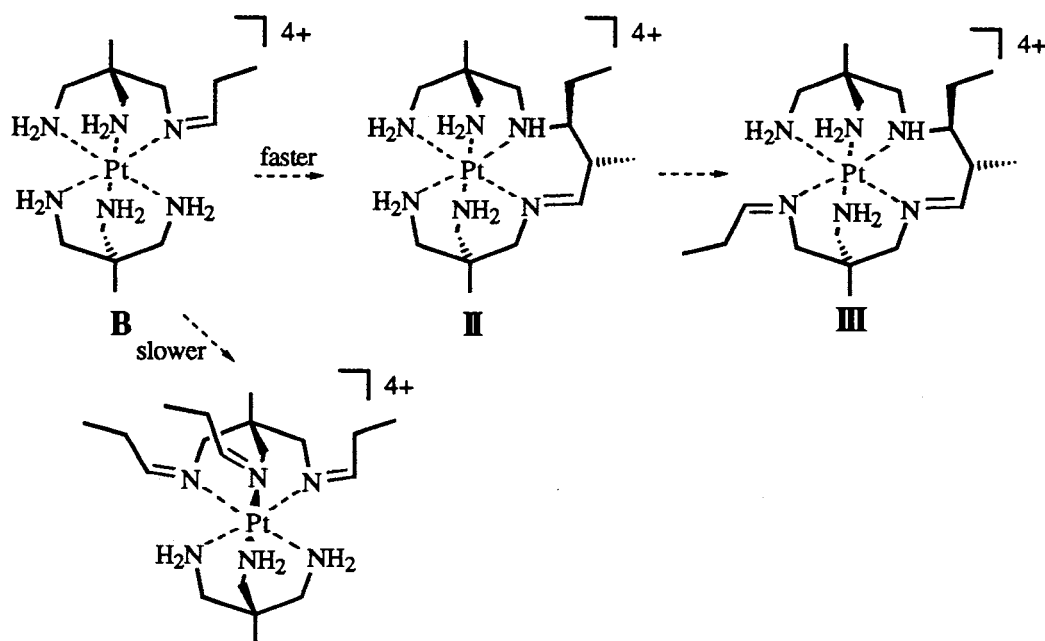


Scheme 3.15: Unlikely routes for the synthesis of $[\text{Pt}(\text{Et}_2\text{-Me}_6\text{-N}_6\text{-tetracosanediimine})]^{4+}$ (some amine protons have been omitted for clarity).

It is surprising that an N_6 -tricosanetriimine complex derived from six propanal units (Scheme 3.16), was not detected upon workup of the reaction solution. Dreiding models indicate that this complex and also its tris(propanimine) precursor are not very strained, nor subject to gross steric interactions. It can be argued that the rate of its formation must be slower than the rate of formation of $[\text{Pt}(\text{Et}_2\text{-Me}_6\text{-}N_6\text{-tetracosane-diiimine})]^{4+}$. As propanal is not as reactive as formaldehyde, the rate of its condensation with the template to form the tris(propanimine) intermediate may be slower than the rate of condensation of the propanal carbanion with the first propanimine. In the latter case, cyclisation occurs to form the strap, which is predisposed to form the N_6 -tetracosane-diiimine complex (II to III in Scheme 3.17). Once the first strap has formed, its imine directs subsequent condensations of propanal units with the template such that they occur at amine sites *cis* to the strap imine, connected to the same tame ligand. Addition of the next propanal unit with complex III is by attack by a carbanion on the imine, and ring closure takes place to form the *trans* strapped complex (C in Scheme 3.16). This is faster than attack to form a *facial*-triimine species. Hence the pathway for the triimine formation is obviated.



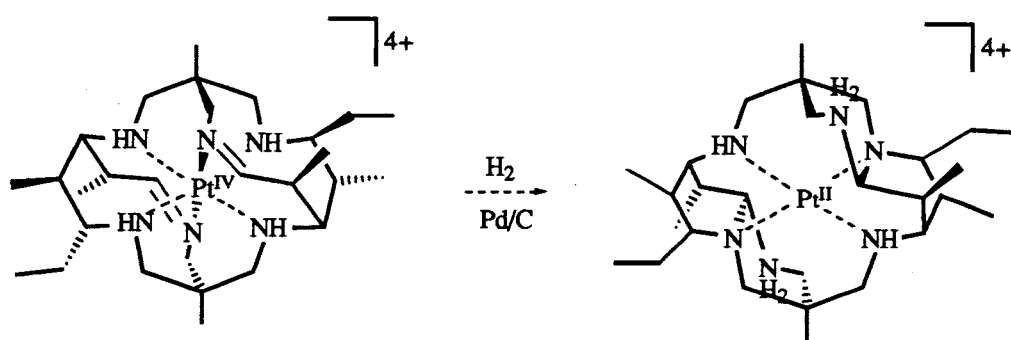
Scheme 3.16. The anticipated intermediate leading to the N_6 -triimine isomer.



Scheme 3.17: Possible competing reactions in the synthesis of $[\text{Pt}(\text{Et}_2\text{-Me}_6\text{-}N_6\text{-tetracosanediiimine})]^{4+}$.

(d) Attempted Selective Reduction of the Imines.

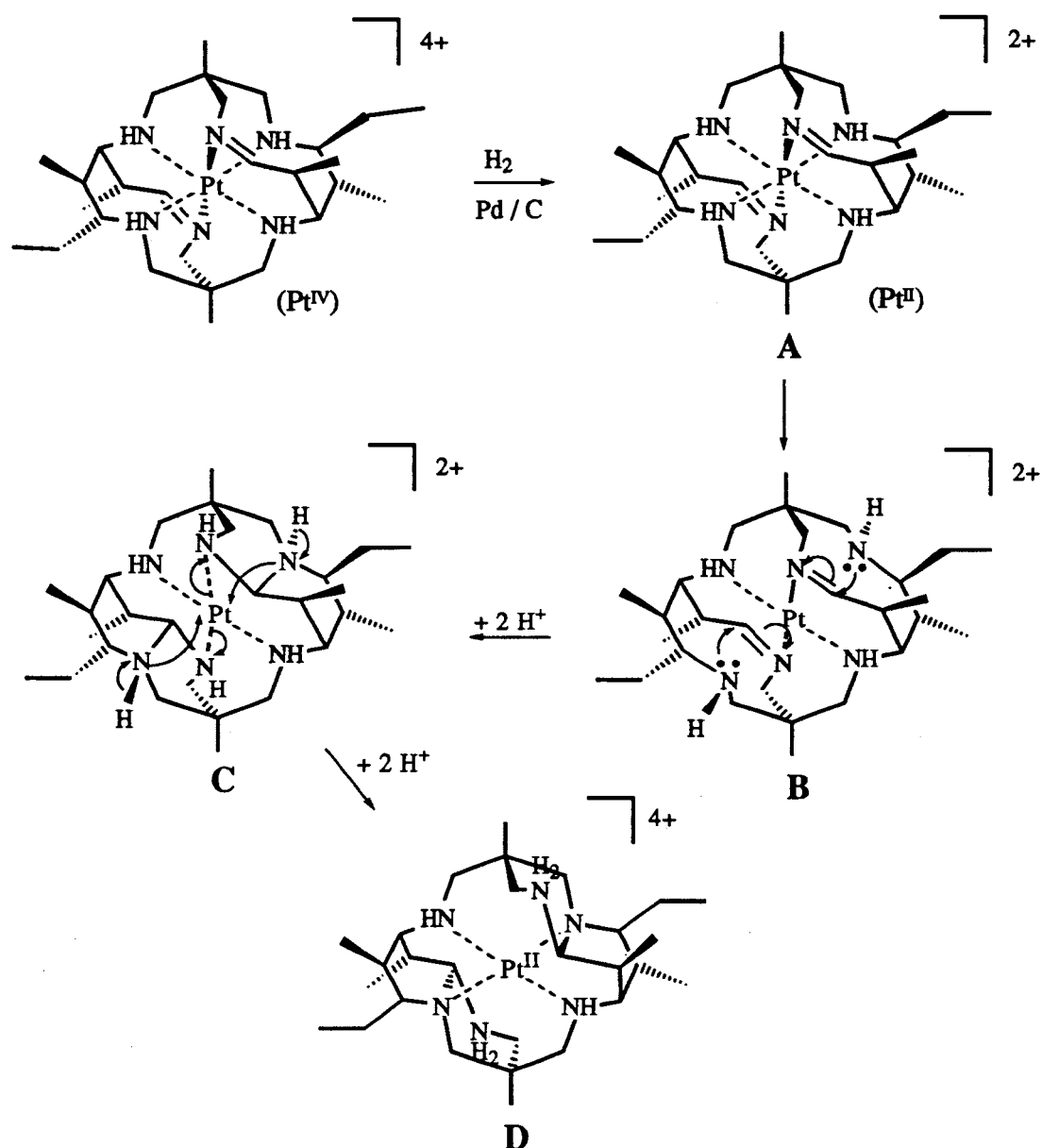
It has not yet been possible to reduce the imines in $[\text{Pt}^{\text{IV}}(\text{Et}_2\text{-Me}_6\text{-N}_6\text{-tetracosanediimine})]^{4+}$ to the fully saturated $[\text{Pt}^{\text{IV}}(\text{Et}_2\text{-Me}_6\text{-N}_6\text{-tetracosane})]^{4+}$, using borohydride or cyanoborohydride as reductants. Many different species, including platinum metal, were produced, too many for successful separation on a small scale. Hydrogenation of the $[\text{Pt}(\text{Et}_2\text{-Me}_6\text{-N}_6\text{-tetracosanediimine})]^{4+}$, however, quantitatively produced a single complex. The ^1H NMR spectrum was complicated but the splitting patterns were reminiscent of the analogous $[\text{Co}(\text{Et}_2\text{-Me}_6\text{-N}_6\text{-tetracosane})]^{3+}$ complex (discussed later) and the analysis of the DQF COSY NMR spectrum implied that the connectivity of the spin systems was not inconsistent with that of the anticipated $[\text{Pt}^{\text{IV}}(\text{Et}_2\text{-Me}_6\text{-N}_6\text{-tetracosane})]^{4+}$ complex. The DEPT NMR spectrum, however, was inconsistent with such a complex. Only after the crystal structure of this product was obtained did it become clear that hydrogenation had resulted in reduction of the octahedral $\text{Pt}(\text{IV})$ centre to square planar $\text{Pt}(\text{II})$. This was accompanied by extensive ligand rearrangement, to form pentacyclo- $[\text{Pt}^{\text{II}}(\text{Et}_2\text{-Me}_6\text{-N}_6\text{-tetracosane})_2\text{H}]^{4+}$ (Scheme 3.18). The crystal structure showed that the coordinated imines in the $\text{Pt}(\text{IV})$ precursor had each condensed with two adjacent amines and that these formerly imine nitrogen donors had dissociated from the $\text{Pt}(\text{II})$ centre. The ligand possesses two pairs of fused six-membered rings, one pair on each side of the large macrocycle. Two new stereogenic centres were created (originating from each imine) to form a total of 16 stereogenic sites.



Scheme 3.18: Product arising from hydrogenation of $[\text{Pt}^{\text{IV}}(\text{Et}_2\text{-Me}_6\text{-N}_6\text{-tetracosanediimine})]^{4+}$.

A mechanism for the synthesis of pentacyclo-[Pt^{II}(Et₂-Me₆-N₆-tetracosane2H)]⁴⁺ is proposed in Scheme 3.19. Reduction of the octahedral Pt(IV) ion to Pt(II) occurs via an unidentified green transient (possibly a Pt(III) complex) giving rise to intermediate A. Since Pt(II) favours square planar geometry,⁴⁰ dissociation of what were the longest Pt-N bonds in the [Pt^{IV}(Et₂-Me₆-N₆-tetracosanediimine)]⁴⁺ precursor is likely (Pt^{IV}-N=2.109(7) Å), to form a PtN₄²⁺ species, intermediate B. Both dissociated nitrogen atoms attack their adjacent coordinated imines, as shown in intermediate B. This process gives rise to intermediate C, which has two additional six-membered rings, one on each side of the ligand. Dreiding models show that this complex is very strained. Reoordination of the two nitrogen atoms takes place, accompanied by concomitant dissociation of what were the original imine nitrogen atoms, (as indicated in intermediate C) to form the product D. In an alternative route, formation of the six-coordinate Pt(II) transient occurs (A), followed by rupture of the Pt-N_{imine} bonds, to form a square planar Pt(II) complex. The cross strap is rather strained in the Pt(IV) state and probably in the Pt(II) state, so this dissociation may be favourable. Each adjacent deprotonated coordinated amine would then attack its adjacent uncoordinated imine, yielding the observed product. However, this route is less likely than that proposed in Scheme 3.19, since firstly, uncoordinated imines are less susceptible to nucleophilic attack and secondly, Pt(II) amines are not very acidic and the deprotonation of the specified amine is not likely under the reaction conditions.

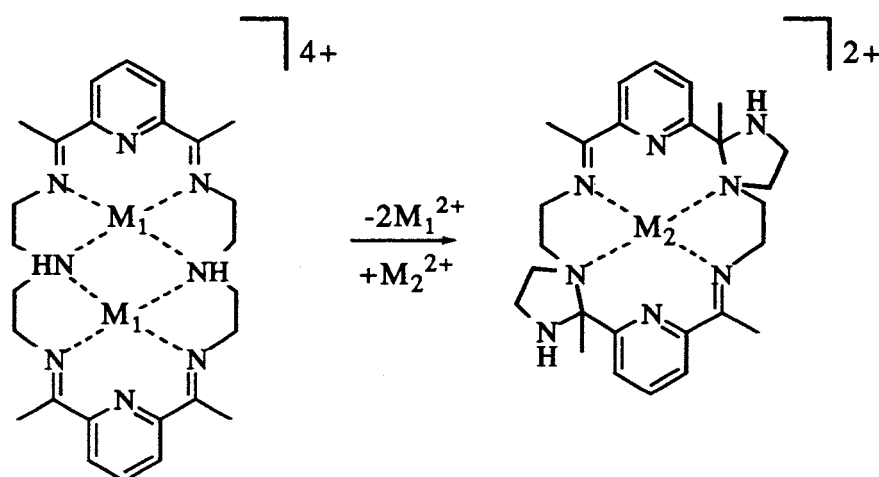
Reoxidation of the pentacyclo-Pt(II) complex to Pt(IV) using dioxygen, hydrogen peroxide, or electrochemical oxidation has not yet been achieved. This is surprising, as the non coordinating nitrogen atoms are not very far away from the metal centre (3.354(7) Å). In comparison, the non-coordinating nitrogen atoms in [Pt(tacn)₂]²⁺ were able to coordinate with the metal centre upon oxidation of the complex to Pt(IV), even though they are further away from the metal centre (3.568 Å).³² The steric demands of the ligand in pentacyclo-[Pt^{II}(Et₂-Me₆-N₆-tetracosane2H)]⁴⁺ may hinder access of oxidants to the Pt(II) ion. These aspects are addressed in more detail in Chapter 4.



Scheme 3.19: Possible mechanism for formation of pentacyclo-[Pt^{II}(Et₂-Me₆-N₆-tetracosane2H)]⁴⁺.

I. Other examples of Intramolecular Nucleophilic Attack

Intramolecular attack by an amine to an imine has been observed previously.⁴¹⁻⁵⁶ One example involves macrocycles obtained from the [2+2] template synthesis of 2,6-diformyl-pyridine with diethylenetriamine (dien) or triethylenetetraamine (trien) with suitable template metal ions.^{41-45,50-55} These complexes have been observed to undergo rearrangement involving intramolecular attack. In these cases, however, the rearrangement is prompted by a mismatch of the ligand cavity and the radius of the metal ion and is generally reversible (Scheme 3.20).



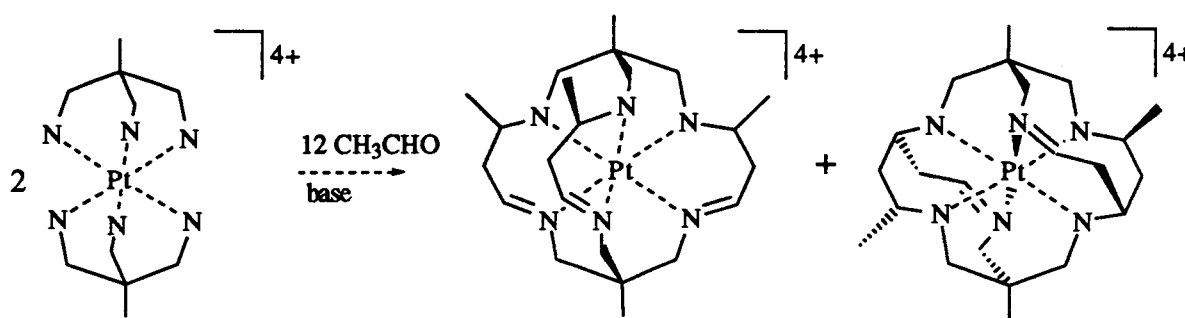
Scheme 3.20: An example of intramolecular rearrangement (the radius of M_1^{2+} is smaller than that of M_2^{2+}).

That $[Pt(Et_2-Me_6-N_6-tetracosanediimine)]^{4+}$ is able to undergo intramolecular nucleophilic attack during reduction is therefore not unusual. However, this rearrangement is prompted not by the mismatch of the metal ion with the ligand cavity, but by the stereochemical demands of the Pt(II) ion, which strongly favour square planar geometries⁴⁰ and the steric preferences of the ligand.

3.4.4. Reaction of $[Pt(tame)_2]^{4+}$ with Acetaldehyde

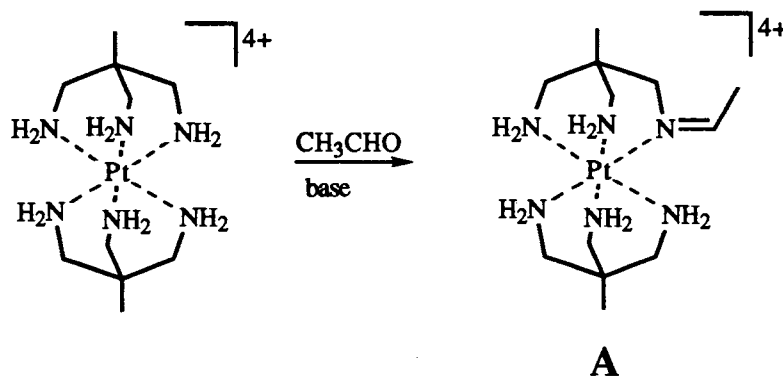
(a) and (b) Synthesis of $[Pt(\beta Me_5-N_6-tricosanetriimine)]^{4+}$ and $[Pt(Me_4-N_6-tetracosanediimine)]^{4+}$

The major products isolated in the reaction of $[Pt(tame)_2]^{4+}$ with acetaldehyde in basic MeCN in a one-pot synthesis are $[Pt(\beta Me_5-N_6-tricosanetriimine)]^{4+}$ and $[Pt(Me_4-N_6-tetracosanediimine)]^{4+}$ (Scheme 3.21). Attempts to alter the relative product composition by changing solvent, temperature or base were unsuccessful. $[Pt(\beta Me_5-N_6-tricosanetriimine)]^{4+}$ is an isomer of the complex produced in the reaction of aqueous formaldehyde and propanal, where the strap methyl substituents are on carbon atoms beta to the imine in the strap instead of alpha.



Scheme 3.21: Two products arising from the reaction of $[\text{Pt}(\text{tame})_2]^{4+}$ with acetaldehyde (amine protons have been omitted for clarity).

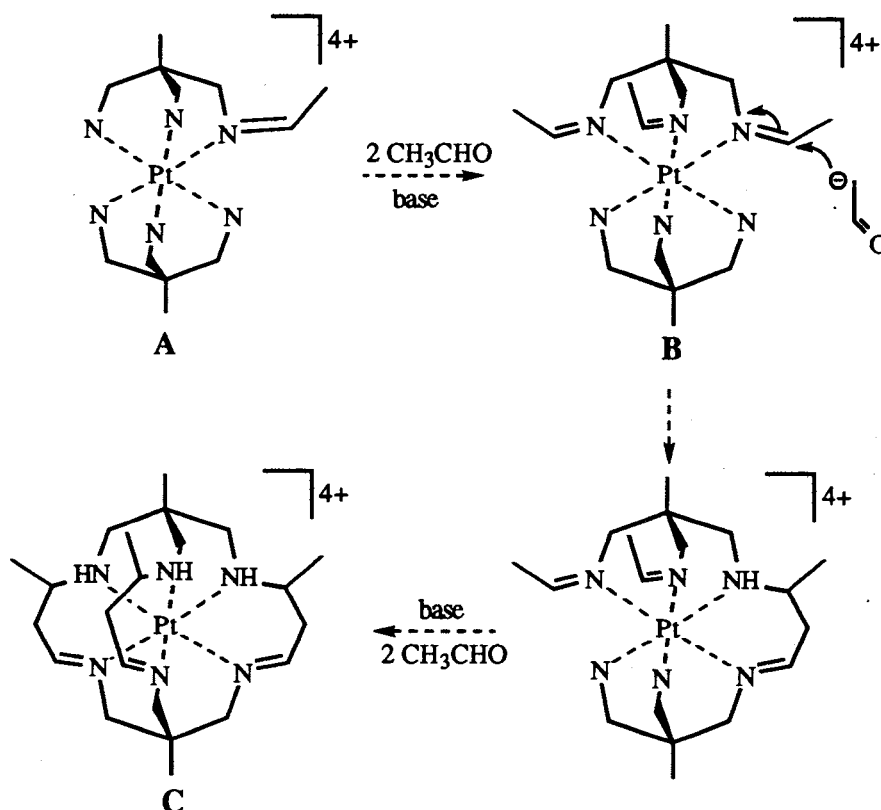
As for the previously discussed condensation reactions, the exact sequence of events in the synthesis of these two complexes is not certain. The regio- and stereoselectivity may be governed by a combination of electronic and steric factors, as discussed previously. The common intermediate for the formation of both complexes is probably the mono(ethanimine) complex, **A** (Scheme 3.22). This is formed by deprotonation of the template $[\text{Pt}(\text{tame})_2]^{4+}$ and then condensation with an acetaldehyde unit. Two competing reactions branch from this intermediate, which give rise to the triimine and the diimine complexes in about the same amounts and this implies that the rates of their formation are similar.



Scheme 3.22: A likely common intermediate in the synthesis of the $[\text{Pt}(\beta\text{Me}_5\text{-}N_6\text{-tricosanetriimine})]^{4+}$ and $[\text{Pt}(\text{Me}_4\text{-}N_6\text{-tetracosanediimine})]^{4+}$ cages.

The proposed mechanism for the formation of $[\text{Pt}(\beta\text{Me}_5\text{-}N_6\text{-tricosanetriimine})]^{4+}$ is shown in Scheme 3.23. The monoethanimine complex, **A**, condenses sequentially with two acetaldehyde units to form the *facial*-tris(ethanimine) species, **B**. As mentioned previously, the site of condensation of these two acetaldehyde units is in part governed by subtle electronic effects, so amines *cis* to the imine on the same tame ligand are thought to be more acidic than those *trans*.^{33,34} Complex **B** reacts sequentially with three acetaldehyde carbanions, in a manner similar to that discussed for the synthesis of

the $[\text{Pt}(\alpha\text{Me}_5\text{-}N_6\text{-tricosanetriimine})]^{4+}$ in Scheme 3.7 and Fig. 3.48, to form the β -triimine analogue, complex C. In this reaction, seven stereogenic centres are created, one from the Pt(IV) ion and two associated with each of the three straps, at the nitrogen and the methine carbon atoms and 48 stereoisomers are possible. For the Δ stereoisomer observed in the crystal structure of the tetrachlorozincate salt, the configurations about the strap methine carbon atoms and nitrogen centres are S and R, respectively, enantiomeric to those observed in the crystal structure of Λ - $[\text{Pt}(\alpha\text{Me}_5\text{-}N_6\text{-tricosanetriimine})](\text{ZnCl}_2)_2$.

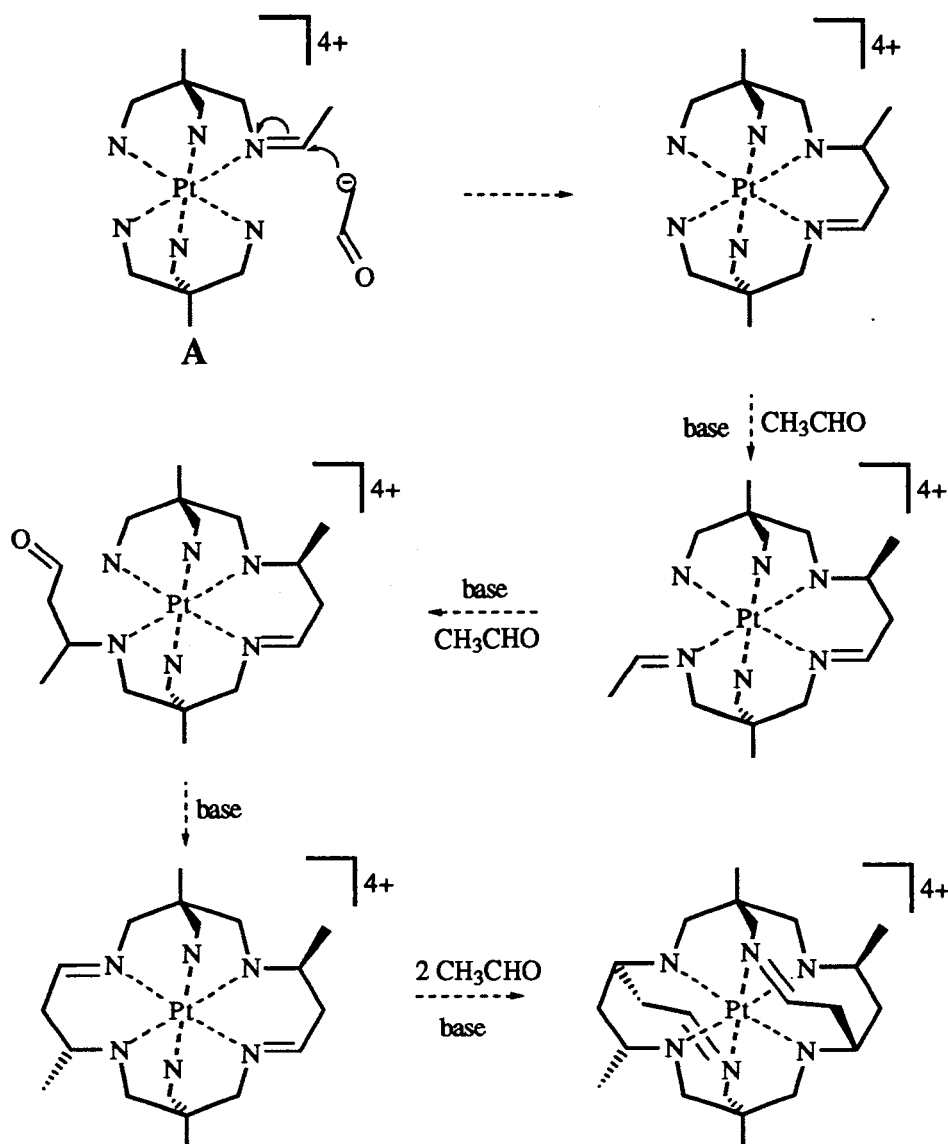


Scheme 3.23: Reaction of $[\text{Pt}(\text{tame})_2]^{4+}$ with acetaldehyde in MeCN to form $[\text{Pt}(\beta\text{Me}_5\text{-}N_6\text{-tricosanetriimine})]^{4+}$ (some amine protons have been omitted for clarity).

The *mer*-triimine isomer was not detected; however, ~50% of the template has not been accounted for. It may have been formed in low yield but it was not isolated from the many other products in the mother liquor.

Scheme 3.24 depicts a possible mechanism for the formation of the $[\text{Pt}(\text{Me}_4\text{-}N_6\text{-tetracosanediimine})]^{4+}$. It is anticipated that the stereoselectivity of this pathway is similar to that discussed for the synthesis of the analogous $[\text{Pt}(\text{Et}_2\text{-Me}_6\text{-}N_6\text{-tetracosanediimine})]^{4+}$ using propanal (Schemes 3.12-3.14). The complex has ten stereogenic centres, but their exact configurations are not certain. The crystals obtained were twinned and therefore not suitable for X-ray analysis. However, the same arguments governing the stereoselectivity of the analogous propanal condensation

reaction may be extended to the acetaldehyde system. It is anticipated that the configurations about the relevant chiral centres in $[\text{Pt}(\text{Et}_2\text{-Me}_6\text{-N}_6\text{-tetracosanediimine})]^{4+}$ and $[\text{Pt}(\text{Me}_4\text{-N}_6\text{-tetracosanediimine})]^{4+}$ are analogous.

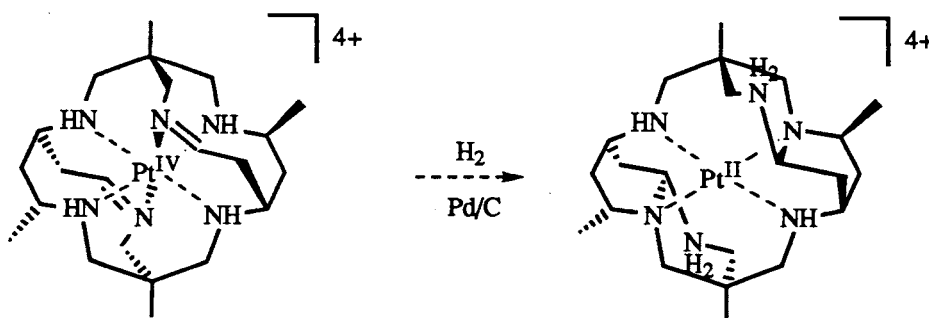


Scheme 3.24: Reaction of $[\text{Pt}(\text{tame})_2]^{4+}$ with acetaldehyde to form $[\text{Pt}(\text{Me}_4\text{-N}_6\text{-tetracosanediimine})]^{4+}$ (some amine protons have been omitted for clarity).

The formation of the two complexes in this reaction may be attributed to the intermediate reactivity of the acetaldehyde and also its steric hindrance compared to formaldehyde (more reactive) and propanal (less reactive and more sterically hindered). Acetaldehyde is able to condense with the template to form a tris(ethanimine) precursor, as does formaldehyde. However, the rate of carbanion condensation with the monoethanimine and subsequent ring closure to form the first strap appears to be competitive with the formation of the tris(ethanimine) species. Once ring closure has occurred, it predisposes the complex to form the N_6 -tetracosanediimine species.

(c) Hydrogenation of the $[Pt(Me_4-N_6-tetracosanediimine)]^{4+}$

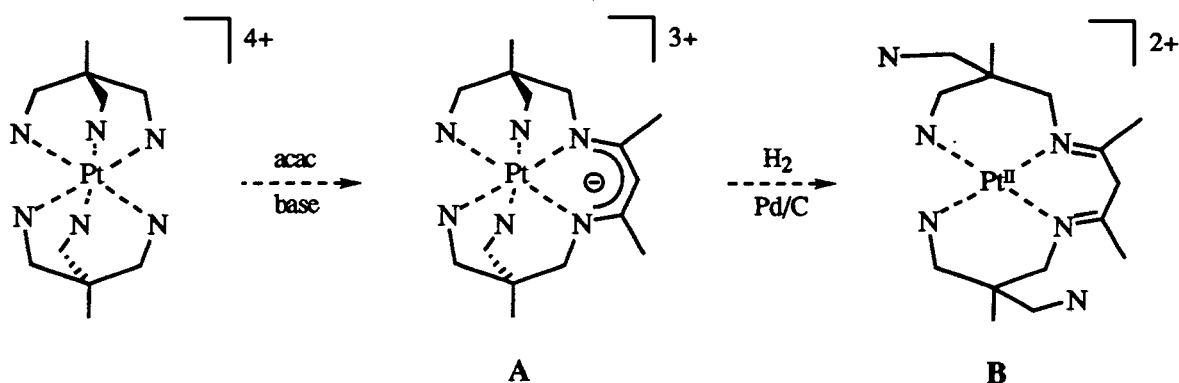
The product isolated from the hydrogenation of $[Pt(Me_4-N_6-tetracosanediimine)]^{4+}$ appears to be structurally similar to the pentacyclo- $[Pt^{II}(Et_2-Me_6-N_6-tetracosane2H)]^{4+}$ isolated from the hydrogenation of the analogous $[Pt(Et_2-Me_6-N_6-tetracosanediimine)]^{4+}$. The colour changes, from orange (deprotonated Pt(IV)) to green and then to colourless, as observed during the hydrogenation of the $[Pt(Me_4-N_6-tetracosanediimine)]^{4+}$, imply that a Pt(II) complex is formed. The NMR spectra of the hydrogenated $[Pt(Me_4-N_6-tetracosanediimine)]^{4+}$ complex are reminiscent of those of pentacyclo- $[Pt^{II}(Et_2-Me_6-N_6-tetracosane2H)]^{4+}$, so it is presumed that rearrangement of the Me_4-N_6 -tetracosanediimine ligand also occurs. The overall process is illustrated in Scheme 3.25. This complex has 12 stereogenic centres; two of which were created during hydrogenation. It is likely that the mechanism is similar to that described in Scheme 3.19 and the configurations about the relevant chiral centres in pentacyclo- $[Pt^{II}(Me_4-N_6-tetracosaneH_2)]^{4+}$ are probably the same as observed in the crystal structure of pentacyclo- $[Pt^{II}(Et_2-Me_6-N_6-tetracosane2H)]Cl_4$.



Scheme 3.25: Hydrogenation of $[Pt^{IV}(Me_4-N_6-tetracosanediimine)]^{4+}$ to pentacyclo- $[Pt^{II}(Me_4-N_6-tetracosaneH_2)]^{4+}$.

3.4.5. Reaction of $[\text{Pt}(\text{tame})_2]^{4+}$ with Acetylacetonone

Condensation of acetylacetonone (acac) with $[\text{Pt}(\text{tame})_2]^{4+}$ produced the 2,4-pentanediiiminate complex (complex A in Scheme 3.26), in a manner similar to that for the condensation of acetylacetonone with $[\text{Pt}(\text{NH}_3)_6]^{4+}$ and $[\text{Pt}(\text{en})_3]^{4+}$.⁷⁻⁹ However, condensation of only one acetylacetonone molecule was observed, even when excess acetylacetonone was used, despite reports that two acetylacetonone units condensed with $[\text{Pt}(\text{NH}_3)_6]^{4+}$.⁹ It is postulated that the formation of the delocalised six-membered diiminate ring resulted in the reduction of amine proton acidity and obviated further condensation.



Scheme 3.26: Reaction of $[\text{Pt}(\text{tame})_2]^{4+}$ with acetylacetonone to form $[\text{Pt}^{\text{IV}}(\text{tame}_2\text{-2,4-pentanediiiminate})]^{3+}$, followed by hydrogenation (some amine protons have been omitted for clarity).

Attempts to reduce the imines by hydrogenation resulted in the reduction of the Pt(IV) state to Pt(II), accompanied by dissociation of two primary amine donors, one from each tame ligand and the loss of the delocalised ring system (complex B in Scheme 3.26). The loss of delocalisation is implied from the ^{13}C NMR spectra, where the imine resonance in the Pt(II) complex occurs at 18 ppm higher than that of the Pt(IV) complex. Additional support for this is from the beta carbon resonance on the diiminate chelate ring, which is shifted to lower frequencies by ~45 ppm. As a square planar geometry is strongly favoured by Pt(II) complexes, dissociation of two nitrogen donor atoms is inevitable. Formation of this complex therefore removed the possibility for further condensation of an acetylacetonone molecule to form the target *tris*-strapped Pt(IV) complex.

Two isomers are possible, the *trans* and *cis* complexes, which have different configurations about the quaternary carbon atom in the same residue. In the former complex, the pendant amines lie on opposite sides of the PtN_4^{2+} plane, whereas the *cis* complex has its pendant amines lying on the same side of the PtN_4^{2+} plane.[§]

It is not clear from the NMR spectra if both complexes are present, or only the *trans* complex. In the latter case, 15 ^{13}C NMR resonances are anticipated if the six-membered chelate rings derived from the same residues are in the more stable flattened chair conformation. Therefore, one of the methyl substituents in a same residue would occupy the equatorial position, whereas the methyl substituent on the opposite same ligand would occupy the axial position. Dreiding models indicate that interconversion of the axial/equatorial methyl substituents is coupled with the "flipping" of the rigid diiminate ring, via skew boat conformations of the same residues. Hence, provided that the same chelate rings favour the chair conformation, it is anticipated that interconversion is slow. Consequently, the same methyl substituents would be in different environments and have different frequencies, as observed in the NMR spectra. However, there is accidental degeneracy for each pair of strap methyl and imine signals and this would account for the apparent simplicity of the ^{13}C NMR spectrum. The accidental degeneracy diminishes for carbon atoms which are further away from the diiminate ring. In addition, in order to generate the square planar geometry favoured by the Pt(II) ion, the formation of the product is likely to involve a pathway which has the least rearrangement. Dissociation of the amines in the axis orthogonal to the diiminate ring requires less reorganisation than the dissociation of those *trans* to the imines. While the former route is predisposed to the formation of the *trans* isomer, it is not clear how the *cis* isomer would form initially. It is not yet clear if *cis/trans* isomerisation is taking place at 298K.

Alternatively, in the case where both isomers are present, then 23 ^{13}C resonances are expected in the ^{13}C NMR spectrum.[†] Only 13 signals are observed however, and this may arise from coincidental overlap of some signals for carbon atoms in similar environments, for example, the imine, strap methylene and strap methyl carbon atoms. If the relatively simple ^{13}C NMR spectrum reflected the presence of both isomers, then it is also required that the same methyl carbon atoms in the *trans* complex

§ The *trans* isomer has the same configurations about the quaternary carbon, whereas the *cis* isomer has opposite configurations.

† The number of different carbon environments anticipated in the *trans* and *cis* isomers are 15 and 8, respectively, as the former complex has no symmetry, while the latter has a mirror plane perpendicular to the diiminate ring.

be in equivalent environments. This might be achieved if the six-membered chelate rings of the same residues adopt a flattened skew boat conformation. Such conformations have been observed previously in cage complexes containing 2,2-dimethyl-1,3-propanediamine chelate rings.⁵⁷

In order to rationalise the NMR spectra, further experiments are under consideration. Firstly, ¹⁹⁵Pt NMR spectra may indicate if there is one or two complexes present. Secondly, temperature dependent NMR spectra may indicate whether interconversion between the apical/equatorial same methyl substituents is occurring, and would also indicate if *cis/trans* isomerisation is possible.

3.4.6. Summary of the Synthesis of the Pt(IV) Large Cavity Cages

Pt(IV) complexes were template synthesised to form stable tri- and diimine complexes with expanded cavities and their syntheses were remarkably stereoregular. The yields were significantly higher compared to analogous template syntheses in nonaqueous media using other metal ions. The scope for these cages may be extended or example, by functionalising the cage straps using other carbonyl compounds in the reaction, such as acetone, acetophenone and iso-butanal. Examining the products and possible isomer composition of such reactions may further illuminate their mechanisms. Selective reduction of the imines without the reduction of the Pt(IV) centre and/or intramolecular rearrangement and requires further investigation. The problem is clearly a mechanistic one, and reagents that only reduce the imines while the Pt(IV) state is maintained need to be found. SnCl₂ in HCl may be a suitable reagent, and this is currently under investigation. Similarly, oxidation of the rearranged Pt(II) complexes is currently underway using chemical methods, for example [IrCl₆]³⁻ as an oxidant, or electrochemical oxidation in a variety of electrolytes and solvents. The saturated Pt(IV) cage complexes are still an important goal, especially in relation to their effect on hydrogen production from water and this aspect will be pursued at a later date.

3.4.7. References

- (1) Boucher, H. A.; Lawrance, G. A.; Lay, P. A.; Sargeson, A. M.; Bond, A. M.; Sangster, J. C.; Sullivan, J. C. *J. Am. Chem. Soc.* **1983**, *105*, 4562.
- (2) Geue, R. J.; Hambley, T. W.; Harrowfield, J. M.; Sargeson, A.; Snow, M. R. *J. Am. Chem. Soc.* **1984**, *106*, 5478, and references therein.
- (3) Geue, R. J.; McDonnell, M. B.; Mau, A. W. H.; Sargeson, A. M.; Willis, A. C. *J. Chem. Soc., Chem. Commun.* **1994**, 667, and references therein.
- (4) Dietrich, B.; Viout, P.; Lehn, J.-M. *Macrocyclic Chemistry*; VCH Verlagsgesellschaft Inc.: New York, 1993, and references therein.
- (5) de Sousa Healy, M.; Rest, A. J. *Adv. Inorg. Chem. and Radiochem.* **1978**, *21*, 1.
- (6) Lindoy, L. F. *The Chemistry of Macrocyclic Ligand Complexes*; Cambridge University Press: Cambridge, 1989.
- (7) Evans, I. P.; Everett, J., G.W.; Sargeson, A. M. *J. Chem. Soc., Chem. Commun.*, **1975**, 139.
- (8) Evans, I. P.; Everett, J., G.W.; Sargeson, A. M. *J. Am. Chem. Soc.* **1976**, *98*, 8041.
- (9) Brawner, S. A.; Lin, I. L. B.; Kim, J.-H.; Everett, J., G.W. *Inorg. Chem.* **1978**, *17*, 1304.
- (10) Spiccia, L., Unpublished observations.
- (11) Giedt, D. C.; Nyman, C. J. *Inorganic Syntheses* **1966**, *8*, 239.
- (12) Osvath, P., Unpublished observations.
- (13) Dwyer, F. P.; Sargeson, A. M. *J. Am. Chem. Soc.* **1959**, *81*, 5272.
- (14) McDonnell, M.; Sargeson, A. M., Unpublished results.
- (15) Ralph, S. F., Personal Communication **1991**.
- (16) Günter, H. *NMR Spectroscopy, An Introduction*; John Wiley and Sons: New York, 1973; Chapter 4.

- (17) Geue, R. J.; Höhn, A.; Ralph, S. F.; Sargeson, A. M.; Willis, A. C. *J. Chem. Soc., Chem. Commun.* **1994**, 1513.
- (18) Pregosin, P. S. *Ann. Rep. NMR Spec.* **1986**, *17*, 285, and references therein.
- (19) Pregosin, P. S. *Coord. Chem. Rev.* **1982**, *44*, 247, and references therein.
- (20) Pesek, J. J.; Mason, W. R. *J. Mag. Reson.* **1977**, *25*, 519, and references therein.
- (21) Sargeson, A. M., Personal Communication **1994**.
- (22) Silverstein, R. M.; Bassler, G. C.; Morill, T. C. *Spectrometric Identification of Organic Compounds*; Wiley: New York, 1981.
- (23) Basolo, F.; Wilks, P. H.; Pearson, R. G.; Wilkins, R. G. *J. Inorg. Nucl. Chem.* **1958**, *6*, 161.
- (24) Mason, W. R. *Coord. Chem. Rev.* **1972**, *7*, 241.
- (25) Chanon, M.; Tobe, M. L. *Angew. Chem., Int. Ed. Engl.* **1982**, *21*, 1.
- (26) Hartley, F. R. *The Chemistry of Platinum and Palladium*; Applied Science Publishers, Ltd.: London, 1973, and references therein.
- (27) Belluco, U. *Organometallic and Coordination Chemistry of Platinum*; Academic Press: London, 1974.
- (28) Basolo, F.; Pearson, R. G. *Inorganic Reaction Mechanisms*; 2nd ed.; John Wiley and Sons: New York, 1967.
- (29) Wilkins, R. G. *Kinetics and Mechanisms of Reactions of Transition Metal Complexes*; 2nd ed.; VCH Publishers. Inc.: New York, 1991, and references therein.
- (30) Anderson, G. K.; Cross, R. J. *Chem. Soc. Rev.* **1980**, *9*, 185, and references therein.
- (31) Bard, A. J.; Parsons, R.; Jordan, J. *Standard Potentials in Aqueous Solutions*; Marcel Dekker Inc.: New York, 1985.
- (32) Wiegardt, K.; Köppen, M.; Swiridoff, W.; Weiss, J. *J. Chem. Soc. Dalton Trans.* **1983**, 1869.
- (33) Adrianova, O. N.; Fedotova, T. N. *Russ. J. Inorg. Chem.* **1970**, *15*, 1272.

- (34) Adrianova, O. N.; Fedotova, T. N. *Russ. J. Inorg. Chem.*, **1980**, *25*, 105.
- (35) Kukushkin, Y. N.; Drokina, Z. V.; Varshaskii, Y. S.; Ivannikova, N. V. *Russ. J. Inorg. Chem.* **1968**, *13*, 1693, and references therein.
- (36) Gainsford, G. J.; Geue, R. J.; Sargeson, A. M. *J. Chem. Soc., Chem. Commun.* **1982**, 233.
- (37) Höhn, A., Unpublished results **1989**.
- (38) Korybut-Daskiewicz, B.; Sargeson, A. M.; Angus, P., Unpublished results.
- (39) Geue, R. J., Personal communication **1990**.
- (40) Cotton, F. A.; Wilkinson, G.; *Advanced Inorganic Chemistry*; 5th ed.; John Wiley and Sons: New York, 1988; Chapter 19.
- (41) Cabral, M. F.; Murphy, B.; Nelson, J. *Inorg. Chim. Acta.*, **1984**, *90*, 169.
- (42) Drew, M. G. B.; Nelson, J.; Nelson, S. M. *J. Chem. Soc., Dalton Trans.*, **1981**, 1691.
- (43) Drew, M. G. B.; Nelson, J.; Nelson, S. M. *J. Chem. Soc., Dalton Trans.*, **1981**, 1678.
- (44) Nelson, S. M.; Knox, C. V.; McCann, M.; Drew, M. G. B. *J. Chem. Soc., Dalton Trans.*, **1981**, 1669.
- (45) Nelson, S. M. *Pure and Appl. Chem.* **1980**, *52*, 2451.
- (46) Ngwenya, M. P.; Chen, D.; Martell, A. E.; Reibenspies, J. *Inorg. Chem.* **1991**, *30*, 2732.
- (47) Menif, R.; Martell, A. E.; Squattrito, P. J.; Clearfield, A. *Inorg. Chem.*, **1990**, *29*, 4723.
- (48) Menif, R.; Martell, A. E. *J. Chem. Soc., Chem. Commun.*, **1989**, 1521.
- (49) Fenton, D. E.; Kitchen, S. J.; Spencer, C. M.; Tamburini, S.; Vigato, P. A. *J. Chem. Soc., Dalton Trans.*, **1988**, 685.
- (50) Fenton, D. E.; Moody, R. *J. Chem. Soc., Dalton Trans.*, **1987**, 219.
- (51) Adams, H.; Bailey, N. A.; Fenton, D. E.; Good, R. J.; Moody, R.; Rodriguez de Barbarin, R. O. *J. Chem. Soc., Dalton Trans.* **1987**, 207.

- (52) Sakiyama, H.; Motoda, K.; Okawa, H.; Kida, S. *Chem. Lett.* **1991**, 1133.
- (53) Motoda, K.; Sakiyama, H.; Matsumoto, N.; Okawa, H.; Kida, S. *Bull. Chem. Soc., Jpn.* **1992**, *65*, 1176.
- (54) Sakiyama, H.; Tokuyama, K.; Matsumura, Y.; Okawa, H. *J. Chem. Soc., Dalton Trans.*, **1993**, 2329.
- (55) Tamburini, S.; Vigato, P. A.; Chiarello, D.; Traldi, P. *Inorg. Chim. Acta.* **1989**, *156*, 271.
- (56) Kahwa, I. A.; Fronczek, F. R.; Selbin, J. *Inorg. Chim. Acta.* **1988**, *148*, 273.
- (57) Sargeson, A. M.; Qin, C. J.; Geue, R. J.; Willis, A. C. **1994**, Unpublished results.

Chapter 4

Electrochemical Behaviour of the Expanded Pt(IV) Cage Complexes

4.1. Introduction

4.1.1. General

One important consequence of encapsulating metal ions with the cage ligands is that reactive oxidation states may be stabilised, as the steric constraints of the ligand hinder substitution and dimerisation reactions. Prime examples include the stabilisation of the reactive d^7 states, such as Co(II)^{1-3} and $\text{Rh(II)}^{4,5}$ in both N_6 -tricosane and sar complexes. It was previously anticipated that similar complexes of the Pt(III) state could also be stabilised from the reduction of analogous Pt(IV) complexes.^{6,7}

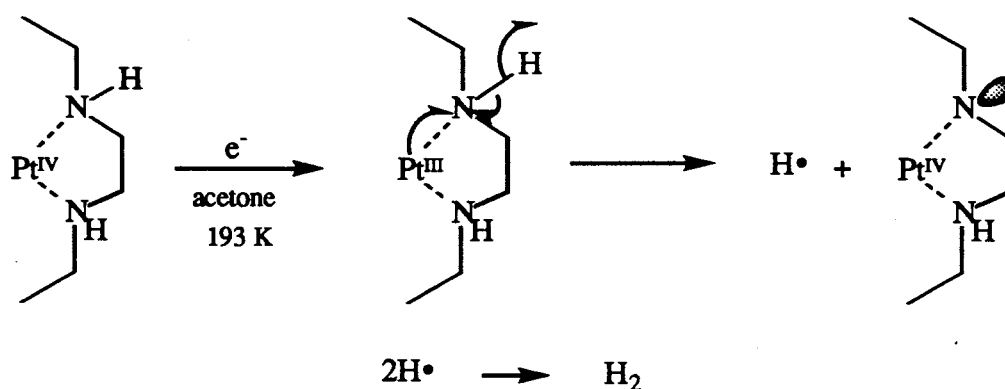
4.1.2. Overview of Pt(III) Complexes

Isolation and characterisation of the intermediate Pt(III) ion is difficult as it readily disproportionates to form discrete Pt(IV) and Pt(II) complexes or dimerises to form diamagnetic mixed valence species, with formally d^6 and d^8 metal centres.⁸⁻¹² In the latter case, the unpaired electron from each Pt(III) centre may be shared between the two metal centres, by way of a direct M-M bond, for example with ligands such as orthophosphate,¹³⁻¹⁵ α -dioximato derivatives,¹⁶ amide,¹⁷ sulfate,¹⁸ pyrophosphite,¹⁹ carboxylate,¹¹ 2-pyridonate^{20,21} and 2-pyrimidonate,²² or across a bridging ligand, for example, bromide in $[\text{Pt}^{\text{II}}(\text{NH}_3)_2\text{Br}_2][\text{Pt}^{\text{IV}}(\text{NH}_3)_2\text{Br}_4]$.^{11,23} and in derivatives of α -pyrrolidonates.¹⁶ Monomeric Pt(III) complexes have been isolated but most contain ligands which enable extensive delocalisation from the metal onto the ligand, such as diphenylglyoxime,²⁴ and dithiolato²⁵⁻²⁷ derivatives and some ligands with sulfur donor atoms, such as 1,4,7-trithiacyclononane (tcn).^{28,29} Stabilisation of reactive metal centres has also been achieved by hindering the approach of incoming species to the metal centre, so that ligand substitution and disproportionation reactions are limited. For example, $[\text{Pt}(\text{C}_6\text{Cl}_5)_4]^-$ contains bulky ligands that prevent close access to the Pt(III) centre.³⁰ Similarly, the ligands 1,4,7-triazacyclononane (tacn)^{29,31-33} and tcn^{28,34-36} have been shown to stabilise the d^7 centres of the ions Rh(II), Pd(III) and Ir(II). These ligands have the potential to coordinate in a facial manner with many metal ions,^{34,37} and often the d^7/d^8 and d^6/d^7 couples are reversible. This reversibility has been attributed to the ability of the ligand to meet readily the preferred steric and electronic requirements for each member of the redox couples.^{29,33,35,38} Unfortunately, the electrochemistry of the $[\text{Pt}(\text{tacn})_2]^{4+/3+}$ and $[\text{Pt}(\text{tacn})_2]^{3+/2+}$ system has not been reported although the Pt(IV) and Pt(II) complexes have been characterised.³⁹ Similarly, the sep and sar ligands coordinate in a hexadentate manner and ligand substitution, dimerisation and disproportionation reactions are restricted.

4.1.3. Electrochemical Behaviour of Pt(IV) Sar Cage Complexes

The stabilisation of Pt(III) within the sar cages has been achieved with limited success.^{6,7} However, one of the unexpected features of these Pt(IV) cage complexes was their different electrochemical behaviour in acetone and in water.^{6,7}

The Pt(IV)/Pt(III) couple is reversible in acetone at low temperature. Under these conditions, the $[\text{Pt}^{\text{III}}(\text{NHOH})_2\text{sar}]^{3+}$ transient has been observed by EPR techniques, where the Pt(III) ion was generated electrochemically and by γ - and pulse radiolysis. Electrochemical studies of Pt(IV) sar complexes (in acetone at low temperature) imply that the processes in Scheme 4.1 take place.^{6,7} The Pt(IV) ion is firstly reduced to Pt(III), which then undergoes homolysis to form a Pt(IV)-N⁻ moiety and a hydrogen atom. Two hydrogen atoms then combine to form dihydrogen on the surface of the electrode.

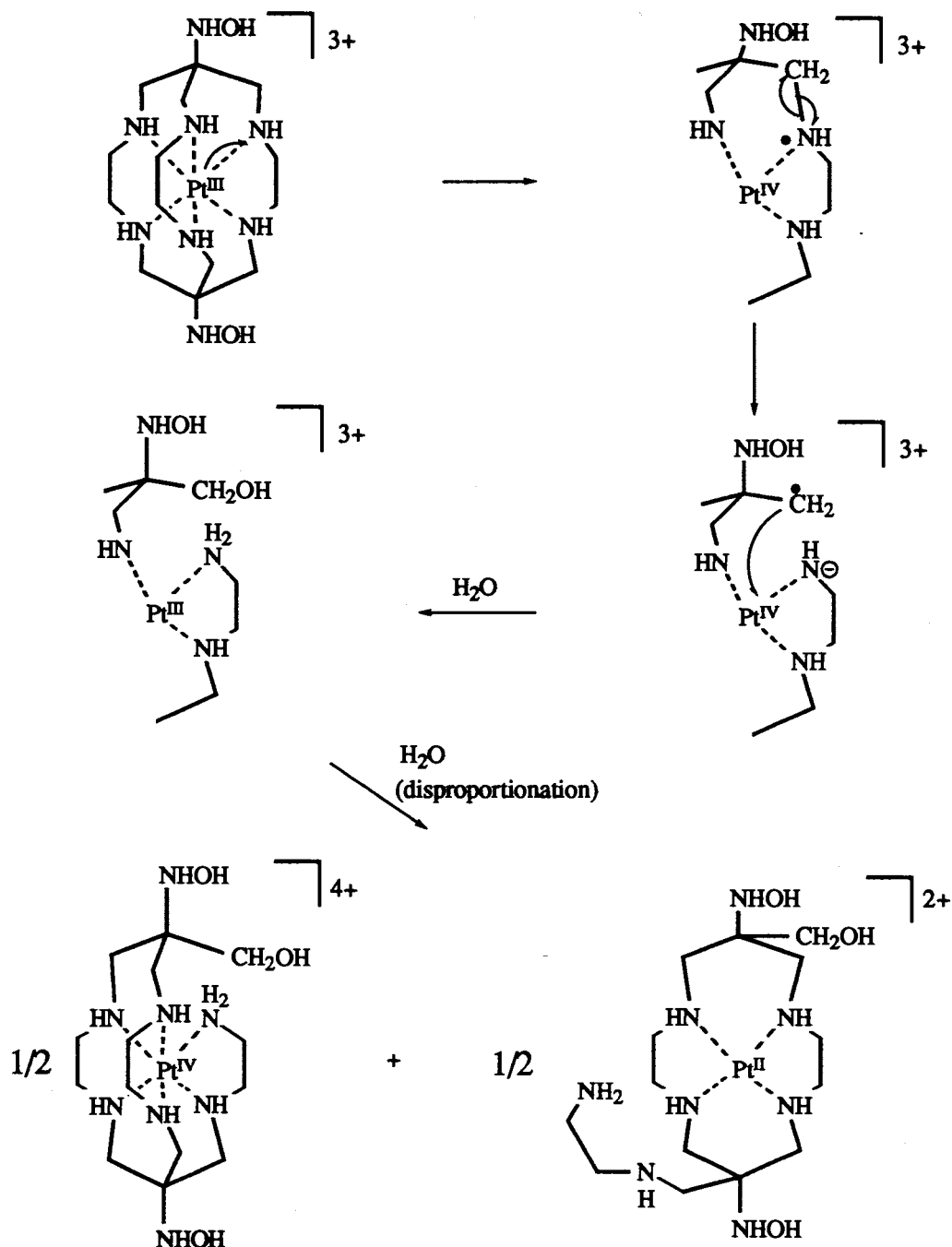


Scheme 4.1: Reduction of $[\text{Pt}((\text{NHOH})_2\text{sar})]^{4+}$, in acetone at low temperature.

This electrochemical behaviour has been attributed to the inability of the ligand to accommodate the larger Pt(III) ion.^{6,7} The seventh electron in the Pt(III) system occupies an antibonding orbital which is aligned along one of the Pt-N axes, therefore the electron density in the Pt-N bond is increased. The electron density in the Pt-N bond spills over into an antibonding orbital of the adjacent N-H bond, leading to its homolytic fission and finally the formation of the Pt^{IV}-N⁻ complex by intramolecular electron transfer. This chemistry is unusual as no other d⁷ sar cage complexes have been observed to behave in this way. If the Pt^{IV}-N⁻ species could be protonated at the amine site, this system might be an effective electrocatalyst for dihydrogen production at low overpotential.

In aqueous media, or in acetone at ambient temperature, however, the Pt(IV)/Pt(III) couples are irreversible.^{6,7} Analysis of the bulk electrolysed solution of the sar cages yielded a mixture of both Pt(II) and Pt(IV) macrocyclic complexes and no dihydrogen evolution was observed at the electrode surface. A possible mechanism for

rupture is depicted in Scheme 4.2. Reduction to the Pt(III) species occurs, and instead of fission of an N-H bond to form a hydrogen radical, the electron density migrates to the antibonding orbital of the N-C bond in the cap. The ligand framework then ruptures at the N-C bond, to form an N anion which then protonates, and a carbon radical in the cap. Intramolecular electron transfer takes place, regenerating the Pt(III) ion, which then disproportionates to afford Pt(II) and Pt(IV) macrocyclic complexes. This rupture of the cage removed any possibility for catalytic H₂ production.



Scheme 4.2: Rupture of the Pt(III) species (in aqueous media or in acetone at ambient temperature).

It is not clear why ligand rupture occurs at two different sites of the ligand framework, depending on solvent and temperature. At least three factors should be considered in attempting to explain the inability of the sar cages to contain the Pt(III) ion:

(1) The solvent appears to influence the direction of migration of electron density within the Pt(III) complex. The rupture of the N-H bond is preferred in the less polar acetone, while the N-C bond is ruptured in water, a more polar solvent. This is unexpected, as the amine proton was anticipated to be more acidic in aqueous media than in acetone.⁷

(2) How substituents influence the electrochemical behaviour of the sar Pt cages has not yet been assessed. The rupture of the cage framework appeared to be more rapid in the $[\text{Pt}(\text{NO}_2)_2\text{sar}]^{3+}$ system than the $[\text{Pt}(\text{NHOH}_2)_2\text{sar}]^{3+}$ and $[\text{Pt}(\text{sep})]^{3+}$ complexes.⁴⁰ The nitro substituents in the former complex may facilitate the migration of electron density into the ligand cap. However, the unsubstituted $[\text{Pt}(\text{sar})]^{4+}$ has not been isolated, so this aspect has not yet been addressed.

(3) Rupture of the ligand may be driven by the Pt(III) ion being too large for the cavity of the sar cage ligand. A ligand with a larger cavity may alleviate this problem. Like Pt(III), monomeric Rh(II) complexes are rare and usually have only been detected electrochemically or by pulse radiolysis.⁸ It has been noted that the reduction of the Rh(III)/*N*₆-tricosane cages to the Rh(II) analogues is more favourable than the reduction of the Rh(III) sar complexes. For example, the reduction potential for the $[\text{Rh}(\text{Me}, \text{NH}_2\text{-}N_6\text{-tricosane})]^{3+/2+}$ couple is 0.4 V more positive⁵ than the homologous $[\text{Rh}(\text{NH}_2)_2\text{sar}]^{3+/2+}$ couple,⁴ implying that the *N*₆-tricosane ligand stabilises the Rh(II) ion more effectively than the sar ligands. The Ir(III)/Ir(II) *N*₆-tricosane analogue has not yet been synthesised for comparison. On the basis that the Rh(III)/Rh(II) cage couple is accessible and is reversible, the analogous $[\text{Pt}(N_6\text{-tricosane})]^{4+/3+}$ couple may also be reversible. The Pt(III) ion may be more readily accommodated in the expanded cage. This chapter explores this aspect namely, the effect of ligand size on the electrochemistry of Pt(IV) and Pt(II) hexamine cage complexes, essentially, $[\text{Pt}(\alpha\text{Me}_5\text{-}N_6\text{-tricosanetriimine})]^{4+}$, $[\text{Pt}(\text{Et}_2\text{-Me}_6\text{-}N_6\text{-tetracosanediimine})]^{4+}$ and pentacyclo- $[\text{Pt}(\text{Et}_2\text{-Me}_6\text{-}N_6\text{-tetracosane}2\text{H})]^{4+}$.

4.2. Experimental

4.2.1. Electrochemistry

The electrochemical equipment and procedures were described previously in Chapter 2.8. The electrolytes used were either 0.1 M NaClO₄, 0.1 M NaCl, 0.1 M HCl, 0.1 M CF₃COOH, 1 M CF₃COOH, 1 M H₂SO₄ or 1 M HCl in aqueous media. The electrolytes used for investigating the electrochemistry in non aqueous media were also discussed in Chapter 2.8. As different reference electrodes were used, the potentials cited in the text are referenced to the normal hydrogen electrode (NHE), in order to allow comparison between experiments, unless otherwise specified. All experiments were undertaken at 295 K.

(a) Electrochemical generation of [Pt^{II}(tame₂H)₂](CF₃COO)₄.

Controlled potential electrolysis of [Pt(tame)₂]Cl₄ (100 mg) in 0.1M CF₃COOH (15 mL) at -800 mV vs SCE using a mercury pool working electrode was undertaken. The electrolysis indicated that ~2 electrons per Pt ion had been passed. After electrolysis for 5.8 hours, the solution was decanted off the mercury pool and then evaporated to dryness to yield a white powder that was characterised by NMR spectroscopy.

NMR (δ (ppm), D₂O) [Pt^{II}(tame)₂2H](CF₃COO)₄: ¹H: 1.20 (s, 3H, CH₃) 2.74 (t of d of d, 4H, CH₂), 3.10 (s, 2H, CH₂) 5.08 (broad s, NH₂), 5.35 (broad s, NH₂). ¹³C: 18.4, 37.3, 46.1, 48.9, 49.2.

4.3. Results

4.3.1. General

No responses were observed using glassy carbon or platinum disc electrodes in the cyclic voltammograms (CV's) of $[\text{Pt}^{\text{IV}}(\alpha\text{Me}_5\text{-N}_6\text{-tricosanetriimine})]^{4+}$, $[\text{Pt}^{\text{IV}}(\text{Me}_4\text{-N}_6\text{-tetracosanediimine})]^{4+}$, $[\text{Pt}^{\text{IV}}(\text{Et}_2\text{-Me}_6\text{-N}_6\text{-tetracosanediimine})]^{4+}$ and pentacyclo- $[\text{Pt}^{\text{II}}(\text{Et}_2\text{-Me}_6\text{-N}_6\text{-tetracosane2H})]^{4+}$ in neutral or acidic media (0.1 M NaClO_4 , 0.1 M NaCl , 0.1 M HClO_4 , 1 M HClO_4 , 0.1 M HCl and 1 M HCl) between 0 to ± 1.0 V (vs SCE). Similarly, no responses were observed with the gold disc electrode in neutral media, although slight responses were observed in 0.1 M HCl for some of the Pt(IV) complexes, whose reduction potentials were located close to that for the evolution of hydrogen. Responses were observed in the range 0.7 to -0.7 V (vs SCE) using an edge plane pyrolytic graphite (EPG) electrode and in the range $+0.1$ to -1.5 V (vs $\text{Ag}/\text{AgCl}/\text{KCl}_{(\text{sat.})}$ or SCE) using a hanging mercury drop electrode (HMDE) in aqueous media. The CV's using the last two electrodes showed high current responses. Adsorption of the reactant and/or the product on the HMDE often deformed the voltammetric responses and this behaviour was particularly noticeable in neutral solution.

4.3.2. $[\text{Pt}^{\text{IV}}(\text{tame})_2]^{4+}$

The CV of $[\text{Pt}^{\text{IV}}(\text{tame})_2]^{4+}$ in 1 M HClO_4 using an HMDE is shown in Fig. 4.1. An irreversible response is evident at $E_{\text{pc}} = -0.20$ V (vs NHE, 100 mVs^{-1}). The response is also irreversible in 0.1 M NaClO_4 , although it is distorted in this medium, presumably due to weak adsorption. The reduction potentials in acid or neutral media did not differ significantly. Bulk electrolysis at -0.80 V vs SCE in 0.1 M CF_3COOH indicated that 1.8 electrons per Pt(IV) ion were consumed. The ^1H and ^{13}C NMR spectra of the bulk electrolysis product showed that a single isomer of $[\text{Pt}^{\text{II}}(\text{tameH})_2]^{4+}$ had been formed. This indicates that the irreversible response in Fig. 4.1 is a two electron process, corresponding to the reduction of Pt(IV) to Pt(II). The peak potentials for the reduction of $[\text{Pt}^{\text{IV}}(\text{tame})_2]^{4+}$ in 1 M HClO_4 , 0.1 M NaClO_4 and 1 M H_2SO_4 , at various scan rates are listed in Table 4.1.

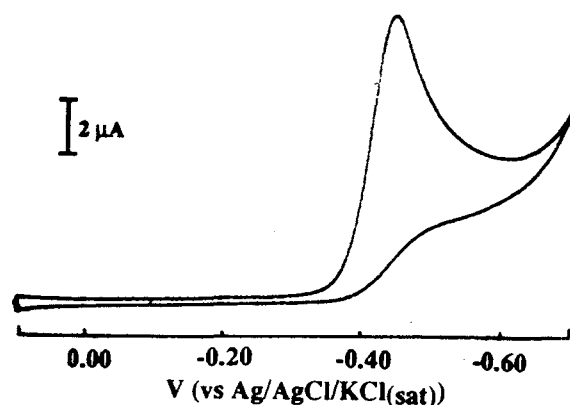


Figure 4.1: Cyclic voltammogram of $[\text{Pt}^{\text{IV}}(\text{tame})_2]^{4+}$ in 1 M HClO_4 (100 mVs^{-1} , vs $\text{Ag}/\text{AgCl}/\text{KCl}_{(\text{sat.})}$, HMDE).

Table 4.1: Reduction potentials for $[\text{Pt}(\text{tame})_2]^{4+}$ under various conditions (V vs NHE, HMDE, 295 K).

Scan Rate (mVs^{-1})	E_{pc} (V vs NHE)		
	0.1 M NaClO_4	1 M HClO_4	1 M H_2SO_4
20	-0.23	-0.19	
50	-0.22		
100	-0.21	-0.20	-0.27
200	-0.20		-0.28
500	-0.19		-0.29

2. $[\text{Pt}^{\text{IV}}(\alpha\text{Me}_5\text{-N}_6\text{-tricosanetriimine})]^{4+}$

The CV of $[\text{Pt}^{\text{IV}}(\alpha\text{Me}_5\text{-N}_6\text{-tricosanetriimine})]^{4+}$ in 1 M H_2SO_4 using an HMDE shows an irreversible response at $E_{\text{pc}} = +0.06 \text{ V}$ (vs NHE, 200 mVs^{-1}) (Fig. 4.2(a)). The CV's in 0.1 M HCl using an EPG electrode and at different scan rates all show irreversible responses at $E_{\text{pc}} = +0.03$ and $+0.01 \text{ V}$ (vs NHE), at 50 and 900 mVs^{-1} , respectively (Fig. 4.2(b)). The CV in 0.1 M HCl using a gold disc electrode shows an irreversible response at $E_{\text{pc}} = +0.02 \text{ V}$ (vs NHE, 50 mVs^{-1}) (Fig. 4.2(c)). However, the peak current (i_{pc}) was significantly greater using the EPG electrode than that obtained for the gold electrode. The potentials at which hydrogen evolution occurred using the gold electrode, in the presence and absence of $[\text{Pt}^{\text{IV}}(\alpha\text{Me}_5\text{-N}_6\text{-tricosanetriimine})]^{4+}$ in

0.1 M HCl are very similar (Figs 4.2(c)(i,ii) and 4.2 (c)(iii)). Therefore, this complex is not effective as a catalyst for the electroproduction of hydrogen.

It is proposed that the irreversible response is due to a two electron process, corresponding to the reduction of Pt(IV) to Pt(II), by analogy with the reduction of $[\text{Pt}^{\text{IV}}(\text{tame})_2]^{4+}$ and the related cage complex $[\text{Pt}^{\text{IV}}(\text{Et}_2\text{-Me}_6\text{-N}_6\text{-tetracosanediimine})]^{4+}$. The data for the electrochemistry of $[\text{Pt}^{\text{IV}}(\alpha\text{Me}_5\text{-N}_6\text{-tricosanetriimine})]^{4+}$ recorded under a variety of conditions are listed in Table 4.2.

Table 4.2: Reduction Potentials of $[\text{Pt}^{\text{IV}}(\alpha\text{Me}_5\text{-N}_6\text{-tricosanetriimine})]^{4+}$ under different conditions (V vs NHE, 295 K).

Scan rate (mVs^{-1})	E_{pc} (V vs NHE)		
	HMDE	EPG [†]	Au [†]
	1 M H ₂ SO ₄	0.1 M HCl	0.1 M HCl
20	+0.08		
50	+0.08	+0.03	+0.02
100	+0.07		
200	+0.06		
500	+0.06		
900		-0.01	

†,

Recorded by Dr. C. Shi.

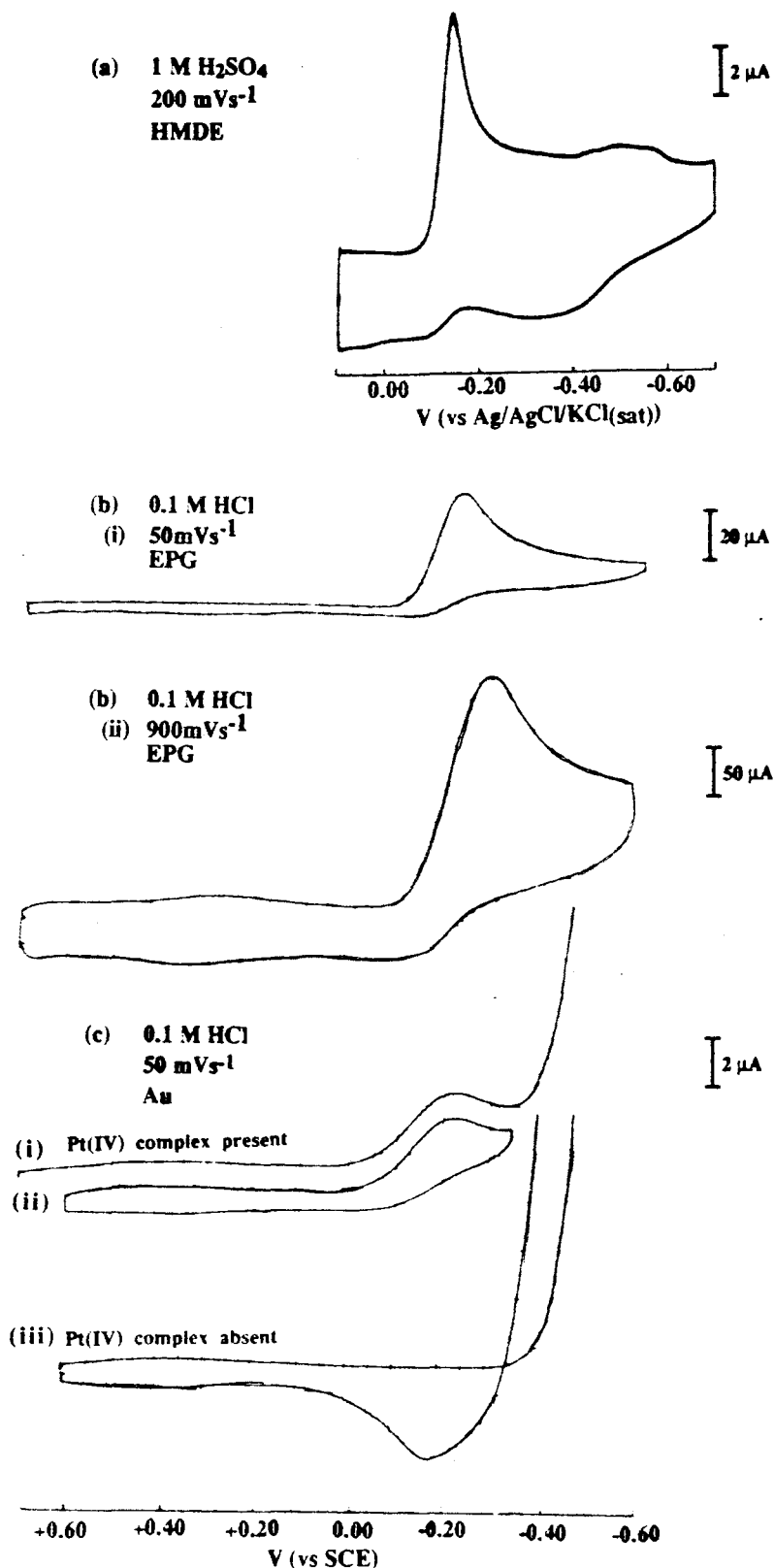


Figure 4.2: Cyclic voltammograms of $[\text{Pt}(\alpha\text{Me}_5\text{-N}_6\text{-tricosanetriimine})]^{4+/2+}$. (a) 1 M H₂SO₄ (200 mVs⁻¹, vs Ag/AgCl/KCl_(sat.)) HMDE); (b) 0.1 M HCl (i) 50 mVs⁻¹ and (ii) 900 mVs⁻¹ (vs SCE, EPG electrode);[§] (c) 0.1 M HCl (i) and (ii) in the presence of $[\text{Pt}(\alpha\text{Me}_5\text{-N}_6\text{-tricosanetriimine})]^{4+}$, (iii) in the absence of $[\text{Pt}(\alpha\text{Me}_5\text{-N}_6\text{-tricosanetriimine})]^{4+}$ (50 mVs⁻¹, vs SCE, Au electrode).[§]

[§]. Recorded by Dr. C. Shi.

3. [Pt^{IV}(Me₄-N₆-tetracosanediimine)]⁴⁺

The CV's of [Pt^{IV}(Me₄-N₆-tetracosanediimine)]⁴⁺ in 1 M H₂SO₄ and 0.1 M NaClO₄ using an HMDE are presented in Fig. 4.3(a) and (b), respectively. Irreversible responses were observed in both electrolytes and are attributed to the reduction of the Pt(IV) to Pt(II) state, by analogy with the reduction of [Pt^{IV}(tame)₂]⁴⁺ and the related cage complex [Pt^{IV}(Et₂-Me₆-N₆-tetracosanediimine)]⁴⁺. The peak potentials for [[Pt^{IV}(Me₄-N₆-tetracosanediimine)]⁴⁺ in 0.1 M NaClO₄ and 1 M H₂SO₄ at different scan rates are listed in Table 4.3. In 0.1 M NaClO₄, the irreversible response was accompanied by a sharp prewave which is attributed to strong adsorption of the product.^{41,42} Its potential was independent of scan rate ($E_{pc} = -0.32$ V vs NHE). The reduction potentials of the diffusion controlled responses moved to more negative values as the scan rate increased, indicating that product is weakly adsorbed on the electrode. The sharp prewave was not observed in the acidic medium, however the responses in 1 M H₂SO₄ were sharper than expected for a diffusion controlled response, and also moved to more negative potentials as the scan rate was increased. This implies that the product is weakly adsorbed on the electrode in 1 M H₂SO₄. The responses occur at more positive potentials in acid media than in neutral solution as the complexes are fully protonated under these conditions.

Table 4.3: Scan rate dependence of the reduction potential for the [Pt^{IV}(Me₄-N₆-tetracosanediimine)]^{4+/2+} couple (V vs NHE, HMDE, 295 K).

Scan Rate (mVs ⁻¹)	E_{pc} (V vs NHE)	
	0.1 M NaClO ₄	1 M H ₂ SO ₄
20	-0.32	-0.04
50	-0.32 _{ads} , -0.37	-0.05
100	-0.33 _{ads} , -0.42	-0.05
200	-0.35 _{ads} , -0.48	-0.06
500	-0.28 _{ads} , -0.50	-0.06

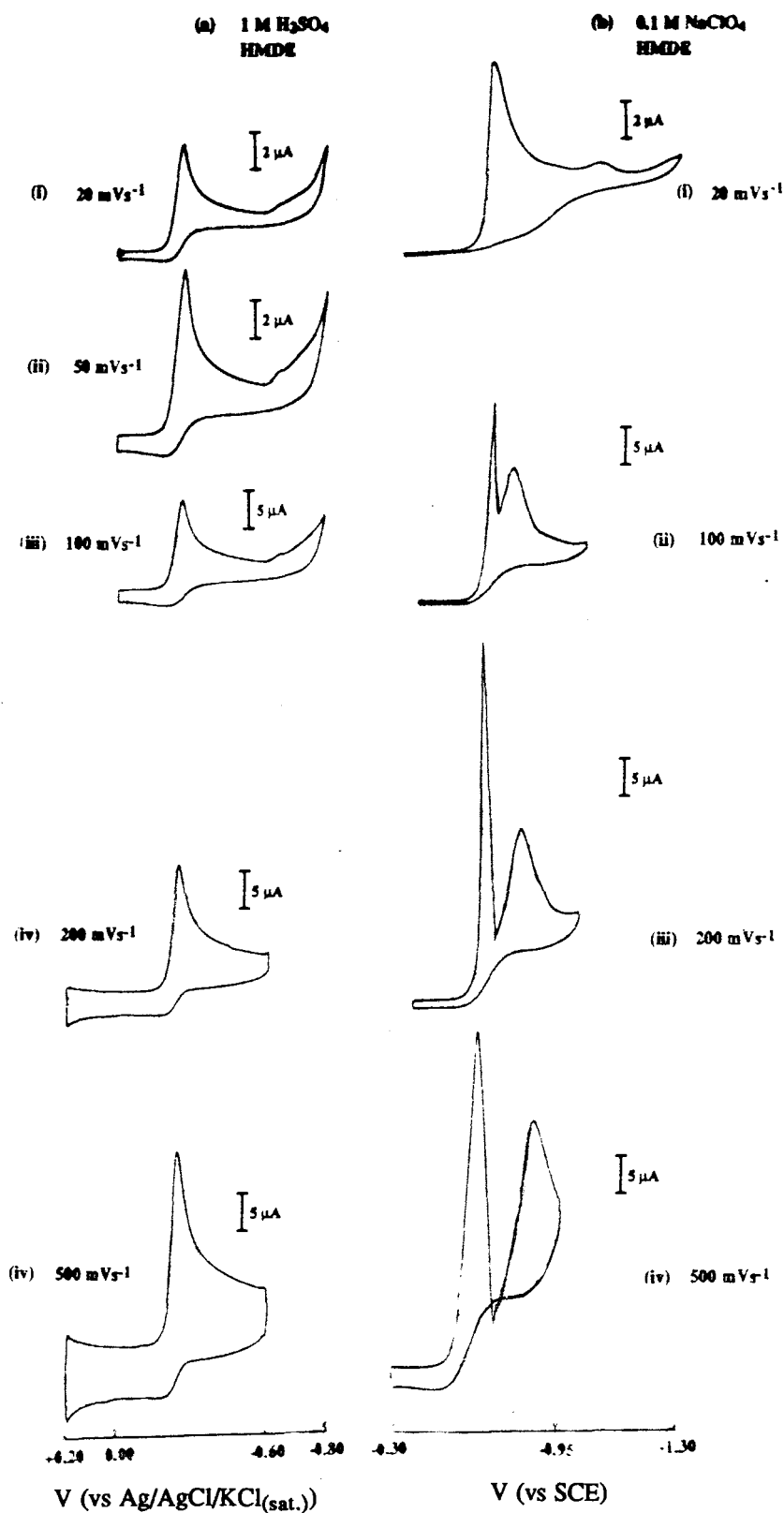


Figure 4.3: Cyclic voltammograms of $[\text{Pt}^{\text{IV}}(\text{Me}_4\text{-N}_6\text{-tetracosanediimine})]^{4+/2+}$.
 (a) 1 M H_2SO_4 at (i) 20 mVs^{-1} , (ii) 50 mVs^{-1} , (iii) 100 mVs^{-1} , (iv) 200 mVs^{-1} , (v) 500 mVs^{-1} (vs Ag/AgCl/KCl_(sat.), HMDE); (b) 0.1 M NaClO_4 (i) 20 mVs^{-1} (ii) 100 mVs^{-1} , (iii) 200 mVs^{-1} , (iv) 500 mVs^{-1} (vs SCE, HMDE).

4. [Pt^{IV}(Et₂-Me₆-N₆-tetracosanediimine)]⁴⁺

(a) Electrochemistry using the EPG and Au disc electrodes

(i) Aqueous Media

The CV's of [Pt^{IV}(Et₂-Me₆-N₆-tetracosanediimine)]⁴⁺ in HCl using the EPG and gold disc electrodes each show an irreversible response (Fig. 4.4), and the peak potentials at different scan rates are tabulated in Table 4.4. The peak currents were higher using the EPG electrodes than those using the gold disc electrodes. The irreversible response was established as a two electron process from the rotating disc electrode experiments (described later) and is attributed to the reduction of the Pt(IV) complex to a Pt(II) species. The reduction potentials are more positive in acidic media, as the complexes are fully protonated under these conditions. The potentials for hydrogen evolution in the presence and absence of [Pt^{IV}(Et₂-Me₆-N₆-tetracosanediimine)]⁴⁺ in 0.1 M HCl are very similar (Figs 4.4(c)(i and ii) and Fig. 4.3(c)(iii)). Therefore, this complex is not effective as a catalyst for the electroproduction of hydrogen.

(ii) Non Aqueous Media

The reduction potentials for the responses in nonaqueous media are listed in Table 4.4. A quasireversible response was observed in acetone using the gold disc electrode, in the range +400 to -100 mV, at $E_{1/2} \sim 0.13$ V ($\Delta E_p = 164$ mV) vs Ag/AgCl/LiCl_(sat. acetone) (Fig. 4.5(a)). The quasireversible response became irreversible ($E_{pc} = +0.05$ V vs Ag/AgCl/LiCl_(sat. acetone)) when the potential window was extended to include an irreversible response which appeared at a more negative potential, $E_{pc} = -0.48$ V (vs Ag/AgCl/LiCl_(sat. acetone)) (Fig. 4.5(b)). The quasireversible response is likely to be due to the Pt(IV)/Pt(II) couple. The large peak separation is attributed to structural rearrangement that accompanies the reduction of the six-coordinate Pt(IV) centre to the square planar Pt(II) ion. The more positive potentials in acetone compared to those in aqueous media are consistent with the behaviour observed for the Pt(IV) sar and sep type cages.^{6,7} No responses were observed in 50% acetone:water using the gold, platinum or glassy carbon disc electrodes. The irreversible response at $E_{pc} = -0.48$ (vs Ag/AgCl/LiCl_(sat. acetone)) had a greater current than that at $E_{pc} = +0.05$ V (vs Ag/AgCl/LiCl_(sat. acetone)) due to an irreversible multi electron process. This response could be attributed to reduction of the imines.

Similar behaviour was observed in MeCN. The quasireversible response at $E_{1/2} = +0.03$ V ($\Delta E_p = 258$ mV) vs Ag/AgCl/KCl_(sat.) became irreversible ($E_{pc} = -0.13$ V (vs Ag/AgCl/KCl_(sat.))) when the potential window was extended to include the irreversible response at $E_{pc} = -0.77$ V (vs Ag/AgCl/KCl_(sat.)).

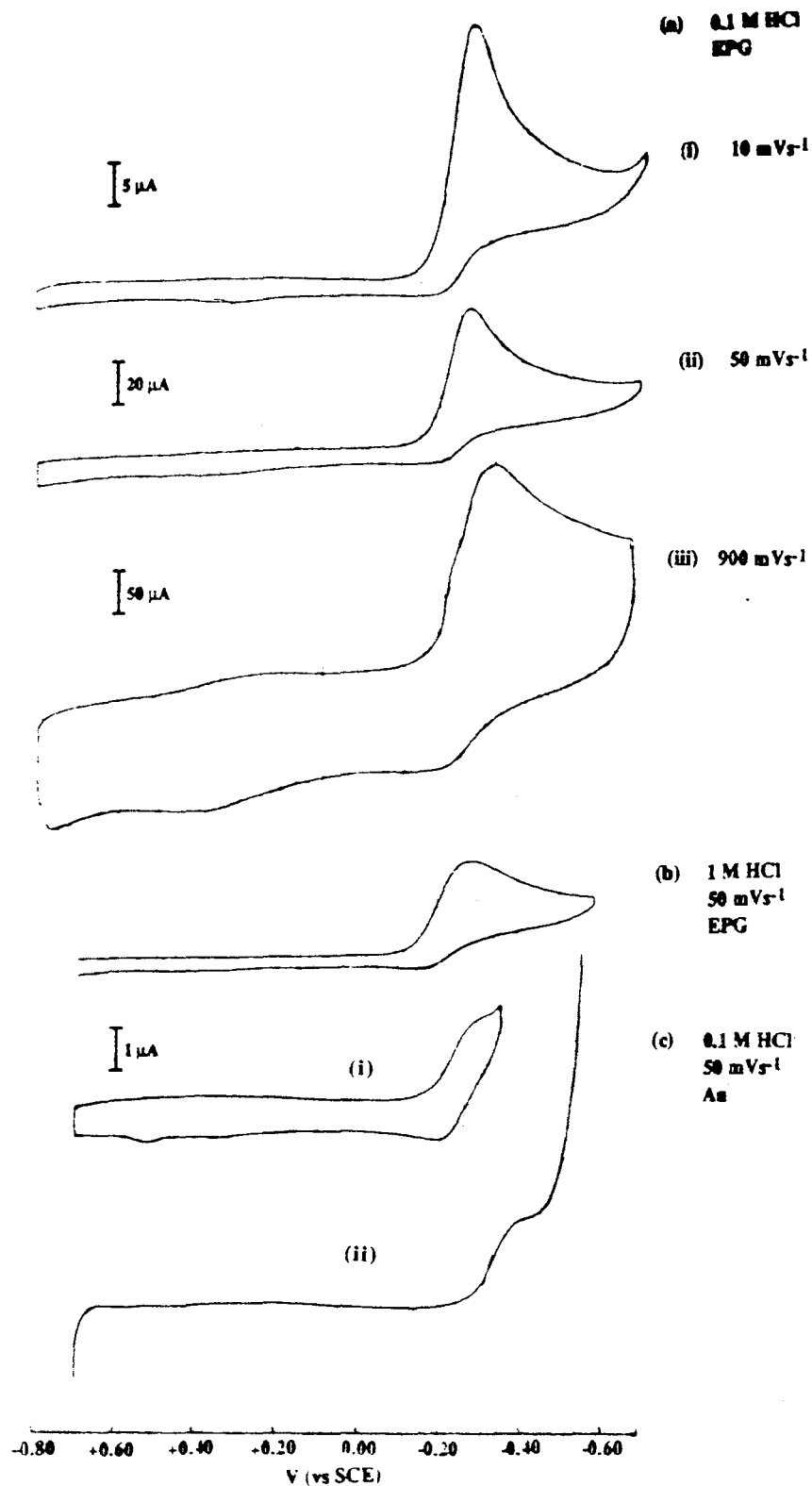


Figure 4.4: Cyclic voltammograms of $[\text{Pt}^{\text{IV}}(\text{Et}_2\text{-Me}_6\text{-N}_6\text{-tetracosanediimine})]^{4+}$ using the EPG electrode. (a) 0.1 M HCl (i) 10, (ii) 50, (iii) 900 mVs^{-1} ; (b) in 1 M HCl (50 mVs^{-1}); (c) gold electrode, 0.1 M HCl (50 mVs^{-1}) (i) range +0.7 to -0.4 V (ii) range +0.7 to -0.6 V in the presence of $[\text{Pt}^{\text{IV}}(\text{Et}_2\text{-Me}_6\text{-N}_6\text{-tetracosanediimine})]^{4+}$ (vs SCE)[§]

[§] Recorded by Dr. C. Shi.

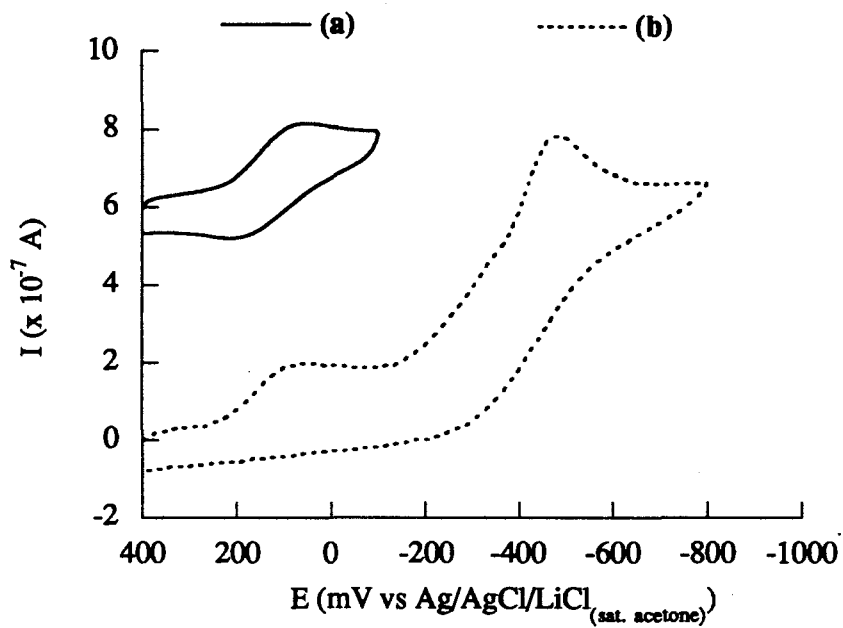


Figure 4.5: Cyclic voltammograms of $[\text{Pt}^{\text{IV}}(\text{Et}_2\text{-Me}_6\text{-N}_6\text{-tetracosanediimine})]^{4+}$ in acetone. (a) 400 to -100 mV (b) 400 to -800 mV (50 mVs^{-1} , vs $\text{Ag}/\text{AgCl}/\text{LiCl}_{(\text{sat. acetone})}$), 0.1 M TMAH, 293 K, Au electrode).

Table 4.4: Electrochemistry of $[\text{Pt}^{\text{IV}}(\text{Et}_2\text{-Me}_6\text{-N}_6\text{-tetracosanediimine})]^{4+}$ under various conditions (V vs NHE, 295 K).

Scan rate (mVs^{-1})	HMDE			EPG [†]		Au		Pt
	E_{pc} (V vs NHE)			E_{pc} (V vs NHE)		E_{pc} (V vs NHE) [‡]		$E_{1/2}$ (V) [¶]
	0.1 M NaCl	1 M H ₂ SO ₄	1 M HCl [†]	0.1 M HCl	1 M HCl	0.1 M HCl [†]	Acetone ($E_{1/2}$) [‡]	MeCN
10				-0.03		+0.00		
20		-0.02						0.01 (295)
50	-0.10.	-0.02	+0.01	-0.02	-0.04*	+0.01	+0.13 (164), $E_{\text{pc}} =$ -0.48*	
100	-0.12	-0.03					+0.12 (135)	+0.03, (258), $E_{\text{pc}} =$ -0.77 [§]
200	-0.14	-0.04						
500		-0.05						-0.01 (254)
900			-0.01	-0.08				
1000								-0.01 (233)

†, Recorded by Dr. C. Shi; [‡], in acetone, $E_{1/2}$ in V vs Ag/AgCl/LiCl(sat. acetone); [¶], in MeCN, V vs Ag/AgCl/KCl(sat) ($E_{1/2}(\text{Fc}^{+/0}) = +308.8$ mV Ag/AgCl/KCl(sat)); *, The half wave potential at $E_{1/2} = +0.13$ V becomes irreversible ($E_{\text{pc}} = +0.047$ V) when the potential window includes the irreversible response at $E_{\text{pc}} = -0.48$ V. The latter response has twice the current than that at +0.047 V; [§], The half wave potential at $E_{1/2} = +0.03$ V becomes irreversible ($E_{\text{pc}} = -0.13$ V) when the potential window includes the irreversible response at $E_{\text{pc}} = -0.77$ V. The latter response has twice the current than that at +0.077 V.

(b) Electrochemistry using the Rotating Disc Electrode (RDE).

The bulk electrochemical reduction of $[\text{Pt}^{\text{IV}}(\text{Et}_2\text{-Me}_6\text{-N}_6\text{-tetracosanediimine})]^{4+}$ at -0.8 V vs SCE using a stirred mercury pool working electrode showed that only 1.5 electrons per Pt(IV) complex had been consumed after three hours, when the current became negligible. The product, a Pt(II) complex, was found to passivate the mercury surface, preventing complete electrolysis. The ¹H and ¹³C NMR spectra of the bulk electrolysis product indicated that it was the same complex as that isolated from the

hydrogenation of $[\text{Pt}^{\text{IV}}(\text{Et}_2\text{-Me}_6\text{-N}_6\text{-tetracosanediimine})]^{4+}$. The number of electrons involved in the reduction of $[\text{Pt}^{\text{IV}}(\text{Et}_2\text{-Me}_6\text{-N}_6\text{-tetracosanediimine})]^{4+}$ was established using the rotating disc electrode (RDE). Figure 4.6 depicts the responses for the reduction of $[\text{Pt}^{\text{IV}}(\text{Et}_2\text{-Me}_6\text{-N}_6\text{-tetracosanediimine})]^{4+}$ using an EPG RDE in 0.1 M HCl at different angular velocities.

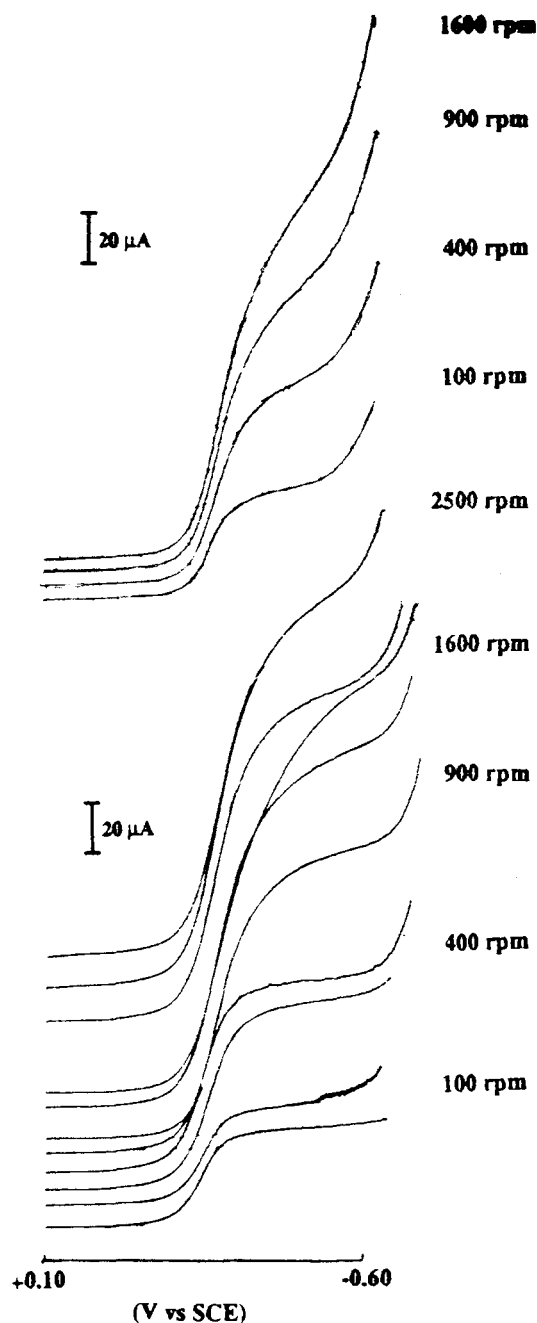


Figure 4.6: Reduction of $[\text{Pt}^{\text{IV}}(\text{Et}_2\text{-Me}_6\text{-N}_6\text{-tetracosanediimine})]^{4+}$ using the EPG RDE, at 50 mVs^{-1} .[§]

[§], Recorded by Dr. C. Shi.

The number of electrons involved in the response was calculated from the Koutecky-Levich equation:

$$i_l = 0.62n\mathcal{F}AD_o^{\frac{2}{3}}C_o^*\omega^{\frac{1}{2}}\nu^{-\frac{1}{6}}$$

where i_l = the limiting current, n = the number of electrons, \mathcal{F} = Faraday's constant, A = the area of the electrode (0.32 cm^2), D_o = the diffusion coefficient, C_o^* = concentration of the electroactive species in the bulk solution ($0.63 \times 10^{-3} \text{ M}$), ω = angular velocity ($2\pi \times \text{rps}$) of the disc and ν = the kinematic viscosity ($0.01 \text{ cm}^2\text{s}^{-1}$). The diffusion coefficient for $[\text{Co}(\text{Me}_5\text{-N}_6\text{-tricosanetriimine})]^{3+}$ was used ($2.72 \times 10^{-6} \text{ cm}^2\text{s}^{-1}$, derived in Appendix D) and this value is consistent with that obtained for $[\text{Co}(\text{sar})]^{3+}$.⁴³ The use of this diffusion coefficient is justified as $[\text{Pt}^{\text{IV}}(\text{Et}_2\text{-Me}_6\text{-N}_6\text{-tetracosanediimine})]^{4+}$ is deprotonated under these conditions, so the complex would have an effective charge of +3 and have similar dimensions as that for the Co(III) species. Table 4.5 lists the dependence of the limiting current (i_l) on angular velocity (ω) and the calculated number of electrons involved. Two electrons are involved in the electrochemical reduction of $[\text{Pt}^{\text{IV}}(\text{Et}_2\text{-Me}_6\text{-N}_6\text{-tetracosanediimine})]^{4+}$ in 0.1 M HCl. It is therefore likely that the responses observed for the similar Pt(IV) cage complexes presented in this work are also due to the Pt(IV)/(II) couple.

Table 4.5: Dependence on the limiting current with angular velocity and the calculated number of electrons.

	ω (rpm, rads^{-1})	i_l (μA)	n^{\S}
experiment 1	2,500	128	1.56
	1,600	120	1.83
	900	106	2.16
	400	68	2.07
	100	34	2.07
experiment 2	1,600	108	1.65
	900	88	1.79
	400	67	2.04
	109	38	2.22

[§], Calculated using diffusion coefficient for $[\text{Co}(\text{Me}_5\text{-N}_6\text{-tricosanetriimine})]^{3+}$, $D_o = 2.72 \times 10^{-6} \text{ cm}^2\text{s}^{-1}$

(c) *Electrochemistry using the HMDE*

The CV of $[\text{Pt}^{\text{IV}}(\text{Et}_2\text{-Me}_6\text{-N}_6\text{-tetracosanediimine})]^{4+}$ in 1 M HCl at 50 mVs^{-1} (using the HMDE), showed a two electron irreversible response at $E_{\text{pc}} = +0.01 \text{ V}$ (vs NHE) (Fig. 4.7(a)). At 900 mVs^{-1} , no oxidative wave was discernible (Fig. 4.7(b)). The response was also irreversible in 0.1 M NaCl and 1 M H_2SO_4 at scan rates 20 to 500 mVs^{-1} . The wave was grossly distorted in 0.1 M NaCl, presumably due to adsorption. The reduction potential was slightly pH dependent, being more positive in acidic solution than in neutral solution. This is probably due to the complex being fully protonated in the 1 M acid. The reduction potentials for this response in 0.1 M NaCl, 1 M H_2SO_4 and 1 M HCl at different scan rates using the HMDE are listed in Table 4.4.

The CV's of $[\text{Pt}^{\text{IV}}(\text{Et}_2\text{-Me}_6\text{-N}_6\text{-tetracosanediimine})]^{4+}$, in 0.1 M and 1 M CF_3COOH using the HMDE, also showed a two electron irreversible response at $E_{\text{pc}} = \sim 0 \text{ V}$ (vs NHE at 20 mVs^{-1}) (Fig. 4.8). However, the potential shifted to more negative values as the scan rate increased and an oxidation wave became apparent (Figs 4.8(b-e)). The oxidation potential was essentially independent of scan rate, $E_{\text{pa}} = +0.04 \text{ V}$ (vs NHE). These data imply that the reactant was weakly adsorbed on the electrode.^{41,42} At slow scan rates, the complex has time to desorb slowly and react, but at fast scan rates there appears to be a degree of reversibility. This reversibility is anion dependent, as no oxidation wave was observed in 1 M HCl, 0.1 M NaCl or 1 M H_2SO_4 , even at fast scan rates.

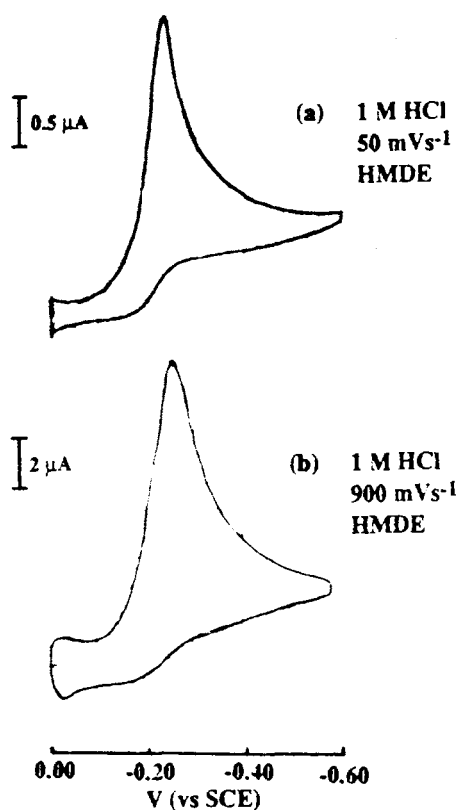


Figure 4.7: Cyclic voltammogram of $[\text{Pt}^{\text{IV}}(\text{Et}_2\text{-Me}_6\text{-N}_6\text{-tetracosanediimine})]^{4+}$ in 1 M HCl at (a) 50 (b) 900 mVs^{-1} (vs SCE, HMDE).[§]

[§] Recorded by Dr. C. Shi.

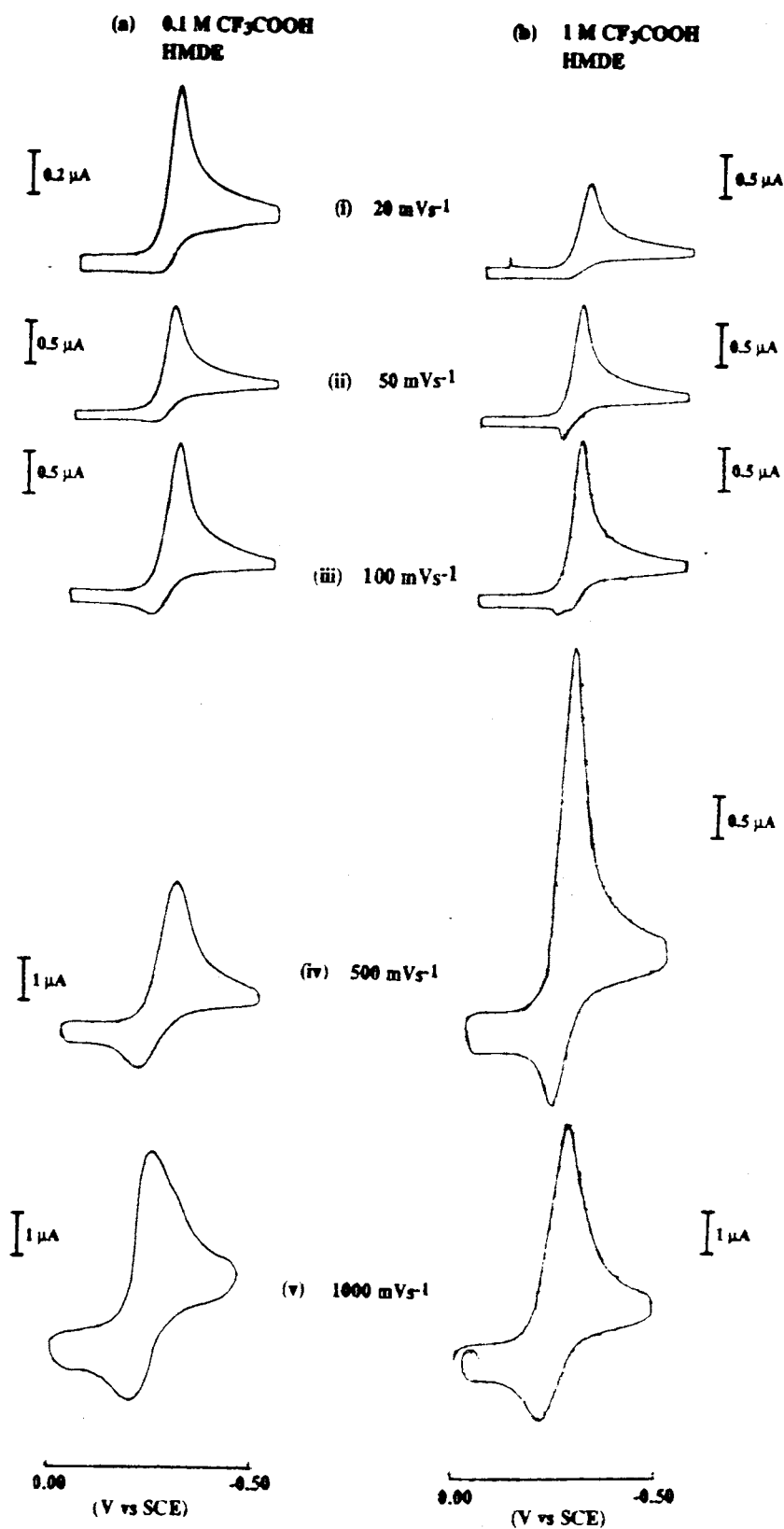


Figure 4.8: Cyclic voltammograms of $[\text{Pt}^{\text{IV}}(\text{Et}_2\text{-Me}_6\text{-N}_6\text{-tetracosanediimine})]^{4+}$ in 0.1 M CF₃COOH and 1 M CF₃COOH[§] at (a) 20, (b) 50, (c) 100, (d) 500, (e) 1000 mVs⁻¹, (vs SCE, HMDE).

[§]. Recorded by Dr. C. Shi.

The peak potentials and currents for the reduction (E_{pc} , i_{pc}) and oxidation (E_{pa} , i_{pa}) waves in 0.1 and 1 M CF_3COOH are listed in Table 4.6. In 1 M CF_3COOH at 100 mVs^{-1} , two peaks are noted in the oxidation scan, possibly due to an adsorption controlled response ($E_{pa} = +0.04\text{ V}$) and a diffusion controlled response ($E_{pa} = +0.02\text{ V}$). At faster scan rates, the wave at $E_{pa} = +0.04\text{ V}$ is swamped by that at $E_{pa} = +0.02\text{ V}$ (vs NHE).

Table 4.6: Comparison of the Peak Potentials of $[Pt^{IV}(Et_2-Me_6-N_6-tetracosanediimine)]^{4+}$ with pentacyclo- $[Pt^{II}(Et_2-Me_6-N_6-tetracosane2H)]^{4+}$, in CF_3COOH (vs NHE, 295 K).

Scan rate (mVs^{-1})	$[Pt^{IV}(Et_2-Me_6-N_6-tetracosanediimine)]^{4+}$				pentacyclo- $[Pt^{II}(Et_2-Me_6-N_6-tetracosane2H)]^{4+}$	
	0.1 M CF_3COOH		1 M CF_3COOH §		0.1 M CF_3COOH §	
	E_{pc} (V) (i_{pc} , μA)	E_{pa} (V) (i_{pa} , μA)	E_{pc} (V) (i_{pa} , μA)	E_{pa} (V) (i_{pa} , μA)	E_{pa} (V)	E_{pc} (V)
10					0.05	0.01
20	0.01 (0.80)		-0.01 (1.0)			
50	0.00 (1.25)	0.04 (0.30)	0.01 (1.35)	0.04 (0.35)	0.06	0.01
100	-0.01 (1.75)	0.04 (0.45)	0.00 (1.8)	0.05 (0.35) 0.02 (0.30)	0.06	0.01
500	-0.04 (3.35)	0.04 (1.25)	-0.02 (4.3)	0.02 (1.25)	0.08	-0.00
1000	-0.05 (4.00)	0.06 (1.75)	-0.02 (5.3)	0.02 (2.0)		

§: Recorded by Dr. C. Shi

The multiply scanned CV's demonstrate how the adsorbed species contribute to the electrochemistry of the $[Pt^{IV}(Et_2-Me_6-N_6-tetracosanediimine)]^{4+}$ system (Fig. 4.9). The peak potentials of the first cycle ($E_{pc}(1)$ and $E_{pa}(1)$) and of the last cycle ($E_{pc}(i)$ and $E_{pa}(i)$, for $i > 1$) are listed in Table 4.7. The CV response remained irreversible when it was cycled at 50 mVs^{-1} in 0.1 M CF_3COOH (Fig. 4.9(a)). The current of the reduction wave (i_{pc}) decreased significantly before it reached a limiting value after about 4 scans. The multiply scanned CV's at both 200 mVs^{-1} and 500 mVs^{-1} are depicted in

Figs 4.9(b-c). After the first cycle, the reduction potential ($E_{pc(i)}$) shifted to a slightly more positive value ($E_{pc} \sim -0.02$ V vs NHE) compared that of the first cycle ($E_{pc(1)}$). This response also moved to more positive potentials as the scan rate was increased, again, in contrast to the behaviour of the first cycle. The oxidation potential for the reverse wave, however, remained the same during the cycling and was also independent of scan rate ($E_{pa} = +0.06$ V vs NHE). When the CV was cycled at both 200 and 500 mVs^{-1} , the i_{pc} also decreased on successive scans and reached a limiting value after about 7 cycles. In contrast, at each scan rate the current for the oxidative scan remained constant during the cycling. However, after about 7 cycles at 500 mVs^{-1} , the response appeared to be quasireversible, with a half wave potential at $E_{1/2} = +0.02$ V (vs NHE), with a peak separation of $\Delta E_p = 84$ mV and $i_{pc}:i_{pa}^{-1}$.

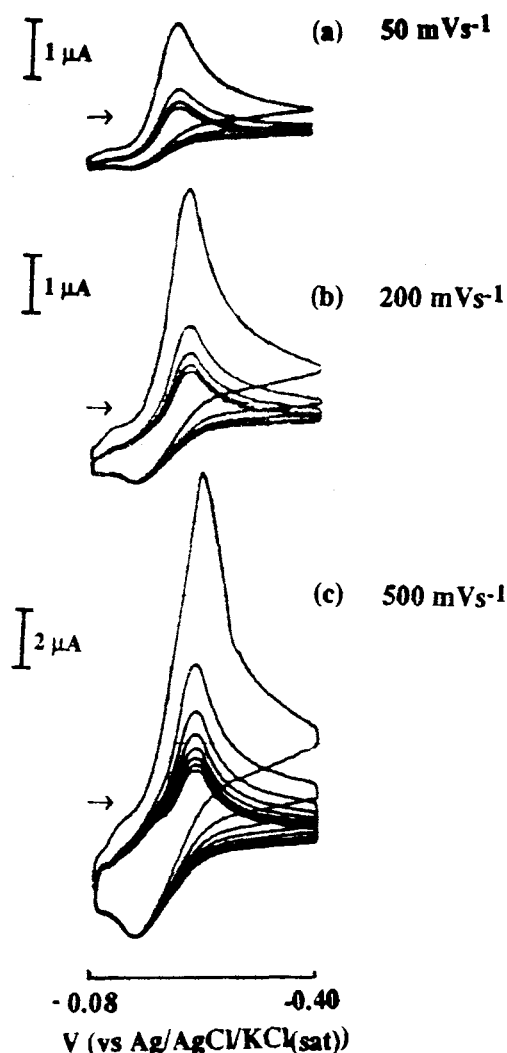


Figure 4.9: Multiple scanned cyclic voltammograms of $[Pt^{IV}(Et_2-Me_6-N_6-tetracosanediimine)]^{4+}$ in 0.1 M CF_3COOH at (a) 50, (b) 200, (c) 500 mVs^{-1} (vs $Ag/AgCl/(KCl_{(sat.)})$, HMDE).

Table 4.7: Peak potentials for the multiply scanned CV's of $[\text{Pt}^{\text{IV}}(\text{Et}_2\text{-Me}_6\text{-N}_6\text{-tetracosanediiimine})]^{4+}$ in 0.1 M CF_3COOH (V vs NHE, HMDE, 295 K).

scan rate (mVs^{-1})	$E_{\text{pc}(1)}$	$E_{\text{pc}(i)}$	E_{pa}
50	-0.00 ₅	-0.01	—
200	-0.02 ₁	-0.02	+0.06
500	-0.03	-0.02	+0.06

Clearly, in CF_3COOH both the reactant and the product are weakly adsorbed. This is apparent from the unusual shape of the reduction waves, especially those of the first cycles, which are sharper than expected for purely diffusion controlled responses. That the reactant is weakly adsorbed was evident from the shift of $E_{\text{pc}(1)}$ to more negative potentials as the scan rate increased,^{41,42} yet support for a weakly adsorbed product is evident from the multiply scanned CV's, which showed a shift of $E_{\text{pc}(i)}$ with increasing scan rates to more positive values after the first scan. The progressive decrease in i_{pc} to a limiting value and the essentially constant i_{pa} indicate that a steady state of the adsorbed species is reached after several cycles. It is likely that both partners of the redox couple contribute to this behaviour. Finally, the peak to peak separation ($\Delta E_{\text{p}(i)}$) for the quasireversible system at 500 mVs^{-1} is too large to be consistent with an electrochemically reversible two electron process, especially if associated with adsorption. However, the quasireversible response may be attributed to a weakly adsorbed $\text{PtN}_6^{4+}/\text{PtN}_4^{2+}$ system where the electron transfer is coupled with reversible coordination changes required for the six-coordinate Pt(IV) state and the four-coordinate Pt(II) state. Large peak separations have also been observed for other Pt(IV)/(II) tetraamine couples.⁴⁴⁻⁴⁶

5. Pentacyclo- $[\text{Pt}^{\text{II}}(\text{Et}_2\text{-Me}_6\text{-N}_6\text{-tetracosane2H})]^{4+}$

(a) Electrochemical behaviour on the HMDE

The electrochemical behaviour of the pentacyclo- $[\text{Pt}^{\text{II}}(\text{Et}_2\text{-Me}_6\text{-N}_6\text{-tetracosane2H})]^{4+}$ ion is different to that observed for the Pt(IV) parent diimine complex under the same conditions. The CV's of the pentacyclo- $[\text{Pt}^{\text{II}}(\text{Et}_2\text{-Me}_6\text{-N}_6\text{-tetracosane2H})]^{4+}$ ion in 0.1 M CF_3COOH at different scan rates all show an oxidation wave at $E_{\text{pa}} = \sim +0.06 \text{ V}$ (at 100 mVs^{-1}) whose peak potential was slightly dependent on scan rate (Figs 4.10(a-d)). A reduction wave was also observed at $E_{\text{pc}} = +0.01 \text{ V}$ (vs NHE) whose potential was essentially independent of scan rate. The peak potentials are listed in Table 4.6. The shapes of the CV's were not consistent with a diffusion

controlled process, probably due to adsorption of both the reactant and product. The peak potentials of both the reduction and oxidation waves progressively move to slightly more negative values with multiple scans (Fig. 4.11). This may have been due to slight changes in the activity of the adsorbed species.⁴⁷ The current of both responses decreased progressively over successive scans and became negligible after 7 cycles, presumably due to passivation of the mercury surface under these conditions. These experiments indicate that the adsorbed Pt(II) complex can only be reversibly oxidised and reduced for a limited period. The large peak to peak separation is attributed to the coordination changes between the four-coordinate Pt(II) and the six-coordinate Pt(IV) state which is coupled to the electron transfer. It is clear that the behaviour is not the same as that of the parent Pt(IV) complex even though the potentials for the reductions are similar.

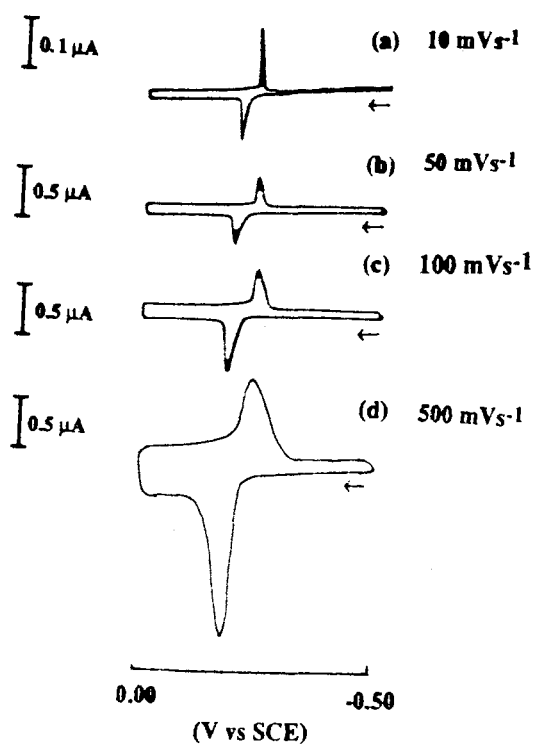


Figure 4.10: Cyclic voltammograms of pentacyclo-[Pt^{II}(Et₂-Me₆-N₆-tetracosane₂H)]⁴⁺ in 0.1 M CF₃COOH (a) 10 (b) 50 (c) 100 (d) 500 mVs⁻¹ (vs SCE, HMDE).[§]

[§], Recorded by Dr. C. Shi.

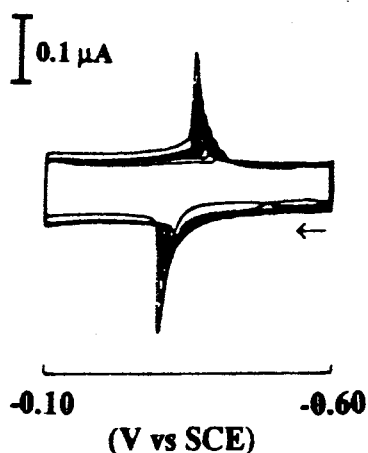


Figure 4.11: Cyclic voltammogram of pentacyclo-[Pt^{II}(Et₂-Me₆-N₆-tetracosane2H)]⁴⁺ in 0.1 M CF₃COOH, 7 scans (50 mVs⁻¹, V vs SCE, HMDE).[§]

[§] Recorded by Dr. C. Shi.

The bulk electrochemical oxidation of pentacyclo-[Pt^{II}(Et₂-Me₆-N₆-tetracosane2H)]⁴⁺ in 0.1 M CF₃COOH at 0 V vs SCE using a mercury pool working electrode was unsuccessful. The current decreased rapidly during the oxidation, presumably due to the passivation of the mercury surface by adsorption of pentacyclo-[Pt^{II}(Et₂-Me₆-N₆-tetracosane2H)]⁴⁺. This occurred even when the mercury pool was vigorously agitated by bubbling with nitrogen and stirring the surface with a magnetic flea. The behaviour is consistent with the decrease in current observed for the multiply scanned CV's for this complex.

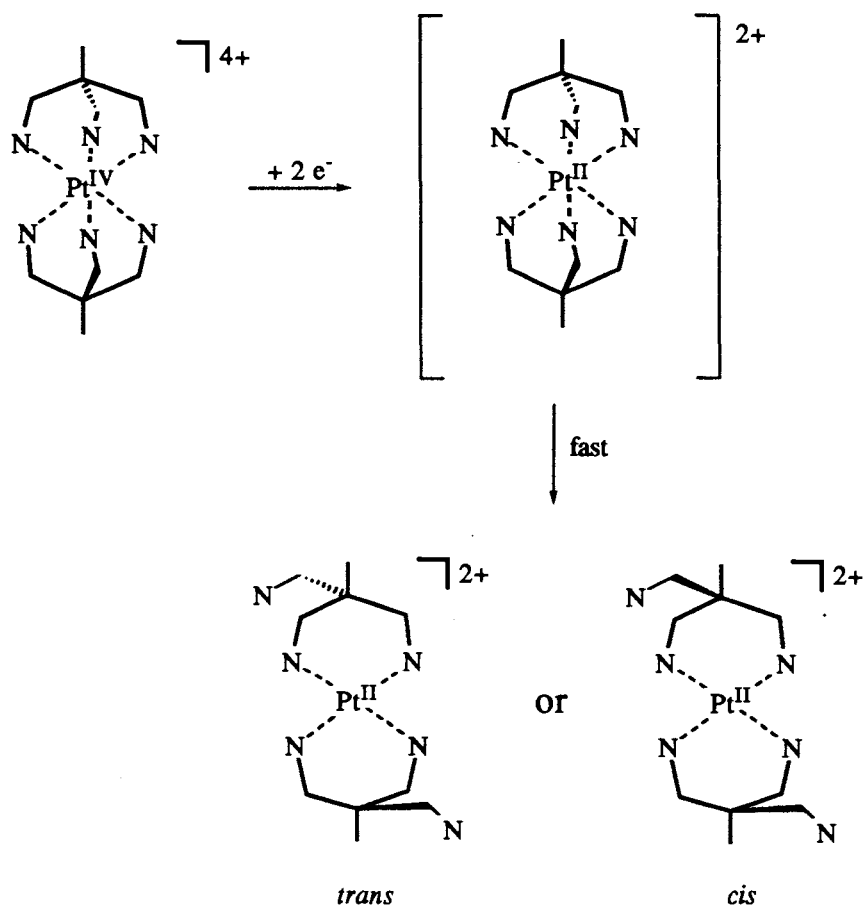
4.4. Discussion

4.4.1. General

Much of the Pt(IV) reduction chemistry was irreversible in aqueous media on the HMDE, gold disc and EPG electrodes. Bulk electrolysis of $[\text{Pt}^{\text{IV}}(\text{tame})_2]^{4+}$ and $[\text{Pt}^{\text{IV}}(\text{Et}_2\text{-Me}_6\text{-N}_6\text{-tetracosanediimine})]^{4+}$ both gave rise to single Pt(II) complexes, which were characterised by ^1H and ^{13}C NMR spectroscopy. The irreversible response for $[\text{Pt}^{\text{IV}}(\text{Et}_2\text{-Me}_6\text{-N}_6\text{-tetracosanediimine})]^{4+}$ was shown to involve a two electron transfer. The irreversible responses observed in the CV's of the remaining related Pt(IV) cages are therefore likely to correspond to the reduction of the Pt(IV) state to Pt(II) which is accompanied by dissociation of two nitrogen donors to achieve the square planar geometry for Pt(II). Both the hydrogenation and bulk electrochemical reduction of $[\text{Pt}^{\text{IV}}(\text{Et}_2\text{-Me}_6\text{-N}_6\text{-tetracosanediimine})]^{4+}$ gave rise to the same Pt(II) product. Therefore, it is concluded that the mechanisms for these processes are similar and this most likely holds for analogous Pt(IV) cage complexes as well.

4.4.2. $[\text{Pt}^{\text{IV}}(\text{tame})_2]^{4+}$

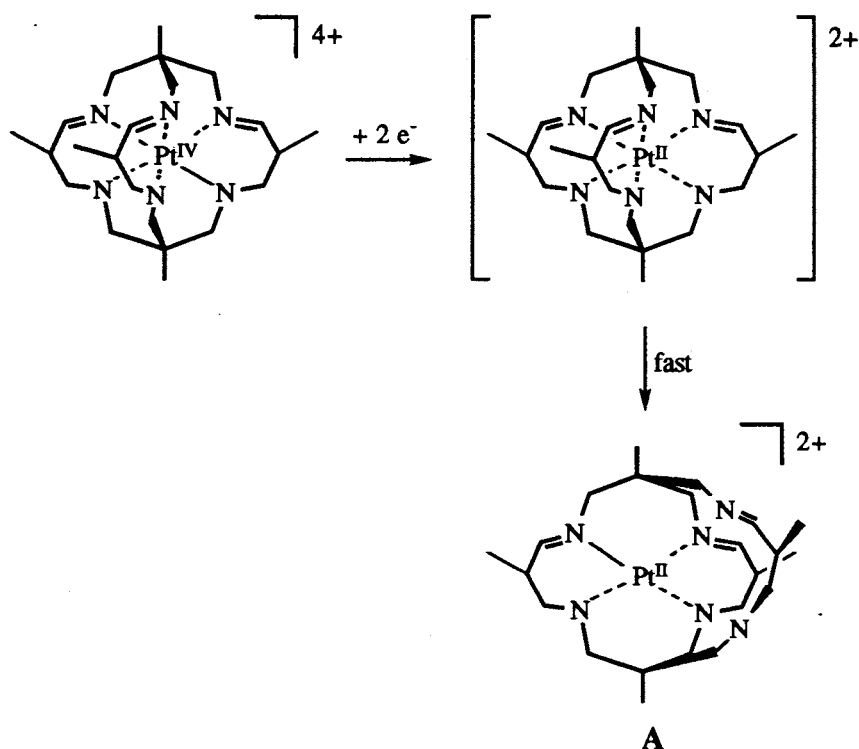
The electrochemistry of $[\text{Pt}(\text{tame})_2]^{4+}$ is relatively straightforward. Reduction of the Pt(IV) complex to Pt(II) involves dissociation of two nitrogen donor atoms as shown in Scheme 4.3. Although bulk reduction of the Pt(IV) complex to the square planar Pt(II) complex appears to give rise to only one product, it is not yet certain if this species is the *trans* or a *cis* isomer. In the *cis* case, the amine groups dissociate on different tame ligands, as dissociation of amine groups on the same tame ligand would not give rise initially to the square planar geometry favoured by the Pt(II) ion. The *trans* isomer and *cis* isomer would give rise to relatively simple ^1H and ^{13}C NMR spectra, as they have C_{2v} or C_{2h} symmetry, respectively, and therefore a structural analysis of the Pt(II) product would be desirable. It is likely that two nitrogen donor atoms *trans* to each other dissociate since this path requires the least reorganisation. Similar stereochemistry has been observed for $[\text{Pt}(\text{tacn})_2]^{2+}$, where the two uncoordinated nitrogen atoms lie on opposite sides of the PtN_4^{2+} plane.³⁹ However, for some cage types, specific steric demands may favour *cis* dissociation.



Scheme 4.3: Electrochemical reduction of $[\text{Pt}^{\text{IV}}(\text{tame})_2]^{4+}$ (amine protons have been omitted for clarity).

4.4.3. $[\text{Pt}^{\text{IV}}(\alpha\text{Me}_5\text{-N}_6\text{-tricosanetriimine})]^{4+}$

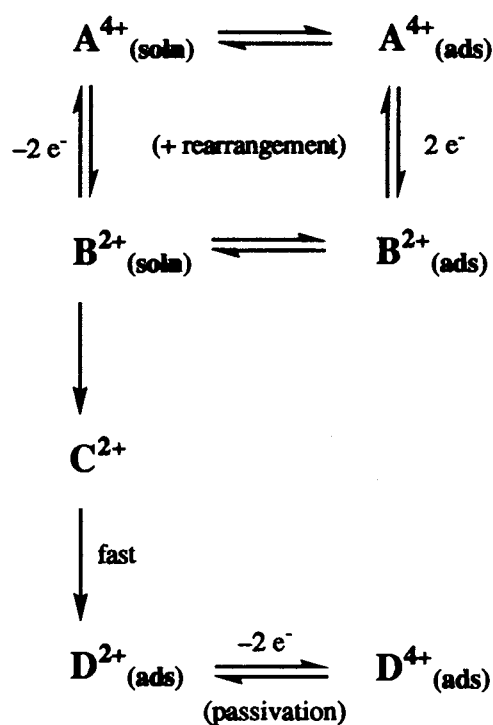
The proposed pathway for the reduction of $[\text{Pt}^{\text{IV}}(\alpha\text{Me}_5\text{-N}_6\text{-tricosanetriimine})]^{4+}$ to square planar Pt(II) is outlined in Scheme 4.4. The mechanism is argued to be similar to that proposed for the hydrogenation (Section 3.4.3.b). The ^{13}C NMR spectra acquired during the hydrogenation imply that the initially reduced complex has a pseudo mirror plane. The NMR spectra indicate that two nitrogen donors *cis* to each other, on the same strand dissociate (A). Similar stereochemistry has been observed for $[\text{Pt}^{\text{II}}((\text{NH}_3)_2\text{sar})]^{4+}$ ⁴⁸ and $[\text{Pd}^{\text{II}}((\text{NH}_3)_2\text{sar})]^{4+}$.⁴⁸ Dissociation of two nitrogen atoms *trans* to each other is unlikely to produce the pseudo symmetry observed in the NMR spectra during hydrogenation (discussed previously in Chapter 3.4.3.b). Subsequent decomposition was observed in the hydrogenation, and decomposition also occurs in the electrochemistry. Presumably the decomposition route is the same for both these processes.



Scheme 4.4: Electrochemical reduction of $[\text{Pt}^{\text{IV}}(\alpha\text{Me}_5\text{-N}_6\text{-tricosanetriimine})]^{4+}$ (amine protons have been omitted for clarity).

4.4.4. $[\text{Pt}^{\text{IV}}(\text{Et}_2\text{-Me}_6\text{-N}_6\text{-tetracosanediimine})]^{4+}$

The electrochemical behaviour of the $[\text{Pt}^{\text{IV}}(\text{Me}_4\text{-N}_6\text{-tetracosanediimine})]^{4+}$ and $[\text{Pt}^{\text{IV}}(\text{Et}_2\text{-Me}_6\text{-N}_6\text{-tetracosanediimine})]^{4+}$ complexes was complicated, but was similar in both systems. As a well-defined product in the reduction of $[\text{Pt}^{\text{IV}}(\text{Et}_2\text{-Me}_6\text{-N}_6\text{-tetracosanediimine})]^{4+}$ was isolated, the following discussion therefore focuses on the electrochemical behaviour of the latter complex. It is anticipated that the mechanism is the same for the structurally related $[\text{Pt}^{\text{IV}}(\text{Me}_4\text{-N}_6\text{-tetracosanediimine})]^{4+}$. The reduction of $[\text{Pt}^{\text{IV}}(\text{Et}_2\text{-Me}_6\text{-N}_6\text{-tetracosanediimine})]^{4+}$ on the CV timescale does not immediately lead to the product obtained from bulk electrolysis, (pentacyclo- $[\text{Pt}^{\text{II}}(\text{Et}_2\text{-Me}_6\text{-N}_6\text{-tetracosane}2\text{H})]^{4+}$) and the latter complex appears to be resistant to both chemical and bulk electrochemical oxidation. The different electrochemistry of these two complexes implies that two connected reaction manifolds are required to explain the observations. An interpretation of the electrochemical behaviour of the Pt(IV) and Pt(II) complexes on short and long timescales is summarised in Scheme 4.5. In the first manifold, the parent Pt(IV) and its immediately reduced product are cycled. This process is essentially chemically reversible in CF_3COOH , at least over a short period. Over longer timescales, and also in other electrolytes, the second manifold becomes competitive and different Pt(II) and Pt(IV) complexes are cycled.



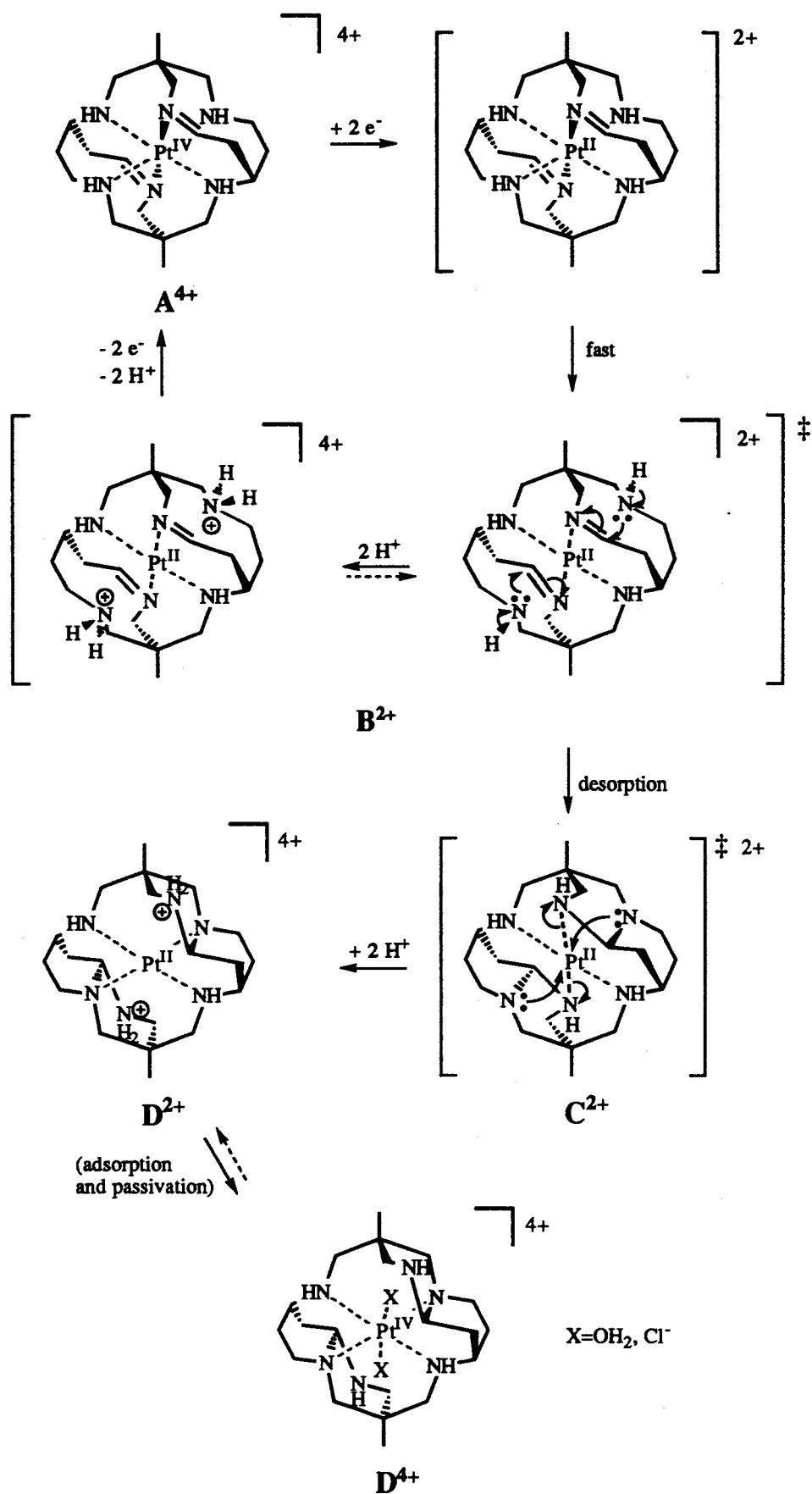
Scheme 4.5: Summary of the electrochemical behaviour of $[\text{Pt}^{\text{IV}}(\text{Et}_2\text{-Me}_6\text{-N}_6\text{-tetracosanediimine})]^{4+}$.

The $[\text{Pt}^{\text{IV}}(\text{Et}_2\text{-Me}_6\text{-N}_6\text{-tetracosanediimine})]^{4+}$ ion from the solution ($\text{A}^{4+}_{(\text{soln})}$) adsorbs weakly on the surface of the electrode to form $\text{A}^{4+}_{(\text{ads})}$. Both $\text{A}^{4+}_{(\text{soln})}$ and $\text{A}^{4+}_{(\text{ads})}$ undergo a two electron reduction which is coupled with rapid inner sphere rearrangement to give a square planar Pt(II) species, $\text{B}^{2+}_{(\text{soln})}$ and $\text{B}^{2+}_{(\text{ads})}$ respectively. At fast scan rates, low pH and in the absence of coordinating anions like Cl^- , both the two electron transfer and subsequent rearrangement between the $\text{A}^{4+}/\text{B}^{2+}$ system are chemically reversible. This accounts for the quasireversibility of the first manifold under these conditions. The large peak to peak separation is consistent with a chemically reversible coordination change that accompanies the two electron transfer. The fate of both $\text{B}^{2+}_{(\text{ads})}$ and $\text{B}^{2+}_{(\text{soln})}$ depends on the scan rate, the acidity and the supporting electrolyte. At slow scan rates, in neutral media or in a relatively high concentration of Cl^- , $\text{B}^{2+}_{(\text{ads})}$ desorbs to form $\text{B}^{2+}_{(\text{soln})}$ which rapidly rearranges to give firstly complex C^{2+} and then D^{2+} before it can reoxidise to A^{4+} . Complex $\text{D}^{2+}_{(\text{ads})}$ may be reversibly oxidised to form $\text{D}^{4+}_{(\text{ads})}$, although passivation of the electrode surface eventually occurs.

The proposed structures of B^{2+} , C^{2+} and D^{4+} are shown in Scheme 4.6. The parent Pt(IV) complex (A^{4+}) is reduced to a short lived six-coordinate Pt(II) intermediate. Rupture of what had been the two longest Pt-N bonds (in the Pt(IV) state) occurs to form the four-coordinate Pt(II) species, B^{2+} . In CF_3COOH , at fast scan rates, B^{2+} is reoxidised to A^{4+} faster than it can desorb and rearrange to form intermediate C^{2+} . The dissociated amine groups in $B^{2+}_{(soln)}$ would be protonated in CF_3COOH , since the exo-amines in Pt(II) complexes are quite basic. In these circumstances, the rate of intramolecular condensation in protonated B^{2+} to give C^{2+} would be slower. Under these conditions, when protonated B^{2+} is reoxidised to the much more acidic Pt(IV) state (A^{4+}), deprotonation of the pendant amino groups occurs and subsequently re-coordinate with the metal centre.

At slower scan rates, desorption of $B^{2+}_{(ads)}$ allows the intramolecular cyclisation to become competitive. The dissociated amines in $B^{2+}_{(soln)}$ condense irreversibly with the adjacent coordinated imines, to form intermediate C^{2+} which then rapidly rearranges to form D^{2+} , which has been structurally characterised. When D^{2+} is oxidised to D^{4+} , it is not likely that the pendant amine groups would simply re-coordinate, as Dreiding models show that such a complex would be severely sterically strained; hence the structure of the D^{4+} is not clear. A coordinating anion, such as Cl^- or H_2O , could occupy the two sites and this may explain the electrolyte dependence on this system. Once formed, complex D^{2+} does not revert to the original reactant and the system remains in the second manifold.

There is obviously a close link between the electrochemical behaviour and the hydrogenation reaction, since their reactant and products are the same. In this respect, the structures proposed in Scheme 4.6, are rather realistic in a broad sense, and is also consistent with the electrochemical observations.



Scheme 4.6: A feasible mechanism for the electrochemical reduction of the [Pt(N₆-tetracosanediimine)]⁴⁺ species.

Clearly, the electrochemical behaviour of $[\text{Pt}^{\text{IV}}(\text{Et}_2\text{-Me}_6\text{-N}_6\text{-tetracosanediimine})]^{4+}$ and pentacyclo- $[\text{Pt}^{\text{II}}(\text{Et}_2\text{-Me}_6\text{-N}_6\text{-tetracosane2H})]^{4+}$ is not fully characterised, as it is a very complex system. It would be desirable to examine the electrolyte, solvent and pH dependence of the system in more detail. The structural rearrangement leading to the formation of D^{2+} is an unusual intramolecular reaction, but its inability to regenerate A^{4+} is not surprising as the product D^{2+} is very stable.

One of the major goals of this work, namely, the synthesis of catalysts for the evolution of hydrogen was not accomplished, due to lack of stabilisation of the Pt(III) state. Such stabilisation may be possible if the reduction of the imine to the amine could be achieved, without reduction of Pt(IV) to Pt(II). In order to avoid this problem, other routes for selective reduction of the imines need are necessary, or alternative strategies to the synthesis of these types of Pt(IV) cages should be sought. The presence of softer donor atoms, such as sulfur, may help to stabilise the Pt(III) ion and work is underway to synthesise Pt(IV) cage complexes with mixed nitrogen and sulfur donors.

4.4.5. References

- (1) Geue, R. J.; Hambley, T. W.; Harrowfield, J. M.; Sargeson, A.; Snow, M. R. *J. Am. Chem. Soc.* **1984**, *106*, 5478, and references therein.
- (2) Ralph, S. F., Personal Communication **1991**.
- (3) Geue, R. J.; Höhn, A.; Ralph, S. F.; Sargeson, A. M.; Willis, A. C. *J. Chem. Soc., Chem. Commun.* **1994**, 1513.
- (4) Harrowfield, J. M.; Herlt, A. J.; Lay, P. A.; Sargeson, A. M. *J. Am. Chem. Soc.* **1983**, *105*, 5503.
- (5) Geue, R. J.; McDonnell, M. B.; Mau, A. W. H.; Sargeson, A. M.; Willis, A. C. *J. Chem. Soc., Chem. Commun.* **1994**, 667, and references therein.
- (6) Lay, P. A. Ph.D. Thesis, Australian National University, 1981, Chapter 5.
- (7) Boucher, H. A.; Lawrance, G. A.; Lay, P. A.; Sargeson, A. M.; Bond, A. M.; Sangster, J. C.; Sullivan, J. C. *J. Am. Chem. Soc.* **1983**, *105*, 4562.
- (8) Pandey, K. K. *Coordination Chemistry Reviews* **1992**, *121*, 1, and references therein.
- (9) Cotton, F. A.; G. Wilkinson *Advanced Inorganic Chemistry*; 5th ed.; John Wiley and Sons: New York, 1988, Chapter 19.
- (10) Roundhill, D. M. *Comprehensive Coordination Chemistry*; Pergamon Press: 1987, and references therein; Vol. 5.
- (11) Woollins, J. D.; Kelly, P. F. *Coord. Chem. Rev.* **1985**, *65*, 115, and references therein.
- (12) Ginzburg, S. I.; Ezerskaya, N. A.; Prokof'eva, I. V.; Fedorenko, N. V.; Shlenskaya, V. I.; Bel'skii, N. K. In *Analytic Chemistry of Platinum Metals*; P. Schelnitz, Ed.; John Wiley and Sons: New York, 1975.
- (13) Appleton, T. G.; Hall, J. R.; Neale, D. W.; Ralph, S. R. *Inorg. Chim. Acta.* **1983**, *77*, 191.
- (14) Conder, H. L.; Cotton, F. A.; Falvello, L. R.; Han, S.; Walton, R. A. *Inorg. Chem.* **1983**, *22*, 1887.
- (15) Cotton, F. A.; Falvello, L. R.; Han, S. *Inorg. Chem.* **1982**, *21*, 1709.

- (16) Baxter, L. A. M.; Heath, G. A.; Raptis, R. G.; Willis, A. C. *J. Am. Chem. Soc.* **1992**, *114*, 6944, and references therein.
- (17) Cini, R.; Fanizzi, F. P.; Intini, F.; Natile, G. *J. Am. Chem. Soc.* **1991**, *113*, 7804.
- (18) Bancroft, D. P.; Cotton, F. A.; Falvello, L. A.; Han, S.; Schwotzer, W. *Inorg. Chim. Acta* **1984**, *87*, 147.
- (19) Alexander, K. A.; Bryan, S. A.; Fronczek, F. R.; Fultz, W. C.; Rheingold, A. L.; Roundhill, D. M.; Stein, P.; Watkins, S. F. *Inorg. Chem.* **1985**, *24*, 2803.
- (20) Hollis, L. S.; Roberts, M. M.; Lippard, S. J. *Inorg. Chem.* **1983**, *22*, 3637.
- (21) Peterson, E. S.; Bancroft, D. P.; Min, D.; Cotton, F. A.; Abbott, E. H. *Inorg. Chem.* **1990**, *29*, 229, and references therein.
- (22) Schöllhorn, H.; Eisenmann, P.; Thewalt, U.; Lippert, B. *Inorg. Chem.* **1985**, *25*, 3384.
- (23) Hartley, F. R. *The Chemistry of Platinum and Palladium*; Applied Science Publishers, Ltd.: London, 1973, and references therein.
- (24) Endres, H.; Keller, H. J.; van der Sand, H.; Dong, V. Z. *Naturforsch* **1978**, *33b*, 843, and references therein.
- (25) Kirms, R.; Dietzsch, W.; Solov'ev, B. V. *J. Inorg. Nucl. Chem* **1977**, *39*, 1157.
- (26) Forbes, C. E.; Gold, A.; Holm, R. H. *Inorg. Chem.* **1971**, *10*, 2479.
- (27) Larin, G. M.; Zvereva, G. A.; Shchelokov, R. N. *Koord. Khim.* **1979**, *3*, 148.
- (28) Blake, A. J.; Gould, R. O.; Holder, A. J.; Hyde, T. I.; Lavery, A. J.; Odulate, M. O.; Schröder, M. *J. Chem. Soc., Chem. Commun.* **1987**, 119.
- (29) Schröder, M. *Pure and Appl. Chem.* **1988**, *60*, 517, and references therein.
- (30) Usón, R.; Forniés, J.; Tomás, M.; Menjón, B.; Sünkel, K.; Bau, R. *J. Chem. Soc. Chem. Commun.* **1984**, 751, and references therein.
- (31) Fortier, D.; McAuley, A.; Subramanian, S.; Whitcombe, T. W. In *International Congree of Pure and Applied Chemistry*; Manchester, U.K., September 1985.

- (32) McAuley, A.; Whitcombe, T. W. *Inorg. Chem.* **1988**, *27*, 3090, and references therein.
- (33) Blake, A. J.; Gordon, L. M.; Holder, A. J.; Hyde, T. I.; Reid, G.; Schröder, M. *J. Chem. Soc., Chem. Commun.* **1988**, 1452, and references therein.
- (34) Blake, A. J.; Schröder, M. *Advances in Inorganic Chemistry* **1990**, *35*, 1, and references therein.
- (35) Blake, A. J.; Holder, A. J.; Hyde, T. I.; Roberts, Y. V.; Lavery, A. J.; Schröder, M. *J. Organomet. Chem.* **1987**, *323*, 261, and references therein.
- (36) Blake, A. J.; Holder, A. J.; Hyde, T. I.; Schröder, M. *J. Chem. Soc., Chem. Commun.* **1987**, 987.
- (37) Chadhuri, P.; Wieghardt, K. *Prog. Inorg. Chem.* **1987**, *35*, 329.
- (38) Hunter, G.; McAuley, A.; Whitcombe, T. W. *Inorg. Chem.* **1988**, *27*, 2634, and references therein.
- (39) Wieghardt, K.; Köppen, M.; Swiridoff, W.; Weiss, J. *J. Chem. Soc. Dalton Trans.* **1983**, 1869.
- (40) Boucher, H. A.; Sargeson, A. M., Unpublished observations.
- (41) Wopschall, R. H.; Shain, I. *Anal. Chem.* **1967**, *39*, 1514, and references therein.
- (42) Bard, A. J.; Faulkner, L. R. *Electrochemical Methods, Fundamentals and Applications*; John Wiley and Sons: New York, 1980; Chapter 12, and references therein.
- (43) M. H. Jensen M.Sc. Thesis, The Technical University of Denmark, Lyngby, Denmark, 1992.
- (44) Bernhardt, P. V.; Lawrance, G. A.; Patalinghug, W. C.; Skelton, B. W.; White, A. H.; Curtis, N. F.; Siriwardena, A. *J. Chem. Soc., Dalton Trans.* **1990**, 2853. A typographical error was noted in this paper for the reduction potential of the $[\text{Pt}(\textit{trans}\text{-diammac})]^{4+/2+}$ couple. The correct values for the peak potentials are $E_{\text{pa}} = +0.32$ and $E_{\text{pc}} = +0.1$ V (vs NHE), therefore the peak to peak separation is $\Delta E_{\text{p}} = 210$ mV (P.V. Bernhardt, personal communication), not 50 mV, as described in the paper.
- (45) Lai, C-N.; Hubbard, A. T. *Inorg. Chem.* **1972**, *11*, 2081.

- (46) Wakine, D.; Heeg, M. J.; Endicott, J. F.; Ochrymowycz, L. A. *Inorg. Chem.* **1991**, *30*, 3691, and references therein.
- (47) Bond, A. M., Personal Communication **1994**.
- (48) Spiccia, L., Unpublished observations.

Chapter 5

Synthesis and Properties of Cobalt(III) Cage Complexes

5.1. Introduction

5.1.1. General

The encapsulation of metal ions with cage ligands, such as sar, has provided insight into the reactivity, redox chemistry, electron transfer and spectral behaviour of a range of metal ion complexes.^{1,2} By altering structural features of the cage ligand, namely the donor atoms, peripheral substituents on the ligand and the cavity size, the properties of the metal ion may be altered in a profound manner. These effects have been detailed in Chapter 1. The effect of altering the M-N bond length on the cage properties, however, has received only minor attention. Only two types of relatively symmetric cages have been isolated which have atypical M-N bond lengths, namely N_6 -tricosane^{3,4} and absar^{5,6} cages. It is also of interest to assess the effect of rigidity on the behaviour of the encapsulated metal ions. In this chapter, the effects both of expanding the cage and increasing the ligand rigidity on properties of the $\text{CoN}_6^{3+/2+}$ cage chromophore are addressed.

5.1.2. Overview of $[\text{Co}(\text{Me}_5\text{-}N_6\text{-tricosane})]^{3+}$

The most obvious way to vary the ligand size is to modify the number of atoms in the ligand skeleton. Relevant examples include sartacn⁷ and N_6 -tricosane^{3,4} (Fig. 5.1). In the first instance, the change is associated with the tacn cap and in the second example, an additional carbon atom is incorporated in the straps connecting the tame caps. This work deals with complexes related to the latter type.

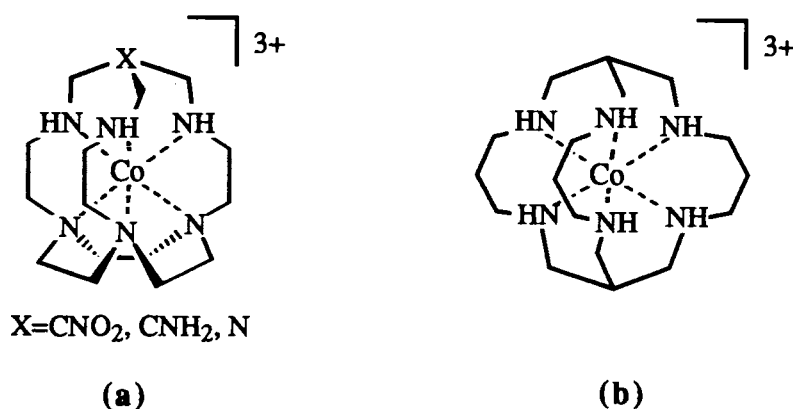


Figure 5.1: (a) $[\text{M}(\text{sartacn})]^{n+}$ and (b) $[\text{M}(N_6\text{-tricosane})]^{n+}$.

The $\text{Me}_5\text{-}N_6\text{-tricosane}$ cage has recently demonstrated how the spectral, redox and electron transfer properties of the $\text{Co}(\text{III})$ ion have been altered compared to the smaller sar analogues.

(a) Spectral Properties

The ligand field bands arising from the ${}^1A_{1g}(O_h) \rightarrow {}^1T_{1g}$ and ${}^1T_{2g}$ transitions for $[Co(Me_5-N_6\text{-tricosane})]^{3+}$ are red shifted by 30–40 nm⁴ compared to those of the sar analogues.⁸ The weaker ligand field for $[Co(Me_5-N_6\text{-tricosane})]^{3+}$ is attributed to the decreased orbital overlap arising from its longer Co(III)-N distance. The average Co(III)-N bond lengths for $[Co(Me_5-N_6\text{-tricosane})]^{3+}$ and $[Co(sep)]^{3+}$ are 2.022(4) Å⁴ and 1.981(2) Å,⁹ respectively. The trigonal distortion about the CoN_6^{3+} core is not likely to contribute to the decrease in orbital overlap as the twist angles about the CoN_6^{3+} core are about the same for both types of complexes (the twist angles about the CoN_6^{3+} core for $[Co(Me_5-N_6\text{-tricosane})]^{3+}$ and $[Co(sep)]^{3+}$ are $66 \pm 0.5^\circ$ ⁴ and 55° ,⁸ respectively, compared to the octahedral value of 60°).

(b) Redox Properties

The reduction potential for the $[Co(Me_5-N_6\text{-tricosane})]^{3+/2+}$ couple ($E_{1/2} = 0.08$ V vs NHE)⁴ is 0.56 V more positive than that for $[Co(Me_2\text{-sar})]^{3+/2+}$,¹⁰ implying that the ligand cavity in the former complex stabilises the larger Co(II) ion better than can the sar system. Molecular mechanics studies for saturated $CoN_6^{3+/2+}$ systems have indicated that the difference in the strain energy between the two members of the redox couple is an important component of the free energy change upon reduction.^{11,12} In the $[Co(Me_5-N_6\text{-tricosane})]^{3+/2+}$ system, the Co(III)-N bond length is longer than optimal and this would destabilise the Co(III) state relative to its Co(II) state. The release of strain energy during reduction to Co(II) is expected to be larger for the $N_6\text{-tricosane}$ system than for the sar system and this would provide a larger driving force for the reduction. This is manifested in the large positive shift in the reduction potential for the $[Co(Me_5-N_6\text{-tricosane})]^{3+/2+}$ couple relative that of the analogous sar cage.

(c) Electron Transfer Rates

The encapsulation of metal ions with the sar and $N_6\text{-tricosane}$ cages dramatically increases the self exchange rate constants (k_{ex}), relative to acyclic saturated $CoN_6^{3+/2+}$ couples. The electron transfer rates for both sar and $N_6\text{-tricosane}$ Co(III)/Co(II) couples are $\sim 10^5$ times greater than for nonencapsulated analogues (e.g., $k_{ex} = 5 \times 10^{-5} \text{ M}^{-1}\text{s}^{-1}$ for $[Co(en)_3]^{3+/2+}$).^{13,14} A current hypothesis ascribes the fast electron transfer of the cages to the increased strain in their ground states for both members of the redox couple. The reorganisation energy required to overcome the activation barrier is less for the encapsulated than for nonencapsulated complexes.¹⁵ Preliminary studies have indicated that the effect of expanding the cage framework appears to be relatively small compared to the effect of encapsulation, as there is little difference in the self exchange rate constants between the sar and the $[Co(Me_5-N_6\text{-tricosane})]^{3+/2+}$ systems (respectively,

$k_{\text{ex}} \sim 2.1 \text{ M}^{-1}\text{s}^{-1}$ ¹⁴ and $0.40 \text{ M}^{-1}\text{s}^{-1}$ ⁴). However, further examination of a wider range of cage complexes with different frameworks and Co-N bond lengths is necessary to sustain the strain argument.

5.1.3. Effect of Ligand Rigidity

(a) $[M(\text{sar})]^{n+}$ Cage Complexes

Subtle changes in the cavity size may also be achieved by altering the conformation of the cage complexes;¹⁶⁻²⁰ for example, by twisting the orientation of the caps from C_3 to D_3 symmetry, the latter complex has a slightly more constricted cavity.^{16,17} Another mechanism involves changes in the alignment of the C-C bonds derived from the ethylenediamine straps. These may be *parallel* (Fig. 5.2(a)) or *oblique* (Fig. 5.2(b)) to the C_3 axis, giving rise to the *lel* or *ob* conformers, respectively.

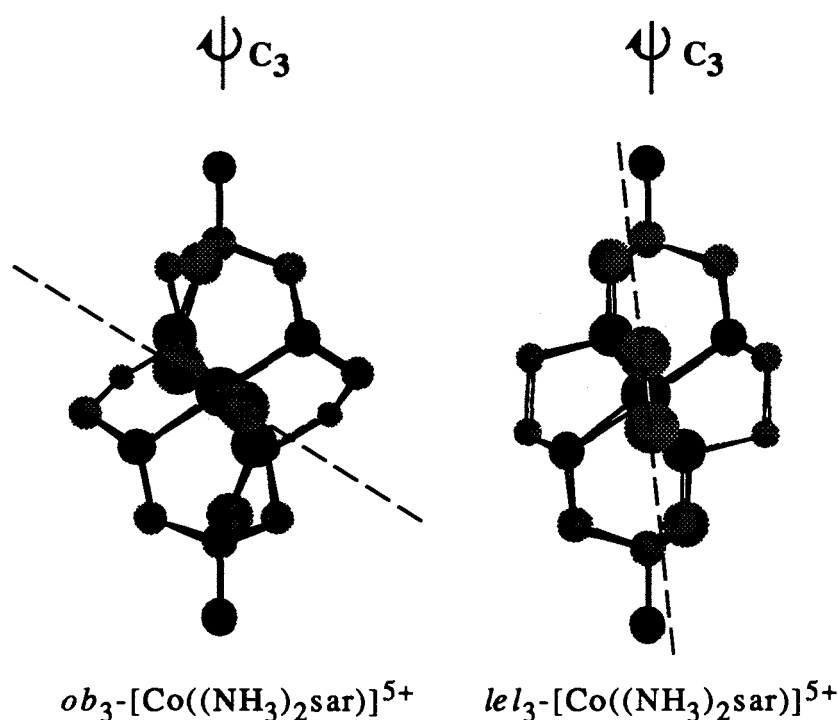


Figure 5.2: (a) *lel*₃ and (b) *ob*₃- $[\text{Co}(\text{NH}_3)_2\text{sar}]^{5+}$

Measurements of physical properties, such as electron transfer rates, may depend on the distribution of conformers present, each of which may have subtly differing electronic properties.²¹ Current evaluation indicates that the bulk of the Co(III) sar complexes are *lel*₃ in aqueous solution and that interconversion between the *lel*₃ and *ob*₃ isomers is fast at 298 K.^{8,12,18} However, addition of substituents on the ethylenediamine residues can stabilise either the *ob*₃ or *lel*₃ conformations, as exemplified in *fac*- $[\text{Co}(\text{NH}_2)_2\text{Me}_3\text{sar}]^{3+}$ (Fig. 5.3). Interconversion of *lel*₃- $[\text{Co}(\text{NH}_2)_2\text{Me}_3\text{sar}]^{3+}$ and *ob*₃- $[\text{Co}(\text{NH}_2)_2\text{Me}_3\text{sar}]^{3+}$ is not observed at 298 K.¹⁶ The different properties of the two species are also revealed in their spectroscopy and

electrochemistry. A comparison of the absorption spectra of *fac*- $lel_3[Co((NH_2)_2Me_3sar)]^{3+}$ with the *ob*₃ analogue shows that the *lel*₃ complex has a weaker ligand field, a higher molar absorption coefficient and has a more positive Co(III)/Co(II) reduction potential than its *ob*₃ isomer.^{16,17,20} On these grounds, it has been postulated that the *lel*₃ isomer has slightly longer Co-N bond lengths than the *ob*₃ isomer.^{16,17}

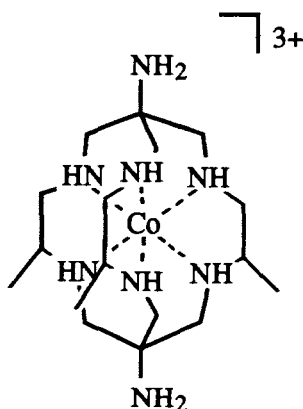


Figure 5.3: *fac*- $[Co((NH_2)_2Me_3sar)]^{3+}$

(b) $[M(N_6\text{-tricosane})]^{n+}$ Complexes

Recent studies indicate that $[M(Me_5\text{-}N_6\text{-tricosane})]^{n+}$ complexes are less able to undergo conformational changes. Molecular mechanics calculations of the Co(III), Cr(III) and Zn(II) complexes predict four conformational minima.²² These conformational minima all have C_3 symmetry, the absolute configurations about all six nitrogen donors are the same and all six-membered chelate straps have a flattened chair conformation.²² The lowest energy conformation (with a twist angle of 66.5) is significantly more stable than the others for a range of M-N bond distances between 1.9–2.35 Å.²² This configuration has been observed in the crystal structures of the smaller ions, viz: Cr(III), Co(III) and Zn(II).²³ A fifth isomer with trigonal prismatic geometry has also been predicted, where the configurations about the nitrogen donors in the two tame caps are catoptric. This configuration has only been observed for larger ions, such as Cd(II) and Hg(II).²³ Conformational changes associated with three six-membered chelate rings of the straps (from chair to skew boat) are not very likely for any of these complexes, as the methyl substituents prefer to occupy the equatorial position of the six-membered chelate ring. Other conformers associated with the six-membered chelate ring, namely the skew boat, are much more strained. In contrast, unsubstituted $[M(Me_2\text{-}N_6\text{-tricosane})]^{n+}$ complexes are expected to be more flexible in this respect. However, only the Rh(III) complex of this ligand been isolated³ and it has the same conformation observed with the Cr(III), Co(III) and Zn(II) complexes. Other

examples where ligand rigidity may affect electron transfer and spectral properties include those of the considerably more rigid $[M(N_6\text{-tetracosane})]^{n+}$ type.

5.1.4. Synthetic Strategies for Expanded Cavity Cages

The synthetic routes for cage complexes with longer Co-N bond lengths were addressed in Chapter 1. These complexes were essentially $[\text{Co}(\text{Me}_x\text{-}N_6\text{-tricosanetriimine})]^{3+}$ ($x=5,8$) and their saturated analogues $[\text{Co}(\text{Me}_x\text{-}N_6\text{-tricosane})]^{n+}$ ($x=5, n=3$; $x=8, n=2$). Briefly, the triimine complexes were synthesised using $[\text{Co}(\text{tame})_2]^{3+}$ as a template to direct a series of base catalysed condensation reactions with paraformaldehyde and either propanal (for $x=5$) or 2-methylpropanal (for $x=8$). Reduction of the imines with BH_4^- yielded the saturated ligand complexes. Interestingly, when this methodology was extended to the $[\text{Pt}(\text{tame})_2]^{4+}$ template, a number of new cage complexes were synthesised, where six aldehyde molecules had condensed to form $[\text{Pt}(\text{R}_2, \text{R}'_6\text{-}N_6\text{-tetracosanediimine})]^{4+}$ (Fig. 5.4, where $\text{R} = \text{Et}$, $\text{R}' = \text{Me}$ or $\text{R} = \text{Me}$, $\text{R}' = \text{H}$). These were discussed extensively in Chapter 3. It was not possible to reduce the imines while retaining the integrity of the Pt(IV) cage. It was anticipated that if the analogous $[\text{Co}(N_6\text{-tetracosanediimine})]^{3+}$ complexes could be similarly synthesised, then selective reduction of the imines would give the saturated $[\text{Co}(N_6\text{-tetracosane})]^{3+}$ analogues. Furthermore, there is a possibility of isolating two cages from the acetaldehyde reactions, $[\text{Co}(\text{Me}_4\text{-}N_6\text{-tetracosanediimine})]^{3+}$ and $[\text{Co}(\beta\text{Me}_5\text{-}N_6\text{-tricosanetriimine})]^{3+}$, with C_i and C_3 symmetry, respectively. In this chapter, the template synthesis of $[\text{Co}(\text{Et}_2\text{-Me}_6\text{-}N_6\text{-tetracosanediimine})]^{3+}$, $[\text{Co}(\text{Me}_4\text{-}N_6\text{-tetracosanediimine})]^{3+}$ and $[\text{Co}(\beta\text{Me}_5\text{-}N_6\text{-tricosanetriimine})]^{3+}$ will be addressed.

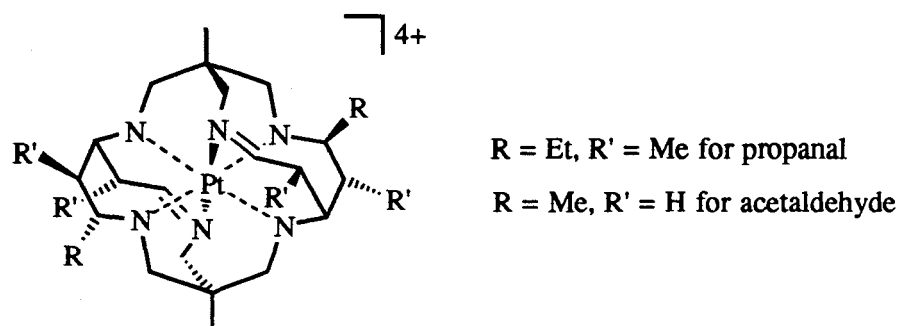


Figure 5.4: $[\text{Pt}(\text{R}_2, \text{R}'_6\text{-}N_6\text{-tetracosanediimine})]^{4+}$ (amine protons have been omitted for clarity).

5.1.5. New Scope for Cage Chemistry

The synthesis of expanded cavity cages leads to the possibility of encapsulating larger metal ions which are otherwise too large for the sar ligands. For example, the synthesis of $[\text{Pb}(\text{Me}_5\text{-}N_6\text{-tricosane})]^{2+}$ has been achieved,²³ whereas the insertion of Pb(II) into the sar cages has not been achieved. Similarly, the larger Cu(I) ion is tolerated in the (Me₅-N₆-tricosane) ligand, as demonstrated by the reversible $[\text{Cu}(\text{Me}_5\text{-}N_6\text{-tricosane})]^{2+/1+}$ couple.²³ In contrast, the $[\text{Cu}(\text{sar})]^{2+/1+}$ couple is irreversible and the Cu(I) ion is rapidly extruded from the sar ligand on the millisecond timescale.²⁴ The N₆-tetracosane cages proposed here may also stabilise larger ions and hinder ligand dissociation by virtue of their cross straps. It is anticipated that free N₆-tetracosane cage ligands could be obtained by extrusion of Co(II) ion from the cage complex in analogy to the synthesis of the free sar and Me₅-N₆-tricosane ligands.^{25,26} The free N₆-tetracosane ligand could then be used to encapsulate other metal ions and their chemistry investigated.

5.2. Experimental

5.2.1. Synthesis

(a) (19,23-diethyl-1,5,9,13,20,24-hexamethyl-3,7,11,15,18,22-hexaazatricyclo[10.4.4.4⁴⁻⁹]tetracos-3,11-diene)cobalt(III) trichloride
 ([Co(Et₂-Me₆-N₆-tetracosanediimine)]Cl₃)

[Co(tame)₂]Cl₃ (5.01 g) was added to a suspension of anhydrous NaClO₄ (15 g) in acetonitrile (100 mL). Propanal (10 equivalents, 9.3 mL) was added to this suspension, followed by triethylamine (5 equivalents, 8.9 mL). Within five minutes of addition of the triethylamine, the reaction mixture changed from orange to rainforest green (in the absence of NaClO₄, the colour change of the reaction took over 30 minutes). The reaction was quenched after two hours with concentrated hydrochloric acid (~10 mL) to form an apricot coloured suspension. This suspension was diluted to 1 L with distilled water to form an orange solution and sorbed on a (5 x 20 cm) column of Dowex 50W-X2 cation exchange resin, which was then washed with water (500 mL) and 1 M HCl (1 L). The complex was eluted with 4 M HCl. The eluate was evaporated to dryness, redissolved in water (1 L) and the solution was then loaded onto a (10 x 120 cm) column of SP-Sephadex cation exchange resin. The resin was washed with water (750 mL) and the complexes were eluted with acidified K₂SO₄ (0.2 M, pH~2.5, using H₂SO₄). Three bands were separated. The first was a fast moving red band which was not identified since after desalting, it gave a broad, featureless ¹H NMR spectrum. The second band (bright orange) was sorbed onto a (10 x 5 cm) column of Dowex (50W-X2) cation exchange resin which was washed with water (1 L), 1 M HCl (1 L) and the complex eluted with 4 M HCl (1 L). The 4 M HCl band was evaporated to near dryness to give an orange suspension. The suspension was filtered and the residue was washed with a minimum of iced water to give the partially encapsulated complex, [(12,19-diethyl-1,5,9,13,20-pentamethyl-3,7,11,15,18,22-hexaazabicyclo[10.4.4]docosa-3,14-diene)cobalt(III)] trichloride ([Co(Et₂-Me₅-N₆-docosanediimine)]Cl₃). The third band from the SP-Sephadex resin (apricot orange) was sorbed onto a (10 x 5 cm) column of Dowex (50W-X2) cation exchange resin which was washed with water (1 L), 1 M HCl (1 L) and the complex eluted with 4 M HCl (1 L). The 4 M HCl band was evaporated to near dryness to yield an apricot suspension. After filtering and washing with iced water, [Co(Et₂-Me₆-N₆-tetracosanediimine)]Cl₃ was isolated. Crystals of the chloride salt suitable for an X-ray crystallographic analysis were grown from a saturated solution (4-5 mg in 0.5 mL in D₂O). The [Co(Et₂-Me₅-N₆-docosanediimine)]³⁺ isolated from the second band was converted to [Co(Et₂-Me₆-N₆-tetracosanediimine)]³⁺ when treated with additional propanal (10 equivalents) and triethylamine (3 equivalents) in acetonitrile and anhydrous NaClO₄. Yield [Co(Et₂-Me₅-

N_6 -docosanediiimine)]Cl₃: 26 %. Anal. Calc. for [C₂₅H₅₀Cl₃CoN₆].2H₂O: C, 47.21; H, 8.56; N, 13.21. Found: C, 47.44; H, 8.62; N, 12.62. Yield [Co(Et₂-Me₆-N₆-tetracosanediiimine)]Cl₃.5H₂O: 30% . Anal. Calc. for [C₂₈H₅₄Cl₃CoN₆].5H₂O: C, 46.06; H, 8.84; N, 11.51; Cl, 14.57. Found: C, 46.15; H, 9.32; N, 11.30; Cl, 14.97.

NMR [Co(Et₂-Me₅-N₆-docosanediiimine)]Cl₃; (δ (ppm), D₂O): ¹H: 0.85 (t, 3H), 0.94 (s, 3H), 0.97 (t, 3H, overlaps with signal at 1.02 (s, 3H)), 1.06 (d, 3H, ³J_{H-H}= 9 Hz), 1.36 (d, 1H, ²J_{H-H}= 6. Hz), 1.48 (d, 1H, ²J_{H-H}= 6 Hz), 1.54-1.75 (m, 1H), 1.75-1.94 (m, 1H), 2.12-2.08 (two overlapping m's, 2H), 2.25 (broad d, 1H), 2.30-2.43 (m, 1H), 3.47 (d, 1H, ²J_{H-H}= 14 Hz), 2.50, 2.55 (two overlapping d's, 2H, ²J_{H-H}= 13 Hz), 2.08-2.20 (m, 2H), 3.18-3.12 (m, 1H), 3.28 (d, 1H, ²J_{H-H}= 13 Hz), 3.54 (d, 1H, ²J_{H-H}= 13 Hz), 3.60-3.61 (m, 2H), 3.90 (d, 1H, ²J_{H-H}= 12 Hz), 4.13 (d, 1H, ²J_{H-H}= 13 Hz), 8.04 (s, 1H), 8.29 (s, 1H).

¹³C: 12.0, 12.5, 15.5, 16.0, 20.9, 21.6, 21.8, 23.4, 23.5, 33.8, 37.1, 37.9, 38.5, 38.8, 44.4, 48.8, 50.2, 52.1, 60.1, 63.5, 65.1, 66.5, 67.6, 190.0 (imine), 194.5 (imine).

NMR [Co(Et₂-Me₆-N₆-tetracosanediiimine)]Cl₃; (δ (ppm), D₂O): ¹H: 0.97 (t, 3H, H₈) 1.09 (s, 3H, H₁), 1.16 (d, 3H, H₁₀), 1.52 (d, 3H, H₁₃), 1.67 (multiplet, 1H, H_{7a}), 1.87 (2 overlapping multiplets, 2H, H_{7a} and H₉), 2.27 (d, 1H, H_{5a}), 2.41 (d, 1H, H_{5b}), 2.54 (broad s, 1H, H₁₁), 2.67 (d, 1H, H_{3a}), 2.85 (multiplet, 1H, H₆), 3.24 (d, 1H, H_{3b}, partially overlapped by H_{4a}), 3.29 (d, 1H, H_{4a}), 3.80 (multiplet, 1H, H₁₂), 4.67 (d, 1H, H_{4b}), 8.04 (s, 1H, H₁₄).

¹³C: 13.7 (C₈); 15.3 (C₁₃); 20.3 (C₁₀); 21.6 (C₁); 24.8 (C₇); 33.6 (C₉); 37.4 (C₂); 38.4 (C₁₂); 48.9 (C₅); 53.4 (C₃); 61.8 (C₆); 62.6 (C₁₁); 65.4 (C₄); 193.4 (C₁₄).

²J_{H-H} (Hz): ²J_{3a-3b}= 13.1; ²J_{4a4b}= 13.5; ²J_{5a-5b}= 13.7; ²J_{7a-7b}= 14.2. ³J_{H-H} (Hz): ³J_{6-7a}= 7.9; ³J_{6-7b}= 2.5; ³J_{7a,b-8}= 7.1 ; ³J₆₋₉= 7.9; ³J₉₋₁₀= 6.9; ³J₉₋₁₁= 2.7; ³J₁₁₋₁₂= 2.5; ³J₁₂₋₁₃= 7.9; ³J₁₃₋₁₄= 2.8. ⁴J_{H-H} (Hz): ⁴J_{3a-5b}= 2.8; ⁴J_{4b-5a}= 2.8; ⁴J_{4a-14}= 2.9; ⁴J_{4a-14}= 5.8. ⁵J_{H-H} (Hz): ⁵J_{4a-12}= 5.4.

Electronic Spectra [Co(Et₂-Me₆-N₆-tetracosanediiimine)]Cl₃; (water, pH~5.5):

λ_{\max} (nm)=480 (ϵ , 110 M⁻¹cm⁻¹), 239 (ϵ , 17,300 M⁻¹cm⁻¹).

(~0.01 M NaOH, pH~11.5): λ_{\max} (nm)=618 (ϵ , 299 M⁻¹cm⁻¹), 420 (ϵ , 330 M⁻¹cm⁻¹), 342 (ϵ , 513 M⁻¹cm⁻¹), 230 (ϵ , 6,740 M⁻¹cm⁻¹), 202 (ϵ , 6,320 M⁻¹cm⁻¹).

Reduction Potential [Co(Et₂-Me₆-N₆-tetracosanediiimine)]^{3+/2+} (V vs SCE, (ΔE_p (mV)) 0.2 M NaCl, glassy carbon): -0.441 V (65) at 100 mV s⁻¹ and -0.440 V (86) at 15,000 mV s⁻¹.

(b) (6,14-diethyl-1,5,9,13,20,23-hexamethyl-3,7,11,15,18,22-hexaazatricyclo [10.4.4.4⁴⁻⁹]tetracosane)cobalt(III) trichloride tetrahydrate
 ([Co(Et₂-Me₆-N₆-tetracosane)]Cl₃.4H₂O)

[Co(Et₂-Me₆-N₆-tetracosanediimine)]Cl₃ (6.4 g) was dissolved in water (100 mL) and the pH of the solution adjusted to ~10 (Na₂CO₃), to yield a rainforest green solution. This solution was treated with excess NaBH₄ (1.5 g) and the reaction was stirred for 3 hours. The reaction mixture was loaded on a (5 x 20 cm) column of Dowex (50W-X2) cation exchange resin, in the sodium form.[§] The resin was washed with water (1 L) and the complex was left on the resin for 24 hours to ensure that any Co(II) species that formed during the BH₄⁻ treatment was oxidised to Co(III). The resin was washed with 1 M HCl (500 mL) and 4 M HCl. This 4 M HCl band was evaporated to dryness, redissolved in water and loaded on a (100 x 10 cm) column of SP-Sephadex cation exchange resin. The resin was washed with water (500 mL) and the complex eluted with (0.2 M) Na₂-(+)-tartrate. Three bands eluted in the following order: a narrow yellow band, which eluted rapidly and was discarded; a purple band and a pink band. The purple band was sorbed onto a (10 x 5 cm) column of Dowex (50W-X2) cation exchange resin which was washed with water (1 L), 1 M HCl (1 L) and 4 M HCl (1 L). The 4 M HCl band was evaporated to near dryness to yield a purple oil, whose ¹H NMR spectrum was very complicated and the product was therefore not identified. The eluate from the pink band was sorbed onto a (10 x 5 cm) column of Dowex (50W-X2) cation exchange resin which was washed with water (1 L), 1 M HCl (1 L) and the complex was eluted with 4 M HCl (~700 mL). The 4 M HCl band was evaporated to near dryness and dark pink crystals were obtained which were filtered and washed with iced water. The crystals were recrystallised from hot water to give [Co(Et₂-Me₆-N₆-tetracosane)]Cl₃.4H₂O. Yield: ~ 54%, based on [Co(tame)₂]Cl₃. Anal. Calc. for [C₂₈H₅₈Cl₃CoN₆].4H₂O: C, 46.96; H, 9.29; N, 11.73; Cl, 14.85. Found: C, 46.57; H, 9.49 N, 11.35; Cl, 14.95.

NMR [Co(Et₂-Me₆-N₆-tetracosane)]Cl₃; (δ (ppm), D₂O): ¹H: 0.97 (d, 3H, cross strap CH₃, H₁₃), 1.00 (s, 3H, cap CH₃, H₁), 1.08 (t, 3H, ethyl CH₃, H₈), 1.19 (d, 3H, strap CH₃, H₁₀), 1.79-1.88 (multiplet, 1H, ethyl CH₂, H_{7a}), 1.99-2.03 (overlapping multiplet and d, 2H, ethyl CH₂, H_{7b}, and cap CH₂, H_{4a}, centred at 2.03), 2.19-2.24 (multiplet, 1H, strap CH, H₉), 2.39 (overlapping broad s and two d's, combined 3H, strap CH, H₁₁, 2 x cap CH₂'s, H_{5a} and H_{3a} both centred at ~2.37), 2.44 (broad d, 1H,

[§] it was anticipated that acid assisted extrusion of the Co(II) from the cage would occur, but this was not observed. In hindsight, the use of Na⁺ form of the Dowex cation exchange resin is probably not necessary.

cross strap CH, H₁₂), 2.52 (overlapping d of d's, 2H, cross strap CH₂, H_{14a,b}), 2.74, (d, 1H, cap CH₂, H_{3b}), 2.82-2.86 (multiplet, 1H, strap CH, H₆), 3.25 (d, 1H, cap CH₂, H_{5b}), 3.65 (d, 1H, cap CH₂, H_{4b}).

¹³C: 13.2 (C₈), 15.9 (C₁₃), 21.2 (C₁₀), 22.2 (C₁), 26.0 (C₇), 29.7 (C₁₁), 31.1 (C₁₂), 38.1 (C₂), 48.2 (C₃), 53.0 (C₅), 56.5 (C₄), 56.7 (C₁₄), 60.4 (C₆), 62.9 (C₉).

²J_{H-H} (Hz): ²J_{3a-3b}= 13.4; ²J_{4a-4b}= 14.8; ²J_{5a-5b}= 12.5; ²J_{7a-7b}= 13.6; ²J_{14a-14b}= 13.9. ³J_{H-H} (Hz): ³J_{6-7a}= 6.3; ³J_{6-7b}= 2.6; ³J_{7a,b-8}= 7.4; ³J₆₋₉= 11.6; ³J₉₋₁₀= 6.8; ³J₉₋₁₁= 3.7; ³J₁₁₋₁₂=not observed; ³J₁₂₋₁₃= 6.1; ³J_{13-14a}= 5.8; ³J_{13-14b}=not observed. ⁴J_{H-H} (Hz): ⁴J_{4a-5b}= 4.9; ⁴J_{4b-5a}= 4.4.

Electronic Spectrum [Co(Et₂-Me₆-N₆-tetracosane)]Cl₃; (water, pH~5.5):
λ_{max}=498 nm (ε, 147 M⁻¹cm⁻¹), 258 nm (ε, 37,200 M⁻¹cm⁻¹).

Reduction Potential [Co(Et₂-Me₆-N₆-tetracosane)]^{3+/2+} (V vs SCE, ΔE_p (mV), 0.2 M NaCl, glassy carbon): -0.474 V (69), at 100 mV s⁻¹ and -0.488 V (91) at 15,000 mV s⁻¹.

(c) *Attempted Extrusion of the Cobalt Ion from [Co(Et₂-Me₆-N₆-tetracosane)]Cl₃*

I. Reduction using Zinc in Hydrochloric Acid

[Co(Et₂-Me₆-N₆-tetracosane)]Cl₃ (50 mg) was suspended in water (25 mL) and the solution was heated to 90° C to dissolve the complex. An equivalent volume of 6 M HCl (~25 mL) was slowly added. The solution was purged with nitrogen for 30 minutes and after which zinc dust (~500 mg) was slowly added. The solution became colourless after heating the solution for ~20 minutes, indicating that the Co(III) complex had been reduced to Co(II). The solution was heated under nitrogen and aliquots of acid (6 M HCl, ~5 mL) were added after one and two hours. After 4 hours, acid was again added to reduce the pH to <1. A colourless precipitate resulted and after filtration in air, slowly became pink. The ¹H NMR spectrum of the pink compound indicated that it was [Co(Et₂-Me₆-N₆-tetracosane)]Cl₃.

II. Reduction using Zinc and Sodium Sulfide in Base

[Co(Et₂-Me₆-N₆-tetracosane)]Cl₃ (10 mg) was suspended in water (5 mL) and the solution was heated to 90° C in order to dissolve the complex. The solution was basified with Na₂CO₃ to pH~11, to afford a dark green solution. The solution was purged with nitrogen for 10 minutes after which an excess of zinc dust (~50 mg) was added. The solution turned colourless, indicating that [Co(Et₂-Me₆-N₆-tetracosane)]²⁺ had formed. Na₂S (~10 mg) was then added to the solution. The solution remained

colourless, even after heating for one hour under a nitrogen blanket. (The black CoS precipitate would have formed had extrusion been successful). When the reaction mixture was exposed to air, the solution again became green, indicating that the Co(III) ion was still complexed with the cage ligand and after 12 hours, an orange solution was formed. This orange complex has not yet been identified.

(d) Reactions of $[Co(tame)_2]^{3+}$ with Acetaldehyde

$[Co(tame)_2]Cl_3$ (0.89 g) was added to a suspension of anhydrous $NaClO_4$ (2 g) in MeCN (10 mL). Acetaldehyde (40 equivalents, 6.23 mL) and diisopropylethylamine (2 equivalents, 0.97 mL) was added and a deep green colour developed. The reaction was quenched after 30 minutes with concentrated HCl (1 mL). The resulting orange suspension was diluted in water to 500 mL and sorbed onto a (10 x 3 cm) column of Dowex 50W-X2 cation exchange resin. The resin was washed with water (1 L), then 1 M HCl (500 mL) and 4 M HCl (500 mL). The 4 M HCl band was evaporated to dryness to yield a dark orange oil. The orange oil was redissolved in water (~500 mL) and sorbed onto a (3 x 30 cm) column of SP-Sephadex cation exchange resin. The resin was washed with water (1 L) and 0.1 M K_2SO_4 . A broad orange band slowly moved down the column. This band was sorbed on a (3 x 10 cm) column of Dowex 50W-X2 cation exchange resin, which was washed with water (500 mL), then 1 M HCl (1 L) and the complexes eluted with 4 M HCl (500 mL). The 4 M HCl band was evaporated to dryness to yield an orange oil which was then redissolved in a minimum volume of water (~50 mL). The pH of the solution was adjusted to ~10 with Na_2CO_3 , and excess $NaBH_4$ (0.21 g) was added. The reaction was quenched after 15 minutes by sorbing the reaction mixture onto a (3 x 10 cm) column of Dowex (50W-X2) cation exchange resin (Na^+ form). The resin was washed with water (500 mL) and the complex was left on the resin for 24 hours to ensure that any Co(II) species resulting from the treatment with BH_4^- was reoxidised to Co(III). The resin was washed with 1 M HCl (500 mL) and 4 M HCl (500 mL). The 4 M HCl band was evaporated to dryness to yield an orange oil. The oil was dissolved in water and then sorbed onto a (50 x 3 cm) column of SP-Sephadex cation exchange resin. The resin was washed with water (500 mL) and then with (0.1 M) $Na_2(+)$ -tartrate. Two very diffuse orange bands separated and these fractions were desalted on Dowex 50W-X2 cation exchange resin. The 1H NMR spectra of each of these bands were complicated, indicating that many species had been formed.

The above procedure was repeated for $[Co(tame)_2]Cl_3$ (0.27 g) in a solution of anhydrous $NaClO_4$ (1 g) MeCN (5 mL), except that this mixture was cooled to ~275 K prior to addition of diisopropylethylamine (2 equivalents, 3 mL) and acetaldehyde (30 equivalents, 1.41 mL). However, no green colour was observed after 10 minutes. The temperature was raised to about ~283 K after which the green colour developed and more acetaldehyde was added (~15 equivalents, 0.7 mL). The reaction was quenched

with concentrated HCl (1 mL) after 30 minutes to form an orange suspension. The reaction mixture was worked up in a similar manner to that described for the previous reaction. After treatment with NaBH₄ followed by chromatographing on SP-Sephadex cation exchange resin, three diffuse bands were separated. These fractions were desalted on Dowex 50W-X2 cation exchange resin. The ¹H NMR spectra of each of these bands were complicated, indicating that many species had been formed. Attempts to separate further the bands using SP-Sephadex and 0.1 M NaCl and 0.05 M Na₃-citrate eluants were not successful. Attempts to crystallise a solid using the anions ZnCl₄²⁻, ClO₄⁻, CF₃SO₃⁻ and PF₆⁻ were also unsuccessful.

5.2.2. Procedures

The procedures and equipment used for the electrochemical measurements, NMR and absorption spectra, were described in Chapter 2. All measurements were performed using solutions of the chloride salt in aqueous media, unless otherwise specified.

The self exchange rate constant for the [Co(Et₂-Me₆-N₆-tetracosane)]^{3+/2+} couple was determined by Dr P. Osvath via a cross reaction of [Co(Et₂-Me₆-N₆-tetracosane)]²⁺ (0.12 mM, after mixing) with an excess of [Co(azacapten)]³⁺ (2.04 mM, after mixing). The measurements were performed under a pseudo first order excess of [Co(azacapten)]³⁺ at an ionic strength of 0.2 M NaCl and at 298 K. The [Co(Et₂-Me₆-N₆-tetracosane)]²⁺ was generated by reduction of its Co(III) analog with zinc in a strictly inert atmosphere in a disposable glove bag. The absorbance changes were monitored at both λ = 378 and 487 nm as the [Co(Et₂-Me₆-N₆-tetracosane)]²⁺ was oxidised using an Applied Photophysics stopped flow spectrophotometer, Model SF.17 MV, coupled to an Archimedes 410/1 computer. The data was treated using standard algorithms provided by the instrument and all data gave good fits for a single exponential decay.

Molecular mechanics calculations for the [Co(Et₂-Me₆-N₆-tetracosane)]^{3+/2+}, [Co(Me₅-N₆-tricosane)]^{3+/2+}, [Co(*trans*-diammac)]^{3+/2+} and [Co(*cis*-diammac)]^{3+/2+} couples were undertaken by Dr. P.V. Bernhardt. The strain energies were minimised using the program MOMECC-87.²⁷ The contributions due to solvent interactions were not included in the calculations. The force fields used for the Co(III) and Co(II) states for the [Co(Et₂-Me₆-N₆-tetracosane)]^{3+/2+}, [Co(Me₅-N₆-tricosane)]^{3+/2+}, [Co(*trans*-diammac)]^{3+/2+} and [Co(*cis*-diammac)]^{3+/2+} calculations have been defined previously.^{12,27} The reported calculations for the [Co(*trans*-diammac)]^{3+/2+} system¹² were for a different conformation and were recalculated.²²

5.3. Results

5.3.1. Reaction of Propanal with $[\text{Co}(\text{tame})_2]^{3+}$

(a) Synthesis of $[\text{Co}(\text{Et}_2\text{-Me}_6\text{-N}_6\text{-tetracosanediimine})]^{3+}$

Treating $[\text{Co}(\text{tame})_2]^{3+}$ with propanal in basic MeCN in the presence of NaClO_4 produced the partially strapped complex $[\text{Co}(\text{Et}_2\text{-Me}_6\text{-N}_6\text{-docosanediimine})]\text{Cl}_3$ and the fully strapped complex $[\text{Co}(\text{Et}_2\text{-Me}_6\text{-N}_6\text{-tetracosanediimine})]\text{Cl}_3$ in reasonable yields. The initially low yield of the latter cage and the isolation of $[\text{Co}(\text{Et}_2\text{-Me}_6\text{-N}_6\text{-docosanediimine})]\text{Cl}_3$ in about the same yield indicated that the reaction was quenched too early. Further treatment of the partially strapped complex with propanal in MeCN/triethylamine/ NaClO_4 gave the fully encapsulated $[\text{Co}(\text{Et}_2\text{-Me}_6\text{-N}_6\text{-tetracosanediimine})]\text{Cl}_3$, so that its overall yield was ~55%.

The other by-products that had formed during the reaction were not identified. The yield of the by-products was higher than that for the Pt(IV) reaction and additional workup on SP-Sephadex cation exchange resin was essential prior to isolation of the complex. About 45% of the template was not accounted for.

I. Properties of $[\text{Co}(\text{Et}_2\text{-Me}_6\text{-N}_6\text{-tetracosanediimine})]\text{Cl}_3$

This complex is apricot orange in colour but in base ($\text{pH} > 9$) it is green, implying that it was deprotonated under these mildly basic conditions. The orange chloride salt is sparingly soluble in water and is also less soluble than the analogous Pt(IV) complex. This poor solubility influenced the conditions under which the physical measurements were acquired. The perchlorate salt is sparingly soluble in MeCN. The cation is also more stable at pH 5.5 than the analogous Pt(IV) complex; however, in solutions more than a week old, loss of a propanal residue was evident.

II. Crystal Structure of $[\text{Co}(\text{Et}_2\text{-Me}_6\text{-N}_6\text{-tetracosanediimine})]\text{Cl}_3 \cdot 5\text{H}_2\text{O}$

The structure of $[\text{Co}(\text{Et}_2\text{-Me}_6\text{-N}_6\text{-tetracosanediimine})]\text{Cl}_3 \cdot 5\text{H}_2\text{O}$ was established by X-ray crystallographic analysis. The ORTEP diagram and the numbering scheme of the cation in $[\text{Co}(\text{Et}_2\text{-Me}_6\text{-N}_6\text{-tetracosanediimine})]\text{Cl}_3 \cdot 5\text{H}_2\text{O}$ is depicted in Fig. 5.5. The interatomic distances and angles are listed in Table 5.1. Other crystallographic data are tabulated in Appendix E(I).

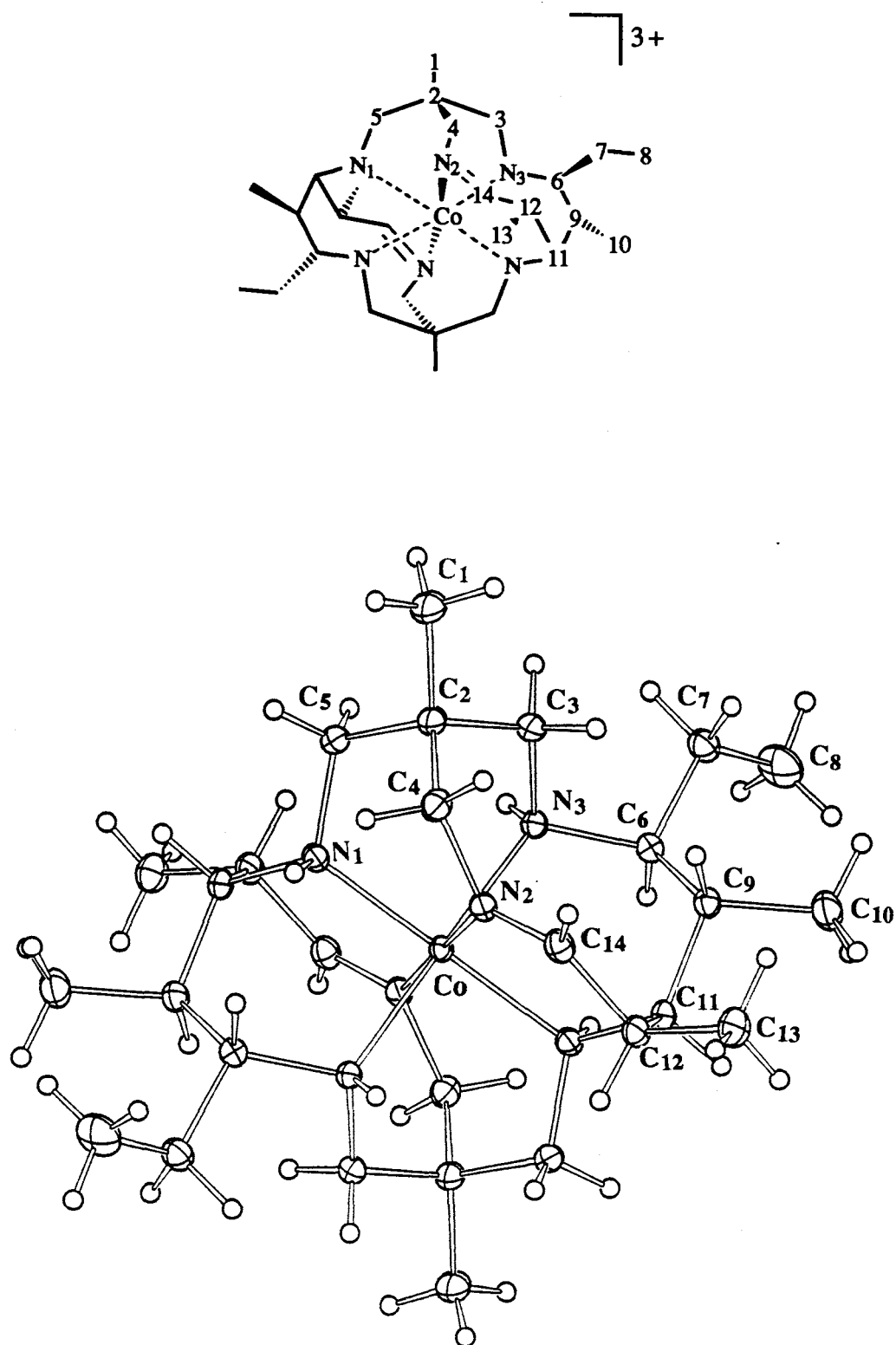


Figure 5.5: ORTEP diagram of the cation in $[\text{Co}(\text{Et}_2\text{-Me}_6\text{-N}_6\text{-tetracosanediimine})]\text{Cl}_3 \cdot 5\text{H}_2\text{O}$.

Table 5.1: Bond lengths and angles for non-hydrogen atoms of the cation in [Co(Et₂-Me₆-N₆-tetracosanediimine)]Cl₃.5H₂O (space group = P2₁/n).

Bond	Distance (Å)
Co-N(1)	1.979(2)
Co-N(2)	1.961(2)
Co-N(3)	2.029(2)

Bond [§]	Distance (Å)	Bond [§]	Distance (Å)
N(1)-C(5)	1.485(3)	N(1)-C(11)	1.485(3)
N(2)-C(4)	1.484(3)	N(2)-C(14)	1.273(3)
N(3)-C(3)	1.503(3)	N(3)-C(6)	1.518(3)
C(1)-C(2)	1.529(3)	C(2)-C(5)	1.524(3)
C(2)-C(4)	1.529(3)	C(2)-C(3)	1.519(3)
C(6)-C(7)	1.545(3)	C(6)-C(9)	1.548(3)
C(7)-C(8)	1.520(3)	C(9)-C(10)	1.532(3)
C(9)-C(11)'	1.560(3)	C(11)'-C(12)	1.529(3)
C(12)-C(13)	1.529(3)	C(12)-C(14)	1.491(3)

Bond Angles [§]	Degrees	Bond Angles [§]	Degrees
N(1)-Co-N(2)	87.0(1)	N(1)-Co-N(3)	92.7(1)
N(1)-Co-N(2)'	93.0(1)	N(2)-Co-N(3)'	95.9(1)
N(1)-Co-N(3)'	87.3(1)	N(2)-Co-N(3)	84.1(1)
N(1)-C(5)-C(2)	108.6(2)	N(2)-C(4)-C(2)	109.8(2)
N(3)-C(3)-C(2)	114.4(2)	N(3)-C(6)-C(7)	110.1(2)
N(3)-C(6)-C(9)	110.3(2)	C(5)-N(1)-C(11)'	112.7(2)
N(1)'-C(11)-C(12)	109.5(3)	C(3)-N(3)-C(6)	109.3(2)
N(2)-C(14)-C(12)	125.7(2)	C(4)-N(2)-C(14)	115.3(2)
N(1)'-C(11)-C(9)	110.7(2)	Co-N(1)-C(5)	116.7(1)
Co-N(2)-C(4)	116.6(1)	Co-N(2)-C(14)	127.2(1)
Co-N(3)-C(6)	117.4(1)	Co-N(1)-C(11)'	116.5(1)
Co-N(3)-C(3)	115.1(1)	C(1)-C(2)-C(4)	108.6(2)
C(1)-C(2)-C(5)	110.2(2)	C(5)-C(2)-C(4)	110.3(2)
C(1)-C(2)-C(3)	108.1(2)	C(4)-C(2)-C(3)	110.7(2)
C(5)-C(2)-C(3)	108.8(2)	C(7)-C(6)-C(9)	113.9(2)
C(6)-C(7)-C(8)	113.5(2)	C(6)-C(9)-C(10)	112.5(2)
C(6)-C(9)-C(11)	113.7	C(10)-C(9)-C(11)	108.8
C(9)-C(11)-C(12)	114.6(2)	C(11)-C(12)-C(14)	110.1
C(11)-C(12)-C(13)	112.3	C(13)-C(12)-C(14)	108.6(2)

§ Primes indicate atoms generated by the symmetry operation (1-x, 1-y, 1-z)

The structure shows that a total of six propanal molecules had condensed with the $[\text{Co}(\text{tame})_2]^{3+}$ template to form an achiral complex with C_i symmetry. The Co(III) ion lies at a centre of inversion and is slightly distorted from octahedral. The pair of Co-N_{imine} bond lengths are the shortest of the three independent Co-N bonds, but are still long for bonds of this type. This is presumably a consequence of the steric constraints of the ligand. The second pair of Co-N_{amine} bond lengths are typical for bond lengths of this type, whilst the last pair are significantly longer, and ranks as one of the longest reported for Co(III)-N_{amine} bonds. The six-membered chelate rings of the tame caps have skewboat conformations. There are two six-membered chelate rings linking the two tame caps, such that the two remaining amines are *trans* to each other and both these chelate rings are in the skewboat conformation. Both "straps" are derived from the condensation of two propanal residues. Each strap has a propanal residue linked to one of the remaining *trans* amine groups, to give rise to two more six-membered chelate rings. These "cross straps" adopt a flattened skewboat conformation, as a consequence of their imine. Fourteen chiral centres were generated in the reaction, ten associated with the carbon framework and four associated with the secondary nitrogens. On one side of the complex, the chiral carbon atoms C₂, C₆, C₉, C₁₁ and C₁₂ have S,S,S,S and R configurations, respectively. The secondary nitrogens N₁ and N₃ both have the S configuration. The chiral centres on one side of the complex have configurations enantiomeric to those on the other side of the inversion centre. The conformations of the chelate rings and configurations about all chiral centres are the same as those observed in the analogous Pt(IV) complex. The numbering system used for the X-ray analysis is also used in the following NMR spectral assignments.

III. NMR Spectroscopy of $[\text{Co}(\text{Et}_2\text{-Me}_6\text{-N}_6\text{-tetracosanediimine})]^{3+}$

The ^1H NMR spectrum of $[\text{Co}(\text{Et}_2\text{-Me}_6\text{-N}_6\text{-tetracosanediimine})]\text{Cl}_3$ in D_2O is complicated by the overlapping of different ^1H resonances and complex splitting patterns (Fig. 5.6(a)). The resolution was improved by use of a 500 MHz spectrometer. The splitting pattern of the ^1H NMR spectrum shows some similarities to that for the analogous Pt(IV) complex at pH~1 (see Chapter 3). However, assignment of the proton signals was relatively easy for the Co(III) complex due to the lack of proton exchange on carbon atoms alpha to the imines (H₁₂) with the solvent and also ^{59}Co coupling is not a problem. The assignment of the ^1H NMR spectrum and estimation of the smaller coupling constants was aided by the DQF COSY spectrum (Appendix F). Assignment of the signals was also aided by analogy with the spectrum of the saturated complex (discussed later).

All the methylene protons not related by symmetry are magnetically inequivalent and are observed as pairs of doublets ($H_{3a,3b}$, $H_{4a,4b}$, $H_{5a,5b}$ and $H_{7a,7b}$). The magnetically inequivalent methylene protons of the strap ethyl group (H_{7a} and H_{7b}) are observed as a pair of multiplets centred at 1.67 ppm and 1.87 ppm. Long range coupling between some pairs of cap methylene protons (viz: H_{3a-5b} and H_{4b-5a}) was apparent from the DQF COSY spectrum (Appendix F) where ${}^4J_{3a-5b} \sim 2.8$ and ${}^4J_{4b-5a} \sim 2.8$ Hz. Each of the pairs of protons forms part of a "W" conformation which favours long range coupling.²⁸ Such couplings have not been observed previously in either the N_6 -tricosane or sar cage Co(III) complexes. Coupling has been observed in [Co(*cis*-diammac)]³⁺ (${}^4J=2.5$ Hz),²⁹ and this has been attributed to the inflexibility of this complex. Similarly, the long range coupling observed for these N_6 -tetracosane complexes is therefore attributed to the ligand rigidity. Surprisingly, long range coupling of the cap proton H_{4b} (4.67 ppm) with protons H_{12} and H_{14} in the cross strap (3.80 and 8.04 ppm, respectively) was apparent from intense cross peaks in the DQF COSY spectrum (${}^4J_{14-4b}=5.8$ Hz, ${}^5J_{12-4b}=5.4$ Hz). These pairs of protons also form part of a "W" conformation. The magnitude of this long range coupling across the imine is comparable with 5J coupling constants associated with alkenes and other conjugated systems.²⁸ Strong coupling is not observed for the same set of protons after reduction of the imines, implying that the spin transmission is enhanced by the imine π system. The poor resolution of some signals (namely, H_6 , H_9 , H_{11} and H_{12}) is mostly due to the small coupling between adjacent spin systems, which reflects their unfavourable dihedral angles (Appendix F lists relevant dihedral angles). Longer range coupling also appears to contribute to the lack of resolution of some signals. These small couplings were manifested in the DQF COSY spectrum, where the structures of the relevant cross peaks were more complex than was anticipated.

The ${}^{13}\text{C}$ NMR spectrum in D_2O showed the 14 anticipated resonances (Fig. 5.6(b)), unlike that of the analogous Pt(IV) complex. The assignment of the ${}^{13}\text{C}$ NMR spectrum was deduced from the HMQC spectrum (Appendix F).

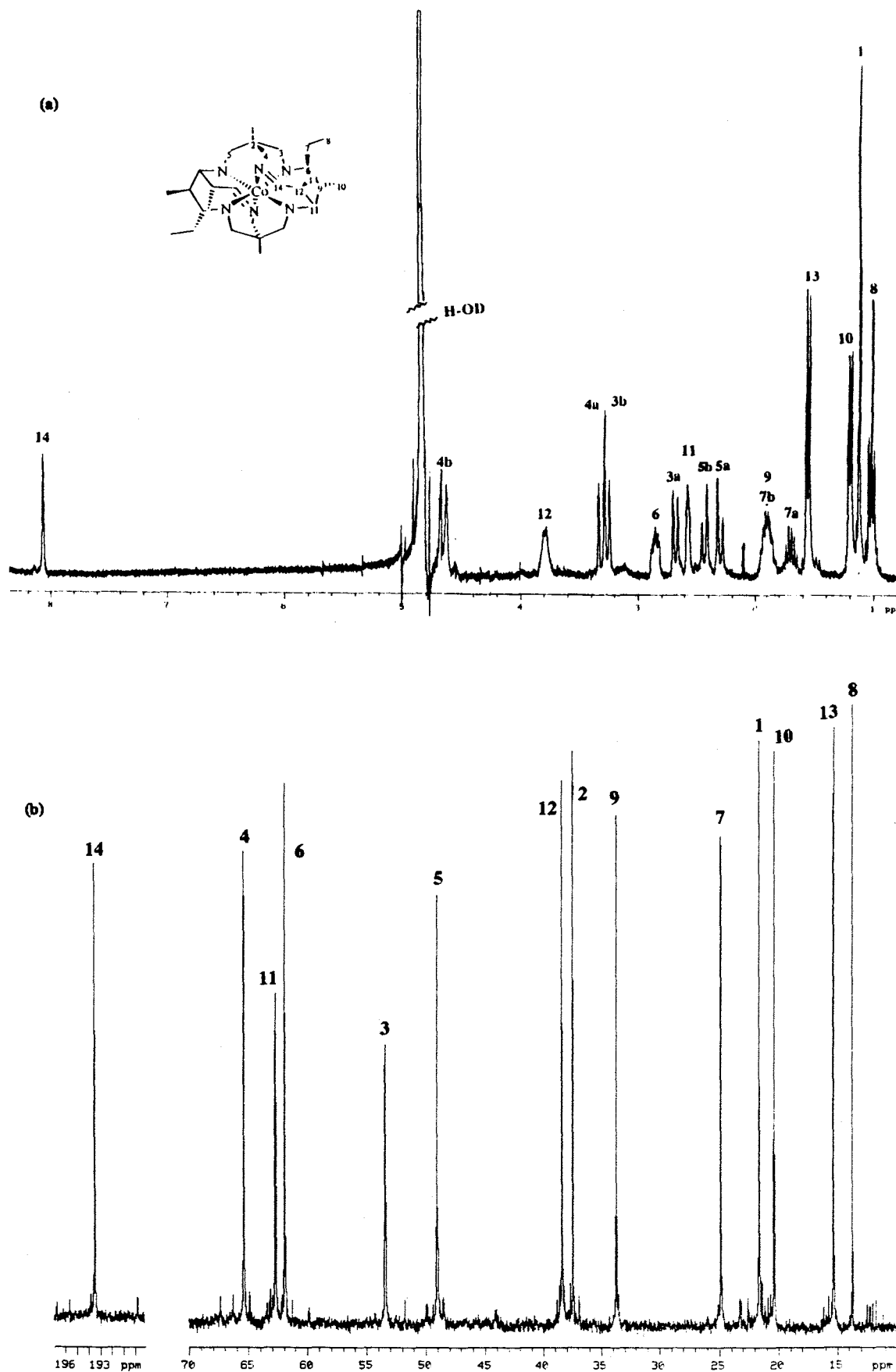


Figure 5.6: 500 MHz ^1H NMR and (b) 300 MHz ^{13}C NMR spectra of $[\text{Co}(\text{Et}_2\text{-Me}_6\text{-N}_6\text{-tetracosanediimine})]\text{Cl}_3$ in D_2O .

(b) Decomposition Products of [Co(Et₂-Me₆-N₆-tetracosanediimine)]³⁺

At pH > 6 one of the imines slowly hydrolyses, resulting in loss of a propanal residue. The ¹H NMR spectrum of this complex was complicated and only a partial assignment of the signals was made (Appendix F). It was also identical with the ¹H NMR spectrum of [Co(Et₂-Me₅-N₆-docosanediimine)]³⁺ from the second band obtained after workup of the reaction mixture on SP-Sephadex cation exchange resin. Notable peaks include two unique imine and seven methyl signals. The APT spectrum (Appendix F) was also complex and consisted of 25 carbon resonances, including two imine signals (at 190.0 and 194.5 ppm) and seven methyl signals at 12.0, 12.5, 15.5, 16.0, 20.9, 21.6 and 21.8 ppm. The APT spectrum shows that there are 15 carbon atoms with an odd number of protons and 10 carbon atoms with an even number of protons, which is consistent with the proposed structure. The microanalysis of the chloride salt gave a C₂₅:N₆ ratio. Crystals of the chloride salt were grown in D₂O and are currently awaiting X-ray crystallographic analysis.

5.3.2. Reduction of [Co(Et₂-Me₆-N₆-tetracosanediimine)]³⁺

I. Properties of [Co(Et₂-Me₆-N₆-tetracosane)]Cl₃

The imines were reduced selectively with NaBH₄ at pH~10.5 to give [Co(Et₂-Me₆-N₆-tetracosane)]Cl₃. This complex has a solubility similar to that of the diimine precursor in water. The acetate salt is slightly more soluble than the chloride salt in water. The triflate and perchlorate anions are sparingly soluble in water, the ClO₄⁻ salt is also sparingly soluble in MeCN. It is stable indefinitely in water.

II. Crystal Structure of [Co(Et₂-Me₆-N₆-tetracosane)]Cl₃.4H₂O

The structure was established by X-ray crystallographic analysis. The ORTEP diagram for the cation and its numbering scheme is depicted in Fig. 5.7. Interatomic distances and angles are listed in Table 5.2. Other crystallographic data are listed in Appendix E(II). The numbering system here is also used to describe the NMR spectra.

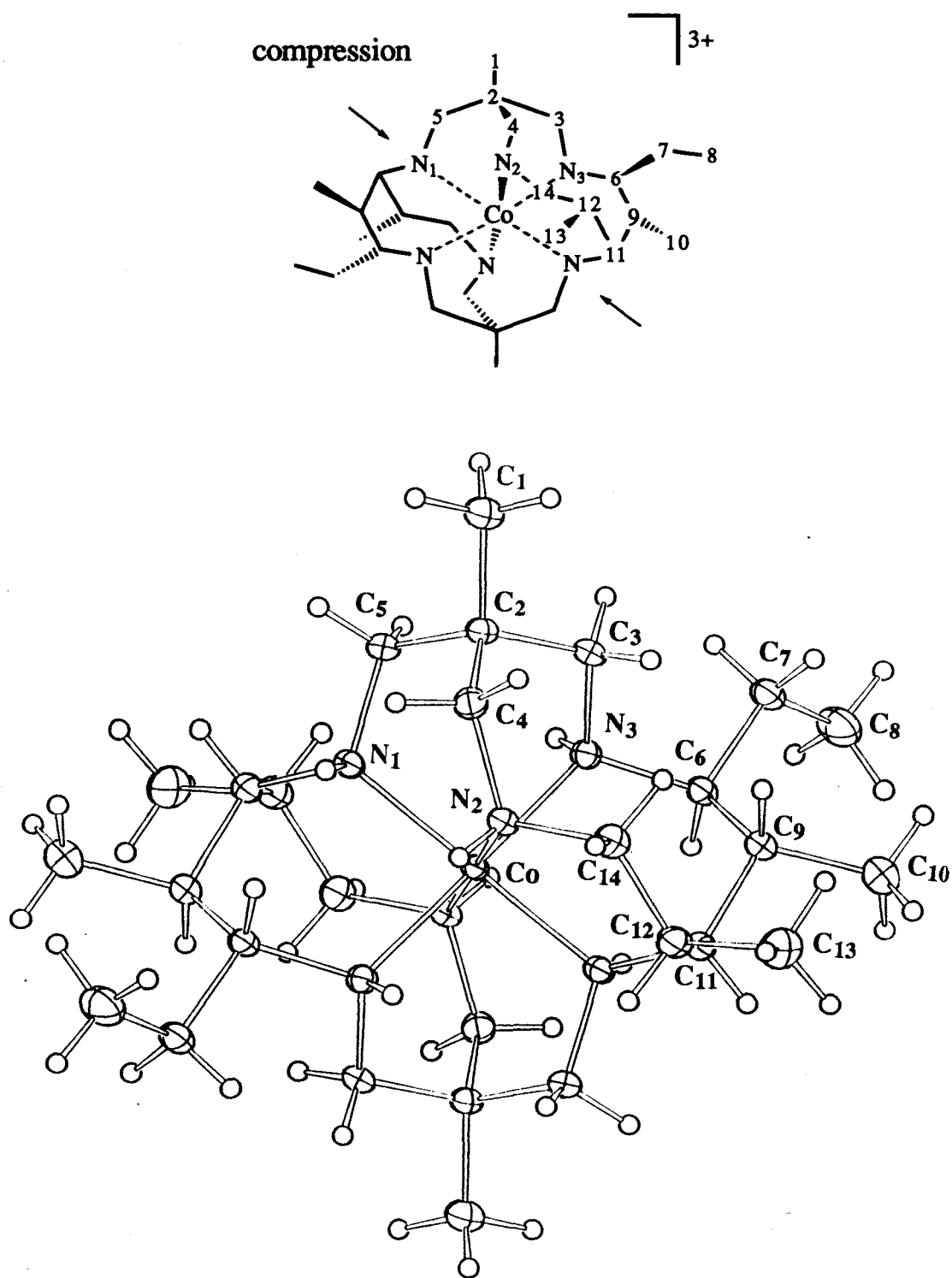


Figure 5.7: ORTEP diagram of the cation in $[\text{Co}(\text{Et}_2\text{-Me}_6\text{-N}_6\text{-tetracosane})]\text{Cl}_3 \cdot 4\text{H}_2\text{O}$.

Table 5.2: Bond lengths and angles for non-hydrogen atoms of the cation in [Co(Et₂-Me₆-N₆-tetracosane)]Cl₃.4H₂O (space group = PZ₁/n).

Bond	Distance (Å)
Co-N(1)	1.974(2)
Co-N(2)	2.030(2)
Co-N(3)	2.030(2)

Bond§	Distance (Å)	Bond§	Distance (Å)
N(1)-C(5)	1.489(3)	N(1)-C(11)'	1.489(3)
N(2)-C(4)	1.513(3)	N(2)-C(14)	1.501(3)
N(3)-C(3)	1.505(3)	N(3)-C(6)	1.520(3)
C(1)-C(2)	1.525(3)	C(2)-C(5)	1.529(3)
C(2)-C(4)	1.536(3)	C(2)-C(3)	1.518(3)
C(6)-C(7)	1.549(3)	C(6)-C(9)	1.528(3)
C(7)-C(8)	1.517(4)	C(9)-C(10)	1.537(4)
C(9)-C(11)	1.559(3)	C(11)-C(12)	1.516(4)
C(12)-C(13)	1.526(4)	C(12)-C(14)	1.501(3)

Bond Angles§	Degrees	Bond Angles§	Degrees
N(1)-Co-N(2)	84.9	N(1)-Co-N(3)	93.4
N(1)-Co-N(1)'	180.0	N(1)-Co-N(2)'	95.1
N(1)-Co-N(3)'	86.1	N(2)-Co-N(3)	88.4
N(2)-Co-N(2)'	180.0	N(2)-Co-N(3)'	91.6
N(3)-Co-N(3)'	180.0	Co-N(1)-C(5)	114.3
Co-N(1)-C(11)'	118.2	C(5)-N(1)-C(11)'	113.5
Co-N(2)-C(4)	113.6	Co-N(2)-C(14)	123.0
C(4)-N(2)-C(14)	107.0	Co-N(3)-C(3)	115.4
Co-N(3)-C(6)	118.9	C(3)-N(3)-C(6)	111.1
C(1)-C(2)-C(5)	109.6	C(1)-C(2)-C(4)	108.3
C(1)-C(2)-C(3)	108.0	C(5)-C(2)-C(4)	110.3
C(5)-C(2)-C(3)	109.6	C(4)-C(2)-C(3)	111.1
N(1)-C(5)-C(2)	108.9	N(2)-C(4)-C(2)	112.9
N(3)-C(3)-C(2)	113.1	N(3)-C(6)-C(7)	110.4
N(3)-C(6)-C(9)	111.3	C(7)-C(6)-C(9)	113.5
C(6)-C(7)-C(8)	113.3	C(6)-C(9)-C(10)	112.2
C(6)-C(9)-C(11)	114.0	C(10)-C(9)-C(11)	108.8
C(9)-C(11)-C(12)	114.4	C(9)-C(11)-N(1)'	110.8
C(12)-C(11)-N(1)'	111.4	C(11)-C(12)-C(13)	111.1
C(11)-C(12)-C(14)	113.4	C(13)-C(12)-C(14)	107.8
N(2)-C(14)-C(12)	116.0		

§ Primes indicate atoms generated by the symmetry operation (-x, 1-y, -z)

The achiral complex has C_i symmetry with the Co(III) ion at a centre of inversion. The reduction of the imines resulted in a substantial increase of the Co-N₂ bond length by 0.069 Å, such that it became comparable with that of Co-N₃. The Co-N₁ and Co-N₃ bond lengths are about the same as those in the parent imine structure. The Co(III) ion is therefore tetragonally compressed along the Co-N₁ axis. The average Co(III)-N bond length in the complex is longer than typical for Co(III) hexamine complexes and the Co-N₂ and Co-N₃ bonds rank amongst the longest reported for complexes of this type. Table 5.3 lists the bond lengths of some related Co(III)-N hexamine complexes. The conformations of the chelate rings in the complex are essentially the same as those described for the parent diimine structure, except for the chelate rings which form the cross straps, which changed from the skewboat to the chair conformation. There are 16 chiral centres in the complex, 10 arising from carbon sites in the ligand and 6 arising from the secondary nitrogen atoms. The configurations about C₂, C₆, C₉, C₁₁, C₁₂ are S,S,S,R,S, respectively, while the configurations about the secondary nitrogens N₁, N₂, N₃ and are S,S,S respectively. The chiral centres on one side of the molecule have configurations enantiomeric to those on the other side of the inversion centre.

III. NMR Spectroscopy of [Co(Et₂-Me₆-N₆-tetracosane)]³⁺

The one dimensional ¹H NMR spectrum was complicated by overlapping resonances and complex splitting patterns (Fig. 5.8(a)). The resolution was improved by use of a 500 MHz spectrometer.

The methylene protons not related by symmetry are magnetically inequivalent and are observed as pairs of doublets (H_{3a,3b}, H_{4a,4b}, H_{5a,5b}, H_{7a,b} and H_{14a,14b}). The NOESY spectrum (Appendix F) was helpful for assigning the cap methylene protons. The DQF COSY spectrum (Appendix F) indicated that long range coupling was operative between some of the cap methylene protons, which form part of a "W" conformation (⁴J_{4a-5b} = 4.9; ⁴J_{4b-5a} = 4.4 Hz), however the long range coupling over the what were the imine protons to the same cap proton H_{4b} (⁴J_{14-4b} and ⁵J_{12-4b}) was not apparent. The poorly resolved signals for H₆, H₉, H₁₁ and H₁₂ are a reflection of their small coupling with the relevant spin systems due to unfavourable dihedral angles (Appendix F). Small long-range couplings also contributed to the lack of resolution, as manifested in the complicated structure of the cross peaks in the DQF COSY spectrum.

The DQF COSY, TOCSY and NOESY spectra (Appendix F) were essential for assignment of the one dimensional ¹H NMR spectrum and were also helpful in assignment of the resonances in other complexes of this type ([Co(Et₂-Me₆-N₆-tetracosanediimine)]³⁺, [Pt(Et₂-Me₆-N₆-tetracosanediimine)]⁴⁺ [Pt(Me₄-N₆-tetracosanediimine)]⁴⁺ and to some extent, the Pt(II) complexes).

The one dimensional ^{13}C NMR spectrum consisted of the expected 14 resonances (Fig. 5.8(b)). The assignments were deduced from the HMQC spectrum (Appendix F).

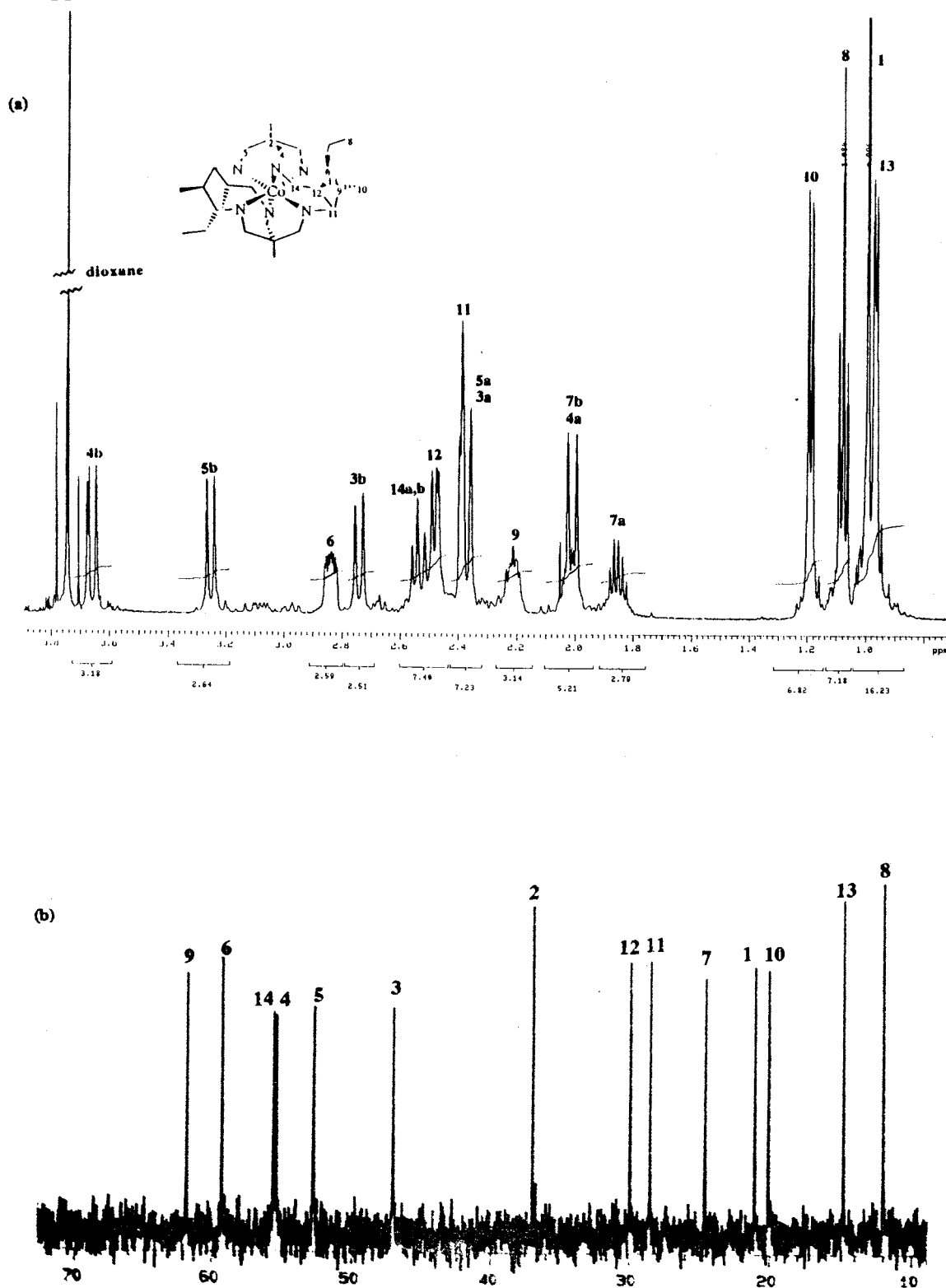


Figure 5.8: (a) 500 MHz ^1H NMR and (b) 300 MHz ^{13}C NMR spectra of $[\text{Co}(\text{Et}_2\text{-Me}_6\text{-N}_6\text{-tetracosane})]\text{Cl}_3$ in D_2O .

(c) Attempted Extrusion of Co(II) from [Co(Et₂-Me₆-N₆-tetracosane)]³⁺

Extrusion of the Co(II) ion from [Co(Et₂-Me₆-N₆-tetracosane)]²⁺ was attempted unsuccessfully by treatment of the Co(III) complex with zinc/HCl under nitrogen. This route has been successful for metal ion extrusion from some sar³⁰ and N₆-tricosane ligands.²³ Although the Co(III) complex was easily reduced to the Co(II) species, subsequent addition of excess hydrochloric acid to the reaction led to precipitation of the colourless [Co(Et₂-Me₆-N₆-tetracosane)]Cl₂, rather than the anticipated extrusion of the metal ion. The Co(II) complex reoxidised in air during filtration. An attempt to extrude the Co(II) ion using sulphide in basic media under nitrogen was also unsuccessful.

5.3.3. Condensation of [Co(tame)₂]³⁺ with Acetaldehyde

(a) Attempted Synthesis of [Co(Me₄-N₆-tetracosanediimine)]³⁺ and [Co(^βMe₅N₆-tricosanetriimine)]³⁺

The reaction of [Co(tame)₂]³⁺ with acetaldehyde and diisopropylethylamine in MeCN at both 295 and 275 K produced many complexes and the separation and characterisation of these complexes by cation exchange chromatography was not successful. The target complexes, [Co(Me₄-N₆-tetracosanediimine)]³⁺ and [Co(^βMe₅-N₆-tricosanetriimine)]³⁺, were not identified. Fractional crystallisation of the imine complexes was unsuccessful. Treatment of the orange products with BH₄⁻ at pH~10 did not improve the separation of the many complexes on SP-Sephadex cation exchange resin. Fractional crystallisation of this reduced mixture was also unsuccessful.

5.3.4. Electronic Spectra

The absorption spectra for [Co(Et₂-Me₆-N₆-tetracosanediimine)]Cl₃ and [Co(Et₂-Me₆-N₆-tetracosane)]Cl₃ in water (pH~5.5) each exhibit two bands, arising from the ¹A_{1g}(O_h) → ¹T_{1g} transition and a charge transfer band (Fig. 5.9). The band arising from the second spin allowed ¹A_{1g}(O_h) → ¹T_{2g} transition for both complexes was obscured by the usually intense charge transfer band. The absorption maxima and corresponding molar absorption coefficients for these complexes are listed in Table 5.3, along with those of some related Co(III) hexamine complexes. The energy of the ¹A_{1g}(O_h) → ¹T_{1g} band for [Co(Et₂-Me₆-N₆-tetracosane)]Cl₃ is lower than that for other acyclic and sar-type CoN₆³⁺ chromophores. The molar absorption coefficients of this band for both [Co(Et₂-Me₆-N₆-tetracosanediimine)]³⁺ and [Co(Et₂-Me₆-N₆-tetracosane)]³⁺ are relatively high compared with the octahedral parent, [Co(NH₃)₆]³⁺ and also are both slightly larger than those for the [Co(Me₅-N₆-tricosane)]³⁺ and the [Co(Me₅-N₆-tricosanetriimine)]³⁺, respectively. This implies that the symmetries about

the CoN_6^{3+} cores for the N_6 -tetracosane complexes are lower than those for the N_6 -tricosane complexes. The absorption spectrum of $[\text{Co}(\text{Et}_2\text{-Me}_6\text{-}N_6\text{-tetracosanediimine})]\text{Cl}_3$ in 0.01 M NaOH (pH~11.5) is shown in Fig. 5.10. The absorption maxima of the three bands at $\lambda_{\text{max}} = 618 \text{ nm}$ ($\epsilon, 300 \text{ M}^{-1}\text{cm}^{-1}$), 420 nm ($\epsilon, 330 \text{ M}^{-1}\text{cm}^{-1}$) and 342 nm ($\epsilon, 513 \text{ M}^{-1}\text{cm}^{-1}$) indicate that this complex is tetragonally distorted under these conditions. Deprotonation at the amine sites is likely to introduce such distortion.

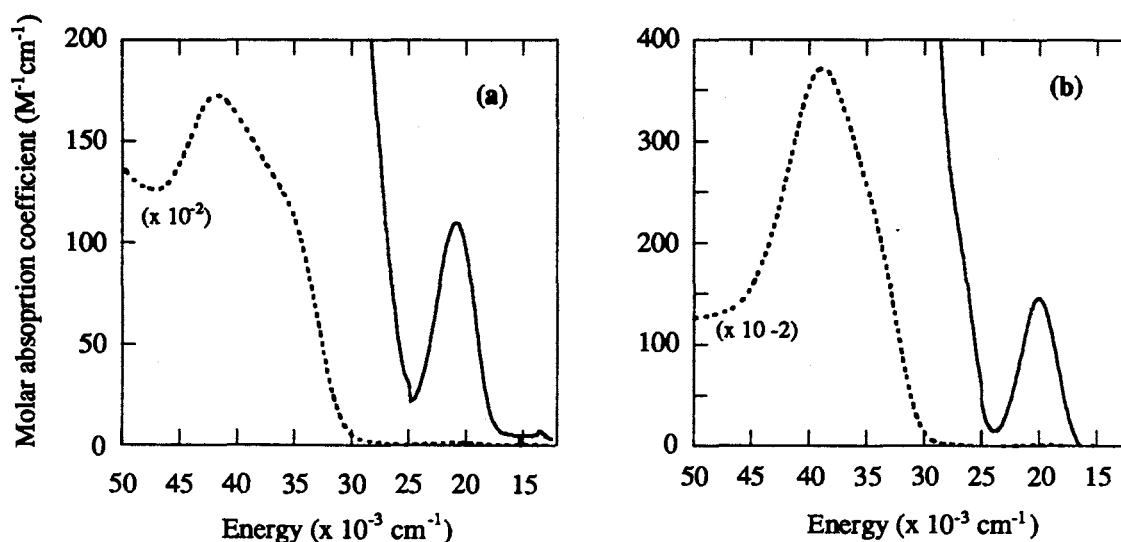


Figure 5.9: Absorption Spectra of (a) $[\text{Co}(\text{Et}_2\text{-Me}_6\text{-}N_6\text{-tetracosanediimine})]\text{Cl}_3$ and (b) $[\text{Co}(\text{Et}_2\text{-Me}_6\text{-}N_6\text{-tetracosane})]\text{Cl}_3$ in water (pH~5.5).

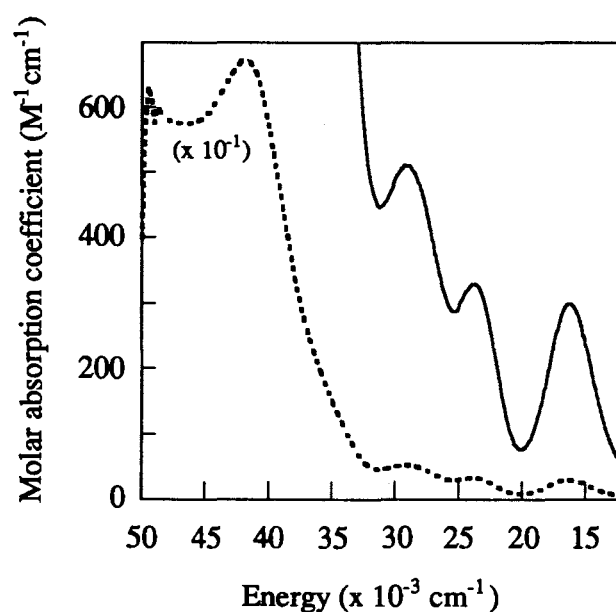


Figure 5.10: Absorption Spectrum of $[\text{Co}(\text{Et}_2\text{-Me}_6\text{-}N_6\text{-tetracosanediimine})]\text{Cl}_3$ in 0.01 M NaOH (pH~11.5).

Table 5.3: Spectroscopic data, reduction potentials, Co(III)-N bond lengths, and self exchange rate constants (k_{ex}) for some Co(III) hexaamine complexes.

Complex	λ_{max} (nm) ϵ_{max} ($M^{-1}cm^{-1}$)	$E_{1/2}$ (V vs NHE) [¶]	Co(III)-N (Å)	k_{11} ($M^{-1}s^{-1}$)
[Co(NH ₃) ₆] ³⁺ ³¹	203 (19,000) 339 (47) 474 (58)	-0.02 ¹⁴	1.960(6) ³²	2×10^{-7} ¹¹
[Co(en) ₃] ³⁺ ³¹	213 (12,700) 339 (85) 467 (93)	-0.17 ¹⁴	1.964(3) ⁹	5×10^{-5} ¹³
[Co(Metacn) ₂] ³⁺ ³¹	463 (85), 340 (78)	-0.41	1.974(5) ³³	0.19
[Co(tame) ₂] ³⁺ ³¹	229 (19,400) 345 (76) 472 (81)	-0.43	1.972(3) ³⁴	
[Co(<i>trans</i> -diammac)] ³⁺ ³⁵	218 (16,900) 328 (76) 447 (73)	-0.61	1.937(2), 1.936(2), 1.946(2),	900 [§]
[Co(sar)] ³⁺ ⁶ [Co(NH ₂) ₂ sar] ³⁺ [Co(NH ₃) ₂ sar] ⁵⁺	242 (19,650) 343 (107) 471 (135)	-0.40 ⁶ -0.30 ⁶ 0.04 ⁶	1.978 ³⁶	2.1 ¹⁴
[Co(sep)] ³⁺ ³⁷	340 (116) 472 (109)	-0.30 ⁶	1.981(2) ⁹	5.1
[Co(Me ₅ -N ₆ - tricosanetriimine)] ³⁺ ¹⁰	343 (135) 468 (107)	-0.19		
[Co(Me ₅ -N ₆ -tricosane)] ³⁺ ⁴	265 (20,100) 370 (102) 516 (80)	0.08	2.010(4) 2.032(4)	0.4
[Co(Et ₂ -Me ₆ -N ₆ - tetracosanediimine)] ³⁺	239 (17,329) 480 (110)	-0.20	1.961(2), 1.979(2), 2.029(2)	
[Co(Et ₂ -Me ₆ -N ₆ - tetracosane)] ³⁺	258 (37,175) 498 (147)	-0.23	2.030(2) x 2, 1.974(2)	200

[¶] 0.2 M NaCl, at 293 K. [§] k_{ex} for this complex was obtained using Zn(I) in the cross reaction.³⁵

5.3.5. Electrochemistry of the Co(III) N_6 -tetracosane Complexes

The $\text{CoN}_6^{3+/2+}$ reduction potentials of the $[\text{Co}(\text{Et}_2\text{-Me}_6\text{-}N_6\text{-tetracosanediimine})]^{3+/2+}$ and $[\text{Co}(\text{Et}_2\text{-Me}_6\text{-}N_6\text{-tetracosane})]^{3+/2+}$ couples and also for some related complexes are listed in Table 5.3. The cyclic voltammograms (CV's) of the $[\text{Co}(\text{Et}_2\text{-Me}_6\text{-}N_6\text{-tetracosanediimine})]^{3+/2+}$ and $[\text{Co}(\text{Et}_2\text{-Me}_6\text{-}N_6\text{-tetracosane})]^{3+/2+}$ couples at 100 mVs^{-1} are depicted in Fig. 5.11(a) and (b), respectively. Both CV's show a reversible response corresponding to the Co(III)/Co(II) couple. The reduction potential of the $[\text{Co}(\text{Et}_2\text{-Me}_6\text{-}N_6\text{-tetracosanediimine})]^{3+/2+}$ couple is 34 mV more positive than that for the $[\text{Co}(\text{Et}_2\text{-Me}_6\text{-}N_6\text{-tetracosane})]^{3+/2+}$ couple. The CV's for the $[\text{Co}(\text{Et}_2\text{-Me}_6\text{-}N_6\text{-tetracosanediimine})]^{3+/2+}$ and $[\text{Co}(\text{Et}_2\text{-Me}_6\text{-}N_6\text{-tetracosane})]^{3+/2+}$ couples at $15,000 \text{ mV s}^{-1}$ are depicted in Fig. 5.11(c) and (d), respectively. For both complexes, a degree of reversibility is still observed at fast scan rates, implying that electron transfer is quite fast.

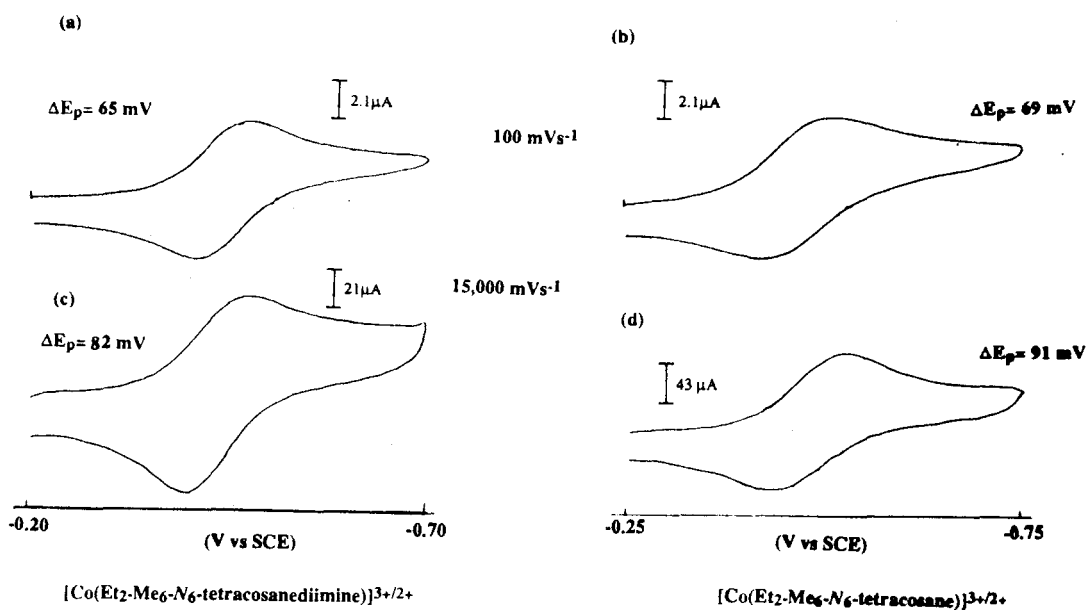


Figure 5.11: Cyclic voltammograms of (a) $[\text{Co}(\text{Et}_2\text{-Me}_6\text{-}N_6\text{-tetracosanediimine})]^{3+/2+}$ and (b) $[\text{Co}(\text{Et}_2\text{-Me}_6\text{-}N_6\text{-tetracosane})]^{3+/2+}$ at 100 mV s^{-1} and (c) $[\text{Co}(\text{Et}_2\text{-Me}_6\text{-}N_6\text{-tetracosanediimine})]^{3+/2+}$ and (d) $[\text{Co}(\text{Et}_2\text{-Me}_6\text{-}N_6\text{-tetracosane})]^{3+/2+}$ at $15,000 \text{ mV s}^{-1}$, (0.2 M NaCl, glassy carbon; 295 K).

No imine centred responses were observed in the range 0 to -1.1 V vs SCE in aqueous media or in the range 0 to -1.9 V vs SCE in MeCN (0.1 M TBAClO₄, Pt working electrode). In MeCN, the reduction potential for the [Co(Et₂-Me₆-N₆-tetracosanediiimine)]^{3+/2+} couple is 95 mV more positive than for the saturated complex ($E_{1/2} = -685$ and -780 mV vs Fc⁺⁰, respectively). The lack of imine centred responses in this window may be due to their reduction potentials being more negative than -1.9 V. Alternatively, in the absence of a proton source, reduction of the imines is not likely, particularly as MeCN is not a very strong proton donor.

5.3.6. Self Exchange Rate Constants

The self exchange rate constant for the [Co(Et₂-Me₆-N₆-tetracosane)]^{3+/2+} couple was deduced from the rate constant for the cross reaction of [Co(Et₂-Me₆-N₆-tetracosane)]²⁺ with an excess of [Co(azacpten)]³⁺ using the Marcus cross relation:^{38,39}

$$k_{12} = \sqrt{(k_{11}k_{22}K_{12}f_{12})}$$

$$\ln f_{12} = \frac{(\ln K_{12})^2}{4 \ln(k_{11}k_{22} / Z^2)}$$

where k_{12} = the rate constant for the cross reaction, k_{11} and k_{22} = self exchange rate constants for each component of the cross reaction, K_{12} = the equilibrium constant, f = a frequency factor and Z = the collision frequency = $10^{11} \text{ M}^{-1}\text{s}^{-1}$. These values are compiled in Table 5.4. The reduction potential for the [Co(azacpten)]^{3+/2+} couple is 0.12 V vs NHE (0.2 M NaCl) and its self exchange rate constant (k_{11}) is $2.2 \times 10^4 \text{ M}^{-1}\text{s}^{-1}$.⁴⁰ The self exchange rate constant for the [Co(Et₂-Me₆-N₆-tetracosane)]^{3+/2+} couple was evaluated as $\sim 200 \text{ M}^{-1}\text{s}^{-1}$, which is considerably larger than that for saturated CoN₆^{3+/2+} chromophores. Table 5.3 lists the self exchange rate constants for some related CoN₆^{3+/2+} couples.

Table 5.4: Data utilised in the cross reaction between [Co(azacpten)]³⁺ and [Co(Et₂-Me₆-N₆-tetracosane)]²⁺ (0.2 M NaCl, 298K).

$k_{\text{obs}} (\text{s}^{-1})$	k_{12} ($\text{M}^{-1}\text{s}^{-1}$)	k_{11} ($\text{M}^{-1}\text{s}^{-1}$)	$\Delta E_{1/2}$ (mV)	K_{12}	f_{12}	k_{22} ($\text{M}^{-1}\text{s}^{-1}$)
95 ± 10	9.4×10^4	2.2×10^4	-208	3.3×10^3	0.63	200

5.4. Discussion

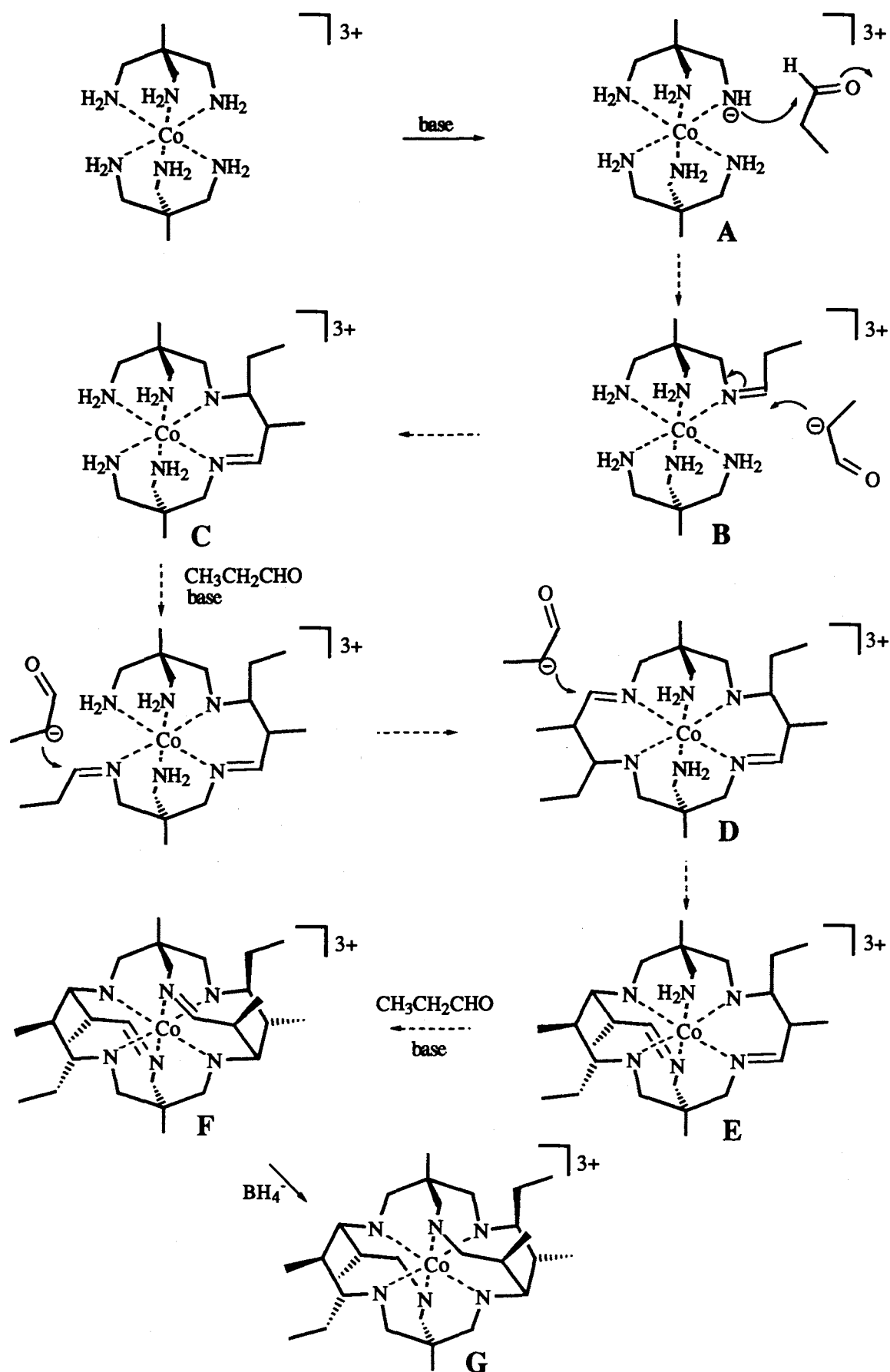
5.4.1. Synthesis

(a) $[\text{Co}(\text{Et}_2\text{-Me}_6\text{-N}_6\text{-tetracosanediimine})]^{3+}$

Two complexes were isolated from the base catalysed condensation of $[\text{Co}(\text{tame})_2]^{3+}$ with propanal in acetonitrile, namely, $[\text{Co}(\text{Et}_2\text{-Me}_6\text{-N}_6\text{-tetracosanediimine})]\text{Cl}_3$ and $[\text{Co}(\text{Et}_2\text{-Me}_5\text{-N}_6\text{-docosanediimine})]\text{Cl}_3$. As the latter complex can be readily synthesised from the former in the presence of excess propanal and base, it is proposed that the partially strapped $[\text{Co}(\text{Et}_2\text{-Me}_5\text{-N}_6\text{-docosanediimine})]^{3+}$ complex is the penultimate intermediate in the synthesis of $[\text{Co}(\text{Et}_2\text{-Me}_6\text{-N}_6\text{-tetracosanediimine})]^{3+}$. In addition, the $[\text{Co}(\text{Et}_2\text{-Me}_6\text{-N}_6\text{-tetracosanediimine})]^{3+}$ slowly decomposes to the N_6 -docosanediimine complex in solutions where the $\text{pH} \geq 5.5$.

As the configurations about the stereogenic centres for $[\text{Co}(\text{Et}_2\text{-Me}_6\text{-N}_6\text{-tetracosanediimine})]^{3+}$ are identical to those in the analogous Pt(IV) complex obtained under similar conditions, it is likely that the mechanism is very similar to that proposed for the analogous Pt(IV) complex which was discussed extensively in Chapter 3.4 (Schemes 3.6-3.8). An abbreviated mechanism for the synthesis of $[\text{Co}(\text{Et}_2\text{-Me}_6\text{-N}_6\text{-tetracosanediimine})]^{3+}$ is depicted in Scheme 5.1.

The template deprotonates to form intermediate **A** which condenses with a propanal molecule, to form the propanimine species, **B**. The subsequent order of condensation reactions is probably governed by a combination of electronic and steric effects. A propanal carbanion attacks the imine in **B** to form a pendant carbonyl, which is in turn attacked by an amine on the opposite tame cap, so forming the first strap, **C**. There is some evidence that the amines *cis* to a coordinated imine are more acidic than those *trans* in Pt(IV) amine complexes.⁴¹⁻⁴³ This result has been used to rationalise the observed regioselectivity in many of the mixed aldehyde condensation reactions with the Pt(IV) hexaamine complexes (Chapter 3). This concept may be extended to the Co(III) hexaamine systems, where similar regio- and stereoselectivity has been observed. For example, in the synthesis of $[\text{Co}(\text{Me}_5\text{-N}_6\text{-tricosanetriimine})]^{3+}$, the major cage product is the *facial*-triimine isomer, where all three imines lie on the same face of the octahedron. No *meridional* isomer was detected in the reaction mixture,^{10,23} and likewise in analogous Pt(IV) N_6 -tricosanetriimine systems.



Scheme 5.1: Proposed mechanism for the synthesis of $[Co(Et_2-Me_6-N_6-tetracosane)]^{3+}$ (amine protons have been omitted for clarity).

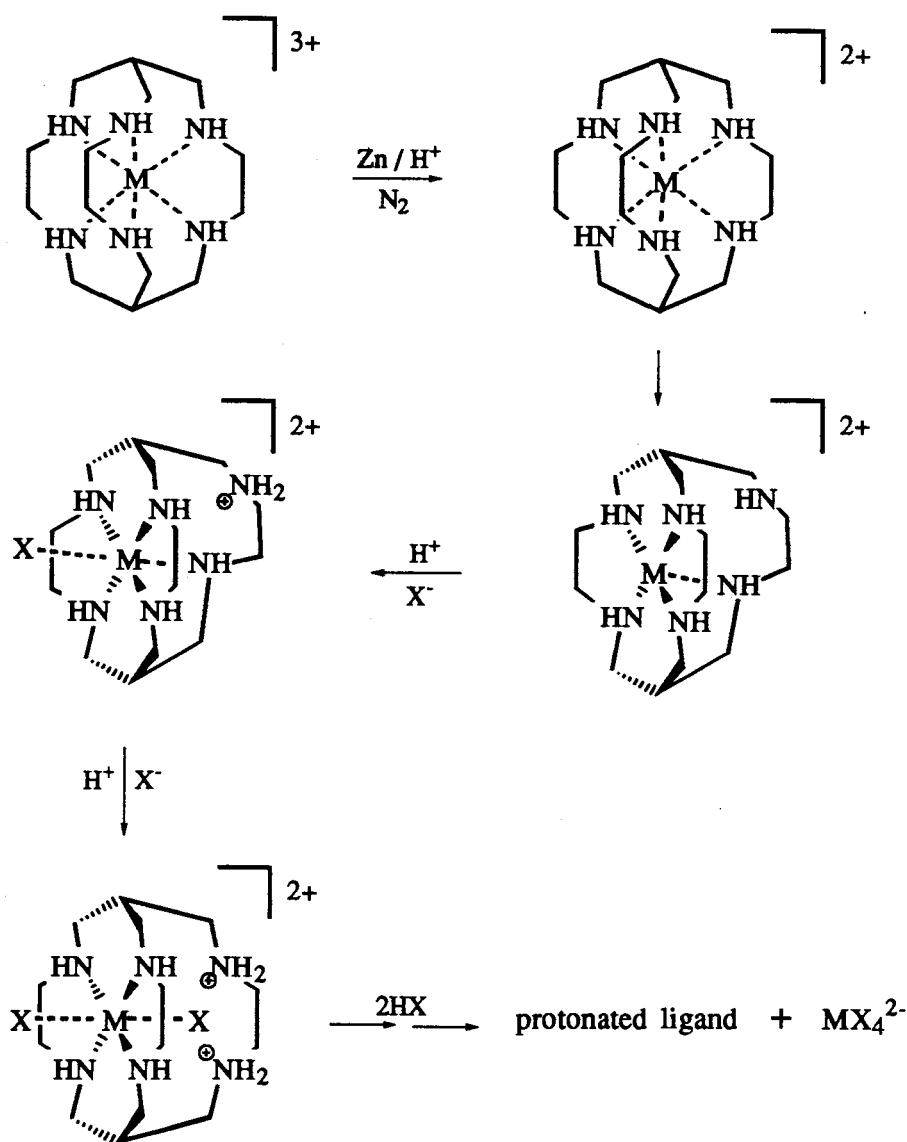
In this reaction, it is likely that the third propanal molecule condenses with an amine, *cis* to the imine in complex C, on the same tame cap, to form a propanimine as shown. This imine is then attacked by a propanal carbanion to form a pendant carbonyl. Dreiding models have shown that this pendant carbonyl is very favourably aligned with the amine in the opposite tame cap, such that it can only condense at this site, so forming the second strap, as shown in D. The imines are located *trans* to each other in intermediate D, as are the primary amines, and the latter cannot be readily linked. Hence, once D has formed, formation of a triimine complex (with C_3 symmetry) is not feasible. Sequential condensation of each of the strap imines with the fifth and sixth propanal units form the cross straps, to form firstly $[Co(Et_2-Me_5-N_6\text{-docosanediiimine})]^{3+}$, E, then the fully encapsulated N_6 -tetracosanediiimine complex, F. Reduction of the imines in F is accomplished by treating complex F with BH_4^- under basic conditions, to yield $[Co(Et_2-Me_6-N_6\text{-tetracosane})]^{3+}$, G.

The lower yield obtained for $[Co(Et_2-Me_6-N_6\text{-tetracosanediiimine})]^{3+}$ compared to the Pt(IV) system may be due to the less acidic coordinated amine protons of the $[Co(\text{tame})_2]^{3+}$ template. Condensation of the aldehydes with the deprotonated amine sites is slower and competing side reactions, such as self condensation of the aldehydes, become more competitive, limiting the availability of the reagents for reaction with the template. It is not clear why there was a relatively higher yield for the synthesis of $[Co(Et_2-Me_6-N_6\text{-tetracosane})Cl_3]$ compared to that for $[Co(Me_5-N_6\text{-tricosane})]^{3+}$. It may be that methylene bridged species form relatively easily and/or irreversibly in reactions involving methanimine intermediates, whereas they form less readily from propanimine intermediates.

(c) *Attempted Extrusion of Cobalt from $[Co(Et_2-Me_6-N_6\text{-tetracosane})]^{3+}$*

It was anticipated that other metal ions besides Co(III) could be encapsulated in the $Et_2-Me_6-N_6$ -tetracosane cage. For this, it was necessary to isolate first the free ligand by extruding the relatively more labile Co(II) ion from $[Co(Et_2-Me_6-N_6\text{-tetracosane})]^{2+}$, which was generated by reduction of the Co(III) complex by zinc in acid media. The difficulty in removing the Co(II) ion from the $Et_2-Me_6-N_6$ -tetracosane cage using the Zn/HCl strategy is attributed essentially to the inflexibility of the ligand, in contrast to the sar and N_6 -tricosane complexes. A mechanism for the extrusion of a labile metal ion (M^{2+}) from the bicyclic complex has been proposed (Scheme 5.2) and is based on observations made for the extrusion of CuX_4^{2-} from $[Cu(\text{sar})]^{2+}$ in the presence of HX ($X=Cl^-, Br^-$).¹ Similar mechanisms have been postulated for the extrusion of the Hg(II),¹ and Mn(II)²⁶ ions from the sar ligand. In the cobalt system, reduction by Zn/HX to the Co(II) ion occurs, followed by rupture of an M-N bond. In excess acid, the amine protonates. This inhibits its recoordination with the metal ion and instead, an anion coordinates with the metal ion. The second amine donor on the same

ligand strand dissociates and it also protonates in excess acid. The protonated amines move away from the metal ion and expose it to other coordinating anions. The metal ion is eventually extruded as the MX_4^{n-} ion. The ability of the ligand strap to fold back and expose the metal ion to coordinating anions is central to the extrusion mechanism. The cross straps in the N_6 -tetracosane system however, probably impede such movement. The incoming anions have restricted access to the metal ion and this slows its rate of extrusion. Furthermore, the poor solubility of the chloride salt of the Co(II) complex in the presence of excess HCl limits this strategy. The solubility problem may be overcome using H_2SO_4 as the acid, as sulfate salts are generally more soluble. Alternatively, HBr as the strong acid will allow higher temperatures to be attained, which would ensure that the Co(II) complex remains in solution, such that extrusion has time to take place. Finally, stronger coordination ligands, such as CN^- , might remove the Co(II) ion from the N_6 -tetracosane cages.



Scheme 5.2: Metal ion extrusion from the sar cages.

More soluble cobalt N_6 -tetracosane cages are desired. The greater solubility for the lesser alkyl substituted $[\text{Pt}(\text{Me}_4\text{-}N_6\text{-tetracosanediimine})]\text{Cl}_4$ compared to $[\text{Pt}(\text{Et}_2\text{-Me}_6\text{-}N_6\text{-tetracosanediimine})]\text{Cl}_4$ was observed previously (Chapter 3.4) and similar behaviour is anticipated in the analogous $[\text{Co}(\text{Me}_4\text{-}N_6\text{-tetracosane})]\text{Cl}_n$ system ($n = 2,3$). Unfortunately, condensation reactions of $[\text{Co}(\text{tame})_2]^{3+}$ with acetaldehyde did not yield $[\text{Co}(\text{Me}_4\text{-}N_6\text{-tetracosanediimine})]^{3+}$ (or $[\text{Co}(\beta\text{Me}_5\text{-}N_6\text{-tricosane})]^{3+}$) in a recognisable quantity. Attempts to limit self condensation of the aldehydes and other side reactions by lowering the temperature and adding extra acetaldehyde during the reaction were unsuccessful. It may be necessary to limit further the concentration of acetaldehyde in solution. In the same way as availability of monomeric formaldehyde was limited, a polymeric source of acetaldehyde (metaldehyde) could be useful for slow release of monomeric acetaldehyde units *in situ*.

5.4.2. Properties of $[\text{Co}(\text{Et}_2\text{-Me}_6\text{-}N_6\text{-tetracosanediimine})]^{3+}$ and $[\text{Co}(\text{Et}_2\text{-Me}_6\text{-}N_6\text{-tetracosane})]^{3+}$

One of the aims in this work was to examine how the spectral, electrochemical and electron transfer properties of cobalt cage complexes were altered by increasing the size of the cage and also increasing by the rigidity of the ligand. These properties for $[\text{Co}(\text{Et}_2\text{-Me}_6\text{-}N_6\text{-tetracosanediimine})]^{3+}$ and $[\text{Co}(\text{Et}_2\text{-Me}_6\text{-}N_6\text{-tetracosane})]^{3+}$ were surprising in many respects. The following discussion compares these complexes with those of other Co(III) cage complexes, in particular, with the related large cages $[\text{Co}(\text{Me}_5\text{-}N_6\text{-tricosane})]^{3+}$ and its N_6 -triimine analogue, which have comparable Co(III)-N bond lengths.

(a) Electronic Spectroscopy

Both $[\text{Co}(\text{Et}_2\text{-Me}_6\text{-}N_6\text{-tetracosanediimine})]^{3+}$ and $[\text{Co}(\text{Et}_2\text{-Me}_6\text{-}N_6\text{-tetracosane})]^{3+}$ have a lower than typical energy for the absorption band arising from the $^1A_{1g}(\text{O}_h) \rightarrow ^1T_{1g}$ transition compared to other saturated CoN_6^{3+} chromophores. The energy of the band for the diimine complex is $\sim 750 \text{ cm}^{-1}$ higher than that for the saturated analogue. This is attributed to the slightly shorter Co(III)-N bond lengths and also the coordinated imines which exert an inherently stronger field on the metal ion than the saturated amines. This energy difference is likewise observed in the analogous spectra for the $[\text{Co}(\text{Me}_5\text{-}N_6\text{-tricosane})]^{3+}$ and $[\text{Co}(\text{Me}_5\text{-}N_6\text{-tricosanetriimine})]^{3+}$ complexes, where the energy of the band for the first spin allowed transition for the N_6 -triimine complex is 1990 cm^{-1} higher than for the saturated amine complex.^{10,23} The $^1A_{1g}(\text{O}_h) \rightarrow ^1T_{2g}$ band for both $[\text{Co}(\text{Et}_2\text{-Me}_6\text{-}N_6\text{-tetracosanediimine})]^{3+}$ and $[\text{Co}(\text{Et}_2\text{-Me}_6\text{-}N_6\text{-tetracosane})]^{3+}$ is obscured by an unusually intense charge transfer band.

Similar overlap of the second spin allowed transition band by the charge transfer band has been observed previously in the spectra of the (*S,S*) and *meso*-[Co(dppn)₃]³⁺ complexes⁴⁴ (dppn = 1,2-diphenyl-1,3-propanediamine). The red shift of the charge transfer band in the *N*₆-tetracosane complexes is consistent with the observed behaviour of [Co(Me₅-*N*₆-tricosane)]³⁺ and the sar complexes (Fig. 5.12) compared to acyclic Co(III) hexamine complexes

The spectrum of [Co(Et₂-Me₆-*N*₆-tetracosanediimine)]³⁺ at pH~11.5 is reminiscent of that for a tetragonally distorted complex. This distortion probably arises from the deprotonation of an amine proton leading to a short Co-N bond for the amido ion and a longer Co-N bond *trans* to it, as observed in the crystal structure of [Co((NO₂)₂sar-H)]²⁺.⁴⁵ This complex has a similar spectrum,⁴⁵ as does [Co(Me₅-*N*₆-tricosanetriimine)]³⁺ in basic solution,²³ although the band maxima for [Co((NO₂)₂sar-H)]²⁺ are blue shifted due to the stronger ligand field arising from the shorter Co(III)-N bond lengths inherent in the sar systems.

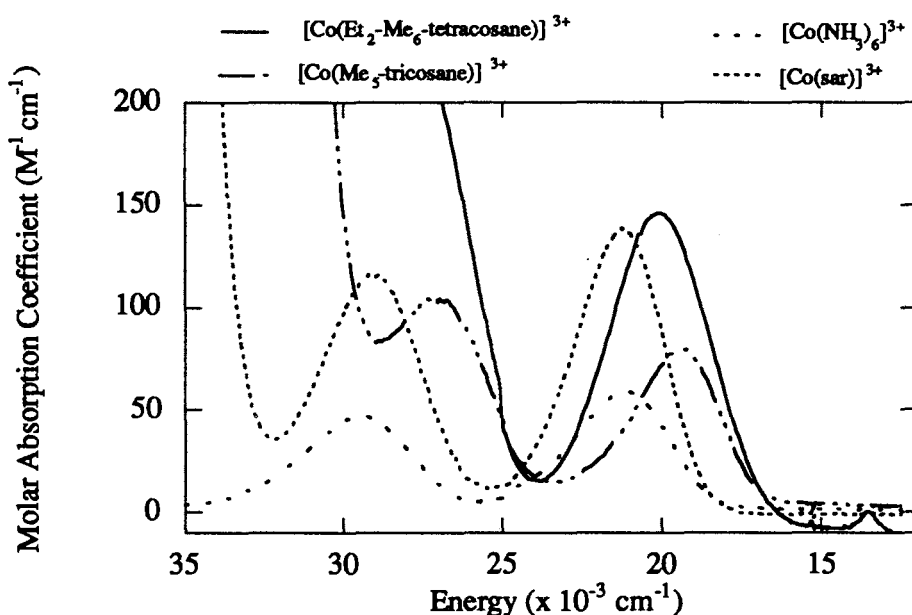


Figure 5.12: Absorption spectra of [Co(Et₂-Me₆-*N*₆-tetracosanediimine)]³⁺, [Co(Me₅-*N*₆-tricosane)]³⁺, [Co(sar)]³⁺ and [Co(NH₃)₆]³⁺ in water (pH~5.5)

Attempts to predict the energies of the first spin allowed transition for transition metal complexes have been made previously.^{12,46-51} A systematic study examining the effect of the types of distortion has been undertaken, namely, by trigonally twisting or elongating/compressing the CoN₆³⁺ chromophore.⁵⁰ However, this work indicates that only the correlation with the Co(III)-N bond with the energy of the ¹A_{1g}→¹T_{1g}(O_h) band is meaningful⁵⁰ (Fig. 5.13). The Co(III) complexes used in the correlation are

tabulated in Appendix G. They were selected on the basis that they had good crystal data ($R \leq 5\%$), were relatively symmetric and also possessed either all primary or all secondary amines, with the exception of *mer*-[Co(dpt)₂]³⁺ and [Co(*trans*-diammac)]³⁺ which contain both primary and secondary amines. The former complex was included as it is one of the few examples with longer than typical Co(III)-N bond lengths,⁵² while the latter complex was included as it has one of the shortest Co(III)-N bond lengths reported.³⁵ Unfortunately, the absorption spectrum of the complex with the shortest Co(III)-N bond lengths ([Co(C₆H₉N₃)₂](NO₃)₃, where Co(III)-N_{av} = 1.92 Å)⁵³ has not been reported, so this complex is excluded from the correlation. At the extremes of the Co(III)-N range, [Co(*trans*-diammac)]³⁺ has one of the strongest ligand fields²⁹ whereas [Co(Me₅-N₆-tricosane)]³⁺ has one of the weakest ligand fields,⁴ and is indicative of its long Co(III)-N bond lengths. The [Co(Et₂-Me₆-N₆-tetracosane)]³⁺ complex strengthens this correlation, as this complex lies in a region where points are scarce — its longer than typical Co(III)-N bond lengths result in the anticipated weakened ligand field.

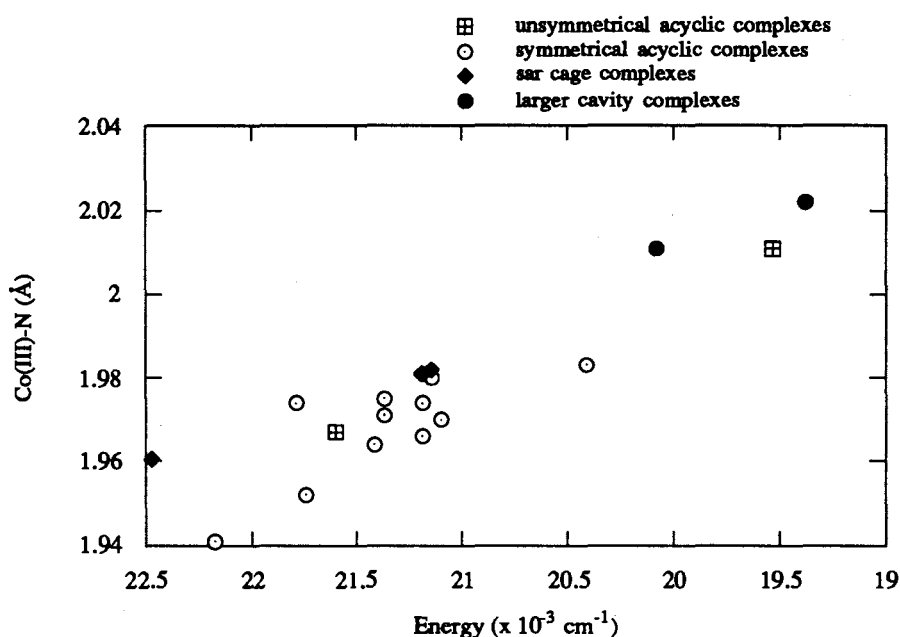


Figure 5.13: Correlation between the energy of the ${}^1A_{1g} \rightarrow {}^1T_{1g}(O_h)$ transition and the Co(III)-N bond lengths for a number of Co(III) hexaamine complexes (correlation coefficient = 0.93).

(b) *Electrochemistry*

The reduction potential for the [Co(Et₂-Me₆-N₆-tetracosane)]^{3+/2+} couple is more negative than the [Co(Me₅-N₆-tricosane)]^{3+/2+} couple. This may be attributed to the greater relief of steric strain upon reduction from the Co(III) to the Co(II) state for the [Co(Et₂-Me₆-N₆-tetracosane)]^{3+/2+} couple, which provides a greater driving force for the

reduction. These complexes crudely fit the observed relation between $\{U(\text{III})-U(\text{II})\}$ and the $\text{CoN}_6^{3+/2+}$ reduction potential (Fig. 5.14). The difference in the strain energies ($\{U(\text{III})-U(\text{II})\}$) between the Co(III) and Co(II) states for the $[\text{Co}(\text{Et}_2\text{-Me}_6\text{-N}_6\text{-tetracosane})]^{3+/2+}$ and $[\text{Co}(\text{Me}_5\text{-N}_6\text{-tricosane})]^{3+/2+}$ couples are listed in Appendix G, as well as those for some related $\text{CoN}_6^{3+/2+}$ couples.^{12,22} Complexes which have larger $\{U(\text{III})-U(\text{II})\}$ values than that for the strain free $[\text{Co}(\text{NH}_3)_3]^{3+/2+}$ couple are thought to stabilise their Co(II) state better than its Co(III) state, relative to the $[\text{Co}(\text{NH}_3)_3]^{3+/2+}$ couple. These systems are $[\text{Co}(\text{tn})_3]^{3+/2+}$, $[\text{Co}(\text{tacn})_2]^{3+/2+}$, *mer*- $[\text{Co}(\text{dien})_2]^{3+/2+}$, $[\text{Co}(\text{sep})]^{3+/2+}$, *mer*- $[\text{Co}(\text{dpt})]^{3+/2+}$, $[\text{Co}(\text{Et}_2\text{-Me}_6\text{-N}_6\text{-tetracosane})]^{3+/2+}$ and $[\text{Co}(\text{Me}_5\text{-N}_6\text{-tricosane})]^{3+/2+}$ and the implication follows that their reduction potentials should be more positive than that for the $[\text{Co}(\text{NH}_3)_3]^{3+/2+}$ couple. This is clearly not the case for the $[\text{Co}(\text{sep})]^{3+/2+}$, $[\text{Co}(\text{tacn})_2]^{3+/2+}$, *mer*- $[\text{Co}(\text{dpt})]^{3+/2+}$ and $[\text{Co}(\text{Et}_2\text{-Me}_6\text{-N}_6\text{-tetracosane})]^{3+/2+}$ couples. However, the crude correlation might be improved by scrutinising the strain energy differences for all of these couples. The force fields used for calculating the energies of the both the Co(III) and Co(II) states are currently being examined for their deficiencies.¹⁹ In addition, calculations of this type do not include the solvent contributions to the strain energies, and these play an important role in the redox energetics of such complexes.⁵⁴

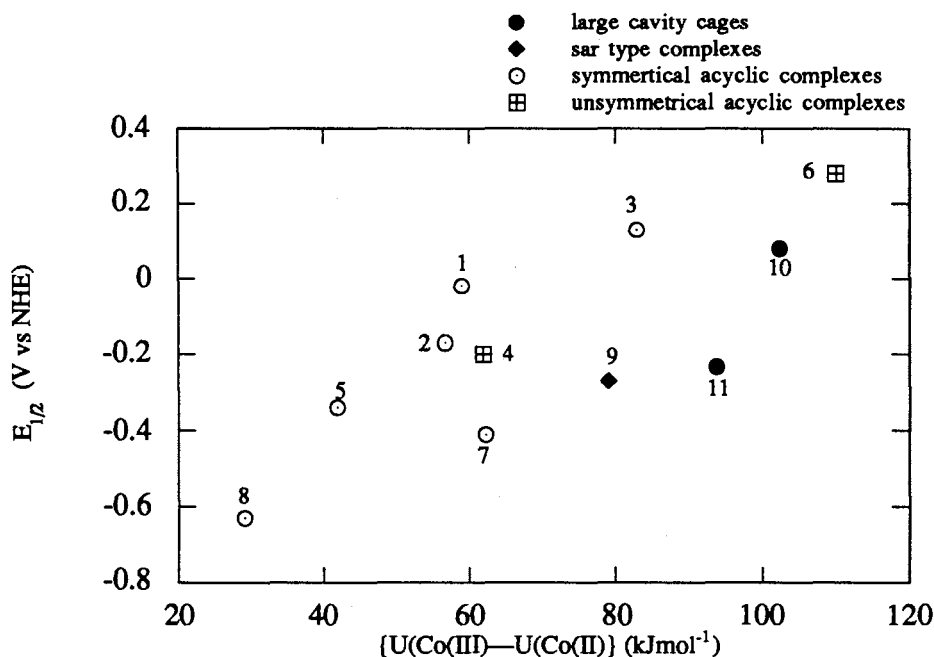


Figure 5.14: Plot of Co(III)/Co(II) reduction potential and the difference in strain energies for a number of $\text{CoN}_6^{3+/2+}$ complexes (correlation coefficient = 0.82, The complexes used in the correlation are tabulated in Appendix G).

I. Effect of Imines Incorporated into the Cage Framework

The more positive reduction potential observed for the $[\text{Co}(\text{Et}_2\text{-Me}_6\text{-N}_6\text{-tetracosanediimine})]^{3+/2+}$ couple than that of its saturated analogue may be attributed to both electronic and strain factors. Imines in the ligand framework have the potential to withdraw electron density from the metal centre via back bonding, which stabilises the Co(II) state. This also has been realised in some $\text{RuN}_6^{3+/2+}$ cage systems.⁵⁵ On the other hand, the reduction potential for the $[\text{Co}(\text{Et}_2\text{-Me}_6\text{-N}_6\text{-tetracosanediimine})]^{3+/2+}$ couple is more positive than the $[\text{Co}(\text{Me}_5\text{-N}_6\text{-tricosanetriimine})]^{3+/2+}$ couple, even though the latter complex contains more coordinated imines. Incorporation of imines in the ligand framework in the N_6 -tricosanetriimine system may reduce its flexibility, so diminishing the ability of the ligand to expand to accommodate the larger Co(II) ion. This has also been exemplified in the $[\text{Co}(\text{Mesar})]^{3+/2+}$ (Fig. 5.15(a)) and the $[\text{Co}(\text{Mesarimine})]^{3+/2+}$ couples (Fig. 5.15(b)), whose reduction potentials are essentially the same ($E_{1/2} = -0.41^6$ and -0.47^{10} V vs NHE, respectively). The means by which coordinated imines introduce strain into the cage complexes has not yet been assessed, as force fields for unsaturated $\text{CoN}_6^{3+/2+}$ systems have not yet been developed.

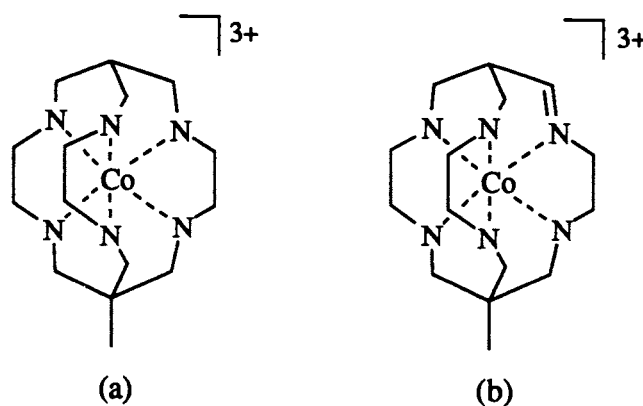


Figure 5.15: (a) $[\text{Co}(\text{Mesar})]^{3+}$ and (b) $[\text{Co}(\text{Mesarimine})]^{3+}$ (amine protons have been omitted for clarity),

(c) Correlation between Spectroscopic and Electrochemical Properties

A correlation between the energy of the ${}^1\text{A}_{1g} \rightarrow {}^1\text{T}_{1g}(\text{O}_h)$ band for the CoN_6^{3+} chromophore and the $\text{CoN}_6^{3+/2+}$ reduction potential has been claimed.^{31,48} This correlation is depicted in Fig. 5.16 for a range of acyclic and cage complexes with the $\text{CoN}_6^{3+/2+}$ chromophore. The complexes used in this correlation are listed in Appendix G. Of the sar complexes, only the unsubstituted cages (viz: $[\text{Co}(\text{sar})]^{3+/2+}$ and $[\text{Co}(\text{Me}_2\text{sar})]^{3+/2+}$) were included, as it would not be meaningful to compare the properties of the substituted cages with those of the unsubstituted acyclic analogues. Although the points for the encapsulated complexes appear to lie on a different line from

the acyclic complexes, the gradient seems to be roughly the same. It has been noted however, that the basis of this correlation is not clear, as the reduction potential depends on the properties of both members of the redox couple and not just on those of the Co(III) state.^{12,31,56} In these systems, such a correlation could arise if the energetics of the reduction are dominated by those of the Co(III) state. This might be achieved if the solvent contributions are more important in the Co(III) state than in the Co(II) state. An examination of the dependency of the $\text{CoN}_6^{3+/2+}$ reduction potential with different solvents might illuminate this aspect.

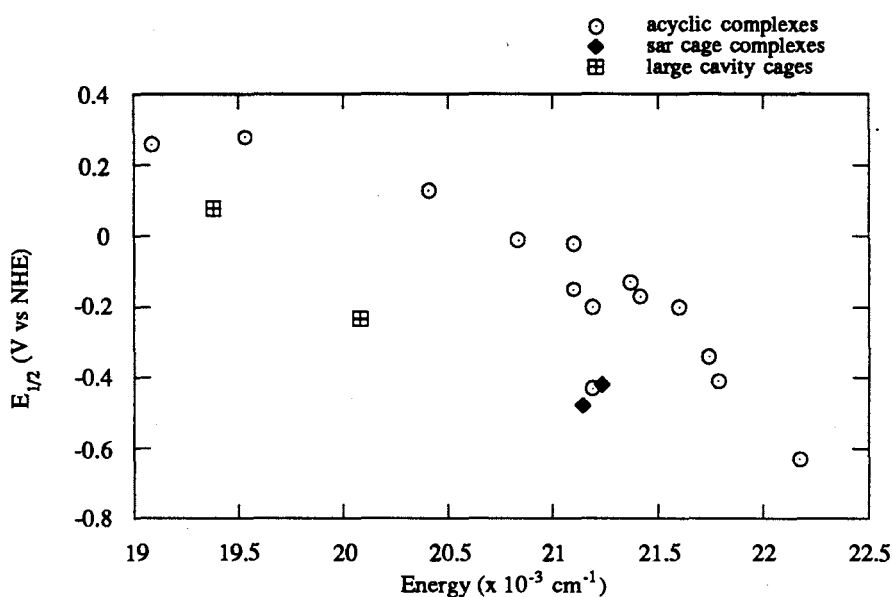


Figure 5.16: Plot of Co(III)/Co(II) reduction potential and energy of the first spin allowed transition for a number of Co(III) hexamine complexes (The complexes used in this correlation are tabulated in Appendix G).

(d) Self Exchange Rate Constant

The deduced self exchange rate constant (k_{ex}) for the $[\text{Co}(\text{Et}_2\text{-Me}_6\text{-N}_6\text{-tetracosane})]^{3+/2+}$ couple is one of the largest yet reported for a saturated $\text{CoN}_6^{3+/2+}$ couple. It is 10^2 times greater than those of the $\text{CoN}_6^{3+/2}$ sar¹⁴ and N_6 -tricosane⁴ type cage complexes and 10^{7-9} times faster than those of the non encapsulated $\text{CoN}_6^{3+/2+}$ complexes (Table 5.3). It is not clear why the electron transfer rate is significantly faster for the $[\text{Co}(\text{Et}_2\text{-Me}_6\text{-N}_6\text{-tetracosane})]^{3+/2+}$ couple compared with the other $\text{CoN}_6^{3+/2+}$ cage couples. One reason may be that both the Co(II) and Co(III) states are more destabilised compared to the other hexamine cage complexes. Comparing the

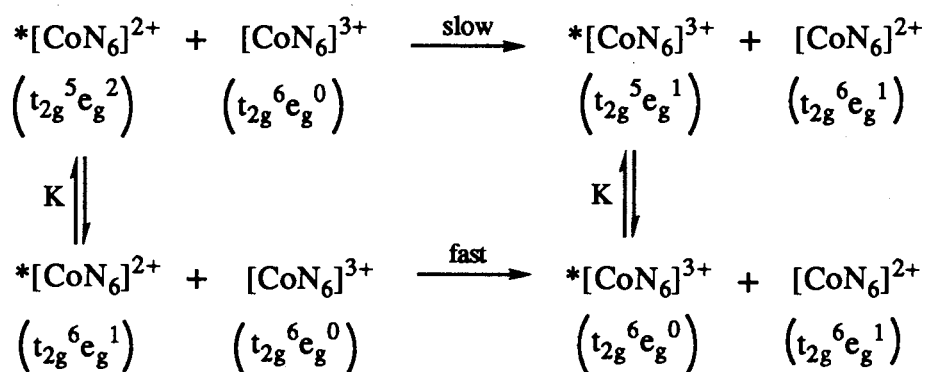
geometries about the metal ion provides a rough estimate of the relative strain in the complexes. The steric constraints of the N_6 -tetracosane ligand dominate the overall stereochemistry so that the metal ion is forced to adopt the unexpected tetragonally compressed geometry, as observed in the crystal structure of the Co(III) complex. The symmetry about the Co(II) is not yet clear, as crystals of this complex have not yet been grown for an X-ray crystallographic analysis. However, the energy minimised structure for $[\text{Co}(\text{Et}_2\text{-Me}_6\text{-}N_6\text{-tetracosane})]^{2+}$ predicts that the $\text{Co}N_6^{2+}$ chromophore is also tetragonally compressed.²² Three different types of Co(II)-N bonds are predicted and are listed in Table 5.5 (along with the Co(II)-N bond lengths for related complexes). It was surprising that there is a substantial difference between the shortest and longest Co(II)-N bonds of 0.1 Å. The tetragonal distortion in both states probably increases their strains and thereby the activation barrier for electron transfer is reduced. Similar tetragonal distortion has been observed in the crystal structure of the $[\text{Co}(\textit{trans}\text{-diammac})]^{3+}$ complex³⁵ and has likewise been predicted for its Co(II) analogue.²² The $[\text{Co}(\textit{trans}\text{-diammac})]^{3+/2+}$ couple has been argued to undergo fast electron transfer, but the self exchange rate constant was deduced by a very indirect route.³⁵ In contrast, crystal structures of $\text{Co}N_6^{2+}$ sar and analogous acyclic complexes have essentially octahedral configurations. In particular, the Co(II) ion in $[\text{Co}(\text{Me}_5\text{-}N_6\text{-tricosane})]^{2+}$ is also predicted to be approximately octahedral,²² and the electron transfer rate for this complex is similar to that for the $\text{Co}N_6^{3+/2+}$ sar complexes.

Table 5.5: Co(III)-N and Co(II) bond lengths for some hexamine complexes

Complex	Co(III)-N average (Å)	Co(II)-N average (Å)
$[\text{Co}(\text{NH}_3)_6]^{3+}$	$1.960(6) \times 6^{57}$	2.166×6^{32}
$[\text{Co}(\text{en})_3]^{3+}$	$1.964(3) \times 6^{58}$	2.160×6^{11}
$[\text{Co}(\text{Metacn})_2]^{3+}$	$1.974(5) \times 6^{33}$	$2.158 \times 6^{59}\text{¶}$
$[\text{Co}(\textit{trans}\text{-diammac})]^{3+35}$	$1.937(2) \times 4$ $1.946(2) \times 2$	2.097×4 $2.136 \times 2^{\S}$
$[\text{Co}(\text{NH}_3)_2\text{sar}]^{5+}$	1.978×6^{36}	$2.179 \times 6^{\S}$
$[\text{Co}(\text{sep})]^{3+}$	$1.981(2) \times 6^9$	2.164×6^8
$[\text{Co}(\text{Me}_5\text{-}N_6\text{-tricosane})]^{3+}$	$2.010(4) \times 3$ $2.032(4) \times 3^4$	2.183×3 $2.172 \times 3^{\S}$
$[\text{Co}(\text{Et}_2\text{-Me}_6\text{-}N_6\text{-tetracosane})]^{3+}$	$2.030(2) \times 4$ $1.974(2) \times 2$	2.208×2 2.104×2 $2.188 \times 2^{\S}$

¶ Value is for $[\text{Co}(\text{tacn})_2]^{2+}$; § Co(II)-N bond lengths predicted using molecular mechanics using published force fields.²²

An alternative explanation for the fast self exchange rates observed for the $\text{CoN}_6^{3+/2+}$ sar and N_6 -tricosane couples may arise from a more favourable high spin-low spin equilibrium for the Co(II) ion.⁸ Since the expression for the self exchange rate constant contains a term first order in $[\text{Co(II)}]$, an increase in the concentration of the low spin configuration for Co(II) may increase the rate of electron transfer (Scheme 5.3).⁶⁰ This argument has been rejected previously on the grounds that the absorption spectra and magnetic properties of the Co(II) complexes of both the CoN_6^{2+} sar cages and its acyclic analogues are similar,⁸ where the Co(II) ion is in the high spin state. Although the essentially colourless $[\text{Co}(\text{Et}_2\text{-Me}_6\text{-}N_6\text{-tetracosane})]\text{Cl}_2$ precipitate isolated from the attempted extrusion reactions implies that the configuration of the Co(II) ion is predominantly high spin, spectral changes would not be detected if only 1% of the low spin configuration were present. The low spin state for the Co(II) ion may be relatively more accessible if the tetragonal distortion predicted for the $[\text{Co}(\text{Et}_2\text{-Me}_6\text{-}N_6\text{-tetracosane})]^{2+}$ state is realised. It is anticipated that the self exchange rate constant for the low-spin Co(II) / low spin Co(III) reaction would be comparable to that observed for cage couples with high field donor atoms which enforce the low spin configuration in the Co(II) state (such as in the N_3S_3 and S_6 sar cages, $k_{\text{ex}} \sim 10^4 \text{ M}^{-1}\text{s}^{-1}$).⁴⁰ The 10^2 fold increase in the rate constant observed for the $[\text{Co}(\text{Et}_2\text{-Me}_6\text{-}N_6\text{-tetracosane})]^{3+/2+}$ couple compared to the sar analogues is therefore not unreasonable.



Scheme 5.3: High spin-low spin equilibrium for self exchange between Co(III) and *Co(II).

The spectral and redox properties of $[\text{Co}(\text{Et}_2\text{-Me}_6\text{-}N_6\text{-tetracosane})]^{3+}$ are consistent with other Co(III) hexaamine complexes with similar Co(III)-N bond lengths. However, why its large self exchange rate constant is so large needs further exploration. Examining the spectral properties of the Co(II) complex and its X-ray crystallographic analysis may clarify this behaviour. The Co(II) complex is stable in an inert atmosphere and crystals should be relatively easy to grow. The electron transfer rates for a range of other $\text{CoN}_6^{3+/2+}$ complexes whose metal ions are not in octahedral fields should be inspected further. Examples include the $[\text{Co}(\textit{trans}\text{-diammac})]^{3+/2+}$, unsubstituted $[\text{Co}(\textit{absar})]^{3+/2+}$ and $\textit{trans}\text{-}[\text{Co}(\text{NH}_2)_2(\text{cyclam})]^{3+/2+}$ couples.

5.4.3. References

- (1) Sargeson, A. M. *Pure and Appl. Chem.* **1986**, *58*, 1551, and references therein.
- (2) Sargeson, A. M. *Pure and Appl. Chem.* **1984**, *56*, 1603, and references therein.
- (3) Geue, R. J.; McDonnell, M. B.; Mau, A. W. H.; Sargeson, A. M.; Willis, A. *C. J. Chem. Soc., Chem. Commun.* **1994**, 667.
- (4) Geue, R. J.; Höhn, A.; Ralph, S. F.; Sargeson, A. M. *J. Chem. Soc., Chem. Commun.* **1994**, 1513.
- (5) Clark, I. J.; Geue, R. J.; Engelhardt, L. M.; Harrowfield, J. M.; Sargeson, A. M.; White, A. H. *Aust. J. Chem.* **1993**, *46*, 1485.
- (6) Bond, A. M.; Lawrance, G. A.; Lay, P. A.; Sargeson, A. M. *Inorg. Chem.* **1983**, *22*, 2010.
- (7) Hammershøi, A.; Lawrance, G. A.; Sargeson, A. M. *Aust. J. Chem.* **1986**, *39*, 2183.
- (8) Creaser, I. I.; Geue, R. J.; Harrowfield, J. M.; Herlt, A. J.; Sargeson, A. M.; Snow, M. R.; Springborg, J. *J. Am. Chem. Soc.* **1982**, *104*, 6016, and references therein.
- (9) Dubicki, L.; Ferguson, J.; Geue, R. J.; Sargeson, A. M. *Chem. Phys. Lett.* **1980**, *74*, 393, and references therein.
- (10) Höhn, A., Unpublished results. **1989**.
- (11) Geselowitz, D. *Inorg. Chem.* **1981**, *20*, 4457.
- (12) Hambley, T. W. *Inorg. Chem.* **1988**, *27*, 2496, and references therein.
- (13) Dwyer, F. P.; Sargeson, A. M. *J. Phys. Chem.* **1961**, *65*, 1892.
- (14) Creaser, I. I.; Sargeson, A. M.; Zanella, A. W. *Inorg. Chem.* **1983**, *22*, 4022.
- (15) Geue, R. J.; Pizer, R.; Sargeson, A. M. In *183rd ACS National Meeting*; Las Vegas, 1982.
- (16) Hendry, A. J. Ph.D. Thesis, Australian National University, 1986.

- (17) Hendry, A. J.; Naidoo, K. J.; Thornton, D. A. *J. Chem. Soc., Chem. Commun.* **1989**, 998.
- (18) Comba, P. *Inorg. Chem.* **1989**, *28*, 426.
- (19) Bygott, A., Work in progress. **1990-1994**.
- (20) Geue, R. J.; Hendry, A. J.; Sargeson, A. M. *J. Chem. Soc., Chem. Commun.* **1989**, 1646.
- (21) Bond, A. M.; Hambley, T. W.; Mann, D. R.; Snow, M. R. *Inorg. Chem.* **1987**, *26*, 2257, and references therein.
- (22) Bernhardt, P. V., Unpublished results **1993**.
- (23) Ralph, S. F., Personal communication. **1990-1993**.
- (24) Creaser, I. I.; Harrowfield, J. M.; Lawrance, G. A.; Mulac, W.; Sangster, D.; Sargeson, A. M.; Schmidt, K.; Sullivan, J. C. *J. Coord. Chem.* **1991**, *23*, 389.
- (25) Creaser, I. I., Unpublished results.
- (26) Anderson, P. A.; Creaser, I. I.; Dean, C.; Harrowfield, J. M.; Horn, E.; Martin, L. L.; Sargeson, A. M.; Snow, M. R.; Tiekink, E. R. T. *Aust. J. Chem.* **1993**, *46*, 449, and references therein.
- (27) Hambley, T. W.; Hawkins, C. J.; Palmer, J. A.; Snow, M. R. *Aust. J. Chem.* **1981**, *551*, 33.
- (28) Günter, H. *NMR Spectroscopy, An Introduction*; John Wiley and Sons: New York, 1973, Chapter 4, and references therein.
- (29) Bernhardt, P. V.; Comba, P.; Hambley, T. W. *Inorg. Chem.* **1993**, *32*, 2804.
- (30) Bottomley, G. A.; Clark, I. J.; Creaser, I. I.; Engelhardt, L. M.; Geue, R. J.; Hagen, K. S.; Harrowfield, J. M.; Lawrance, G. A.; Lay, P. A.; Sargeson, A. M.; See, A. J.; Skelton, B. W.; White, A. H.; Wilner, F. R. *Aust. J. Chem.* **1994**, *47*, 143, and references therein.
- (31) Hendry, P.; Ludi, A. *Advances in Inorganic Chemistry*, **1990**, *35*, 117, and references therein.
- (32) Freeman, H. C. *Inorg. Chem.* **1991**, *30*, 3499.
- (33) Mikami, M.; R., K.; Konno, M.; Saito, Y. *Acta Crystallog.* **1977**, *B33*, 1485.

- (34) Geue, R. J.; Snow, M. R. *Inorg. Chem.* **1977**, *16*, 231.
- (35) Bernhardt, P. V.; Lawrance, G. A.; Hambley, T. W. *J. Chem. Soc., Dalton Trans.* **1989**, 1059, and references therein.
- (36) Horn, E.; Snow, M. R.; Tiekink, E. R. T. **1993**, Unpublished results.
- (37) Creaser, I. I.; Harrowfield, J. M.; Herlt, A. J.; Sargeson, A. M.; Geue, R. J.; Snow, M. R. *J. Am. Chem. Soc.* **1977**, *99*, 3181.
- (38) Marcus, R. A. *Discuss. Faraday. Soc.* **1960**, *29*, 21.
- (39) Marcus, R. A. *Annu. Rev. Phys. Chem.* **1964**, *15*, 155.
- (40) Osvath, P.; Sargeson, A. M.; Skelton, B. W.; White, A. H. *J. Chem. Soc., Chem. Commun.* **1991**, 1035, and references therein.
- (41) Adrianova, O. N.; Fedotova, T. N. *Russ. J. Inorg. Chem.* **1970**, *15*, 1272.
- (42) Adrianova, O. N.; Fedotova, T. N. *Russ. J. Inorg. Chem.*, **1980**, *25*, 105.
- (43) Kukushkin, Y. N.; Drokina, Z. V.; Varshaskii, Y. S.; Ivannikova, N. V. *Russ. J. Inorg. Chem.* **1968**, *13*, 1693, and references therein.
- (44) Arakawa, S.; Kashiwabara, K.; Fujita, J.; Saito, Y. *Bull. Chem. Soc., Jpn.* **1977**, *50*, 2108.
- (45) Geue, R. J.; Hambley, T. W.; Harrowfield, J. M.; Sargeson, A. M.; Snow, M. R. *J. Am. Chem. Soc.* **1984**, *106*, 5478.
- (46) Ballhausen, C. J. *Introduction to Ligand Field Theory*; McGraw-Hill Book Co.: New York, N.Y., 1962.
- (47) Bernhardt, P. V.; Comba, P. *Inorg. Chem.* **1993**, *32*, 2798, and references therein.
- (48) Wieghardt, K.; Schimdt, W.; Herrmann, W.; Küppers, H.-J. *Inorg. Chem.* **1983**, *22*, 2953, and references therein.
- (49) Ventur, D.; Wieghardt, K.; Nuber, B.; Weiss, J. Z. *Anorg. Allg. Chem.* **1987**, *551*, 33.
- (50) Brorson, M., Unpublished results **1994**.

- (51) Lever, A. B. P. *Inorganic Electronic Spectroscopy*; 2nd ed.; Elsevier Science Publishers: New York, 1984.
- (52) Hambley, T. W.; Searle, G. H.; Snow, M. R. *Aust. J. Chem.* **1982**, *35*, 1285.
- (53) Schwesinger, R.; Piontek, K.; Littke, W.; Schweikert, O.; Prinzbach, H.; Krüger, C.; Tsay, Y.-H. *Tet. Lett.* **1982**, *23*, 2427.
- (54) Lay, P. A. *J. Phys. Chem.* **1986**, *90*, 878.
- (55) Bull, D. B. Ph.D. Thesis, Australian National University, 1991.
- (56) Lintvedt, R. L.; Fenton, D. E. *Inorg. Chem.* **1980**, *19*, 569.
- (57) Figgis, B. N.; Skelton, B. W.; White, A. H. *Aust. J. Chem.* **1979**, *32*, 417.
- (58) Templeton, D. H.; Zalkin, A.; Ruben, H. W.; Templeton, L. K. *Acta Crystallogr.* **1979**, *B35*, 1608.
- (59) Küppers, H. J.; Neves, A.; Pomp, C.; Venur, D.; Wieghardt, K.; Nuber, B.; Weiss, J. *Inorg. Chem.* **1986**, *25*, 2400, and references therein.
- (60) Basolo, F.; Pearson, R. *Mechanisms of Inorganic Reactions*; 2nd ed.; John Wiley and Sons: New York, 1967.

Chapter 6

Synthesis and Properties of Expanded Chromium(III) Cage Complexes

6.1. Introduction

6.1.1. General

When electromagnetic radiation is absorbed by a photoactive molecule, the distribution of electron density within the molecule is altered such that the reactivity, spectral and thermodynamic properties of the excited state may be dramatically different from those of the ground state. The molecule returns to its resting configuration in a number of ways, for example, by emitting a photon, transferring energy to other systems, or reacting to form a new species. How the structure of the species influences the relative rates of relaxation of excited-states has received much attention, particularly with a view to understanding and controlling photochemically induced reactions. The Cr(III) ion has been extensively studied as a probe for such issues.¹⁻¹² Its excited-state processes are profoundly influenced by the nature of the donor atom and by the geometry, electronic structure and rigidity of the complexing ligand.^{2,11} This study addresses the excited state behaviour of a range of Cr(III) saturated hexamine complexes,[†] whose geometries are approximately octahedral.[§] Particular attention is given to the effect of encapsulation of the Cr(III) ion with the sarcophagine and *N*₆-tricosane ligands.

6.1.2. General Spectroscopy for Cr(III) Hexamine Complexes

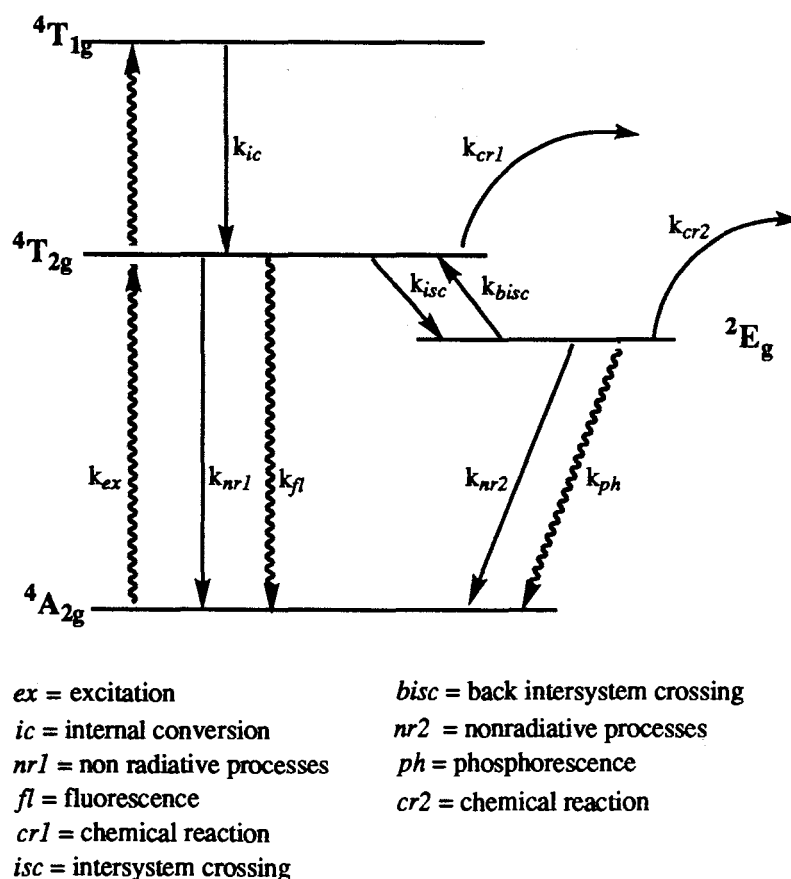
For a simple transition metal ion complex, $MX_6^{n\pm}$, in a strictly octahedral ligand field, d-d transitions are electric dipole forbidden,¹⁴ but they may have a modest intensity arising from magnetic dipole coupling and static or dynamic deformation of the octahedral field.^{2,6} Static mechanisms refer to the effect of the ligand field symmetry about the metal ion. The average field exerted by the donor atoms on the metal ion over time may not be purely octahedral but for example, trigonally distorted. As a result, the transition becomes more probable due to the mixing of states in the diminished symmetry. Dynamic mechanisms increase the probability of the transition by coupling the vibrational modes of the ligand with the electronic transition moment. Vibrational fine structure in the band may sometimes be observed. The spin selection rule also influences the probability of a transition and the band structure. Transitions involving

[†] The term hexamine refers complexes with saturated nitrogen donors only, unless otherwise specified.

[§] Although the site symmetry of the Cr(III) complex may be less than O_h , the microsymmetry of the CrN_6^{3+} chromophore is approximately octahedral.¹³ Therefore, for simplicity, the notation used in this thesis describing the electronic transitions is based on the complexes having octahedral symmetry.

changes in spin are formally prohibited, but these may be observed due to magnetic dipole and spin-orbit coupling.^{2,14}

The relative energy levels of the excited states for a generic Cr(III) hexaamine complex in an octahedral field are depicted in Scheme 6.1. Three spin-allowed transitions are possible in the UV/visible region and these arise from the ground state ${}^4A_{2g}(\text{O}_h) \rightarrow {}^4T_{2g}$ (from 4F), ${}^4T_{1g}$ (from 4F) and ${}^4T_{1g}$ (from 4P) transitions. The former two transitions typically occur at about 460 and 350 nm respectively, while the latter is usually obscured by a charge transfer band in the UV region.^{2,14} Transitions from the ground state (${}^4A_{2g}(\text{O}_h)$) to the upper quartet states (${}^4T_{2g}$ and ${}^4T_{1g}$) occur from the non-bonding t_{2g}^3 configuration to antibonding orbitals with the configurations $t_{2g}^2e_g^1$. The equilibrium geometries of these quartet states are distorted as a consequence of the occupation of the antibonding orbitals.^{1,15} These bands are rather broad as they are sensitive to small fluctuations in ligand field strength,^{14,16} and vibronic and spin-orbit coupling.¹⁴



Scheme 6.1: Relative energy levels and routes for relaxation for a generic CrN_6^{3+} species in an octahedral field.

Three spin-forbidden transitions are possible, arising from the ${}^4A_{2g}(O_h) \rightarrow {}^2E_g$ (from 2G), ${}^2T_{1g}$ (from 2G) and ${}^2T_{2g}$ (from 2G) transitions. For octahedral Cr(III) hexaamine complexes, the ${}^4A_{2g}(O_h) \rightarrow {}^2E_g$ (2G), ${}^2T_{1g}$ (2G) transitions frequently have similar energies, occurring in the region 640-700 nm.¹ The ${}^4A_{2g}(O_h) \rightarrow {}^2T_{2g}$ transition is often obscured by that of the ${}^4A_{2g}(O_h) \rightarrow {}^4T_{2g}$.¹ The ${}^4A_{2g}(O_h) \rightarrow {}^2E_g$ transition involves a pairing of spin within the non bonding t_{2g}^3 orbitals and is relatively independent of the ligand field strength.^{2,6} The equilibrium geometry of the 2E_g state should be very similar to that of the ground state, since little configurational change is required.^{6,17} The 0-0 transition is formally forbidden, but it may be observed as a result of magnetic and spin-orbit coupling with the ${}^4T_{2g}$ state and vibrational coupling.^{6,14,17,18} Most of the intensity is distributed in the vibronic side bands and the 0-0 transition itself is weak. As the field becomes less octahedral due to static mechanisms, the 0-0 transition becomes more probable and its intensity relative to that of the vibrational bands increases.¹

The processes arising from excitation of a generic Cr(III) hexaamine ion with octahedral micro symmetry are depicted in Scheme 6.1. The complex absorbs a photon of suitable energy which results in the promotion of an electron into the spin-allowed quartet states, ${}^4T_{2g}$ or ${}^4T_{1g}$, with a rate constant, $k_{ex} \sim 10^{15} \text{ s}^{-1}$.¹⁹ Internal conversion from the upper quartet states to the lowest lying vibrational level of the lowest electronic state (${}^4T_{2g}$) is very rapid,²⁰ its rate constant has been estimated as $k_{ic} \sim 10^{11} \text{ s}^{-1}$.²¹ From the ${}^4T_{2g}$ state, the species may release its energy either by reacting to form a new chemical species, with a rate constant k_{cr1} , by transmitting its energy into the ligand, the surrounding solvent system, or a quenching molecule, with a rate constant k_{nr1} , or by emitting a photon (fluorescence) with a rate constant k_f . However, for Cr(III) hexaamine complexes, fluorescence has not been observed,^{1,11} so k_f is considered to be negligible. Processes associated with relaxation of the ${}^4T_{2g}$ state are fast; the lifetime of this state has been estimated as $<10^{-12} \text{ s}$.²² Alternatively, the electron may cross into the 2E_g state (referred to as intersystem crossing) and for Cr(III) hexaamine complexes for example, this process is generally efficient ($k_{isc} > 10^7 \text{ s}^{-1}$).^{1,21,23-25} The 2E_g state relaxes to the ground state, with mechanisms similar to those described for the ${}^4T_{2g}$ state. It may relax through vibrational excitation of the immediate environment (k_{nr2}). Important non-radiative mechanisms for this process include coupling of skeletal vibrational modes and high frequency N-H and C-H stretching modes with the electronic transition moment.^{1,26,27} The excited state may deactivate by crossing back to the upper ${}^4T_{2g}$ state if the upper vibrational levels of the 2E_g potential surface overlap sufficiently with the ${}^4T_{2g}$ surface. Clearly, back intersystem crossing is sensitive to the energy difference between the two states.^{1,4,5,9-11,28} It may be possible that the 2E_g state reacts to form a new complex (k_{cr2}). For many Cr(III) hexaamine complexes, ligand dissociation has been claimed to be an important contribution to the k_{cr2}

term,^{21,28} however, there is some doubt about this possibility.²⁹⁻³⁴ Another proposed pathway involves the formation of a transient ground state intermediate of higher coordination number. The rate constant for this mechanism, however, is incorporated in the k_{cr2} term.^{8,35} Lastly, the excited 2E_g state may deactivate by emitting a photon (phosphorescence, $k_{ph} \sim 10^3-10^9 \text{ s}^{-1}$).²¹ The overall rate constant for depletion of the 2E_g state may therefore be expressed by k_i .^{6,9,21,36,37}

$$k_i = k_{bisc} + k_{cr2} + k_{nr2} + k_{ph} \quad (6.1)$$

All upper states are capable of emitting a photon, but emission generally occurs from the lowest lying excited state,^{1,11,20,38} as internal conversion rates are much faster than radiative relaxation rates.^{20,39} For Cr(III) hexaamine complexes, emission takes place from the 2E_g state and the relative rates of radiative and competing relaxation pathways determine the lifetime of the excited state. The lifetime (τ) of the excited state is related to the inverse of the sum of all the rate constants, k_i , of the processes which deplete the population of the 2E_g state.

$$\tau = \frac{1}{\sum_i k_i} \quad (6.2)$$

The lifetime of the 2E_g state is therefore dependent on the nature of the ligand, which governs the magnitude of the rate constants. The manner in which the ligand structure can influence the spectroscopic processes is demonstrated by comparing the Cr(III) cage complexes with the nonencapsulated Cr(III) hexaamine analogues. The spectral properties of sar Cr(III) complexes compared to nonencapsulated analogues were unexpected.^{7,40}

(a) The lifetimes of the 2E_g state of the $[\text{Cr}(\text{X}_2\text{sar})]^{3+}$ complexes ($\text{X}=\text{H}, \text{NH}_2, \text{NO}_2, \text{Cl}$) are all $<10 \text{ ns}$ at 293 K,^{7,40,41} whereas the 2E_g state lifetime for the nonencapsulated analogue, $[\text{Cr}(\text{en})_3]^{3+}$, is $1.85 \mu\text{s}$.³¹ Table 6.1 lists the 2E_g state lifetimes of analogous Cr(III) hexaamine complexes.

Table 6.1: 2E_g state lifetimes of some Cr(III) hexaamine complexes at 298 and 77 K.

Complex	77 τ (μs)	298 τ (μs)
$[\text{Cr}(\text{NH}_3)_6]^{3+}$	70 ⁴²	2.2 ³¹
$[\text{Cr}(\text{en})_3]^{3+}$	120 ⁴²	1.85 ³¹
$[\text{Cr}(\text{tn})_3]^{3+}$	133 ⁴²	3.1 ⁴³
$[\text{Cr}(\text{sen})]^{3+}$ ⁴⁴	171	0.01
$[\text{Cr}((\text{NH}_2)_2\text{sar})]^{3+}$ ^{7,40}	65	$<10 \text{ ns}$
$[\text{Cr}(\text{sar})]^{3+}$ ^{7,40}	60	$<10 \text{ ns}$

(b) The temperature dependence of the 2E_g state lifetimes of the $[\text{Cr}(\text{NH}_2)_2\text{sar}]^{3+}$ and $[\text{Cr}(\text{en})_3]^{3+}$ ions are depicted in Fig. 6.1.⁴⁰ The lifetimes of the sar cages follow the same pattern as that observed for other Cr(III) hexaamine complexes. Namely, at low temperatures, the lifetime of the 2E_g state is independent of temperature, but as the temperature increases, a threshold region is reached where a thermally activated process for decay becomes effective. For the sar complexes, the threshold temperature regions are unexpectedly low (150-170 K), much lower than that of $[\text{Cr}(\text{en})_3]^{3+}$ (220-250 K).

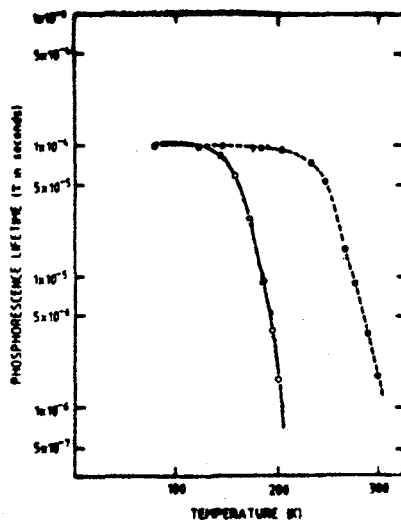


Figure 6.1: 2E_g lifetimes as a function of temperature for $[\text{Cr}(\text{NH}_2)_2\text{sar}]^{3+}$ (full line) and $[\text{Cr}(\text{en})_3]^{3+}$ (dashed line), in MeOH:H₂O (3:1) (reproduced from reference 40).

(c) The emission spectra of the sar complexes exhibited a more intense 0-0 transition and vibrational fine structure was poorly resolved (Fig. 6.2). In contrast, some vibrational fine structure was observed in the emission spectra for $[\text{Cr}(\text{en})_3]^{3+}$ and $[\text{Cr}(\text{NH}_3)_6]^{3+}$ (Fig. 6.2).^{38,45}

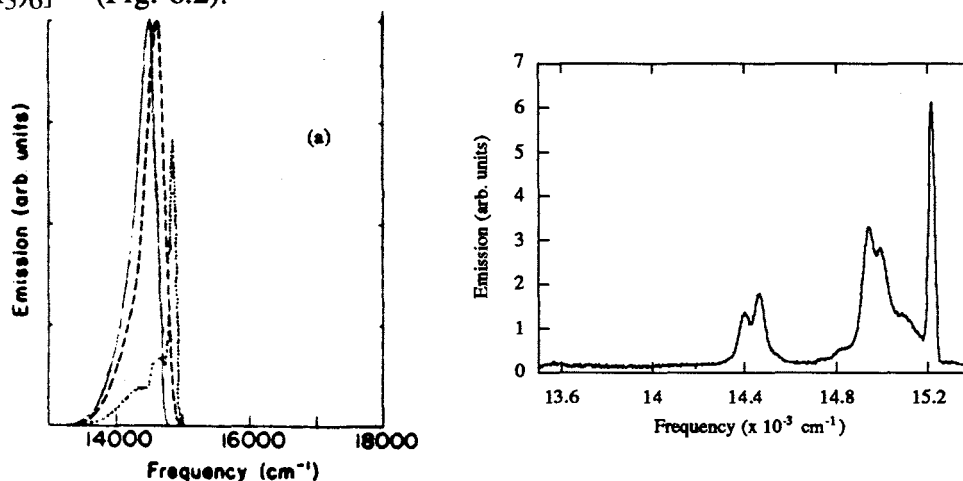


Figure 6.2: Emission spectra of (a) $[\text{Cr}(\text{NH}_2)_2\text{sar}]^{3+}$ (full line), $[\text{Cr}(\text{sar})]^{3+}$ (dashed line) and $[\text{Cr}(\text{en})_3]^{3+}$ (dotted line) in water, 77 K (reproduced from reference 7) and (b) $[\text{Cr}(\text{NH}_3)_6]^{3+}$ (2:1 ethylene glycol:water, 77 K, measured by Hans Riesen).

(d) The intensity of the absorption bands arising from the ${}^4A_{2g}(O_h) \rightarrow {}^4T_{2g}$ and ${}^4T_{1g}$ transitions for the sar cage complexes (Fig. 6.3) are significantly higher than those for the corresponding bands of the parent complex, $[Cr(NH_3)_6]^{3+}$ and the nonencapsulated analogue, $[Cr(en)_3]^{3+}$ (Fig. 6.3).

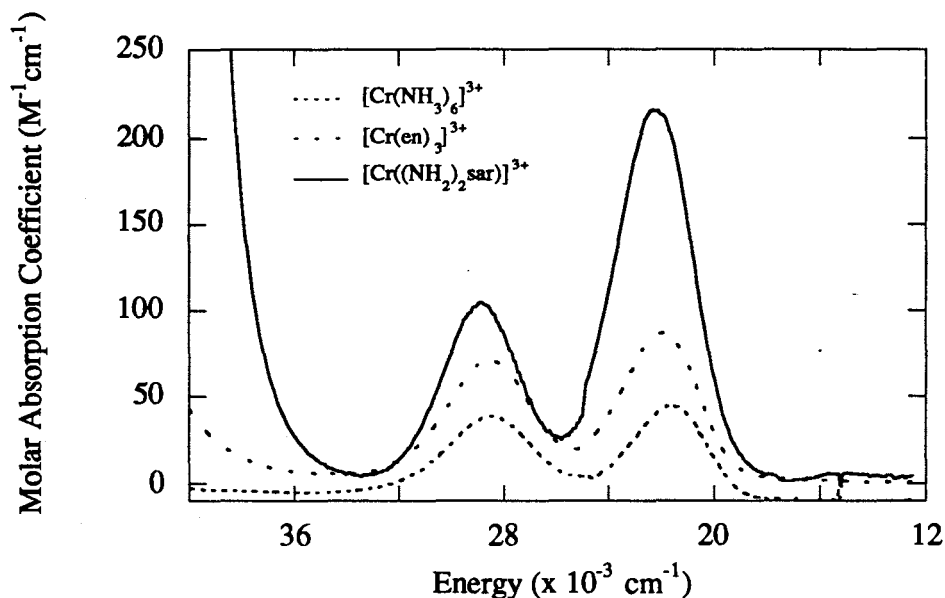


Figure 6.3: Absorption spectra of $[Cr((NH_2)_2sar)]^{3+}$, $[Cr(en)_3]^{3+}$ and $[Cr(NH_3)_6]^{3+}$ in water at 295 K.

It is not clear why the 2E_g state lifetimes of Cr(III) sar complexes are so short at room temperature (both < 10 ns). The effect of substituents at the apical position on the cage ligand does not alter this behaviour.⁴¹ In order to address this issue, each of the relaxation pathways described in equation 6.1 should be examined and compared with the spectral behaviour of other encapsulated Cr(III) complexes with different cage ligand frameworks, such as N_6 -tricosane and sar (Fig. 6.4).

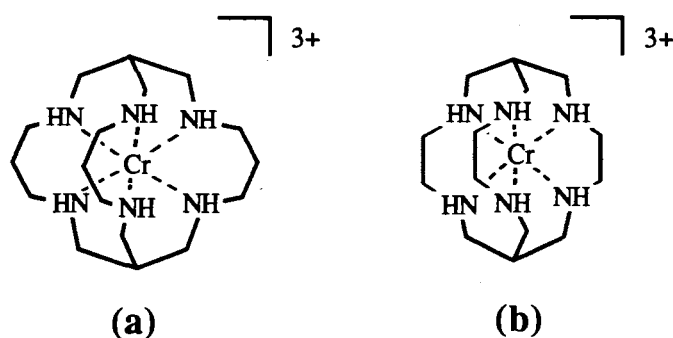
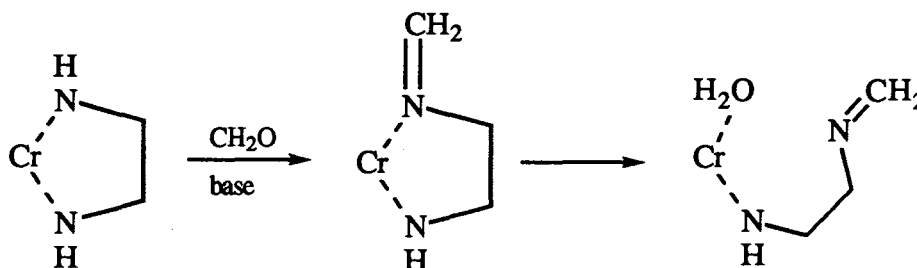


Figure 6.4: (a) N_6 -tricosane and (b) sar.

6.1.3. Synthesis of Cr(III) Cage Complexes

The Cr(III) ion has been complexed with hexadentate ligands, using a labile Cr(II) species as an intermediate. Subsequent oxidation by air of the Cr(II) species affords $[\text{Cr}(\text{L})]^{3+}$, where $\text{L} = ((\text{NH}_2)_2\text{sar})$,^{7,40} sar ,^{7,40} $((\text{NH}_2)_2\text{-Me}_3\text{sar})$,⁴⁶ (Cl_2sar) ,⁴⁷ $((\text{OH})_2\text{sar})$,⁴⁷ $((\text{NO}_2)_2\text{sar})$,⁴⁷ N_5Ssar ,⁴⁸ sen ,^{44,49,50} stn ⁵⁰ and $(\text{Me}_5\text{-N}_6\text{-tricosane})$.⁵¹ While the substitution step to form the Cr(II) complexes may be quantitative, the yield for the synthesis of the free ligand may be low and so limit the usefulness of this strategy. Such is the case with the synthesis of $[\text{Cr}(\text{Me}_5\text{-N}_6\text{-tricosane})]^{3+}$.⁵¹ The free $(\text{Me}_5\text{-N}_6\text{-tricosane})$ ligand is derived⁵¹ from strapping reactions around $[\text{Co}(\text{tame})_2]^{3+}$ which produces $[\text{Co}(\text{Me}_5\text{-N}_6\text{-tricosane})]^{3+}$ in ~20% yield.⁵² The cobalt ion is extruded from the complex and the free $\text{Me}_5\text{-N}_6\text{-tricosane}$ ligand is complexed with Cr(II), the overall yield for this procedure is ~5-10%, based on the template $[\text{Co}(\text{tame})_2]^{3+}$.⁵¹

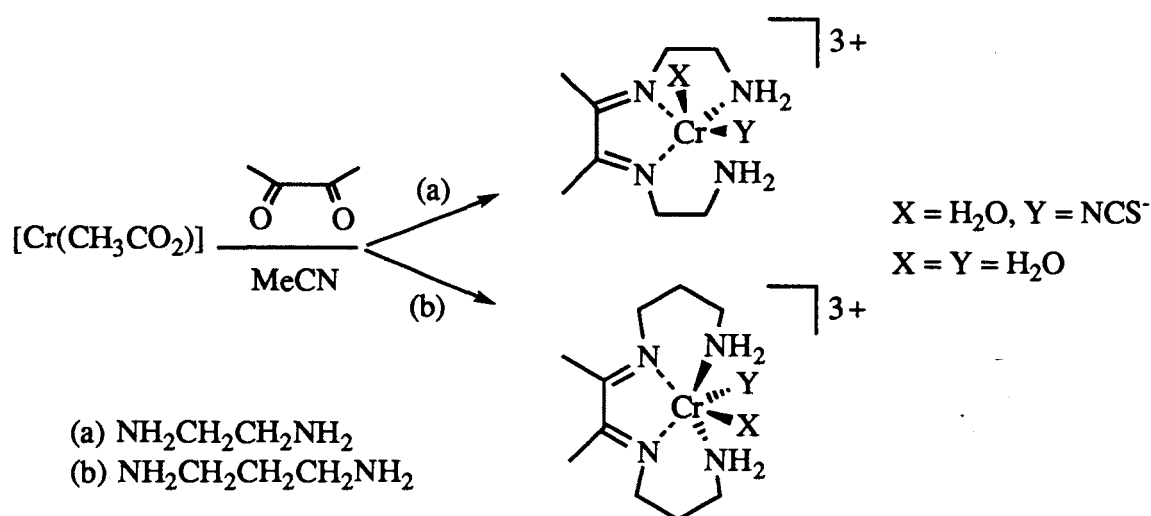
It was anticipated that recently modified template methods would improve the chances of synthesising $[\text{Cr}(\text{Me}_x\text{-N}_6\text{-tricosane})]^{3+}$ ($x=2,5,8$) directly. Surprisingly, attempts to encapsulate the Cr(III) ion by the capping route (described in Chapter 1) have been disappointing,⁴⁰ especially since the Cr(III)-N bond lengths are comparable to those of other inert metal ions where capping reactions have been successful, viz: for $[\text{M}(\text{en})_3]^{n+}$, where $\text{M}=\text{Co}(\text{III})$,^{53,54} $\text{Ir}(\text{III})$,^{55,56} $\text{Rh}(\text{III})$ ^{55,56} and $\text{Pt}(\text{IV})$.⁵⁷ Capping reactions require the formation of imine intermediates as shown in Scheme 6.2; and for the Cr(III) reactions, these are thought to be unstable and to readily undergo ligand dissociation⁴⁰ thus limiting this synthetic strategy.



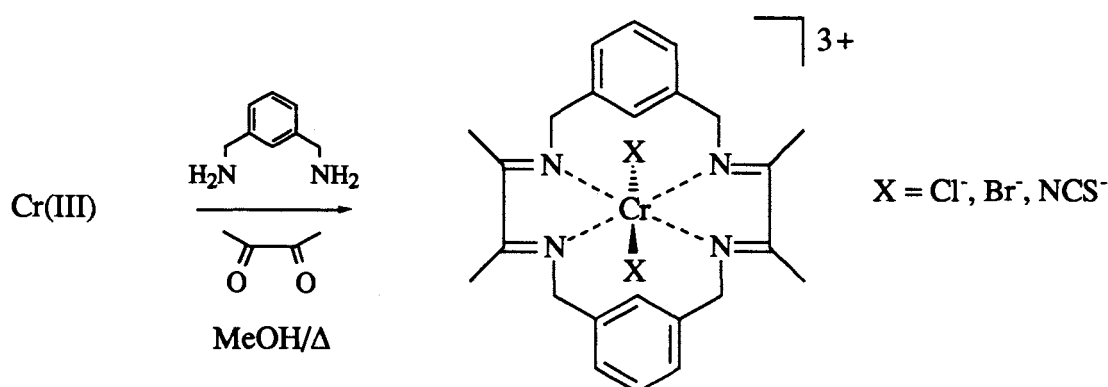
Scheme 6.2: Dissociation of imine precursors in the capping reactions of $[\text{Cr}(\text{en})]^{3+}$.

A claim for the synthesis of $[\text{Cr}(\text{sep})]^{3+}$ via template methods has been made,⁵⁸ but this supposed complex was poorly characterised. No microanalysis or crystal structure was reported. Furthermore, the published emission spectrum and its ${}^2\text{E}_g$ state lifetime were very similar to those of the starting material, $[\text{Cr}(\text{en})_3]^{3+}$. The spectral properties of this supposed cage complex are also grossly different from the other $[\text{Cr}(\text{sar})]^{3+}$ type cages. Subsequent attempts to repeat the published synthesis have been unsuccessful.^{47,59}

Few Schiff base template syntheses using Cr(III) as a template have been reported. Schemes 6.3⁶⁰ and 6.4⁶¹ show two examples where Cr(III) salts have reacted with diketones and coordinated amines. These complexes were characterised by UV/visible and IR spectroscopy and microanalysis. No structural data were reported.



Scheme 6.3: Template synthesis of Cr(III) complexes.



Scheme 6.4: Template synthesis of Cr(III) macrocycles (the Cr(III) template was not specified).

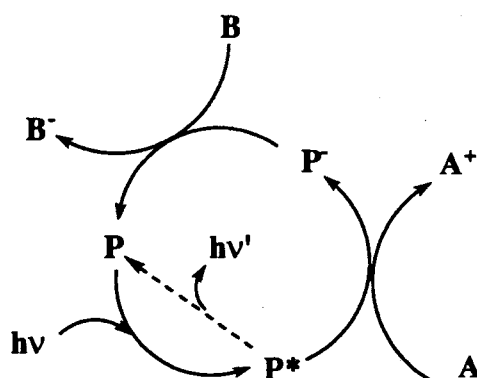
The use of multidentate ligands in Cr(III) templates may reduce the disposition of the imine intermediates to dissociation; the additional binding sites of the ligand should increase the kinetic stability of the intermediate imines formed during condensation. Rigid ligands may also restrict the movement of the donor atoms away from the metal ion. The tridentate tame ligand forms templates superior to the bidentate ethylenediamine and trimethylenediamine ligands. Similarly, hexadentate ligands, such as sen and stn, have been shown to be even better templates in capping reactions with Co(III)⁶²⁻⁶⁴ and Rh(III)⁶⁵ ions, respectively. Preliminary capping reactions of $[\text{Cr}(\text{sen})]^{3+}$ have been attempted but these were not successful.⁵⁰ Possibly, the reaction

conditions were too severe to ensure the survival of the critical intermediates. Firstly, the condensation reactions were carried out in water. In this solvent, condensation of the reactive imines may be less controlled. More stable methylene bridged species may form from intramolecular condensation of the imines with adjacent amine sites before they react with the carbanion to form the cage complex. Secondly, it is not unreasonable to assume that the intermediates are photosensitive and that this too may enhance their propensity towards dissociation. These two problems may be eliminated with relative ease. The reactivity of the imines during the reaction may be retarded by carrying out the condensation reactions in acetonitrile. Controlling the reactivity of the imine intermediates has been achieved to a degree with some Co(III) hexaamine complexes in this solvent^{59,66,67} and the behaviour of Cr(III) imine complexes may be similar. In addition, excluding light from the system during the condensation reactions and work up where basic conditions are necessary may inhibit the putative photoinduced dissociation reactions of the imine intermediates.

The possibility of capping $[\text{Cr}(\text{stn})]^{3+}$ and strapping $[\text{Cr}(\text{tame})_2]^{3+}$ to form the cage complexes $[\text{Cr}(\text{Me}_2\text{-}N_6\text{-tricosanemonoimine})]^{3+}$ and $[\text{Cr}(\text{Me}_5\text{-}N_6\text{-tricosanetriimine})]^{3+}$ respectively, should be examined. One reason for the lack of success in capping $[\text{Co}(\text{stn})]^{3+}$ and $[\text{Co}(\text{tn})_3]^{3+}$ might be that the shorter Co-N bonds may not allow favourable conformations to be achieved during the final stages of capping.⁶⁷ Longer Cr(III)-N bond lengths (e.g., Cr(III)-N = 2.08 Å, for $[\text{Cr}(\text{en})_3]^{3+}$ ⁶⁸) may better suited for capping $[\text{Cr}(\text{stn})]^{3+}$, especially as these bond lengths are comparable to those where capping reactions have been successful, namely, for $[\text{Rh}(\text{stn})]^{3+}$ and $[\text{Rh}(\text{sen})]^{3+}$ (e.g., Rh(III)-N = 2.06 Å for $[\text{Rh}(\text{en})_3]^{3+}$).⁶⁵ In addition, template reactions with $[\text{Cr}(\text{tame})_2]^{3+}$ have not yet been attempted, yet this complex has much potential for template reactions of this type.

6.1.4. Suitability of the Cr(III)/Cr(II) Couple in the Photocatalytic Cycle

The encapsulated Cr(III) complexes are not as susceptible to photodecomposition and therefore it was anticipated that $[\text{Cr}(\text{Me}_5\text{-}N_6\text{-tricosane})]^{3+}$ might function as a photocatalyst, as illustrated in Scheme 6.5. In this photocatalytic cycle, photosensitiser P absorbs a photon of light to become a strong oxidant (P^*), which then oxidises substrate A and is concomitantly reduced to P^- . Substrate B is then reduced by P^- and the catalyst, P, is regenerated. The $^*[\text{Cr}(\text{bpy})_3]^{3+}/[\text{Cr}(\text{bpy})_3]^{2+}$ couple has been claimed to function as a photocatalyst in such a manner.⁶⁹⁻⁷⁴ The energy of the $^2E_g \rightarrow ^4A_{2g}$ transition for $[\text{Cr}(\text{bpy})_3]^{3+}$ occurs at 13760 cm^{-1} , which correlates to an excited state potential of 1.72 eV^\ddagger for the $^*[\text{Cr}(\text{bpy})_3]^{3+}$ above its ground state. The ground state $[\text{Cr}(\text{bpy})_3]^{3+}/[\text{Cr}(\text{bpy})_3]^{2+}$ couple is reversible, with a reduction potential of -0.26 V vs NHE. Therefore, the excited state reduction potential for the $^*[\text{Cr}(\text{bpy})_3]^{3+}/[\text{Cr}(\text{bpy})_3]^{2+}$ couple is $+1.4 \text{ V}$, which implies that $^*[\text{Cr}(\text{bpy})_3]^{3+}$ is a powerful oxidant. The Cr(III) sar complexes, however are not suitable photosensitisers, as their 2E_g state is $<10 \text{ ns}$ at 298 K . However, the effect of increasing the cage size might increase the lifetime, as similar to the Rh(III) chemistry.⁶⁵



Scheme 6.5: Simplified photocatalytic cycle for the oxidation of substrate A and the reduction of substrate B, using photosensitiser P.

One of the criteria governing the effectiveness of a photocatalytic cycle is that the photosensitiser should be resistant to decomposition in the oxidation states attained

[‡] The excited state reduction potential, $E\{^*\text{Cr}(\text{III})/\text{Cr}(\text{II})\}$, was calculated from:

$$E\{^*\text{Cr}(\text{III})/\text{Cr}(\text{II})\} = E\{\text{Cr}(\text{III})/\text{Cr}(\text{II})\} + E_{0-0}\{^*\text{Cr}(\text{III})/\text{Cr}(\text{II})\}$$

where $E^0\{\text{Cr}(\text{III})/\text{Cr}(\text{II})\}$ is the ground state reduction potential, and $E_{0-0}\{^*\text{Cr}(\text{III})/\text{Cr}(\text{II})\}$ is estimated from the energy of the 0-0 transition of the excited state: $8000 \text{ cm}^{-1} = 1 \text{ eV}$.⁷⁵

during the cycle. In the proposed system, the labile Cr(II) ion would be formed. Few studies have addressed stabilisation and isolation of Cr(II) cage complexes or even nonencapsulated Cr(II) hexaamine complexes, as they are readily oxidised and are quite susceptible to ligand dissociation. Some Cr(II) hexaamine complexes have been observed, but none have been structurally characterised and only their reflectance spectra have been recorded. These include substituted ethylenediamine⁷⁶⁻⁷⁸ diethylenetriamine (dien) and triethylenetetraamine (trien),^{76,79} substituted [14]aneN₄,^{78,80,81} [15]aneN₄ complexes.^{82,83} However, the [Cr((NH₂)₂sar)]^{3+/2+},^{7,40} [Cr(sar)]^{3+/2+},^{7,40} and [Cr(tacn)₂]^{3+/2+}⁸⁴ couples have reversible responses at $E_{1/2} = -1.11$ ($\Delta E_p = 70$ mV), -1.14 ($\Delta E_p \sim 70$ mV at scan rates >10 V s⁻¹), -1.14 V ($\Delta E_p = 63$ mV) vs NHE, respectively, implying that dissociation is slower than for the nonencapsulated analogues, such as [Cr(NH₃)₆]^{3+/2+} and [Cr(en)₃]^{3+/2+}. It is anticipated that the (Me₅-N₆-tricosane) ligand will be able to stabilise the Cr(II) ion and it may be able to participate in photocatalytic cycles, in the manner described in Scheme 6.6.

In this chapter, template syntheses of Cr(III) (N₆-tricosane) complexes are explored using the capping⁶⁵ and strapping⁵² strategies discussed in Chapter 1. The properties of these complexes are examined. Particular issues to be addressed are a comparison of the spectroscopic behaviour of Cr(III) hexaamine complexes with the emphasis on those derived from N₆-tricosane and the sar cages and the potential use of the N₆-tricosane cages as photocatalysts.

6.2. Experimental

6.2.1. Synthesis

(a) [tripyridyltrichlorochromium(III)]. $[Cr(py)_3Cl_3]$

The preparation of $[Cr(py)_3Cl_3]$ has been described previously.⁸⁵ Anhydrous $CrCl_3$ (26.4 g) and pyridine (100 ml) are introduced in a 1.5 L round bottom flask and stirred. A water condenser was fitted and a Vigreux column was inserted on top of the condenser. The pink slurry was slowly heated to reflux temperature. A vigorous reaction was expected,⁸⁵ but not observed in this reaction. After refluxing for 6 hours, the reaction was cooled and ice cold water (500 mL) was added. Dark green crystals were collected and washed with a small amount of ice cold water. The green crystals were refluxed in a Soxhlet extractor for 2 days with $CHCl_3$. The solvent was evaporated to yield a green powder. Yield: 60%

The best yields for the templates $[Cr(tame)_2]Cl_3$ and $[Cr(stn)]Cl_3$ were obtained when using dry solvents and exposure to light was minimal.

(b) Bis(1,1,1-tris(aminomethyl)ethane)chromium(III) trichloride monohydrate ($[Cr(tame)_2]Cl_3 \cdot H_2O$)

Ethanol was dried using literature methods⁸⁶ and dry ethanol (400 mL) was introduced into a hot, three necked r.b. flask (1 L) fitted with a water condenser and purged with nitrogen for 30 minutes. $[Cr(py)_3Cl_3]$ (30.0 g) was added to the ethanol followed by tame (2.1 equivalents, 17.8 g), zinc dust (5%, 0.5 g) and triethylamine (3 equivalents, 32.5 mL). Immediately after addition of base, the reaction suspension became purple and after a further 15 minutes it became yellow, indicating the formation of $[Cr(tame)_2]Cl_3$. The reaction was refluxed for a further 6 hours in the dark. The reaction suspension was allowed to cool and then filtered. The residue was washed with ice water and cold ethanol to remove most of the purple species before it was dissolved in 0.5 M HCl (1 L) and then sorbed on a column (20 x 5 cm) of Dowex 50W-X2 cation exchange resin. The resin was washed with water (1 L), 1 M HCl (1.5 L) and the complex eluted with 3 M HCl. The eluate was evaporated to near dryness and the bright yellow crystals were filtered, washed with a small volume of isopropanol and dried *in vacuo*. Yield: 70 %. The chloride salt was converted to the triflate salt and also to the perchlorate salt using methods previously described in Chapter 2. Anal. Calc. for $[C_{10}H_{30}Cl_3CrN_6]0.25HCl \cdot H_2O$: Cr, 12.38; C, 28.61; H, 7.74; N, 20.02; Cl, 27.44. Found: Cr, 12.53; C, 29.09; H, 7.92; N, 20.23; Cl, 27.07. Electronic spectrum (water, λ_{max} nm (ϵ , $M^{-1}cm^{-1}$): 444 (67), 343 (51).

Reduction Potential for $[\text{Cr}(\text{tame})_2]^{3+/2+}$ at 100 mVs^{-1} (E_p , V vs Ag/AgCl/KCl_(sat), 0.1 M NaClO₄, HMDE): -1.39 V .

(c) *1,1,1-tris(5-amino-2-azapentyl)ethane chromium(III) trichloride monohydrochloride* ($[\text{Cr}(\text{stn})\text{Cl}_3]\text{HCl}$).

The method used was similar to that described for the synthesis of $[\text{Cr}(\text{tame})_2]\text{Cl}_3$. Dry ethanol (400 mL) was introduced under nitrogen into a clean dry 3 necked r.b. flask (1 L) fitted with a water condenser. The ethanol was purged with nitrogen for 30 minutes. $[\text{Cr}(\text{py})_3\text{Cl}_3]$ (10.3 g) was added to the ethanol, followed by stn (1 equivalent, 7.5 g), triethylamine (2 equivalents, 7.4 mL) and zinc dust ($\sim 0.2 \text{ g}$). After ~ 20 minutes the solution became purple and as the reaction proceeded, a yellow suspension developed, indicating that $[\text{Cr}(\text{stn})]\text{Cl}_3$ had formed. The suspension was refluxed for 6 hours. After cooling, the suspension was filtered to yield a yellow solid which was washed with ice water and cold ethanol to remove most of the purple species before it was dissolved in 0.5 M HCl and loaded on a (10 x 50 cm) column of Dowex (50W-X2) cation exchange resin. After thoroughly washing the resin with water (1 L), then 1 M HCl (1.5 L), the complex was eluted with 3 M HCl. The eluate was evaporated to near dryness, to yield bright yellow crystals, which were washed with ethanol and then isopropanol. The complex was dried *in vacuo*. Yield: 85 %. Anal. Calc. for $[\text{C}_{15}\text{H}_{36}\text{Cl}_3\text{CrN}_6]0.25\text{HCl}\cdot 3.5\text{H}_2\text{O}$: C, 33.93; H, 8.21; N, 15.83; Cl, 21.70; Found: C, 33.37; H, 8.91; N, 16.44; Cl, 22.27.

Electronic spectrum (water, λ_{max} nm (ϵ , $\text{M}^{-1}\text{cm}^{-1}$): 456 (58), 353 (64).

Reduction Potential for $[\text{Cr}(\text{stn})]^{3+/2+}$ at 100 mVs^{-1} ($E_{1/2}$, V vs Ag/AgCl/KCl_(sat), ΔE_p (mV) 0.1 M NaClO₄, HMDE): -1.18 V (287).

(d) *(1,5,9,13,20-pentamethyl-3,7,11,15,18,22-hexaazabicyclo[7.7.7]tricosane)chromium(III) trichloride* ($[\text{Cr}(\text{Me}_5\text{-N}_6\text{-tricosane})]\text{Cl}_3$)

(e) *(5,13,20-trishydroxymethyl)-(1,5,9,13,20-pentamethyl-3,7,11,15,18,22-hexaazabicyclo[7.7.7]tricosane)chromium(III) chloride*. ($[\text{Cr}(\text{Me}_5\text{-(CH}_2\text{OH)}_3\text{-N}_6\text{-tricosanetriimine})]\text{Cl}_3$)

The best yields were obtained when the reaction and the subsequent purification steps were performed in the dark.

$[\text{Cr}(\text{tame})_2]\text{Cl}_3\cdot\text{H}_2\text{O}$ (6.2 g) was added to a suspension of anhydrous NaClO₄ (25 g) in acetonitrile (90 mL) and stirred. Propanal (10 equivalents, 11.5 mL), followed by paraformaldehyde (~ 4 equivalents, 1.9 g) and then triethylamine (4.5 equivalents, 10 mL) were added. The reaction was quenched after 4 hours with the addition of concentrated HCl (5 mL). The resulting brown suspension was diluted to 1 L to form a

clear red solution which was sorbed on a (50 x 10 cm) column of Dowex 50W-X2 cation exchange resin. The resin was washed with H₂O (1 L) and 1 M HCl (2 L) and the band containing the trimine products was eluted with 6 M HCl (2 L). Evaporation to near dryness afforded a red oil which was redissolved in H₂O (2 L) and sorbed onto a (10 x 20 cm) column of SP-Sephadex cation exchange resin. The resin was washed with water (1 L) and an orange band was eluted using 0.5 M K₂SO₄ (pH ~ 2.5, using H₂SO₄). This step removes most of the side products and polymeric components and aids separation of the desired product at later stages. The resulting orange eluate was sorbed onto a (5 x 10 cm) column of Dowex 50W-X2 cation exchange resin, which was washed with water (1 L), 1 M HCl (1 L) and 6 M HCl (1 L). The 6 M HCl band was evaporated to form a dark orange oil, redissolved in water (500 mL) and then sorbed onto a (10 x 50cm) column of SP-Sephadex cation exchange resin. The resin was washed and the complex and 2 bands were separated using 0.2 M K₂SO₄ (acidified with H₂SO₄ to pH = 2.5) as the eluant. The first band was red and rapidly moved off the column and was discarded. The second orange band slowly moved off the column and was sorbed onto a (5 x 10 cm) column of Dowex 50W-X2 cation exchange resin which was then washed with water (1 L), 1 M HCl (1 L) and an orange band was eluted with 6 M HCl. The 6 M HCl band, containing the [Cr(Me₅-N₆-tricosanetriimine)]³⁺ complexes, was evaporated to dryness. The resulting orange oil (~ 6 g) was redissolved in water (minimum volume, 100 mL), the pH adjusted to 11 (using Na₂CO₃) and treated with NaBH₄ (~ 3 equivalents, 1.0 g). After 2 hours, the reaction was quenched by pouring the reaction solution into 4 M HCl (200 mL). The resulting dark orange solution was diluted to 1 L with water and sorbed onto a (5 x 10 cm) column of Dowex 50W-X2 cation exchange resin, which was washed with water (1 L) and 1 M HCl (1 L) and the complexes eluted with 6 M HCl. The 6 M HCl band was evaporated to dryness and sorbed on a (10 x 50 cm) column of SP-Sephadex cation exchange resin, which was washed with water (1 L), then with 0.2 M K₂SO₄ (pH ~ 2.5, using H₂SO₄). Three bands were eluted in order: yellow, dark orange, yellow, the second band overlapped both yellow bands. The bands were each loaded onto (3 x 20 cm) columns of Dowex 50W-X2 cation exchange resin, which were washed with water (500 mL), then 1 M HCl (1 L) and the complexes eluted with 4 M HCl. The 4 M HCl eluates of the first and third bands were evaporated to near dryness, and the resulting yellow residues were recrystallised from HCl and dried *in vacuo*. The 4 M HCl eluate of the second band was also evaporated to yield a red oil. Attempts to indentify its composition by fractional crystallisation using the anions tetrachlorozincate, chloride, perchlorate and triflate were unsuccessful. The complex isolated from the first yellow band is believed to have additional formaldehyde condensed with the methine carbons of the straps to form [Cr(Me₅-(CH₂OH)_x-N₆-tricosaneimine)]Cl₃ (x = 2,3) (Yield~8 %) while the complex isolated from the third band was [Cr(Me₅-N₆-tricosane)]Cl₃ (Yield~9 %).

Anal. Calc. for $[C_{25}H_{48}Cl_3CrN_6O_3]6H_2O$: C, 39.24; H, 8.17; N, 10.98; Cl, 13.90; Cr, 6.9. Found: C, 39.58; H, 8.21; N, 11.09; Cl, 13.90.

electrospray mass spectrum (H_2O/CH_3OH , chloride salt, 50 V) m/z: 546.7, 536.7, 519.5, 508.6, 500.7, 478.6, 468.6, 432.6, 322.6, 316.6, 288.6, 256.5, 251.1, 237.0, 217.0, 159.0, 59.1. electrospray mass spectrum (MeCN, chloride salt, 40 V) m/z: 649.4, 564.7, 512.6, 501.7, 501.1, 478, 473.3, 433.2, 288.7, 251.3, 273, 216.8, 201.2, 188, 169.5, 149, 141.2, 138.5. electrospray mass spectrum (MeCN, chloride salt, 50 V) m/z: 538.0, 502.7, 501.6, 500.3, 474.3, 472.9, 433.3, 317.1, 289.7, 282, 273.7, 216.6, 146.3.

Electronic spectrum of $[Cr(Me_5-(CH_2OH)_3-N_6-tricosanetriimine)]Cl_3$ (water, λ_{max} nm (ϵ , $M^{-1}cm^{-1}$): 444 (ϵ , 58.6), 346 (ϵ , 60.7), 216 (ϵ , 10.690).

Reduction Potential $[Cr(Me_5-(CH_2OH)_3-N_6-tricosanetriimine)]^{3+/2+}$ at 100 mVs^{-1} , ($E_{1/2}$, V vs $Ag/AgCl/KCl_{(sat)}$, ΔE_p (mV) 0.1 M $NaClO_4$, HMDE): -1.39 (30) V (adsorption peak).

Anal. Calc. for $[C_{22}H_{48}Cl_3CrN_6]1HCl.6H_2O$: C, 37.77; H, 8.79; N, 12.01; Cl, 20.27. Found: C, 37.62; H, 8.29; N, 11.68; Cl, 20.53.

electrospray mass spectrum ($H_2O/MeCN$, chloride salt, 50V) m/e: 482.3, 446.3, 223.7. Electronic spectrum of $[Cr(Me_5-N_6-tricosane)]Cl_3$ (water, λ_{max} nm (ϵ , $M^{-1}cm^{-1}$): 460 (57), 358 (60).

Reduction Potential $[Cr(Me_5-tricosane)]^{3+/2+}$ at 100 mVs^{-1} , ($E_{1/2}$, V vs $Ag/AgCl/KCl_{(sat)}$, ΔE_p (mV) 0.1 M $NaClO_4$, HMDE): -1.19 V (75).

(f) Attempted synthesis of (1,9-dimethyl-3,7,11,15,18,22-hexaazabicyclo[7.7.7]tricosane)chromium(III) trichloride ($[Cr(Me_2-N_6-tricosane)]Cl_3$

I. Reaction of $[Cr(stn)]Cl_3$ with Propanal

$[Cr(stn)]Cl_3$ (0.9 g) was suspended in a solution of anhydrous $NaClO_4$ (3g) dissolved in acetonitrile (20 mL). The reaction vessel was wrapped in foil and stirred. Propanal (4 equivalents, 0.6 mL), paraformaldehyde (3 equivalents, 0.2 g) and then triethylamine (2 equivalents, 0.6 mL) were added to the suspension. After one hour, the reaction was quenched with concentrated HCl (1 mL). The resulting red-brown suspension was diluted in water to 500 mL and sorbed onto a (20 x 3 cm) column of Dowex 50W-X2 cation exchange resin. The resin was washed with water (1 L), then 1 M HCl (1 L) and a red band was eluted using 4 M HCl (1 L). The 4 M HCl band was evaporated to dryness, redissolved in small fraction of water (100 mL) and again evaporated to dryness. The red oil that ensued was redissolved in water (500 mL) and sorbed onto a short (5 x 10 cm) column of SP-Sephadex cation exchange resin, in order

to remove by products and polymeric species. The resin was washed with water (1 L) and a broad red band was eluted with 0.2 M K_2SO_4 (pH ~ 2.5, using H_2SO_4). This band was sorbed onto a short (3 x 10 cm) column of Dowex 50W-X2 cation exchange resin, which was then washed with water (1 L), 1 M HCl (1 L) and a red band was eluted using 4 M HCl (1 L). The 4 M HCl band was evaporated to dryness, redissolved in a minimum volume of water (~50 mL) and the pH adjusted to ~10.5 using Na_2CO_3 . $NaBH_4$ (0.08 g) was then added to the solution. The reaction was quenched 1 hour later by addition of the dark orange reaction solution to 4 M HCl (20 mL). The reaction solution was diluted to 1 L and sorbed onto a (10 x 3 cm) column of Dowex 50W-X2 cation exchange resin. The resin was washed with water (1 L), 1 M HCl (1 L) and a red band was eluted with 4 M HCl (1 L). The 4 M HCl band was evaporated to dryness, then diluted to 500 mL with water and loaded onto a (40 x 5 cm) column of SP-Sephadex cation exchange resin. The resin was washed with water (1 L) and then 0.1 M K_2SO_4 . A small red band rapidly moved off the column, followed by a broad red diffuse band and separation of this main band was not successful using the eluants 0.05 and 0.1 M K_2SO_5 or 0.05 M NaCl. The many complexes in the main band were therefore not identified.

II. Reaction of $[Cr(tame)_2]^{3+}$ with Acetaldehyde

$[Cr(tame)_2](ClO_4)_3$ (1.06 g) was suspended in a solution of anhydrous $NaClO_4$ (3g) dissolved in acetonitrile (20 mL). The reaction vessel was wrapped in foil and stirred. Acetaldehyde, (10 equivalents, 1.0 mL), paraformaldehyde (4 equivalents, 0.22 g) and then triethylamine (3 equivalents, 0.78 mL) were added to the suspension. After three hours, the reaction was quenched with concentrated HCl (1 mL). The resulting red-brown suspension was diluted in water to 500 mL and sorbed onto a (20 x 3 cm) column of Dowex 50W-X2 cation exchange resin. The resin was washed with water (1 L), then 1 M HCl (1 L) and the complex eluted with 4 M HCl (1 L). The 4 M HCl fraction was evaporated to dryness, redissolved in small fraction of water (100 mL) and evaporated again to dryness to yield a red oil. This oil was redissolved in water (500 mL) and sorbed onto a short (5 x 10 cm) column of SP-Sephadex cation exchange resin, in order to remove by products and polymeric species. The resin was washed with water (1 L) and a red band was eluted with 0.2 M K_2SO_4 (pH ~ 2.5, using H_2SO_4). The red band was sorbed on a short (3 x 10 cm) column of Dowex 50W-X2 cation exchange resin, which was then washed with water (1 L), 1 M HCl (1 L) and the complexes eluted with 4 M HCl (1 L). The 4 M HCl fraction was evaporated to dryness, redissolved in a minimum volume of water (~50 mL) and the pH was raised to 10 using Na_2CO_3 , before adding $NaBH_4$ (three equivalents, 0.2 g) to the solution. The reaction was quenched after 1 hour by pouring the red solution into 4 M HCl (1 L). The reaction solution was diluted to 1 L and sorbed onto a (10 x 3 cm) column of Dowex 50W-X2

cation exchange resin. The resin was washed with water (1 L), 1 M HCl (1 L) and a red band was eluted with 4 M HCl (1 L). The red band was evaporated to dryness, then diluted to 500 mL with water and loaded onto a (40 x 5 cm) column of SP-Sephadex cation exchange resin. The resin was washed with water (1 L) and then 0.1 M K₂SO₄. A fast moving red band was separated from a very diffuse red band, but separation of the broad second band was not successful using the eluants 0.05 and 0.1 M K₂SO₄ or 0.05 M NaCl. The many complexes in this main band were not identified.

(g) Other Cr(III) Hexamine Complexes

[Cr(NH₃)₆]Cl₃ was prepared by A.M. Sargeson according to literature methods⁸⁷ and was used without further purification. [Cr(en)₃]Cl₃ and [Cr(tn)₃]Cl₃ was synthesised by R.J. Geue, according to literature methods⁸⁸ and both complexes were recrystallised from HCl and ethanol. [Cr(sen)]Cl₃ and the cages [Cr(Cl₂sar)]Cl₃, [Cr((OH)₂sar)]Cl₃, [Cr(NO₂sar)]Cl₃, [Cr(NH₂)₂sar)]Cl₃ and [Cr(sar)]Cl₃ were synthesised by I.I. Creaser and were used without further purification. The synthesis of the latter two cage complexes has been described elsewhere,⁴⁰ while the remaining complexes were synthesised using a similar strategy. *Le*₃-[Cr(NH₃)₂(Me₃)-sar)]Cl₅ was synthesised by A.J. Hendry using free *le*₃-(NH₃)₂(Me₃)-sar)H₂ ligand, whose synthesis has been described elsewhere.^{46 54,89,90} The complex was recrystallised from HCl.

6.2.2. Procedures

Electronic absorption spectra of the spin allowed bands were recorded using a Hewlett Packard 8450 A UV/visible spectrophotometer with 1 cm quartz cells.

The absorption spectra of the ⁴A_{2g}(O_h)→²E_g transition for saturated solutions of [Cr(tame)]Cl₃, [Cr(stn)]Cl₃ and [Cr(Me₅-N₆tricosane)]Cl₃ were recorded using a single-beam microcrystal absorption spectrometer, which has been described previously.⁹¹ The solutions were millipore filtered into 1 cm quartz cells prior to acquisition of data to remove any crystalline material, and the concentration of the solution determined from the absorbance of the quartet bands.

Emission spectra were acquired using a continuous wave Spectra Physics 171 Ar⁺ ion laser, in conjunction with a Spex 1404 (0.85m) double monochromator and the phosphorescence was detected by a RCA C31034 photomultiplier tube. The data was stored and worked up on the VAX, using standard software. The ²E_g state lifetimes were measured using the 337 nm line from a PRA LN1000 N₂ laser (500 ps pulse width, 1 mW) as the irradiating source. Quantum yields of phosphorescence were measured relative to that of [Cr(NH₃)₆]³⁺ (φ_{ph} = 0.0033)²³ in a (1:1) ethylene glycol:H₂O glass at liquid nitrogen temperatures.

The photostabilities of the $[\text{Cr}(\text{Me}_5\text{-N}_6\text{-tricosane})]^{3+}$ and $[\text{Cr}(\text{stn})]^{3+}$ complexes were assessed by irradiating acidic solutions of the complexes (~ 1 mM, $\text{pH}=2$). The intensities of the ${}^2\text{E}_g$ emission for these complexes were monitored during irradiation with a Spectra Physics Ar⁺ ion laser (50 mW) at 488 nm.

The ${}^2\text{E}_g$ lifetime dependence with pD was measured in duplicate, using solutions of $[\text{Cr}(\text{Me}_5\text{-N}_6\text{-tricosane})]\text{Cl}_3$ (0.98 mM) in solutions of 0.5 M NaCl/D₂O at pD = <0, -0.2, 1.0, 1.1, 2.0, 2.0, 3.1, 3.1, 4.3, 4.2, 5.1, 5.2, 7.2, 6.9, 8.2, 8.7, 9.3. The pD of the solutions were determined from pH indicator paper (Merck, with an error of ± 0.1), immediately prior to irradiation.

The ${}^2\text{E}_g$ lifetime dependence with $[\text{Fe}(\text{CN})_6]^{4-}$ concentration was measured using solutions with a constant concentration of $[\text{Cr}(\text{Me}_5\text{-N}_6\text{-tricosane})]\text{Cl}_3$ (1.03 mM), in 0.52 M NaCl in D₂O. The concentration of $[\text{Cr}(\text{Me}_5\text{-N}_6\text{-tricosane})]\text{Cl}_3$ used for examining the dependence of the ${}^2\text{E}_g$ state lifetime on $[\text{I}^-]$ was 0.459×10^{-4} M, in 1.0 M KCl, at $\text{pH} = 5.5 \pm 0.1$. The concentration of the following quenchers disodium oxalate, sodium azide, tetrasodium ethylenediaminetetraacetate (Na₄EDTA) and tetrasodium 1,2-diaminocyclohexanetetraacetate (Na₄DCTA) was ~ 0.1 M. The concentration of $[\text{Cr}(\text{Me}_5\text{-N}_6\text{-tricosane})]\text{Cl}_3$ used in these experiments was ~ 5 mM and the $\text{pH} \sim 4-5$. Table 6.2 lists the concentrations of the quenchers and $[\text{Cr}(\text{Me}_5\text{-N}_6\text{-tricosane})]\text{Cl}_3$ and the anticipated products for irreversible electron transfer. All solutions were purged with argon prior to irradiation. CO₂ measurements were performed using a CO₂ electrode (CM-1 Microelectrodes, Inc). The light source used for the CO₂ experiments was a Varian model PS150-8 xenon lamp (EIMAC division), set at ~ 7 A. A CuSO₄ heat filter with quartz windows was used between the lamp and the solution, along with an ultra violet filter to block out light at wavelengths less than 460 nm. The irradiation cell is illustrated in Fig. 6.5.

Table 6.2: Relative concentration of the quenchers to the $[\text{Cr}(\text{Me}_5\text{-N}_6\text{-tricosane})]\text{Cl}_3$ used and the anticipated products arising from electron transfer in all quenching experiments. $\text{pH} \sim 4$ for all experiments, unless specified.

Quencher, Q	[Q] [†] (M)	[Cr] [‡] (mM)	anticipated products
Na ₂ C ₂ O ₄	0.11	4.9	CO ₂
Na ₄ DCTA	0.099	5.1	CO ₂
Na ₄ EDTA	0.102	5.4	CO ₂
NaN ₃	0.11 (pH=4.5) 0.13 (pH=5.3)	5.32 4.43	N ₂

[†] [Q] = concentration of quencher, Q; [‡] [Cr] = [concentration of $\text{Cr}(\text{Me}_5\text{-N}_6\text{-tricosane})]^{3+}$.

Background solutions containing only the quencher and only $[\text{Cr}(\text{Me}_5\text{-N}_6\text{-tricosane})]\text{Cl}_3$ were irradiated for 15 minutes, during which the CO_2 electrode was turned on. Solutions containing both the quencher and $[\text{Cr}(\text{Me}_5\text{-N}_6\text{-tricosane})]\text{Cl}_3$ were irradiated for up to 20 minutes.

A VG Micromass spectrometer was used for the detection of N_2 , focussed on $m/e = 28$ and later on 29 and 30. The cell used during the irradiation is illustrated in Fig. 6.6. This cell consists of a glass cylinder over a teflon membrane, which is permeable to nitrogen, but impermeable to water. Underneath the teflon membrane is an evacuated cavity with an inlet to the two liquid nitrogen traps, which are themselves connected to the mass spectrometer. The traps serve to remove possible traces of water and HCl . The cell was sealed using a perspex plug. The light source used for the N_2 experiments was a Voigtländer VP135 quartz halogen projector light source 200 W.

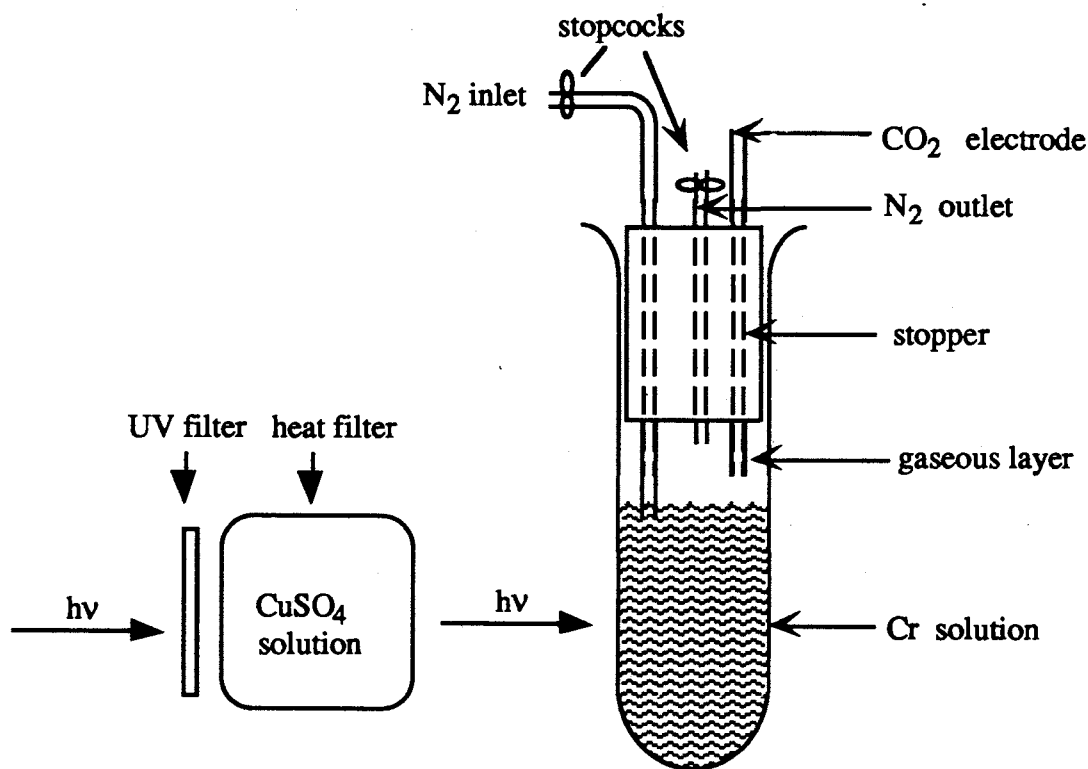


Figure 6.5: Irradiation cell used for detection of CO_2

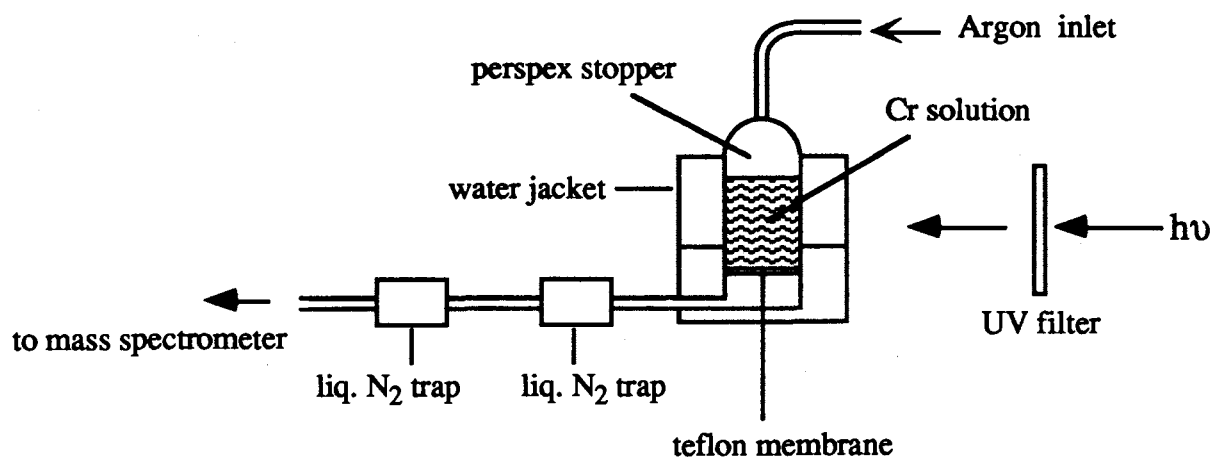


Figure 6.6: Irradiation cell used for detection of N_2 .

To a solution of PVA in water, a saturated solution of $[Cr(Me_5-N_6-tricosane)](CH_3CO_2)_3$ was added and thoroughly mixed. The mixture was dropped onto a microscope slide to cover an area of $\sim 1.5\text{ cm}^2$ and allowed to slowly evaporate, to avoid bubbles in the film. Drops of this solution were intermittently added to the drying film to increase its thickness, until a film of $\sim 1.5\text{ mm}$ had formed. Using Araldite[®], a section of the film was mounted onto a brass disc having a small aperture (2 mm^2), with the film covering the hole. The film was irradiated at 620 nm, using an Ar^+ laser, with the appropriate filters, for 30 minutes. No colour change was observed, the film remained yellow, indicating that the $[Cr(Me_5-N_6-tricosane)]^{3+}$ ion had not undergone net electron exchange with the PVA matrix. The wavelength of irradiating laser was changed to 488 nm. After 30 minutes of irradiation, again no colour change was evident. The film was then irradiated for a further hour and still no colour change was observed. The energy of the irradiating laser beam was increased for a third time to 337 nm using an N_2 laser, and after 5 minutes of irradiation into the charge transfer band, the film singed.

The molecular mechanics calculations were performed by Dr. P.V. Bernhardt, using the program MOMECC-87⁹² and published force fields.⁹³ No attempt was made to include the contribution due to solvent interactions. The strain energies were calculated using

$$U_{\text{tot}} = \sum E_b + \sum E_\theta + \sum E_\varphi + \sum E_{\text{nb}}$$

where U_{tot} = the total strain energy, E_b = bond deformation energy, E_θ = valence angle deformation energy, E_φ = the torsion angle deformation energy and E_{nb} = the nonbonded interaction energy. These terms have been defined previously.^{93,94}

6.3. Results

6.3.1. Synthesis

(a) Synthesis of the Templates, $[\text{Cr}(\text{tame})_2]\text{Cl}_3$ and $[\text{Cr}(\text{stn})]\text{Cl}_3$

The treatment of $[\text{Cr}(\text{py})_3\text{Cl}_3]$ with each of the ligands tame and stn (L) and a trace amount of zinc dust in ethanol produced respectively $[\text{Cr}(\text{tame})_2]\text{Cl}_3$ and $[\text{Cr}(\text{stn})]\text{Cl}_3$. The yields were increased from ~30% to ~80% when the reactions were performed in dry ethanol under a blanket of nitrogen. Reduction of $[\text{Cr}(\text{py})_3\text{Cl}_3]^{3+}$ by the zinc formed the labile Cr(II) species, around which substitution took place and subsequent oxidation of the $[\text{CrL}]^{2+}$ complex by $[\text{Cr}(\text{py})_3\text{Cl}_3]^{3+}$ afforded the Cr(III) templates.

(b) Synthesis of the $[\text{Cr}(\text{Me}_5\text{-N}_6\text{-tricosane})]^{3+}$ -Type Complexes

The reaction and subsequent workup were undertaken in the dark to minimise possible photodissociation of the imine intermediates. Two complexes were isolated in a 1:1 ratio from the treatment of $[\text{Cr}(\text{tame})_2]\text{Cl}_3$ with propanal and paraformaldehyde in the presence of triethylamine and NaClO_4 in acetonitrile, followed by treatment with BH_4^- . The microanalysis, electrochemistry, absorption and emission spectra of the second yellow complex to elute from the SP-Sephadex cation exchange column are identical to that of $[\text{Cr}(\text{Me}_5\text{-N}_6\text{-tricosane})]\text{Cl}_3$, which has also been synthesised by introducing the Cr(III) ion into the free $\text{Me}_5\text{-N}_6\text{-tricosane}$ ligand.⁵¹ However, the yield of $[\text{Cr}(\text{Me}_5\text{-N}_6\text{-tricosane})]\text{Cl}_3$ using the template method is higher than that obtained using the substitution strategy.

The structure of the first complex to elute from the SP-Sephadex cation exchange column is not clear. The microanalysis, electrochemistry, absorption spectrum and electrospray mass spectra are not inconsistent with a cage complex where additional formaldehyde units had condensed with the methine carbon atom, alpha to the imine on the strap. It is not clear how many formaldehyde units are present. The microanalysis gives an empirical formula of $\text{C}_{25}\text{N}_6\text{Cl}_3$, implying that three additional formaldehyde units had condensed with the complex. However, this is inconsistent with the electrospray mass spectrum (Appendix H), which implies that there are only two additional formaldehyde units present. On the basis of the electrospray mass spectra, electrochemistry and absorption spectra, a possible structure for the complex is $[\text{Cr}(\text{Me}_5\text{-(CH}_2\text{OH)}_2\text{-N}_6\text{-tricosanediimine})]\text{Cl}_3$ (Fig. 6.7). Attempts to grow suitable crystals for a crystallographic analysis using the anions Cl^- , Br^- , ClO_4^- , CF_3SO_3^- and ZnCl_4^{2-} were not successful.

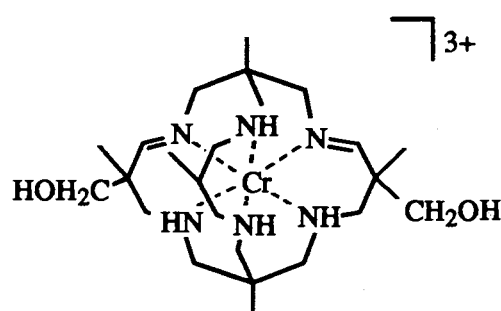


Figure 6.7: Possible structure of the first complex to elute from the SP-Sephadex cation exchange column.

The best yields for both complexes were obtained when the by-products and polymeric species were removed by chromatographing on SP-Sephadex cation exchange resin prior to treatment of the reaction mixture with BH_4^- at $\text{pH} \sim 10.5$. These species obscured separation of the products during the later stages of workup by cation exchange chromatography. Only after reduction and separation of the products on cation exchange resin was it apparent that two products had been formed. The mobility of the hydroxymethyl species on the column is presumably aided by the greater ability of the hydroxyl groups to hydrogen bond with the eluant. Isolation of the unsubstituted triimine intermediate was not successful either by cation exchange chromatography or fractional crystallisation. The use of the triflate salt of the $[\text{Cr}(\text{tame})_2]^{3+}$ template gave rise to the same products, although slightly better yields were achieved when the chloride salt (in the presence of anhydrous NaClO_4) was used.

(c) Attempted Synthesis of $[\text{Cr}(\text{Me}_2\text{-N}_6\text{-tricosane})\text{Cl}_3$

The reaction of $[\text{Cr}(\text{stn})]\text{Cl}_3$ with propanal and paraformaldehyde in the presence of triethylamine and NaClO_4 in acetonitrile in an attempt to form the $[\text{Cr}(\text{Me}_2\text{-N}_6\text{-tricosanemonoimine})]^{3+}$ ion resulted in the formation of many products. Similarly, the reaction of $[\text{Cr}(\text{tame})_2]^{3+}$ with acetaldehyde and paraformaldehyde in basic acetonitrile, in an attempt to form a similar complex ($[\text{Cr}(\text{Me}_2\text{-N}_6\text{-tricosanetriimine})]^{3+}$) also gave rise to many different products. The organic residues and polymeric species from both reactions were each removed from their reaction mixtures by cation exchange chromatography using both Dowex and SP-Sephadex cation exchange resin. As it was anticipated that the imine intermediates were too unstable to isolate, the reaction mixtures were each treated with BH_4^- in basic aqueous media. This would have given rise to the saturated forms of the fully encapsulated complexes, while the partially encapsulated complexes were expected to dissociate to yield the unencapsulated chromium ion and organic residues. In both systems however, attempts to separate the many products by cation exchange chromatography or fractional crystallisation were unsuccessful.

6.3.2. Electrochemistry of Cr(III) Hexaamine Complexes

The $\text{CrN}_6^{3+/2+}$ reduction potential for the complexes presented here are listed in Table 6.3, along with those of other relevant $\text{CrN}_6^{3+/2+}$ complexes. The cyclic voltammograms (CV's) of $[\text{Cr}(\text{tame})_2]^{3+}$, $[\text{Cr}(\text{sen})]^{3+}$ and $[\text{Cr}(\text{stn})]^{3+}$ are depicted in Fig. 6.8. The $[\text{Cr}(\text{tame})_2]^{3+/2+}$ couple was irreversible while the $[\text{Cr}(\text{sen})]^{3+/2+}$ and $[\text{Cr}(\text{stn})]^{3+/2+}$ couples were quasireversible. When scan rates slower than 100 mVs^{-1} and 50 mVs^{-1} were used for the $[\text{Cr}(\text{sen})]^{3+/2+}$ and $[\text{Cr}(\text{stn})]^{3+/2+}$ couples respectively, the mercury drop dislodged. The CV's of $l\text{el}_3\text{-}[\text{Cr}(\text{NH}_2)_2\text{-Me}_3\text{sar}]^{3+}$, $[\text{Cr}(\text{OH})_2\text{sar}]^{3+}$ and $[\text{Cr}(\text{NO}_2)_2\text{sar}]^{3+}$ exhibited reversible Cr(III)/Cr(II) couples (Fig. 6.9). The CV of $[\text{Cr}(\text{NO}_2)_2\text{sar}]^{3+}$ exhibited two multielectron reductions at -0.58 and -0.62 V vs $\text{Ag}/\text{AgCl}/\text{KCl}_{(\text{sat.})}$, which are attributed to the reduction of each nitro substituent. These responses occur at about the same potential as that in the analogous cobalt system, which were attributed to the reduction of the nitro substituents to hydroxylamine.⁹⁵ Therefore, the reduction potential of the Cr(III)/Cr(II) couple quoted is likely to be that for the $[\text{Cr}(\text{NHOH})_2\text{sar}]^{3+/2+}$ couple. The CV's of the $[\text{Cr}(\text{Me}_5\text{-}N_6\text{-tricosane})]^{3+}$ and the putative $[\text{Cr}(\text{Me}_5\text{-(CH}_2\text{OH)}_2\text{-}N_6\text{-tricosanediimine})]^{3+}$ complexes exhibited sharp responses, and in the CV of $[\text{Cr}(\text{Me}_5\text{-}N_6\text{-tricosane})]^{3+}$, a reversible diffusion controlled Cr(III)/Cr(II) response was observed at more negative potentials (Fig. 6.10). This behaviour is attributed to strong adsorption of the product⁹⁶ in the Cr(III)/Cr(II) couple. Similar adsorption behaviour has been observed in the electrochemistry of the Cr(III)/Cr(II) couples of the sar complexes.^{40,97} The reduction potential for the adsorption response for the $[\text{Cr}(\text{Me}_5\text{-}N_6\text{-tricosane})]^{3+/2+}$ couple is 0.37 V more positive than that of the $[\text{Cr}(\text{Me}_5\text{-(CH}_2\text{OH)}_2\text{-}N_6\text{-tricosanediimine})]^{3+/2+}$ couple. It is anticipated that the diffusion controlled response for the $[\text{Cr}(\text{Me}_5\text{-(CH}_2\text{OH)}_2\text{-}N_6\text{-tricosanediimine})]^{3+/2+}$ couple is more negative than that of the adsorption response, but is obscured by that for the reduction of the solvent. As the hydroxymethyl substituents are unlikely to influence significantly the reduction potential (like the apical substituents of the sar complexes), the negative shift for this couple is attributed to the presence of imines, which diminish the ability of the cage to accommodate the larger Cr(II) ion. Similar behaviour has been observed with the $[\text{Co}(\text{Me}_5\text{-}N_6\text{-tricosane})]^{3+/2+}$ and $[\text{Co}(\text{Me}_5\text{-}N_6\text{-tricosanetriimine})]^{3+/2+}$ system.⁵¹ The two irreversible responses in the oxidation scan in the CV of $[\text{Cr}(\text{Me}_5\text{-(CH}_2\text{OH)}_2\text{-}N_6\text{-tricosanediimine})]^{3+}$ (Fig. 6.10(a)) are possibly attributed to a two-step oxidation for the hydroxyl substituents, firstly to the aldehyde (at $E_{\text{pa}} = -1.15 \text{ V}$ vs $\text{Ag}/\text{AgCl}/\text{KCl}_{(\text{sat.})}$) and then to the carboxylate (at $E_{\text{pa}} = -0.18 \text{ V}$ vs $\text{Ag}/\text{AgCl}/\text{KCl}_{(\text{sat.})}$). These oxidation responses however, have not yet been fully characterised and work is currently underway to determine their origin.

Irreversible multiple electron transfer responses were observed at more negative potentials in the CV's of $[\text{Cr}(\text{Me}_5\text{-N}_6\text{-tricosane})]^{3+}$ ($E_{\text{pc}} = -1.47$ V vs Ag/AgCl/KCl_(sat.)) and $lel_3\text{-}[\text{Cr}((\text{NH}_2)_2\text{-Me}_3\text{sar})]^{3+}$ ($E_{\text{pc}} = -1.38$ V vs Ag/AgCl/KCl_(sat.)). The responses may be due to reduction of Cr(III) to Cr(II), followed by ligand rupture or ligand dissociation, as has been postulated for the sar complexes.⁴⁰ The multi-electron processes could not be observed for $[\text{Cr}(\text{sen})]^{3+}$ and $[\text{Cr}(\text{stn})]^{3+}$ as attempts to scan to more negative potentials resulted in the mercury drop dislodging.

The Cr(III)/Cr(II) reduction potential of these complexes does not appear to be greatly influenced by the cavity size. There is only a slight shift to more positive potentials for complexes with longer Cr(III)-N bond lengths (Table 6.3). The Cr(III)-N bond lengths for complexes whose structures have not yet been reported have been calculated using molecular mechanics⁹⁸ and published force fields.⁹³ Similarly, the presence of substituents on the ligand framework does not greatly influence the $\text{CrN}_6^{3+/2+}$ reduction potential, in contrast to the analogous $\text{CoN}_6^{3+/2+}$ couple. The range of reduction potentials for all the $\text{CrN}_6^{3+/2+}$ couples was 0.28 V, yet the range for the saturated $\text{CrN}_6^{3+/2+}$ sar cages is only 0.09 V (excluding the highly charged $[\text{Cr}(\text{NH}_3)_2\text{R}_3\text{sar}]^{5+/4+}$ couples, R=Me, H).

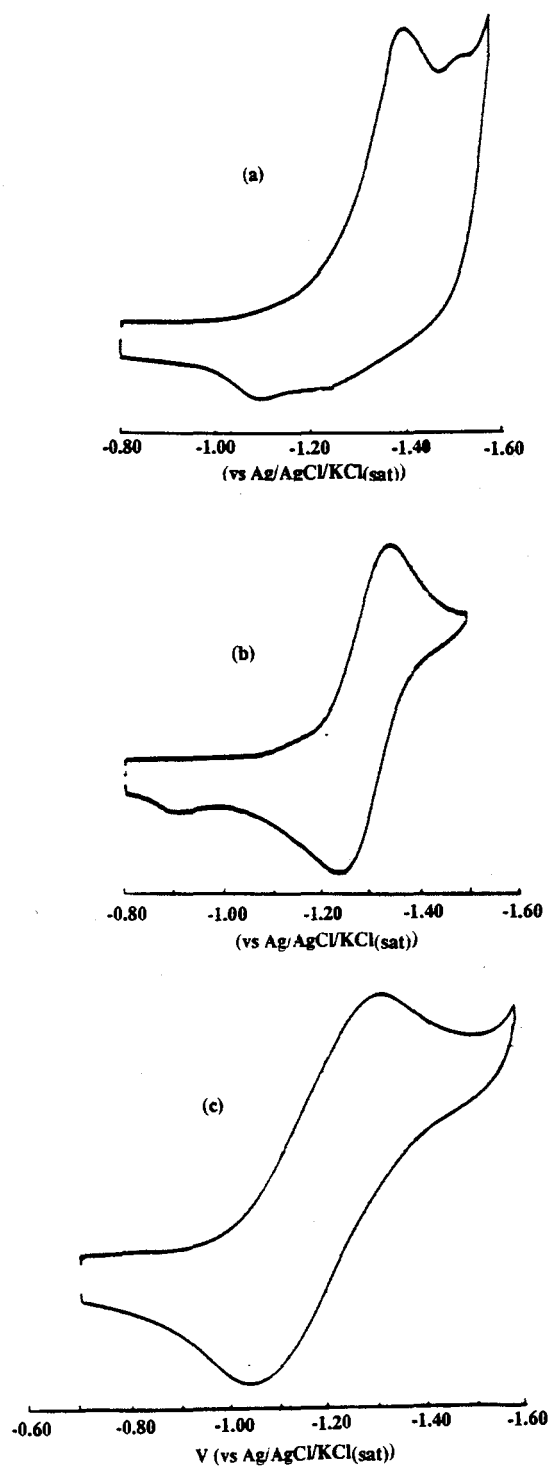


Figure 6.8: Cyclic voltammograms of (a) $[\text{Cr}(\text{tame})_2]^{3+/2+}$ (b) $[\text{Cr}(\text{sen})]^{3+/2+}$ (c) $[\text{Cr}(\text{stm})]^{3+/2+}$ (0.1 M NaClO_4 ; 100 mV s^{-1} HMDE; 293 K).

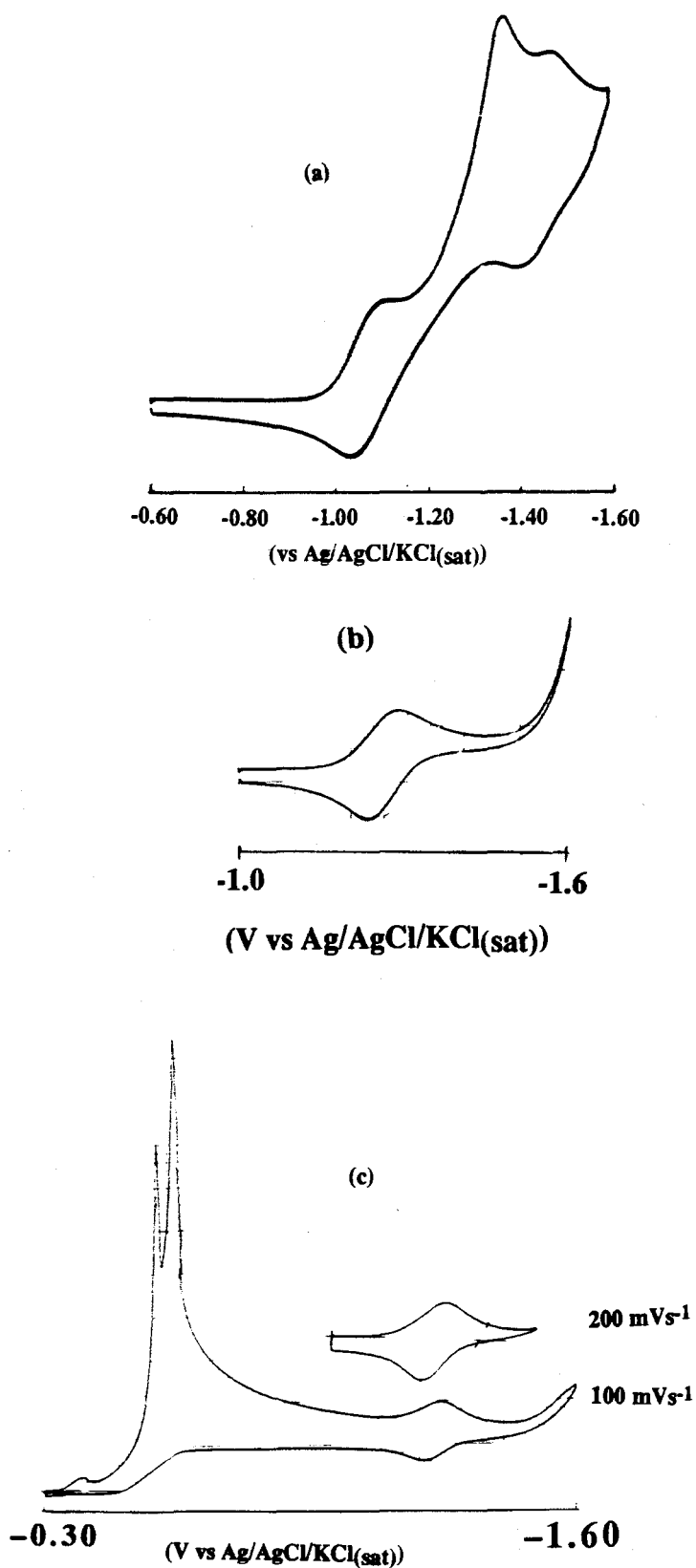


Figure 6.9: Cyclic voltammograms of (a) $1el_3-[Cr((NH_3)_2-Me_3sar)]^{5+/4+}$ (b) $[Cr(OH)_2sar]^{3+/2+}$ and (c) $[Cr(NO_2)_2sar]^{3+/2+}$ (0.1 M $NaClO_4$; 200 mVs^{-1} ; HMDE; 293 K).

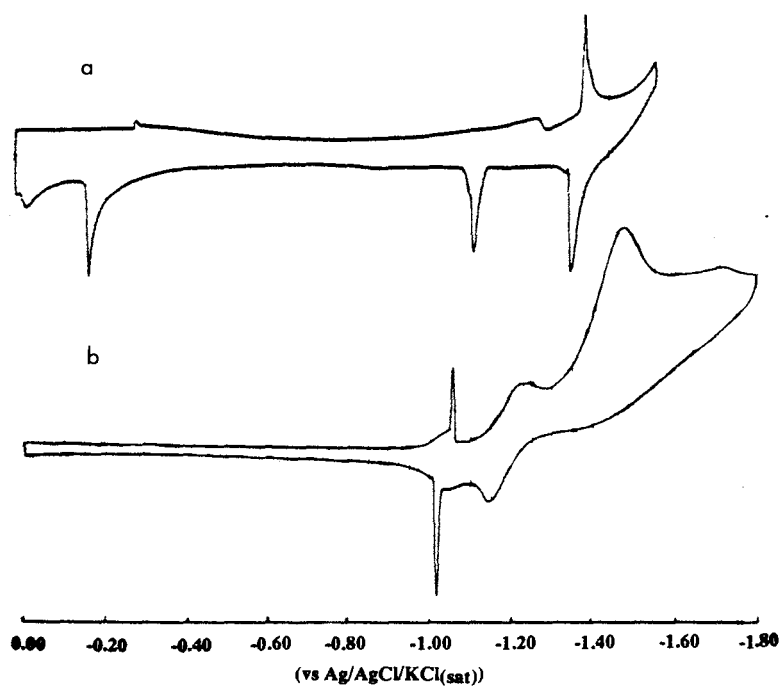


Figure 6.10: Cyclic voltammograms of (a) $[\text{Cr}(\text{Me}_5-(\text{CH}_2\text{OH})_2\text{-}N_6\text{-tricosanediimine})]^{3+/2+}$ (100 mV s^{-1}) and (b) $[\text{Cr}(\text{Me}_5\text{-}N_6\text{-tricosane})]^{3+/2+}$ (200 mV s^{-1}) (0.1 M NaClO_4 ; HMDE; 293 K).

Table 6.3: Reduction potential of Cr(III)/Cr(II) hexaamine couples and Cr(III)-N bond lengths. (0.1 M NaClO₄, 100 mV s⁻¹, HMDE, 295 K)

Complex	E _{1/2} (V vs NHE) (ΔE _p , mV)	Cr(III)-N (Å)
[Cr(NH ₃) ₆] ^{3+/2+}	-1.17 ^{†99}	2.064 ⁶⁸
[Cr(en) ₃] ^{3+/2+}	-1.14 ^{†99}	2.0795 ¹⁰⁰
[Cr(m) ₃] ^{3+/2+}	—	2.093 _(av) ¹⁰¹
[Cr(tacn) ₂] ^{3+/2+}	-1.14 (63) ^{§,84}	2.071 [‡]
[Cr(tame) ₂] ^{3+/2+}	-1.19 [†]	2.0738 [‡]
[Cr(sen)] ^{3+/2+}	-1.10 (97)	2.07(1) [‡]
[Cr(stn)] ^{3+/2+}	-0.98 (287)	2.0977 2.1001 [‡]
[Cr(sar)] ^{3+/2+}	-1.14 (70) ^{7,40}	
[Cr((NHOH) ₂ sar)] ^{3+/2+}	-1.05 (40.3)	
[Cr((OH) ₂ sar)] ^{3+/2+}	-1.07 (56.4)	
[Cr((NH ₂) ₂ sar)] ^{3+/2+}	-1.11 (70) ^{7,40}	2.071 ⁴⁰
[Cr((NH ₃) ₂ sar)] ^{5+/4+}	-0.81 (70) ^{7,40}	
<i>lel</i> ₃ -[Cr((NH ₃) ₂ -Me ₃ -sar)] ^{5+/4+}	-0.86 (55)	2.068 2.073 [‡]
[Cr(Me ₅ -N ₆ -tricosane)] ^{3+/2+}	-0.82 (34)* -0.99 (75)	2.1066 ¹⁰²
[Cr(Me ₅ (CH ₂ OH) ₂ -N ₆ -tricosanediimine)] ^{3+/2+}	-1.19 (30)*	
[Cr(<i>cis</i> -diammac)] ^{3+/2+}	-0.91 ^{†103}	
[Cr(<i>trans</i> -diammac)] ³⁺	-1.06 (150) ^{103,104}	2.035 2.039 2.065 ¹⁰⁴

† Irreversible response. § Measured in 0.1 M LiClO₄ at 50 mVs⁻¹. ‡ Calculated from strain minimised structures predicted from molecular mechanics by P.V. Bernhardt. ¶ Crystal Structure by B. Skelton and A. White. * Response due to adsorption.

6.3.3. Electronic Spectra

(a) Absorption Spectra of the Cr(III) Hexaamine Complexes

The absorption maxima and molar absorption coefficients for the bands arising from the ${}^4A_{2g}(O_h) \rightarrow {}^4T_{1g}$, ${}^4T_{2g}$ and 2E_g transitions at 298 K for the $[Cr(\text{tame})_2]^{3+}$, $[Cr(\text{stn})]^{3+}$, $lel_3-[Cr((NH_2)_2\text{-Me}_3\text{sar})]^{3+}$, $[Cr(\text{Me}_5\text{-}N_6\text{-tricosane})]^{3+}$ and $[Cr(\text{Me}_5\text{-(CH}_2\text{OH)}_2\text{-}N_6\text{-tricosanediimine})]^{3+}$ complexes are listed in Table 6.4. The energies and corresponding molar absorption coefficients of the transitions for $[Cr(\text{Me}_5\text{-(CH}_2\text{OH)}_2\text{-}N_6\text{-tricosanediimine})]^{3+}$ and $[Cr(\text{Me}_5\text{-}N_6\text{-tricosane})]^{3+}$ are similar to those reported for acyclic Cr(III) hexaamine complexes. The energy of the ${}^4A_{2g}(O_h) \rightarrow {}^4T_{2g}$ band for the $[Cr(\text{Me}_5\text{-(CH}_2\text{OH)}_2\text{-}N_6\text{-tricosanediimine})]^{3+}$ complex is higher than that of $[Cr(\text{Me}_5\text{-}N_6\text{-tricosane})]^{3+}$, which implies that the former complex has a stronger ligand field. The stronger ligand field may be attributed to the presence of imines in the ligand framework, as a similar shift has been observed in the ${}^1A_{1g}(O_h) \rightarrow {}^1T_{1g}$ bands for the $[Co(\text{Me}_5\text{-}N_6\text{-tricosanetriimine})]^{3+}$ and $[Co(\text{Me}_5\text{-}N_6\text{-tricosane})]^{3+}$ complexes.⁵² The absorption spectrum for the $lel_3-[Cr((NH_2)_2\text{-Me}_3\text{sar})]^{3+}$ ion is similar to that of the $[Cr(\text{sar})]^{3+}$ and $[Cr((NH_2)_2\text{sar})]^{3+}$ ions, namely, that the molar absorption coefficient of the ${}^4A_{2g}(O_h) \rightarrow {}^4T_{2g}$ band is approximately double that of the ${}^4A_{2g}(O_h) \rightarrow {}^4T_{1g}$ band. The differences in the intensities and energies of the bands arise from distortions away from octahedral symmetry.¹⁴ The distortions for these complexes may be quantified using the trigonal twist and polar angles which are defined in Fig. 6.11 respectively. The values for these angles for the complexes are also tabulated in Table 6.4. For complexes with strictly octahedral symmetry, these angles are 60° and 54.7° , respectively.

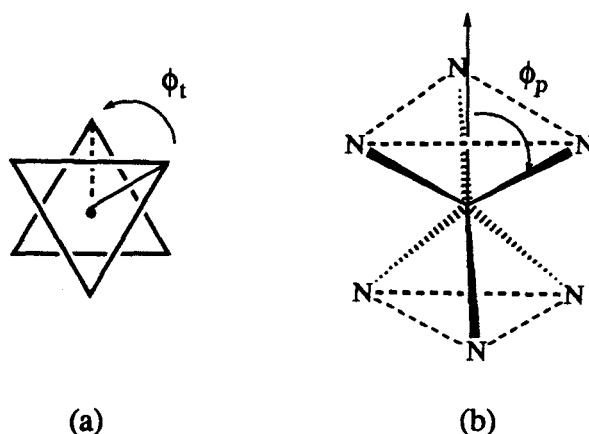


Figure 6.11: Defining the (a) trigonal twist (ϕ_t) and (b) polar angles (ϕ_p).

The absorption bands originating from the ${}^4A_{2g}(O_h) \rightarrow {}^2E_g$ transition for the $[Cr(tame)_2]^{3+}$, $[Cr(stn)]^{3+}$ and $[Cr(Me_5-N_6-tricosane)]^{3+}$ ions are depicted in Figs 6.12. These spectra all show a narrow 0-0 transition of low intensity, which is accompanied by vibrational fine structure on the high energy side. This implies that the complexes are centrosymmetric. The structure of the ${}^4A_{2g}(O_h) \rightarrow {}^2E_g$ band in the absorption spectra of $[Cr(tame)_2]^{3+}$, $[Cr(stn)]^{3+}$ $[Cr(Me_5-N_6-tricosane)]^{3+}$ is similar to that of their corresponding emission bands (see later), except that most of the vibrational fine structure instead lies on the low energy side. This implies that the equilibrium geometries for the 2E_g and ${}^4A_{2g}$ states are similar.

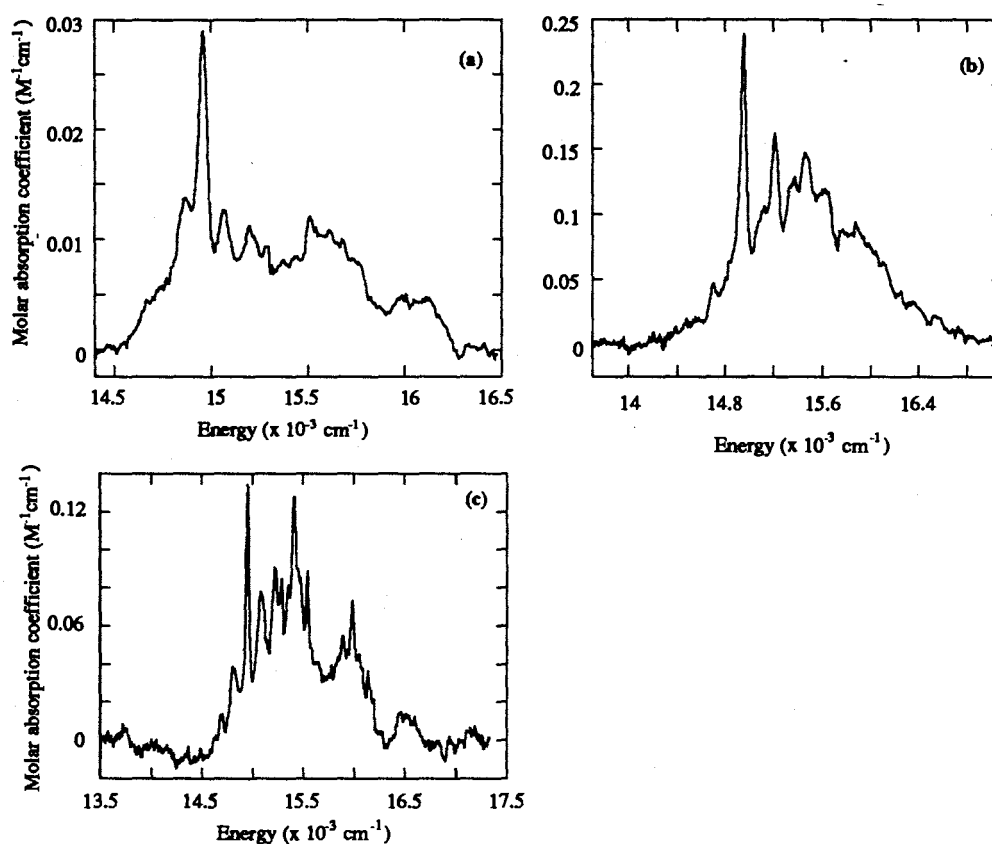


Figure 6.12: Absorption spectra of the band arising from the ${}^4A_{2g}(O_h) \rightarrow {}^2E_g$ transition of (a) $[Cr(tame)_2]Cl_3$; (b) $[Cr(stn)]Cl_3$; (c) $[Cr(Me_5-N_6-tricosane)]Cl_3$ (298 K, H_2O).

Table 6.4: Absorption and emission maxima for relevant Cr(III) hexaamine complexes.

Complex	${}^4A_{2g} \rightarrow {}^4T_{1g} \rightarrow {}^4T_{2g}$	${}^4A_{2g} \rightarrow {}^2E_g$ †	${}^2E_g \rightarrow {}^4A_{2g}$	ϕ_t □	ϕ_p †
[Cr(NH ₃) ₆] ³⁺	346 (37) 462 (44)	654(0.1) ^{25,38}	657 ³⁸	60	54.7
[Cr(en) ₃] ³⁺	351 (70) 462 (86)	669 ³⁸	668 ³⁸	53.5	54.9
[Cr(tn) ₃] ³⁺	355 (48) 464 (55)	666 ³⁸	664 ³⁸	65.2	52.9 54.5
[Cr(tacn) ₂] ³⁺	340 (64) 439 (88) ⁸⁴	679.1 (0.3) ¹⁰⁵	682.1 ¹⁰⁵	53‡	
[Cr(taetacn)] ^{3+ 44}	358 (198) 467 (264)		690		
[Cr(taptacn)] ^{3+ 44}	352 (325) 462 (267)		671		
[Cr(tame) ₂] ³⁺	343 (51) 444 (67)	668 (~0.2)	671.3	64.1‡	53.6‡
[Cr(sen)] ³⁺	347 (62) 450 (85)		675 ⁴⁴	50.8	
[Cr(stn)] ³⁺	353 (64) 456 (58)	670.1 (0.24)	668.8	63.2‡	53.6 53.6‡
[Cr(sar)] ^{3+ 7,40}	347 (91) 447 (156) 457 (153)	683.5 (0.8)	685.4		
[Cr((NH ₂) ₂ sar)] ^{3+ 7,40}	346 (109) 447 (208) 456 (203)	686.3 (~0.8)	688.7	49	53.8 54.5
[Cr((NH ₂) ₂ -Me ₃ sar)] ³⁺	347 (78) 448 (149)		687.8		
[Cr(Me ₅ -(CH ₂ OH) ₂ -N ₆ -tricosanediimine)] ³⁺	346 (61) 444 (59)		674.3		
[Cr(Me ₅ -N ₆ -tricosane)] ³⁺	358 (60) 460 (57)	669.4	668	66.5	52.1 54.0
[Cr(<i>trans</i> -diammac)] ^{3+ 103,104}	332 (32) 427 (55)	663 (0.05) 681 (0.2)	680.5 682.0		
[Cr(<i>cis</i> -diammac)] ^{3+ 103}	350 (68) 452 (128)	684 (0.5) 670 (0.3) 662 (0.1)			
<i>trans</i> - [Cr([14]aneN ₄ (NH ₃) ₂)] ^{3+ 106}	334 (50) 420 (36) 445 (32)		672 ¹⁰⁷		

† λ_{\max} (nm) ϵ_{\max} , (M⁻¹cm⁻¹). ‡ ϕ_t and ϕ_p values are calculated from strain minimised structures predicted from molecular mechanics by P.V. Bernhardt. □ Twist angle. † Polar angle.

(b) Absorption spectrum of the electrochemically generated $[\text{Cr}(\text{Me}_5\text{-N}_6\text{-tricosane})]^{2+}$ ion

The absorption spectrum of $[\text{Cr}(\text{Me}_5\text{-N}_6\text{-tricosane})](\text{ClO}_4)_3$ in MeCN at 298 K prior to reduction was the same as that observed in water. The optically transparent thin layer electrode (OTTLE) cell was cooled to 253 K and the absorption spectrum recorded (Fig. 6.13(a), $\nu_{\text{max}} = 21,800 \text{ cm}^{-1}$ (ϵ , $58 \text{ M}^{-1}\text{cm}^{-1}$); $27,400 \text{ cm}^{-1}$ (ϵ , $59 \text{ M}^{-1}\text{cm}^{-1}$)). This was identical to that recorded at room temperature. The complex was then reduced at -1.15 V vs Ag/AgCl and the visible spectrum acquired at fifteen minute intervals. Within the first 15 minutes, an intense band at $\nu_{\text{max}} \sim 26,600 \text{ cm}^{-1}$ developed, but its absorption was off scale (Fig. 6.13(b)). A broad band of low intensity was also apparent at $\nu_{\text{max}} \sim 16,800 \text{ cm}^{-1}$ ($\epsilon_{t=15\text{min}}$, $13 \text{ M}^{-1}\text{s}^{-1}$). The rate of charge accumulation approached zero after 2.5 hours of reduction, indicating that reduction to Cr(II) neared completion. The spectrum after 2.5 hours of reduction was consistent with that for a high spin CrN_6^{2+} chromophore¹⁴ (Fig. 6.14). Two bands were observed at $\nu_{\text{max}} = 26,600 \text{ cm}^{-1}$ (ϵ_{max} , $915 \text{ M}^{-1}\text{cm}^{-1}$) and $16,800 \text{ cm}^{-1}$ (ϵ_{max} , $28 \text{ M}^{-1}\text{cm}^{-1}$). The former band is attributed to a CT transition, whilst the broad band is attributed to at least two overlapping spin allowed bands originating from the ${}^5\text{B}_{1g}(\text{O}_h) \rightarrow {}^5\text{B}_{2g}$ (from ${}^5\text{T}_{2g}$) and ${}^5\text{E}_g$ (from ${}^5\text{T}_{2g}$) transitions.¹⁴ The potential was reset to 0 V and the complex reoxidised. The spectrum was recorded at 1.5 hour intervals for 19.5 hours. The final spectrum exhibits two absorption maxima at $\nu_{\text{max}} = 22,000 \text{ cm}^{-1}$ (ϵ , $61.8 \text{ M}^{-1}\text{cm}^{-1}$) and $27,500 \text{ cm}^{-1}$ (ϵ , $144.2 \text{ M}^{-1}\text{cm}^{-1}$) (Fig. 6.15). Although the molar absorption coefficients are slightly higher than that for the spectrum of the starting material, the energies of the bands are consistent with that of the $[\text{Cr}(\text{Me}_5\text{-N}_6\text{-tricosane})]^{3+}$, implying that the reoxidation had not quite reached completion.

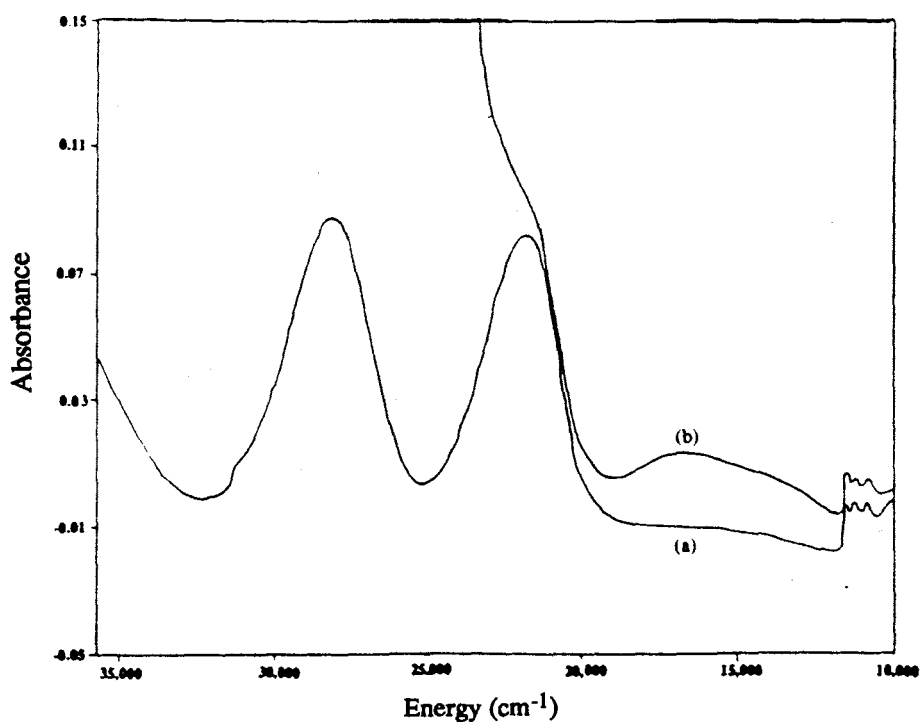


Figure 6.13: Absorption spectrum of $[\text{Cr}(\text{Me}_5\text{-N}_6\text{-tricosane})](\text{ClO}_4)_3$ (a) prior to reduction, (b) after 15 minutes of reduction at -1.15 V vs Ag/AgCl (MeCN, 253 K).

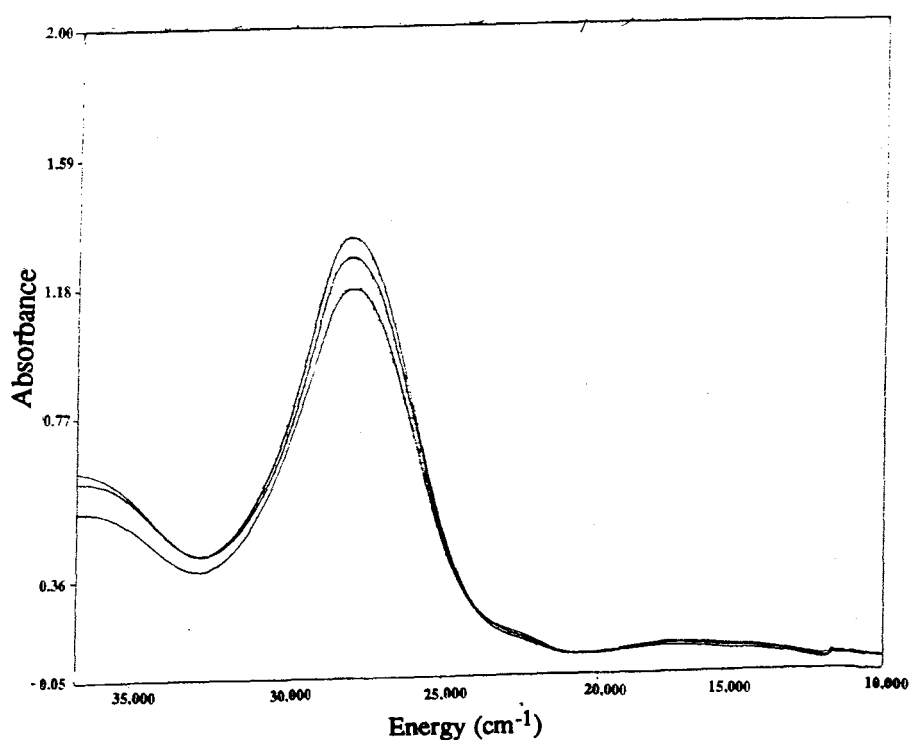


Figure 6.14: Absorption spectra of $[\text{Cr}(\text{Me}_5\text{-N}_6\text{-tricosane})](\text{ClO}_4)_3$ after 2.5 hours of reduction at -1.15 V vs Ag/AgCl; middle spectrum (MeCN, 253 K). Each spectrum is recorded at intervals of 15 minutes.

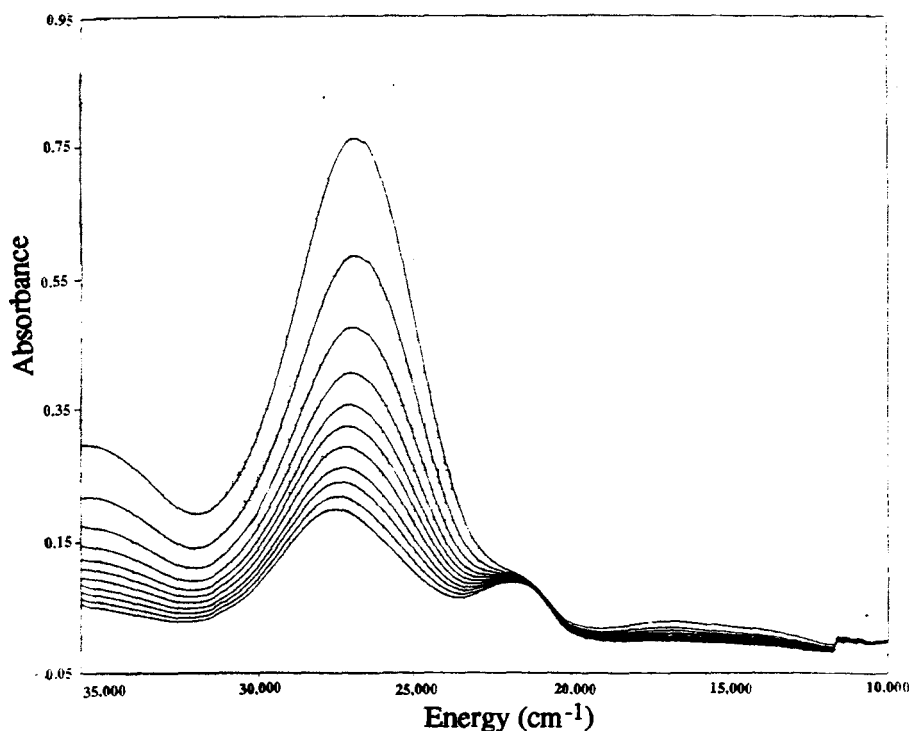


Figure 6.15: Absorption spectra of $[\text{Cr}(\text{Me}_5\text{-N}_6\text{-tricosane})](\text{ClO}_4)_3$ after 19.5 hours of oxidation at 0 V vs Ag/AgCl; bottom spectrum (MeCN, 253 K). Each spectrum is recorded at intervals of 1.5 hours.

(c) Emission Spectra

The wavelengths for the 0–0 emission from the spin forbidden ${}^2\text{E}_g \rightarrow {}^4\text{A}_{2g}(\text{O}_h)$ transition of the $[\text{Cr}(\text{tame})_2]^{3+}$, $[\text{Cr}(\text{stn})]^{3+}$ and $[\text{Cr}(\text{Me}_5\text{-N}_6\text{-tricosane})]^{3+}$ complexes at 298 K and liquid nitrogen temperatures are listed in Table 6.4. The emission spectra for these complexes are depicted in Figs 6.16–6.18. The emission at 298 K was <10 ns for the $lel_3\text{-}[\text{Cr}((\text{NH}_2)_2\text{-Me}_3\text{sar})]^{3+}$ and only its emission spectra at 77 K is presented (Fig. 6.20). The emission spectrum for $[\text{Cr}(\text{Me}_5\text{-(CH}_2\text{OH)}_2\text{-N}_6\text{-tricosanediimine})]^{3+}$ at 77 K is depicted in Fig. 6.19. ${}^2\text{E}_g$ emission was not observed at 298 K for this complex. For comparison, the emission spectrum of the parent ion $[\text{Cr}(\text{NH}_3)_6]^{3+}$ is depicted in Fig. 6.21. The emission spectra at 77 K of the complexes $[\text{Cr}(\text{tame})_2]^{3+}$, $[\text{Cr}(\text{stn})]^{3+}$, $[\text{Cr}(\text{Me}_5\text{-(CH}_2\text{OH)}_2\text{-N}_6\text{-tricosanediimine})]^{3+}$ and $[\text{Cr}(\text{Me}_5\text{-N}_6\text{-tricosane})]^{3+}$ show a 0–0 transition accompanied by vibrational fine structure on the low energy side. These bands are associated with transitions from the vibrational ground state of the ${}^2\text{E}_g$ state to excited vibrational levels in the ${}^4\text{A}_{2g}$ state. The emission spectra at 298 K for the $[\text{Cr}(\text{tame})_2]^{3+}$, $[\text{Cr}(\text{stn})]^{3+}$ and $[\text{Cr}(\text{Me}_5\text{-N}_6\text{-tricosane})]^{3+}$ ions show vibrational fine structure on both sides of the 0–0 transition. The vibrational bands on the higher energy side are associated with transitions from the vibrationally excited levels of the ${}^2\text{E}_g$ state to the vibrational ground state of the ${}^4\text{A}_{2g}$ state.³⁷ The structure of the emission spectrum for $lel_3\text{-}[\text{Cr}((\text{NH}_2)_2\text{-Me}_3\text{sar})]^{3+}$ ions has a relatively more intense 0–0

transition compared to that of the previous three complexes and vibrational structure is not well-resolved. It is reminiscent of the emission spectra of the related Cr(III) sar complexes.⁷

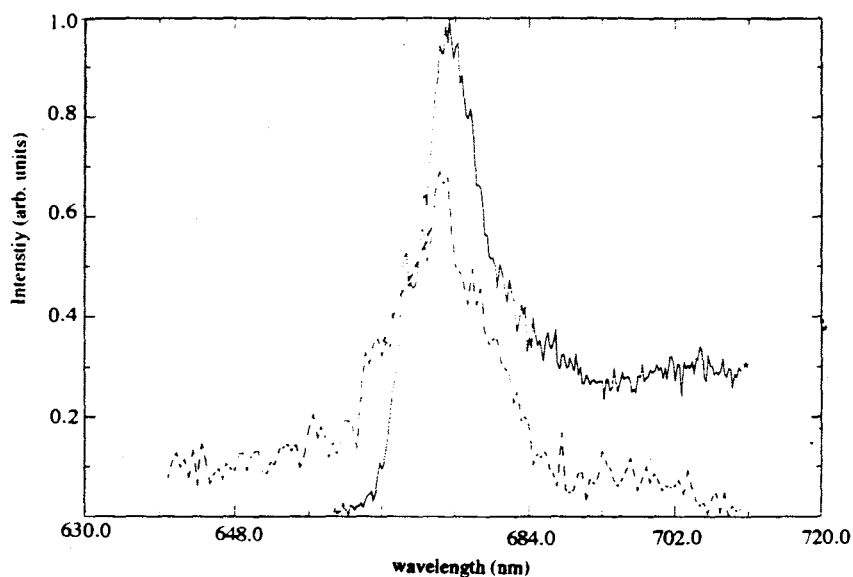


Figure 6.16: Emission spectrum at 298 K (dotted line) and 77 K (bold line) of [Cr(tame)₂]Cl₃. (1:1 DMSO: water glass) (measured by H. Riesen).

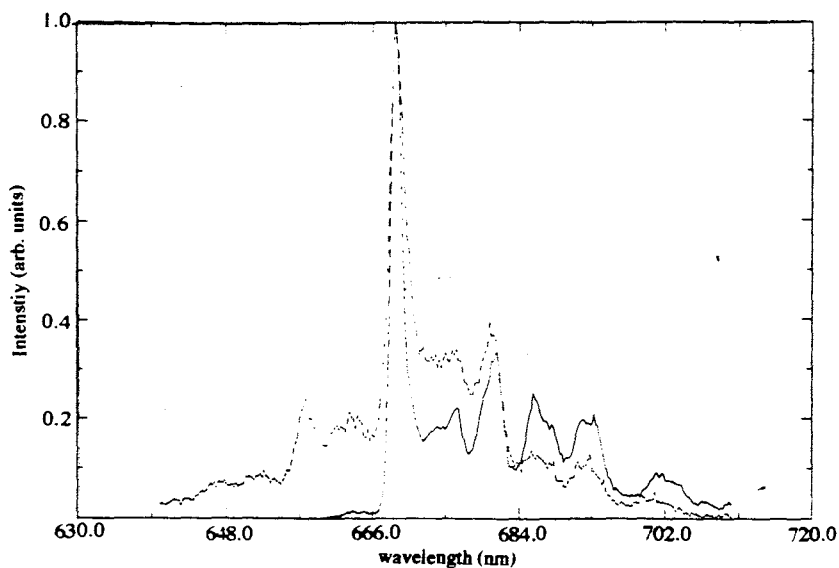


Figure 6.17: Emission spectrum at 298 K (dotted line) and 77 K (bold line) of [Cr(stn)]Cl₃. (1:1 DMSO: water glass) (measured by H. Riesen).

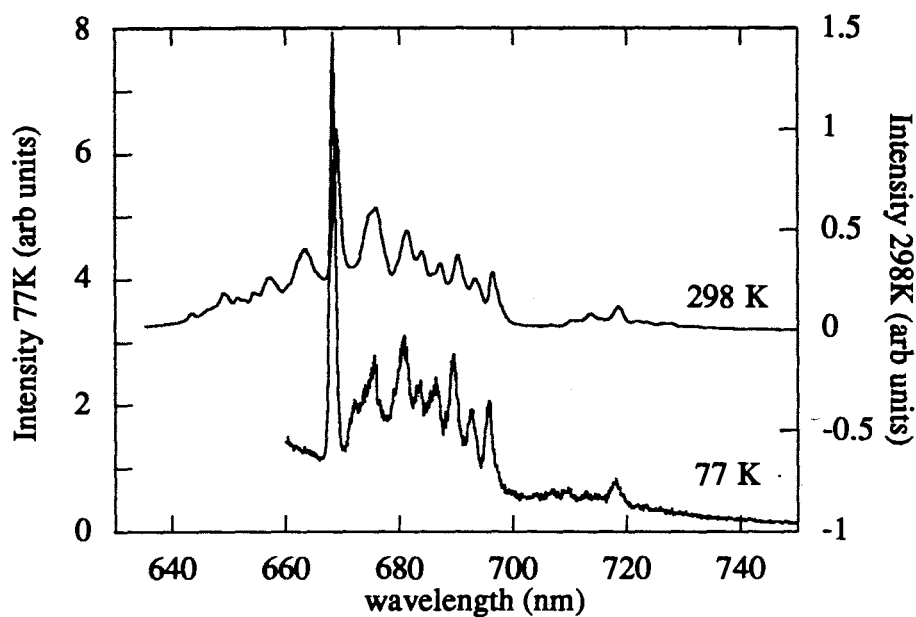


Figure 6.18: Emission spectrum at 298 K (H₂O) and 77 K of [Cr(Me₅-N₆-tricosane)]Cl₃ (2:1 ethylene glycol: water glass) (measured by H. Riesen)

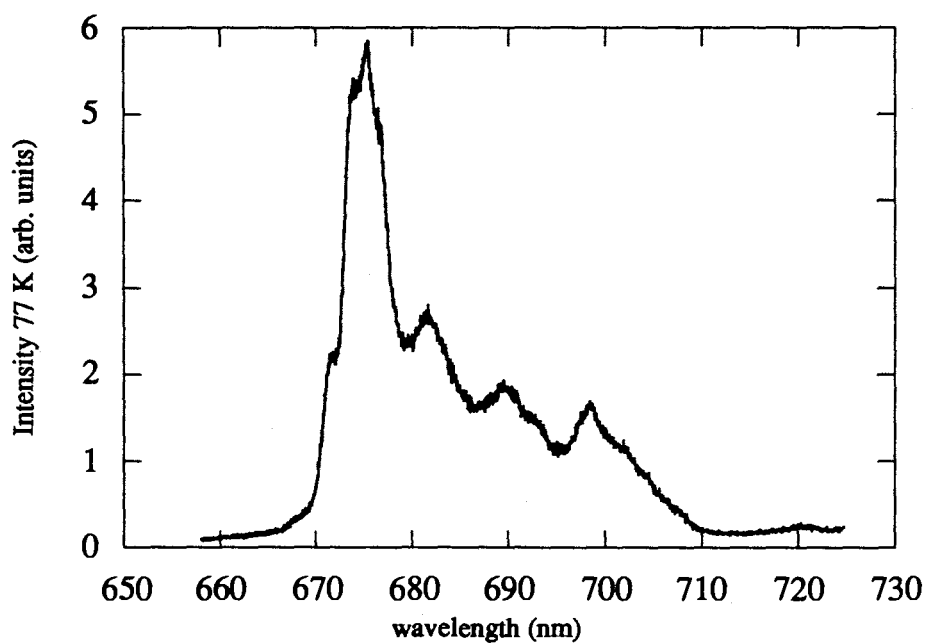


Figure 6.19: Emission spectrum at 77 K of [Cr(Me₅(CH₂OH)₂-N₆-tricosanediiimine)]Cl₃ (1:1 DMF:water glass).

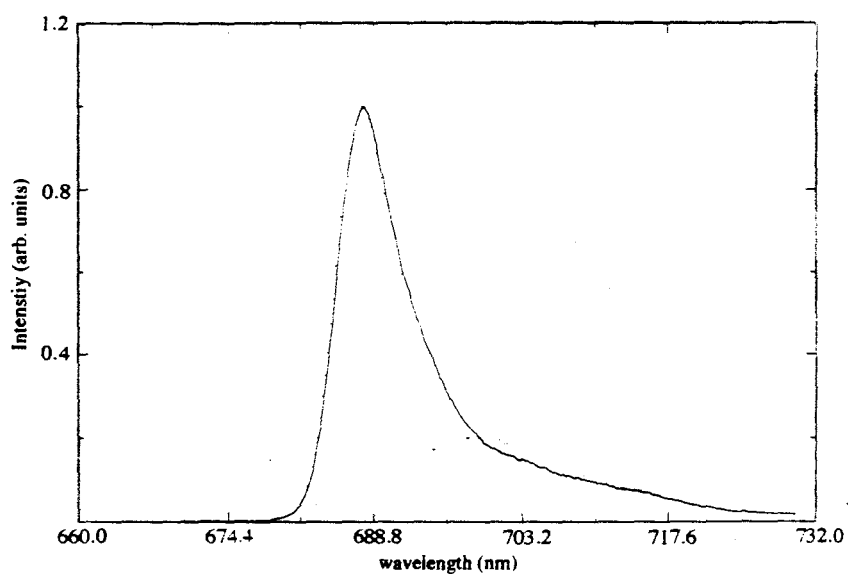


Figure 6.20: Emission spectrum at 77 K of lel_3 -[Cr((NH₂)₂-Me₃sar)]Cl₃. (1:1 DMSO: water glass) (measured by H. Riesen).

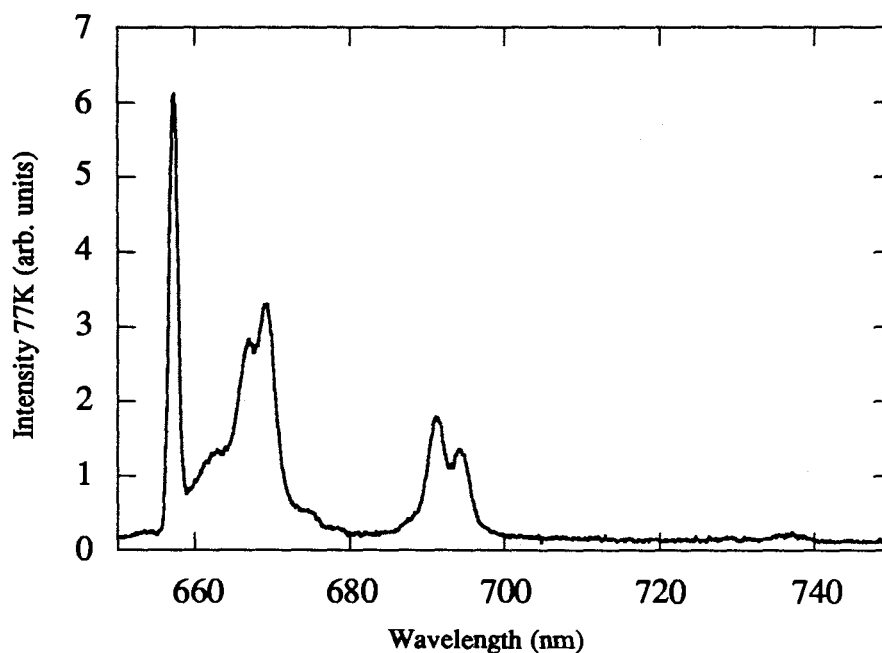


Figure 6.21: Emission spectrum at 77 K of [Cr((NH₃)₆)]Cl₃ (2:1 ethylene glycol:water glass) (measured by H. Riesen).

The 2E_g state lifetimes (in either H_2O , D_2O , 1:1 DMSO/ H_2O or 2:1 ethylene glycol/ H_2O glass) for the ions $[Cr(tame)_2]^{3+}$, $[Cr(stn)]^{3+}$, $[Cr(Me_5-N_6-tricosane)]^{3+}$, $lel_3-[Cr((NH_2)_2-Me_3sar)]^{3+}$ were measured at 298 K and 77 K and they are listed in Table 6.5, along with those of other relevant Cr(III) hexaamine complexes. The 2E_g state behaviour of the $lel_3-[Cr((NH_2)_2-Me_3sar)]^{3+}$ ion was similar to those reported for the analogous cage complexes $[Cr((NH_2)_2sar)]^{3+}$ and $[Cr(sar)]^{3+}$.^{7,40} Namely, the lifetime was <10 ns at 298 K, but measurable at 77 K. The 2E_g state lifetimes of the $[Cr(tame)_2]^{3+}$ and $[Cr(stn)]^{3+}$ complexes only increased by ten and five times, respectively, upon cooling to 77 K. Most interestingly, the lifetime of the 2E_g state for the $[Cr(Me_5-N_6-tricosane)]^{3+}$ ion at 298 K (235 μs) was found to be the longest recorded for saturated Cr(III) hexaamines, being $\sim 10^2$ and at $>10^4$ times that for the nonencapsulated and sar complexes, respectively. Cooling this complex to liquid nitrogen temperatures only doubled its 2E_g state lifetime. It appears that the lifetimes at low temperature are not markedly influenced by the small distortion from octahedral symmetry, as the lifetimes are all about the same, regardless of the ϕ_t and ϕ_p (Table 6.4). The quantum efficiencies for phosphorescence (ϕ_{ph}) for these complexes at liquid nitrogen temperatures are listed in Table 6.5, along with those for other relevant Cr(III) hexaamine systems. In this region, the quantum efficiency of the $[Cr((NH_2)_2sar)]^{3+}$ ion is larger than that of the $[Cr(Me_5-N_6-tricosane)]^{3+}$ ion.

The 2E_g state lifetime of the $[Cr(Me_5-N_6-tricosane)]^{3+}$ ion decreased slightly with increasing ionic strength; at 293 K in 0.5 M and 5 M NaCl it was 235 and 140 μs , respectively. The 2E_g state lifetime was dependent on pD, and this dependency is depicted in Fig. 6.22. The lifetime was highest in the pD range $\sim 2-4$. Above pD ~ 6 , the lifetime decreased sharply as quenching by OH^- became efficient. Similar quenching of the 2E_g state by OH^- has been noted for the $[Cr(NH_3)_6]^{3+}$,³² $[Cr(en)_3]^{3+}$ ¹⁰⁸ and $[Cr(tn)_3]^{3+}$ ^{34,109} ions. At very low pD (<1), the lifetime is also diminished. This behaviour is reminiscent of that at high NaCl concentration, and may be attributed to an ion pairing effect, but this needs to be established.

Table 6.5: Spectroscopic data for relevant Cr(III) hexamine complexes.

Complex	${}^{77}\tau$ (μs) [§]	${}^{298}\tau$ (μs) [§]	$\phi_{\text{ph}}^{\square}$ ($\times 10^{-3}$)	$\phi_{\text{cr}}^{\theta}$
$[\text{Cr}(\text{NH}_3)_6]^{3+}$	73* (5404*) ¹	2.2 (3.6) ^{31\infty\ddagger 31}	3.3 ^{†23}	0.45
$[\text{Cr}(\text{en})_3]^{3+}$	127* ^{††} 42,110 (4800* ^{††}) ¹¹⁰	1.5 ^{\infty} ,7.40 (2.27 ^{\infty\ddagger}) ³¹	9 ^{†23}	0.37
$[\text{Cr}(\text{tn})_3]^{3+}$	138* ^{††} 110 (4800* ^{††}) ¹¹⁰	3.1 ⁴³ (3.5) ¹¹⁰	6.5 ^{†42}	0.15 ⁴³
$[\text{Cr}(\text{chxn})_3]^{3+}$	96 ^{1,8}	0.9 ⁰⁸		
$[\text{Cr}(\text{tactn})_2]^{3+}$	345* ^{1,105} (3226*) ^{1,105}	40* ^{8,105} (51*) ^{8,105}	1.1 ¹⁰⁵	<10 ⁻³ ⁴⁴
$[\text{Cr}(\text{taetacn})]^{3+}$ ^{44,111}	114* (1000 ^{\infty\infty})	4 $\times 10^{-3}$ *		0.27
$[\text{Cr}(\text{taptacn})]^{3+}$ ^{44,111}	265* (4300*)	179* (850*)		0.01
$[\text{Cr}(\text{tame})_2]^{3+}$	120*	18*		
$[\text{Cr}(\text{sen})]^{3+}$ ⁴⁴	171 ^{\diamond} (2960 ^{\diamond})	0.01 ^{\diamond}		
$[\text{Cr}(\text{stn})]^{3+}$	242*	53*		
$[\text{Cr}(\text{sar})]^{3+}$ ^{7,40}	60 ^{\infty}	<10 ns		2 $\times 10^{-5}$
$[\text{Cr}((\text{NH}_2)_2\text{sar})]^{3+}$ ^{7,40}	65 ^{\infty} (790)	<10 ns (12 ms [†])	20	2 $\times 10^{-5}$
$[\text{Cr}((\text{NH}_2)_2\text{Me}_3\text{sar})]^{3+}$	17*	<10 ns		
$[\text{Cr}(\text{Me}_5\text{-}N_6\text{-tricosane})]^{3+}$	440 [†]	235 ^{\infty} (1510 ^{\infty})	8.7 [†]	
<i>trans</i> - $[\text{Cr}([\text{14}] \text{ane}N_4(\text{NH}_3)_2)]^{3+}$ ¹⁰⁶	180 ^{††} (3720 ^{††})	136 ^{††} (1620 ^{††})		~0
<i>cis</i> - $[\text{Cr}([\text{14}] \text{ane}N_4(\text{NH}_3)_2)]^{3+}$ ¹⁰⁶	116 ^{††} (1580 ^{††})	1.0 ^{††} (1.2 ^{††})		0.2
$[\text{Cr}(\text{trans-diammac})]^{3+}$ ¹⁰⁴	150 ^{\text{¥}} (3300 ^{\text{¥}})	2 (PVA)		

§ Values in brackets refer to N-deuterated samples. \square Quantum yield of phosphorescence. θ Quantum yield of chemical reaction. ∞ H₂O or D₂O. * Measured in dmso/H₂O or D₂O (1:1). ** measured in dmso/alcohol (1:1). \ddagger 293 K. \dagger ethylene glycol:water (2:1). $\ddagger\ddagger$ 35 K. \diamond DMF/CHCl₃. $\infty\infty$ (dmso/0.01M CF₃SO₃H). \ddagger 203 K. $\dagger\dagger$ DMSO. ¥ crystalline solid, 80 K.

The changes in intensity of the 2E_g emission of the $[\text{Cr}(\text{stn})]^{3+}$ and $[\text{Cr}(\text{Me}_5\text{-}N_6\text{-tricosane})]^{3+}$ complexes in acid solution during continuous irradiation are depicted in Fig. 6.23. The intensity of the emission for the $[\text{Cr}(\text{stn})]^{3+}$ ion rapidly decreased within seconds due to photoinduced ligand dissociation. In contrast, the emission intensity for the $[\text{Cr}(\text{Me}_5\text{-}N_6\text{-tricosane})]^{3+}$ ion remained constant during 5000 seconds of irradiation. Clearly, the encapsulated Cr(III) complexes are significantly less susceptible to photodecomposition than the nonencapsulated and partially encapsulated complexes.

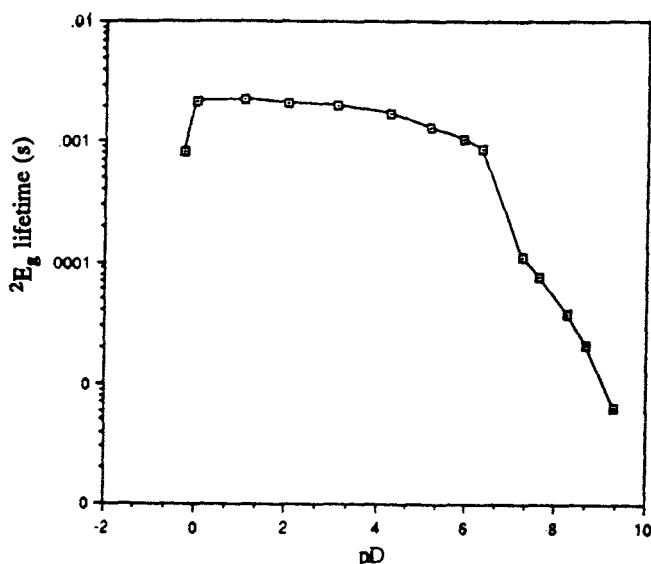


Figure 6.22: 2E_g state lifetime dependence on pD (in 0.5 M NaCl).

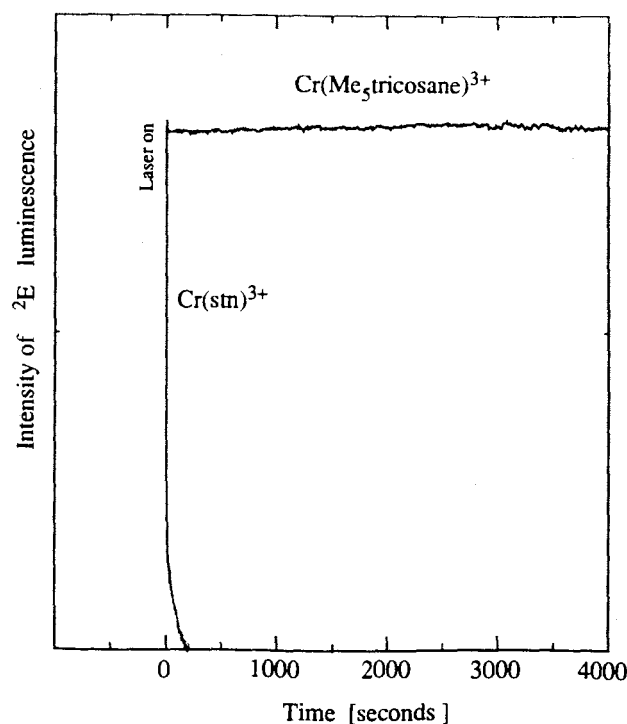


Figure 6.23: Photostabilities of the $[\text{Cr}(\text{stn})]^{3+}$ and $[\text{Cr}(\text{Me}_5\text{-}N_6\text{-tricosane})]^{3+}$ ions in acid solution. (mM solutions, pH=2, Ar^+ 488 nm excitation) (Measured by H. Riesen).

6.3.3. Conformational Analysis

The minimised strain energies of the conformers of the $[\text{Cr}(\text{sar})]^{3+}$ ion are listed in Table 6.6.⁹⁸ The conformation with the predicted lowest energy was C_2lel_2ob , which is different to that observed on the crystal structure of $[\text{Cr}(\text{NH}_2)_2\text{sar}]\text{Cl}_3$ (C_3lel_3).⁴⁰ However, there is very little difference in energy between these structures and this may be overcome by lattice effects.

Table 6.6: Minimised strain energies of the conformers of $[\text{Cr}(\text{sar})]^{3+}$ (in kJmol^{-1}).⁹⁸

D_3lel_3'	D_3lel_3	C_3lel_3	C_2lel_2ob	C_2lelob_2	D_3ob_3
90	91	87*	86‡	92	102

*, indicates conformer observed in the crystal structure. ‡, indicates the conformer with the lowest energy predicted by molecular mechanics (P.V. Bernhardt).

The minimised strain energies of the $[\text{Cr}(\text{Me}_5\text{-}N_6\text{-tricosane})]^{3+}$ conformers are listed on Table 6.7.⁹⁸ There are four conformational minima arising from different configurations of the cap. All of these conformations have C_3 symmetry (the nomenclature for these conformers has been described elsewhere),⁹⁰ and the three six-membered chelate rings of the straps connecting the two tame caps are in the chair conformation, with the methyl substituents in the equatorial position. However, only two conformations have accessible energies (their twist angles being 66.5° and 62°), as the other conformers are too high in energy to be considered. The conformation observed in the crystal structure of $[\text{Cr}(\text{Me}_5\text{-}N_6\text{-tricosane})](\text{ZnCl}_4)_{1.5}$ is the same as that conformation predicted to have the lowest energy.^{51,112}

Table 6.7: Minimised strain energies of the conformers of $[\text{Cr}(\text{Me}_5\text{-}N_6\text{-tricosane})]^{3+}$ (in kJmol^{-1}).⁹⁸

$C_3(\text{S,R})$ ($\phi_t=66.5^\circ$)	$C_3'(\text{R,R})$ ($\phi_t=62^\circ$)	$C_3''(\text{R,S})$ ($\phi_t=53^\circ$)	$C_3'''(\text{S,S})$ ($\phi_t=69^\circ$)	chair/skew boat ($C_3(\text{S,R})$)
158‡*	179	206	206	188

*, indicates conformer observed in the crystal structure. ‡, indicates the conformer with the lowest energy predicted by molecular mechanics (P.V. Bernhardt).

6.3.5. Quenching Experiments

The reduction potential for the ground state $[\text{Cr}(\text{Me}_5\text{-N}_6\text{-tricosane})]^{3+}/[\text{Cr}(\text{Me}_5\text{-N}_6\text{-tricosane})]^{2+}$ couple is -0.99 V vs NHE. The reduction potential for the $(^2\text{E}_g)[\text{Cr}(\text{Me}_5\text{-N}_6\text{-tricosane})]^{3+}/[\text{Cr}(\text{Me}_5\text{-N}_6\text{-tricosane})]^{2+}$ couple is estimated to be ~ 0.9 V vs NHE. In order to examine the possibility of electron transfer as a mechanism for quenching the $^2\text{E}_g$ state, it was necessary to detect the products that would have been formed had electron transfer occurred. To minimise the possibility of back electron transfer, quenchers which were anticipated to undergo irreversible electron transfer were examined. For example, the oxidation of EDTA, DCTA, $\text{C}_2\text{O}_4^{2-}$ and N_3^- would form gaseous products, namely, CO_2 from the first three quenchers, and N_2 would form from N_3^- .

(a) N_2 Experiments

The mass spectrometer was focussed to $m/z = 28$. No N_2 above the background in the spectrometer was detected before, during or after one hour of irradiation of solutions containing (a) only NaN_3 and (b) both NaN_3 and $[\text{Cr}(\text{Me}_5\text{-N}_6\text{-tricosane})]^{3+}$. A solution containing ^{15}N enriched NaN_3 (35 atm %) and $[\text{Cr}(\text{Me}_5\text{-N}_6\text{-tricosane})]^{3+}$ was also irradiated. No N_2 evolution (mass $m/z = 28$) was detected before, during or after irradiation over 1.5 hours. The beam was then focussed at $m/z = 29$ and the cell irradiated for 20 minutes and again no nitrogen was detected. Finally, the beam was focussed at $m/z = 30$ and the cell irradiated for a further 20 minutes, during which no nitrogen evolution was detected.

(b) CO_2 evolution

During irradiation of the solutions, possible changes in concentration of CO_2 were monitored with the CO_2 electrode. When DCTA was used as the donor, the readings for the solutions during 10 minutes of irradiation were stable $-(225\text{-}227)$ and $-(202\text{-}212)$ mV. Similarly, when EDTA was used as the donor, the readings during irradiation over 20 minutes ranged from $-(210\text{ to }219)$ and $-(202\text{ to }215)$ mV. The reading observed in the $\text{C}_2\text{O}_4^{2-}$ experiments ranged from $-(409\text{-}404)$ mV over 20 minutes. In all of these cases, the reading remained stable and low, indicating that a negligible amount of CO_2 was present in the reaction vessel and that none evolved as a result of the irradiation.

The result of the experiments described above did not clarify the dominant mechanism for excited state quenching. Either energy transfer or electron transfer, followed by rapid back electron transfer before the products are able to separate may be possible routes for deactivation. The quenchers I^- and polyvinyl alcohol (PVA) were selected as they had been previously claimed to quench the 2E_g state for $[Cr(bpy)_3]^{3+}$ by reductive electron transfer.^{69,72,113,114} Quenching with I^- was anticipated to form I_2 and furthermore, the mechanism for quenching by the monoatomic I^- ion would have been only by electron transfer. A film of PVA containing $[Cr(bpy)_3]Cl_3$ has been shown to undergo irreversible electron transfer with the excited $[Cr(bpy)_3]^{3+}$ ion,¹¹⁴ resulting in cross linking and further polymerisation of the PVA matrix in the vicinity of the irradiated complex. The blue Cr(II) species was trapped within the polymer matrix and reoxidation to the yellow Cr(III) ion was not observed even days after irradiation. It was anticipated that similar behaviour might result for the excited state of $[Cr(Me_5-N_6-tricosane)]^{3+}$.

(c) Quenching with Iodide

A slight decrease in the 2E_g state lifetime was observed for solutions containing both 0.5 M KI / 0.5 M KCl and $[Cr(Me_5-N_6-tricosane)]Cl_3$ at a constant ionic strength when irradiating at 488 nm. (Table 6.8). This implies that the quenching by I^- is not efficient, although it does indicate that electron transfer is possible. In contrast, the lifetime of the 2E_g state of the $[Cr(bpy)_3]^{3+}$ ion is <10 ns under the same conditions. This implies that the quenching the excited state of $[Cr(bpy)_3]^{3+}$ ion by I^- is more efficient than for the $[Cr(Me_5-N_6-tricosane)]$, especially as the 2E_g state lifetime in the former case is considerably shorter compared to the cage.

Table 6.8: 2E_g state lifetime dependency of $[Cr(Me_5-N_6-tricosane)]^{3+}$ with KI (concentration of $[Cr(Me_5-N_6-tricosane)]Cl_3 = 0.5$ mM, H_2O , $pH \sim 5.5 \pm 0.1$, 295 K).

	τ (μs)	
	$[Cr(Me_5-N_6-tricosane)]^{3+}$	$[Cr(bpy)_3]^{3+}$
0.5 M KCl / 0.5 M KI	106	<10 ns
1 M KCl	188	22

(d) Quenching in PVA

The acetate salt of $[\text{Cr}(\text{Me}_5\text{-N}_6\text{-tricosane})]^{3+}$ complex was the most soluble in the PVA matrix. The triflate, perchlorate and chloride salts formed microcrystals in the film when the PVA solution dried. Irradiation of the film at 488 nm for extended periods did not give rise to any colour change of the film. Similarly, irradiation of the film at 327 nm did not produce a colour change. Irradiation at higher wavelengths caused the film to burn.

(e) Quenching with $[\text{Fe}(\text{CN})_6]^{4-}$

Table 6.9 lists the dependency of the ${}^2\text{E}_g$ state lifetime of the $[\text{Cr}(\text{Me}_5\text{-N}_6\text{-tricosane})]^{3+}$ ion with concentration of $[\text{Fe}(\text{CN})_6]^{4-}$. The rate constants for quenching were calculated from the Stern-Volmer relation: $\tau_0/\tau = 1 + k_q\tau_0[\text{Q}]$,¹¹⁵ which is depicted in Fig. 6.24. The average quenching rate constant ($7.2 \times 10^7 \text{ M}^{-1}\text{s}^{-1}$) was estimated from the data at low concentrations, as at high quencher concentrations, the lifetime reached a constant value. This suggests that the cage and $[\text{Fe}(\text{CN})_6]^{4-}$ had formed an ion pair.

Table 6.9: ${}^2\text{E}_g$ state lifetime dependency of $[\text{Cr}(\text{Me}_5\text{-N}_6\text{-tricosane})]^{3+}$ with $\text{K}_4[\text{Fe}(\text{CN})_6]$ (D_2O , 298 K, 0.5 M NaCl, pH~5, concentration of $[\text{Cr}(\text{Me}_5\text{-N}_6\text{-tricosane})]^{3+} = 1.03 \text{ mM}$).

$\text{K}_4[\text{Fe}(\text{CN})_6]$ (M)	${}^2\text{E}_g$ lifetime (μs)	k_q ($\text{M}^{-1}\text{s}^{-1}$)
1.05×10^{-3}	110	7.40×10^6
1.03×10^{-4}	113	7.30×10^7
1.03×10^{-5}	410	1.06×10^8
1.03×10^{-6}	678	1.27×10^8
0	744	1340

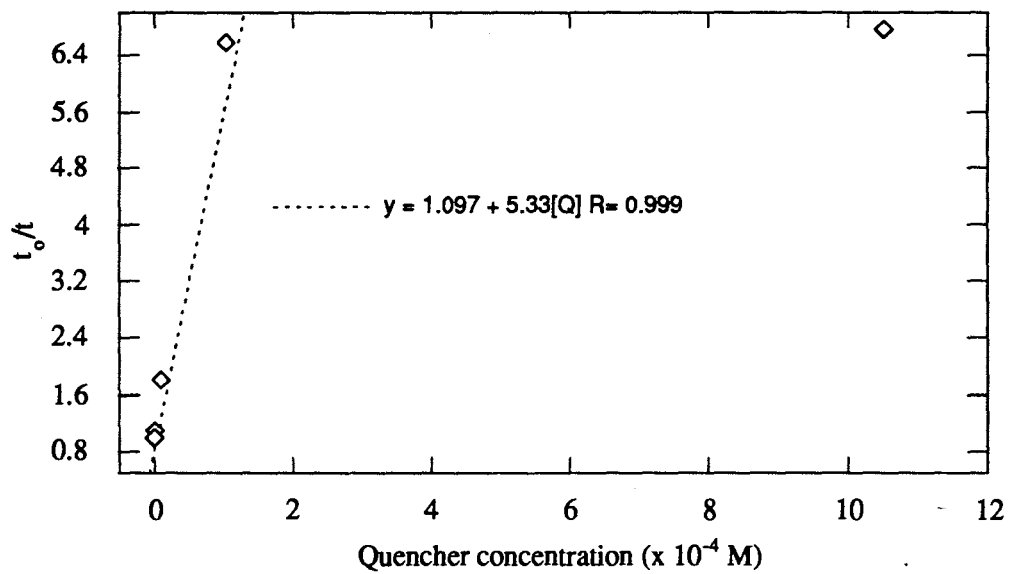


Figure 6.24: Stern Volmer plot for the quenching of $^*[Cr(Me_5-N_6-tricosane)]^{3+}$ by $[Fe(CN)_6]^{4-}$.

6.4. Discussion

6.4.1. Template Synthesis of Chromium(III) Hexamine Complexes

(a) Template Synthesis of $[\text{Cr}(\text{Me}_5\text{-N}_6\text{-tricosane})]^{3+}$ and $[\text{Cr}((\text{CH}_2\text{OH})_2\text{-Me}_5\text{-N}_6\text{-tricosanediimine})]^{3+}$

A rare example of a template synthesis about the Cr(III) ion using the Schiff base strategy was developed. Two complexes were isolated from the reaction of $[\text{Cr}(\text{tame})_2]^{3+}$ with propanal, paraformaldehyde and triethylamine in acetonitrile followed by treatment with borohydride, whose structures are proposed in Fig. 6.25 — $[\text{Cr}(\text{Me}_5\text{-N}_6\text{-tricosane})]^{3+}$ and $[\text{Cr}((\text{CH}_2\text{OH})_2\text{-Me}_5\text{-N}_6\text{-tricosanediimine})]^{3+}$.

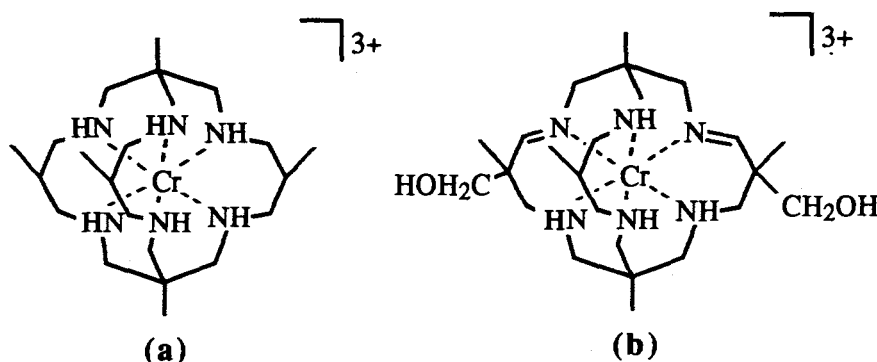
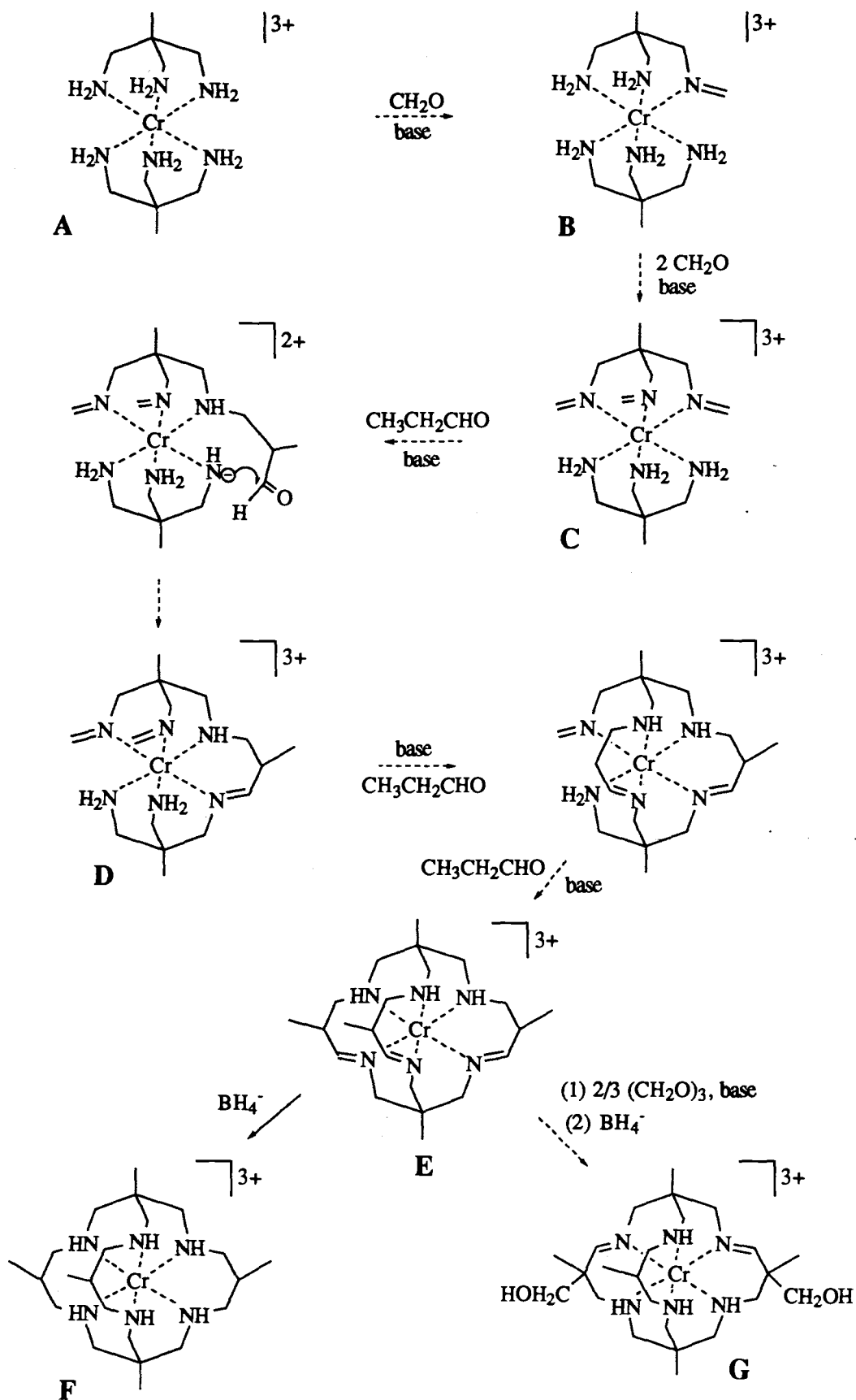


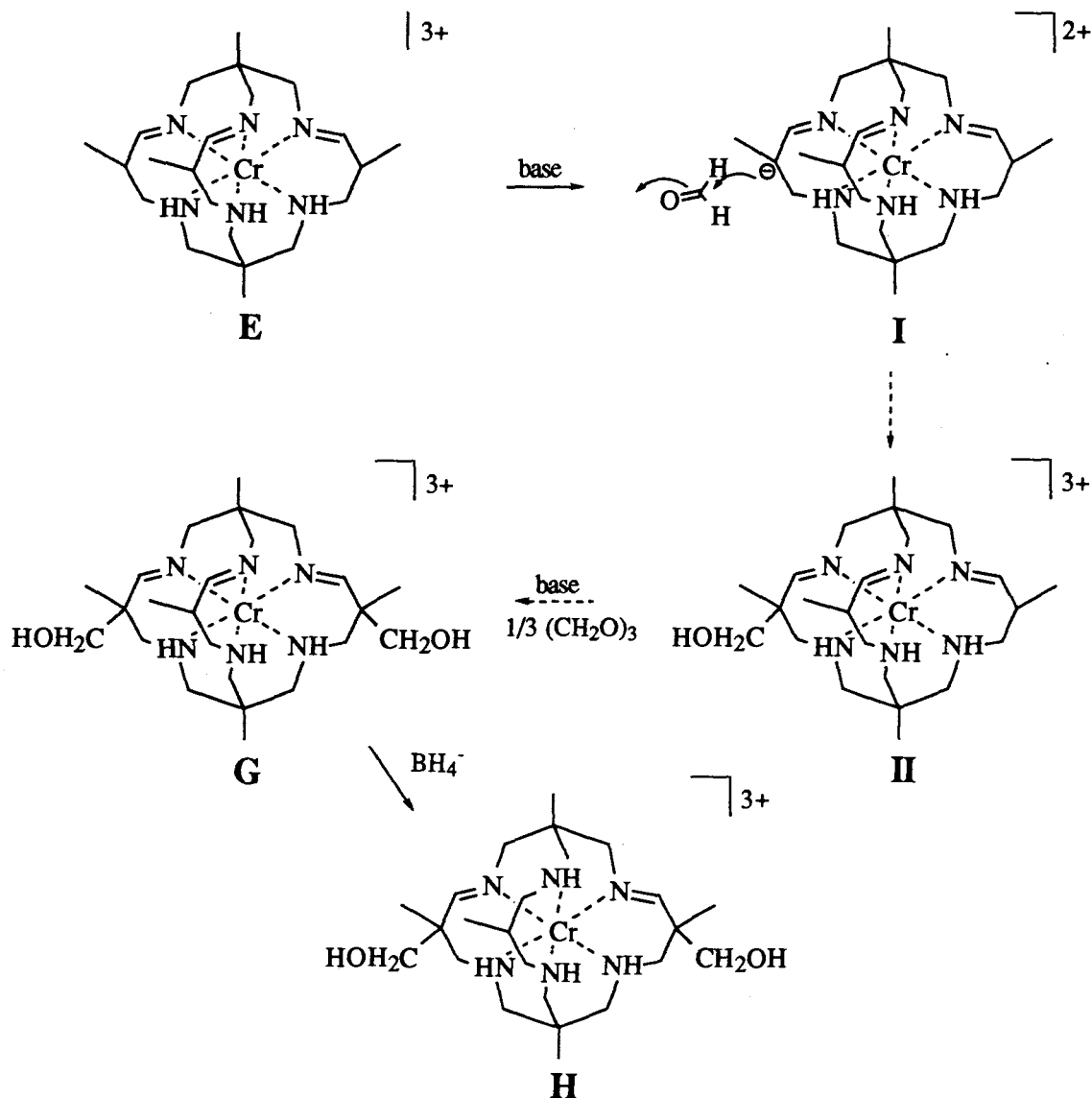
Figure 6.25: (a) $[\text{Cr}(\text{Me}_5\text{-N}_6\text{-tricosane})]^{3+}$ and (b) $[\text{Cr}((\text{CH}_2\text{OH})_2\text{-Me}_5\text{-N}_6\text{-tricosanediimine})]^{3+}$.

It is proposed that the series of condensation reactions and the intermediates leading to the formation of the Cr(III) cage complexes is similar to that for the formation of the analogous Pt(IV) N_6 -tricosanetriimine cage complexes as discussed in Chapter 3.4.ii.a. Hence, only an abbreviated mechanism is presented in Scheme 6.6. The $[\text{Cr}(\text{tame})_2]^{3+}$ template (A) deprotonates and condenses with a formaldehyde unit to form the mono(methanimine) intermediate (B). Amines *cis* to the first imine are anticipated to be more acidic than those which are *trans*, as has been deduced from the analogous Pt(IV) reactions and also by others.^{116,117} Two more formaldehyde units subsequently condense with amines *cis* to the coordinated imine, on the same tame ligand, giving rise to the tris-methanimine intermediate (C). A propanal carbanion attacks one of the coordinated methanimines. The resulting pendant carbonyl condenses with an adjacent deprotonated amine on the opposite tame ligand, to form the first strap (D). This process is repeated twice more to form $[\text{Cr}(\text{Me}_5\text{-N}_6\text{-tricosanetriimine})]^{3+}$ (E).



Scheme 6.6: Template synthesis of $[\text{Cr}(\text{Me}_5\text{-N}_6\text{-tricosane})]^{3+}$ and $[\text{Cr}((\text{CH}_2\text{OH})_2\text{-Me}_5\text{-N}_6\text{-tricosanediiimine})]^{3+}$

It is likely that the imines in this complex lie on the same face of the octahedron, as observed with all other N_6 -tricosanetriimine complexes so far investigated, viz: $[\text{Pt}(\alpha,\beta\text{Me}_5\text{-}N_6\text{-tricosanetriimine})]^{4+}$ (Chapter 3) and $[\text{Co}(\text{Me}_x\text{-}N_6\text{-tricosanetriimine})]^{3+}$ ($x=5,8$).^{51,52,66} The imines in $[\text{Cr}(\text{Me}_5\text{-}N_6\text{-tricosanetriimine})]^{3+}$ (E) are selectively reduced with BH_4^- , to afford the saturated complex, $[\text{Cr}(\text{Me}_5\text{-}N_6\text{-tricosane})]^{3+}$ (F). Furthermore, in E, the methine protons alpha to the imine in the strap are sufficiently acidic and are able to condense further with formaldehyde to form intermediate I and then the di-hydroxymethyl-tricosanetriimine complex G, as depicted in Scheme 6.7. Treatment of G with borohydride yielded the product H, whose structure has not yet been completely resolved. The electrospray mass spectrum indicates that reduction of G did not yield the fully saturated $[\text{Cr}((\text{CH}_2\text{OH})_2\text{-Me}_5\text{-}N_6\text{-tricosane})]^{3+}$ and it may be that the imine in two straps bearing the hydroxymethyl substituents are slower to reduce and longer reduction times or more powerful reductants may be necessary.



Scheme 6.7: Proposed mechanism for functionalisation of the cage at the straps.

The lower yield of the Cr(III) cages, compared to those obtained from the analogous reaction around $[\text{Pt}(\text{tame})_2]^{4+}$, is attributed to the lower acidity of the amines of the Cr(III) template. The side reactions (e.g., self condensation of the aldehydes, formation of other types of cages such as N_6 -tetracosane-type complexes and dissociation of partially formed cages) are more competitive in the Cr(III) condensation reactions. However, the combined yield for both Cr(III) cage Me_5 - N_6 -tricosane complexes (~20% total) is comparable to that obtained in the corresponding strapping reaction around Co(III) to form $[\text{Co}(\text{Me}_5\text{-}N_6\text{-tricosane})]^{3+}$.⁵² Furthermore, the potential exists for the addition of other substituents at the strap methine site in the triimine species (E).

(b) Attempted Synthesis of $[\text{Cr}(\text{Me}_2\text{-}N_6\text{-tricosane})]^{3+}$

The attempted synthesis of $[\text{Cr}(\text{Me}_2\text{-}N_6\text{-tricosane})]^{3+}$ by both the strapping and capping routes was not successful. Both methods gave rise to a range of monomeric and polymeric species which have not yet been characterised. In the $[\text{Cr}(\text{tame})_2]^{3+}$ strapping reaction, the high reactivity of acetaldehyde may have limited its success. Self condensation of the acetaldehyde would have been efficient under the basic reaction conditions, so its concentration was reduced. To circumvent this, it may be necessary to add acetaldehyde slowly during the course of the reaction. In addition, the coordinated imine intermediates may be susceptible to bridge formation, by analogy with the methylene bridges in Co(III) systems,¹¹⁸ but this is not so likely, as the Cr-N bond length is considerably longer than that of the Co-N bond. These processes may be suppressed by using metaldehyde as the source of acetaldehyde. Other side reactions may include ligand dissociation⁴⁷ and formation of a number of different products, such as (Me_4 - N_6 -tetracosanediimine) and (β Me_5 - N_6 -tricosanetriimine) complexes, as observed for analogous condensation reactions using $[\text{Pt}(\text{tame})_2]^{4+}$ template (Chapter 3).

It was surprising that the capping route using $[\text{Cr}(\text{stn})]^{3+}$, propanal and paraformaldehyde in acetonitrile was also unsuccessful, as this template has M-N bond lengths comparable to the successfully capped $[\text{Rh}(\text{stn})]^{3+}$ template. It is likely that base catalysed imine dissociation is faster for Cr(III)⁴⁷ than for Rh(III) and this would obviate the template strategy.

6.4.2. Electrochemistry

The Cr(III)/Cr(II) reduction potentials for the sar and N_6 -tricosane complexes are very similar to those of the $[\text{Cr}(\text{en})_3]^{3+/2+}$ and strain free parent $[\text{Cr}(\text{NH}_3)_6]^{3+/2+}$ couples. The effect of encapsulation and also the expansion of the cage did not dramatically shift the Cr(III)/Cr(II) reduction potential, in contrast with the corresponding Co(III)/Co(II) systems. The reduction potential of the $[\text{Cr}(\text{Me}_5\text{-}N_6\text{-tricosane})]^{3+/2+}$ couple is only 0.18 V more positive than that of the $[\text{Cr}(\text{NH}_3)_6]^{3+/2+}$ couple and only 0.12 V and 0.15 V more positive than that of the $[\text{Cr}((\text{NH}_2)_2\text{sar})]^{3+/2+}$ and $[\text{Cr}(\text{sar})]^{3+/2+}$ couples, respectively, compared to 0.38 V for the analogous cobalt complexes. This is surprising, as the difference in the Cr(III)-N bond length in $[\text{Cr}(\text{Me}_5\text{-}N_6\text{-tricosane})]^{3+}$ and $[\text{Cr}((\text{NH}_2)_2\text{sar})]^{3+}$ is not negligible (0.04 Å). Similarly, there is only a 0.07 V difference between the complexes with the shortest (Cr(*trans*-diammac))³⁺) and longest Cr(III)-N bond lengths ($[\text{Cr}(\text{Me}_5\text{-}N_6\text{-tricosane})]^{3+}$), yet the difference in the Cr(III)-N bond lengths for these complexes is not insignificant (0.06 Å). The unexpectedly small variation in the reduction potential with cage size is not clear. The Cr(II) ion may have less demanding stereochemistry and the energy required to distort the complex would be small. The differences in the strain energies between the Cr(III) and Cr(II) states may be similar for most of these complexes. However, the strain in the Cr(II) complex has not yet been evaluated due to the lack of a Cr(II) force field. Such a force field might be developed from a crystal structure of a suitable complex. Preliminary investigations show that $[\text{Cr}(\text{sar})](\text{CF}_3\text{SO}_3)_2$ dissolved in acetonitrile is stable after one week in an argon atmosphere, but no crystals were isolated. Crystals suitable for X-ray analysis might be obtained from a less soluble system, such as $[\text{Cr}(\text{sar})]\text{Cl}_2$ and this is currently under investigation.

6.4.3. Absorption and Emission Spectra

(a) Spin Allowed Transitions

The energies and molar absorption coefficient for the bands derived from the ${}^4\text{A}_{2g}(\text{O}_h) \rightarrow {}^4\text{T}_{2g}$ and ${}^4\text{T}_{1g}$ transitions for $[\text{Cr}(\text{Me}_5\text{-(CH}_2\text{OH)}_2\text{-}N_6\text{-tricosanediimine})]^{3+}$ and $[\text{Cr}(\text{Me}_5\text{-}N_6\text{-tricosane})]^{3+}$ are not very different from the nonencapsulated Cr(III) hexamine complexes. This implies that the ligand field and microsymmetry about the Cr(III) ion for all of these complexes are similar. In contrast, the higher molar absorptivities and the significantly inequivalent intensities of the two quartet bands observed for the Cr(III) sar complexes^{7,40} implies the CrN_6^{3+} chromophore is more distorted from octahedral symmetry than for the Cr(III) N_6 -tricosane and the nonencapsulated complexes. This distortion reduces the rigour of the symmetry

selection rules for the transitions so that the latter become more probable and therefore more intense. The types of distortion are primarily compression/elongation along the C_3 axis and trigonal twisting about the C_3 axis. These distortions are quantified by the polar angle, ϕ_p , and twist angle, ϕ_t , respectively. The polar angles for all the Cr(III) hexaamine complexes, including the sar complexes here do not deviate greatly from the octahedral value of 54.7° . In contrast, the range of twist angles is larger ($49\text{--}66.5^\circ$) compared to the octahedral value of 60° . The Cr(III) sar complexes are the most trigonally twisted ($\phi_t = 49^\circ$) and this type of distortion may be responsible for the higher molar absorption coefficients and the differences in the intensities of the two quartet bands.

(b) Spectroelectrochemistry

The spectrum of the electrochemically generated $[\text{Cr}(\text{Me}_5\text{-N}_6\text{-tricosane})]^{2+}$ (in acetonitrile, 253 K) is similar to that reported for other high spin Cr(II) hexaamines (in water, 293 K).^{14,76-78,119} It is not clear why reoxidation of the Cr(II) species was notably slower than the initial reduction, especially as the Cr(III)/Cr(II) couple is reversible on the CV timescale. The labile Cr(II) state may have undergone stereochemical rearrangement to form an isomer which could more readily accommodate the larger Cr(II) ion (e.g., a trigonal prismatic cage). This stereochemistry may be the more stable form for Cr(II) and in order to regenerate the preferred C_3 stereochemistry about Cr(III) ion, rearrangement would be necessary. Similar behaviour may have occurred with the bulk electrochemical reduction of $[\text{Cr}(\text{NH}_2)_2\text{sar}]^{3+}$ (Fig. 6.26), followed by reoxidation to reform the Cr(III) species.⁹⁷ The absorption spectrum of the reduced Cr(II) complex was not recorded. The spectrum recorded after reoxidation was largely that of $[\text{Cr}(\text{NH}_2)_2\text{sar}]^{3+}$ and this implies that the Cr(II) ion largely remains within the cage on the bulk electrolytic timescale. One aspect of the spectrum of the regenerated $[\text{Cr}(\text{NH}_2)_2\text{sar}]^{3+}$ is that the band arising from the ${}^4A_{2g}(\text{O}_h) \rightarrow {}^4T_{1g}$ transition for the reoxidised material was higher in intensity than that of the starting material, as observed for the reoxidised $[\text{Cr}(\text{Me}_5\text{-N}_6\text{-tricosane})]^{3+}$ system. This phenomenon might be due to a mechanism similar to that proposed for the $[\text{Cr}(\text{Me}_5\text{-N}_6\text{-tricosane})]^{3+/2+}$ system, but it is not established at this time. Crystallisation of both Cr(II) cage complexes for X-ray structural analyses would be helpful for elucidating this problem.

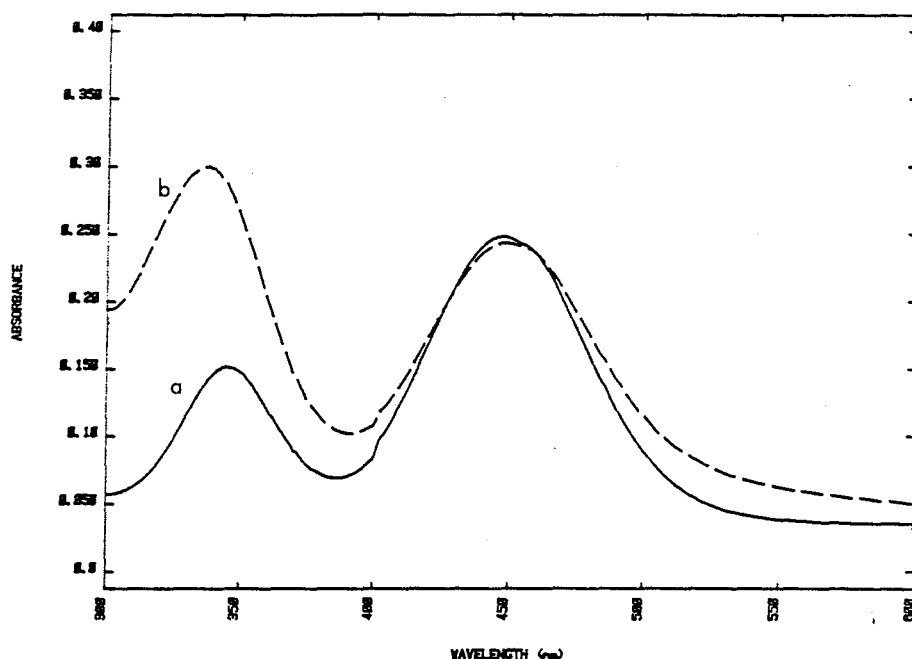


Figure 6.26: Absorption Spectra for $[\text{Cr}(\text{NH}_2)_2\text{sar}]^{3+}$ (a) before reduction (b) after reduction, followed by reoxidation. (298 K, in 0.1 M NaClO_4) (reproduced from reference 97).

(c) Spin Forbidden Transitions

The energies of the 0–0 band arising from the spin forbidden ${}^4\text{A}_{2g}(\text{O}_h) \leftrightarrow {}^2\text{E}_g$ transition for the $[\text{Cr}(\text{tame})_2]^{3+}$, $[\text{Cr}(\text{stn})]^{3+}$ and $[\text{Cr}(\text{Me}_5\text{-N}_6\text{-tricosane})]^{3+}$ complexes are very similar to those observed for related Cr(III) hexaamine complexes, occurring at ~ 670 nm. In a strictly octahedral field, this transition is electric dipole forbidden but magnetic dipole allowed and this is reflected in the very low molar absorption coefficients $\epsilon_{\text{max}} \sim 0.1\text{--}0.8 \text{ M}^{-1}\text{cm}^{-1}$. Most of the intensity is distributed into the vibrational side bands, like other Cr(III) hexaamines with octahedral microsymmetry,² and the relative intensity of the 0–0 transition compared to the vibrational side bands is sensitive to distortions from octahedral symmetry.¹¹ These data indicate that the symmetry about the Cr(III) ion is octahedral.

6.4.4. Comparison of the Lifetimes of the 2E_g State.

It was surprising that the 2E_g state lifetime of the $[\text{Cr}(\text{Me}_5\text{-N}_6\text{-tricosane})]^{3+}$ ion was so long lived at 298 K, in contrast to those of the Cr(III) sar cages and the nonencapsulated complexes. The 2E_g state lifetime at 298 K for the $[\text{Cr}(\text{Me}_5\text{-N}_6\text{-tricosane})]^{3+}$ complex is at least $\sim 10^4$ times longer than that for the Cr(III) sar complexes, and is the longest recorded to date for a Cr(III) hexaamine complex at both 77 and 298 K in solution. The following discussion addresses why these two types of cage complexes have such vastly different 2E_g lifetimes.

The 2E_g state lifetime for Cr(III) hexaamine complexes depends on the number and efficiency of the deactivation pathways. Their absolute and relative rates (in equation 6.1) should be addressed before attempting to explain the different lifetimes observed for the series of Cr(III) hexaamine complexes presented here. The processes which contribute to the observed relaxation rate constant (k_i) of the 2E_g state were briefly described in the introduction.

$$\frac{1}{\tau} = k_i = k_{nr2} + k_{cr2} + k_{bisc} + k_{ph} \quad (6.1)$$

The non radiative term (k_{nr2}) contains temperature independent and dependent terms, k^0 and $k(T)$, respectively (equation 6.3). Dynamic processes associated with ligand skeletal motions are the main contributors to the $k(T)$ term, whereas k^0 is dominated by static mechanisms, namely, the average symmetry of the ligand field exerted by the donor atoms on the Cr(III) ion.

$$k_{nr2} = k^0 + k(T) \quad (6.3)$$

At 77 K, the lifetimes of all of the Cr(III) hexaamine complexes considered here have reached limiting values. Vibrational mechanisms and putative chemical reactions are considerably damped at this temperature so the corresponding terms for these processes, $k(T)$ and k_{cr2} , are negligible. The back intersystem crossing rate constants (k_{bisc}) are also likely to be negligible for all Cr(III) hexaamine complexes as the energy differences between the absorption maxima for the bands arising from the ${}^4A_{2g}(\text{O}_h) \rightarrow {}^4T_{2g}$ and the 2E_g transitions are large.^{4-6,9,11,106,107,110,111,120} It is likely that this process is dependent on the energies of the equilibrium geometries of the ${}^4T_{2g}$ and 2E_g states.^{11,120} The values range from 6420 to 8760 cm^{-1} (for $[\text{Cr}(\text{NH}_3)_6]^{3+}$ to $[\text{Cr}(\textit{trans}\text{-diammac})]^{3+}$, respectively) and is too large for even thermally induced back intersystem crossing. It therefore follows that the overall rate constant for the 2E_g deactivation at 77 K could be reduced to:

$$k_i = k_{ph} + k^0 \quad (6.4)$$

At 77 K, the 2E_g lifetimes of the Cr(III) complexes appear to be much the same. The average value is 160 μ s; the difference is at most a factor of ~ 3 . This implies that the dominant contribution to the deactivation rate at low temperature is from the k_{ph} and k^0 terms (equation 6.4). The small variations in the lifetime at low temperature may arise from static mechanisms originating from subtle differences in the stereochemistry imposed by the ligand on the Cr(III) ion. Given that the lifetimes of these complexes are similar at 77 K, slight deviations from octahedral microsymmetry do not appear to contribute significantly to the rate of relaxation. Even trigonal twisting from octahedral symmetry by as much as 11° , as for the Cr(III) sar complexes, does not appear to have a significant effect on the lifetime in the temperature independent region.

Although vibrational processes are mostly damped at 77 K, they are not eliminated. One such pathway at low temperature is the coupling of the high energy N-H stretching mode with the transition moment. The lifetimes of the complexes at 77 K increase approximately 10-20 times upon deuteration of the N centres (excluding the $[\text{Cr}(\text{NH}_3)_6]^{3+}$ ion, which increases by ~ 40 times) and appears to be roughly dependent on the number of N-H oscillators present.^{12,42,105,121} It is not clear if an increase in temperature alters the relative effectiveness of these modes.

As the temperature increases, other pathways which deplete the 2E_g state become accessible, and this is manifest by a rapid decrease in the 2E_g state lifetime in a threshold temperature regime for all complexes except the $[\text{Cr}(\text{Me}_5\text{-}N_6\text{-tricosane})]^{3+}$ ion up to 300 K. Such pathways include ligand dissociation (k_{cr2}) and thermally activated non radiative processes $k((T))$.

That the Cr(III) hexamine complexes are able to undergo photoinduced chemical reactions, such as ligand dissociation, has been widely discussed.^{8,21,33-35,122-124} Whether photoinduced substitution occurs from the 2E_g state or the ${}^4T_{2g}$ state has been the subject of considerable controversy. One reason for supporting the 2E_g state argument mainly arose because its lifetime is longer than the ${}^4T_{2g}$ state²¹ and that it therefore had more time to undergo ligand dissociation (The lifetime of the 2E_g state is $\sim 10^{-3}$ – 10^{-8} s compared to that of the ${}^4T_{2g}$ state, which has been estimated as $\sim 10^{-10}$ – 10^{-12} s).²² The ${}^4T_{2g}$ state however, has a more suitable configuration for dissociation reactions, as the act of promoting an electron into the e_g antibonding levels leads to elongation of Cr(III)-N bonds^{15,32} and dissociation of a ligating group would be facilitated. In contrast, the configuration for the 2E_g state is very similar to the ${}^4A_{2g}$ ground state,¹⁷ which is substitution inert. Recent experiments using the $[\text{Cr}(\text{NH}_3)_6]^{3+}$ and $[\text{Cr}(\text{en})_3]^{3+}$ ions in both ethylene glycol:water and in a PVA film support the ${}^4T_{2g}$ pathway.^{30,114} No photosubstitution was observed when the 2E_g state of these complexes was directly populated, even during prolonged irradiation.^{30,114} However,

irradiation into the ${}^4T_{2g}$ state using a blue laser resulted in prompt photosubstitution. This clearly indicates that the ${}^4T_{2g}$ state is largely responsible for photoinduced ligand dissociation. Similar conclusions have been reached by others using solutions of the complexes $[Cr(NH_3)_6]^{3+}$,³² $[Cr(tn)_3]^{3+}$ ¹⁰⁹ and $[Cr(en)_3]^{3+}$.¹⁰⁸

In contrast, the cage complexes are significantly more photostable in the visible region, as amply demonstrated by prolonged irradiation of the $[Cr(Me_5-N_6\text{-tricosane})]^{3+}$ ion at 488 nm in acidic media. The phosphorescence intensity is invariant even after 5000 s of continuous irradiation, whereas the intensity of the 2E_g emission for partially encapsulated $[Cr(stn)]^{3+}$ drops to zero within microseconds under the same conditions. In addition, the quantum yield for photodecomposition for the Cr(III) sar complexes is $<10^{-4}$ times that for the nonencapsulated complexes.^{7,40} Photoinduced ligand substitution is impeded by the steric constraints of the cage complexes. If the M-N bond ruptures, the nitrogen donor atom is unable to move away from the metal ion during the lifetime of the excited state, unlike the nonencapsulated systems. Furthermore, if ligand dissociation were an important decay route, it is anticipated that the rates of excited state decay would be comparable for both types of cages. It is therefore unlikely that the dramatic difference in the lifetimes of the Cr(III) sar complexes and the $[Cr(Me_5-N_6\text{-tricosane})]^{3+}$ ion is due to ligand dissociation. It should also be noted that a proposed associative pathway^{8,35} is not feasible in the cage systems; the steric constraints of the cage complexes would hinder the coordination of a seventh donor group. Furthermore, there has been no evidence for increased coordination with any of the Cr(III) sar systems^{7,40} or with the $[Cr(Me_5-N_6\text{-tricosane})]^{3+}$ ion.

Clearly, deactivation by chemical reaction and static mechanisms are not responsible for the rapid phosphorescence decay of the Cr(III) sar complexes after the threshold temperature region has been attained. Thermally activated processes, such as vibronic coupling, are probably the dominant contributors to the decay. The ten-fold increase in the lifetime upon deuteration for all complexes at both 77 and 298 K shows that the N-H stretching vibrations are important to $k(T)$. The N-H vibrations however, cannot account for the spectacularly different lifetimes of the $[Cr(Me_5-N_6\text{-tricosane})]^{3+}$ and the sar complexes. If this were the dominant pathway, then the decay rates are expected to be the same for complexes with the same number of N-H oscillators, for example, the Cr(III) sar complexes, $[Cr(Me_5-N_6\text{-tricosane})]^{3+}$ and $[Cr(tacn)_2]^{3+}$. However, the temperature dependent threshold region for each of these complexes is grossly different, the Cr(III) sar complexes have a notably lower threshold temperature regime (150 – 200 K)^{7,40} compared to the other nonencapsulated Cr(III) hexamine complexes (~220 – 250 K).^{4,104,105} In contrast, the threshold temperature for the $[Cr(Me_5-N_6\text{-tricosane})]^{3+}$ ion appears not to have been attained even at 298 K. The different temperature threshold regions imply that a very efficient relaxation process for

the Cr(III) sar complexes exists, which is absent for $[\text{Cr}(\text{Me}_5\text{-N}_6\text{-tricosane})]^{3+}$. The nature of these processes has not been established. Most of the other Cr(III) complexes decay by way of ligand dissociation and are therefore not considered further. In order to simplify this issue only the encapsulated complexes will be addressed.

(a) *The Effect of Ligand Rigidity on the 2E_g State Lifetime.*

It is possible that vibrational processes associated with the ligand skeleton are responsible and the efficiency of these processes would depend on the flexibility of the complex. Complexes which undergo rapid conformational changes could couple these motions with the transition moment. The sar complexes are able to undergo conformational changes such as twisting the ligand caps to change the symmetry from C_3 to D_3 . Other possible conformational changes involve the alignment of the C-C bond of the ethylenediamine chelate strap with the C_3 axis. The C-C bond may be oblique (*ob*) or parallel (*lel*) to the C_3 axis, giving rise to complexes having ob_3 , ob_2lel , $oblel_2$ or lel_3 conformations. The strain energies of the various conformers arising from such motions for unsubstituted sar complexes have been estimated using molecular mechanics for a number of metal ions.^{54,125,126} For example, in one calculation for $[\text{Co}(\text{sar})]^{3+}$,¹²⁵ the differences in energies and the barriers to interconversion between the D_3ob_3 , D_3lel_3 , C_3lel_3 , C_2lel_2ob and C_2lelob_2 conformers are small. Interconversion between the conformers is rapid on the ^1H NMR timescale in diamagnetic Co(III) systems and they have not been damped, even at 178 K.

Extending the strain energy concept to the 2E_g state of the Cr(III) cages provides a useful gauge for comparing the relative rigidity of the Cr(III) sar and N_6 -tricosane complexes. As there is no force field available for excited state Cr(III) complexes (or any other excited state metal ion), the energies of the conformations were calculated using a ground state force field.^{93,98} The equilibrium geometries in the ground $^4A_{2g}$ and 2E_g states are similar and it is anticipated that the relative energies of the conformers are similar. It is unlikely that a change of electron spin in a non bonding orbital to attain the 2E_g state will drastically alter the properties of the complex.^{§,17} This is confirmed in part by the coincidence of the 0-0 transition in the absorption and emission spectra for the $^4A_{2g} \leftrightarrow ^2E_g$ transition. Therefore, although the absolute energies of the conformers are

§ It should be noted that the ground state force field should not be used to calculate the strain energies of the excited quartet states and the distribution of the electrons in these states is very different from that of the ground state.

not meaningful, their relative energies may be a useful guide for gauging the ease of interconversion of conformers in the excited state.

Molecular mechanics calculations of $[\text{Cr}(\text{sar})]^{3+}$ ⁹⁸ estimate that the energies of the conformational minima are very similar. The process of interconversion results in a variation in microsymmetry about the CrN_6^{3+} chromophore such that the rigour of the symmetry selection rules is diminished. The movement of the ligand induces vibrations which could couple with the transition moment, thereby increasing the probability of the transition. Therefore the flexibility of the Cr(III) sar cages enhances the rate of 2E_g state decay. The barrier for cap twisting ($C_3lel_3 \leftrightarrow D_3lel_3$) appears to be lower than that for *ob/lel* interconversion. Cap twisting is probably a more facile process and therefore a more likely mechanism for 2E_g state relaxation than strap interconversion (see Fig. 6.27). The implications of the results for the $[\text{Cr}(\text{sar})]^{3+}$ conformers may be extended to other Cr(III) sar complexes with apical substituents (NH_2 , Cl, etc), as they are unlikely to affect the barriers to interconversion.

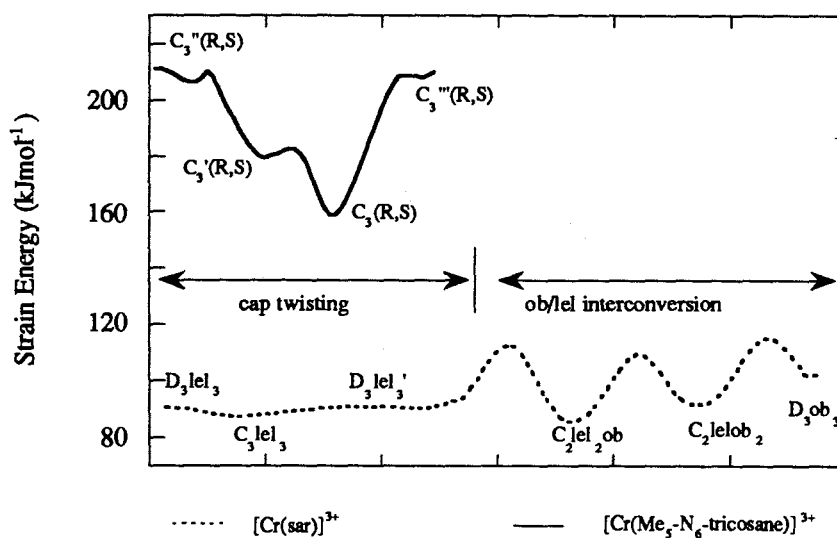


Figure 6.27: Potential energy surface for predicted conformers of (a) $[\text{Cr}(\text{sar})]^{3+}$ (dotted line) and (b) $[\text{Cr}(\text{Me}_5\text{-N}_6\text{-tricosane})]^{3+}$ (solid line).⁹⁸

In contrast, conformer interconversion is more difficult for the $[\text{Cr}(\text{Me}_5\text{-}N_6\text{-tricosane})]^{3+}$ ion. Molecular mechanics calculations⁹⁸ predict that the lowest energy conformation[‡] is significantly more stable than other possible conformations (Fig. 6.27). The calculations indicate that it is unlikely that cap twisting is an important mechanism for deactivation in this system. Similarly, interconversion of the chelate rings of the strap from chair to skew boat is unfavoured, as peripheral methyl substituents on these chelate rings prefer to be in the equatorial position. On the basis of the ground state calculations, it is anticipated that the excited state complex also exists almost exclusively in one conformer. As the probability for interconversion is not high, there would be relatively fewer skeletal modes available for coupling with the transition moment compared to the Cr(III) sar system. This may explain why this complex has a surprisingly long 2E_g state lifetime compared to those of the Cr(III) sar complexes.

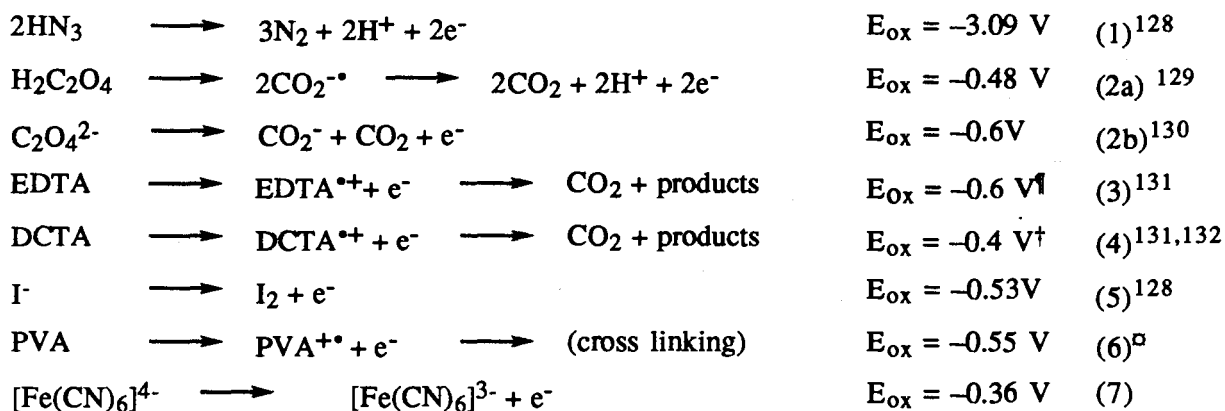
Similar conformational changes are likely in the analogous nonencapsulated systems, but there are fewer degrees of freedom available. This might be why most of the nonencapsulated Cr(III) hexaamines have a higher temperature threshold region than the Cr(III) sar complexes. However, as photodissociation is a dominant mechanism for excited state relaxation, it would be difficult to delineate the relative contributions of the vibrational relaxation pathways and the rate of dissociation to the total deactivation rate.

In summary, the unexpectedly long lifetime of the 2E_g state for the $[\text{Cr}(\text{Me}_5\text{-}N_6\text{-tricosane})]^{3+}$ ion may be attributed to its decreased flexibility. In contrast, the Cr(III) sar complexes (and to an extent, the nonencapsulated complexes) are conformationally labile and the energies of the conformers are not very different. In this context, it would be interesting to examine the spectroscopy of the $[\text{Cr}(\text{Me}_2\text{-}N_6\text{-tricosane})]^{3+}$, as there are no peripheral substituents on the strap to hinder interconversion. Examination of the lifetime of $[\text{Cr}(\text{Me}_3\text{N})_2\text{sar}]^{5+}$ may also add support to this argument. Cap twisting in this complex is expected to be encumbered by the apical Me_3N^+ substituents. Such behaviour has been observed for $[\text{Co}(\text{Me}_3\text{N})_2\text{sar}]^{5+}$.¹²⁷

‡ The conformer with the lowest energy has $C_3(R,S)$ symmetry, a twist angle, ϕ_t , of 66.5° and the six membered chelate rings of the strap are in the chair conformation. It is also the same as that observed in the crystal structure.¹¹²

6.4.5. A Potential Photosensitiser — the $[\text{Cr}(\text{Me}_5\text{-N}_6\text{-tricosane})]^{3+}$ Ion?

As the ${}^2\text{E}_g$ state for the $[\text{Cr}(\text{Me}_5\text{-N}_6\text{-tricosane})]^{3+}$ ion was exceptionally long and photosubstitution was negligible in acid media, it was anticipated that this complex might function as a photosensitiser. The quenchers investigated are able to quench the ${}^2\text{E}_g$ state thermodynamically by a one electron transfer and their oxidation half equations are:



‡ , pH=2.1; ‡ , pH=3.8; $^\square$, The oxidation potential for PVA was not determined. An analogous system is ethylene glycol whose reduction potential is quoted.¹³³

There are two possible routes for quenching the ${}^2\text{E}_g$ state, either by electron transfer or energy transfer. The quenching experiments however, do not indicate which of these pathways is operative. The quenchers azide, oxalate, EDTA, DCTA and PVA which were anticipated to react irreversibly to form gaseous products showed no evidence for net electron transfer. Energy transfer into vibrational modes of these quencher may be a possible route, but electron transfer should not be ruled out. Some evidence for electron transfer arises from the slight decrease in the ${}^2\text{E}_g$ state lifetime of the $[\text{Cr}(\text{Me}_5\text{-N}_6\text{-tricosane})]^{3+}$ ion using I^- as a quencher. However, this pathway is inefficient, as a large excess of I^- is required to decrease the ${}^2\text{E}_g$ state lifetime by a mere 44%. In contrast, the quenching of the excited state $[\text{Cr}(\text{bpy})_3]^{3+}$ complex under the same conditions is considerably more efficient, the rate of excited electron transfer appears to be faster, even though the lifetime of this ion is only a tenth of that for the cage complex. Preliminary experiments show that $[\text{Fe}(\text{CN})_6]^{4-}$ quenches the ${}^2\text{E}_g$ state. In this instance, electron transfer is thought to be dominant as $[\text{Fe}(\text{CN})_6]^{4-}$ has no low energy bands. If electron transfer is the mechanism for quenching, the self exchange rate constant for the $^*[\text{Cr}(\text{Me}_5\text{-N}_6\text{-tricosane})]^{3+}/[\text{Cr}(\text{Me}_5\text{-N}_6\text{-tricosane})]^{2+}$ couple is

estimated as $\sim 500 \text{ M}^{-1}\text{s}^{-1}$, using the Marcus cross relation.^{§ 134,135} The absence of observed net electron transfer may be attributed to rapid back electron transfer occurring prior to the separation of the products. It is anticipated that the back electron transfer rate is even faster than the forward rate, as the driving force for the oxidation of $[\text{Cr}(\text{Me}_5\text{-N}_6\text{-tricosane})]^{2+}$ and reduction $[\text{Fe}(\text{CN})_6]^{3-}$ is very large ($\Delta E = 1.36 \text{ V}$). The ion pairing between $[\text{Cr}(\text{Me}_5\text{-N}_6\text{-tricosane})]^{2+}$ and $[\text{Fe}(\text{CN})_6]^{3-}$ also impedes the separation of products and this enhances the probability of back electron transfer.

Further experiments are required in order to determine whether electron transfer is a possible deactivation route. Examination of the pressure dependence on quenching rate constants could provide some insight into this dilemma.¹³⁶ It is anticipated that the volume of activation would be large and negative if electron transfer was the dominant mechanism for quenching as this process would involve solvent reorganisation, regardless of whether or not back electron transfer occurs. In contrast, solvent reorganisation would be minimal if energy transfer was dominant and the volume of activation would be small.

Although the photoreactivity of the ${}^2\text{E}_g$ state of the $[\text{Cr}(\text{Me}_5\text{-N}_6\text{-tricosane})]^{3+}$ ion was disappointing, the extension of its excited state lifetime is an important result. It is clear that photodissociation of the Cr(III) cages is limited and this is essential for the success of photocyclic reactions. However, currently, the Cr(II) product from the electron transfer reactions is too powerful as a reducing agent and the back electron transfer rates are probably near diffusion controlled. Therefore, it is important to reduce the negative potential in the ground state if these systems are to be useful photocatalysts. Other Cr(III) cage complexes are being sought as potential photosensitisers. For example, it is anticipated that Cr(III) cage complexes with some sulfur donor atoms, would shift the ground state reduction potential to more positive values and therefore reduce the driving force for the putative back electron transfer. Such an example is the analogous N_3S_3 cage complex and work is currently underway to achieve this.⁵⁹

§ using the expression $k_{12} = \sqrt{k_{11} \times k_{22} \times K_{12} \times f}$,

where k_{11} is the self exchange rate constant for the ground state couple of the donor ($2.3 \times 10^4 \text{ M}^{-1}\text{s}^{-1}$ for $[\text{Fe}(\text{CN})_6]^{3-/4-}$), k_{22} is the self exchange rate constant for the acceptor, k_{12} is the rate constant for electron transfer from the donor to the acceptor ($7.2 \times 10^7 \text{ M}^{-1}\text{s}^{-1}$), and K_{12} is the equilibrium constant = $\exp(nF\Delta E/RT)$, (for this system, $\Delta E = 0.51 \text{ V}$, so $K_{12} = 4.22 \times 10^8$) and

$$\ln f_{12} = \frac{(\ln K_{12})^2}{4 \ln(k_{11}k_{22} / Z^2)}$$

where $Z = 10^{11} \text{ M}^{-1}\text{s}^{-1}$.

6.4.6. References

- (1) Forster, L. S. *Chem. Rev.* **1990**, *90*, 331, and references therein.
- (2) Forster, L. S. *Trans. Met. Chem.* **1969**, *5*, 1, and references therein.
- (3) *Concepts in Inorganic Photochemistry*; Adamson, A. W.; Fleischauer, P. D., Eds.; John Wiley and Sons: New York, 1975, and references therein.
- (4) Forster, L. S. *Advances in Photochemistry* **1991**, *16*, 226, and references therein.
- (5) Kemp, T. J. *Prog. Reaction Kinetics* **1980**, *10*, 316, and references therein.
- (6) Fleischauer, P. D.; Fleischauer, P. *Chem. Rev.* **1970**, 199, and references therein.
- (7) Comba, P.; Mau, A. W. H.; Sargeson, A. M. *J. Phys. Chem.* **1985**, *89*, 394, and references therein.
- (8) Endicott, J. F.; Ramasami, T.; Tamilarasan, R.; Lessard, R. B.; Ryu, C. K. *Coord. Chem. Rev.* **1987**, *77*, 1, and references therein.
- (9) Rojas, G. E.; Magde, D. *Inorg. Chem.* **1987**, *26*, 2334.
- (10) Linck, N. J.; Berens, S. J.; Magde, D.; Linck, R. G. *J. Phys. Chem.* **1983**, *87*, 1733.
- (11) Schläfer, H. L.; Gausmann, H.; Witzke, H. *J. Chem. Phys.* **1967**, *46*, 1423.
- (12) Robbins, D. J.; Thomson, A. J. *Mol. Phys.* **1973**, *25*, 1103, and references therein.
- (13) Flint, C. D. *J. Chem. Phys.* **1970**, *52*, 168.
- (14) Lever, A. B. P. *Inorganic Electronic Spectroscopy*; 2nd ed.; Elsevier Science Publishers: New York, 1984.
- (15) Wilson, R. B.; Soloman, E. I. *Inorg. Chem.* **1978**, *17*, 1729.
- (16) Schläfer, H. L.; Gliemann, G. *Basic Principles of Ligand Field Theory*; Wiley: New York, 1969, and references therein.
- (17) Porter, G. B.; Schläfer, H. L. *Z. Phys. Chem. (Frankfurt)* **1963**, *38*, 227.
- (18) Angel, S. M.; DeArmond, M. K. *J. Phys. Chem.* **1984**, *88*, 3407.

- (19) Parker, C. A. *Photoluminescence of Solutions*; Elsevier Publishing Co: Amsterdam, 1968.
- (20) Robinson, G. W.; Frosch, R. P. *J. Chem. Phys.* **1962**, *37*, 1962.
- (21) Schläfer, H. L. *J. Phys. Chem.* **1965**, *69*, 2201.
- (22) Rojas, G. E.; Dupuy, C.; Sexton, D. A.; Magde, D. *J. Phys. Chem.* **1986**, *90*, 87, and references therein.
- (23) Chatterjee, K. K.; Forster, L. S. *Spectrochim. Acta.* **1964**, *20*, 1603.
- (24) DeArmond, K.; Forster, L. S. *Spectrochim. Acta* **1963**, *19*, 1687.
- (25) Adamson, A. W.; Waltz, W. L.; Zinato, E.; Watts, D.; Fleischauer, P. D.; Lindholm, R. D. *Chem. Rev.* **1968**, *68*, 541, and references therein.
- (26) Fucaloro, A. F.; Forster, L. S.; Rund, J. V.; Lin, S. H. *J. Phys. Chem.* **1983**, *87*, 1796, and references therein.
- (27) Endicott, J. F.; Lessard, R. B.; Lynch, D.; Perkovic, M. W.; Ryu, C. K. *Coord. Chem. Rev.* **1990**, *97*, 65, and references therein.
- (28) Waltz, W. L.; Lilie, J.; Lee, S. H. *Inorg. Chem.* **1984**, *23*, 1768.
- (29) Ceulemans, A.; Beyens, D.; Vanquickenborne, L. G. *J. Am. Chem. Soc.* **1982**, *104*, 2988, and references therein.
- (30) Riesen, H.; Manson, N. B.; Krausz, E. *J. Lumin.* **1990**, *46*, 345.
- (31) Walters, R. T.; Adamson, A. W. *Acta. Chem. Scand.* **1979**, *A33*, 53.
- (32) Krause, H. H.; Wasgestian, F. *Inorg. Chim. Acta* **1981**, *49*, 231.
- (33) Kirk, A. D. *Coord. Chem. Rev.* **1981**, *39*, 225, and references therein.
- (34) Kirk, A. D. *Comments Inorg. Chem.* **1993**, *14*, 89.
- (35) Endicott, J. F. *J. Chem. Educ.* **1983**, *60*, 824.
- (36) Adamson, A. W. *J. Phys. Chem.* **1967**, *71*, 798.
- (37) Forster, L. S. In *Concepts of Inorganic Photochemistry*; A. W. Adamson and P. D. Fleischauer, Eds.; John Wiley and Sons: New York, 1975, and references therein.
- (38) Porter, G. B.; Schläfer, H. L. *Z. Phys. Chem. (Frankfurt)* **1964**, *40*, 280.

- (39) Porter, G. B. In *Kinetics of Photophysical Processes*; A. W. Adamson and P. D. Fleischauer, Eds.; John Wiley and Sons: New York, 1975, and references therein.
- (40) Comba, P.; Creaser, I. I.; Gahan, L. R.; Harrowfield, J. M.; Lawrance, G. A.; Martin, L. L.; Mau, A. W. H.; Sargeson, A. M.; Sasse, W. H. F.; Snow, M. R. *Inorg. Chem.* **1986**, *25*, 384, and references therein.
- (41) Moran, G., Unpublished results.
- (42) Wasgestian, F.; Kühn, K.; Kupka, H. *J. Phys. Chem.* **1981**, *85*, 665, and references therein.
- (43) Gowin, E.; Wasgestian, F. *Inorg. Chem.* **1985**, *24*, 3106.
- (44) Perkovic, M. W.; Heeg, M. J.; Endicott, J. F. *Inorg. Chem.* **1991**, *30*, 3140.
- (45) Flint, C. D.; Matthews, A. P. *J. Chem. Soc. Faraday Trans.* **1976**, *72*, 579.
- (46) Hendry, A. J., Unpublished results.
- (47) Creaser, I. I., Unpublished results.
- (48) Bruce, J.; Gahan, L.; Hambley, T. W.; Stranger, R. *J. Chem. Soc., Chem. Commun.* **1993**, 702.
- (49) McDonnell, M., Unpublished observations.
- (50) Maeder, U., Unpublished results.
- (51) Ralph, S. F., Personal Communication.
- (52) Geue, R. J.; Höhn, A.; Ralph, S. F.; Sargeson, A. M. *J. Chem. Soc., Chem. Commun.* **1994**, 1513.
- (53) Creaser, I. I.; Harrowfield, J. M.; Herlt, A. J.; Sargeson, A. M.; Springborg, J.; Geue, R. J.; Snow, M. R. *J. Am. Chem. Soc.* **1977**, *99*, 3181.
- (54) Geue, R. J.; Hambley, T. W.; Harrowfield, J. M.; Sargeson, A. M.; Snow, M. R. *J. Am. Chem. Soc.* **1984**, *106*, 5478.
- (55) Lay, P. A. Ph.D. Thesis, Australian National University, 1981.
- (56) Harrowfield, J. M.; Herlt, A. J.; Lay, P. A.; Sargeson, A. M.; Bond, A. M.; Mulac, W. A.; Sullivan, J. C. *J. Am. Chem. Soc.* **1983**, *105*,

- (57) Boucher, H. A.; Lawrance, G. A.; Lay, P. A.; Sargeson, A. M.; Bond, A. M.; Sangster, D. F.; Sullivan, J. C. *J. Am. Chem. Soc.* **1983**, *105*, 4652.
- (58) Ramasami, T.; Endicott, J. F.; Brubaker, G. R. *J. Phys. Chem.* **1983**, *87*, 5057.
- (59) Angus, P., Personal communication.
- (60) Nair, B. U.; Ramasami, T.; Ramaswamy, D. *Polyhedron* **1983**, *2*, 103.
- (61) Colton, R. *Coord. Chem. Rev.* **1988**, *90*, 1, and references therein.
- (62) Höhn, A.; Geue, R. J.; Sargeson, A. M. *J. Chem. Soc., Chem. Commun.* **1990**, 1473.
- (63) Geue, R. J.; Petri, W. R.; Sargeson, A. M.; Snow, M. R. *Aust. J. Chem.* **1992**, *45*, 1681.
- (64) Geue, R. J.; Korybut-Daskiewicz, B.; Sargeson, A. M. *J. Chem. Soc. Chem. Commun.* **1993**, 1454.
- (65) Geue, R. J.; McDonnell, M. B.; Mau, A. W. H.; Sargeson, A. M.; Willis, A. *C. J. Chem. Soc. Chem. Commun.* **1994**, 667.
- (66) Höhn, A., Unpublished observations.
- (67) Geue, R. J., Personal communication. **1990**.
- (68) Raymond, K. N.; Corfield, P. W. R.; Ibers, J. A. *Inorg. Chem.* **1968**, *7*, 1362.
- (69) Ballardini, R.; Varani, G.; Scandola, F.; Balzani, V. *J. Am. Chem. Soc.* **1976**, *98*, 7432.
- (70) Bolletta, F.; Maestri, M. M.; Moggi, L.; Balzani, V. *J. Chem. Soc., Chem. Commun.* **1975**, 901.
- (71) Ballardini, R.; Varani, G.; Indelli, M. T.; Scandola, F.; Balzani, V. *J. Am. Chem. Soc.* **1978**, *100*, 7219, and references therein.
- (72) Serpone, N.; Jamieson, M. A.; Henry, M. S.; Hoffman, M. Z.; Bolletta, F.; Maestri, M. *J. Am. Chem. Soc.* **1979**, *101*, 2907, and references therein.
- (73) Jamieson, M. A.; Serpone, N.; Hoffman, M. Z. *Coord. Chem. Rev.* **1981**, *39*, 121, and references therein.

- (74) Bakac, A.; Zahir, K.; Espensen, J. H. *Inorg. Chem.* **1988**, *27*, 315, and references therein.
- (75) Sima, J.; Sykora, J. *Coord. Chem. Rev.* **1990**, *12*, 1, and references therein.
- (76) Earnshaw, A.; Larkworthy, L. F.; Patel, K. S. *J. Chem. Soc., (A)* **1969**, 1339.
- (77) Larkworthy, L. F.; Patel, K. S.; Trigg, J. K. *J. Chem. Soc., (A)* **1971**, 2766.
- (78) Larkworthy, L. F.; Nolan, K. B.; O'Brien, P. O. In *Comprehensive Coordination Chemistry*; G. Wilkinson, Ed.; Pergamon Press: 1989; Vol. 3, Chapter 35.
- (79) Pecsok, R. L.; Garber, R. A.; Shields, L. D. *Inorg. Chem.* **1965**, *4*, 447.
- (80) Dei, A.; Mani, F. *Inorg. Chem.* **1976**, *15*, 2574.
- (81) Mani, F. *Inorg. Chim. Acta* **1982**, *60*, 181.
- (82) Samuels, G. J.; Espenson, J. H. *Inorg. Chem.* **1979**, *18*, 2587.
- (83) Samuels, G. J.; Espenson, J. H. *Inorg. Chem.* **1980**, *19*, 233.
- (84) Wieghardt, K.; Schmidt, W.; Herrmann, W.; Küppers, H.-J. *Inorg. Chem.* **1983**, *22*, 2963.
- (85) Taft, J. C.; Jones, M. M. *J. Am. Chem. Soc.* **1960**, *82*, 4196.
- (86) Perrin, D. D.; Armarego, W. L. F. *Purification of Laboratory Chemicals*; Pergamon Press: Exeter, 1988.
- (87) Berman, D.; Bokerman, G.; Parry, R. W. *Inorg. Synth.* **1967**, *10*, 37.
- (88) Pedersen, E. *Acta Chem. Scand.* **1967**, *24*, 3362.
- (89) Hendry, A. J.; Naidoo, K. J.; Thornton, D. A. *J. Chem. Soc., Chem. Commun.* **1989**, 998.
- (90) Hendry, A. J. Ph.D. Thesis, Australian National University, 1986.
- (91) Krausz, E. *Aust. J. Chem.* **1993**, *46*, 1041, and references therein.
- (92) Hambley, T. W.; MOMECC-87, A Program for Strain Energy Minimisation; University of Sydney, 1987.

- (93) Bernhardt, P. V.; Comba, P. *Inorg. Chem.* **1992**, *31*, 2638, and references therein.
- (94) Hambley, T. W.; Hawkins, C. J.; Palmer, J. A.; Snow, M. R. *Aust. J. Chem.* **1981**, *35*, 45, and references therein.
- (95) Bond, A. M.; Lawrance, G. A.; Lay, P. A.; Sargeson, A. M. *Inorg. Chem.* **1983**, *22*, 2010.
- (96) Wopschall, R. H.; Shain, I. *Anal. Chem.* **1967**, *39*, 1535, and references therein.
- (97) Martin, L. L. Ph.D. Thesis, Australian National University, 1986.
- (98) Bernhardt, P. V., Unpublished results **1993-94**.
- (99) Maki, N.; Shimura, Y.; Tsuchida, R. *Bull. Chem. Soc., Jpn.* **1958**, *31*, 413.
- (100) Whuler, P. A.; Brouty, C.; Spinat, P.; Herpin, P. *Acta Crystallogr.* **1975**, *B31*, 2069.
- (101) Terzis, A.; Raymond, K.; Spiro, T. *Inorg. Chem.* **1970**, *9*, 2415.
- (102) Skelton, B.; White, A. H. **1991**, Unpublished results.
- (103) Bernhardt, P. V.; Comba, P.; Hambley, T. W. *Inorg. Chem.* **1993**, *32*, 2804.
- (104) Bernhardt, P. V.; Comba, P.; Curtis, N. F.; Hambley, T. W.; Lawrance, G. A.; Maeder, M.; Siriwardena, A. *Inorg. Chem.* **1990**, *29*, 3208, and references therein.
- (105) Ditze, A.; Wasgestian, F. *J. Phys. Chem.* **1985**, *89*, 426.
- (106) Kane-Maguire, N. A. P.; Wallace, K. C.; Miller, D. B. *Inorg. Chem.* **1985**, *24*, 597.
- (107) Forster, L. S.; Mønsted, O. *J. Phys. Chem.* **1986**, *90*, 5131.
- (108) Cimolino, M. C.; Linck, R. G. *Inorg. Chem.* **1981**, *20*, 3499.
- (109) Kirk, A. D.; Ibrahim, A. M. *Inorg. Chem.* **1990**, *29*, 4848.
- (110) Ditze, A.; Wasgestian, F. *Ber. Bunsenges. Phys. Chem.* **1986**, *90*, 111.
- (111) Perkovic, M. W.; Endicott, J. F. *J. Phys. Chem.* **1990**, *94*, 1217.
- (112) White, A. W. H.; Skelton, B. *Unpublished results* **1991**,

- (113) Juris, A.; Manfrin, M. F.; Maestri, M.; Serpone, N. *Inorg. Chem.* **1978**, *17*,
- (114) Riesen, H., Personal communication.
- (115) Wilkins, R. G. *Kinetics and Mechanisms of Reactions of Transition Metal Complexes*; 2nd ed.; VCH Publishers, Inc.: New York, 1991, and references therein.
- (116) Adrianova, O. N.; Fedotova, T. N. *Russ. J. Inorg. Chem.* **1970**, *15*, 1272.
- (117) Adrianova, O. N.; Fedotova, T. N. *Russ. J. Inorg. Chem.*, **1980**, *25*,
- (118) Gainsford, G. J.; Geue, R. J.; Sargeson, A. M. *J. Chem. Soc., Chem. Commun.* **1982**, 233.
- (119) Earnshaw, A.; Larkworthy, L. F.; Patel, K. S. *J. Chem. Soc., (A)* **1969**, 2276.
- (120) Schläfer, H. L.; Gausmann, H.; Zandler, H.-U. *Inorg. Chem.* **1967**, *6*, 1528, and references therein.
- (121) Streck, W.; Ballhausen, C. J. *Mol. Phys.* **1978**, *36*, 1321, and references therein.
- (122) Adamson, A. W.; Fukuda, R. C.; Walters, R. T. *J. Phys. Chem.* **1981**, *85*, 3206.
- (123) Kirk, A. D. *J. Phys. Chem.* **1981**, *85*, 3205.
- (124) Ballardini, R.; Varani, G.; Wasgestian, F.; Moggi, L.; Balzani, V. *J. Phys. Chem.* **1973**, *77*, 2947.
- (125) Comba, P. *Inorg. Chem.* **1989**, *28*, 426.
- (126) Hambley, T. W. *J. Comp. Chem.* **1987**, *8*, 651.
- (127) Bernhardt, P. V.; Bygott, A. M. T.; Geue, R. J.; Hendry, A. J.; Korybut-Daskiewicz, B. R.; Lay, P. A.; Pladziewicz, J. R.; Sargeson, A. M.; Willis, A. C. *In press* **1994**,
- (128) Lide, D. R. *CRC Handbook of Chemistry and Physics*; 73rd ed.; CRC Publishing Co.: Boca Raton, 1992-1993, and references therein.
- (129) Bard, A. J.; Pauson, R.; Jordan, J. *Standard Potentials in Aqueous Solution*; Marcel Dekker: New York, 1985, p195, and references therein.

- (130) Steffan, C. R.; Bakac, A.; Espenson, J. H. *Inorg. Chem.* **1989**, *28*, 2992, and references therein.
- (131) Meites, L.; Zuman, P. *CRC Handbook of Organic Electrochemistry, Vols I and II*; CRC Publishers: Cleveland, and references therein.
- (132) Stulik, K.; Vydra, F. *J. Electroanal. Chem.* **1968**, *16*, 385, and references therein.
- (133) Bagotzky, V. S.; Vasilyev, Y. B. *Electrochim. Acta* **1964**, *9*, 869.
- (134) Marcus, R. A. *Annu. Rev. Phys. Chem.* **1964**, *15*, 155.
- (135) Marcus, R., A. *Discuss. Faraday. Soc.* **1960**, *29*, 21.
- (136) Stranks, D. R. *Pure Appl. Chem.* **1974**, *38*, 303.

Appendices

Appendix A

A.1. Nomenclature

The complexes were named systematically using IUPAC nomenclature,¹ with particular attention given to rules A1, A11 and A31-A32. To avoid using the cumbersome IUPAC names of the ligand framework, the abbreviations below were adopted. The numbering of the atoms in the ligands are depicted in Fig. A.1.

- (I) sep = sepulchrane = 1,3,6,8,10,13,16,19-octaazabicyclo[6.6.6]icosane
- (II) sar = sarcophagine = 3,6,10,13,16,19-hexaazabicyclo[6.6.6]icosane
- (III) N_6 -tricosane = 3,7,11,15,18,22-hexaazabicyclo[7.7.7]tricosane
- (IV) N_6 -tricosanetriimine = 3,7,11,15,18,22-hexaazabicyclo[7.7.7]tricosane-3,14,18-triene
- (V) N_6 -tetracosane = 3,7,11,15,18,22-hexaazatricyclo[10.4.4.4⁹⁻⁴]tetracosane
- (VI) N_6 -tetracosanediimine = 3,7,11,15,18,22-hexaazatricyclo[10.4.4.4⁹⁻¹⁴]tetracosane-18,22-diene
- (VII) pentacyclo- N_6 -tetracosaneH₂ = 3,7,11,15,18,22-hexaazapentacyclo[10.4.4.4⁴⁻⁹.0⁷⁻²³.0¹⁵⁻¹⁹]tetracosane
- (VIII) N_6 -docosanediimine = 3,7,11,15,18,22-hexaazabicyclo[10.4.4]docosane-3,14-diene

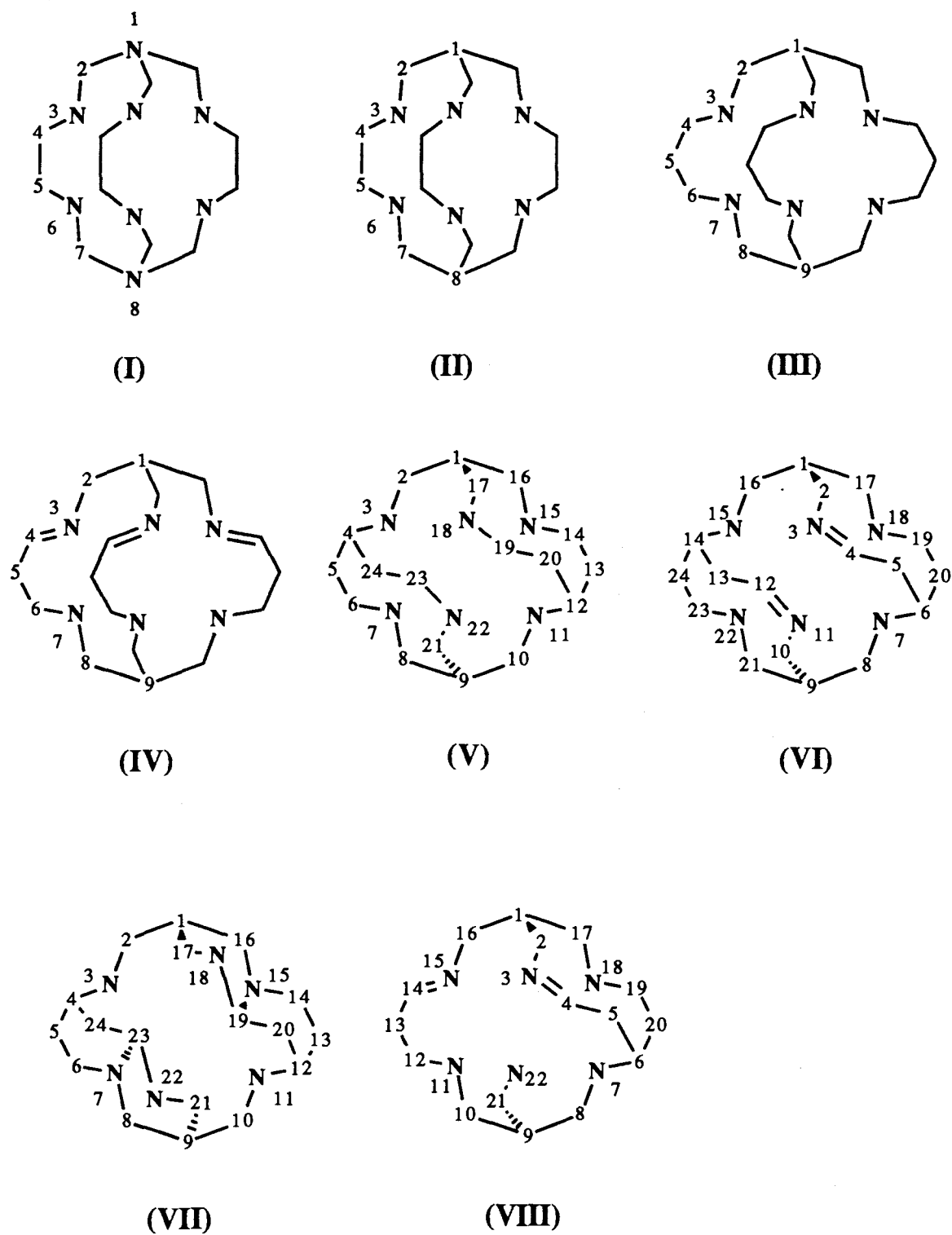


Figure A.1: Numbering system used for cage nomenclature.

References

- (1) *IUPAC Nomenclature of Organic Chemistry, Sections A,B,C,D,E,F and H*;
Pergamon: London, 1979.

Appendix B

I. Crystal Data for [Pt(^αMe₅-N₆-tricosanetriimine)](ZnCl₄)_{1.5}Cl¹

Table B(I).1: Data for [Pt(^αMe₅-N₆-tricosanetriimine)](ZnCl₄)_{1.5}Cl

Empirical formula	C ₂₂ H ₄₅ Cl ₇ N ₆ PtZn _{1.5}
formula weight	934.98
space group	$R\bar{3}c$
Z	12
crystal system	hexagonal
crystal dimensions	0.30 x 0.30 x 0.16 mm
lattice parameters	a=14.711(4) Å, b=14.736(5) Å, c=55.80(1) Å, γ=120°
V	1739(1)Å ³
D(calc'd)	1.778 g cm ⁻³
F ₀₀₀	5532
radiation	Mo K _α (λ=0.7107Å), graphite monochromated
μ(Mo K _α)	60.61
T	294 K
scan type	ω-0.670
scan width	1.00 + 0.35tanθ
h,k,l (min, max)	-17→17, 0→17, 0→66
N ^o reflections measured	
total	6498
unique	2010
N ^o observations (I>2.5σ(I))	1562
N ^o variables	154
trans factors (min, max)	0.408-0.108
decay	8.1 % decline
Structure Solution	Patterson Methods
Refinement	Full matrix least squares
Function minimised	$R = \Sigma \{ F_o - F_c \} / \Sigma F_o $ $R_w = \Sigma \{ w^{1/2} F_o - F_c \} / \Sigma w^{1/2} F_o $
Least squares weights	4.8/{σ ² (F)+(0.00022)F ² }
p-factor	2.2 x 10 ⁻⁴
Anomalous dispersion	all non hydrogen atoms
Residuals: R; R _w	0.039, 0.046
goodness of fit indicator	4.8
Max. shift/error in final cycle	0.001
Max.; Min. peaks in Final Diff. Map	+1.2 e ⁻ Å ⁻¹ ; -0.8 e ⁻ Å ⁻¹

Data reduction and application of Lorentz, polarisation and absorption corrections were carried out using the Enraf-Nonius Structure Determination Package.² The structure was solved by direct atoms methods using SHELX-86³ and the solution was extended by difference Fourier methods. Hydrogen atoms were included at calculated sites with group isotropic thermal parameters and all other atoms were refined anisotropically. Scattering factors and anomalous dispersion terms used for Pt (neutral Pt) were taken from International Tables⁴ and all others used were those supplied in SHELX-76.⁵ All calculations were carried out using SHELX-76⁵ and plots were drawn using ORTEP.⁶ Listings of observed and calculated structure factors, close non bonded contacts and torsion angles are deposited as an accessory publication.⁷

Table B(I).2: Positional parameters for [Pt(α Me₅-N₆-tricosanetriamine)](ZnCl₄)_{1.5}Cl

	10 ⁴ x	10 ⁴ y	10 ⁴ z
Pt(1)	0	0	3625(1)
N(1)	1061(5)	-81(4)	3849(1)
N(2)	1179(4)	1105(5)	3406(1)
C(1)	0	0	4459(3)
C(2)	0	0	4182(3)
C(3)	684(6)	-434(6)	4093(1)
C(4)	2017(6)	211(6)	3799(1)
C(5)	2560(6)	731(6)	3568(2)
C(6)	3743(6)	1234(8)	3592(2)
C(7)	2251(6)	1548(6)	3494(2)
C(8)	1133(6)	759(6)	3155(1)
C(9)	0	0	3069(3)
C(10)	0	0	2786(3)
Zn(1)	2887(2)	-316(2)	2380(1)
Cl(1)	4474(3)	0	2500
Cl(2)	1910(4)	-1004(4)	2738(1)
Cl(3)	2309(6)	-1386(5)	2066(1)
Cl(4)	5000	0	0
Cl(4')	1468(11)	3134(8)	3211(3)
Cl(5)	7229(22)	0	2500
Cl(5')	2573(17)	2949(16)	2380(3)

Table B(I).3: Thermal parameters ($\times 10^3$) for $[\text{Pt}(\alpha\text{Me}_5\text{-N}_6\text{-tricosanetriimine})](\text{ZnCl}_4)_{1.5}\text{Cl}$

	U_{11}	U_{22}	U_{33}	U_{23}	U_{13}	U_{12}
Pt(1)	22(1)	22(1)	36(1)	0	0	11(1)
N(1)	31(4)	25(4)	38(4)	0(3)	-4(3)	14(3)
N(2)	20(3)	28(4)	43(4)	2(3)	1(3)	10(3)
C(1)	64(8)	64(8)	43(9)	0	0	45(4)
C(2)	45(6)	45(6)	47(10)	0	0	35(3)
C(3)	38(5)	46(5)	39(5)	0(4)	-5(4)	26(5)
C(4)	28(5)	41(5)	53(5)	-3(4)	-5(4)	20(4)
C(5)	27(5)	40(5)	64(6)	-5(5)	0(4)	16(4)
C(6)	43(6)	89(8)	73(7)	-11(6)	0(5)	38(6)
C(7)	27(5)	32(5)	59(6)	2(5)	3(4)	6(4)
C(8)	38(5)	40(5)	38(5)	1(4)	2(4)	18(4)
C(9)	35(5)	35(5)	43(9)	0	0	58(3)
C(10)	58(7)	58(7)	41(9)	0	0	22(4)
Zn(1)	59(2)	69(2)	119(3)	13(2)	-9(2)	28(2)
Cl(1)	98(7)	57(3)	92(3)	0	0	61(6)
Cl(2)	48(3)	63(4)	153(6)	-15(4)	15(4)	31(3)
Cl(3)	107(6)	87(5)	100(5)	-11(4)	-41(5)	53(4)
Cl(4)	41(9)	7(7)	278(50)	-40(19)	-42(22)	-4(7)
Cl(4')	39(8)	13(6)	117(10)	7(7)	9(7)	3(5)
Cl(5)	83(25)	197(42)	20(13)	0	0	16(32)
Cl(5')	172(19)	143(16)	62(13)	-29(12)	-16(13)	94(15)

Table B(I).4: Hydrogen atom positional ($\times 10^3$) and thermal ($\times 10^2$) parameters for $[\text{Pt}(\alpha\text{Me}_5\text{-N}_6\text{-tricosanetriimine})](\text{ZnCl}_4)_{1.5}\text{Cl}$

	x	y	z	U_{iso}
HN(2)	99(1)	161(1)	341(1)	5(1)
H(1)	-40(1)	26(1)	451(1)	3(2)
H(3A)	28(1)	-119(1)	410(1)	7(1)
H(3B)	128(1)	-19(1)	420(1)	7(1)
H(4)	242(1)	9(1)	392(1)	7(1)
H(5)	232(1)	19(1)	345(1)	7(1)
H(6A)	407(1)	156(1)	344(1)	7(1)
H(6B)	393(1)	71(1)	363(1)	7(1)
H(6C)	398(1)	176(1)	372(1)	7(1)
H(7A)	273(1)	199(1)	337(1)	7(1)
H(7B)	232(1)	197(1)	363(1)	7(1)
H(8A)	144(1)	137(1)	305(1)	7(1)
H(8B)	154(1)	40(1)	314(1)	7(1)
H(10)	-65(1)	-43(1)	273(1)	3(2)

II. Crystal Data for [Pt^{IV}(Et₂-Me₆-N₆-tetracosanediimine-H)](PF₆)₃·5H₂O⁸

Table B(II).1: Data for [Pt^{IV}(Et₂-Me₆-N₆-tetracosanediimine-H)](PF₆)₃·5H₂O

Empirical formula	C ₂₈ H ₆₃ F ₁₈ Cl ₄ N ₆ O ₅ P ₃ Pt
formula weight	1193.82
space group	<i>C2/c</i>
Z	4
crystal system	monoclinic
N ^o reflections used for unit cell determination (2θ range):	25 (92-99°)
crystal dimensions	0.13 x 0.06 x 0.14 mm
lattice parameters	a=17.203(3) Å, b=14.999(1) Å, c=17.273(2) Å; β=92.41(2)°
V	4453.0(9) Å ³
D(calc'd)	1.781 g cm ⁻³
F ₀₀₀	2391.5
radiation	Cu K _α (λ=1.54178 Å); graphite monochromated
μ(Cu K _α)	80.9 cm ⁻¹
T	299 K
scan type	ω-2θ
scan rate	32.0° min ⁻¹ (in ω) (up to 4 scans)
scan width	(1.05+0.30tanθ)°
h,k,l (min, max)	-19→19, 0→16, 0→19
N ^o unique reflections	3308
N ^o observations (I>3.00σ(I))	2365
N ^o variables	277
trans factors	0.457-0.646
decay	0 % decline
Refinement	full matrix least squares
Residuals: R; R _w	0.042; 0.064
Function minimised	$R = \sum \{ F_o - F_c \} / \sum F_o $ $R_w = \{ \sum w (F_o - F_c)^2 / \sum (w F_o^2) \}^{1/2}$
Least squares weights	$w = 1 / \{ \sigma^2(F) + (0.0009)F^2 \}$
p-factor	9 x 10 ⁻⁴
Anisotropic refinement	all non hydrogen atoms except O(3)
Max. shift/error in final cycle	<0.07
Max.; Min. peaks in Final Diff. Map	0.9 e ⁻ Å ⁻¹ ; -0.8 e ⁻ Å ⁻¹

Data reduction and refinement computations were performed with XTAL3.2.⁹ atomic scattering factors for neutral atoms and dispersion terms were taken from International Tables.⁴ All non hydrogen atoms were located and refined with anisotropic displacement factors. Hydrogen atoms attached to carbon atoms of the cation were placed at calculated position, tetrahedral at the carbon atom, terminal methyl groups assumed to be in the staggered conformation and not refined, but were periodically recalculated. Chemical evidence had indicated that three of the four nitrogen donors in each cation would be protonated. As the cation possess a centre of symmetry in the solid state, this would lead to disorder, the protons either being equally delocalised over the two crystallographic sites (both with occupancy 0.75) or preferring one site over the other (one site with occupancy 1.0, the other 0.5). The former scheme has been adopted here. Some of the fluorine atom displacement factors are very large. Attempts were made to model this motion by disorder, but were not successful. The anions appear rather free to rotate and the anisotropic model has been retained. Refinement was continued until all shift/error ratios were <0.07.

Table B(II).2: Atomic coordinates and equivalent isotropic displacement parameters[§] for the non-hydrogen atoms in [Pt^{IV}(Et₂-Me₆-N₆-tetracosanediimine-H)](PF₆)₃·5H₂O.

	<i>x/a</i>	<i>y/b</i>	<i>z/c</i>	<i>U_{eq}</i>
Pt	0.25000	0.25000	0.50000	0.0301(2)
N(1)	0.2091(4)	0.1749(4)	0.5916(4)	0.037(2)
N(2)	0.2873(4)	0.3395(4)	0.5819(4)	0.037(2)
N(3)	0.1516(4)	0.3340(4)	0.4938(4)	0.037(2)
C(1)	0.1168(6)	0.3517(6)	0.7118(5)	0.057(4)
C(2)	0.1617(5)	0.3173(6)	0.6412(5)	0.042(3)
C(3)	0.1302(5)	0.3698(6)	0.5715(5)	0.041(3)
C(4)	0.2496(5)	0.3332(5)	0.6558(5)	0.043(3)
C(5)	0.1440(5)	0.2165(7)	0.6318(5)	0.042(3)
C(6)	0.1509(5)	0.4029(5)	0.4313(5)	0.037(3)
C(7)	0.0724(6)	0.4504(6)	0.4286(6)	0.052(3)
C(8)	0.0402(7)	0.4721(8)	0.3478(7)	0.072(4)
C(9)	0.2226(5)	0.4639(5)	0.4395(5)	0.044(3)
C(10)	0.2157(6)	0.5456(6)	0.3829(6)	0.053(3)
C(11)	0.3008(5)	0.4179(5)	0.4252(5)	0.038(3)
C(12)	0.3635(5)	0.4357(6)	0.4932(5)	0.048(3)
C(13)	0.3918(6)	0.5284(7)	0.4979(6)	0.063(4)
C(14)	0.3299(5)	0.4077(7)	0.5713(5)	0.048(3)
P(1)	0.2018(2)	0.3457(2)	0.1460(2)	0.075(1)
F(1)	0.271(1)	0.296(1)	0.1712(9)	0.28(1)
F(2)	0.192(1)	0.3587(8)	0.2320(8)	0.27(1)
F(3)	0.233(1)	0.4367(7)	0.1414(7)	0.235(9)
F(4)	0.1326(8)	0.389(1)	0.106(2)	0.37(2)
F(5)	0.223(1)	0.3284(9)	0.0642(6)	0.227(9)
F(6)	0.156(2)	0.2588(9)	0.147(1)	0.27(1)
P(2)	0	0.9835(6)	0.2500	0.123(3)
F(7)	0.0125(9)	1.065(1)	0.3107(8)	0.221(8)
F(8)	0.003(1)	0.918(1)	0.1807(9)	0.31(1)
F(9)	0.0872(7)	0.990(2)	0.2515(9)	0.30(1)
O(1)	0.0172(6)	0.2269(6)	0.4523(7)	0.109(4)
O(2)	0.084(1)	0.7450(8)	0.426(1)	0.19(1)
O(3) [†]	0.053(3)	0.231(2)	0.290(3)	0.23(2)

[§] $U_{eq} = \frac{1}{3} \sum_i \sum_j U_{ij} a_i^* a_j^* a_i a_j$ [†] O(3) has occupancy 0.5 and an isotropic displacement factor.

Table B(II).3: Atomic coordinates and isotropic displacement parameters for the hydrogen atoms in $[\text{Pt}^{\text{IV}}(\text{Et}_2\text{-Me}_6\text{-N}_6\text{-tetracosanediimine-H})](\text{PF}_6)_3 \cdot 5\text{H}_2\text{O}$.

	<i>x/a</i>	<i>y/b</i>	<i>z/c</i>	<i>U</i>
HN(1)‡	0.2466	0.1760	0.6252	0.080
HN(3)‡	0.1142	0.2994	0.4806	0.080
H(1A)	0.0625	0.3429	0.7027	0.080
H(1B)	0.1337	0.3205	0.7574	0.080
H(1C)	0.1277	0.4135	0.7176	0.080
H(3A)	0.0750	0.3705	0.5728	0.080
H(3B)	0.1495	0.4290	0.5759	0.080
H(4A)	0.2574	0.3871	0.6839	0.080
H(4B)	0.2714	0.2850	0.6850	0.080
H(5A)	0.1394	0.1899	0.6813	0.080
H(5B)	0.0968	0.2086	0.6020	0.080
H(6)	0.1544	0.3720	0.3836	0.080
H(7A)	0.0360	0.4132	0.4530	0.080
H(7B)	0.0781	0.5046	0.4567	0.080
H(8A)	0.0767	0.5093	0.3235	0.080
H(8B)	0.0345	0.4178	0.3198	0.080
H(8C)	-0.0087	0.5017	0.3461	0.080
H(9)	0.2252	0.4865	0.4909	0.080
H(10A)	0.2109	0.5242	0.3311	0.080
H(10B)	0.1707	0.5790	0.3943	0.080
H(10C)	0.2600	0.5832	0.3879	0.080
H(11)	0.3204	0.4445	0.3801	0.080
H(12)	0.4070	0.3984	0.4847	0.080
H(13A)	0.4145	0.5427	0.4503	0.080
H(13B)	0.3485	0.5663	0.5053	0.080
H(13C)	0.4294	0.5390	0.5387	0.080
H(14)	0.3420	0.4444	0.6150	0.080

‡. Occupancy 0.75

Table B(II).4: Anisotropic displacement parameters in [Pt^{IV}(Et₂-Me₆-N₆-tetracosanediimine-H)](PF₆)₃·5H₂O.

	<i>U</i> ₁₁	<i>U</i> ₂₂	<i>U</i> ₃₃	<i>U</i> ₁₂	<i>U</i> ₁₃	<i>U</i> ₂₃
Pt	0.0335(3)	0.0299(3)	0.0268(3)	0.0060(2)	0.0002(2)	0.0002(2)
N(1)	0.042(4)	0.036(4)	0.032(4)	0.001(3)	-0.003(3)	-0.002(3)
N(2)	0.040(4)	0.038(4)	0.031(4)	0.005(3)	-0.005(3)	-0.001(3)
N(3)	0.041(4)	0.037(4)	0.033(4)	0.010(3)	0.002(3)	-0.004(3)
C(1)	0.077(7)	0.071(7)	0.023(5)	0.023(5)	0.008(5)	-0.004(4)
C(2)	0.048(5)	0.048(5)	0.030(5)	0.007(4)	-0.004(4)	-0.002(4)
C(3)	0.049(5)	0.048(5)	0.024(4)	0.011(4)	0.000(4)	-0.005(4)
C(4)	0.054(6)	0.042(5)	0.033(5)	-0.003(4)	0.003(4)	0.005(4)
C(5)	0.045(5)	0.047(5)	0.033(5)	0.006(4)	0.003(4)	-0.002(4)
C(6)	0.037(5)	0.035(5)	0.039(5)	0.008(4)	-0.004(4)	0.003(4)
C(7)	0.060(6)	0.044(5)	0.051(6)	0.012(4)	-0.001(5)	-0.003(5)
C(8)	0.072(8)	0.086(8)	0.058(7)	0.021(6)	-0.007(6)	0.029(6)
C(9)	0.063(6)	0.040(5)	0.030(5)	0.013(4)	-0.005(4)	0.003(4)
C(10)	0.054(6)	0.033(5)	0.071(7)	0.002(4)	0.012(5)	0.014(5)
C(11)	0.047(5)	0.035(4)	0.034(5)	0.008(4)	0.000(4)	0.007(4)
C(12)	0.044(5)	0.055(6)	0.044(6)	-0.004(4)	0.003(4)	0.003(5)
C(13)	0.058(6)	0.058(6)	0.073(8)	-0.004(5)	0.002(5)	-0.023(6)
C(14)	0.049(6)	0.056(6)	0.038(6)	0.006(5)	-0.009(4)	-0.007(4)
P(1)	0.079(2)	0.060(2)	0.087(2)	0.010(2)	0.019(2)	0.024(2)
F(1)	0.30(2)	0.30(2)	0.22(2)	0.19(2)	-0.08(2)	0.03(2)
F(2)	0.47(3)	0.18(1)	0.16(1)	0.01(1)	0.16(2)	-0.048(9)
F(3)	0.41(2)	0.102(8)	0.18(1)	-0.09(1)	-0.05(1)	0.010(8)
F(4)	0.091(9)	0.25(2)	0.76(5)	0.06(1)	-0.06(2)	0.07(2)
F(5)	0.38(2)	0.20(1)	0.100(9)	-0.05(1)	0.03(1)	-0.012(8)
F(6)	0.35(3)	0.20(2)	0.26(2)	-0.15(2)	-0.02(2)	0.02(1)
P(2)	0.069(4)	0.214(8)	0.086(4)	0.0	0.009(3)	0.0
F(7)	0.19(1)	0.25(2)	0.23(1)	-0.02(1)	0.04(1)	-0.04(1)
F(8)	0.39(2)	0.32(2)	0.22(1)	0.20(2)	-0.09(2)	-0.14(1)
F(9)	0.11(1)	0.56(3)	0.23(2)	-0.01(1)	-0.03(1)	-0.11(2)
O(1)	0.085(7)	0.095(6)	0.14(1)	-0.018(5)	-0.041(7)	0.033(6)
O(2)	0.13(1)	0.17(2)	0.28(3)	0.005(8)	0.03(2)	-0.08(1)

Anisotropic displacement parameters in the form: $-2p^2(U_{11}h^2a^{*2} + 0\dots + 2U_{12}hka^*b^* + \dots)$.

III. Crystal Data for pentacyclo-[Pt^{II}(Et₂-Me₆-N₆-tetracosaneH₂)Cl₄.9H₂O]¹⁰

Table B(III).1: Data for pentacyclo-[Pt^{II}(Et₂-Me₆-N₆-tetracosaneH₂)Cl₄.9H₂O

Empirical formula	C ₂₈ H ₇₄ Cl ₄ N ₆ O ₉ Pt
formula weight	975.83
space group	R $\bar{3}$ (#148)
Z	9
crystal system; lattice type	trigonal; R-centred
N ^o reflections used for unit cell determination (2 θ range):	25 (56.0-63.8)
crystal dimensions	0.13x0.12x0.08 mm
lattice parameters	a=22.010(1) Å, c=21.927(2) Å
V	9198(1) Å ³
D(calc'd)	1.585 g cm ⁻³
F000	4518.00
radiation	Cu K α (λ =1.54178 Å); graphite monochromated
μ (Cu K α)	90.22 cm ⁻¹
T	213 K
scan type	ω -2 θ
scan rate	16.0°/min (in ω) (up to 4 scans)
scan width	(1.31+0.30tan θ)°
2 θ _{max}	120.1°
N ^o reflections measured (total)	3312
unique	3038 (R_{int} =0.080)
N ^o observations ($I > 3.00\sigma(I)$)	2711
N ^o variables	230
trans factors	0.939-0.994
decay	1.31% decline
Refinement	Full matrix least squares
Residuals: R; R _w	0.043; 0.048
Function minimised	$R = \sum \{ F_o - F_c \} / \sum F_o $ $R_w = \{ (\sum w F_o - F_c)^2 / \sum w F_o^2 \}^{1/2}$
Least squares weights	$1 / \{ \sigma^2(F_o) \} = 4 F_o^2 / \{ \sigma^2(F_o^2) \}$
p-factor	0.004
Anomalous dispersion	all non hydrogen atoms
Max. shift/error in final cycle	<0.01
Max.; Min. peaks in Final Diff. Map	1.47 e ⁻ Å ⁻¹ ; -1.61 e ⁻ Å ⁻¹

The data were corrected for Lorentz and polarisation effects. The structure was solved by heavy-atoms Patterson methods and expanded using Fourier techniques. The non hydrogen atoms were refined anisotropically and all hydrogen atoms in the cation were included at calculated positions and held fixed. Neutral atom scattering factors were taken from International Tables.⁴

Table B(III).2: Atomic Coordinates and Isotropic Displacement Parameters for pentacyclo-[Pt^{II}(Et₂-Me₆-N₆-tetracosaneH₂)Cl₄.9H₂O

atom	x	y	z	B _{eq}
Pt(1)	0.5000	-0.5000	0.0000	1.24(1)
N(1)	0.5807(4)	-0.5205(4)	0.0137(4)	2.0(2)
N(2)	0.4635(4)	-0.5730(4)	-0.1392(3)	1.7(2)
N(3)	0.4386(3)	-0.6028(3)	-0.0318(3)	1.5(2)
C(1)	0.7195(5)	-0.3961(5)	0.1048(4)	2.4(2)
C(2)	0.6408(4)	-0.4257(4)	0.0933(4)	1.7(2)
C(3)	0.3656(4)	-0.6200(4)	-0.0442(4)	1.5(2)
C(4)	0.3911(5)	-0.5844(4)	-0.1508(4)	2.0(2)
C(5)	0.6062(4)	-0.5049(4)	0.0767(4)	1.7(2)
C(6)	0.4376(4)	-0.6534(4)	0.0193(4)	1.8(2)
C(7)	0.3767(5)	-0.7303(4)	0.0136(4)	2.3(2)
C(8)	0.3137(6)	-0.7485(5)	0.0551(6)	4.3(3)
C(9)	0.5090(4)	-0.6523(4)	0.0211(4)	1.5(2)
C(10)	0.5242(5)	-0.6711(5)	0.0830(5)	2.8(2)
C(11)	0.5664(4)	-0.5889(4)	-0.0112(5)	2.1(2)
C(12)	0.5475(4)	-0.5922(4)	-0.0808(4)	1.5(2)
C(13)	0.5636(5)	-0.6421(5)	-0.1160(4)	2.0(2)
C(14)	0.4692(4)	-0.6141(4)	-0.0881(4)	1.5(2)
Cl(1)	0.4953(1)	-0.6112(1)	-0.2664(1)	2.52(5)
Cl(2)	0.3156(1)	0.2301(1)	0.8372(1)	3.64(7)
O(1)	1.0000	0.0000	0.165(1)	11.2(5)
O(2)	0.8836(5)	0.0065(5)	0.1346(4)	6.2(3)
O(3)	0.6666	0.3333	0.3333	11.0(7)
O(4)	0.8744(7)	0.0743(8)	0.9208(6)	9.7(6)
O(4')	0.204(1)	0.049(1)	0.094(1)	14(1)
O(5)	0.8972(8)	0.168(1)	0.9675(10)	16.8(9)
O(5')	0.146(1)	0.0526(9)	0.0372(8)	9.3(7)

Table B(III).3: Hydrogen atom positional parameters and thermal parameters for pentacyclo-[Pt^{II}(Et₂-Me₆-N₆-tetracosaneH₂)Cl₄.9H₂O

atom	<i>x</i>	<i>y</i>	<i>z</i>	<i>U</i> _{iso}
H(01)	0.6183	-0.4865	-0.0102	2.4611
H(02a)	0.4789	-0.5850	-0.1753	2.0951
H(02b)	0.4936	-0.5246	-0.1305	2.0951
H(1a)	0.7256	-0.4208	0.1376	2.9080
H(1b)	0.7408	-0.4014	0.0691	2.9080
H(1c)	0.7408	-0.3477	0.1149	2.9080
H(3a)	0.3396	-0.6675	-0.0570	1.7728
H(3b)	0.3461	-0.6142	-0.0074	1.7728
H(4a)	0.3940	-0.5518	-0.1807	2.3890
H(4b)	0.3620	-0.6308	-0.1654	2.3890
H(5a)	0.5677	-0.5308	0.1034	2.0896
H(5b)	0.6399	-0.5193	0.0823	2.0896
H(6)	0.4323	-0.6359	0.0574	2.1424
H(7a)	0.3608	-0.7380	-0.0275	2.7346
H(7b)	0.3943	-0.7606	0.0235	2.7346
H(8a)	0.3283	-0.7420	0.0966	5.2112
H(8b)	0.2953	-0.7187	0.0458	5.2112
H(8c)	0.2785	-0.7960	0.0488	5.2112
H(9)	0.5014	-0.6906	-0.0040	1.7920
H(10a)	0.4879	-0.7168	0.0939	3.3270
H(10b)	0.5678	-0.6702	0.0820	3.3270
H(10c)	0.5265	-0.6382	0.1123	3.3270
H(11)	0.6083	-0.5910	-0.0082	2.5399
H(12)	0.5750	-0.5465	-0.0976	1.7638
H(13a)	0.5356	-0.6884	-0.1007	2.4439
H(13b)	0.5535	-0.6411	-0.1580	2.4439
H(13c)	0.6118	-0.6279	-0.1113	2.4439
H(14)	0.4435	-0.6625	-0.0984	1.7533
H(1w)	0.9036	0.0544	0.1227	7.4621
H(2w)	0.8492	-0.0183	0.1122	7.4621

Table B(III).4: Anisotropic Displacement Parameters ($\times 10^3$) for pentacyclo-[Pt^{II}(Et₂-Me₆-N₆-tetracosaneH₂)Cl₄.9H₂O

atom	U_{11}	U_{22}	U_{33}	U_{12}	U_{13}	U_{23}
Pt(1)	147(3)	113(3)	209(3)	63(2)	3(2)	-14(2)
N(1)	180(4)	170(4)	470(5)	120(3)	-90(4)	-110(4)
N(2)	210(4)	180(4)	260(4)	80(3)	20(3)	-20(3)
N(3)	150(4)	150(4)	270(4)	80(3)	-20(3)	-10(3)
C(1)	220(5)	280(5)	410(6)	120(4)	0(4)	-20(4)
C(2)	180(5)	140(5)	300(5)	70(4)	-40(4)	-40(4)
C(3)	130(4)	150(4)	250(5)	40(4)	30(4)	-60(4)
C(4)	190(5)	180(5)	350(6)	70(4)	-70(4)	-20(4)
C(5)	210(5)	240(5)	240(5)	130(4)	-30(4)	30(4)
C(6)	230(5)	130(5)	310(5)	80(4)	60(4)	40(4)
C(7)	230(5)	90(5)	500(7)	40(4)	60(5)	30(4)
C(8)	450(7)	270(6)	750(9)	50(6)	300(6)	50(6)
C(9)	230(5)	200(5)	140(4)	110(4)	-40(4)	-40(4)
C(10)	360(6)	240(5)	450(6)	140(5)	-30(5)	50(5)
C(11)	130(5)	120(5)	570(7)	80(4)	-50(4)	-90(4)
C(12)	220(5)	110(4)	220(5)	80(4)	40(4)	30(3)
C(13)	280(5)	200(5)	310(5)	140(4)	50(4)	0(4)
C(14)	210(5)	100(4)	230(5)	60(4)	50(4)	-20(3)
Cl(1)	340(1)	250(1)	300(1)	90(1)	0(1)	-42(10)
Cl(2)	610(2)	360(1)	550(2)	340(1)	-240(1)	-190(1)
O(1)	610(8)	607	3000(3)	303	0	0
O(2)	790(7)	670(6)	870(7)	340(6)	90(6)	-50(5)
O(3)	1000(1)	1004	2200(4)	502	0	0
O(4)	1400(1)	1200(1)	1400(1)	900(1)	200(1)	200(1)
O(4')	1300(2)	2100(3)	2200(3)	1000(2)	700(2)	300(2)
O(5)	1000(1)	2400(3)	3200(3)	900(1)	900(1)	2000(2)
O(5')	1900(2)	1000(1)	900(1)	900(2)	300(1)	100(1)

IV. Crystal Data for [Pt(β Me₅-N₆-tricosanetriimine)](ZnCl₄)(ZnCl₃)₂·0.5H₂O·4HCl¹⁰

Table B(IV).1: Data for [Pt(β Me₅-N₆-tricosanetriimine)](ZnCl₄)(ZnCl₃)₂·0.5H₂O·4HCl

Empirical formula	C ₄₄ H ₉₂ Cl ₂₄ N ₁₂ OPt ₂ Zn ₆
formula weight	2388.23
space group	R $\bar{3}$ (#148)
Z	3
crystal system; lattice type	trigonal; R-centred
N ^o reflections used for unit cell determination	
(2 θ range)	25 (40.5-53.7°)
crystal dimensions	0.15 x 0.15 x 0.12 mm
lattice parameters	a=14.877(6)Å, c=32.48(2)Å
V	6224(5) Å ³
D(calc'd)	1.911 g cm ⁻³
F ₀₀₀	3426.00
radiation	Cu K α (λ =1.54178 Å); graphite monochromated
μ (Cu K α)	152.1 cm ⁻¹
T	296 K
scan type	ω -2 θ
scan rate	16.0° min ⁻¹ (in ω , up to 4 scans)
scan width	(1.47 + 0.30tan θ)
2 θ _{max}	121.2°
N ^o reflections measured (total):	2384
(unique)	1154
N ^o observations ($I > 3.00\sigma(I)$)	607
N ^o variables	64
decay	31.59 % decline
Refinement	Full matrix least squares
Function minimised	$R = \sum \{ F_o - F_c \} / \sum F_o $ $R_w = \{ (\sum w F_o - F_c)^2 / \sum w F_o^2 \}^{1/2}$
Least squares weights	$w = 1 / \{ \sigma^2(F_o) = (4F_o^2) / \sigma^2(F_o) \}$
p-factor	0.024
Anomalous dispersion	all non hydrogen atoms
Residuals: R; R _w	0.175, 0.212
goodness of fit indicator	8.20

The data were corrected for Lorentz and polarisation effects. The structure was solved by heavy-atoms Patterson methods and expanded using Fourier techniques. The non hydrogen atoms were refined anisotropically. Neutral atom scattering factors were taken from International Tables.⁴

Table B(IV).2: Atomic Coordinates and Isotropic Displacement Parameters for [Pt(^{β} Me₅-N₆-tricosanetriimine)](ZnCl₄)(ZnCl₃)₂.0.5H₂O.4HCl

atom	x	y	z	B _{eq}
Pt(1)	1.0000	0.0000	0.7730(2)	6.0(2)
N(1)	0.975(5)	-0.105(5)	0.819(2)	7(1)
N(2)	0.873(5)	-0.074(5)	0.732(2)	6(1)
C(1)	1.0000	0.0000	0.926(7)	15(7)
C(2)	1.0000	0.0000	0.868(3)	5(2)
C(3)	0.991(6)	-0.091(6)	0.857(2)	7(2)
C(4)	0.900(9)	-0.183(8)	0.805(3)	9(2)
C(5)	0.820(8)	-0.242(8)	0.772(3)	10(2)
C(6)	0.781(8)	-0.168(8)	0.749(3)	9(2)
C(7)	0.692(8)	-0.207(8)	0.723(3)	10(2)
C(8)	0.901(5)	-0.086(5)	0.694(2)	5(1)
C(9)	1.0000	0.0000	0.674(6)	10(5)
C(10)	1.0000	0.0000	0.628(4)	7(3)
Zn(1)	0.639(1)	0.040(1)	0.7559(4)	12.3(5)
Cl(1)	0.483(3)	0.007(3)	0.740(1)	19(1)
Cl(2)	0.736(2)	0.054(2)	0.7024(7)	10.4(7)
Cl(3)	0.647(2)	-0.058(2)	0.8050(6)	8.3(5)
Cl(4)	0.719(6)	0.193(6)	0.785(2)	34(3)
O(1)	1.0000	0.0000	0.5000	18(7)

References

- (1) Hambley, T. W., University of Sydney, 1992.
- (2) Enraf-Nonius, Enraf-Nonius Structure Determination Package, Delft, 1985.
- (3) Sheldrick, G. M.; *SHELX-86 Crystallographic Computing 3*; Oxford University Press: 1986, pp 175-189.
- (4) *International Tables for X-ray Crystallography*; Kynoch Press: Birmingham, 1974; Vol. 4.
- (5) Sheldrick, G. M., SHELX-76, A Program for X-ray Crystal Structure Determination, University of Cambridge, 1976.
- (6) Johnson, C. K., ORTEP, A Thermal Ellipsoid Plotting Program, Oak Ridge National Laboratories, 1965.
- (7) Copies are available on application to the Editor-in-Chief, Editorial and Publications Service, CSIRO, 314 Albert Street, East Melbourne, Vic, 3002
- (8) Willis, A. C., Australian National University, 1991.
- (9) Hall, S. R.; Flack, H. D.; Stewart, J. M. In *Universities of Western Australia, Geneva and Maryland*: Perth, 1992.
- (10) Hockless, D. R., Australian National University, 1993.

Appendix C

Supplementary NMR Spectra for Chapter 3.

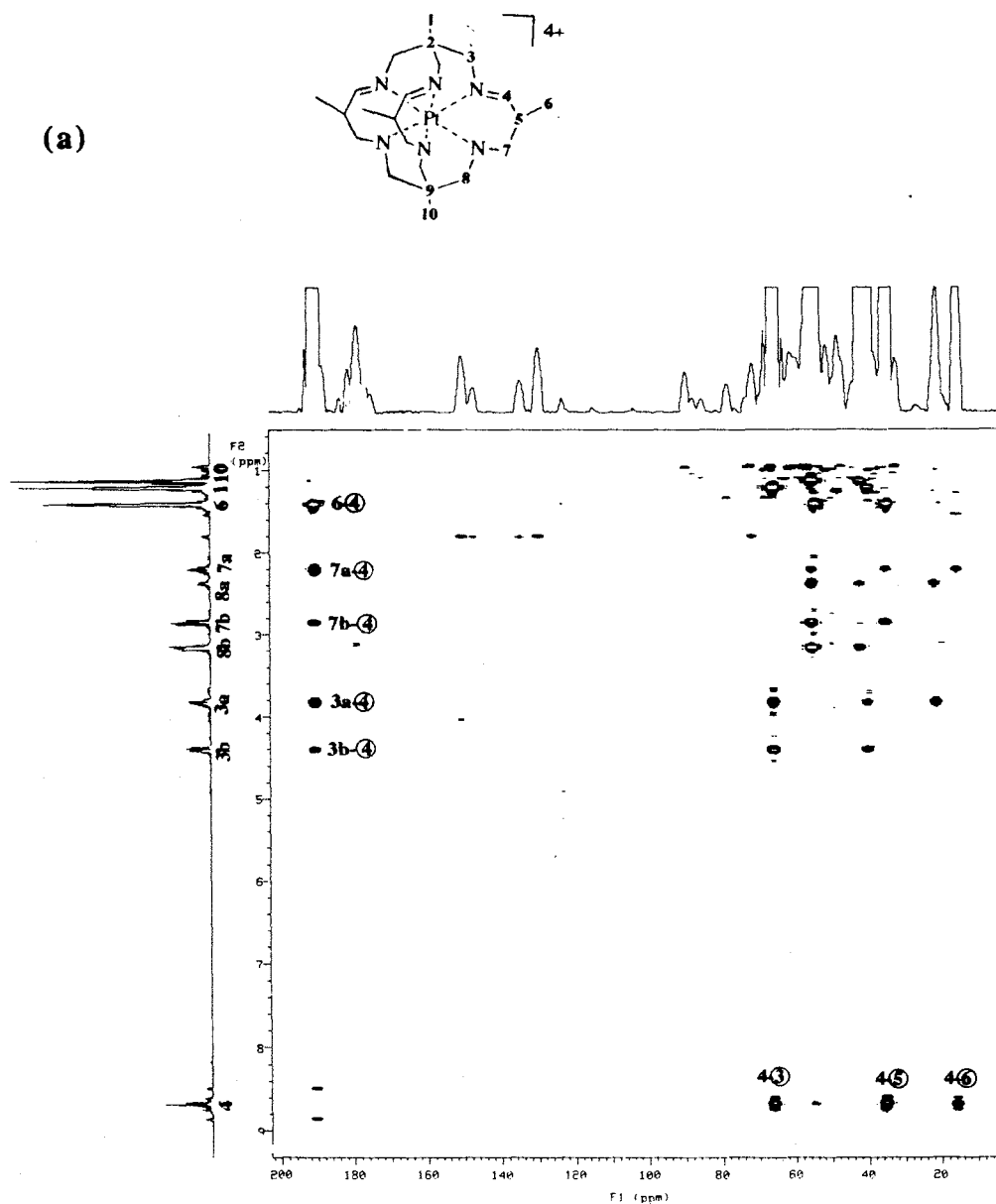
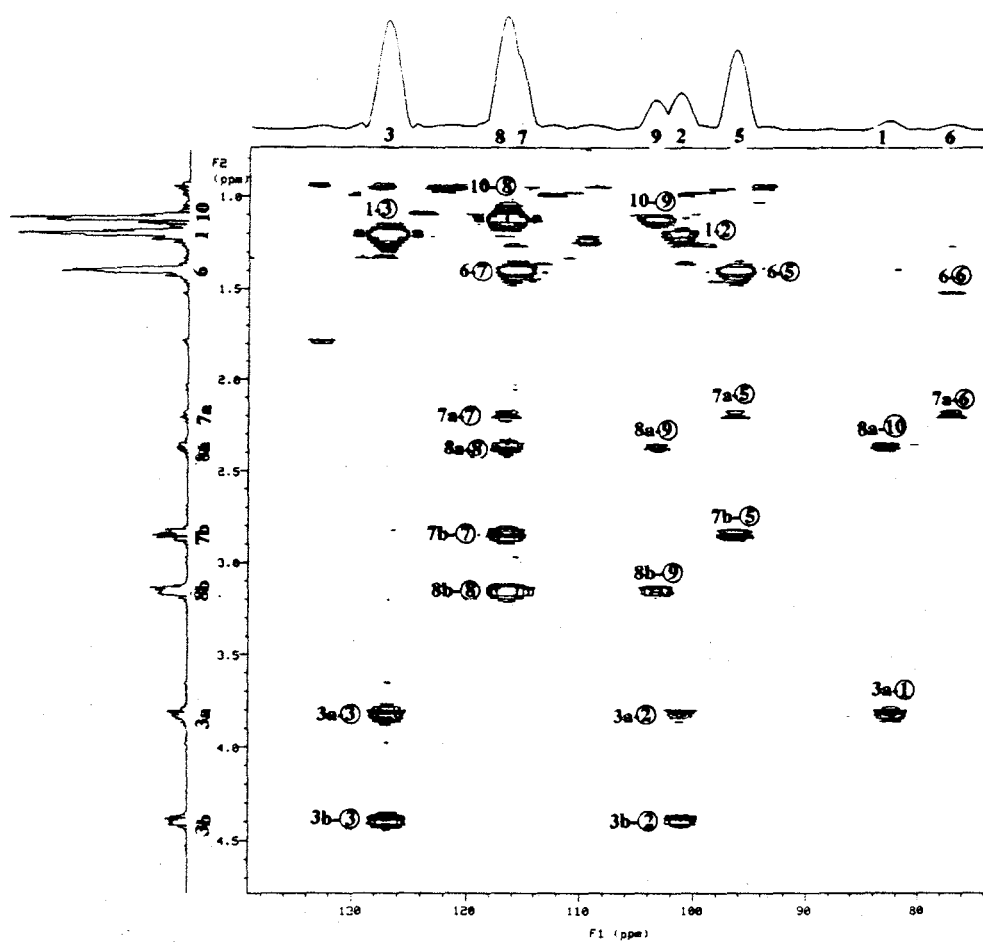


Figure C.1: 500 MHz HMBC spectrum of $[\text{Pt}(\alpha\text{Me}_5\text{-N}_6\text{-tricosanetriimine})]\text{Cl}_4$ in D_2O . np = 4096, sw = 5999.7 Hz, d1 = 1.5s, J=125 Hz, nt = 72, ni = 256, fn = 4096, fn1 = 4096, null = 0, taumb = 0.06 (a) Full spectrum (b) expanded spectrum (Carbon atoms are denoted by circled numbers) ((b) is on the next page).

(b)



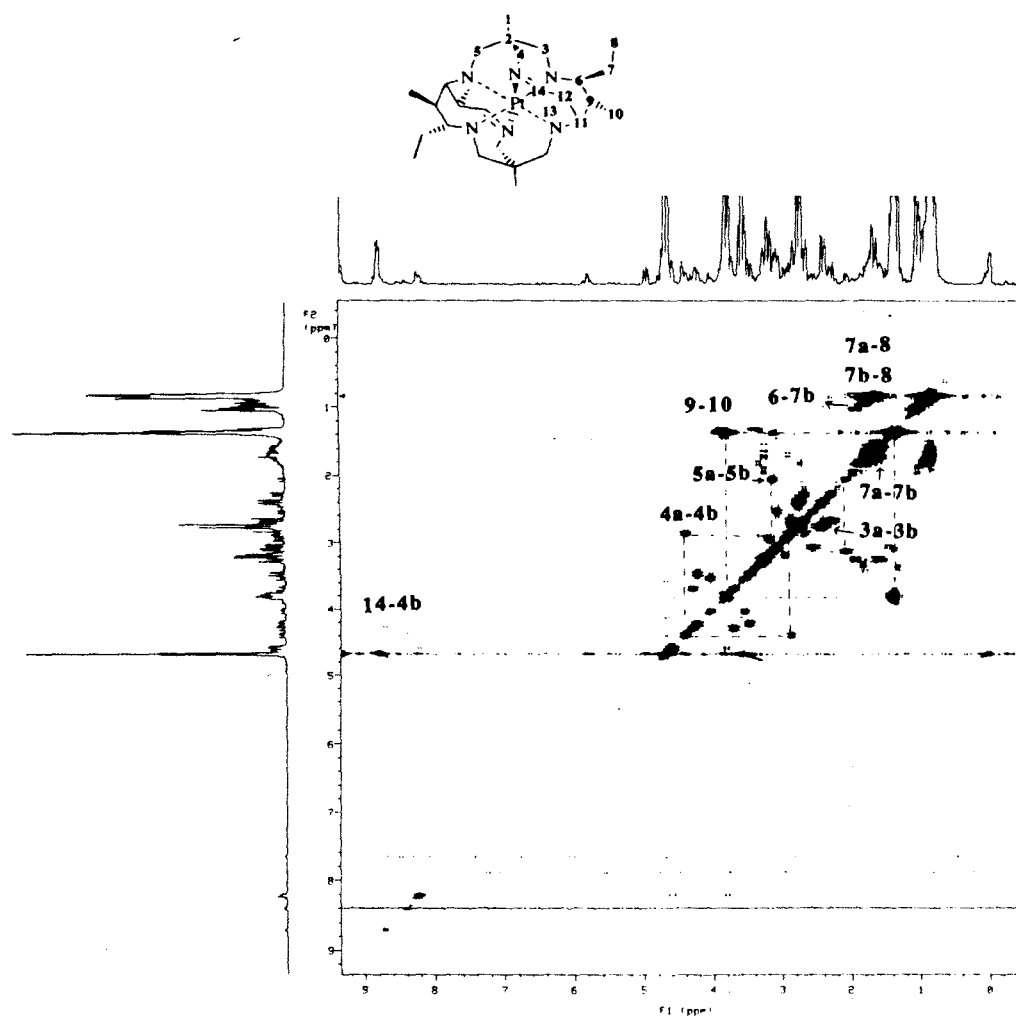


Figure C.2: 300 MHz DQF COSY spectrum of $[\text{Pt}(\text{Et}_2\text{-Me}_6\text{-N}_6\text{-tetracosanediimine})]\text{Cl}_4$ at pH ~ 4 . np = 2048, sw = 2646.9 Hz, d1 = 1.2 s, nt = 168, ni = 220, fn = 4096, fn1 = 4096.

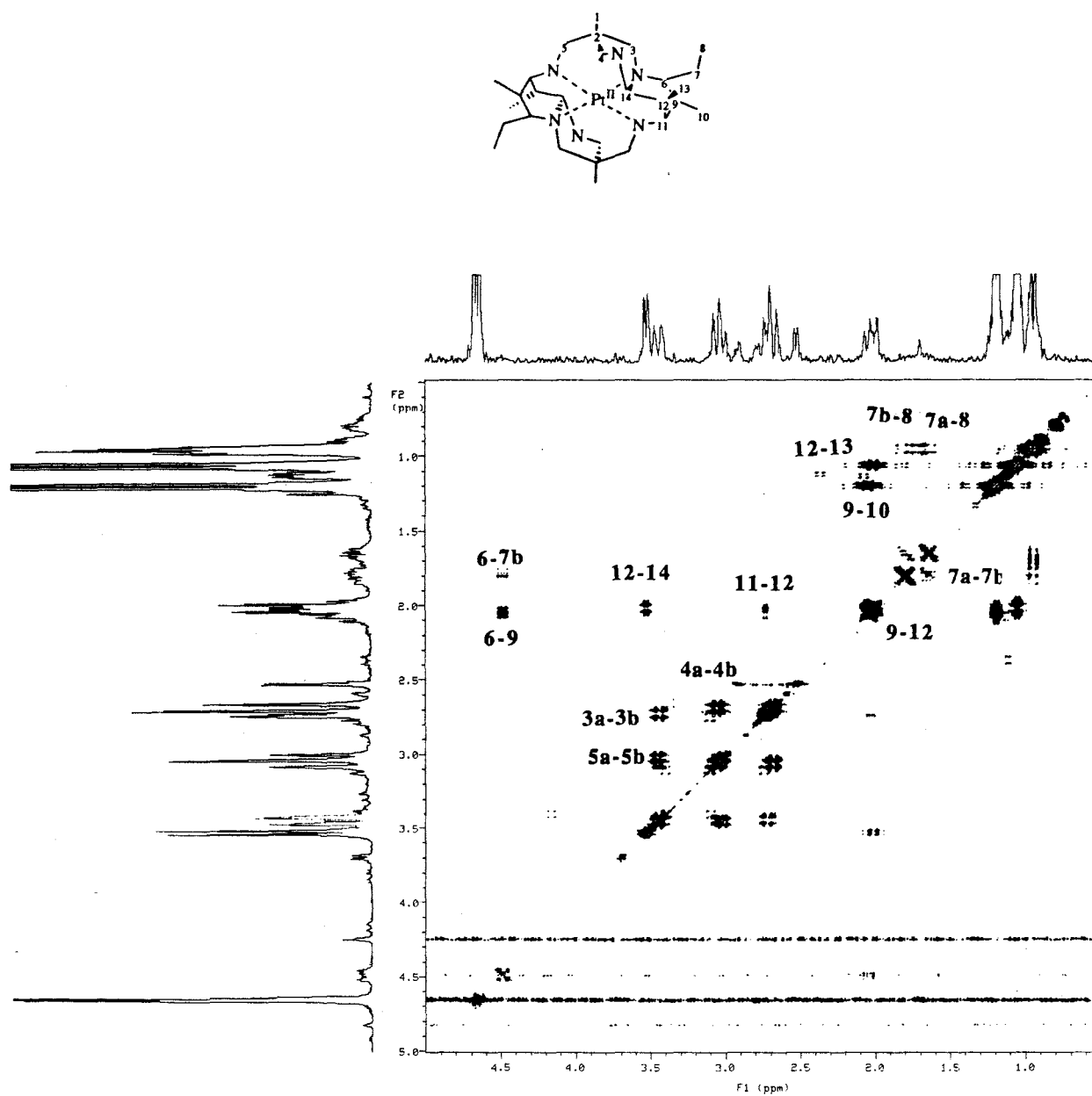


Figure C.3: 300 MHz DQF COSY spectrum of the electrochemically prepared pentacyclo-[Pt^{II}(Et₂-Me₆-N₆-tetracosaneH₂)]⁴⁺. np = 2048, sw = 1753.5 Hz, d1 = 1.5 s, nt = 144, ni = 300, fn = 4096, fn1 = 4096.

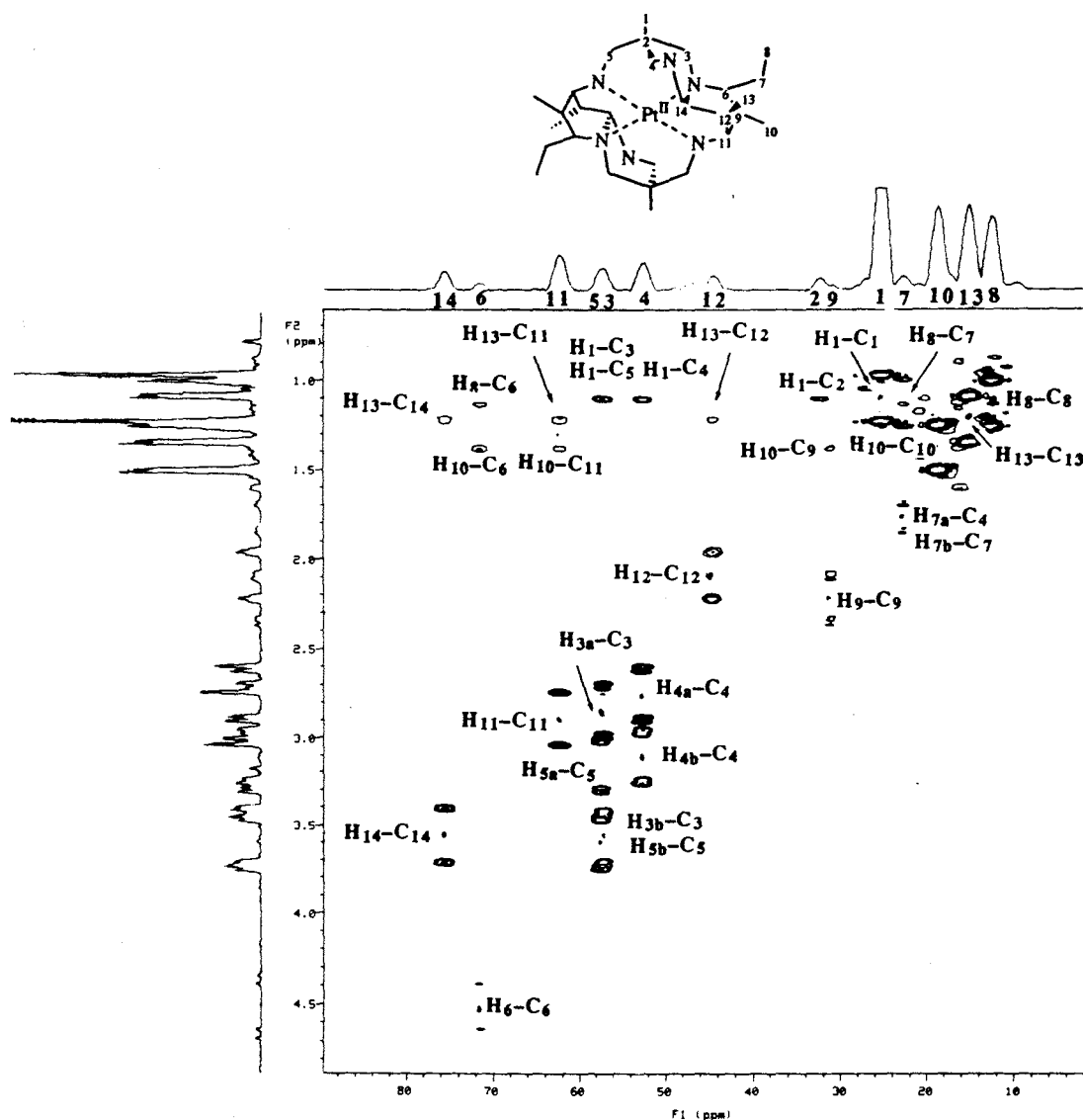
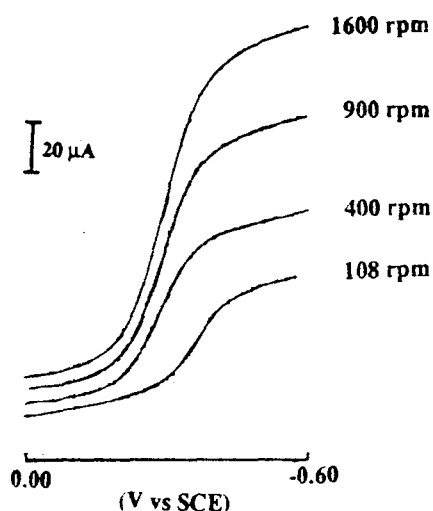


Figure C.4: 500 MHz HMQC spectrum of pentacyclo-[Pt^{II}(Et₂-Me₆-N₆-tetracosaneH₂)]⁴⁺ in D₂O. np = 1024, sw = 2380.0 Hz, d1 = 4s, nt = 64, J = 125 Hz, ni = 256, fn = 2048, fn1 = 2048, mbond = n, null = 0.3, taumb = 0 (Carbon atoms are denoted by circled numbers).

Appendix D

Calculation of the Diffusion Coefficient for $[\text{Co}(\text{Me}_5\text{-N}_6\text{-tricosanetriimine})]^{3+}$ using the Rotating Disc Electrode.

Figure D.1 depicts the responses for the one electron reduction of $[\text{Co}(\text{Me}_5\text{-N}_6\text{-tricosanetriimine})]^{3+}$ to $[\text{Co}(\text{Me}_5\text{-N}_6\text{-tricosanetriimine})]^{2+}$ using an EPG RDE in 0.1 M NaCl. The diffusion coefficient was calculated using the Koutecky-Levich equation. The dependence of the limiting current on angular velocity and the calculated diffusion coefficient for $[\text{Co}(\text{Me}_5\text{-N}_6\text{-tricosanetriimine})]^{3+}$ is listed in Table D.1. The average value for the diffusion coefficient is $2.72 \times 10^{-6} \text{ cm}^2 \text{ s}^{-1}$, which is consistent with the value obtained for $[\text{Co}(\text{sar})]^{3+}$ in 0.2 M KCl, $2.45 \times 10^{-6} \text{ cm}^2 \text{ s}^{-1}$.¹



ω (rpm)	i_p (μA)	D_o ($\times 10^6 \text{ cm}^2 \text{ s}^{-1}$)
108	35.7	3.09
400	62.9	2.71
900	91.4	2.58
1600	120	2.52
average		2.72

Figure D.1: Reduction of $[\text{Co}(\text{Me}_5\text{-N}_6\text{-tricosanetriimine})]^{3+}$ using the EPG RDE, at 50 mV s^{-1} with varying the angular velocity.

Table D.1: Dependence on limiting current with angular velocity and the calculated diffusion coefficient.

References

- (1) M. H. Jensen M.Sc. Thesis, The Technical University of Denmark, Lyngby, Denmark, 1992.

Appendix E

For both Co(III) complexes, data reduction and application of Lorentz, polarisation and absorption corrections were carried out using the Enraf-Nonius Structure Determination Package.¹ The structure was solved by direct atoms methods using SHELX-86² and the solution was extended by difference Fourier methods. Hydrogen atoms were refined with isotropic thermal parameters and all other atoms were refined anisotropically. Scattering factors and anomalous dispersion terms used for Co (neutral Co) were taken from International Tables³ and all others used were those supplied in SHELX-76.⁴ All calculations were carried out using SHELX-76⁴ and plots were drawn using ORTEP.⁵ Listings of observed and calculated structure factors, close non bonded contacts and torsion angles are deposited as an accessory publication.⁶

Table E.(I).1: Crystal Data for [Co(Et₂-Me₆-N₆-tetracosanediimine)]Cl₃.5H₂O.

Empirical formula	C ₂₈ H ₆₄ Cl ₃ CoN ₆ O ₅
formula weight	730.15
space group	<i>P</i> 2 ₁ / <i>n</i>
Z	2
crystal system; lattic type	monoclinic; primitive
N ^o reflections used for unit cell determination	
(2θ range)	25 (2-50)
crystal dimensions	0.35 x 0.40 x 0.36 mm
lattice parameters	a=11.605(3) Å, b=12.152(3) Å, c=12.409(3) Å; β=98.46(2)°
V	1731.0(6) Å ³
D(calc'd)	1.401 g m ⁻³
F ₀₀₀	784
radiation	Mo K _α (λ=0.71069); graphite monochromated
μ(Mo K _α)	7.67
T	294 K
scan type	ω
scan rate	variable
scan width	0.85+0.35tanθ
h,k,l (min, max)	-13→13, 0→1, 0→14
2θ _{max}	50
N ^o reflections measured (total):	3351
N ^o observations	2753 (I>2.5σ(I))
N ^o variables	322
trans factors:	0.801-0.831
decay	0.3% decline
Refinement	Full matrix least squares

Function minimised	$\Sigma w(F_o - F_c)^2 R_w = \{w^{1/2} F_o - F_c \} / \Sigma w^{1/2} F_o $
Least squares weights	$3.3 / \{\sigma^2(F) + (0.00015)F^2\}$
p-factor	1.5×10^{-4}
Anomalous dispersion	all non hydrogen atoms
Residuals: R; R_w	0.033, 0.039
Max. shift/error in final cycle	0.1
Max.; Min peaks in Final Diff. Map	$0.6e^{-1}\text{\AA}^{-1}$; $-0.3e^{-1}\text{\AA}^{-1}$

Table E.(I).2: Positional parameters for [Co(Et₂-Me₆-N₆-tetracosanediimine)]Cl₃.5H₂O

	10 ⁴ x	10 ⁴ y	10 ⁴ z
Co(1)	5000	5000	5000
N(1)	3692(1)	5987(1)	5198(2)
N(2)	4152(1)	3834(1)	5644(1)
N(3)	4164(1)	4407(1)	3566(2)
C(1)	1066(2)	4232(2)	4289(2)
C(2)	2366(2)	4501(2)	4510(2)
C(3)	2939(2)	4017(2)	3593(2)
C(4)	2879(2)	3996(2)	5605(2)
C(5)	2549(2)	5743(2)	4533(2)
C(6)	4805(2)	3566(2)	2971(2)
C(7)	4079(2)	3280(2)	1861(2)
C(8)	4813(3)	3088(3)	960(2)
C(9)	5144(2)	2554(2)	3708(2)
C(10)	5607(3)	1598(2)	3088(2)
C(11)	3954(2)	7184(2)	5264(2)
C(12)	5693(2)	2426(2)	5812(2)
C(13)	5639(3)	1171(2)	5886(2)
C(14)	4528(2)	2882(2)	5943(2)
Cl(1)	3249(1)	6215(1)	1639(1)
Cl(2)	7963(1)	3628(1)	2880(1)
O(1)	7398(3)	4715(5)	788(3)
O(2)	3935(5)	3594(5)	-1794(3)
O(3)	7963(1)	3628(1)	2880(1)

Table E(I).3: Thermal parameters ($\times 10^3$) for [Co(Et₂-Me₆-N₆-tetracosanediimine)]Cl₃.5H₂O.

	U_{11}	U_{22}	U_{33}	U_{23}	U_{13}	U_{12}
Co(1)	18(1)	13(1)	17(1)	0(1)	3(1)	1(1)
N(1)	22(1)	17(1)	17(1)	0(1)	2(1)	0(1)
N(2)	23(1)	18(1)	18(1)	0(1)	4(1)	0(1)
N(3)	20(1)	16(1)	21(1)	0(1)	3(1)	0(1)
C(1)	21(2)	32(2)	44(2)	-4(2)	7(2)	-3(1)
C(2)	19(1)	21(1)	30(2)	-2(1)	4(1)	0(1)
C(3)	20(1)	21(2)	26(2)	-3(1)	1(1)	-1(1)
C(4)	24(2)	21(2)	31(2)	1(1)	11(1)	0(1)
C(5)	20(1)	21(2)	28(2)	-2(1)	2(1)	2(1)
C(6)	23(1)	21(1)	21(1)	-4(1)	4(1)	0(1)
C(7)	31(2)	28(2)	22(2)	-5(1)	1(1)	-1(1)
C(8)	53(2)	65(3)	23(2)	-11(2)	8(2)	-5(2)
C(9)	25(1)	17(1)	25(2)	-2(1)	2(1)	0(1)
C(10)	47(2)	25(2)	35(2)	-10(2)	0(2)	8(2)
C(11)	24(1)	15(1)	26(2)	-1(1)	4(1)	3(1)
C(12)	28(2)	17(1)	24(2)	2(1)	0(1)	1(1)
C(13)	42(2)	20(2)	42(2)	6(1)	3(2)	4(1)
C(14)	32(2)	21(2)	22(2)	0(1)	5(1)	-2(1)
Cl(1)	75(1)	31(1)	35(1)	2(1)	6(1)	6(1)
Cl(2)	52(1)	59(1)	52(1)	-3(1)	12(1)	2(1)
O(1)	83(3)	185(5)	85(3)	-45(3)	22(3)	-49(3)
O(2)	93(3)	203(6)	47(2)	-2(3)	7(2)	7(4)
O(3)	52(1)	59(1)	52(1)	-3(1)	12(1)	2(1)

Table E(I).4: Hydrogen atom positional ($\times 10^3$) and thermal ($\times 10^2$) parameters for $[\text{Co}(\text{Et}_2\text{-Me}_6\text{-N}_6\text{-tetracosanediimine})]\text{Cl}_3 \cdot 5\text{H}_2\text{O}$.

	<i>x</i>	<i>y</i>	<i>z</i>	U_{iso}
HN(1)	356(2)	584(2)	582(2)	1(1)
HN(3)	409(2)	495(2)	315(2)	2(1)
H(1A)	66(2)	438(2)	491(2)	4(1)
H(1B)	73(3)	462(3)	367(3)	5(1)
H(1C)	93(2)	351(2)	411(2)	4(1)
H(3A)	248(2)	421(2)	293(2)	2(1)
H(3B)	295(2)	323(2)	363(2)	2(1)
H(4A)	273(2)	446(2)	620(2)	2(1)
H(4B)	257(2)	330(2)	564(2)	3(1)
H(5A)	199(2)	608(2)	488(2)	2(1)
H(5B)	256(2)	603(2)	375(2)	2(1)
H(6)	552(2)	395(2)	278(2)	2(1)
H(7A)	355(2)	271(2)	197(2)	3(1)
H(7B)	349(2)	387(2)	164(2)	2(1)
H(8A)	517(3)	376(3)	85(3)	8(2)
H(8B)	538(3)	255(4)	116(3)	10(2)
H(8C)	433(3)	298(3)	35(3)	6(1)
H(9)	440(2)	229(2)	399(2)	2(1)
H(10A)	502(2)	131(2)	251(2)	3(1)
H(10B)	633(2)	178(2)	272(2)	5(1)
H(10C)	587(2)	104(2)	358(2)	5(1)
H(11)	325(2)	759(2)	537(2)	2(1)
H(12)	623(2)	268(2)	644(2)	2(1)
H(13A)	637(3)	90(3)	578(2)	5(1)
H(13B)	506(2)	89(3)	538(3)	5(1)
H(13C)	554(2)	96(3)	663(3)	6(1)
H(14)	397(2)	242(2)	625(2)	3(1)
HO(1A)	181(12)	-21(9)	598(13)	40(6)
HO(1B)	198(2)	-9(2)	571(2)	0(1)
HO(2A)	34(5)	-140(5)	659(5)	14(3)
HO(2B)	118(3)	-101(2)	661(3)	0(1)

II. Crystal Data for [Co(Et₂-Me₆-N₆-tetracosane)]Cl₃.4H₂O

Table E(II).1: Crystal Data for [Co(Et₂-Me₆-N₆-tetracosane)]Cl₃.4H₂O

Empirical formula	CoC ₂₈ H ₆₆ N ₆ Cl ₃ O ₄
formula weight	716.16
space group	PZ ₁ /n
Z	2
crystal system	monoclinic
N ^o reflections used for unit cell determination	
(2θ range)	1<θ<25
crystal dimensions	0.35 x 0.38 x 0.23 mm
lattice parameters	a=10.257(6) Å, b=11.165(5) Å, c=15.207(5) Å, β=92.80(3)°
V	1739(1) Å ³
D(calc'd)	1.367 g cm ⁻³
F ₀₀₀	772
radiation	Mo K _α (λ=0.7107); graphite monochromated
μ(Mo K _α)	7.46
T	294 K
R; R _w	0.035, 0.039
scan type	ω-θ
scan width	1.60+0.35tanθ
h,k,l (min, max)	-12→12, 0→13, 0→18
N ^o reflections measured (total):	3352
N ^o observations	2526(I>2.5σ(I))
N ^o variables	325
trans factors:	0.863-0.555
decay	0 % decline
Refinement	Full matrix least squares
Function minimised	$R = \sum (F_o - F_c) / \sum F_o $ $R_w = \{w^{1/2} (F_o - F_c) / \sum w^{1/2} F_o \}$
Least squares weights	2.3/(σ ² (F)+(0.00030)F ²)
p-factor	3 x 10 ⁻⁴
Anomalous dispersion	all non hydrogen atoms
goodness of fit indicator	2.3
Max. shift/error in final cycle	0.02
Max.; Min. peaks in Final Diff. Map	+0.6 e ⁻ Å ⁻¹ ; -0.3 e ⁻ Å ⁻¹

Table E(II).2: Positional parameters for [Co(Et₂-Me₆-N₆-tetracosane)]Cl₃.4H₂O

	10 ⁴ x	10 ⁴ y	10 ⁴ z
Co(1)	0	5000	0
N(1)	1604(2)	5335(2)	-622(1)
N(2)	1109(2)	5380(2)	1107(1)
N(3)	-597(2)	6733(2)	-24(1)
C(1)	2703(3)	8273(3)	342(2)
C(2)	1798(2)	7194(2)	235(2)
C(3)	405(2)	7630(2)	307(2)
C(4)	2170(2)	6291(2)	966(2)
C(5)	1949(3)	6628(2)	-668(2)
C(6)	1938(2)	2965(2)	-297(2)
C(7)	2274(3)	1635(2)	-105(2)
C(8)	3690(3)	1439(3)	193(3)
C(9)	2048(2)	3313(2)	-1262(2)
C(10)	3367(3)	2945(3)	-1618(2)
C(11)	1818(2)	4671(2)	-1451(2)
C(12)	748(3)	4931(2)	-2148(2)
C(13)	1150(3)	4531(3)	-3055(2)
C(14)	538(3)	5672(2)	1972(2)
O(1)	4857(4)	3810(4)	1986(3)
O(2)	5044(5)	5539(5)	3413(3)
Cl(1)	1853(1)	2875(1)	2003(1)
Cl(2)	5000	5000	0

Table E(II).3: Thermal parameters ($\times 10^3$) for $[\text{Co}(\text{Et}_2\text{-Me}_6\text{-N}_6\text{-tetracosane})]\text{Cl}_3 \cdot 4\text{H}_2\text{O}$

	U_{11}	U_{22}	U_{33}	U_{23}	U_{13}	U_{12}
Co(1)	20(1)	14(1)	17(1)	0(1)	3(1)	0(1)
N(1)	26(1)	16(1)	23(1)	0(1)	6(1)	-1(1)
N(2)	25(1)	18(1)	23(1)	0(1)	0(1)	0(1)
N(3)	24(1)	20(1)	21(2)	0(1)	4(1)	-1(1)
C(1)	37(2)	26(2)	48(2)	-6(2)	8(2)	-9(2)
C(2)	23(2)	19(2)	30(2)	-2(1)	4(1)	-6(1)
C(3)	29(2)	16(2)	29(2)	-1(1)	3(1)	-1(1)
C(4)	24(2)	27(2)	27(2)	-4(1)	0(1)	-2(1)
C(5)	28(2)	19(2)	31(2)	1(1)	9(1)	-4(1)
C(6)	23(2)	17(2)	32(2)	-1(1)	5(1)	1(1)
C(7)	31(2)	20(2)	44(2)	0(2)	6(2)	3(1)
C(8)	36(2)	32(2)	74(3)	0(2)	-4(2)	8(2)
C(9)	28(2)	20(2)	33(2)	-3(1)	9(1)	0(1)
C(10)	46(2)	31(2)	52(2)	-2(2)	25(2)	6(2)
C(11)	29(2)	20(2)	25(2)	-3(1)	11(1)	-3(1)
C(12)	38(2)	26(2)	24(2)	1(1)	8(1)	-3(1)
C(13)	57(2)	49(2)	23(2)	-3(2)	11(2)	-11(2)
C(14)	37(2)	30(2)	20(2)	0(1)	2(1)	0(2)
O(1)	84(3)	86(3)	100(4)	-1(3)	-5(3)	1(2)
O(2)	122(4)	118(4)	68(3)	-10(3)	0(3)	7(3)
Cl(1)	84(1)	47(1)	39(1)	14(1)	-3(1)	19(1)
Cl(2)	38(1)	55(1)	68(1)	-15(1)	10(1)	3(1)

Table E(II).3: Hydrogen atom positional ($\times 10^3$) and thermal ($\times 10^2$) parameters for $[\text{Co}(\text{Et}_2\text{-Me}_6\text{-N}_6\text{-tetracosane})]\text{Cl}_3 \cdot 4\text{H}_2\text{O}$.

	<i>x</i>	<i>y</i>	<i>z</i>	U_{iso}
HN(1)	225(2)	506(2)	-22(2)	2(1)
HN(2)	148(3)	476(2)	120(2)	2(1)
HN(3)	-67(2)	681(2)	-56(2)	1(1)
H(1A)	253(2)	870(2)	86(2)	3(1)
H(1B)	257(3)	883(3)	-18(2)	4(1)
H(1C)	366(3)	799(3)	37(2)	4(1)
H(3A)	25(2)	832(3)	-4(2)	3(1)
H(3B)	23(1)	780(2)	91(2)	2(1)
H(4A)	295(2)	587(2)	85(2)	3(1)
H(4B)	234(2)	669(2)	152(2)	2(1)
H(5A)	286(2)	665(2)	-81(2)	3(1)
H(5B)	141(2)	704(2)	-112(2)	2(1)
H(6)	259(2)	347(2)	8(1)	2(1)
H(7A)	201(2)	114(2)	-65(2)	3(1)
H(7B)	174(3)	140(2)	35(2)	3(1)
H(8A)	394(4)	62(5)	29(3)	10(2)
H(8B)	387(3)	185(3)	72(2)	7(2)
H(8C)	426(4)	182(4)	-21(3)	10(2)
H(9)	132(2)	286(2)	-159(2)	3(1)
H(10A)	348(3)	211(3)	-158(2)	6(2)
H(10B)	335(3)	321(3)	-223(2)	6(1)
H(10C)	420(3)	334(3)	-122(2)	6(1)
H(11)	259(3)	496(2)	-163(2)	3(1)
H(12)	58(2)	576(2)	-216(2)	2(1)
H(13A)	204(3)	478(3)	-315(2)	5(1)
H(13B)	52(3)	475(3)	-350(2)	5(1)
H(13C)	115(3)	366(3)	-311(2)	6(2)
H(14A)	38(2)	654(3)	200(2)	3(1)
H(14B)	118(2)	544(2)	243(1)	1(1)
HO(1A)	404(4)	364(4)	199(3)	9(2)
HO(1B)	479(5)	410(5)	155(4)	10(3)
HO(2A)	493(6)	507(5)	309(4)	9(3)
HO(2B)	428(6)	590(6)	325(5)	16(3)

References

- (1) Enraf-Nonius, Enraf-Nonius Structure Determination Package, Delft, 1985.
- (2) Sheldrick, G. M.; *SHELX-86 Crystallographic Computing 3*; Oxford University Press: 1986, pp 175-189.
- (3) *International Tables for X-ray Crystallography*; Kynoch Press: Birmingham, 1974; Vol. 4.
- (4) Sheldrick, G. M., SHELX-76, A Program for X-ray Crystal Structure Determination, University of Cambridge, 1976.
- (5) Johnson, C. K., ORTEP, A Thermal Ellipsoid Plotting Program, Oak Ridge National Laboratories, 1965.
- (6) Copies are available on application to the Editor-in-Chief, Editorial and Publications Service, CSIRO, 314 Albert Street, East Melbourne, Vic, 3002

Appendix F

Supplementary NMR Spectra for Chapter 5.

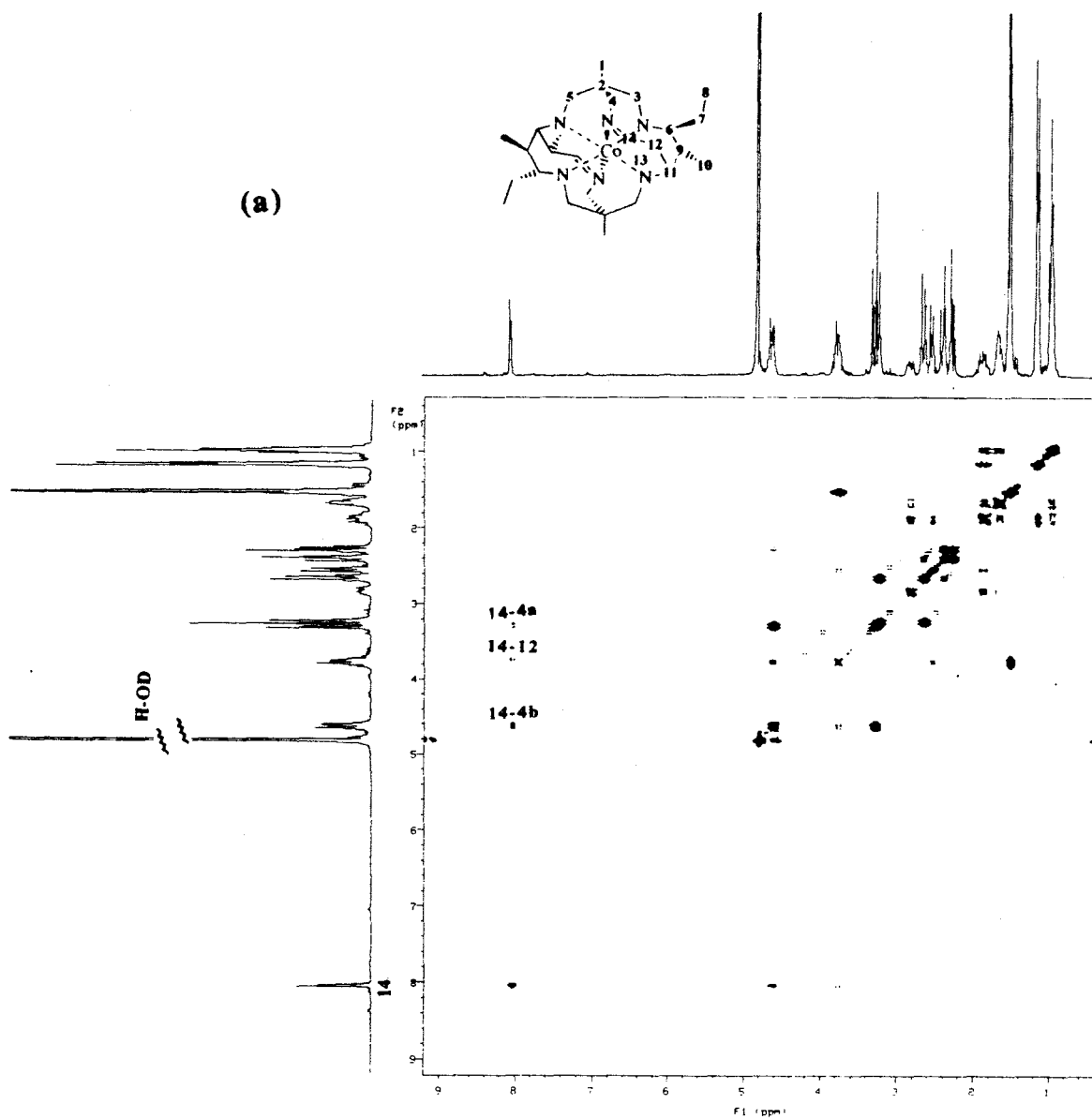
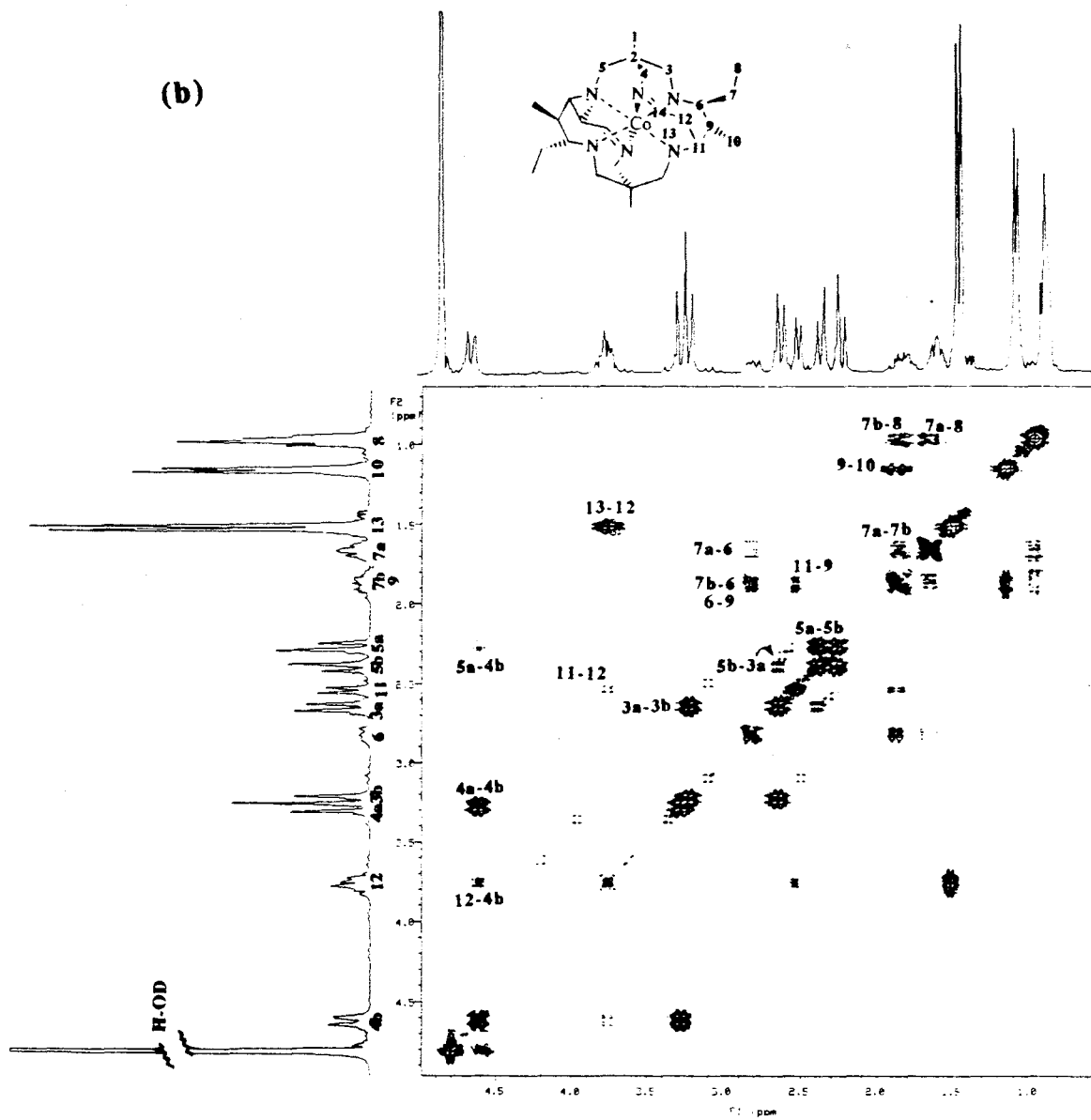


Figure F.1: 500 MHz DQF COSY spectrum of $[\text{Co}(\text{Et}_2\text{-Me}_6\text{-N}_6\text{-tetracosanediimine})]\text{Cl}_3$ in D_2O . $n_p = 2048$, $sw = 2669.5$ Hz, $d_1 = 0.5$ s, $nt = 96$, $ni = 288$, $fn = 4096$, $fn_1 = 4096$. (a) entire spectrum and (next page) (b) expanded spectrum 0-4.5 ppm.



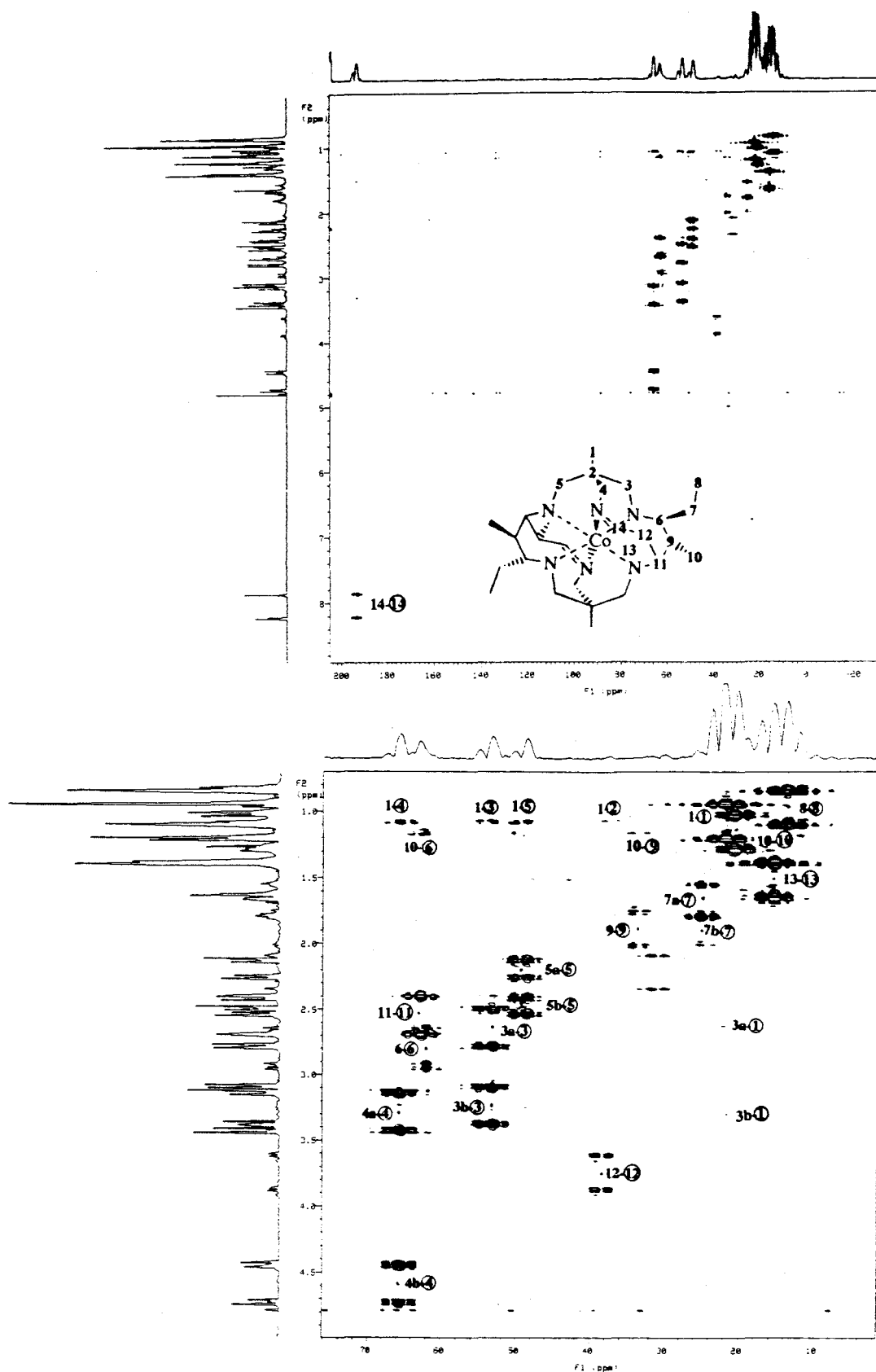


Figure F.2: 500 MHz HMQC spectrum of $[\text{Co}(\text{Et}_2\text{-Me}_6\text{-N}_6\text{-tetracosanediimine})]\text{Cl}_3$ in D_2O . np = 2048, sw = 4354.9 Hz, d1 = 1 s, nt = 352, J = 125 Hz, ni = 128, fn = 2048, fn1 = 2048, mbond = n, null = 0.3, taumb = 0 (a) full spectrum and (b) region 0.6 – 5.5 x 0 – 76 ppm. (Carbon atoms are denoted by circled numbers).

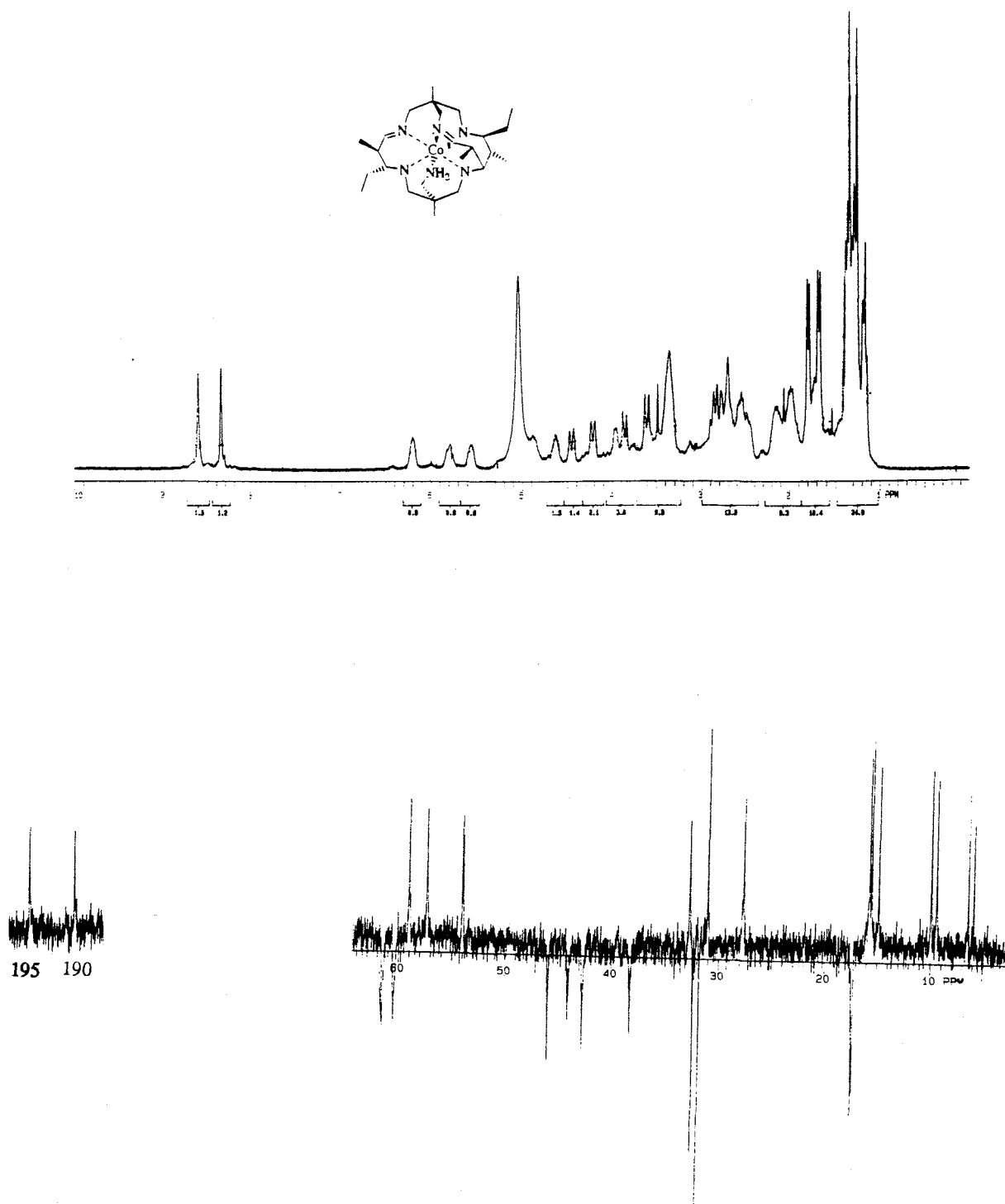


Figure F.3: 300 MHz (a) ^1H and (b) APT NMR spectra of $[\text{Co}(\text{Et}_2\text{-Me}_6\text{-N}_6\text{-docosanediimine})]\text{Cl}_3$ in D_2O .

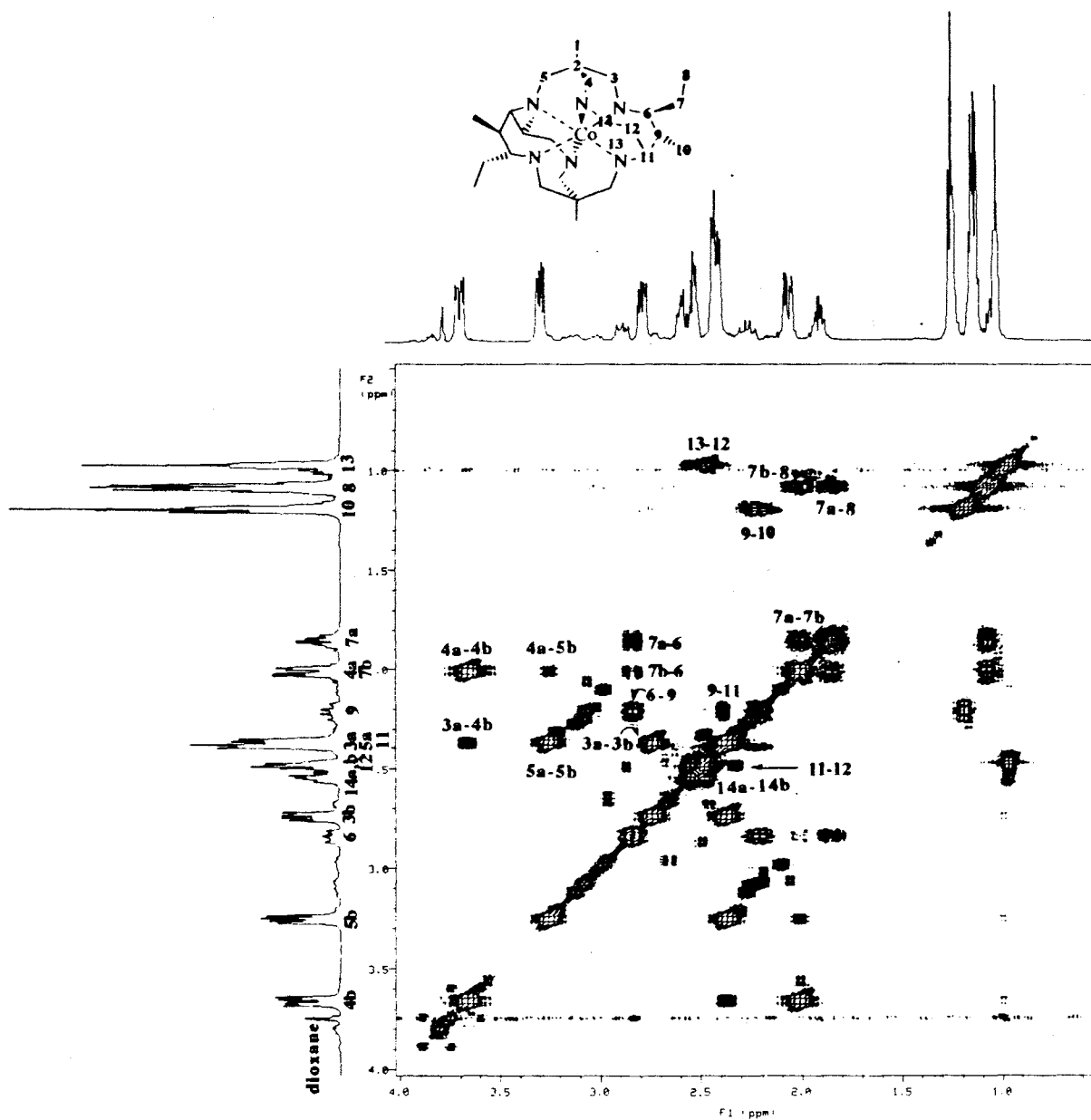


Figure F.4: 500 MHz DFQ COSY spectrum of $[\text{Co}(\text{Et}_2\text{-Me}_6\text{-N}_6\text{-tetracosane})]\text{Cl}_3$ in D_2O . np = 1024, sw = 2400.0 Hz, d1 = 4s, nt = 32, ni = 200, fn = 2048, fn1 = 2048.

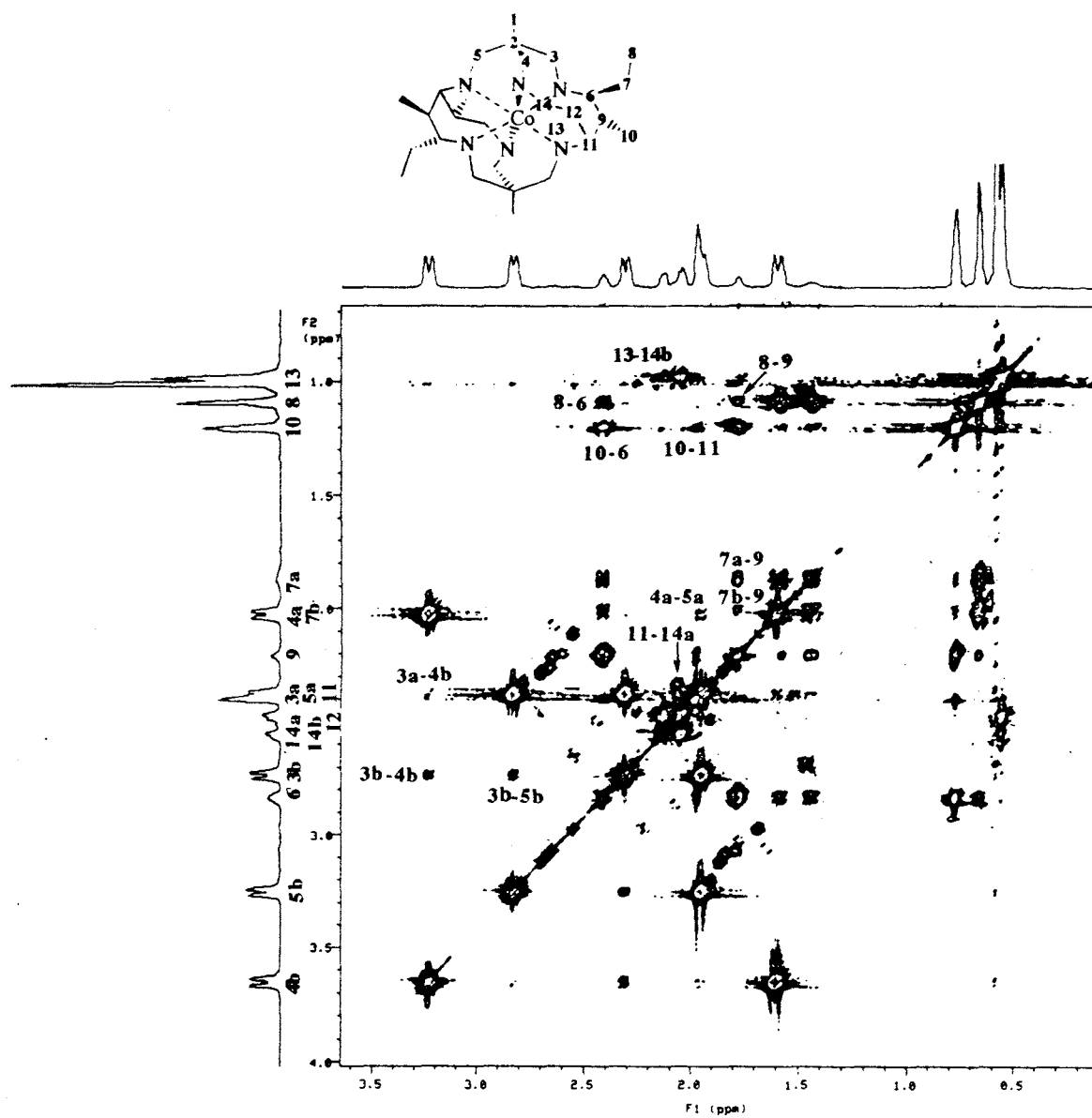


Figure F.5: 500 MHz TOCSY spectrum of $[\text{Co}(\text{Et}_2\text{-Me}_6\text{-N}_6\text{-tetracosane})]\text{Cl}_3$ in D_2O .
 np = 4096, sw = 3000.1 Hz, d1 = 1.8s, nt = 32, ni = 400, mixing time = 0.04, mixing
 sequence = direct correlation, fn = 4096, fn1 = 4096.

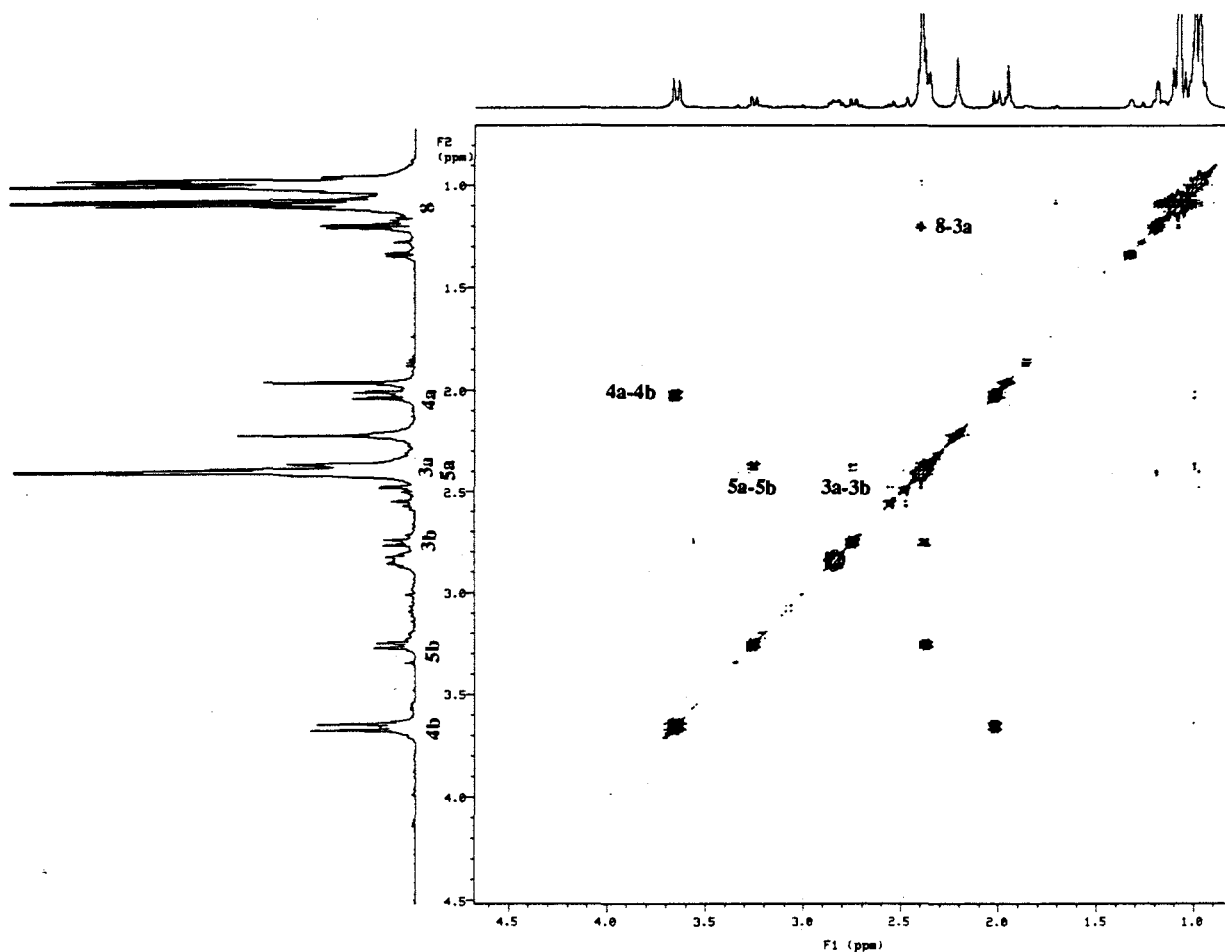


Figure F.6: 500 MHz NOESY spectrum of $[\text{Co}(\text{Et}_2\text{-Me}_6\text{-N}_6\text{-tetracosane})]\text{Cl}_3$ in D_2O .
np = 1024, sw = 2302.8 Hz, d1 = 1.5s, nt = 128, ni = 256, mixing time = 1.0 s, fn = 2048, fn1 = 2048.

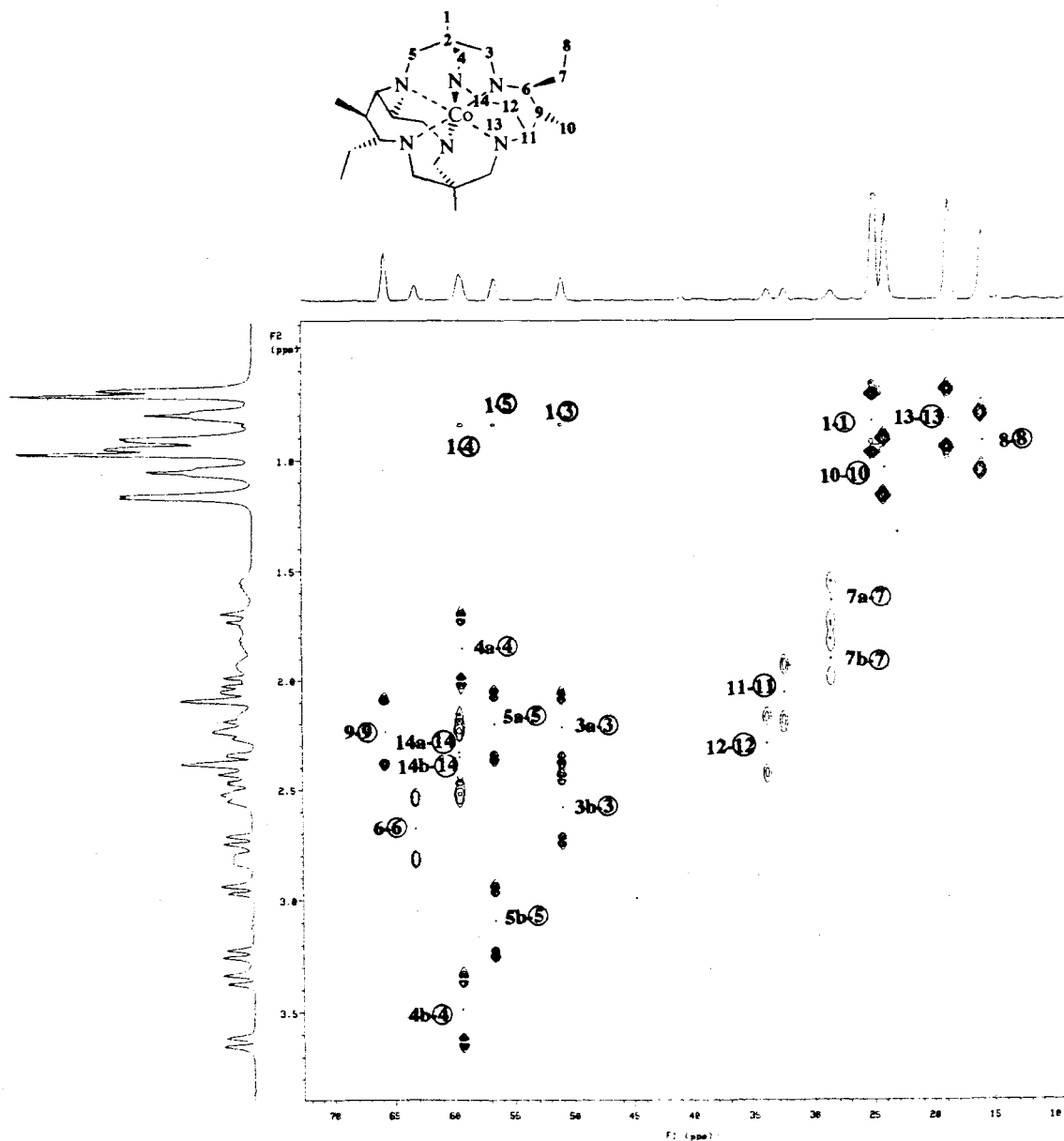


Figure F.7: 500 MHz HMQC spectrum of [Co(Et₂-Me₆-N₆-tetracosane)]Cl₃ in D₂O. np = 1024, sw = 2799.9 Hz, nt = 184, d1 = 1s, J = 125 Hz, ni = 256, fn = , fn1 = mbond = n, null = 0.3, taumb = 0. Carbon atoms are specified by circled numbers.

Table F.1: Vicinal coupling constants and dihedral angles for the cation in [Co(Et₂-Me₆-N₆-tetracosanediimine)]³⁺.Cl₃.5H₂O.

Bond Angles	[Co(Et ₂ -Me ₆ -N ₆ -tetracosanediimine)] ³⁺		
	ϕ	³ J _{calc} (Hz) [†]	³ J _{obs} (Hz) [‡]
H ₆ -C ₆ -C ₇ -H _{7a}	±159.950	8.13	7.9
H ₆ -C ₆ -C ₇ -H _{7b}	±94.357	-0.19	2.5
H ₆ -C ₆ -C ₉ -H ₉	±169.497	8.91	7.9
H ₉ -C ₉ -C ₁₁ -H ₁₁	±128.218	3.47	2.7
H ₁₁ -C ₁₁ -C ₁₂ -H ₁₂	±70.600	0.52	2.5
H ₁₂ -C ₁₂ -C ₁₄ -H ₁₄	±97.970	0.04	2.8

Table F.2: Vicinal coupling constants and dihedral angles for the cation in [Co(Et₂-Me₆-N₆-tetracosane)]³⁺.Cl₃.4H₂O.

Bond Angles	[Co(Et ₂ -Me ₆ -N ₆ -tetracosane)] ³⁺		
	ϕ	³ J _{calc} (Hz) [†]	³ J _{obs} (Hz) [‡]
H ₆ -C ₆ -C ₇ -H _{7a}	±151.400	7.10	6.3
H ₆ -C ₆ -C ₇ -H _{7b}	±93.140	-0.22	2.6
H ₆ -C ₆ -C ₉ -H ₉	±173.828	9.11	11.6
H ₉ -C ₉ -C ₁₁ -H ₁₁	±129.227	3.92	3.7
H ₁₁ -C ₁₁ -C ₁₂ -H ₁₂	±70.126	0.59	—
H ₁₂ -C ₁₂ -C ₁₄ -H _{14a}	±176.189	9.22	5.8
H ₁₂ -C ₁₂ -C ₁₄ -H _{14b}	±57.900	2.00	—

[†] ϕ = dihedral angle. [‡] $^3J_{\text{calc}} = 4.22 - 0.5\cos\phi + 4.5\cos 2\phi$.¹ [‡] $^3J_{\text{obs}}$ estimated from DQF COSY spectrum.

((1) Günter, H. *NMR Spectroscopy, An Introduction*; John Wiley and Sons: New York, 1973, Chapter 4, and references therein.

Appendix G

Table G.1: Data used for correlation between energy of the first spin allowed transition and the Co(III)-N bond length.

Complex	Co(III)-N (Å)	Energy ($\times 10^{-3} \text{ cm}^{-1}$)
[Co(NH ₃) ₆] ³⁺	1.970 ¹	21.10 ²
[Co(en) ₃] ³⁺	1.964 ³	21.413
[Co(tn) ₃] ³⁺	1.983 ⁴	20.49 ²
(+)[Co(<i>R,R</i>)(ptn) ₃] ³⁺	1.988 ⁵	20.75 ²
(-)[Co(<i>R,R</i>)(ptn) ₃] ³⁺	1.984 ⁶	20.53 ²
(+)[Co(<i>R,S</i>)(ptn) ₃] ³⁺	1.993 ⁷	20.37 ²
[Co(Metacn) ₂] ³⁺	1.974 ⁸	21.600
[Co(<i>trans</i> -diammac)] ³⁺	1.9410 ⁹	22.173 ⁹
[Co(tame) ₂] ³⁺	1.974 ¹⁰	21.186 ¹¹
<i>lel</i> ₃ -[Co(chxn) ₃] ³⁺	1.9661 ¹²	21.186
<i>ob</i> ₃ -[Co(chxn) ₃] ³⁺	1.9800 ¹³	21.142
<i>lel</i> ₃ -[Co(pn) ₃] ³⁺	1.9750	21.368
<i>ob</i> ₃ -[Co(pn) ₃] ³⁺	1.9710	21.368
<i>ob</i> ₃ -[Co(tmen) ₃] ^{3+ 14}	1.999	19.841
[Co(tach) ₂] ³⁺	1.987 ¹⁵	20.900 ¹⁶
[Co((NH ₃) ₂ sar)] ⁵⁺	1.9780	21.053
[Co(sep)] ^{3+ 17}	1.981 ¹⁷	21.186
[Co(Me ₅ -N ₆ -tricosane)] ³⁺¹⁸	2.022	19.380
[Co(Et ₂ -Me ₆ -N ₆ -tetracosane)] ³⁺	2.011	20.080
<i>mer</i> -[Co(dien) ₂] ³⁺	1.967 ¹⁹	21.598
<i>mer</i> -[Co(dpt) ₃] ³⁺	2.011 ²⁰	19.531
[Co((Me ₃ N) ₂ sar)] ⁵⁺	1.9605	22.472

Table G.2: Data used in the correlation between the reduction potential and the difference in the strain energies for the Co(III) and Co(II) states.²¹

	Complex	$E_{1/2}$ (V vs NHE)	{U(III)-U(II)} (kJmol ⁻¹)
1	[Co(NH ₃) ₆] ³⁺	-0.02	59
2	[Co(en) ₃] ³⁺	-0.17	57
3	[Co(tn) ₃] ³⁺	0.13	83
4	<i>mer</i> [Co(dien)] ^{3+/2+}	-0.20	62
5	[Co(ptn) ₃] ³⁺	-0.34	42
6	<i>mer</i> -[Co(dpt)] ^{3+/2+}	0.28	111
7	[Co(tacn) ₂] ³⁺	-0.41	62
8	[Co(<i>trans</i> -diammac)] ³⁺	-0.63	29*
9	[Co(sep)] ³⁺	-0.27	79
10	[Co(Me ₅ -N ₆ -tricosane)] ³⁺	0.08	102*
11	[Co(Et ₂ -Me ₆ -N ₆ -tetracosane)] ³⁺	-0.23	94*

* This work; calculated by Dr. P.V. Bernhardt using published force fields for Co(III) and Co(II).²¹

Table G.3: Data used in the correlation between energy of the first spin allowed transition and the $\text{CoN}_6^{3+/2+}$ reduction potential.

Complex	Energy ($\times 10^{-3} \text{ cm}^{-1}$)	$E_{1/2}$ (V vs NHE)
$[\text{Co}(\text{NH}_3)_6]^{3+}$	21.097	-0.02
$[\text{Co}(\text{en})_3]^{3+}$	21.413	-0.17
$[\text{Co}(\text{tn})_3]^{3+}$	20.408	0.13
$[\text{Co}(\text{ptn})_3]^{3+}$	21.739	-0.34
$[\text{Co}(\text{tacn})_2]^{3+}$	21.786	-0.41
$[\text{Co}(\textit{trans}\text{-diammac})]^{3+}$	22.173	-0.63
$[\text{Co}(\textit{tame})_2]^{3+}$	21.186	-0.43
$\textit{lel}_3\text{-}[\text{Co}(\textit{chxn})_3]^{3+}$	21.186	-0.20
$\textit{lel}_3\text{-}[\text{Co}(\textit{pn})_3]^{3+}$	21.368	-0.13
$[\text{Co}(\textit{tmen})_3]^{3+}$	19.841	0.28
$[\text{Co}(\textit{sar})]^{3+}$	21.231	-0.42
$[\text{Co}(\text{Me}_2\textit{sar})]^{3+}$	21.142	-0.48
$[\text{Co}(\text{Me}_5\text{-}N_6\text{-tricosane})]^{3+}$	19.380	0.08
$[\text{Co}(\text{Et}_2\text{-Me}_6\text{-}N_6\text{-tetracosane})]^{3+}$	20.080	-0.23
$\textit{mer}\text{-}[\text{Co}(\textit{dien})_2]^{3+}$	21.598	-0.20
$\textit{mer}\text{-}[\text{Co}(\textit{dpt})_3]^{3+}$	19.531	0.28
$\textit{fac}\text{-}[\text{Co}(\textit{Medien})]^{3+}$	20.833	-0.01
$[\text{Co}(1,4\text{-Medien})]^{3+}$	19.084	0.26
$[\text{Co}(\textit{linpen})]^{3+}$	21.097	-0.15

References

- (1) Figgis, B. N.; Skelton, B. W.; White, A. H. *Aust. J. Chem.* **1979**, *32*, 417.
- (2) Mizukami, F.; Ito, H.; Fujita, J.; Saito, K. *Bull. Chem. Soc., Jpn.* **1972**, *45*, 2129.
- (3) Templeton, D. H.; Zalkin, A.; Ruben, H. W.; Templeton, L. K. *Acta Crystallogr.* **1979**, *B35*, 1608.
- (4) Nagao, R.; Marumo, F.; Saito, Y. *Acta Crystallog.* **1973**, *B29*, 2438.
- (5) Kobayashi, A.; Marumo, F.; Saito, Y. *Acta Crystallog.* **1972**, *B28*, 3591.
- (6) Kobayashi, A.; Marumo, F.; Saito, Y. *Acta Crystallog.* **1973**, *B29*, 2443.
- (7) Sato, S.; Saito, Y. *Acta Crystallog.* **1978**, *B34*, 420.
- (8) Mikami, M.; R., K.; Konno, M.; Saito, Y. *Acta Crystallog.* **1977**, *B33*, 1485.
- (9) Bernhardt, P. V.; Lawrance, G. A.; Hambley, T. W. *J. Chem. Soc., Dalton Trans.* **1989**, 1059, and references therein.
- (10) Geue, R. J.; Snow, M. R. *Inorg. Chem.* **1977**, *16*, 231.
- (11) Ventur, D.; Wieghardt, K.; Nuber, B.; Weiss, J. Z. *Anorg. Allg. Chem.* **1987**, *551*, 33.
- (12) Mizuta, T.; Toshitani, K.; Miyoshi, K.; Yoneda, H. *Inorg. Chem.* **1990**, *29*, 3020.
- (13) Kobayashi, A.; Marumo, F.; Saito, Y. *Acta Crystallog.* **1983**, *C39*, 807.
- (14) Hendry, P.; Ludi, A. *Advances in Inorganic Chemistry*, **1990**, *35*, 117, and references therein.
- (15) Ishii, M.; Umehara, M.; Nakahara, M. *Bull. Chem. Soc. Jpn.* **1987**, *60*, 125.
- (16) Wentworth, R. A. D.; Felton, J. J. *J. Am. Chem. Soc.* **1968**, *90*, 621.
- (17) Dubicki, L.; Ferguson, J.; Geue, R. J.; Sargeson, A. M. *Chem. Phys. Lett.* **1980**, *74*, 393, and references therein.
- (18) Geue, R. J.; Höhn, A.; Ralph, S. F.; Sargeson, A. M. *J. Chem. Soc., Chem. Commun.* **1994**, 1513.

- (19) Okiyama, K.; Sato, S.; Saito, Y. *Acta Crystallog.* **1979**, *B35*, 2389.
- (20) Hambley, T. W.; Searle, G. H.; Snow, M. R. *Aust. J. Chem.* **1982**, *35*, 1285.
- (21) Hambley, T. W. *Inorg. Chem.* **1988**, *27*, 2496, and references therein.

Appendix H

Characterisation of $[\text{Cr}(\text{Me}_5-(\text{CH}_2\text{OH})_2-N_6\text{-tricosanediimine})]\text{Cl}_3$ by electrospray mass spectrometry.

Figure H.1 depicts the electrospray mass spectrum of the first complex to elute off SP-Sephadex cation exchange resin, whose synthesis was described in Chapter 6.2.1.e.

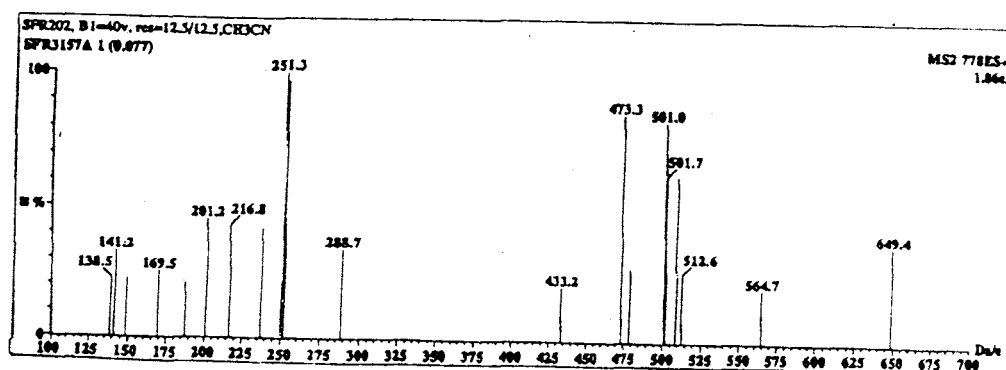


Figure H.1: Electrospray mass spectrum of the first complex to elute from the SP-Sephadex cation exchange resin, (MeCN, 40 V).

Two possible structures are depicted in Figure H.2. Both complexes are anticipated to have similar m/z values and fragmentation patterns. The m/z ratios for ions that might arise from these complexes are listed in Table H.1. The complex with three hydroxymethyl substituents is inconsistent with this mass spectrum, although its empirical formula fits the microanalysis. The saturated form for this complex is also inconsistent with the m/z values in the mass spectrum at 40 V.

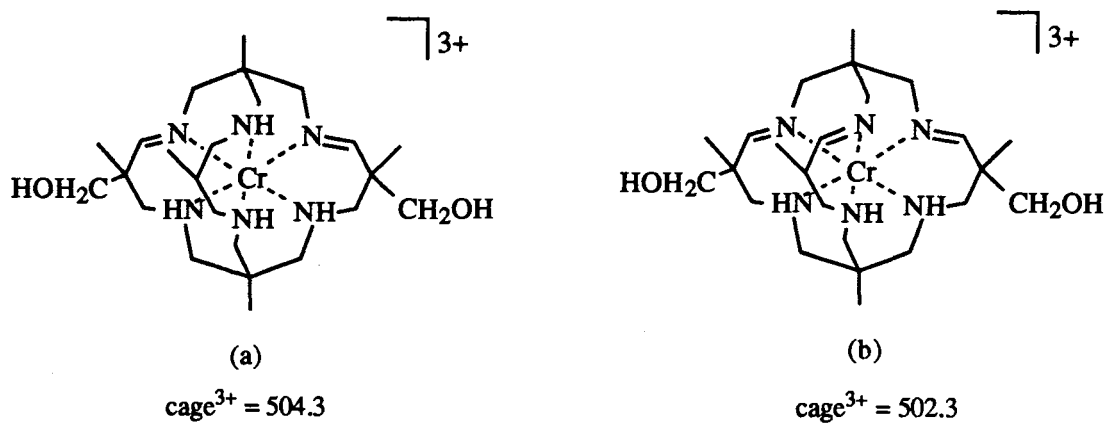


Figure H.2: Possible structures. (a) $[\text{Cr}(\text{Me}_5\text{-(CH}_2\text{OH)}_2\text{-N}_6\text{-tricosanediimine)}]\text{Cl}_3$ (b) $[\text{Cr}(\text{Me}_5\text{-(CH}_2\text{OH)}_2\text{-N}_6\text{-tricosanetriimine)}]\text{Cl}_3$.

Table H.1: m/z ratios for ions that might arise from $[\text{Cr}(\text{Me}_5\text{-(CH}_2\text{OH)}_2\text{-N}_6\text{-tricosanediimine)}]\text{Cl}_3$ and $[\text{Cr}(\text{Me}_5\text{-(CH}_2\text{OH)}_2\text{-N}_6\text{-tricosanetriimine)}]\text{Cl}_3$.

Complex	$[\text{Cr}(\text{Me}_5\text{-(CH}_2\text{OH)}_2\text{-N}_6\text{-tricosanediimine)}]\text{Cl}_3$ (m/z)	$[\text{Cr}(\text{Me}_5\text{-(CH}_2\text{OH)}_2\text{-N}_6\text{-tricosanetriimine)}]\text{Cl}_3$ (m/z)
$[\text{cage}]^{3+}$	168.1	167.4
$[\text{cage-H}^+]^{2+}$	251.7	250.7
$[\text{cage-2H}^+]^+$	502.3	500.3
$[\text{cage-COH-2H}^+]^+$	273.3	271.3
$[\text{cage} + \text{H}^+ + \text{Cl}^-]^+$	287.7	—

Epilogue

" It is absolutely unbelievable how boring people become as soon as they believe their own speeches" ¹

(1) Wood, R. *Kalila and Dimna, Tales for Kings and Commoners, Selected Fables of Bidapai*; Inner Radiations, International Ltd: Rochester, Vermont, 1986.